

62-286
1162-13901

FLIGHT PERFORMANCE HANDBOOK

FOR

POWERED FLIGHT OPERATIONS

SPACE TECHNOLOGY LABORATORIES, INC.

Members of the Technical Staff

Consulting Authors

ALFONSO AMBROSIO

EDWARD MURGES

CLIVE GULVER

JOHN A. JENSEN

DAVID D. WELLS

FREDRICK WHITE

ROGER A. WINE

RE-ORDER No. 62-286

Contract No. 950055

**FLIGHT PERFORMANCE HANDBOOK
FOR
POWERED FLIGHT OPERATIONS**

**Flight Mechanics and Space Vehicle Design,
Empirical Formulae, Analytic Approximations and Graphical Aids**

**Edited by: J. FREDERICK WHITE
Head, Performance Optimization Section
Systems Analysis Department**

March 1962

**Prepared under Prime Contract No. NAS 7-100 to the National Aeronautics
and Space Administration, and Subcontract No. 950055 to the Jet Propulsion
Laboratory, California Institute of Technology, Pasadena, California**

**SPACE TECHNOLOGY LABORATORY, INC.
A Subsidiary of Thompson Ramo Wooldridge, Inc.
One Space Park · Redondo Beach, California**

© Copyright 1962

by

SPACE TECHNOLOGY LABORATORIES, INC.
A Subsidiary of Thompson Ramo Wooldridge, Inc.
One Space Park • Redondo Beach, California
United States of America

FIRST EDITION

ENCLOSURES

11-111-1V-3 pg. ERRATA-V-VI-VII-LX-X-XI	(12)
Chapter 1 - 1-4	(4)
Chapter 2 - 2-126	(126)
Chapter 3 - 3-79	(79)
Chapter 4 - 4-18	(18)
Chapter 5 - 5-96	(96)
Chapter 6 - 6-18	(18)
Chapter 7 - 7-47	(47)
Appendix A - A-24	(24)
Appendix B - B-30	(30)
Appendix C - C-16	(16)
Appendix D - D-16	(16)
Appendix E - E-9	(9)
Addendum - 59A	(59)
Subject Index - 1-15	(15)
Foldout - 1	(1)

TOTAL 573

ERRATA FOR "FLIGHT PERFORMANCE HANDBOOK FOR POWERED FLIGHT OPERATIONS"

PAGE	DESCRIPTION	ERROR	CORRECTION
11		J. Fredrick White	J. Frederick White
vi	second line	Aero Sciences	Aerosciences
vi	middle of second paragraph	Thompson-Ramo	Thompson Ramo
vii		Johns Wiley	John Wiley
vii		Cullen	Culler
xi	under Appendices	Systems Considerations	System Considerations
2-21	3rd line down	Section 3.1.3	page 3-27
2-32	vertical scale on lower curve	50,000 48,000 46,000 44,000	5000 4800 4600 4400
2-43	bottom of curve	Final Orbital Altitude	Final Orbital Altitude (n mi)
2-47	side of curve	Transit Time, T (n.mi.)	Transit Time, T (min)
2-51	bottom of curve	Final Orbital Altitude (min)	Final Orbital Altitude (n.mi.)
2-52	2nd equation	$\mu_e = 1.40766 \times 10^6 \text{ ft}^3/\text{sec}^2$	$\mu_e = 1.40766 \times 10^{16} \text{ ft}^3/\text{sec}^2$
2-65	7)	steps 1 through 7	steps 1 through 6
2-103	paragraph in wrong order -- paragraph entitled <u>Performance Evaluation etc.</u> comes before paragraph entitled <u>Coasting</u>		
2-104	Line under Equation 51 beginning with "where" ending with "planet" should be stripped in under Equation 52.		
2-106	last equation on page	$\dot{\epsilon} = \beta_2 + \theta_2 - \alpha_2$	$\epsilon_2 = \beta_2 + \theta_2 - \alpha_2$
2-110	second line of last para	$I_{sp_{sl}} I_{sp_{vac}} = 0.881$	$I_{sp_{sl}} / I_{sp_{vac}} = 0.881$
2-111	1st equation	$V_I = g_e I_{sp_{vac}} \frac{W_0}{W_{B0}}$	$V_I = g_e I_{sp_{vac}} \ln \frac{W_0}{W_{B0}}$
2-115	middle of page	given by Equation (26) with $\dot{\epsilon} = 0.10$:	given by Equation (26) where $\dot{\epsilon} = 0.10 \text{ deg/sec}$:
2-117	middle page	$\dot{\epsilon} = \dots = 25,345$	24,899
2-125	in nomenclature, 7th item	β_0	β_0
3-3	2nd line from bottom	accures	accrues
3-35	2/3 down page	$\cos \lambda_0 \sin \lambda_z$	$\cos \lambda_L \sin \lambda_z$

ERRATA FOR "FLIGHT PERFORMANCE HANDBOOK FOR POWERED FLIGHT OPERATIONS"

<u>PAGE</u>	<u>DESCRIPTION</u>	<u>ERROR</u>	<u>CORRECTION</u>
3-36	4th line -- add asterisk after V_{BO} and footnote at bottom of page		*Inertial value.
3-36	5th line	fiirst	first
3-36	bottom page	$\theta_1 = R_1/60.76$	$\theta_1 = R_1/60$
3-41	in the equation	t_{BO_1} to impact	t_{BO_1} to impact
3-43	2nd para. 4th line	(Figure 30)	(Figure 25)
3-55	measurement at top of graph	50	500
3-75	1st line	Table 6	Table 3
3-75	bottom page	intial	initial
3-77	top page	$[(154.7)^2 + (87.8)^2 + (54.8)^2]^{1/2}$	$[(92.2)^2 + (61.8)^2 + (42.7)^2]^{1/2}$
4-7		no direction arrows see Figure 2	
4-15	2nd para. 2nd line	data as follows:	data (Table 4, page 3-74) as follows:
18	in nomenclature, 5th from bottom	σ Standard deviation	σ Structure factor-weight to stage weight ratio
5-2	in the footnote	The derivation for --	The derivation of
5-4	equation (7) line is too long--should come only to the end of N		
5-61, 62, 63	Figure title	(Single-Stage Vehicle)	(Single-Stage of Multistage Vehicle)
5-66	2nd para. 8th line	build	built
5-77	next to last line under 15)	condiderabley	considerably
5-83	equation (53b)	$G'(x_1) =$	$G'(x_1)$
5-86	equation (63c)	$\sigma_{INT} w_{O_1}$	$\sigma_{INT_1} w_{O_1}$
5-90	equation (88) move + sign to main line of equation		$x_1 (\sigma_{TK_1} + \sigma_{J_1}) + 1 \quad (88)$
7-12	figure caption	$E_1(\xi_1)$	$E_1(\xi)$
B-2	equation (B.7)	$\cos \lambda \sin A_z$	$\cos \lambda_L \cos A_z$
B-8	first line below diagram	Equation (B.6)	Equation (B.10)
8	Equation (B.27)	\sin^{-1}	$-\sin^{-1} \left(\frac{\tan \lambda_L}{\tan i} \right)$

ERRATA FOR "FLIGHT PERFORMANCE HANDBOOK FOR POWERED FLIGHT OPERATIONS"

<u>PAGE</u>	<u>DESCRIPTION</u>	<u>ERROR</u>	<u>CORRECTION</u>
B-18	equation (63)	$= \frac{\bar{R} \sin \theta}{r_e + h}$	$= \frac{(r_e + h) \sin \theta}{\bar{R}}$
B-18	equation (65)	$\zeta = \sin^{-1} \left(\frac{\bar{R} \sin \theta}{r_e + h} \right) - 90^\circ$	$\zeta = \cos^{-1} \left[\frac{(r_e + h) \sin \theta}{\bar{R}} \right]$
C-16	nomenclature missing		same as Chapter 4's
D-7, -9, and -13	equations (D.36), (D.48), and (D.62)	$= \frac{1}{x_1} \prod_{i=1}^N x_i$	$= \frac{1}{x_1} \prod_{k=1}^N x_k$
12A	line 7	u (t)	u (τ)
28A	2nd paragraph line 5	staionary	stationary

PREFACE

With the advent of the large, high-speed digital computer, many engineers have lost sight of the fact that much worthwhile information can be obtained from only a small amount of data through the use of "rule of thumb" techniques and empirical relations. This fact is especially relevant in the field of preliminary design where flight mechanics and performance evaluation are of particular interest. Here the results of analysis involving approximate input data need not be accurate to eight or ten significant figures. Accuracy within 10 percent is usually satisfactory for preliminary design purposes. Moreover, such aids also reduce the required machine computing time. For example, convergence of the digital machine solution can be accelerated through the use of close initial estimates yielded by empirical approximations. The same empirical approximations in some instances, depending upon the desired accuracy, can eliminate entirely the need for machine runs.

The Jet Propulsion Laboratory, California Institute of Technology, realizing the need for a compilation of such techniques to approximate powered flight performance and vehicle design optimization, awarded a contract in early 1961 to Space Technology Laboratories, Inc., to develop a handbook to be entitled, "Flight Performance Handbook for Powered Flight Operations." The handbook as conceived would enable a person with an engineering background to carry out a realistic design study or mission analysis of existing and conceptual space vehicles. It was intended also that use of the handbook would make possible a quick, reasonably accurate evaluation of vehicle performance without requiring the use of a costly digital computer. The handbook was to be adaptable to a wide variety of missions constrained to "real life" considerations.

At the initiation of the contract all pertinent unclassified material published within STL and by outside sources, was gathered to form a foundation for development of the handbook. The backbone of the performance evaluation portion of the handbook was built around the report "Estimating Performance Capabilities of Boost Rockets,"* P. Dergarabedian and R. P. Ten Dyke, dated 10 September 1959. In the course of the study, it was found necessary to revise, correct and extend the above report to cover a wider range of vehicle parameters and missions. Other portions of the handbook represent a documentation of many techniques previously dispersed throughout the Performance Optimization Section, Systems Analysis Department, as penciled working curves and basic experience. Writing the handbook consisted of documenting this material and providing additional information such that a complete handbook

* STL Document TR-59-0000-00792

Prelace

resulted. The planetary entry portion of the handbook was developed entirely within the Aero Sciences Laboratory, Mechanics Division, and represents a documentation of many heretofore unpublished techniques, an objective survey of relevant literature and considerable original work.

The writing of the handbook was executed under the supervision of Drs. P. Dergarabedian, Director, Systems Research Laboratory, R. M. Page, Manager, and E. H. Tempkins, Associate Manager, Systems Analysis Department. Those making major contributions to the writing of the handbook were: B. A. Wine - Booster Performance Estimation, integration of the Determination of Vehicle Performance section, Vehicle Sizing and Lunar Landing; A. Ambrosio and A. A. Jensen - Planetary Entry; P. D. Burgess - Vacuum Powered Flight Operations and editing of Trajectory Optimization for Powered Flight in Two or Three Dimensions (addendum); H. D. Culver - Performance Margin Concept and Exchange Ratio Analysis; and D. D. Werts - Lunar/Planetary Deboost and Lunar Landing.

In addition to those who developed and wrote major portions, many others made significant contributions in supporting roles: in particular, Dr. E. H. Tempkins aided in the writing of the lunar and interplanetary mission requirements; P. Steiner, acting as consultant, expedited the formulation of the solution for the upper-stage vacuum operation; I. N. Spielberg provided assistance in the area of aerodynamic heating during booster operation; Dr. B. D. Fried, presently of Thompson-Ramo Wooldridge, Inc., contributed material for correlation and inclusion in the addendum; H. R. Wilkinson's research, in support of the writing of Chapter 7, Planetary Entry, led to development of the formulae on the heating associated with entry into planetary atmospheres; R. L. Younkis's investigations resulted in establishing values for the Venus atmospheric model; H. G. Myer studied the approximations for convective heating for various body shapes; and W. Schroder and R. D. Shinkle performed all the general computation and graphical preparation. Ethel E. Johnson edited the rough draft and effected all coordination between the authors, technical writers, technical illustrators, typists, and those who reproduced the book.

This handbook for powered flight operations was made possible by funds granted under JPL Contract Number 950055 and under the JPL technical direction of Dr. S. E. Benesch, assisted by L. A. Baron, W. Brofman, N. R. Haynes, E. Pounder and G. C. Sozio.

Space Technology Laboratories, Inc.
March 1962

ACKNOWLEDGEMENTS

Permission has been granted by the appropriate authorities for the following items in the handbook:

Burton D. Fried, "Trajectory Optimization Problems in Two or Three Dimensions," Space Technology, H. Senter, John Wiley and Sons, Inc., New York, Chapter 4

Glen J. Cullen and Burton D. Fried, "Optimal Trajectories," Journal of Applied Physics, Vol. 37, pages 612 through 619, June 1966, Copyright 1966, Institute of Physics.

CONTENTS

Chapter 1

INTRODUCTION

- | | | |
|-----|--------------------------------|-----|
| 1.1 | PURPOSE, SCOPE AND ASSUMPTIONS | 1-1 |
| 1.2 | USE OF THE HANDBOOK | 1-3 |

Chapter 2

VEHICLE PERFORMANCE ESTIMATION TECHNIQUES

- | | | |
|-------|-----------------------------------------------|------|
| 2.1 | MISSION REQUIREMENTS | 2-2 |
| 2.1.1 | Orbital Missions | 2-3 |
| 2.1.2 | Lunar and Interplanetary Mission Requirements | 2-52 |
| 2.2 | DETERMINATION OF VEHICLE PERFORMANCE | 2-59 |
| 2.2.1 | First Stage Burnout Flight Path Angle | 2-65 |
| 2.2.2 | Cursory Estimation of Performance | 2-68 |
| 2.2.3 | Precise Evaluation of Performance | 2-77 |

Chapter 3

SYSTEM CONSIDERATIONS

- | | | |
|-------|---------------------------------------------|------|
| 3.1 | LAUNCH SITE LIMITATIONS | 3-1 |
| 3.1.1 | Earth's Rotation | 3-1 |
| 3.1.2 | Trajectory Inclination | 3-3 |
| 3.2 | RANGE SAFETY | 3-28 |
| 3.2.1 | Range Safety Constraints and Considerations | 3-28 |
| 3.2.2 | Impact Range and Exit Azimuth | 3-30 |
| 3.3 | LOADS AND AERODYNAMIC HEATING | 3-49 |
| 3.3.1 | Staging | 3-49 |
| 3.3.2 | Maximum Dynamic Pressure | 3-53 |
| 3.3.3 | Heating | 3-53 |
| 3.4 | GUIDANCE AND TRACKING | 3-59 |
| 3.4.1 | Elevation Angle | 3-62 |
| 3.4.2 | Vehicle Angular Displacement | 3-66 |
| 3.4.3 | Look Angle | 3-66 |

CONTENTS

3.5 PERFORMANCE MARGIN CONCEPT	3-57
3.5.1 Discussion of Performance Margin Analysis	3-67
3.5.2 Numerical Example	3-74

Chapter 4

GENERALIZED EXCHANGE RATIO ANALYSIS

4.1 ANALYTICAL RELATIONSHIPS	4-1
4.1.1 Exchange Ratios for an N-Stage Vehicle	4-2
4.1.2 Exchange Ratios for One-Stage Vehicle	4-4
4.2 GRAPHICAL PRESENTATION	4
4.3 NUMERICAL EXAMPLE	4-15

Chapter 5

VEHICLE SIZING

5.1 PAYLOAD RATIO	5-3
5.1.1 One Stage	5-3
5.1.2 Infinite Staging	5-3
5.1.3 Multiple Staging	5-4
5.2 STAGE MASS RATIO	5-5
5.2.1 One Stage	5-5
5.2.2 Infinite Staging	5-6
5.2.3 Multiple Staging	5-6
5.3 OPTIMUM SIZING FOR MINIMUM GROSS WEIGHT-PAYLOAD WEIGHT RATIO	5-64
5.3.1 Constant Structure Factor	5-67
5.3.2 Variable Structure Factor	5-68
5.3.3 Optimum Sizing Nomograph	5-73
5.4 GENERAL OPTIMUM SIZING	5-78
5.4.1 Development of Solution	5-78
5.4.2 Examples	5-80

Chapter 6

LUNAR PLANETARY DEBOOST AND LUNAR LANDING

6.1 LUNAR PLANETARY DEBOOST	6-1
-----------------------------	-----

Contents

xi

6.2	EQUATIONS FOR IMPULSIVE VACUUM DEBOOST	6-3
6.2.1	Equations for Specified Deboost Conditions	6-3
6.2.2	Equations for Specified Entry Conditions	6-7
6.2.3	Planetary Data for Deboost Equations	6-8
6.3	VELOCITY REQUIREMENTS FOR A VERTICAL DESCENT LUNAR LANDING	6-9

Chapter 7

PLANETARY ENTRY

7.1	VEHICLE DESIGN CONSIDERATIONS FOR ATMOSPHERIC ENTRY	7-1
7.1.1	Payload Considerations	7-1
7.1.2	Thermal Protection System	7-2
7.1.3	Loading of the Structural System	7-3
7.1.4	Stability and Dynamic Motion	7-3
7.1.5	Accuracy of Impact Point Prediction	7-4
7.2	ATMOSPHERES OF THE PLANETS	7-4
7.2.1	Earth	7-5
7.2.2	Mars	7-5
7.2.3	Venus	7-8
7.3	GENERAL ENTRY FUNCTION	7-9
7.4	DECELERATION FOR BALLISTIC TRAJECTORIES	7-26
7.5	HEATING FOR PLANETARY ENTRY	7-32
7.5.1	Stagnation Point Heating	7-32
7.5.2	Boundary Layer Transition	7-41
7.5.3	Radiation Heating	7-42

APPENDICES

- A. VEHICLE PERFORMANCE ESTIMATION TECHNIQUES
- B. SYSTEMS CONSIDERATIONS
- C. DEVELOPMENT OF GENERALIZED EXCHANGE RATIOS
- D. VEHICLE SIZING
- E. LUNAR/PLANETARY DEBOOST AND LUNAR LANDING

ADDENDUM

TRAJECTORY OPTIMIZATION FOR POWERED FLIGHT IN TWO OR
THREE DIMENSIONS

CHAPTER 1

INTRODUCTION

1.1 PURPOSE, SCOPE AND ASSUMPTIONS

The "Flight Performance Handbook for Powered Flight Operations" provides the vehicle designer and mission analyst with a tool for rapid design and performance evaluation. Empirical formulae, methods of analytic approximation, and graphical aids have been developed where possible to expedite the required computations. The intent of the handbook is to provide methods applicable to preliminary vehicle design studies that do not require the use of large digital computers, yet yield results accurate enough to permit a valid comparison of design alternatives. At Space Technology Laboratories, Inc., such empirical techniques are often used to generate preliminary vehicle designs and performance for internal use. However, machine integrated trajectory computations are usually made prior to publication of vehicle performance capabilities.

The handbook has been written with the idea that the user will have a basic familiarity with terms and principles associated with space vehicles. A person of two years academic background in engineering could with proper guidance evaluate the performance to be expected from a vehicle design by use of the methods it outlines. The material presented is applicable to vehicles of the current generation. However, similar techniques can be developed for vehicles of future eras by use of the Appendices. No consideration has been given to nuclear or other exotic propulsion systems. The aim of the book has been to encompass as many applicable problems as possible with a minimum number of solutions. Hence, the use of a low altitude parking orbit prior to injection to a higher energy trajectory has been concentrated on since in most cases this is the most nearly optimum mission profile. However, the solutions presented are also applicable to direct-ascent missions.

The handbook covers all the powered flight portions of typical space vehicle trajectories and also planetary entry. For the free flight portions of a vehicle trajectory, the mission analyst is referred to the companion volume* edited by R. W. Wolverton, "Flight Performance Handbook for Orbital Operations."

* "Flight Performance Handbook for Orbital Operations," ed., R. W. Wolverton, Space Technology Laboratories, Inc., September 1961. (Prepared under Contract No. NAS-8-863.)

The subject matter for evaluation of vehicle design is organized herein as follows:

Vehicle Performance Estimation Techniques: 1) mission requirements and 2) determination of vehicle performance.

Systems Considerations: 1) launch site limitations, 2) range safety, 3) loads (accelerations) and aerodynamic heating parameters, 4) trajectory constraints imposed by guidance and tracking requirements, and 5) performance margin for non-nominal vehicle performance.

Generalized Exchange Ratio Analysis: 1) analytic relationships and 2) graphical solutions.

Vehicle Sizing: 1) graphical solution of optimum sizing for minimum gross weight-payload weight ratio, 2) analytical and nomographical solution for minimum gross weight-payload weight ratio for stages of unlike parameters, and 3) general optimum sizing for any criterion.

Lunar/Planetary Deboost and Landing: 1) deboost equations and 2) simplified lunar landing analysis.

Planetary Entry: 1) vehicle design considerations for atmospheric entry, 2) atmospheres of the planets, 3) generalized entry function, 4) deceleration for ballistic trajectories, and 5) heating during planetary entry.

The real utility of this handbook becomes apparent when problems involving flight mechanics and vehicle design require rapid evaluation. Combined with a slide rule and a pad of scratch paper, the "Flight Performance Handbook for Powered Flight Operations," becomes the traveling mission analyst's vade mecum.

The following is a partial list of design methods and procedures currently being used or developed at STL, not presented in this handbook (except 1).

1. Empirical-Method: Method for order of magnitude values.
2. Two-Dimensional Trajectory Computer Programs: Trial-and-error method for parametric studies, a) parameters can be varied by the machine to explore end conditions; b) payload or trajectory energy under constraining conditions can be maximized, based upon a simplified calculus-of-variations model.
3. Three-Dimensional Trajectory Programs: Used in the Atlas, Titan and Minuteman programs for trajectory shaping and performance capability evaluation.

4. Generalized Parametric Study: Computer program used for Titan and Minuteman original design studies, but not complete for application to any other missiles. This program is currently being adapted for use in upper-stage design for space missions.
5. Optimization Program: Based on calculus-of-variations model (vacuum flight) for satellite missions. Program determines pitch program, coast time, and cut-off time.

STL plans to continue studies related to the numerical analysis convergence problem with boundary conditions imposed at the beginning and end of powered flight. Also, the generalized parametric study will be extended to include the optimization of parameters other than just minimum gross weight for a given payload and mission. The calculus of variations is useful in leading to a simple model, but a complete parameter study (partially nonanalytic) is required for final detailed calculations.

Complete optimization in many cases is useless because of uncertainty as to the accuracy of preliminary data. Also, computational evidence has indicated that a true optimization does not differ to any great extent from the parameter studies. However, an increase in the number of variables (to five or more) makes convergence extremely slow and requires many hours of machine time. However, some types of problems of five or more variables, are solved in relatively short times (10 to 20 minutes in IBM 7090 computer) by utilizing good initial estimates provided by empirical nomographs, by breaking the problem into trajectory convergence and vehicle convergence subroutines computed simultaneously, relaxing the convergence limits, and expanding the computing interval.

1.2 USE OF THE HANDBOOK

The material presented has been condensed such that the solution to the problems will be rapid. Only those equations, illustrations, nomographs, graphs, explanations, and instructions are presented in the text that are necessary to perform the actual calculations thereby expediting the solution. All derivations, assumptions, and background have been put in the appendices so that the reader can better understand the methods and extend them to solve problems not included in the scope of the handbook. Where appropriate, examples are provided to illustrate the steps of the solutions, and numerous hints have been provided to aid in solving common problems for which the solutions presented here are not applicable. By no means are all short cuts or approximations to more complex problems included since it is impossible to anticipate the endless number of special mission problems that will arise. However, judicious simplification of relatively complex problems will make them amenable to the methods given and result in solutions having a fair degree of accuracy. Often the

analyst is at first only evaluating an idea for a yes or no answer. For instance, there may be a question as to whether or not a particular combination of vehicle and payload can possibly perform a specific mission. Often the answer to such a problem can be obtained through use of the handbook in a matter of minutes.

A detailed index has been provided to permit rapid reference to specific ideas. The nomenclature for each chapter and appendix has been provided at the end of the chapter or appendix. Also, an attempt has been made to minimize use of the same symbol for different parameters. The English system of units (ft-slug-sec) is used throughout. Unclassified references, readily available, have also been included with each chapter, appendix, and addendum.

This handbook, together with the companion volume, "Flight Performance Handbook for Orbital Operations," provides the mission analyst with the means for studying most problems associated with space missions. Where possible, the format used herein is the same as that used in the handbook covering orbital operations. Because of the different requirements of the contracts under which the two handbooks were written, it was impossible to dovetail the two books perfectly.

In the addendum to this handbook is a discussion of the powered flight trajectory optimization that has been edited from work done by Dr. B. D. Fried at Space Technology Laboratories, Inc. To compliment the addendum and provide a fuller background on the subject, a list of pertinent references on this subject has been included as a bibliography in the addendum.

CHAPTER 2

VEHICLE PERFORMANCE ESTIMATION TECHNIQUES

The material presented in this chapter enables the vehicle designer to estimate a vehicle's performance without necessitating the use of a large digital computer. Two techniques have been developed. The first is a cursory analysis that permits rapid performance evaluation of either a contemplated vehicle or an existing vehicle to a reasonable degree of accuracy. The second analysis is more complete and time consuming, but estimates performance to a relatively high degree of accuracy. The second method is most useful when a vehicle design is fairly well defined. Utilizing both approaches, one can conduct a thorough vehicle design study with a minimum of time and cost. It is suggested that after a vehicle design has been established that an open loop, two-dimensional trajectory be computed on a large computer. This is beneficial since a machine integrated trajectory provides a time-history of the important trajectory parameters during first-stage atmospheric operation, whereas the analyses presented here permit computation only of the end point and critical point conditions.

In order to evaluate a vehicle's performance, first the mission requirements need to be defined. Here the primary emphasis has been placed upon missions that utilize an initial low altitude orbit prior to injection into the transfer trajectory; however, the analyses permit computation of direct ascent trajectories. Mission requirements are defined by a velocity requirement at a particular altitude. In specifying the velocity requirements for the orbital missions, it is assumed that for the low altitude orbits the vehicle flies directly into the orbit, a procedure which is usually found to be optimum. For the higher energy orbits, a Hohmann transfer maneuver is performed from the initial parking orbit. The lunar and interplanetary missions have been defined by velocity bands. The lunar mission has rather narrow velocity bands. Usually, for preliminary lunar performance evaluations, the earth escape velocity is used. For more critical lunar evaluations the velocity band associated with a peculiar transit time can be used. The interplanetary missions, however, have broader velocity bands and consistency in payload capability comparisons of different vehicles necessitates the evaluation of the performance capability for both the high and low velocity requirements. To be taken into consideration in defining the velocity requirements are those constraints imposed upon the trajectory by certain systems considerations and nonnominal vehicle performance. This analysis is detailed in Chapter 3, System Considerations.

Having defined the mission requirements, the vehicle performance capability can be evaluated. The cursory analysis for the booster is based on empirical data developed for representative parametric vehicles; and for the upper stage performance the analysis is computed by a simple analytical approximation. The more precise analysis for the booster is also developed from empirical data and categorizes the performance degradations into gravity, drag, and nozzle-atmosphere pressure (thrust-atmospheric) losses. The upper stage performance precise computation is based upon a very accurate closed-form analytic approximation that permits either the assumption of a constant pitch rate or constant inertial attitude of the vehicle's thrust axis. This analysis has been generalized and could also be used for powered-flight lunar ascent or descent trajectories. This solution, unlike many other solutions, is not constrained by small angle considerations permitting trajectory computations of either vertical or horizontal trajectories.

Included in this chapter is an illustrated example of the precise analysis for a 100-nautical mile parking orbit mission of a two-stage vehicle launched from AMR. The iterative technique required is illustrated and three iterations are performed. Such an analysis performed without the aid of a computer would consume considerable time the first time through. However, after the engineer has become familiar with the solution he should be able to perform the calculations in an hour or two. Also, many short cuts and approximations peculiar to the mission and vehicle being analyzed will be discovered after considerable use of the technique. Programming the upper-stage precise solution on a small digital computer reduces the computation time considerably.

2.1 MISSION REQUIREMENTS

A knowledge of the mission requirements is essential for performance evaluation. With respect to performance, a measure of the mission requirements is a burnout velocity and its associated altitude and flight path angle. In the determination of the optimum mission requirements many considerations other than performance are involved, for example, time of flight, error coefficients of resulting trajectory and communication distance. The methods and techniques for optimizing the mission profile are not included in the scope of this handbook. For such assistance, the reader is referred to the companion volume,¹ "Flight Performance Handbook for Orbital Operations," and the papers, "Interplanetary Navigation," "Three-Dimensional Interplanetary Trajectories," "Analytical and Numerical Studies of Three-Dimensional Trajectories to the Moon," and "Lunar Trajectories."^{2,3,4,5}

2.1.1 Orbital Missions

Graphical and tabular data are presented in this section for use in computing velocity requirements for orbital missions. With respect to performance optimization and system considerations, it is easily shown that, for interplanetary, lunar and orbital flights, it is usually most efficient to park in a low altitude orbit and, at the proper location, to inject and execute a Hohmann transfer⁶ to the proper velocity. From many studies done at STL a parking orbit altitude of about 100 nautical miles has been found to be optimum for most vehicle/mission combinations. Parking at lower altitudes may provide greater performance capability, but heating, orbit life time, and tracking become problems. For systems using a radio guidance system, parking orbit altitudes of about 120 nautical miles are sometimes found to be necessary with respect to elevation angles at burnout. For missions requiring orbit rendezvous a parking altitude of about 300 nautical miles is usually found to be optimum with respect to performance and orbit lifetime. However, even for a parking orbit altitude as low as 300 nautical miles it is often found to be beneficial to park initially at 100 nautical miles and then transfer to the rendezvous parking altitude. In regard to orbit lifetime the reader is referred to Figure 346, page 2-477 of the companion volume,¹ which shows orbit lifetime as a function of circular orbit altitude. It is seen that a satellite having a representative ballistic parameter, $W_O/C_D A$ of 10 lb/ft² has a predicted lifetime at 300 nautical miles of 800 days and at 100 nautical miles of only 0.8 day or 12 revolutions (Figure 345, page 2-475 of the companion volume¹).

Either due to specific mission requirements or vehicle constraints it is sometimes not possible to initially park in a parking orbit. Solid propellant vehicles have the problem of not having restart capability which is required if either a parking orbit-Hohmann transfer maneuver or a parking orbit-lunar or interplanetary injection profile is to be used, and often have relatively short burning times which impair the use of a parking orbit. There are techniques which circumvent these problems but the associated payload degradations may not warrant the use of the parking orbit profile. The method usually employed to alleviate the problem of short burning time is to have a coast phase between stages. This, however, requires attitude stabilization during the coast phase which necessitates a spin table to spin the vehicle or a reaction cold or hot gas attitude control system. The technique used to build in "restart" capability is to size the stage(s) to the exact increment of velocity required. However, this reduces the vehicle's flexibility for use in other missions; it also increases the required performance pad allowance because the dispersions associated with achieving the parking orbit plus each restart must be added algebraically rather than root-sum-square (R.S.S.).

Therefore, in order to reduce all these problems it is sometimes more profitable to use a direct ascent type trajectory. Here the stages are burned sequentially and usually burn out with flight path angles of the order of from 70 to 90 degrees. Probably the most severe systems constraint on this type of trajectory is the fact that the launch window for lunar, interplanetary or synchronous orbits is many times prohibitively short.

Velocity and Orbital Period versus Altitude

1. Velocity. The first figures presented, Figures 1 and 2, show the perigee velocity required, as a function of perigee altitude and orbit eccentricity, for a range in perigee altitudes of 100 to 1,000,000 nautical miles. The associated apogee altitude may be simply evaluated through use of the following equation:

$$h_a = \left[(h_p + r_e) (1 + e) / (1 - e) \right] - r_e$$

where

e = eccentricity

h_a = apogee altitude

h_p = perigee altitude

r_e = radius of the earth (3440 nautical miles).

Given specific apogee and perigee altitudes the eccentricity is

$$e = \frac{h_a - h_p}{(h_a + h_p + 2r_e)}$$

Circular orbit velocity requirements, as a function of orbit altitude, for altitudes of 0 to 20,000 nautical miles are found in Figures 3 through 6, and in tabular form for quick reference in Table 1 for altitudes of 0 to 3000 nautical miles.

2. Orbital Period. Similar figures of the resulting orbital period as a function of perigee altitude and eccentricity are presented in Figures 7 and 8, for a range in perigee altitudes of 100 to 1,000,000 nautical miles.

Circular orbit periods as a function of orbit altitudes for altitudes of 0 to 20,000 nautical miles and are found in Figures 9 through 14, and in tabular form for quick reference in Table 2 for altitudes of 0 to 3000 nautical miles.

Mission Requirements

2-5

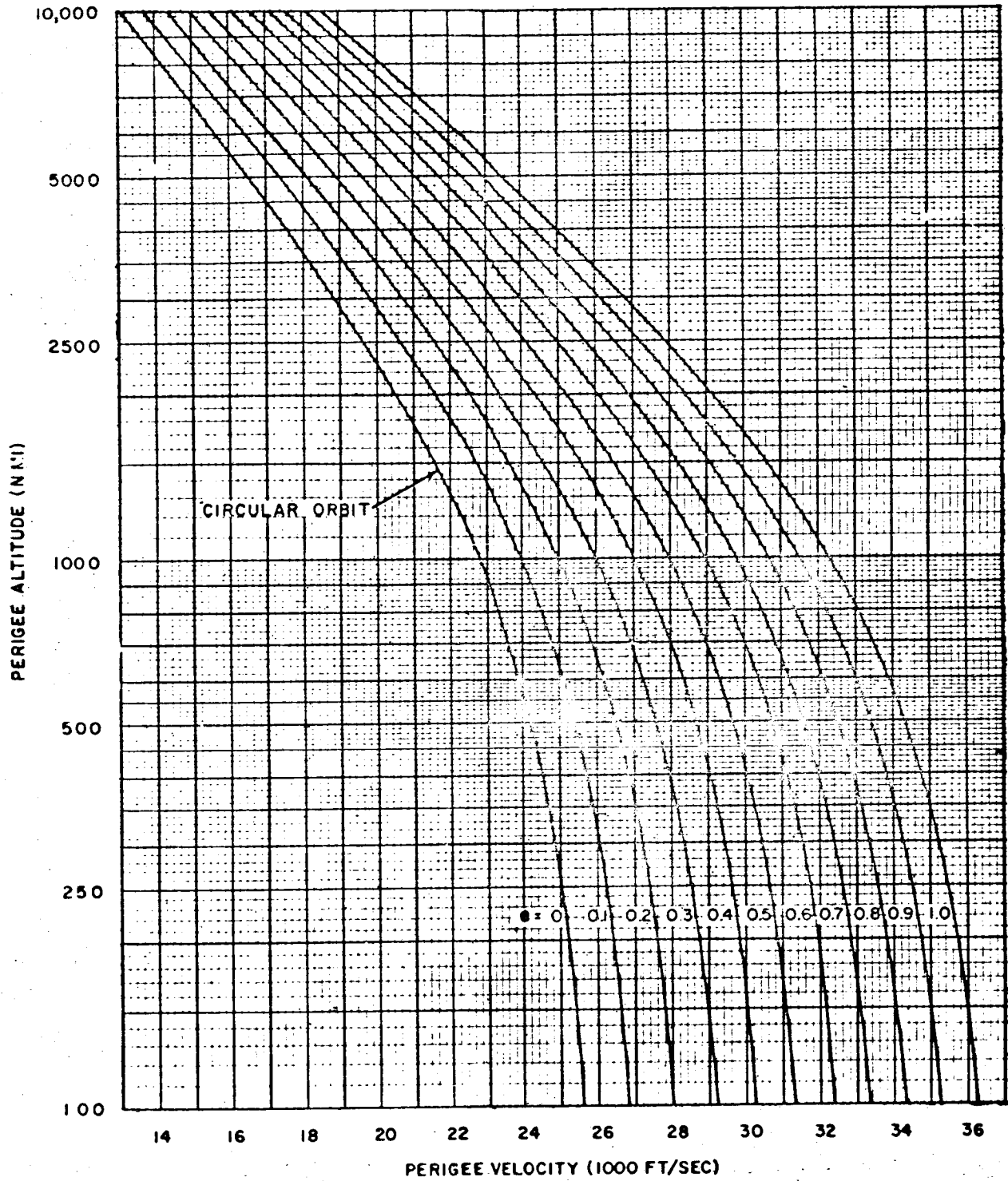


Figure 1. Elliptical Orbital Satellite Velocity

VEHICLE PERFORMANCE ESTIMATION TECHNIQUES

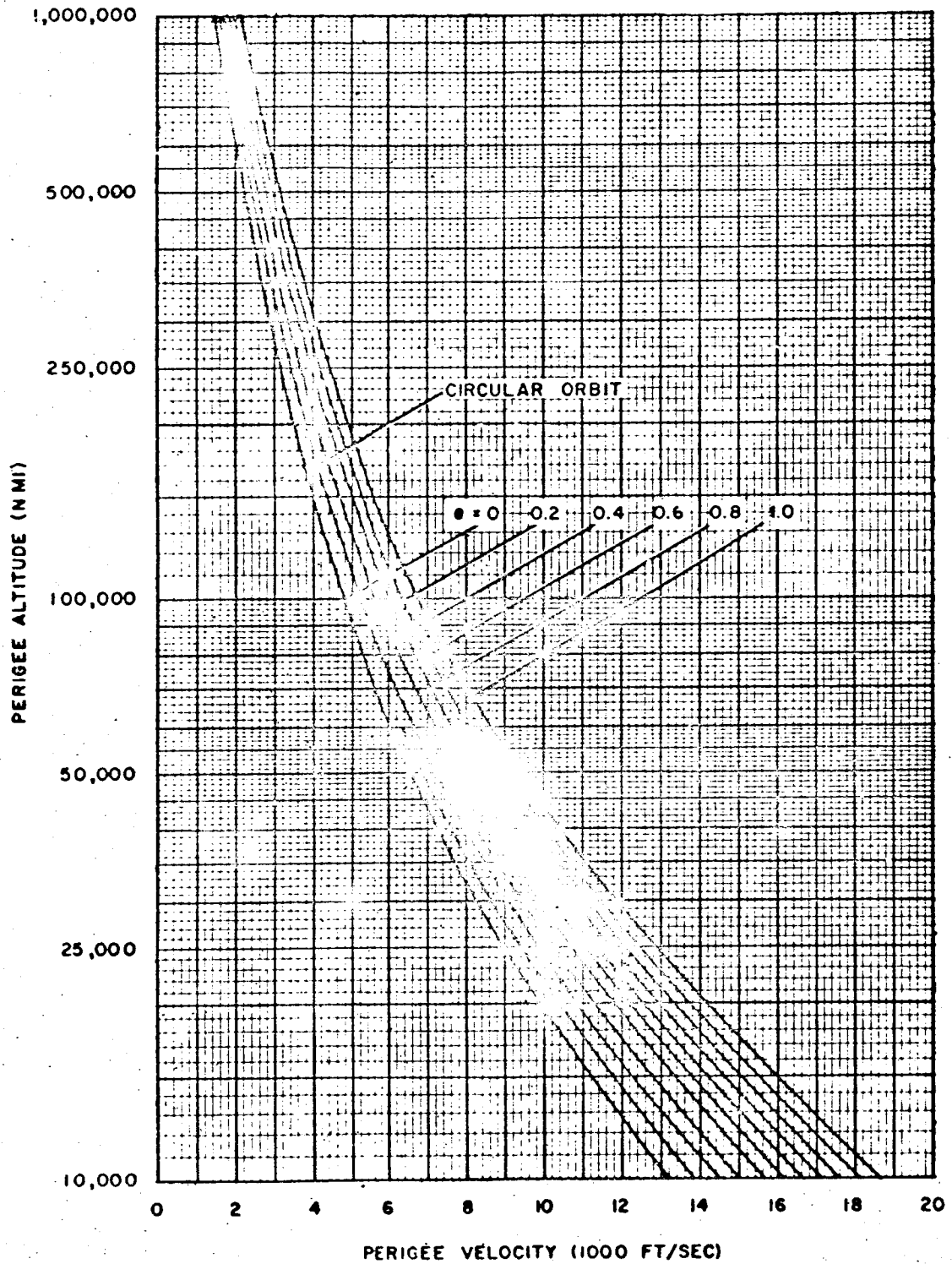


Figure 2. Elliptical Orbital Satellite Velocity

Mission Requirements

2-7

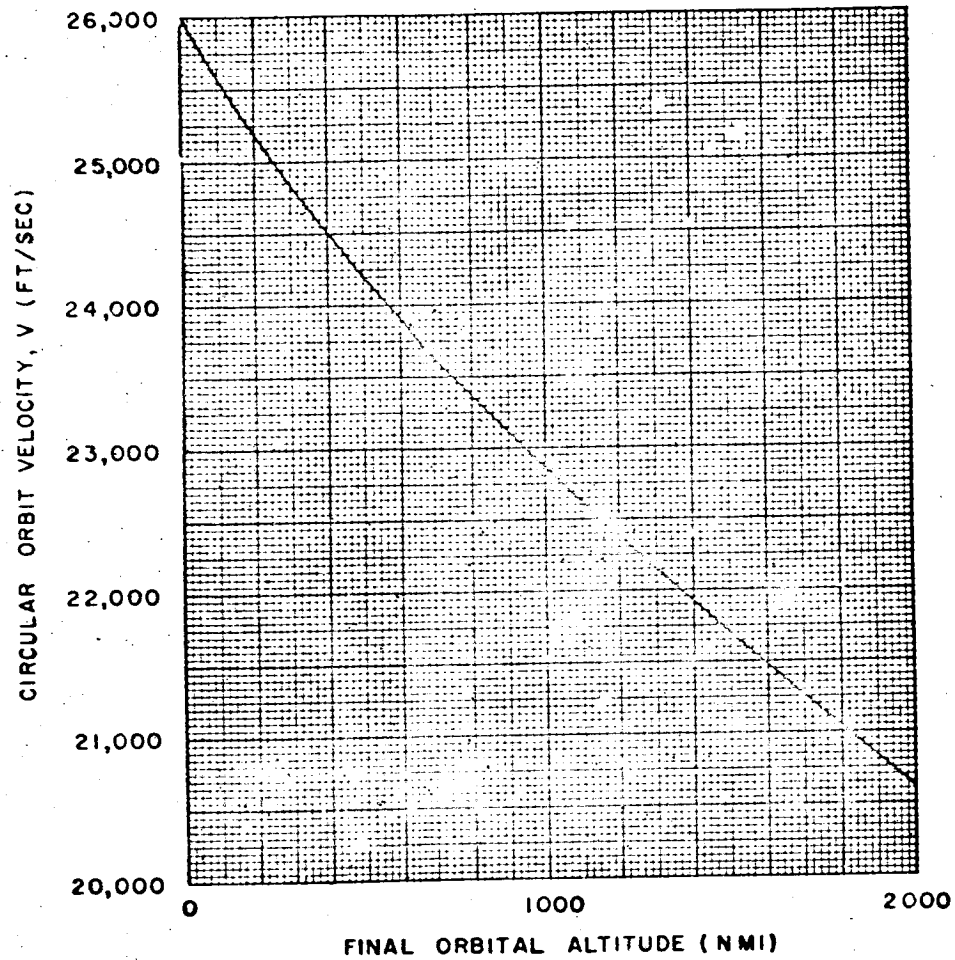


Figure 3. Circular Orbital Satellite Velocity

VEHICLE PERFORMANCE ESTIMATION TECHNIQUES

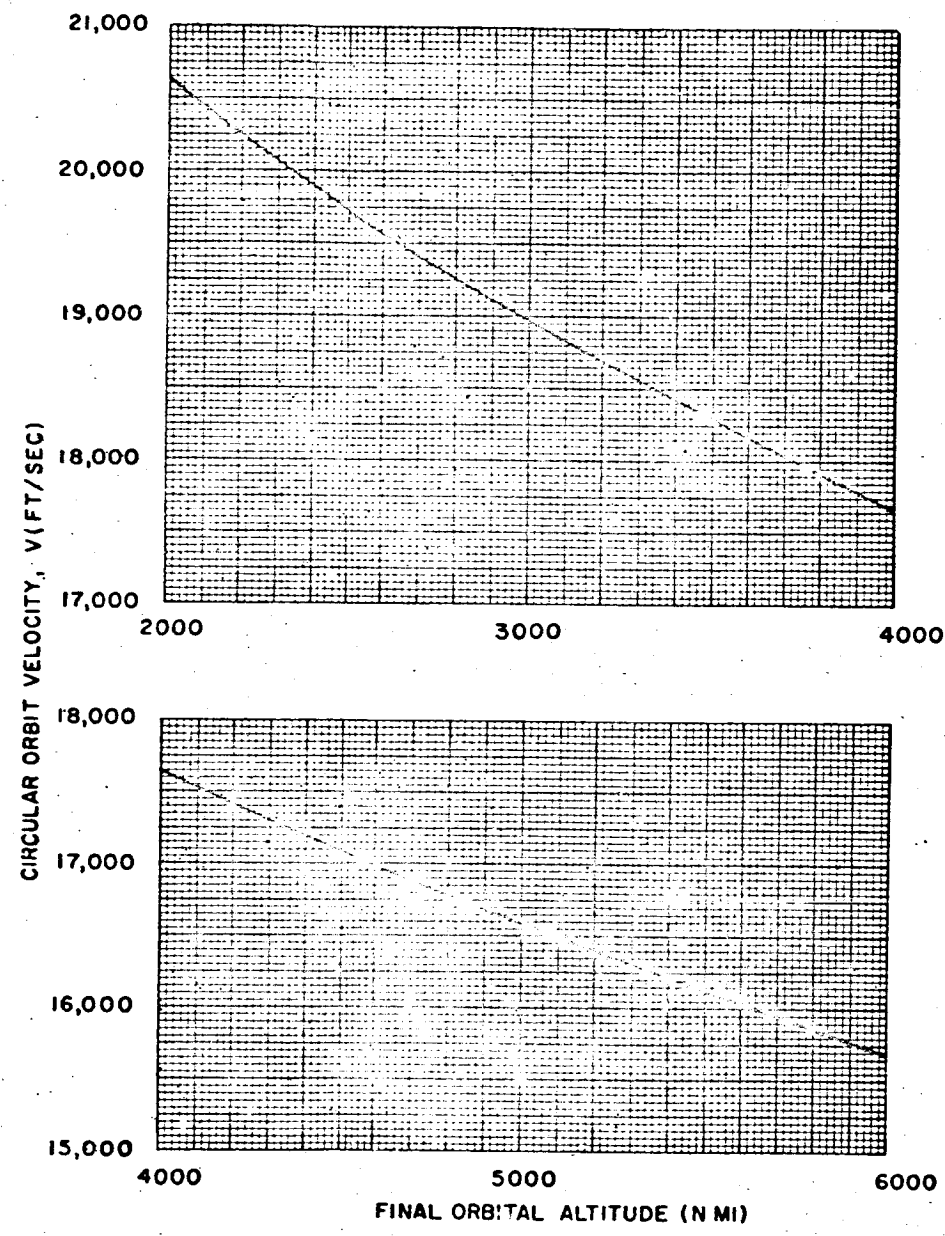


Figure 4. Circular Orbital Satellite Velocity

Mission Requirements

2-9

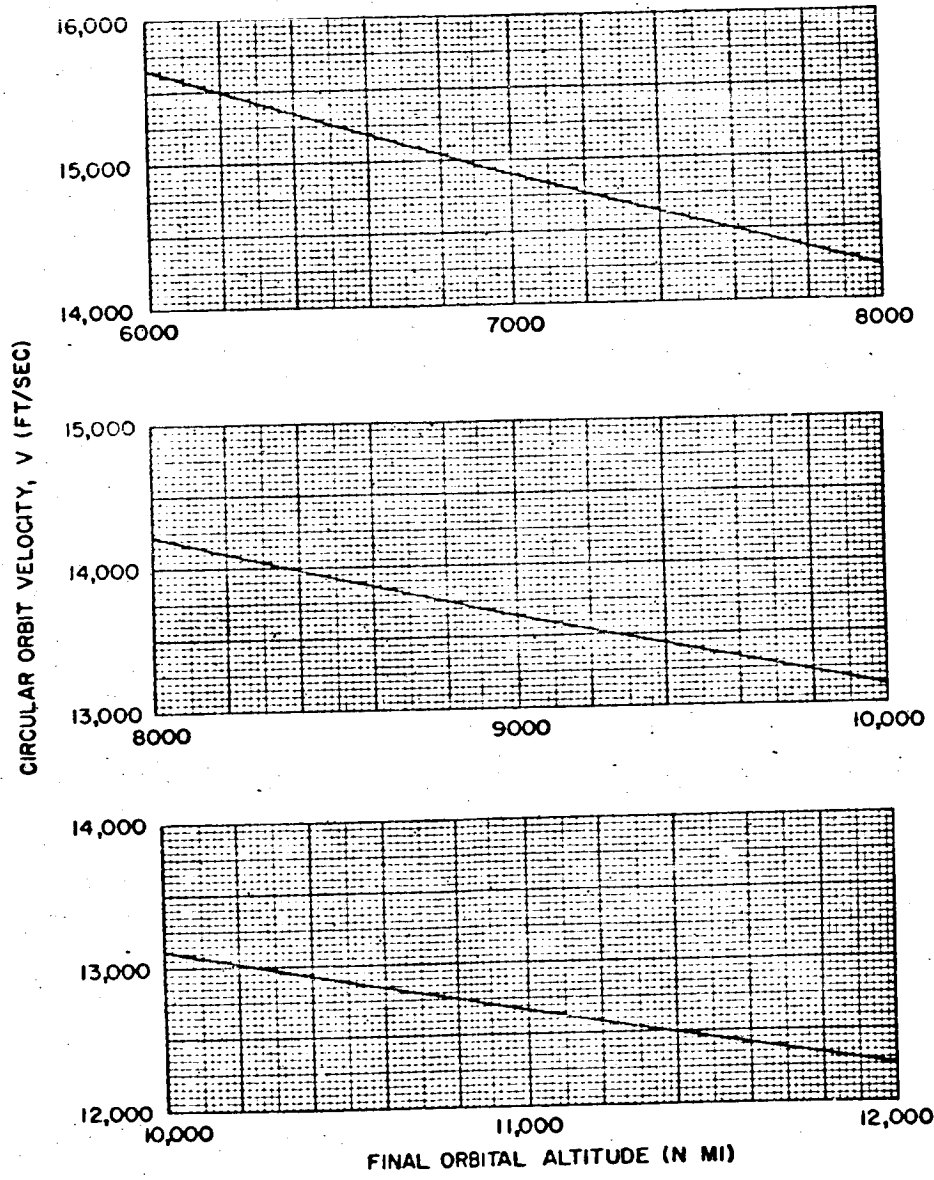


Figure 5. Circular Orbital Satellite Velocity

VEHICLE PERFORMANCE ESTIMATION TECHNIQUES

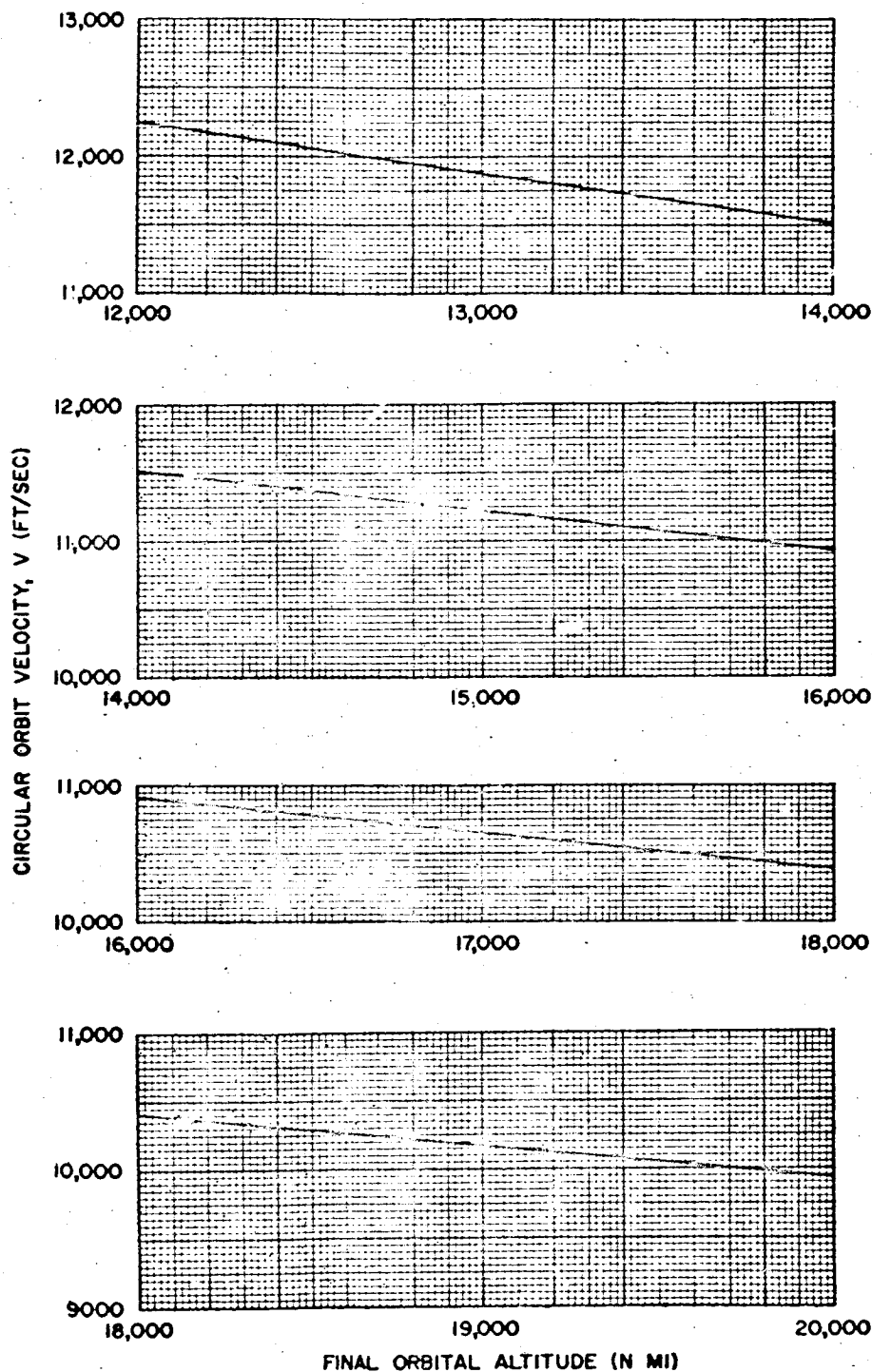


Figure 6. Circular Orbital Satellite Velocity

Mission Requirements

2-11

Table 1. Circular Orbital Satellite Velocity

Altitude (n mi)	Circular Orbital Velocity (ft/sec)									
	0	10	20	30	40	50	60	70	80	90
0	25950	25913	25875	25838	25801	25764	25727	25690	25654	25618
100	25581	25545	25509	25474	25438	25403	25367	25332	25297	25262
200	25228	25193	25159	25124	25090	25056	25022	24988	24955	24921
300	24888	24855	24822	24789	24756	24723	24691	24658	24626	24594
400	24562	24530	24498	24466	24435	24403	24372	24341	24310	24279
500	24248	24217	24187	24156	24126	24096	24066	24036	24006	23976
600	23946	23917	23887	23858	23828	23799	23770	23741	23713	23684
700	23655	23626	23598	23570	23542	23514	23486	23458	23430	23402
800	23375	23347	23320	23292	23265	23238	23211	23184	23157	23130
900	23104	23077	23051	23024	22998	22972	22946	22920	22894	22868
1000	22842	22816	22791	22765	22740	22715	22689	22664	22639	22614
1100	22589	22564	22540	22515	22490	22466	22441	22417	22393	22368
1200	22344	22320	22296	22273	22249	22225	22201	22178	22154	22131
1300	22107	22084	22061	22038	22015	21992	21969	21946	21923	21901
1400	21878	21855	21833	21810	21788	21766	21744	21721	21699	21677
1500	21655	21633	21612	21590	21568	21547	21525	21504	21482	21461
1600	21439	21418	21397	21376	21355	21334	21313	21292	21272	21251
1700	21230	21209	21189	21168	21148	21127	21107	21087	21067	21046
1800	21026	21006	20986	20966	20947	20927	20907	20887	20867	20848
1900	20829	20809	20790	20770	20751	20732	20712	20693	20674	20655
2000	20636	20617	20598	20580	20561	20542	20523	20505	20486	20468
2100	20449	20431	20412	20394	20376	20357	20339	20321	20303	20285
2200	20267	20249	20231	20213	20196	20178	20160	20142	20125	20107
2300	20090	20072	20055	20037	20020	20003	19986	19968	19951	19934
2400	19917	19900	19883	19866	19849	19832	19815	19799	19782	19765
2500	19749	19732	19715	19699	19682	19666	19650	19633	19617	19601
2600	19584	19568	19552	19536	19520	19504	19488	19472	19456	19440
2700	19424	19409	19393	19377	19361	19346	19330	19315	19299	19284
2800	19268	19253	19237	19222	19207	19191	19176	19161	19146	19131
2900	19115	19100	19085	19070	19055	19041	19026	19011	18996	18981
3000	18967									

$$r_e = 0.209029 \times 10^8 \text{ ft}$$

$$\mu_e = 1.40766 \times 10^{16} \text{ ft}^3/\text{sec}^2$$

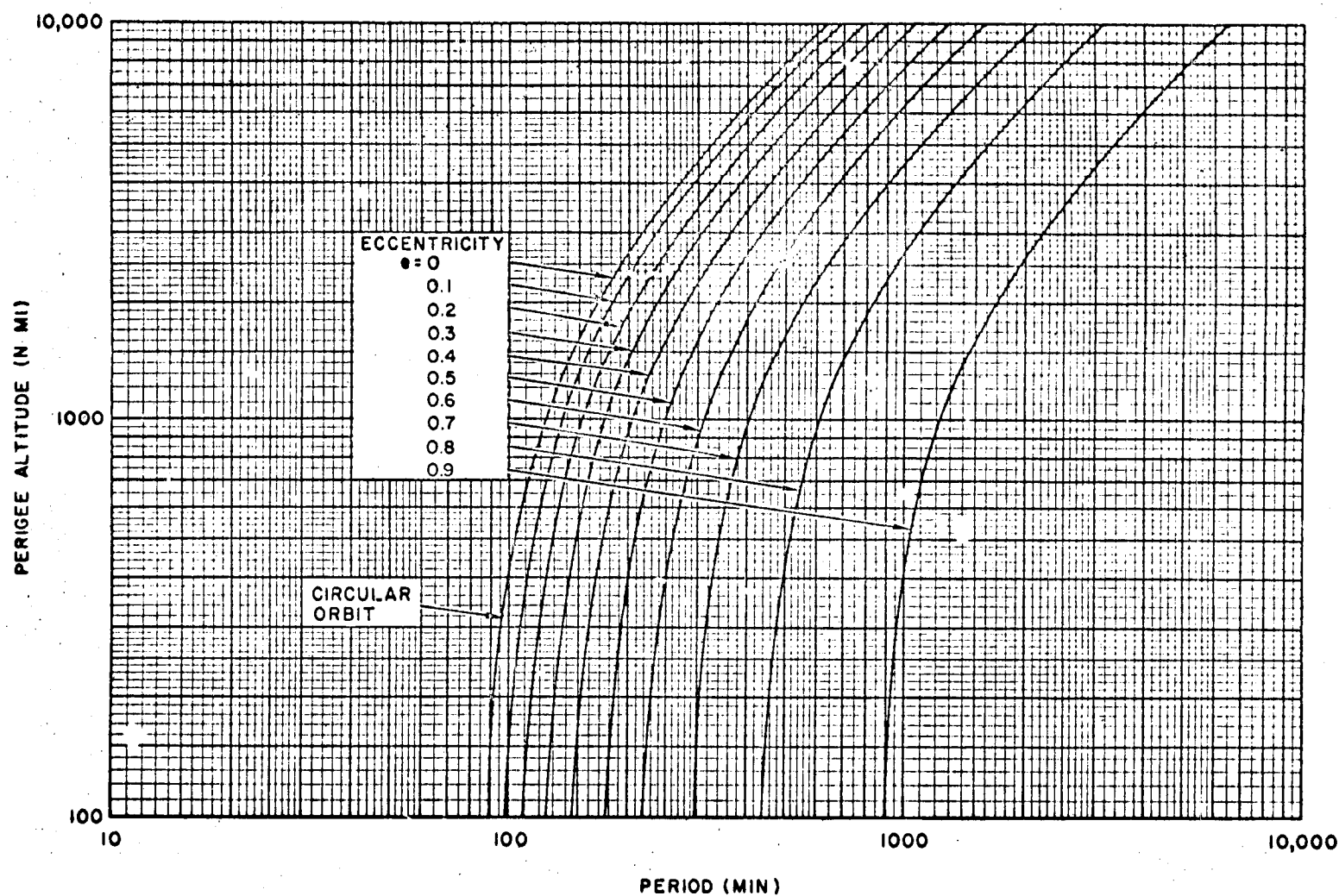


Figure 7. Elliptical Orbital Satellite Period

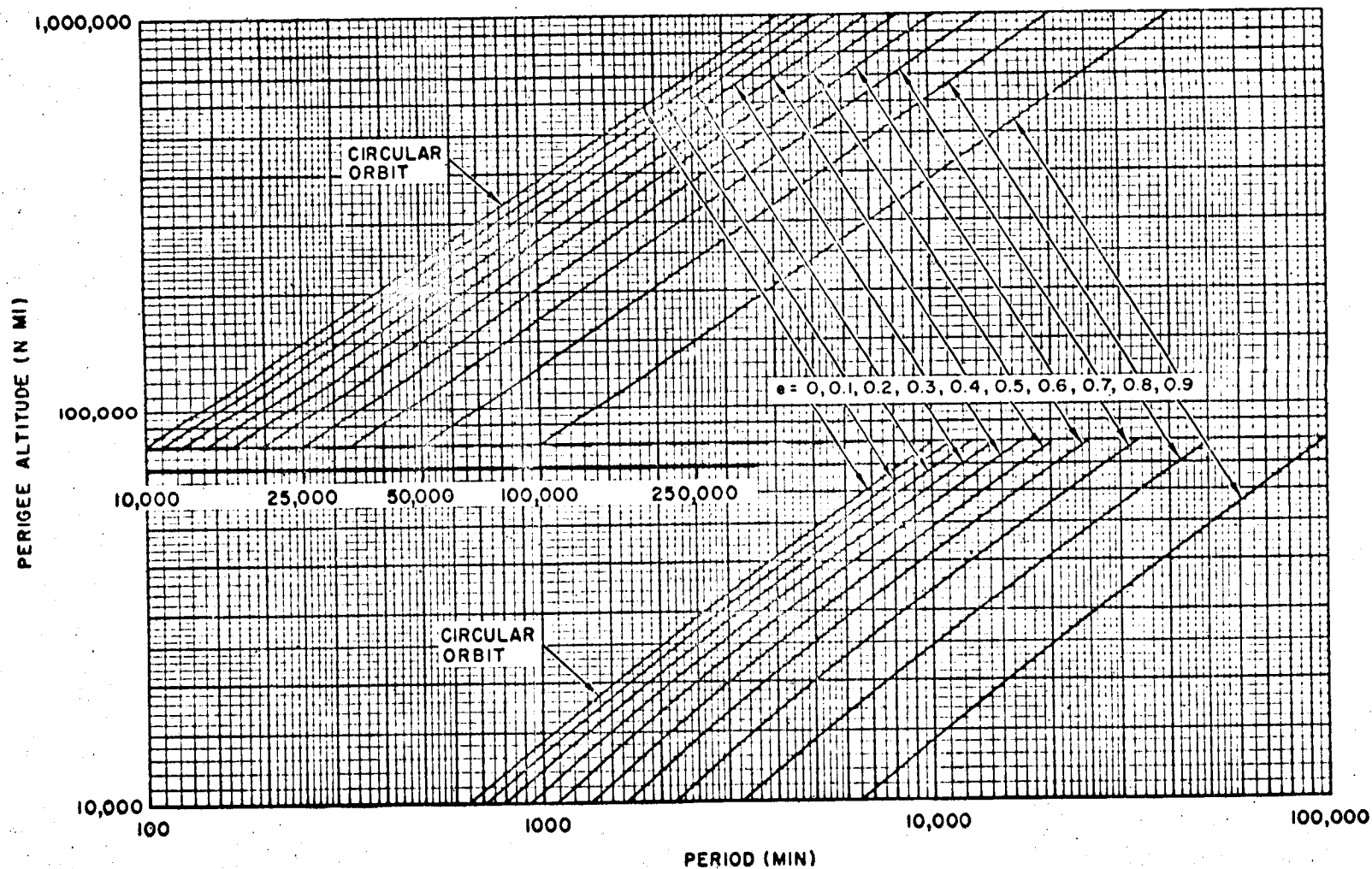


Figure 8. Elliptical Orbital Satellite Period

VEHICLE PERFORMANCE ESTIMATION TECHNIQUES

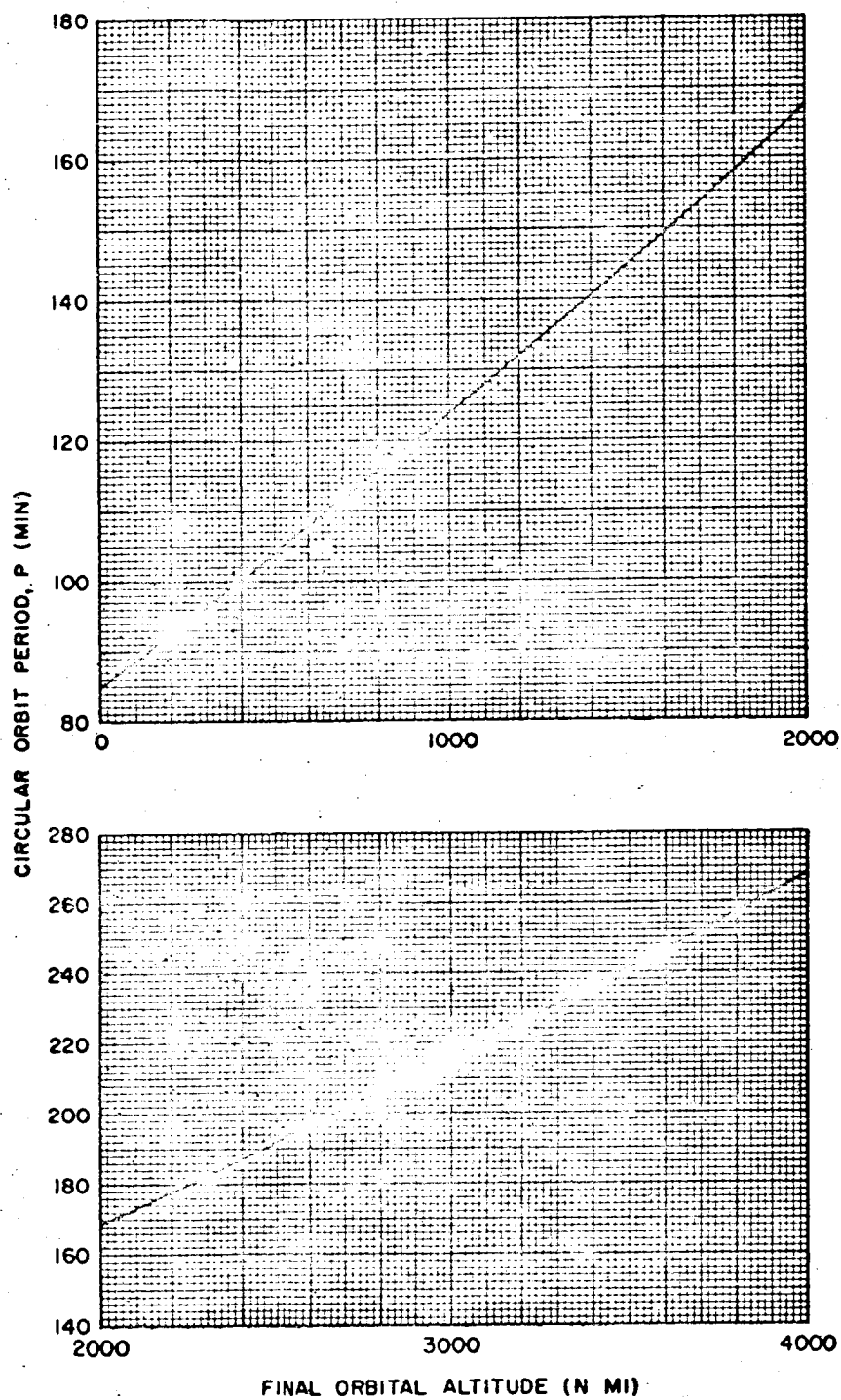


Figure 9. Circular Orbital Satellite Period

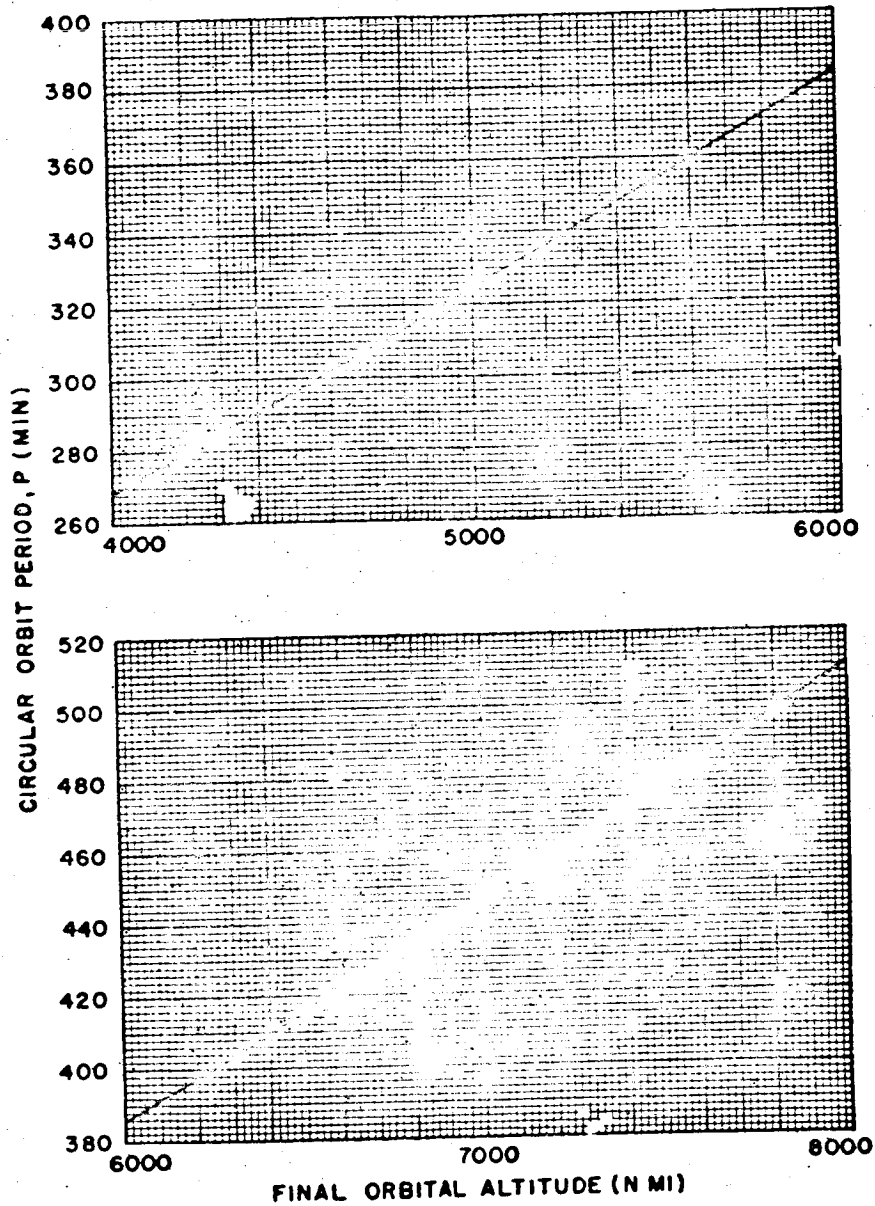


Figure 10. Circular Orbital Satellite Period

VEHICLE PERFORMANCE ESTIMATION TECHNIQUES

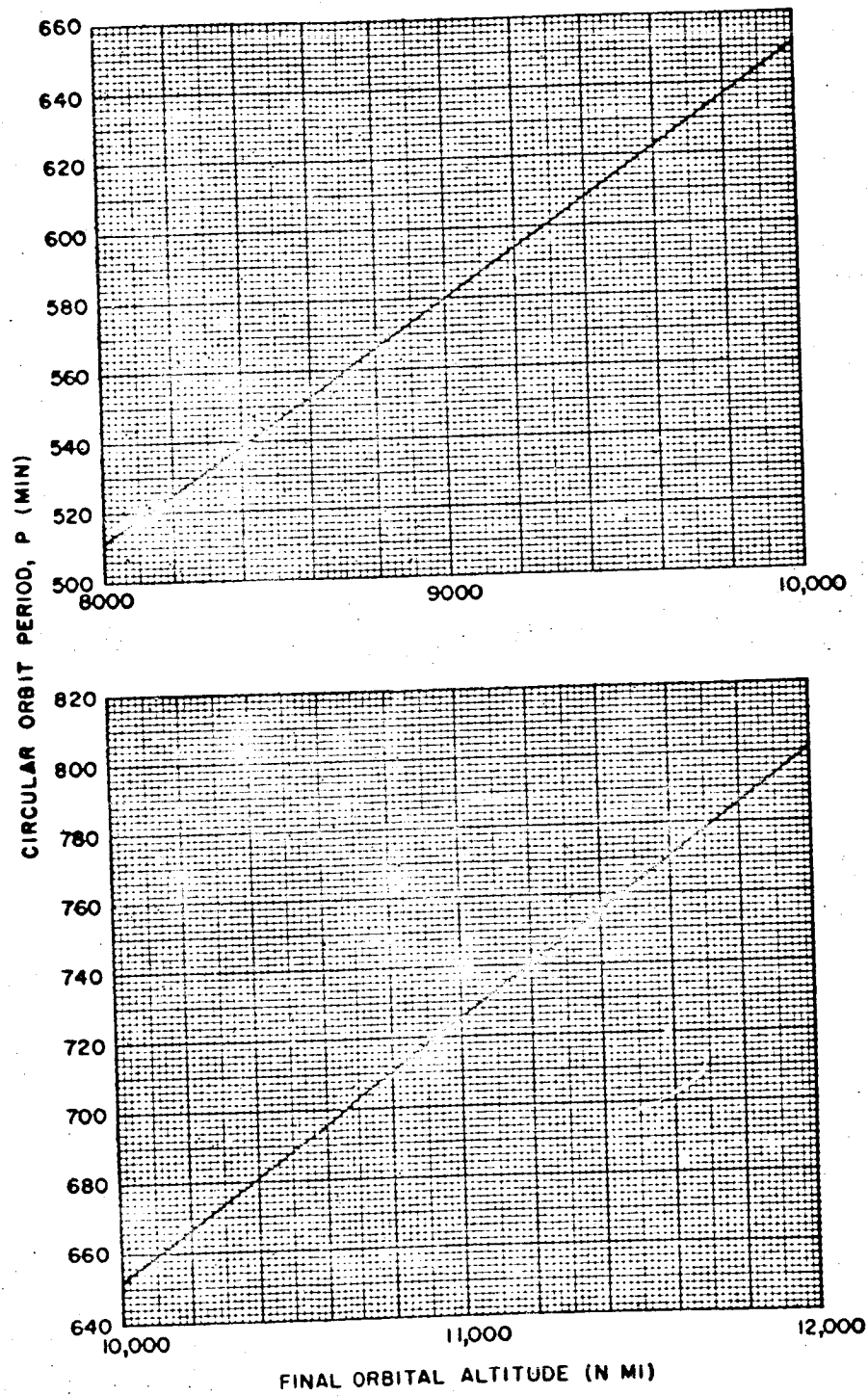


Figure 11. Circular Orbital Satellite Period

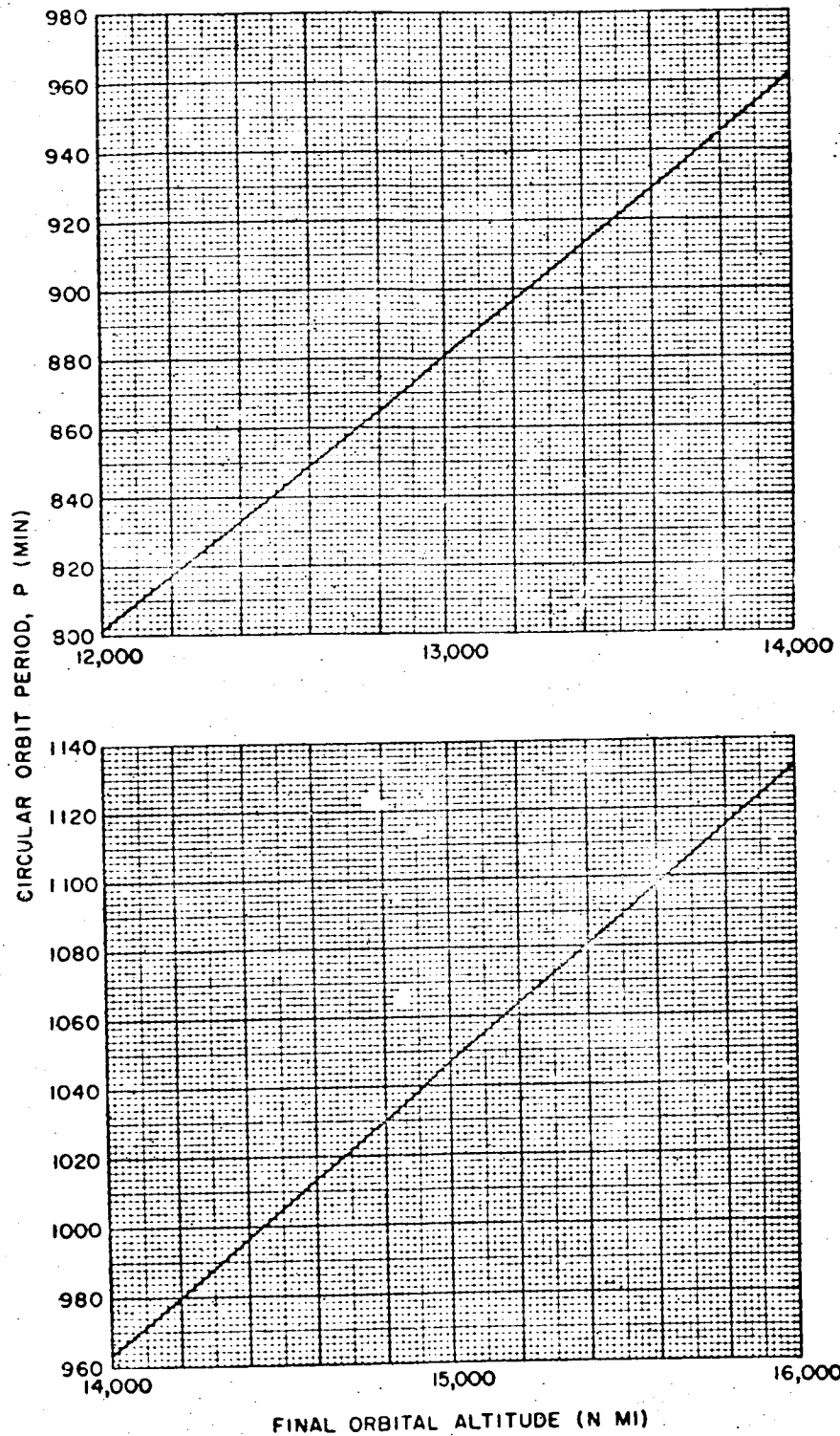


Figure 12. Circular Orbital Satellite Period

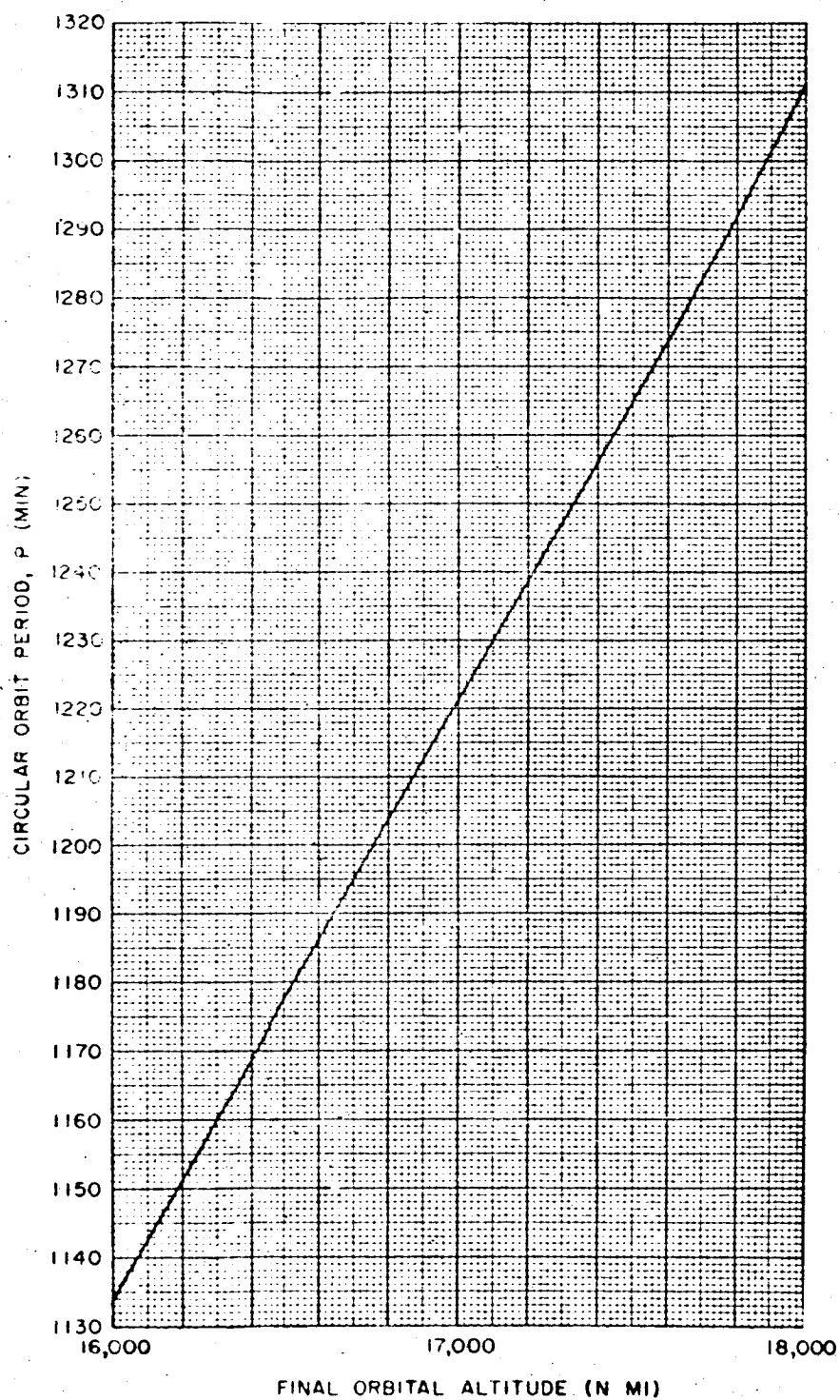


Figure 13. Circular Orbital Satellite Period

Mission Requirements

2-19

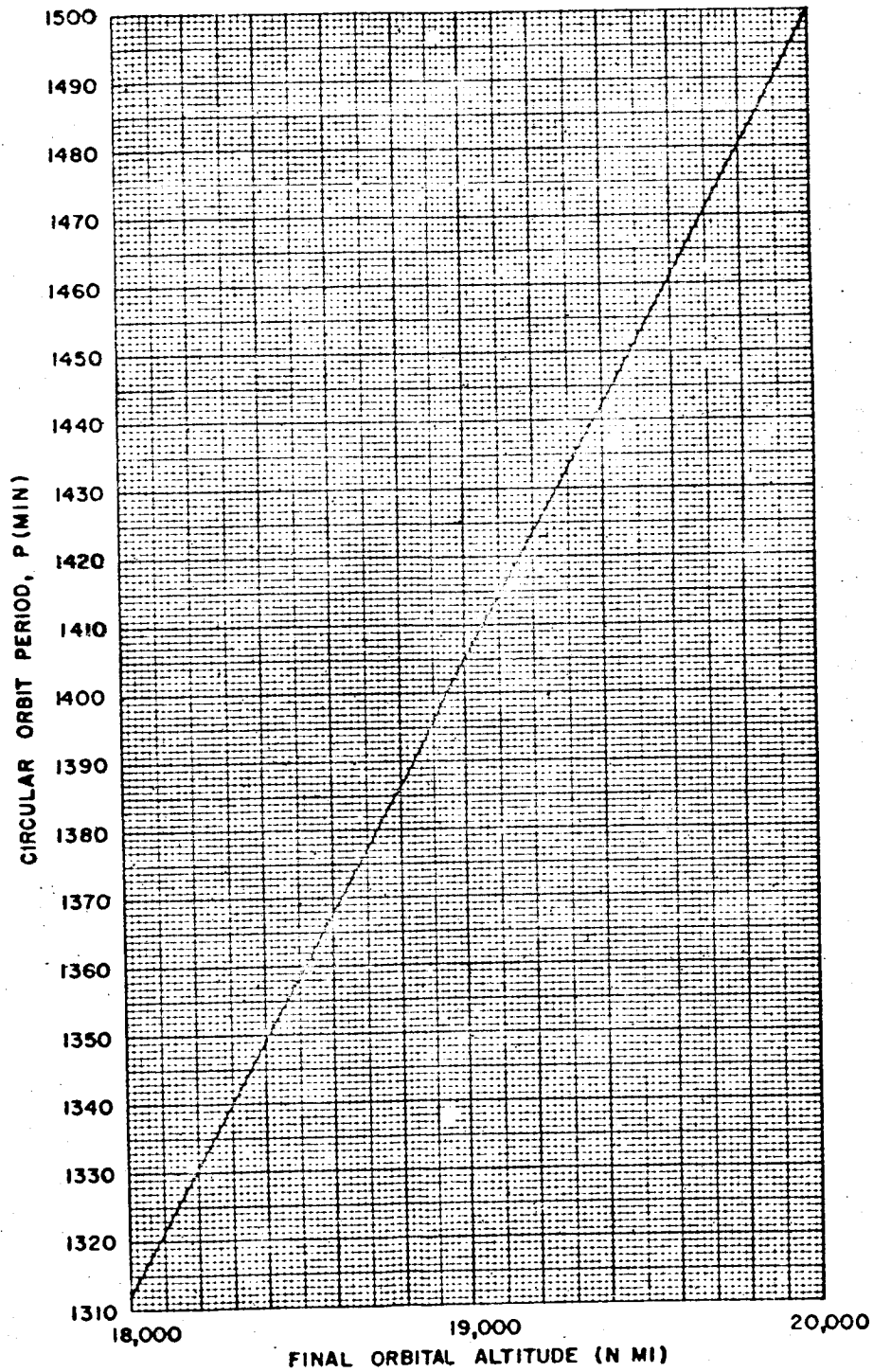


Figure 14. Circular Orbital Satellite Period

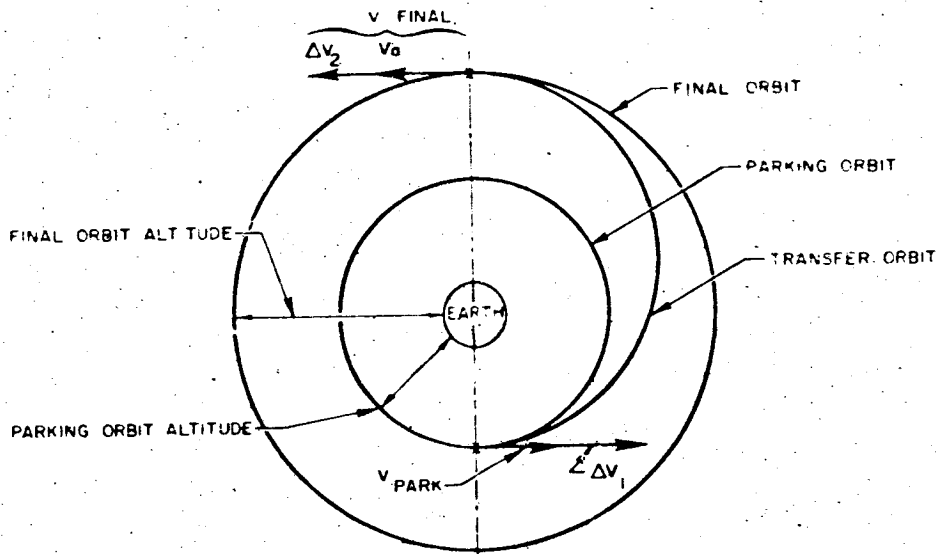
Table 2. Circular Orbital Satellite Period

Altitude (n mi)	Circular Orbital Period (minutes)									
	0	10	20	30	40	50	60	70	80	90
0	84.190	84.451	84.651	85.110	85.566	86.020	86.719	86.921	87.021	87.368
100	87.813	88.255	88.695	89.133	89.133	89.569	90.003	90.434	90.864	91.292
200	91.717	92.141	92.141	92.563	92.982	93.400	93.816	94.231	94.643	95.054
300	95.462	95.869	96.275	96.678	97.080	97.481	97.880	98.277	98.672	99.066
400	99.458	99.849	100.238	100.626	101.012	101.397	101.781	102.163	102.543	102.922
500	103.300	103.676	104.051	104.425	104.797	105.168	105.538	105.906	106.273	106.639
600	107.003	107.729	108.090	108.449	108.808	109.165	109.522	109.877	110.230	110.935
700	111.285	111.635	111.983	112.330	112.676	113.366	113.709	114.051	114.392	114.731
800	115.170	115.745	116.081	116.416	116.750	117.416	117.747	118.077	118.406	119.062
900	119.389	119.715	120.040	120.687	121.069	121.331	121.971	122.290	122.608	123.241
1000	123.557	123.872	124.499	124.811	125.123	125.744	126.053	126.362	126.977	127.283
1100	127.589	128.198	128.501	129.106	129.407	129.708	130.307	130.605	131.200	131.497
1200	132.088	132.382	132.970	133.262	133.554	134.136	134.426	135.004	135.292	135.867
1300	136.153	136.720	137.009	137.576	138.141	138.423	138.984	139.264	139.822	140.100
1400	140.655	140.930	141.484	142.033	142.307	142.853	143.126	143.669	144.210	144.480
1500	145.018	145.554	145.821	146.354	146.885	147.150	147.679	148.205	148.468	148.992
1600	149.513	149.774	150.293	150.811	151.326	151.583	152.096	152.607	153.117	153.371
1700	153.878	154.383	154.887	155.138	155.639	156.139	156.637	157.134	157.628	157.875
1800	158.368	158.859	159.349	159.837	160.327	160.808	161.050	161.533	162.015	162.495
1900	162.973	163.451	163.926	164.401	164.874	165.346	165.816	166.285	166.753	167.219
2000	167.684	168.148	168.611	169.072	169.532	169.991	170.449	170.905	171.360	171.814
2100	172.267	172.718	173.169	173.618	174.066	174.513	174.959	175.625	176.068	176.510
2200	176.951	177.390	177.829	178.266	178.921	179.355	179.789	180.222	180.653	181.299
2300	181.728	182.156	182.583	183.009	183.647	184.070	184.493	184.915	185.545	185.965
2400	186.383	187.009	187.425	187.840	188.461	188.874	189.286	189.902	190.312	190.721
2500	191.332	191.739	192.145	192.752	193.155	193.759	194.161	194.562	195.161	195.560
2600	196.157	196.553	197.147	197.541	198.132	198.525	199.112	199.503	200.088	200.477
2700	201.059	201.446	202.025	202.410	202.986	203.561	203.944	204.516	204.896	205.466
2800	206.033	206.411	206.976	207.352	207.915	208.476	208.849	209.408	209.965	210.336
2900	210.891	211.444	211.996	212.363	212.912	213.460	214.007	214.371	214.915	215.458
3000	215.999									

$$r_e = 0.209029 \times 10^8 \text{ ft}$$

$$\mu_e = 1.40766 \times 10^{16} \text{ ft}^3/\text{sec}^2$$

Hohmann Transfer. The Hohmann transfer⁶ is found to be the minimum energy maneuver for transfer between two circular coplanar earth orbits whose outer orbit has a radius of less than 41,000 nautical miles (see Section 3.1.3 for explanation). The earth Hohmann transfer consists of the addition of an impulsive incremental velocity of magnitude ΔV_1 while parked in a circular orbit, then at an apogee of the transfer orbit an incremental impulsive velocity of sufficient magnitude, ΔV_2 , is added to circularize the orbit. (See schematic diagram below.)



The assumption of instantaneous addition of the velocity tangentially is a realistic approximation for acceleration greater than $1/2 g$. For accelerations of significantly less than $1/2 g$ the reader is referred to the analysis presented in Reference 7.

For the Hohmann transfer analysis presented here representative parking orbit altitudes of from 100 to 300 nautical miles were chosen.

1. ΔV_1 . The initial incremental injection velocity ΔV_1 , required at the parking orbit altitude to transfer to an apogee altitude corresponding to the desired final orbit altitude is presented in Figures 15 and 16 for altitudes of 100 to 1,000,000 nautical miles and more accurately in Figures 17 through 21, for altitudes of 100 to 20,000 nautical miles.

2. ΔV_2 . Similarly, the incremental velocity, ΔV_2 , required to circularize the orbit as the apogee of the transfer orbit is presented in Figures 15 and 16 for altitudes of 100 to 1,000,000 nautical miles and more accurately in Figures 22 through 26, for altitudes of 100 to 20,000 nautical miles.

3. ΔV_T . The sum of ΔV_1 plus ΔV_2 , is presented in Figures 15 and 16 for altitudes of 100 to 1,000,000 nautical miles and more accurately in Figures 27 through 32, for altitudes of 100 to 20,000 nautical miles.

4. Transit Time. A parameter also of interest is the required time to execute the Hohmann transfer, T . The transit time is presented in Figures 33 and 34 for altitudes of 100 to 1,000,000 miles and more accurately in Figures 35 through 44, for altitudes of 100 to 20,000 nautical miles.

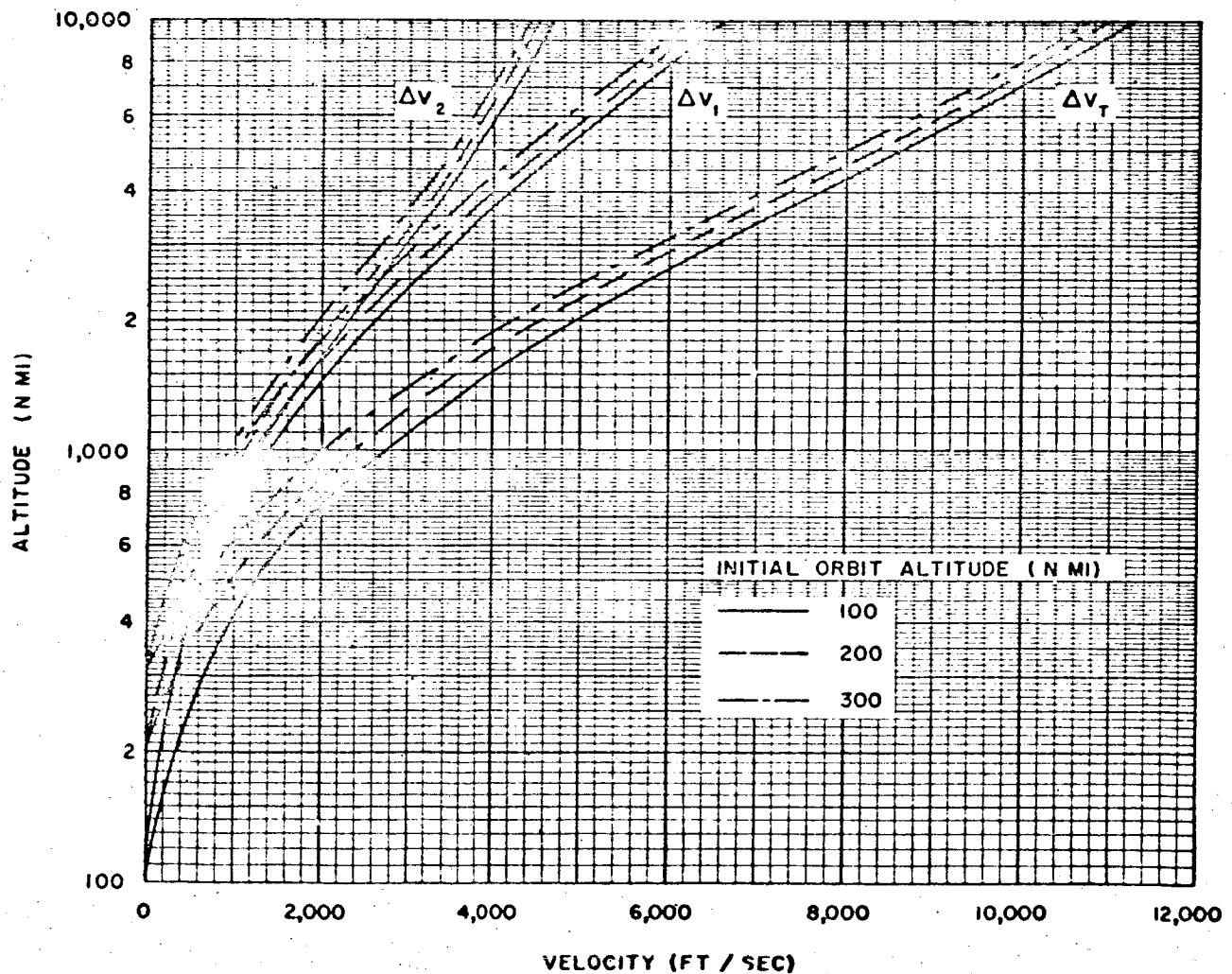


Figure 15. Hohmann Transfer Velocity Requirements

Mission Requirements

2-23

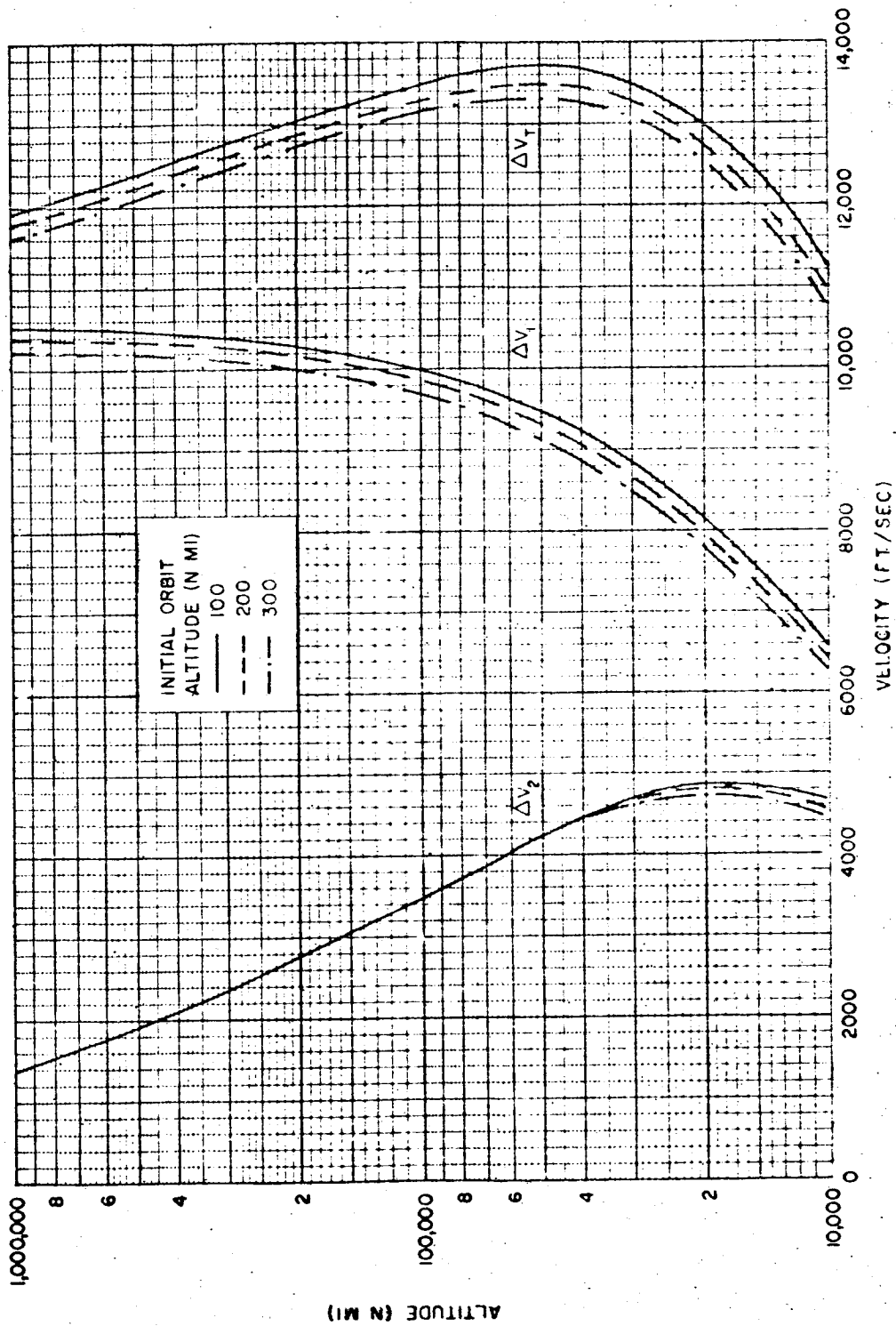


Figure 16. Hohmann Transfer Velocity Requirements

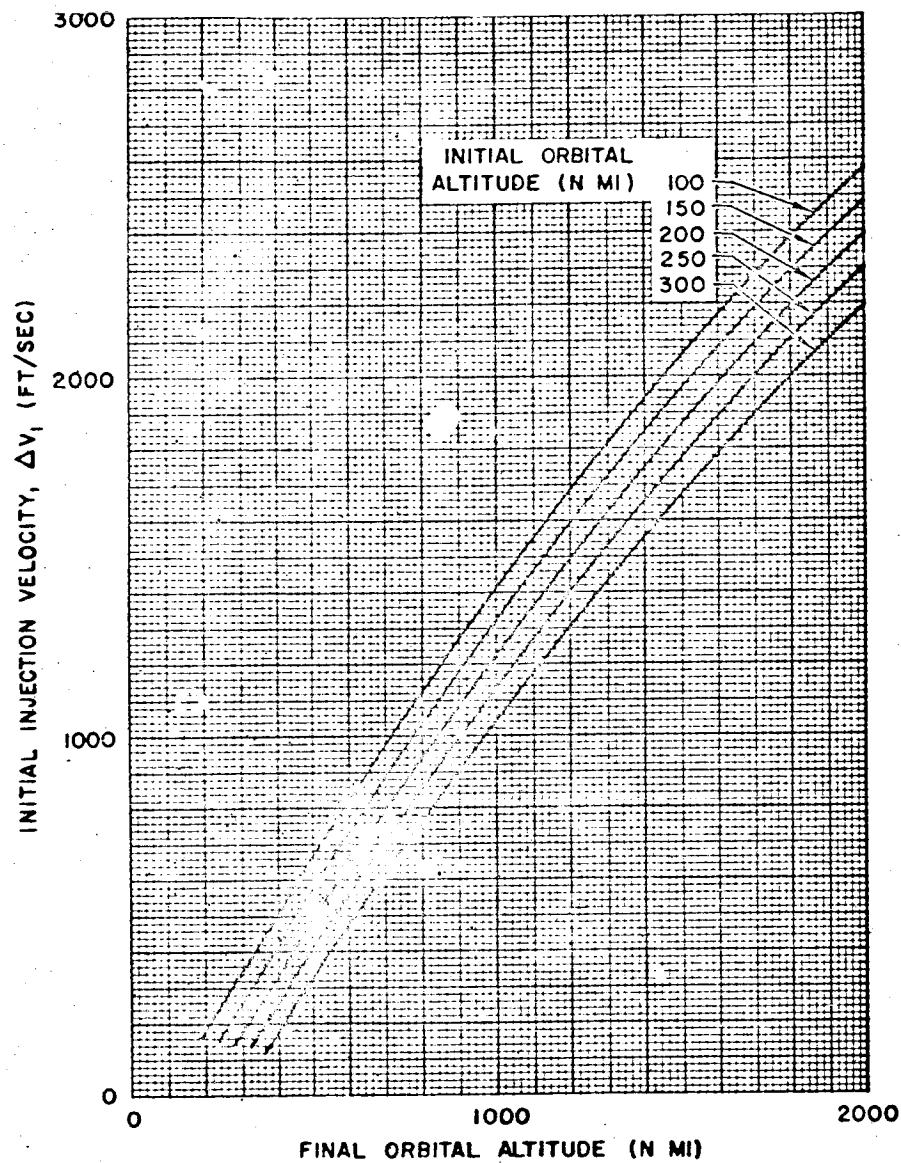


Figure 17. Initial Hohmann Transfer Injection Velocity Requirements

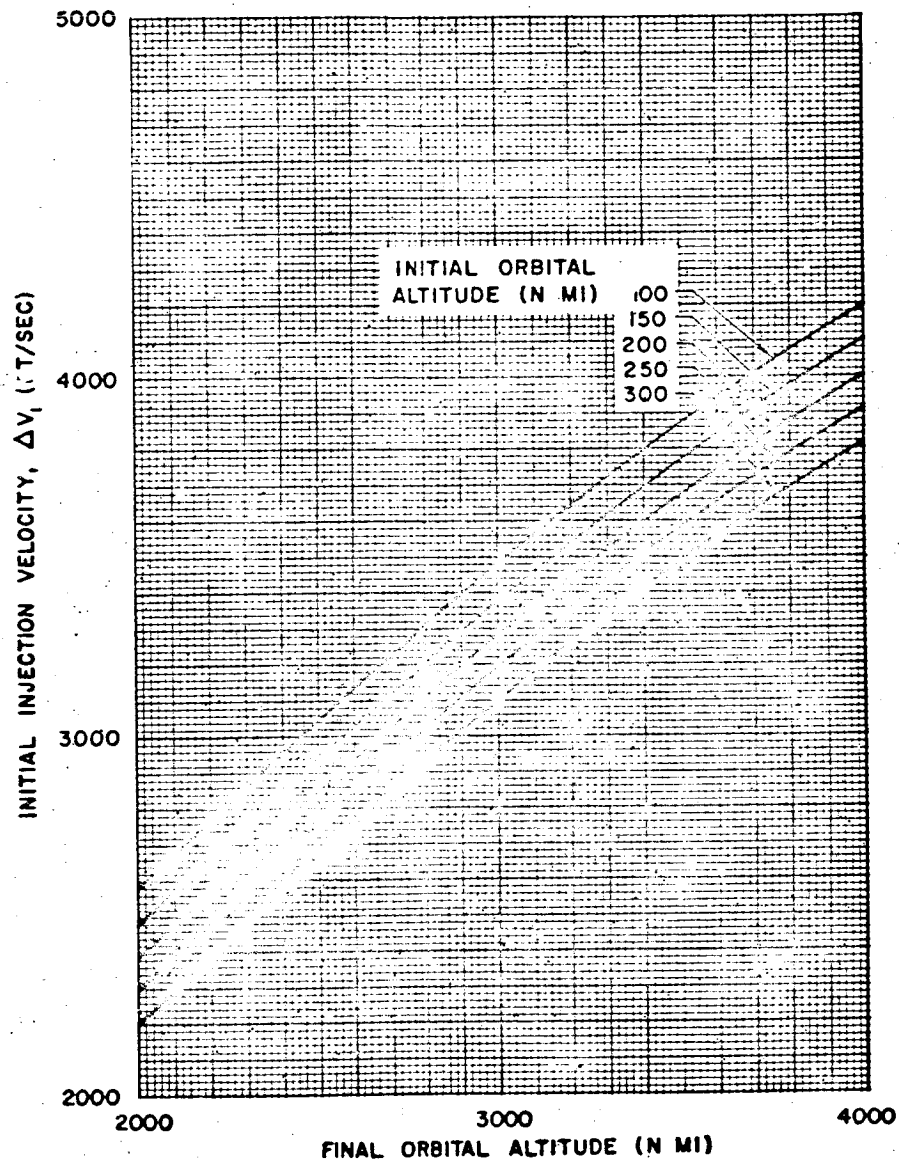


Figure 18. Initial Hohmann Transfer Injection Velocity Requirements

VEHICLE PERFORMANCE ESTIMATION TECHNIQUES

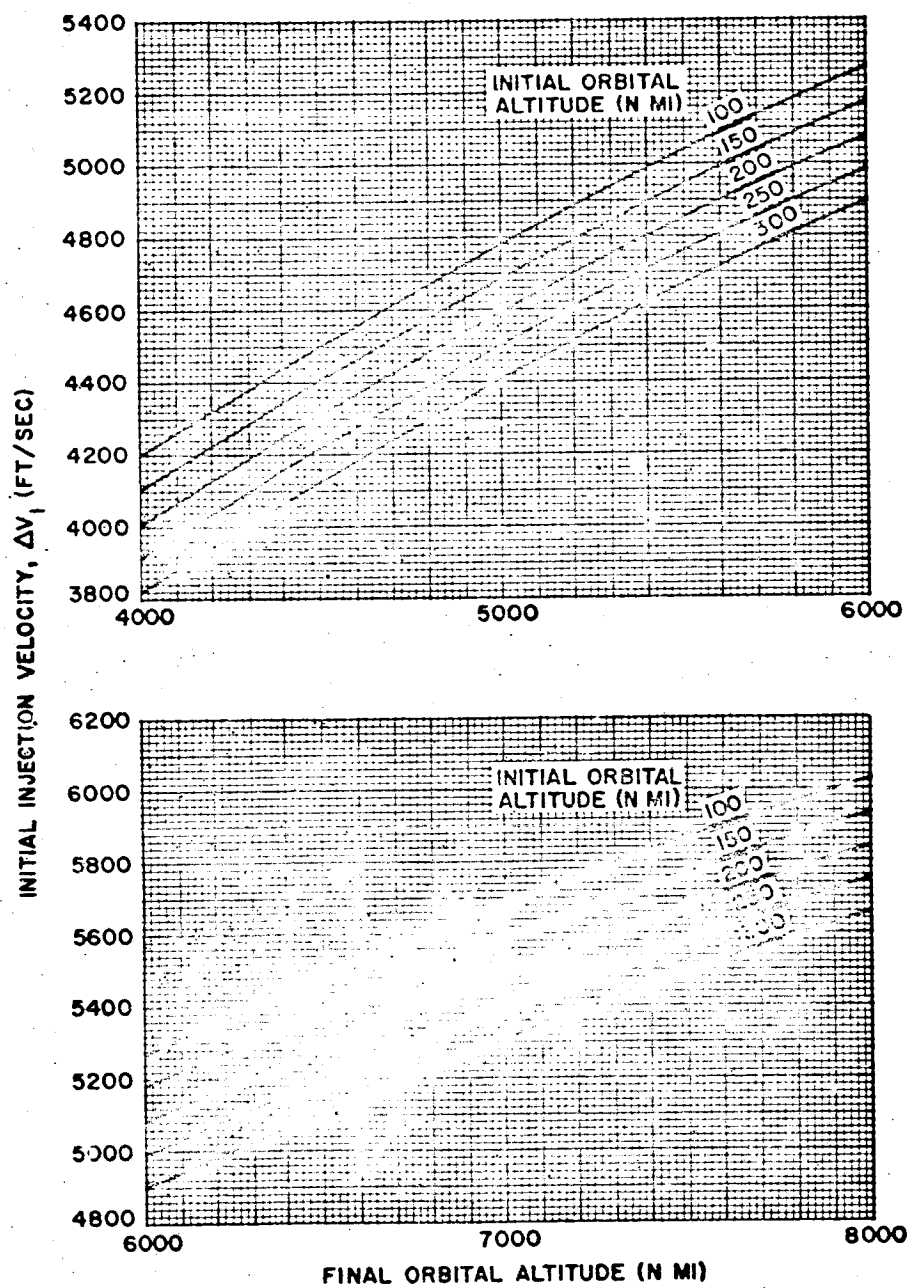


Figure 19. Initial Hohmann Transfer Injection Velocity Requirements

Mission Requirements

2-27

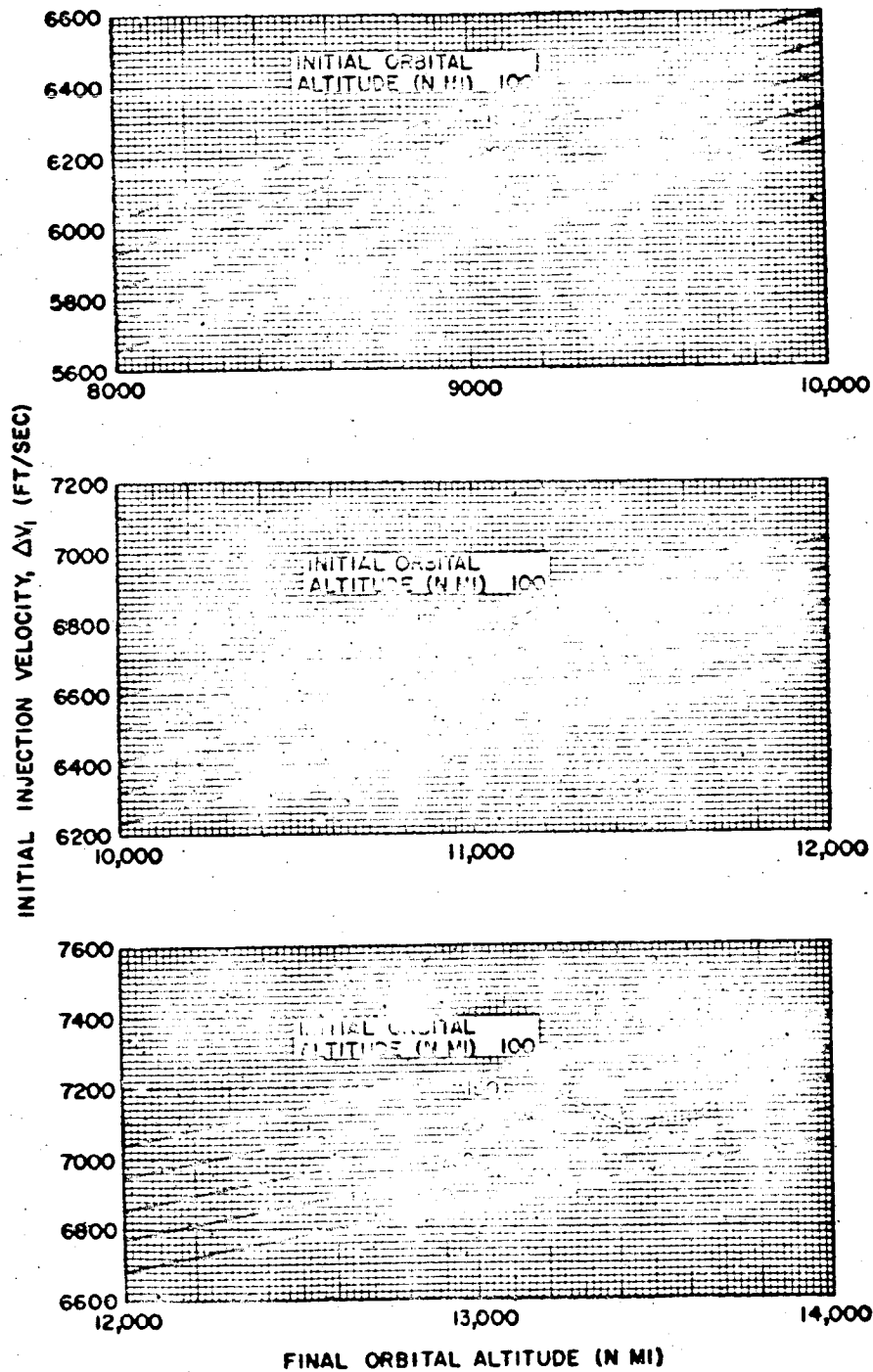


Figure 20. Initial Hohmann Transfer Injection Velocity Requirements

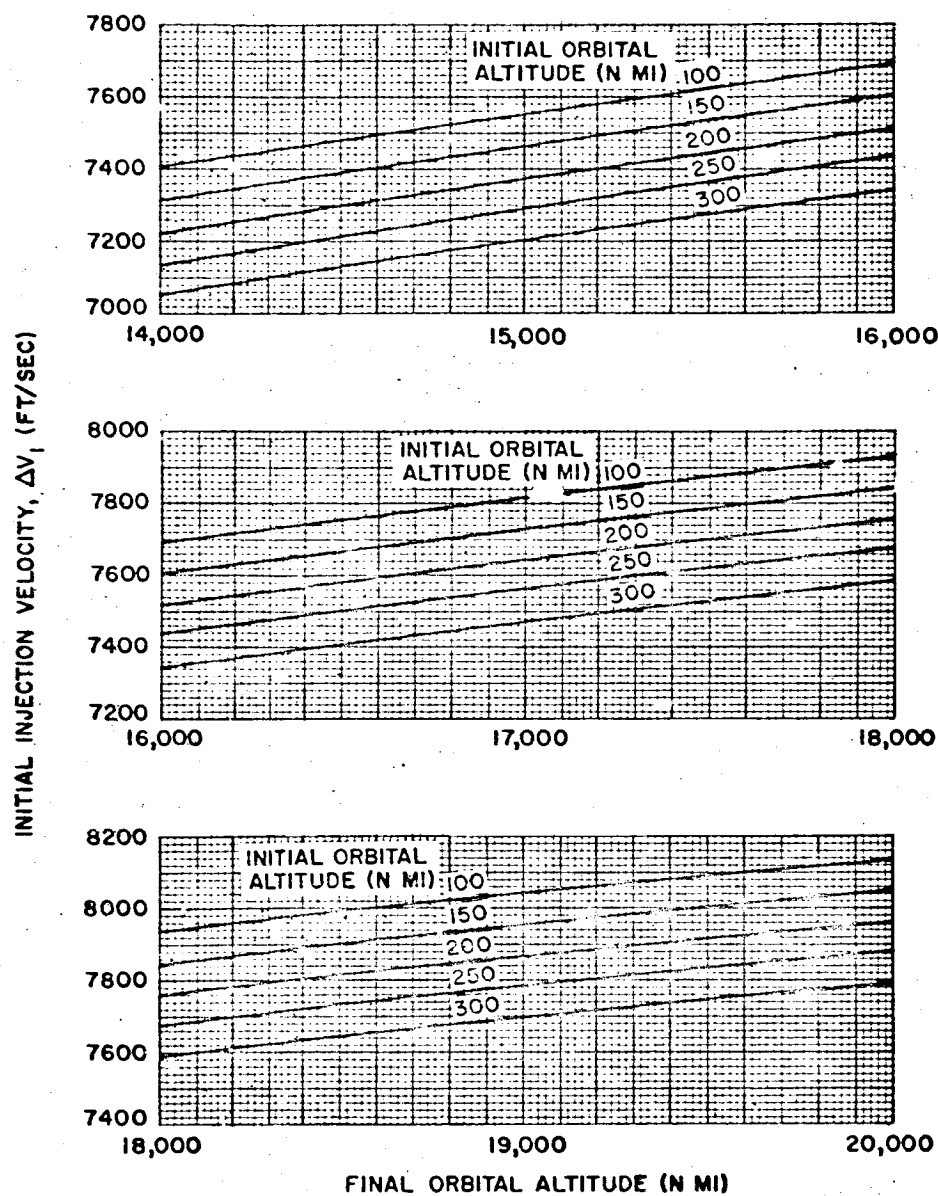


Figure 21. Initial Hohmann Transfer Injection Velocity Requirements

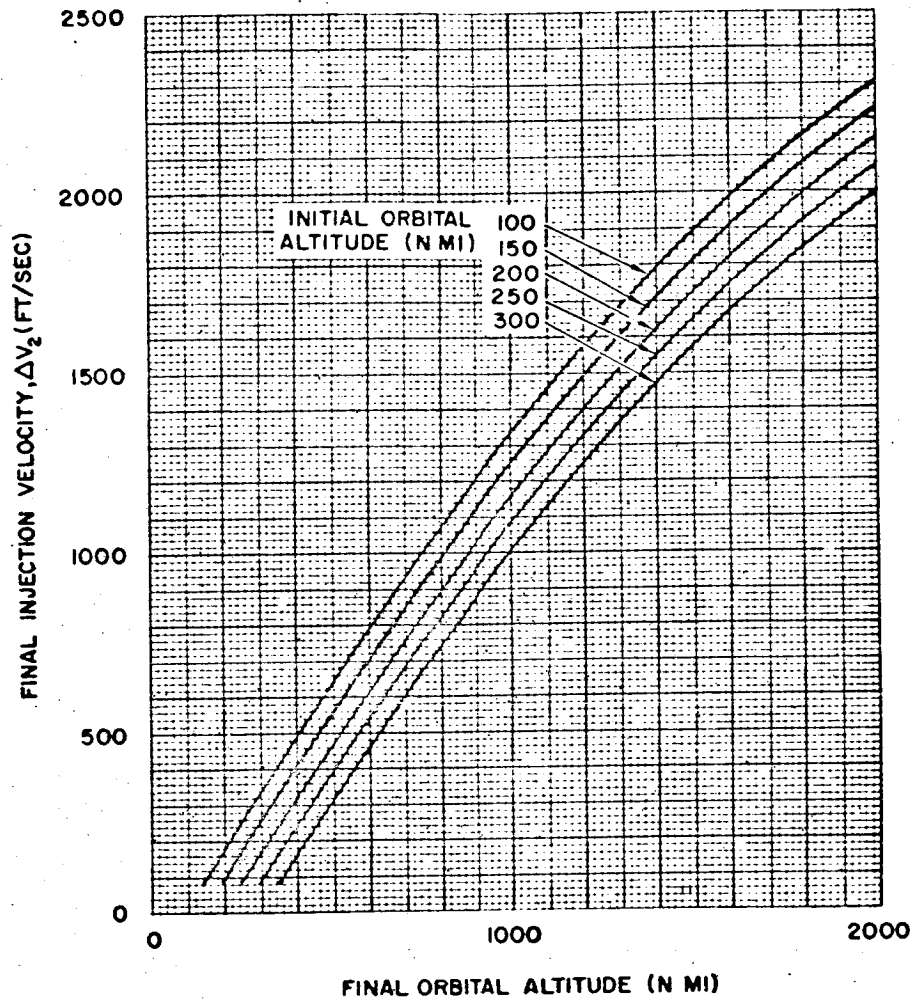


Figure 22. Final Hohmann Transfer Injection Velocity Requirements

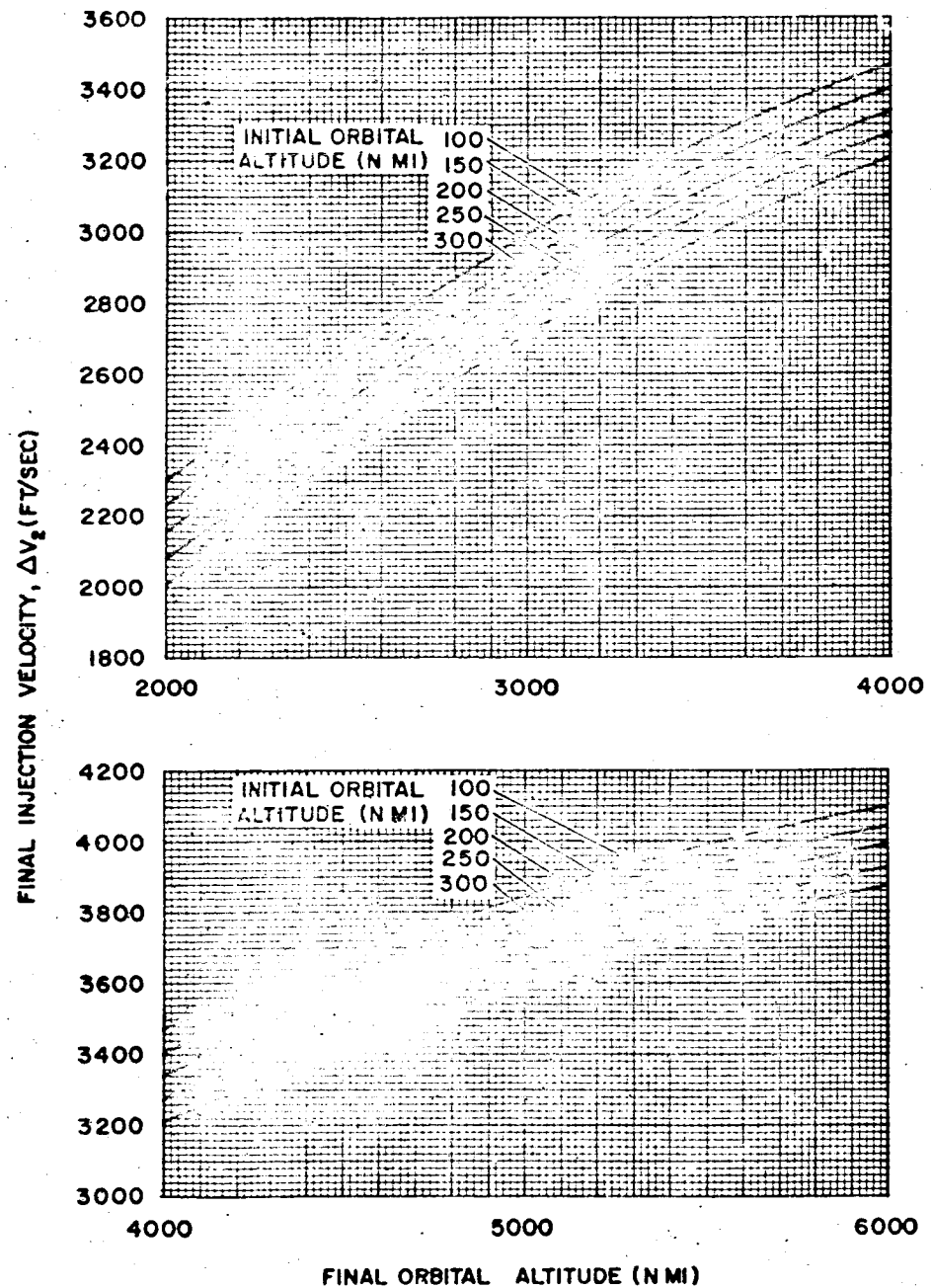


Figure 23. Final Hohmann Transfer Injection Velocity Requirements

Mission Requirements

2-31

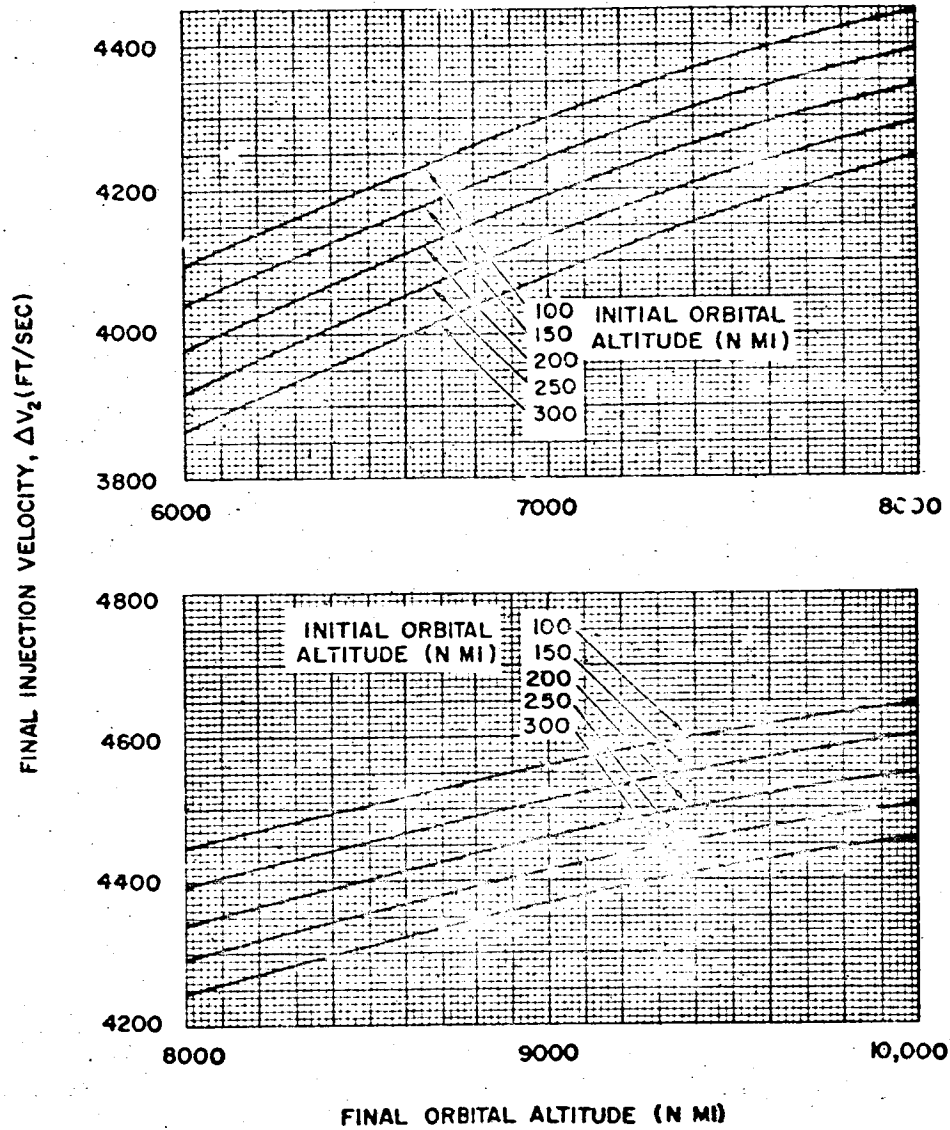


Figure 24. Final Hohmann Transfer Injection Velocity Requirements

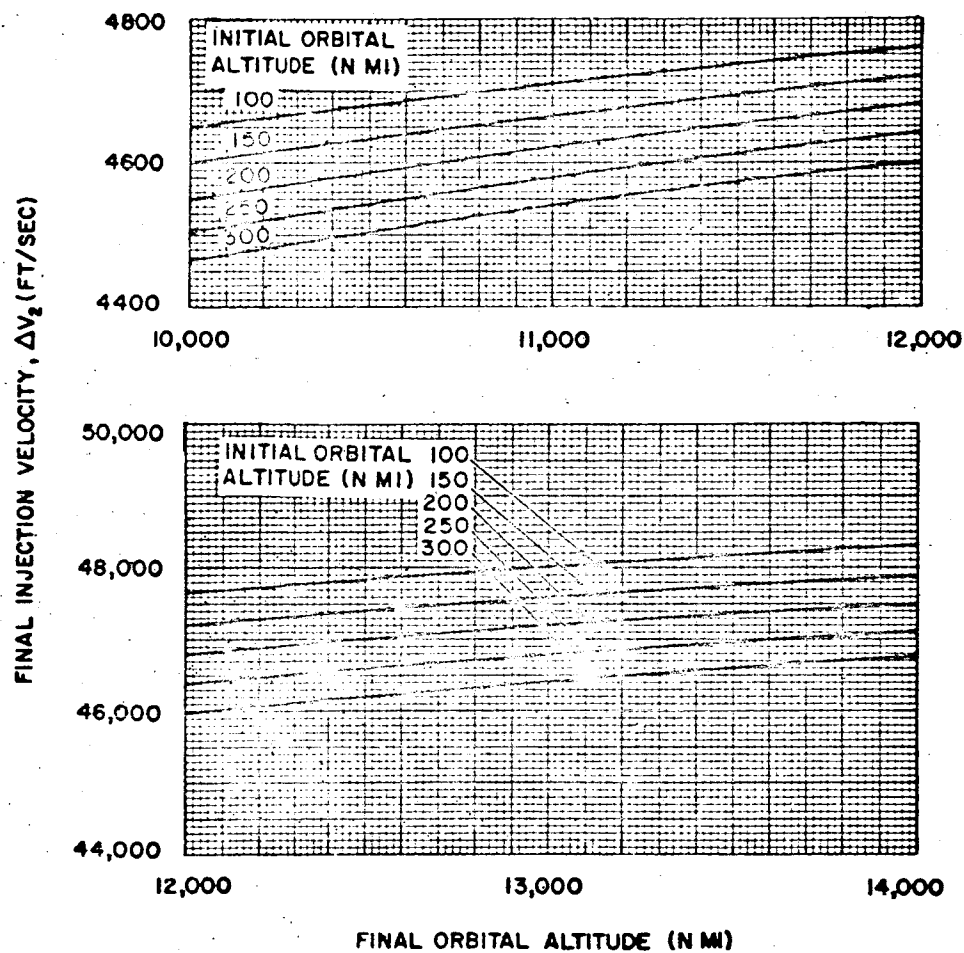


Figure 25. Final Hohmann Transfer Injection Velocity Requirements

Mission Requirements

2-33

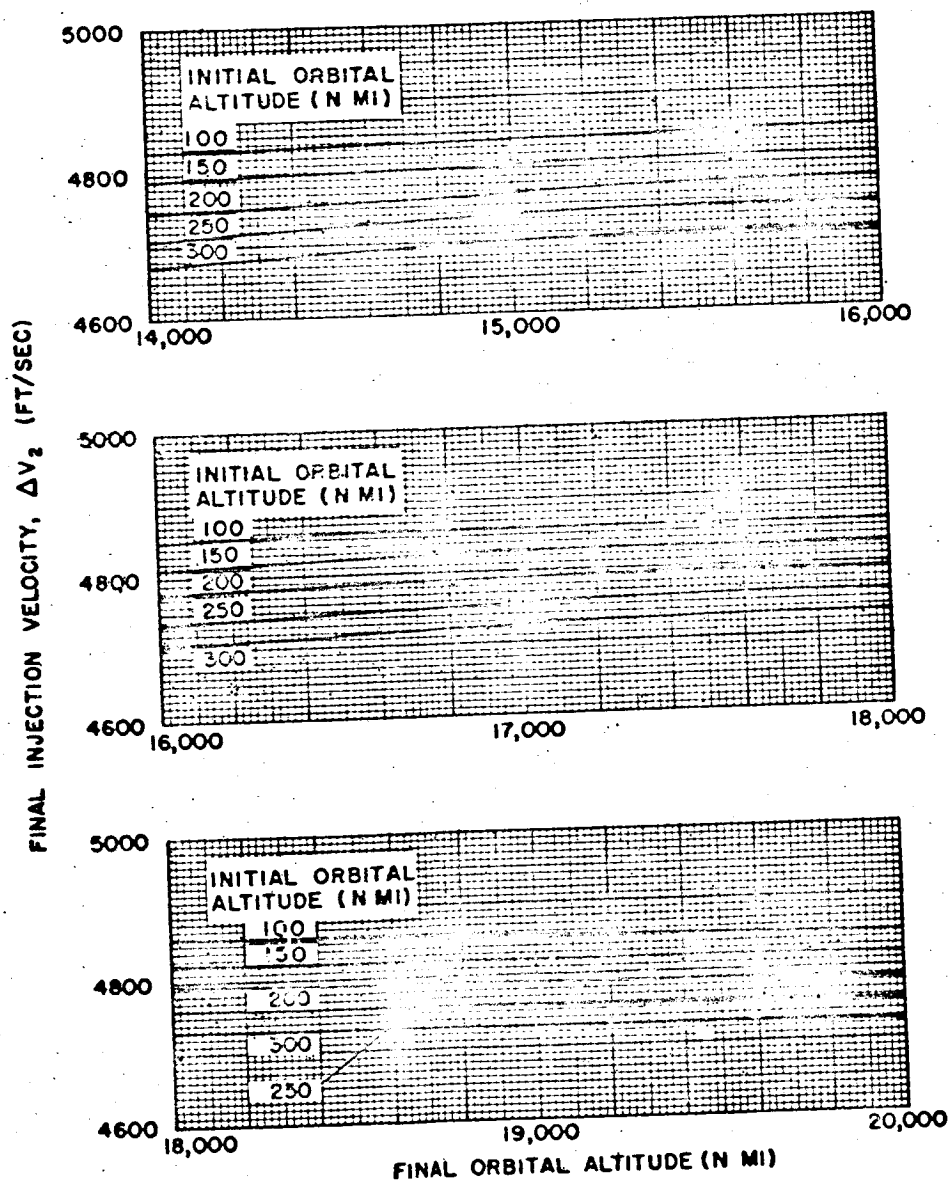


Figure 26. Final Hohmann Transfer Injection Velocity Requirements

VEHICLE PERFORMANCE ESTIMATION TECHNIQUES

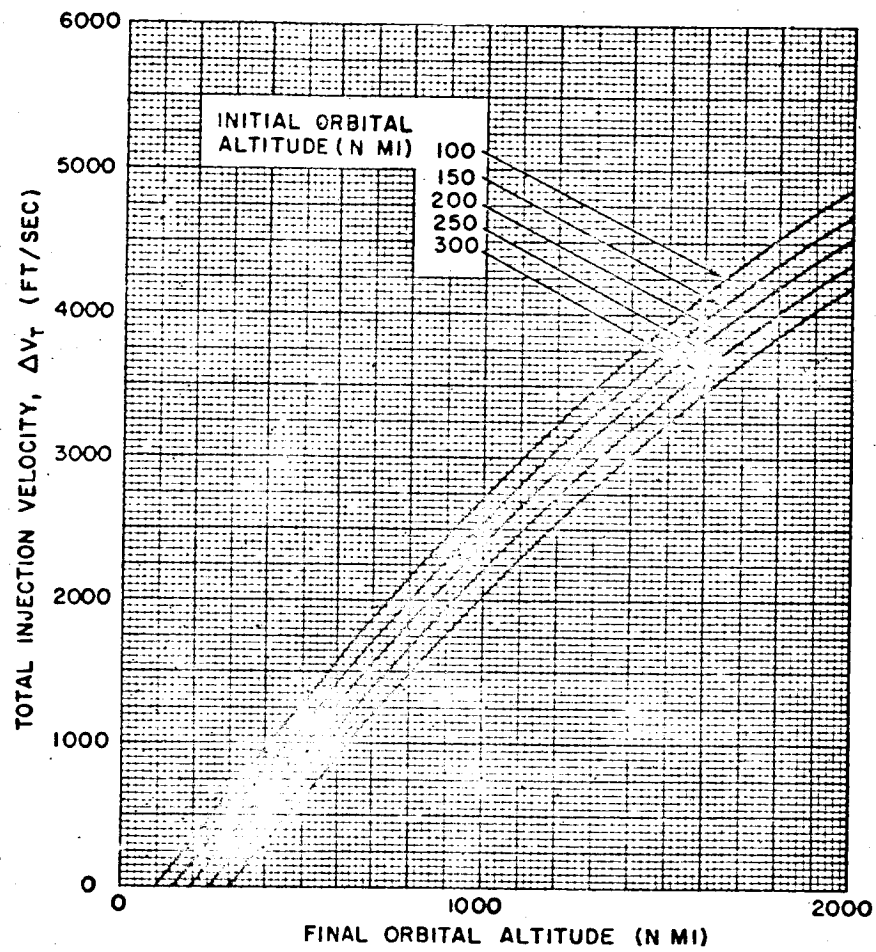


Figure 27. Total Hohmann Transfer Injection Velocity Requirements

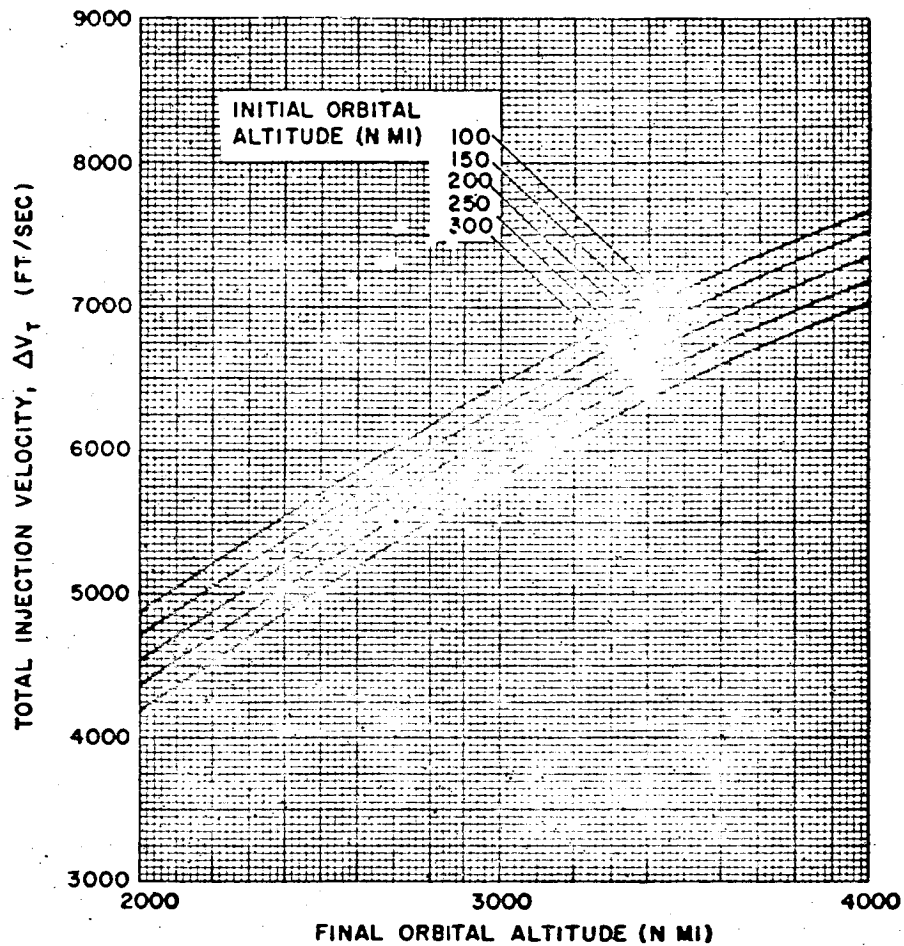


Figure 28. Total Hohmann Transfer Injection Velocity Requirements

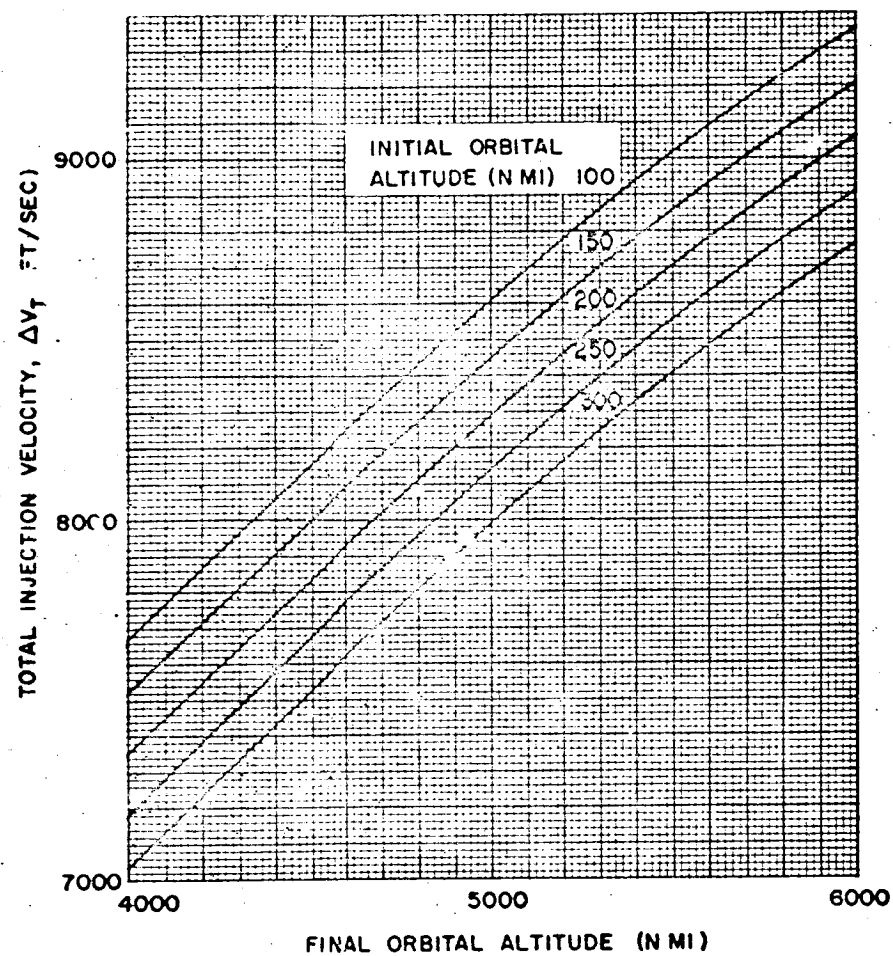


Figure 29. Total Hohmann Transfer Injection Velocity Requirements

Mission Requirements

2-37

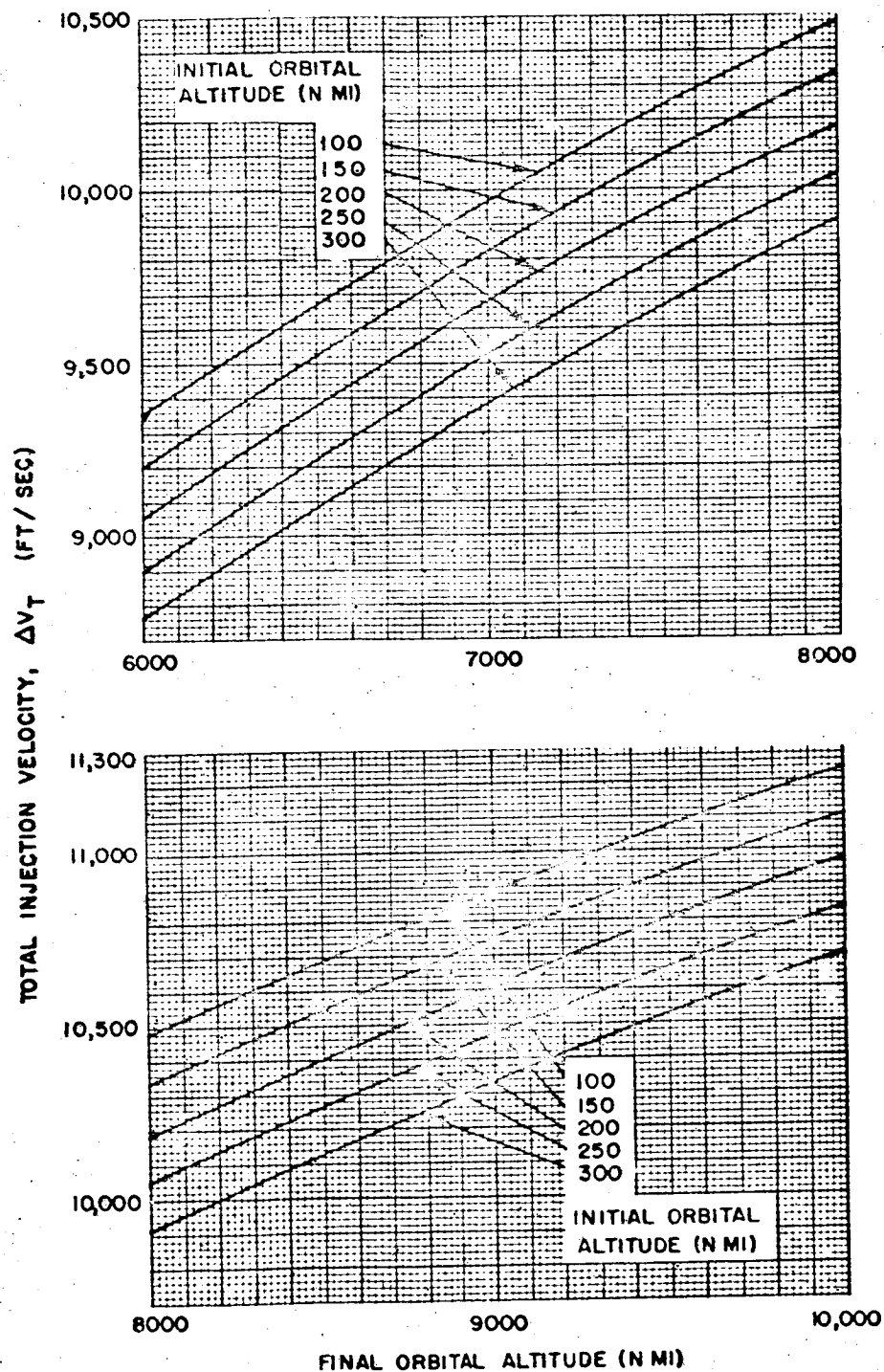


Figure 30. Total Hohmann Transfer Injection Velocity Requirements

VEHICLE PERFORMANCE ESTIMATION TECHNIQUES

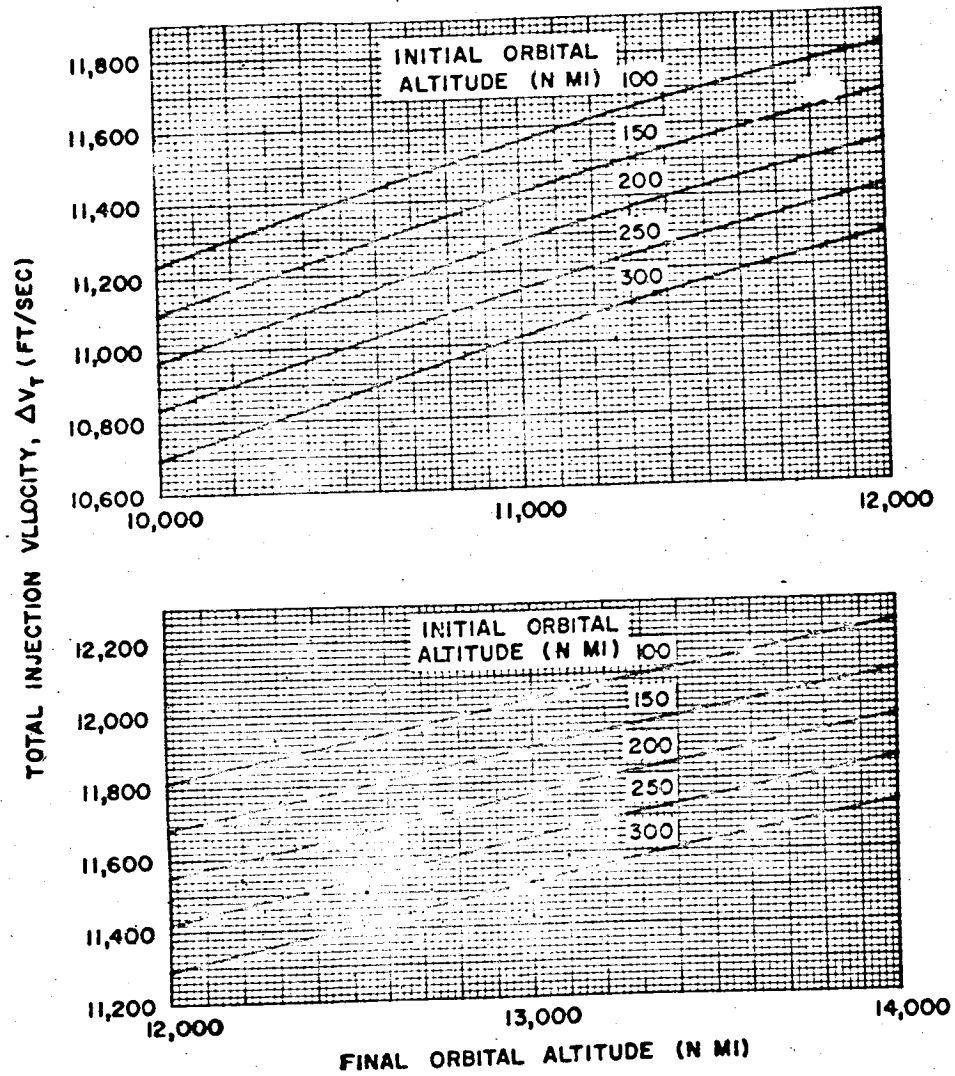


Figure 31. Total Hohmann Transfer Injection Velocity Requirements

Mission Requirements

2-39

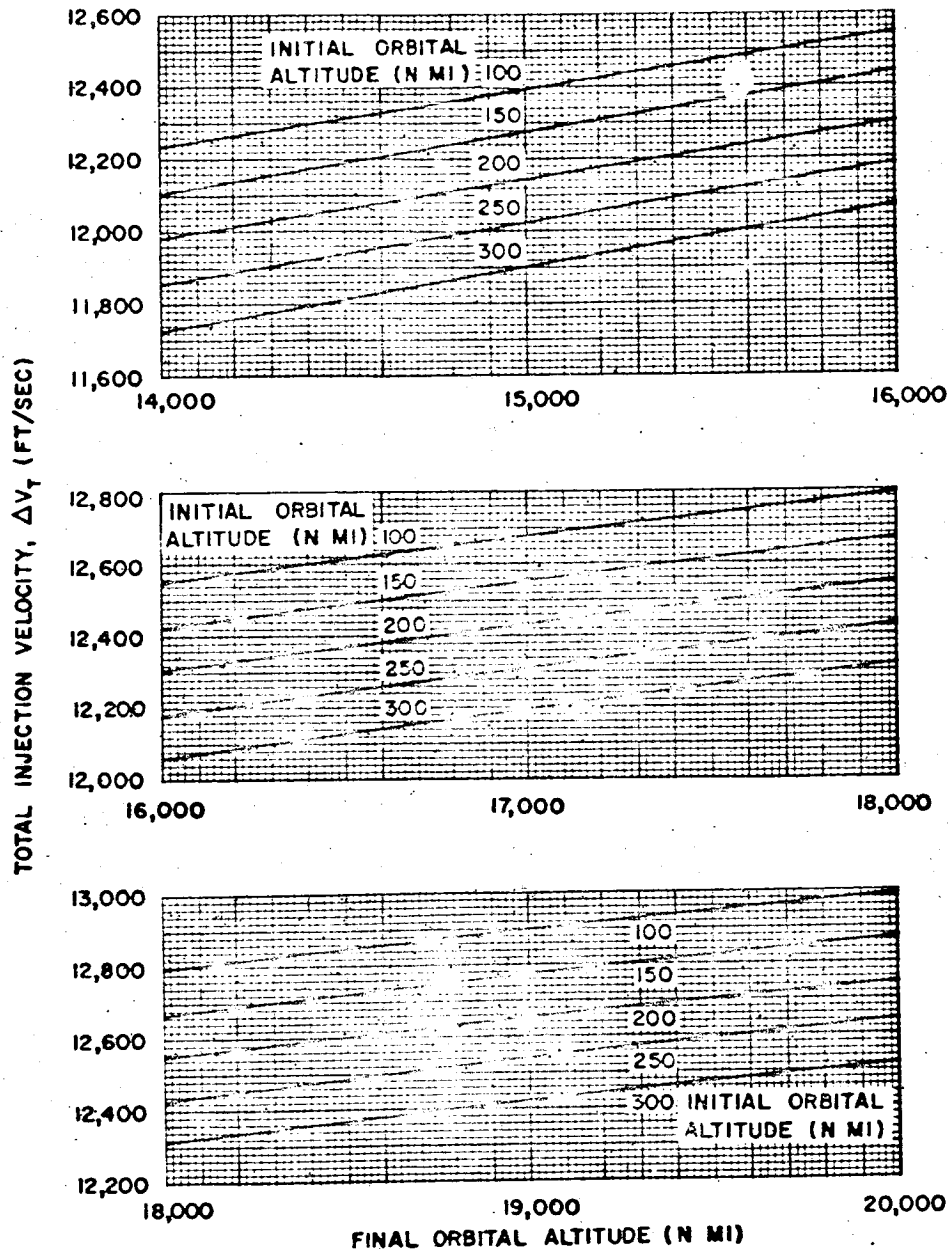


Figure 32. Total Hohmann Transfer Injection Velocity Requirements

VEHICLE PERFORMANCE ESTIMATION TECHNIQUES

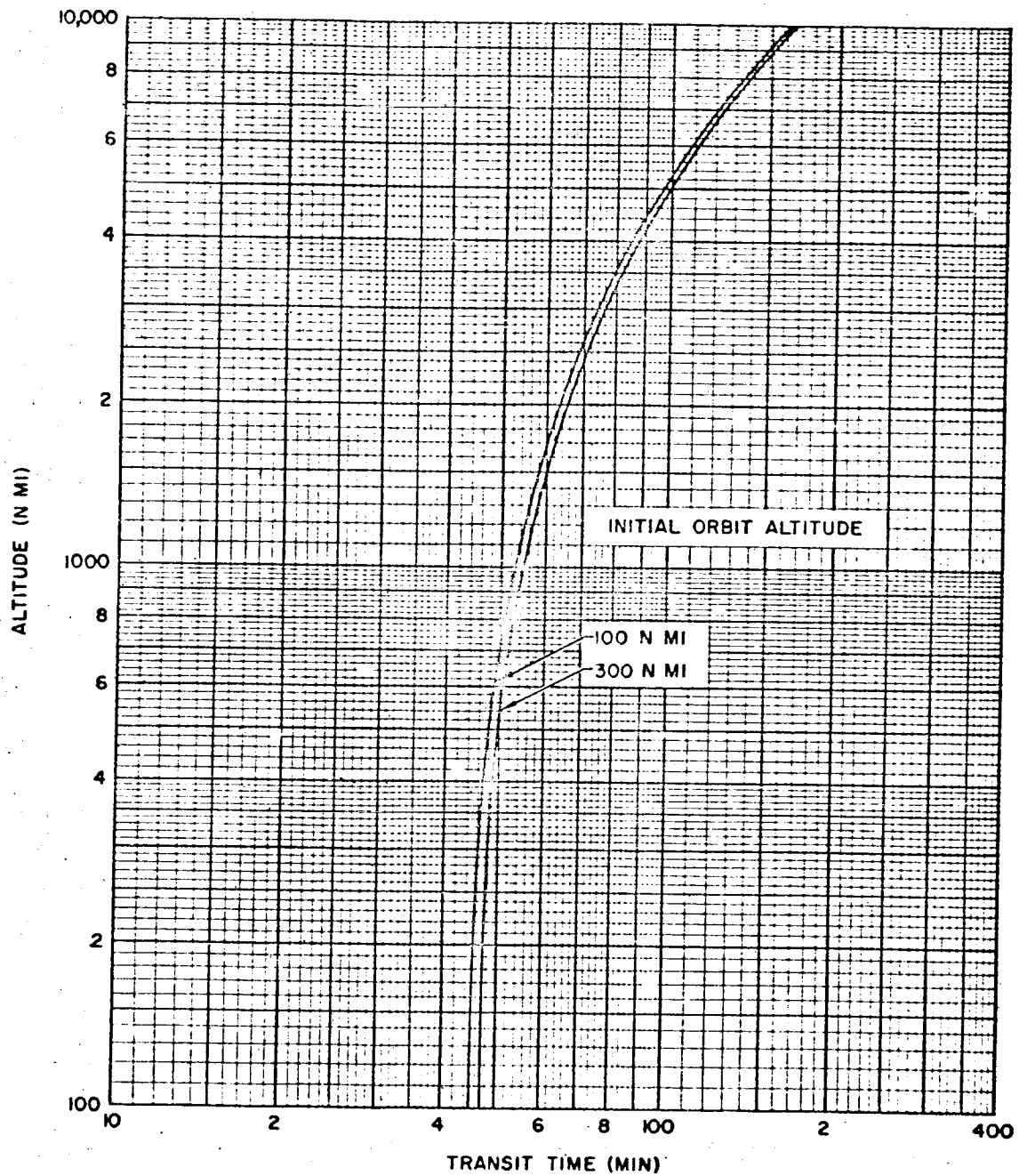


Figure 33. Hohmann Transfer Transit Time

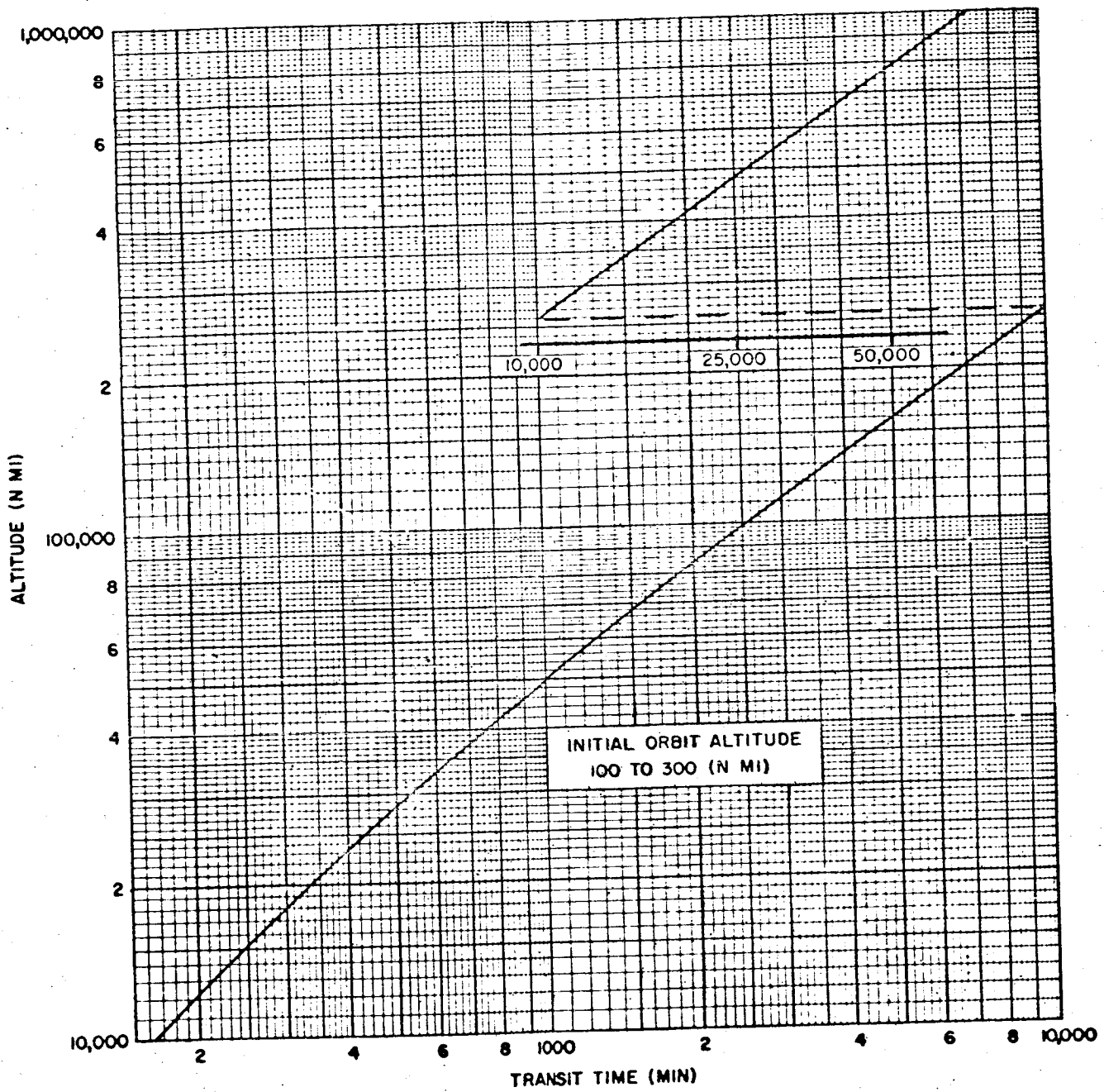


Figure 34. Hohmann Transfer Transit Time

VEHICLE PERFORMANCE ESTIMATION TECHNIQUES

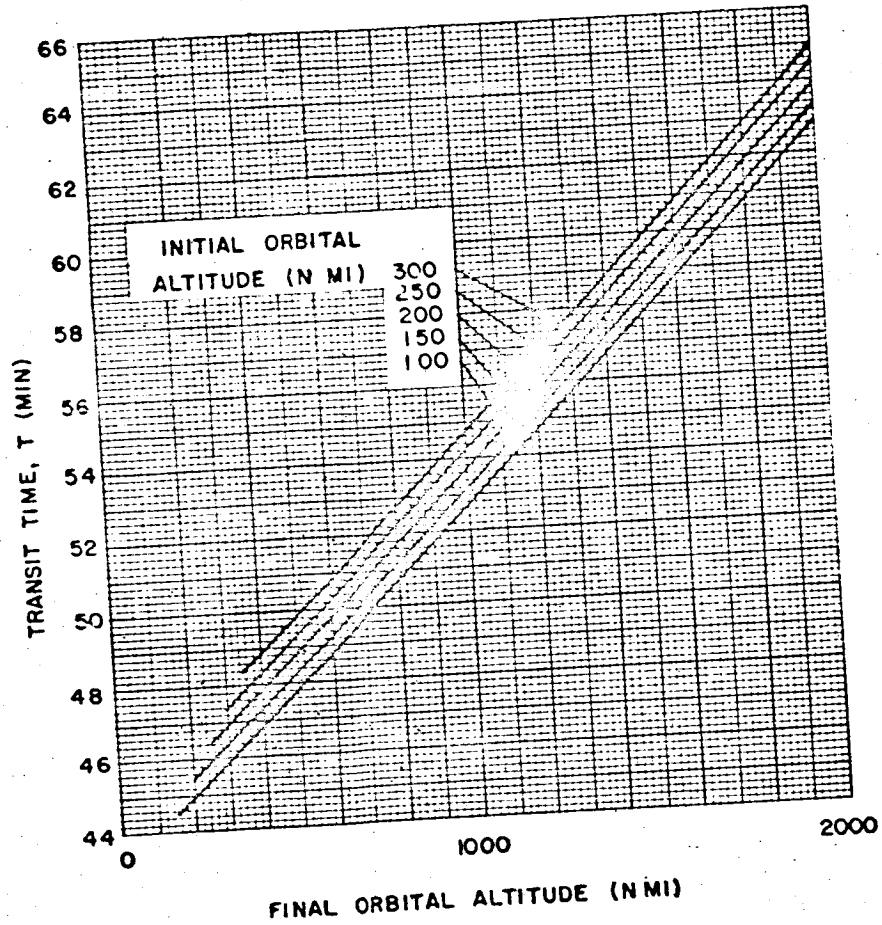


Figure 35. Hohmann Transfer Transit Time

Mission Requirements

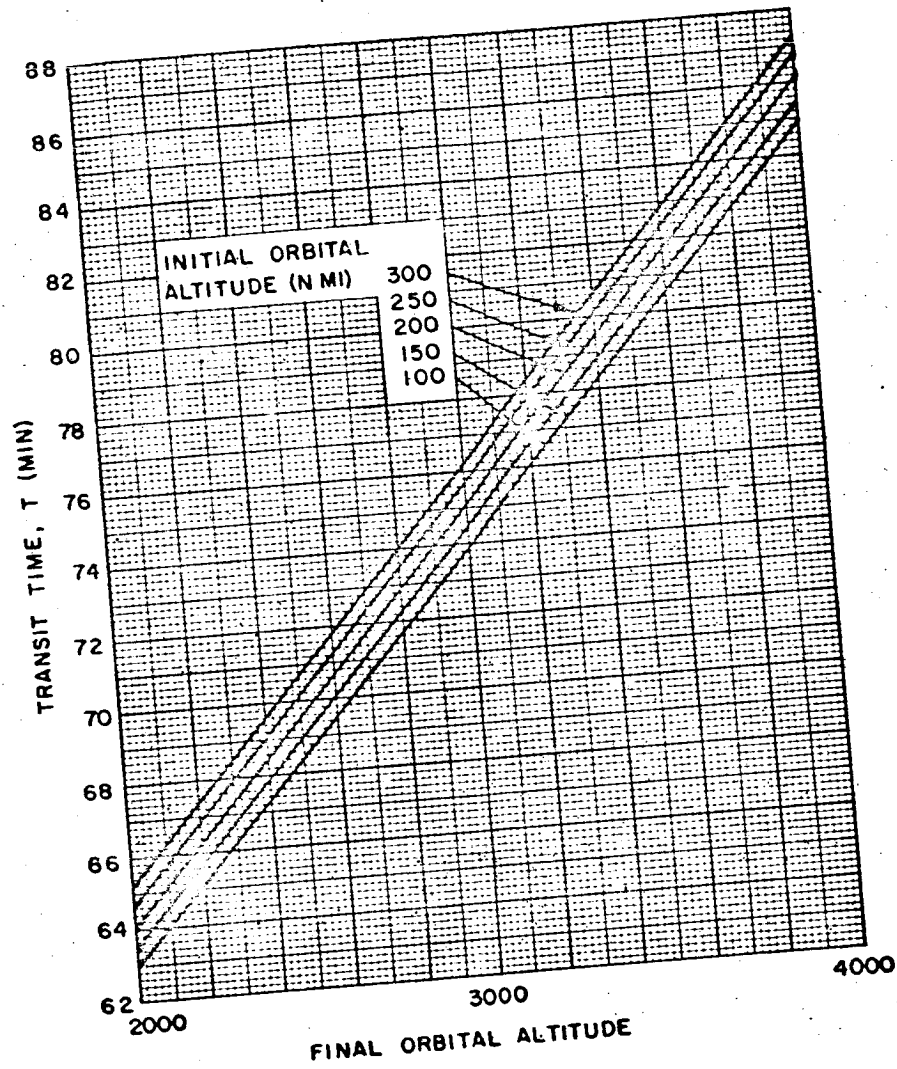


Figure 36. Hohmann Transfer Transit Time

VEHICLE PERFORMANCE ESTIMATION TECHNIQUES

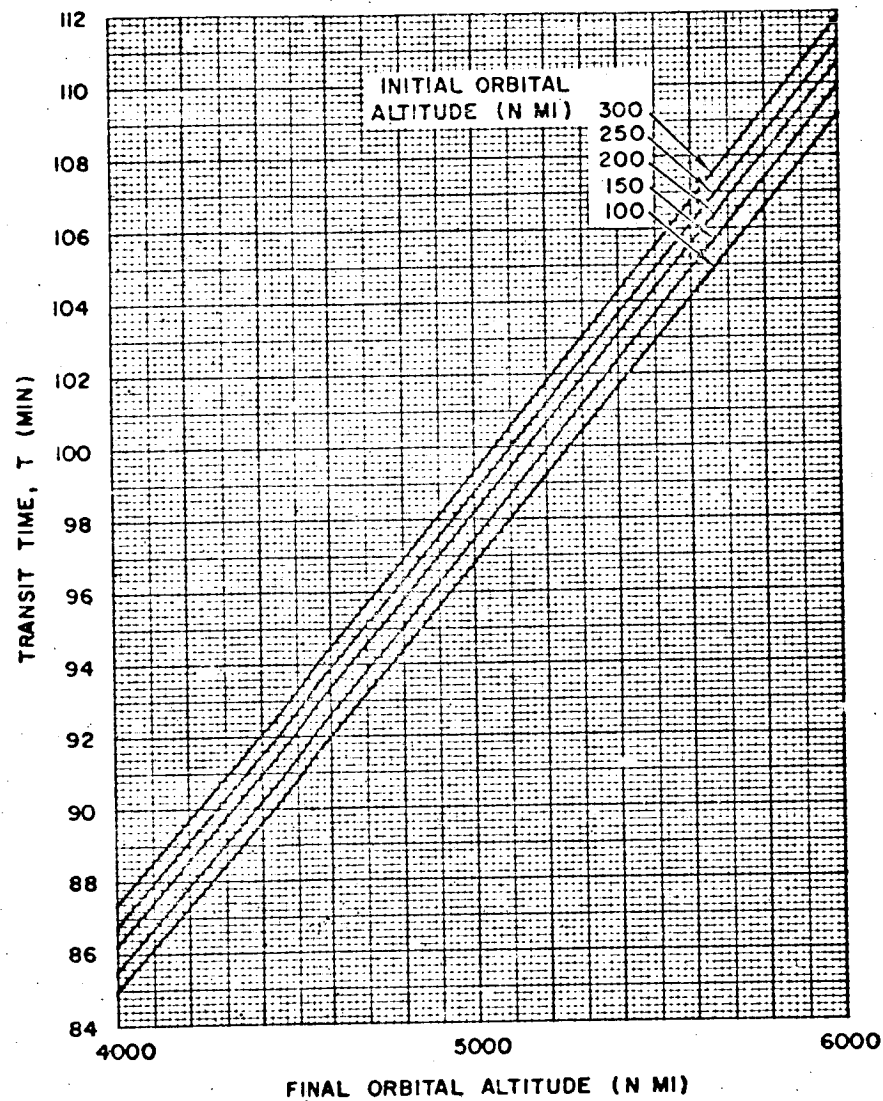


Figure 37. Hohmann Transfer Transit Time

Mission Requirements

245

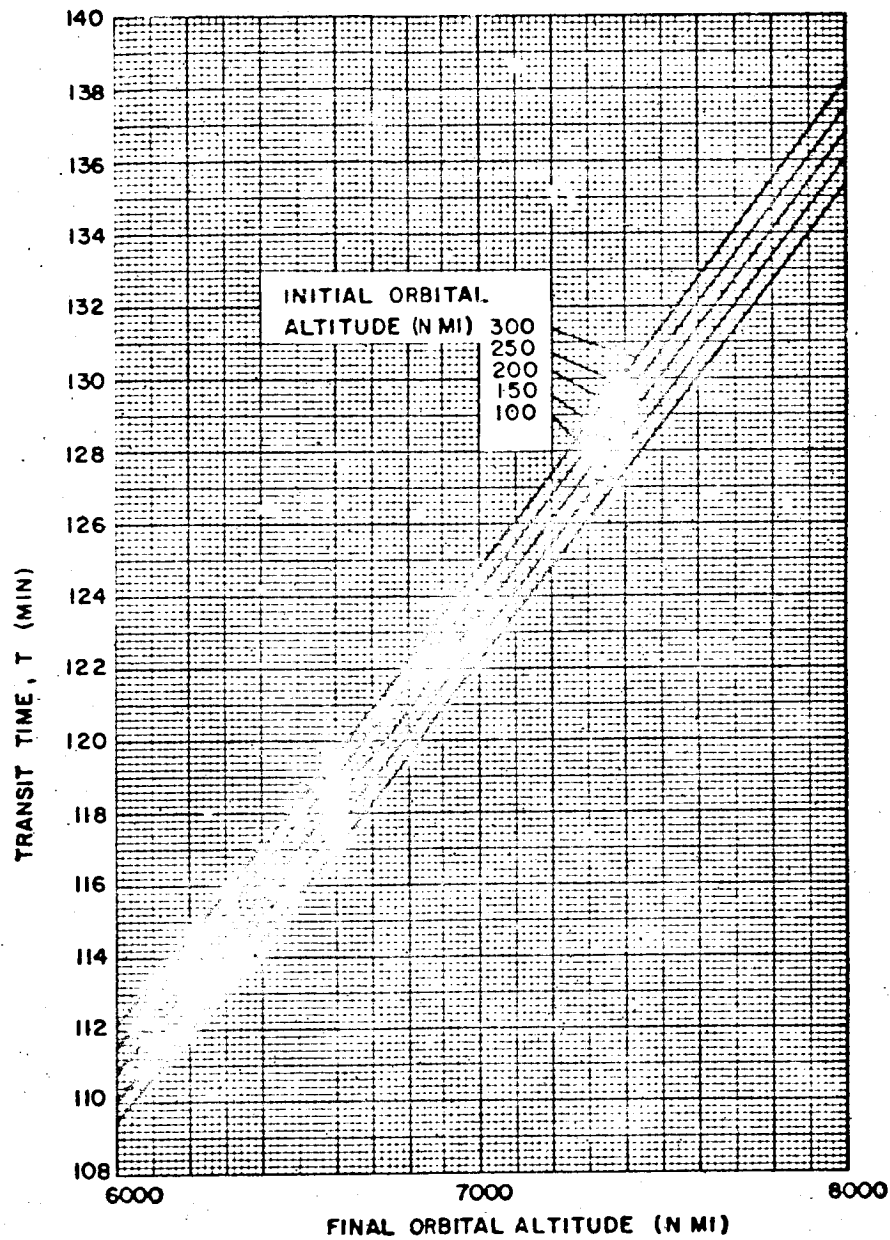


Figure 38. Hohmann Transfer Transit Time

VEHICLE PERFORMANCE ESTIMATION TECHNIQUES

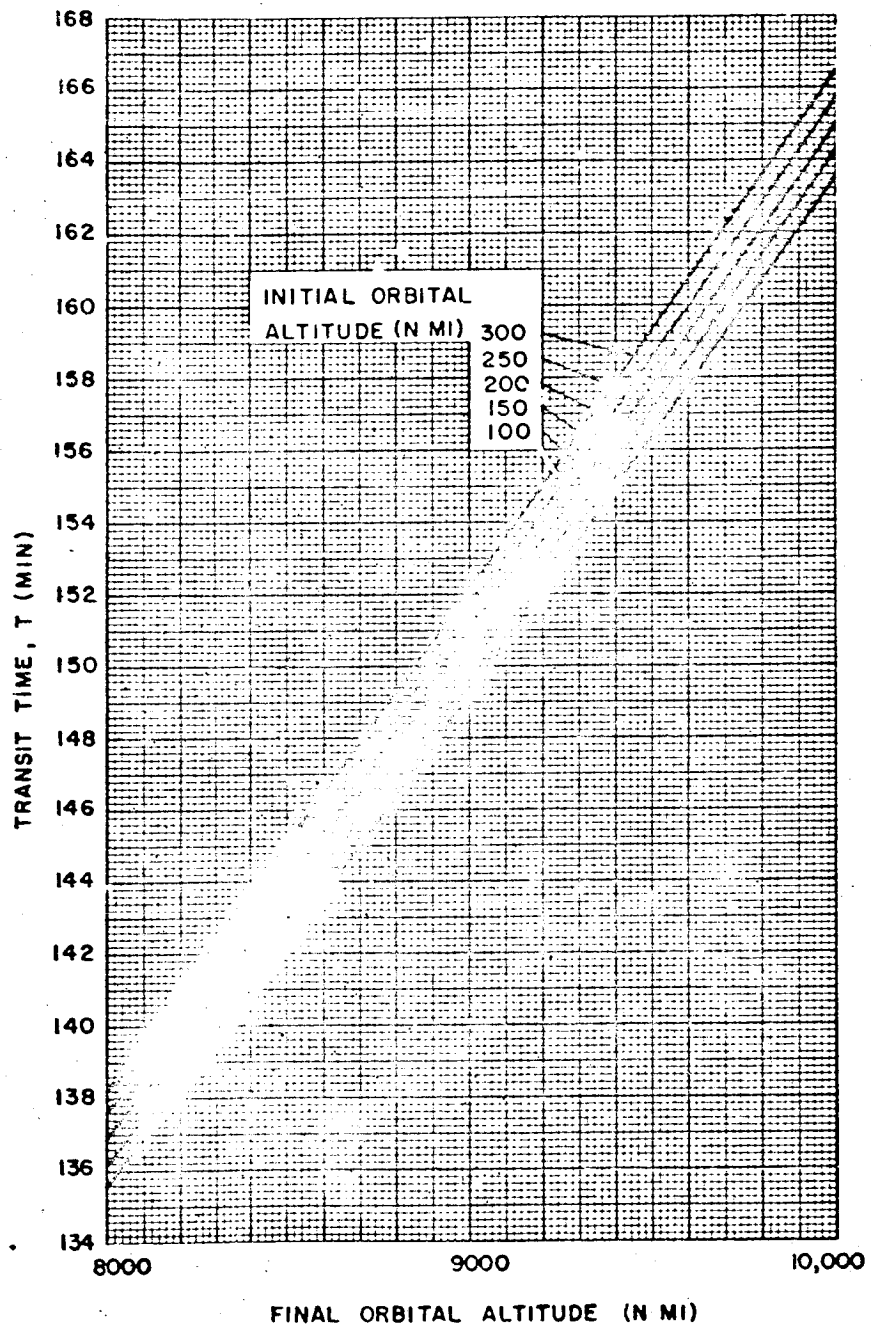


Figure 39. Hohmann Transfer Transit Time

Mission Requirements

2-47

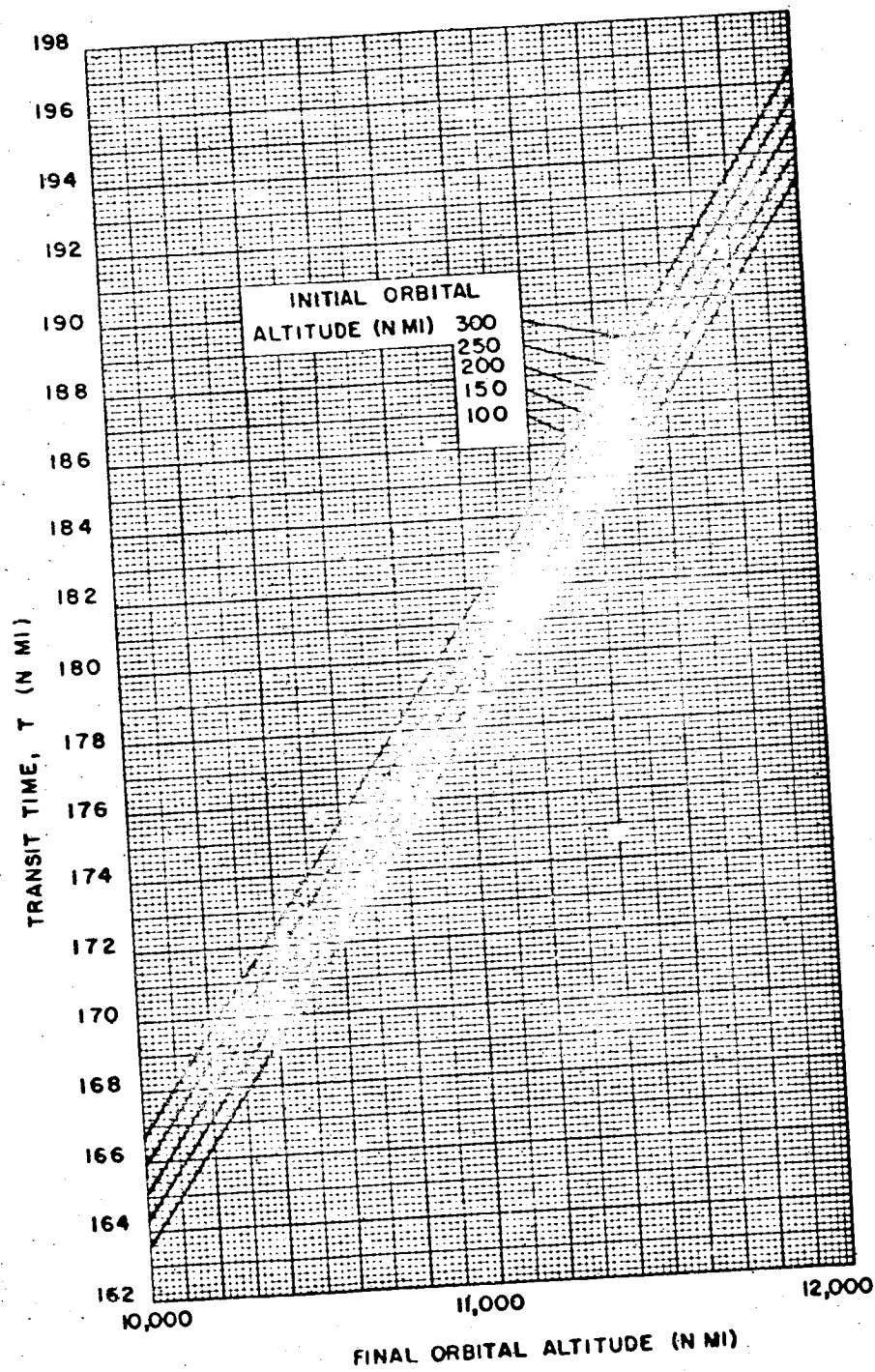


Figure 40. Hohmann Transfer Transit Time

VEHICLE PERFORMANCE ESTIMATION TECHNIQUES

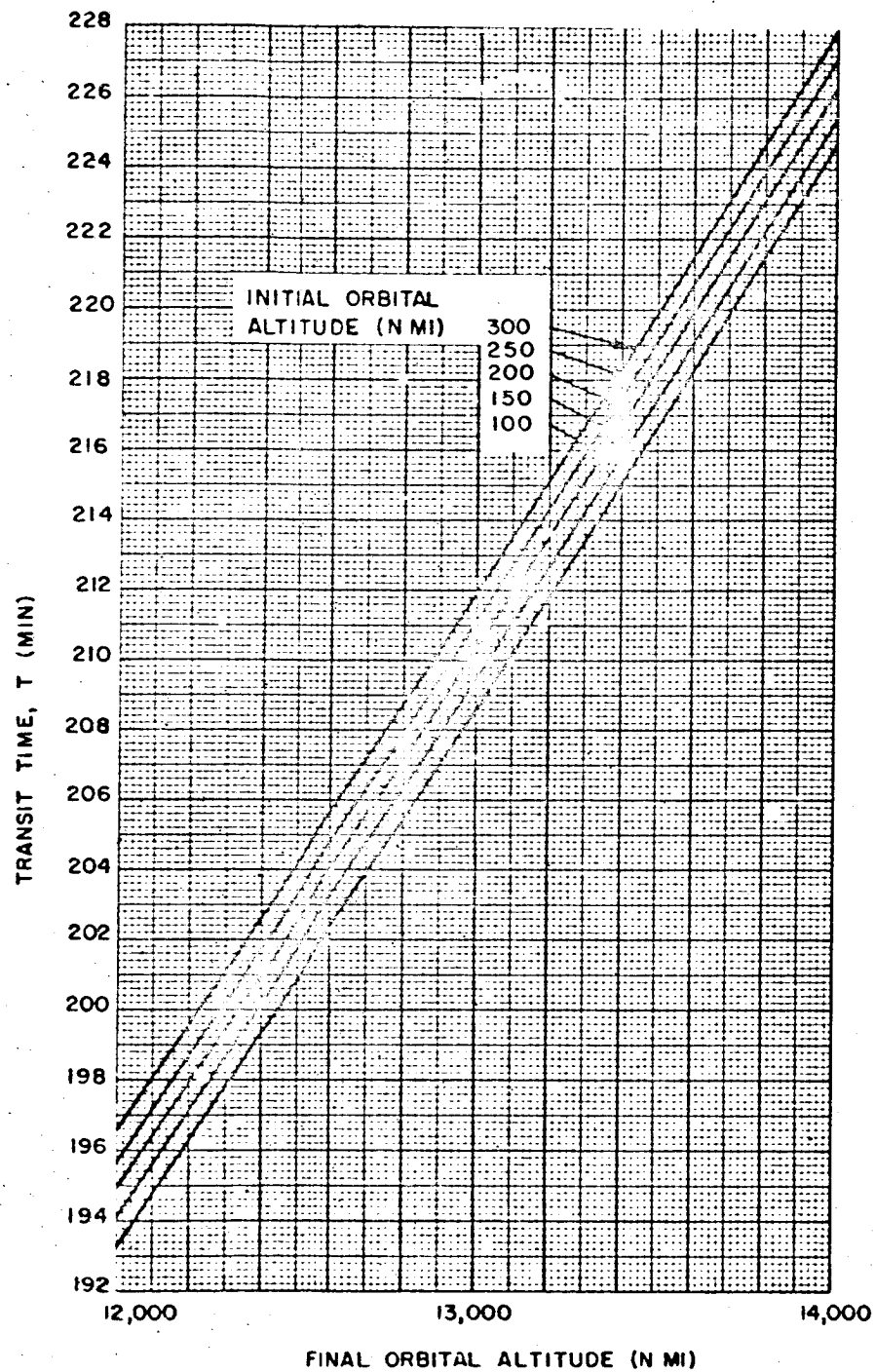


Figure 41. Hohmann Transfer Transit Time

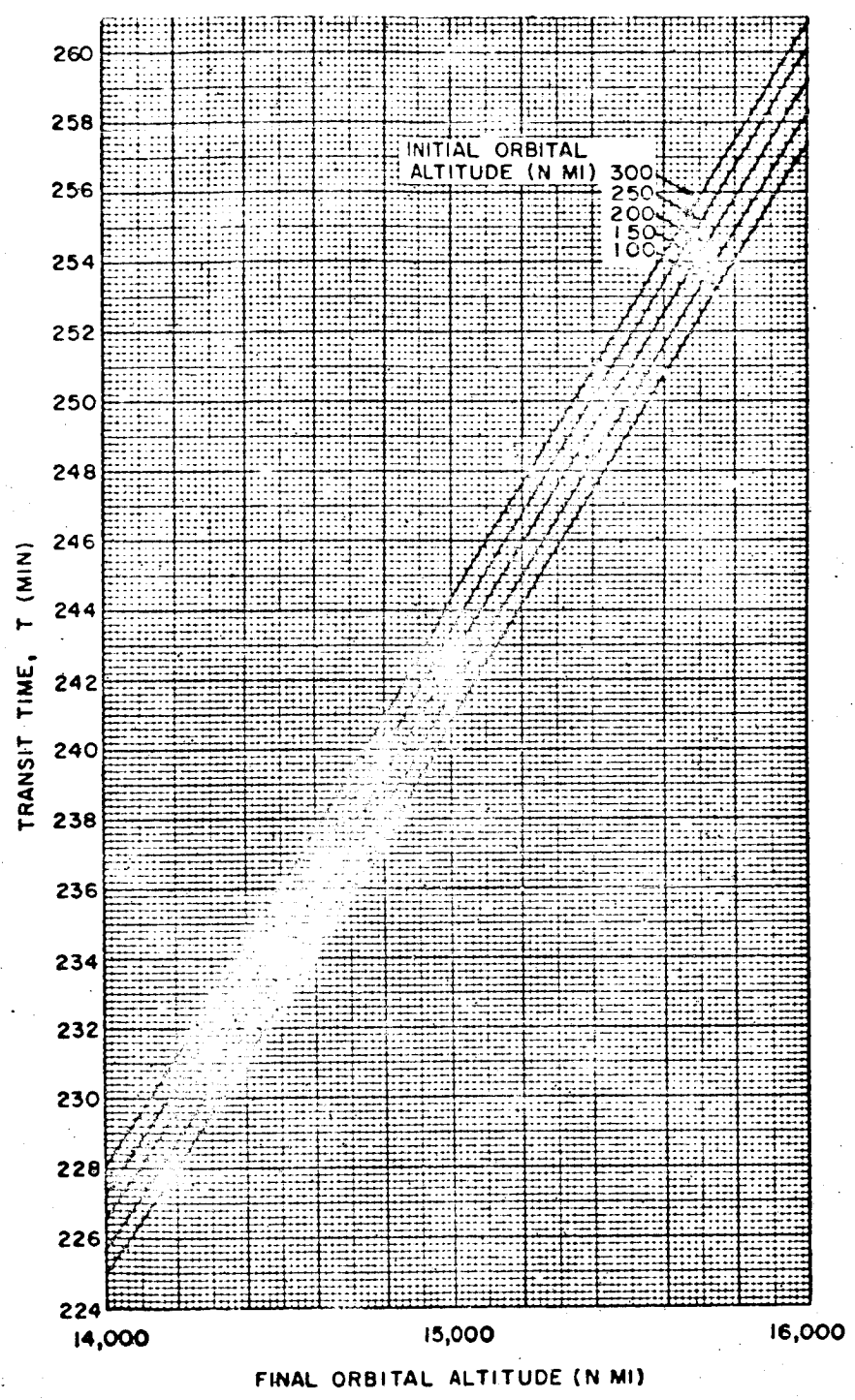


Figure 42. Hohmann Transfer Transit Time

250

VEHICLE PERFORMANCE ESTIMATION TECHNIQUES

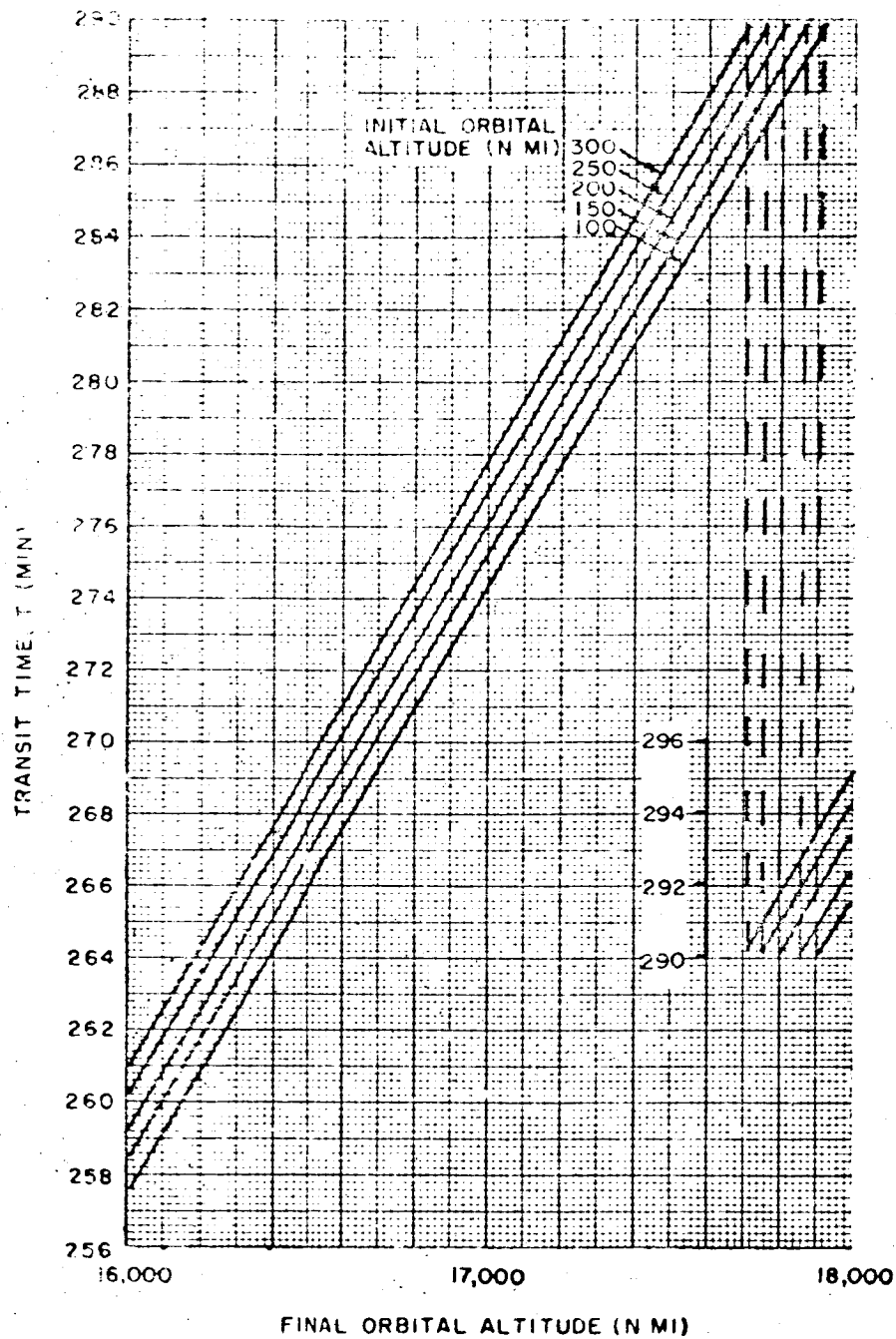


Figure 43. Hohmann Transfer Transit Time

Mission Requirements

2-51

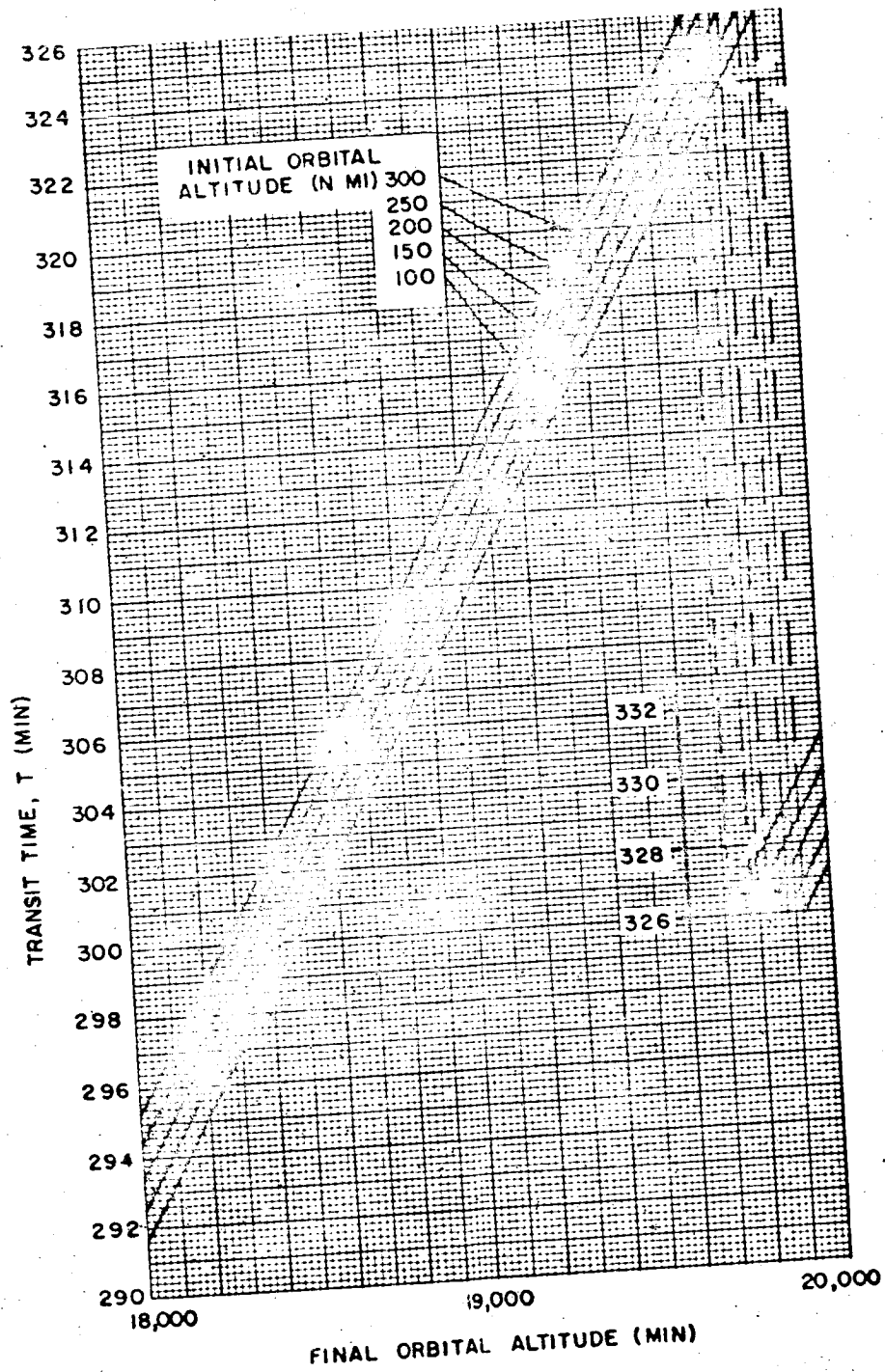


Figure 44. Hohmann Transfer Transit Time

2.1.2 Lunar and Interplanetary Mission Requirements

In preliminary design studies, it is desirable to have standard sets of lunar and interplanetary mission requirements for use in quoting payload capabilities. In the past, much confusion has arisen from quoting for comparison various vehicle payload capabilities for different flight times and/or launch dates. It is difficult to profitably compare vehicle capabilities if the payloads were not computed for the same conditions. Moreover, to add to the confusion, often the flight time and/or launch date for which a particular payload number was computed, are not cited. Therefore, standard sets of injection velocities have been adopted to be used in the performance estimation of lunar and interplanetary missions.

Velocity Requirements for Lunar Missions. For use in evaluating and quoting lunar payload capabilities a range of injection velocities for normal lunar missions is presented here. Figure 45 shows the required injection velocity from a parking orbit altitude of 100 nautical miles as a function of time of flight from injection to the moon. At each flight time, a range of velocities is shown corresponding to trajectories which arrive at the moon when the moon is at perigee and apogee in its orbit about the earth. As with interplanetary trajectories, the velocity required at some other parking orbit altitude, r_1 , may be computed from the equation below to yield the same injection energy.

$$V_1^2 = V_0^2 - \frac{2\mu_e}{r_0} + \frac{2\mu_e}{r_1}$$

where

$$\mu_e = 1.40766 \times 10^6 \text{ ft}^3/\text{sec}^2$$

and

$$r_e = 0.209029 \times 10^8 \text{ ft.}$$

The velocity required for lunar transfer and escape from earth parking orbits, with altitudes of 80 to 300 nautical miles, is presented in Figure 46. The three velocity bands shown in the figure represent lunar transfer times of 50, 66, and 90 hours based on a parking orbit altitude of 100 nautical miles.

The particular velocity (or flight time) to be employed on a mission is usually the result of a comprehensive optimization study considering injected payload weight capability, launch guidance errors, tracking accuracy, tracking station location, midcourse correction, and terminal deboost (if any) fuel requirements. Typically, such analyses for lunar orbiter, soft landing, and circumlunar trajectories have yielded optimum flight times in the range of 60 to 90 hours. Since the total velocity range from 90-hour missions to escape missions is only about 350 ft/sec, and this

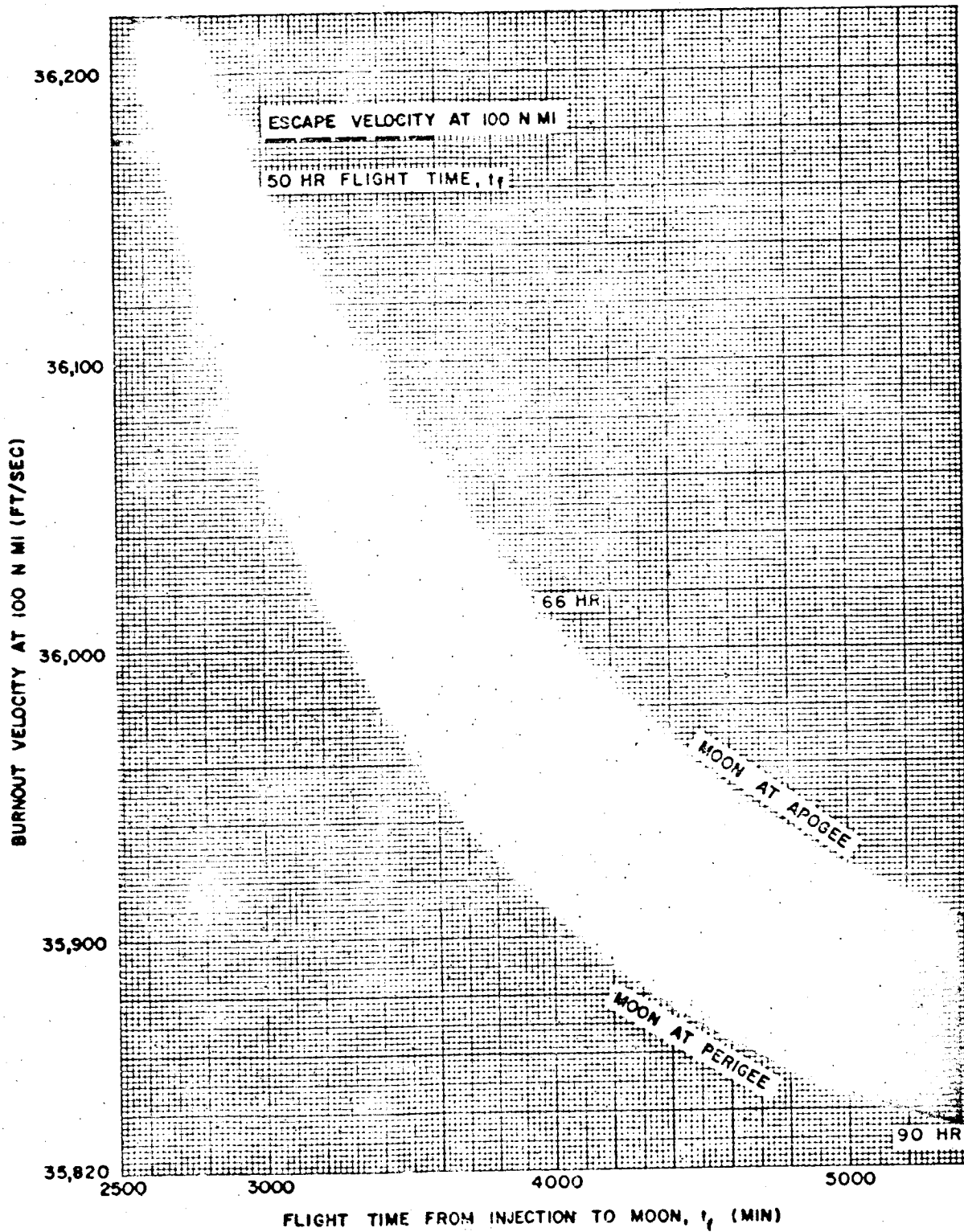


Figure 45. Lunar Mission Requirements

2-54

VEHICLE PERFORMANCE ESTIMATION TECHNIQUES

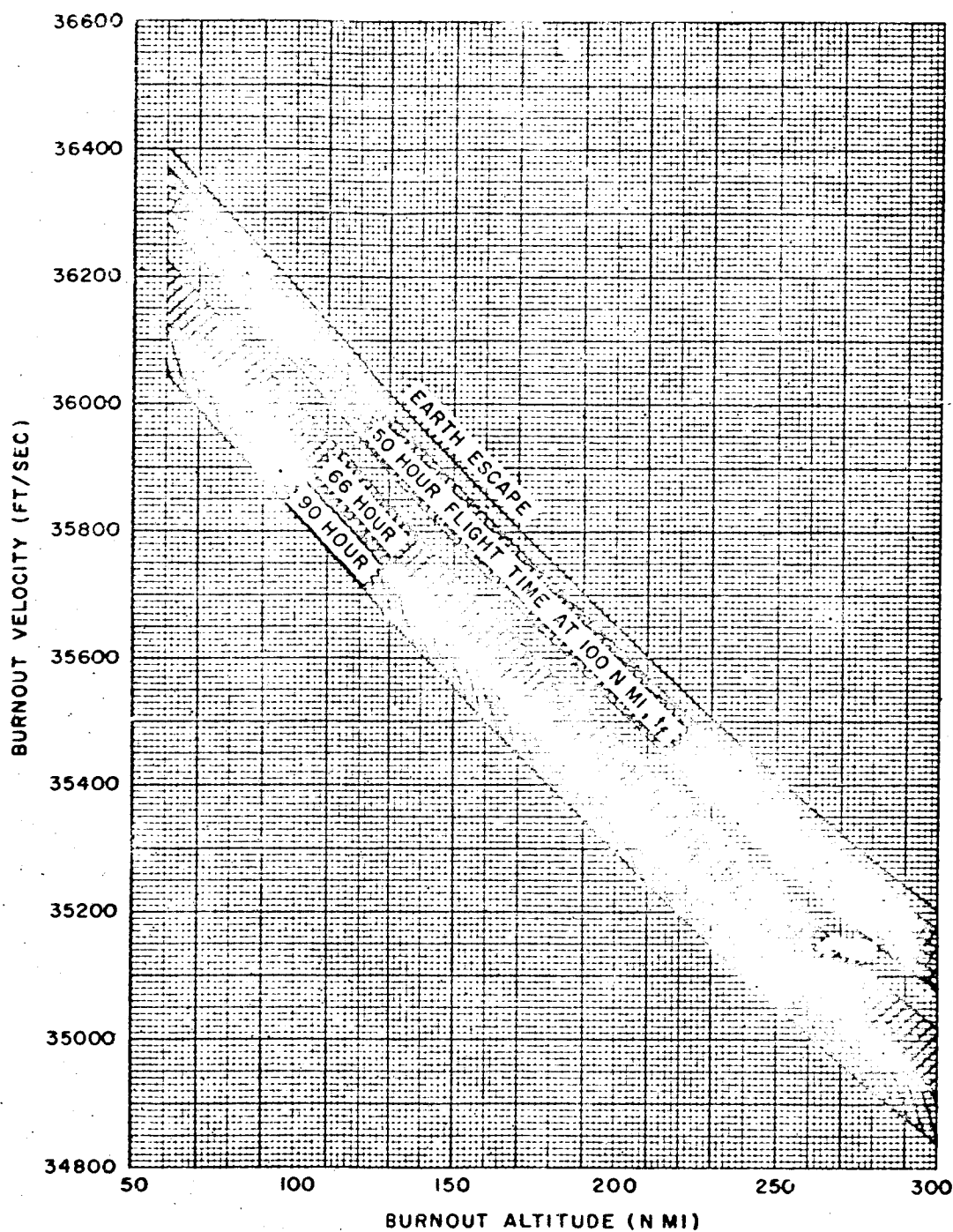


Figure 46. Lunar Mission Requirements

usually represents a small increment in vehicle payload weight capability. It is common in preliminary launch vehicle studies to represent lunar missions by a single number--the earth escape velocity,*

$$V_{\text{escape}} \approx 36,180 \text{ ft/sec at } 100 \text{ n mi}$$

For more exact studies, bands of injection velocities* may be read from Figure 46, corresponding to the flight times of interest such as

$$V_0 = 36,070 \rightarrow 36,160 \text{ ft/sec at } 100 \text{ n mi for } t_f = 50 \text{ hr}$$

$$V_0 = 35,910 \rightarrow 36,010 \text{ ft/sec at } 100 \text{ n mi for } t_f = 60 \text{ hr}$$

$$V_0 = 35,850 \rightarrow 35,910 \text{ ft/sec at } 100 \text{ n mi for } t_f = 70 \text{ hr}$$

The velocities discussed above are inertial velocities and may be partitioned into a component of velocity due to the earth's rotation. Generally, a launch window or range of permissible liftoff times on a given day will be mechanized by varying the launch azimuth and parking orbit coast duration in a systematic way with lift-off time. Typically, the launch window obtainable for a launch azimuth range of 85 to 115 degrees (from AMR) will vary from 2.0 to 5.2 hours depending on the lunar declination. The payload loss, or equivalent velocity requirement, due to not firing at a 90-degree launch azimuth can be estimated simply as shown in Chapter 3, Section 1.

Interplanetary Velocity Requirements for Venus and Mars Missions. Standard sets of Venus and Mars injection velocity requirements are suggested here for use in quoting payload weight capability of vehicles when the specific mission and launch date are unspecified.⁸ In contrast to requirements for lunar trajectories, the range of injection velocities (at a given altitude) for each planet are considerably broader than those for a normal lunar mission.

The normal procedure used in designing an interplanetary flight is as follows: For the year in which the mission is to be launched, curves are computed relating launch date, injection velocity, approach velocity at target planet (for orbiting), earth-planet communication distance on arrival, guidance CEP, flight time, and launch azimuth (for range safety). From these curves an optimum trajectory is chosen to best satisfy the mission objectives. This trajectory will require a particular injection velocity and will thus imply a particular payload weight capability for a given launch vehicle.

* Rounded to 10 ft/sec

The optimum trajectories for each of the above system factors will correspond to quite different injection velocities (and payload weight capabilities). Furthermore, there will be a significant variation in velocity requirements from one launch year to another.

It is desirable to have some standard sets of injection velocities to use in quoting and comparing vehicle performance when the mission requirements and even the year of launch are unknown. In studying a wide variety of Venus and Mars flights over several launch years, it has become apparent that the following ranges of injection velocities cover all "normal mission" requirements:

$$\text{Venus} = V_o = 37,000 \rightarrow 38,500 \text{ ft/sec at } 22(10^6) \text{ ft from center of earth}$$

$$\text{Mars} = V_o = 37,200 \rightarrow 39,000 \text{ ft/sec at } 22(10^6) \text{ ft from center of earth}$$

The requirement is actually that of specifying energy, and the above velocity ranges at $22(10^6)$ ft may be referred to any other convenient injection altitude, r_1 , by the relation

$$V_1^2 = V_o^2 - \frac{2\mu_e}{r_o} + \frac{2\mu_e}{r_1}$$

where $\mu_e = 1.40766 \times 10^{16} \text{ ft}^3/\text{sec}^2$ and $r_e = 0.209029 \times 10^8 \text{ ft}$. In particular the velocity ranges* at a 100 nautical mile parking orbit altitude (above equatorial earth radius) are 37,370 to 38,860 ft/sec at 100 n mi altitude for Venus, and 37,570 to 39,350 ft/sec at 100 n mi altitude for Mars.

The velocity bands as a function of parking orbit altitude for altitudes of 80 to 300 nautical miles for Venus and Mars are presented in Figures 47 and 48, respectively.

The above ranges will include the minimum energy (maximum payload), optimum guidance, and optimum target orbiting trajectories, and will allow for a reduction in Mars communication distance to about 100 million nautical miles (from the typical minimum energy value of 170 million n mi). Alternately, the upper end of the velocity band will allow a launch date window of about 3 months.

*Rounded to 10 ft/sec.

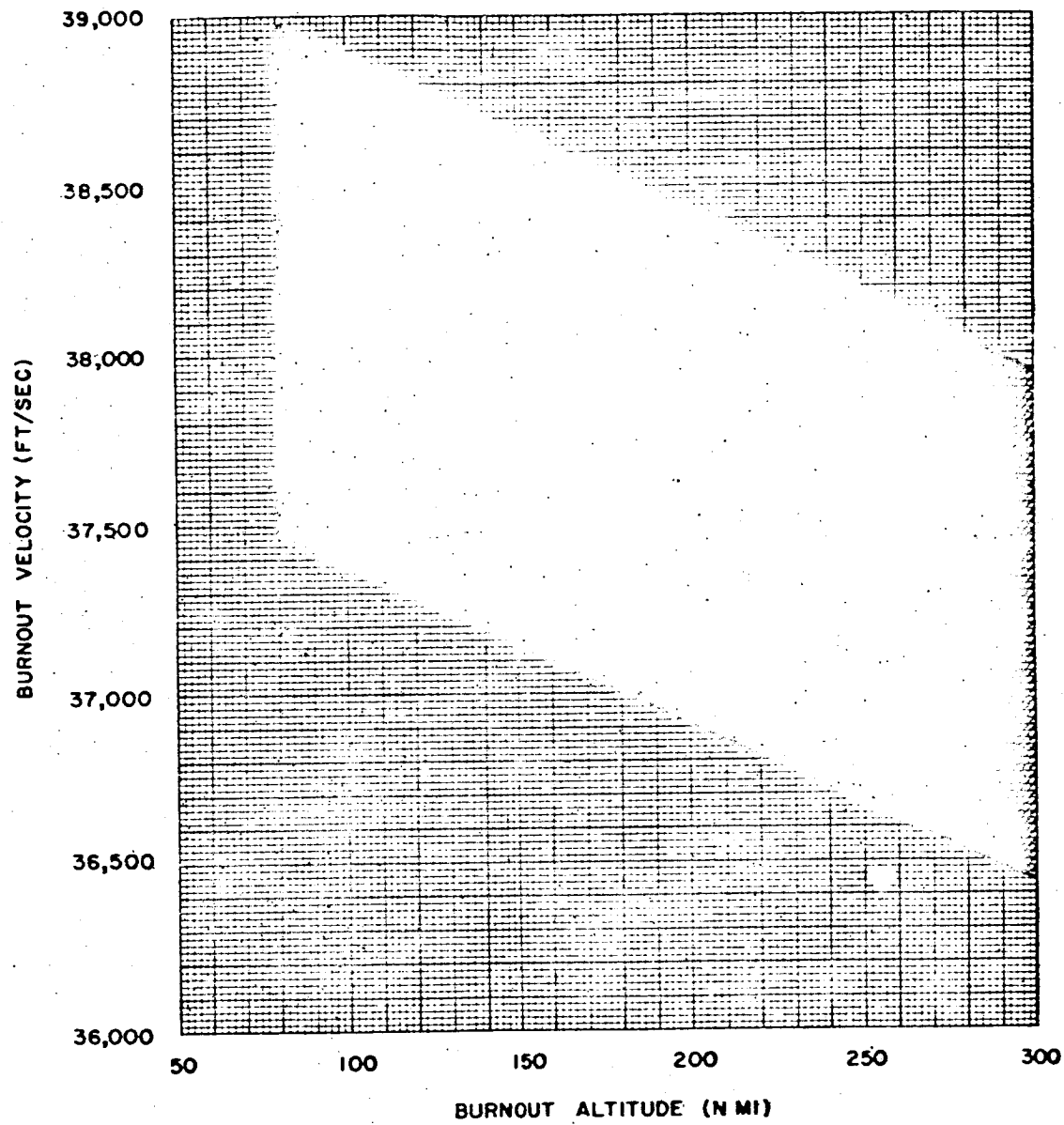


Figure 47. Earth-Venus Mission Requirements

VEHICLE PERFORMANCE ESTIMATION TECHNIQUES

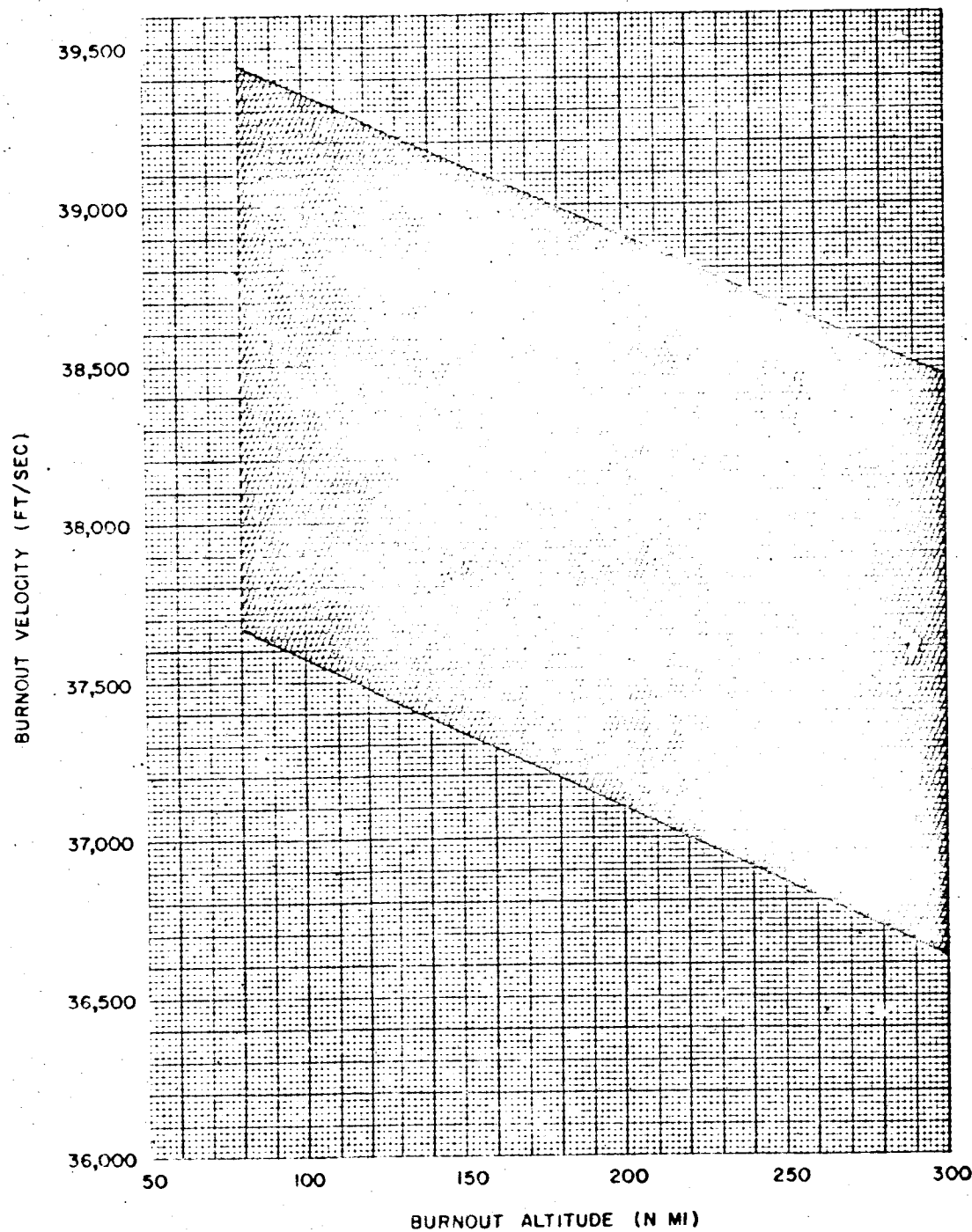
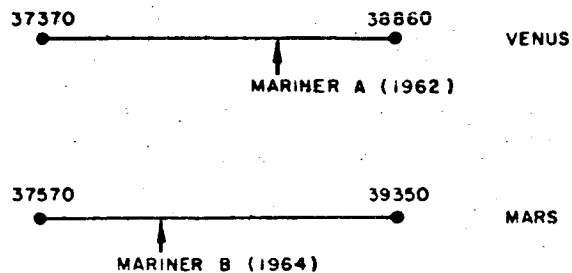


Figure 48. Earth-Mars Mission Requirements

As an example, typical NASA Mariner A and B trajectories for 1962 and 1964 fall within the velocity bands as shown below:



It is recommended that the velocity ranges quoted above be used in all new vehicle payload weight comparisons where specific missions are not involved. Where a curve of payload weight versus injection velocity is not given, payloads corresponding to the ranges should be quoted.

2.2 DETERMINATION OF VEHICLE PERFORMANCE

The determination of vehicle performance after the mission requirements are established can be classified under the two general categories of exact solution and solution by approximate methods. In the exact solution, the equations of motion are solved numerically through the use of a high-speed digital computer. The versatility of the properly written program and the accuracy of the results are very rewarding. However, there are disadvantages to this method. First, the time involved in preparing input data and arranging for computer time is generally long, even though the actual computer time is small. Secondly, the high accuracy of results is usually not required for preliminary design purposes. Finally, the computer run for a set of data does not provide the information to establish trends that are available from analytical or graphical solutions.

Two techniques are available for performance evaluation by approximate methods. One technique uses approximations before the equations of motion are solved. The original expressions are transformed into simpler ones which can be solved by available methods. The second technique makes approximations after solution of the differential equations by a computer. This in essence approximates the solution and not the set of original equations. The first technique usually results in a more general solution, but is difficult to arrive at due to the nonlinearity of the differential equations of motion. The second technique is less general in nature and requires a large body of empirical relationships.

The choice of an approximation technique is made on the basis of convenience to the designer. The equations of motion of the first stage of a vehicle launched from the surface of the earth are complicated and there are interactions due to effects of the atmosphere. Thus, for the first stage the second approximation technique is appropriate for performance evaluation. The vast number of vehicles analyzed in past studies at STL have yielded sufficient data to determine the necessary empirical relationships. This technique was first investigated in Reference 12.

In the case of upper stages, a more general solution is required in order to include the various pitch programs followed by upper stages. Also, the lack of atmospheric effects during upper-stage flight makes the first technique convenient for performance evaluation.

The methods and corresponding data that follow are divided into two sections; a section for cursory performance evaluation, and a section for precise performance evaluation. The data in the cursory analysis section make it possible to evaluate total vehicle performance to within approximately 3 percent of the burnout velocity for a typical orbit mission. This error is considered large, but the short length of time required to arrive at a performance capability warrants the inclusion of such data. On the other hand, the precise computation of losses allows the estimation of burnout velocity within 1 percent of the final value, and all other performance parameters within 5 percent of their final values. This method requires more time due to the iterative procedure required for solution.

The data presented herein can be used to determine the performance of a wide range of booster vehicles. In general, the first stage of the vehicle can have an initial thrust-to-weight ratio of 1.0 to 3.0 with a propellant vacuum specific impulse of 250 to 500 pound-seconds per pound. The first-stage burnout flight path angle can vary from 0 to 90 degrees. The physical size or weight of the vehicle is not limited since the analysis is in parametric form. The range of data allows the analysis of booster stages from present-day vehicles up to and including vehicles of advanced state-of-the-art design using high-energy liquid propellants. The data are not sufficient for nuclear booster stages although the method is certainly valid.

The precise method of evaluation of upper-stage performance essentially has no limitation as to the magnitude of the physical characteristics of the upper stages. Thus, this type of analysis allows even nuclear upper stages to be considered. It must be remembered that assumptions have been made to facilitate the solution of the equations and they must be applied consistently. These assumptions will be pointed out as they appear.

Before presenting the methods used in determining vehicle performance, a description of the assumed trajectory on which the methods are based is necessary (see Figure 49).

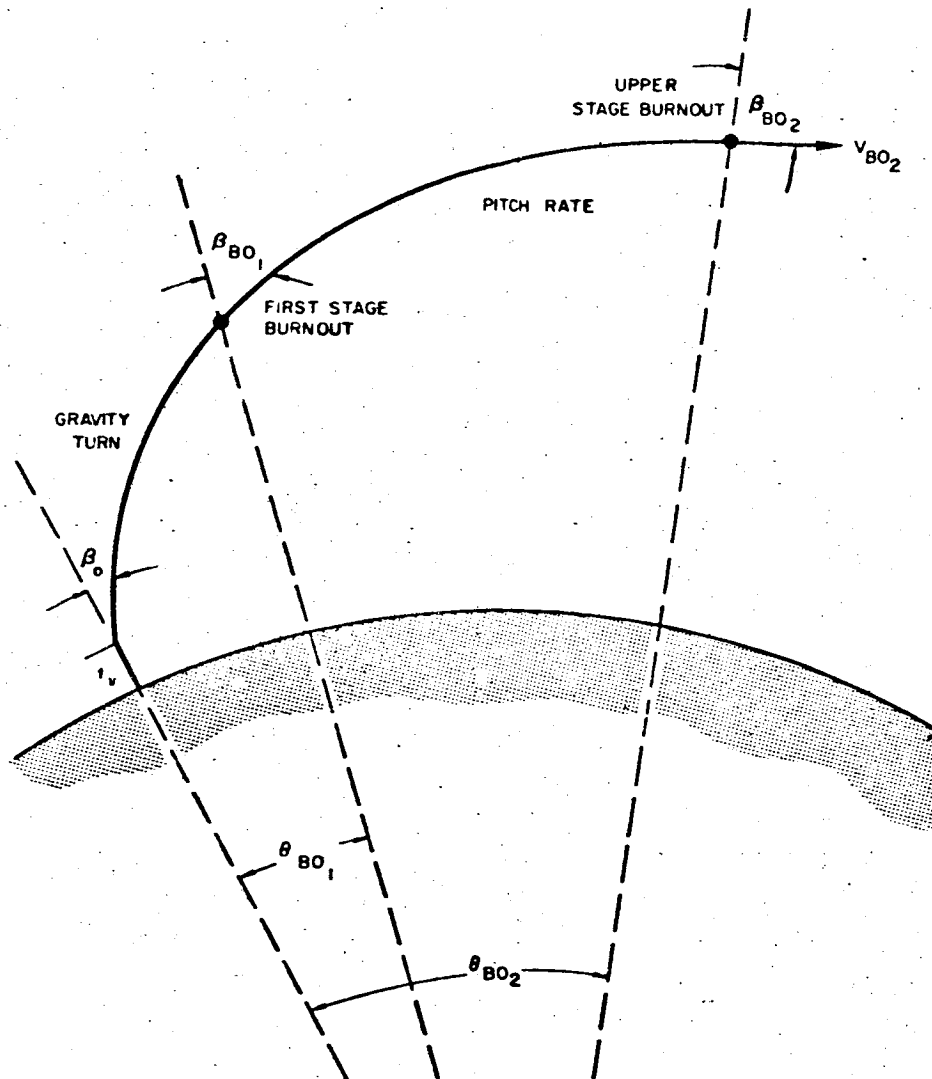


Figure 49. Assumed Typical Trajectory Profile

During the first-stage portion of flight, a gravity turn or "zero angle of attack" trajectory is used to reduce the aerodynamic forces acting on the vehicle. Because a singularity exists at zero initial velocity all vehicles following gravity turn trajectories must be launched vertically and programmed for zero pitch for a short period of time. This period of time is called the vertical rise time, t_v , the length of which is arbitrary but is usually related to the initial thrust-to-weight ratio. After the vertical rise, an artificial "kick angle," instantaneous rotation of the vehicle centerline and velocity vector, is given to the vehicle to initiate the gravity turn. The kick angle is a "tool" used in preliminary trajectory calculations to represent the pitch-over period before the gravity turn. The burnout flight path angle of the first stage is dependent on the magnitude of the kick angle. At first-stage burnout, the vehicle is assumed to be sufficiently out of the atmosphere that the second stage can be flown on a pitch program without regard to aerodynamic effects. In some cases this assumption is not altogether valid, but the error realized in terms of performance is small. At first-stage burnout, the increment in velocity due to the earth's rotational effects is vectorally added to the burnout velocity vector. Thus the upper stages are flown in the inertial reference system, while the first stage is flown in the relative reference system. At this point the upper stages can be coasted or flown with a desired pitch program to burnout.

Past experience has indicated that the coast phases between stages for chill-down, ullage control, etc., have a significant effect on trajectory shaping and thus on overall performance. For this purpose two types of analyses have been included in the section for determining coasting characteristics. The first type is based on the assumption of parabolic motion with constant acceleration. It is a fast and simple method for determining changes in trajectory parameters during a short coast period (less than 60 seconds) due to the previously mentioned conditions of chill-down, ullage control, etc. The second method is based on Kepler's equations of motion along conic sections and gives a more precise but complicated method of determining the changes in trajectory parameters for long coast phases which are typical of vehicles such as Scout.

The analysis for performance evaluation involves two sets of parameters: vehicle design parameters and trajectory parameters. The vehicle design parameters describe the physical characteristics of the vehicle, such as weight, thrusts, specific impulses, drag variations, etc. A set of such design parameters is required in order to analyze performance capabilities. The trajectory parameters are divided into two classes; one class defines the mission, and the other defines vehicle performance. Thus, the problem of determining vehicle performance involves manipulating a set of input data defining the vehicle into a set of trajectory data that are equivalent to the data defining the mission. The required input data are listed below.

Determination of Vehicle Performance

263

First Stage

A	-	Area, used as a reference defining aerodynamic coefficients, ft ²
C_D	-	Drag coefficient as a function of Mach number and based on the reference area A
$I_{sp_{vac}}$	-	Vacuum specific impulse (vacuum thrust divided by flow rate), lb-sec/lb
$I_{sp_{sl}}$	-	Sea-level specific impulse (sea level thrust divided by flow rate), lb-sec/lb
$\frac{T}{W_O}$	-	Initial thrust-to-weight ratio at sea level (based on constant thrust-time variation except as noted)
t_{B_1}	-	First-stage burning time = $\frac{I_{sp_{sl}}}{\left(\frac{T}{W_O}\right)} \left(1 - \frac{1}{r}\right)$, sec
W_O	-	Initial weight, lb
W_{BO}	-	Weight at burnout, lb
r	-	Mass ratio, $\frac{W_O}{W_{BO}}$

Upper Stage

$I_{sp_{vac}}$	-	Vacuum specific impulse, lb-sec/lb
T_{vac}	-	Vacuum thrust, lb
t_{B_u}	-	Upper-stage burning time = $\frac{I_{sp_{vac}}}{\left(\frac{T_{vac}}{W_O}\right)} \left(1 - \frac{1}{r}\right)$, sec
W_O	-	Initial upper-stage weight, lb
$\frac{W_O}{W_{BO}}$	-	Mass ratio, r .

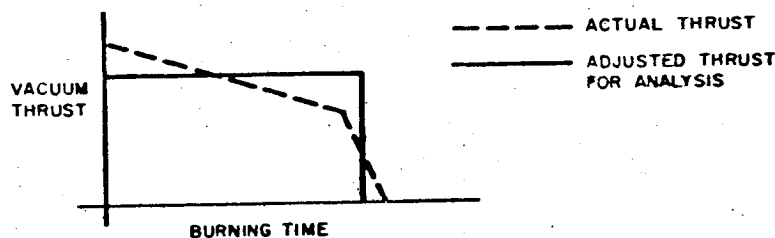
These parameters will be used to determine the following basic trajectory characteristics describing the performance of the vehicle:

$$V_{BO} = \text{Relative velocity at stage burnout (ft/sec)}$$

V_{BO_I}	=	Inertial velocity at stage burnout (ft/sec)
β_{BO}	=	Relative flight path angle at burnout with respect to local vertical (deg)
β_{BO_I}	=	Inertial flight path angle at burnout with respect to local vertical (deg)
h_{BO}	=	Altitude above earth's surface at burnout (ft)
θ_{BO}	=	Range angle from launch site to burnout (deg).

Other trajectory parameters used in overall system considerations are defined in Chapter 3.

It must be pointed out that data for performance evaluation are based on vehicles of constant vacuum thrust (see schematic). For actual vehicles, such as those using solid propellant stages with regressive (or progressive) burning, the vacuum thrust levels must be adjusted to an average constant thrust for use in this analysis. Also, sea-level thrust must be adjusted by the same amount as vacuum thrust to keep the ratio of sea-level specific impulse to vacuum specific impulse constant.



The average vacuum thrust-time history is best found by averaging the vacuum thrust over the burning period prior to tail-off operation and distributing in the tail-off portion rectilinearly at average vacuum thrust and terminating at a time such that the same total tail-off impulse is realized.

In order to clarify the procedure involved in determining the vehicle performance, a listing of the major steps involved is included. These steps essentially follow the time sequence of the actual trajectory mentioned previously. Also, the presentation

of the data and methods will be in the order of the following steps. It is assumed that the data defining both the mission and vehicle have been determined.

- 1) Determine or assume the burnout flight path angle of the first stage.
- 2) Calculate first-stage burnout velocity for the above flight path angle.
- 3) Calculate first-stage burnout altitude and range angle.
- 4) Transform velocity and flight path angle into the inertial system.
- 5) Calculate upper-stage(s) burnout conditions for an assumed pitch program.
- 6) Compare final conditions with the mission requirement.
- 7) Repeat steps 1 through 7 as necessary to obtain final mission conditions within reasonable accuracy.

This sequence of analysis is specifically for the precise computation of vehicle performance. The cursory analysis only determines the burnout velocity to an accuracy of approximately 3 percent for the assumed flight path angles.

2.2.1 First-Stage Burnout Flight Path Angle

As will be seen, the determination of first-stage performance depends on the knowledge of the burnout angle of the first stage. This section presents a method for approximating this flight path angle for low altitude orbit missions which are assumed to be the typical mission of interest for most large booster vehicles. It was mentioned previously that the first-stage burnout angle was determined by the kick angle used at the end of the vertical rise. Thus, the determination of the burnout angle, β_{BO} , is related to the initial kick angle, β_O . The empirical data in Figure 50 indicate the ratio of initial kick angle to vertical rise time required to perform a low-orbit mission. The ratio is dependent on the initial thrust-to-weight ratio and the first-stage mass ratio. The shaded area indicates the spread determined by the various vehicles studied. Generally, the low mass ratio first stages ($r = 2.0$ to 3.5) determined the lower portion of the area while mass ratios greater than 3.5 determined the upper portion. These data were generated for specific values of vertical rise time which are shown in Figure 51 as a function of initial thrust-to-weight ratio.

Since the kick angle is dependent on the vertical rise time, and thus the velocity at the time of kick, the initial thrust-to-weight ratio on the abscissa of Figures 50 and 51 is the actual initial value and not the corrected value for a varying vacuum and sea-level thrust. These are the only two cases where the actual value of initial thrust-to-weight is used if a correction is necessary.

VEHICLE PERFORMANCE ESTIMATION TECHNIQUES

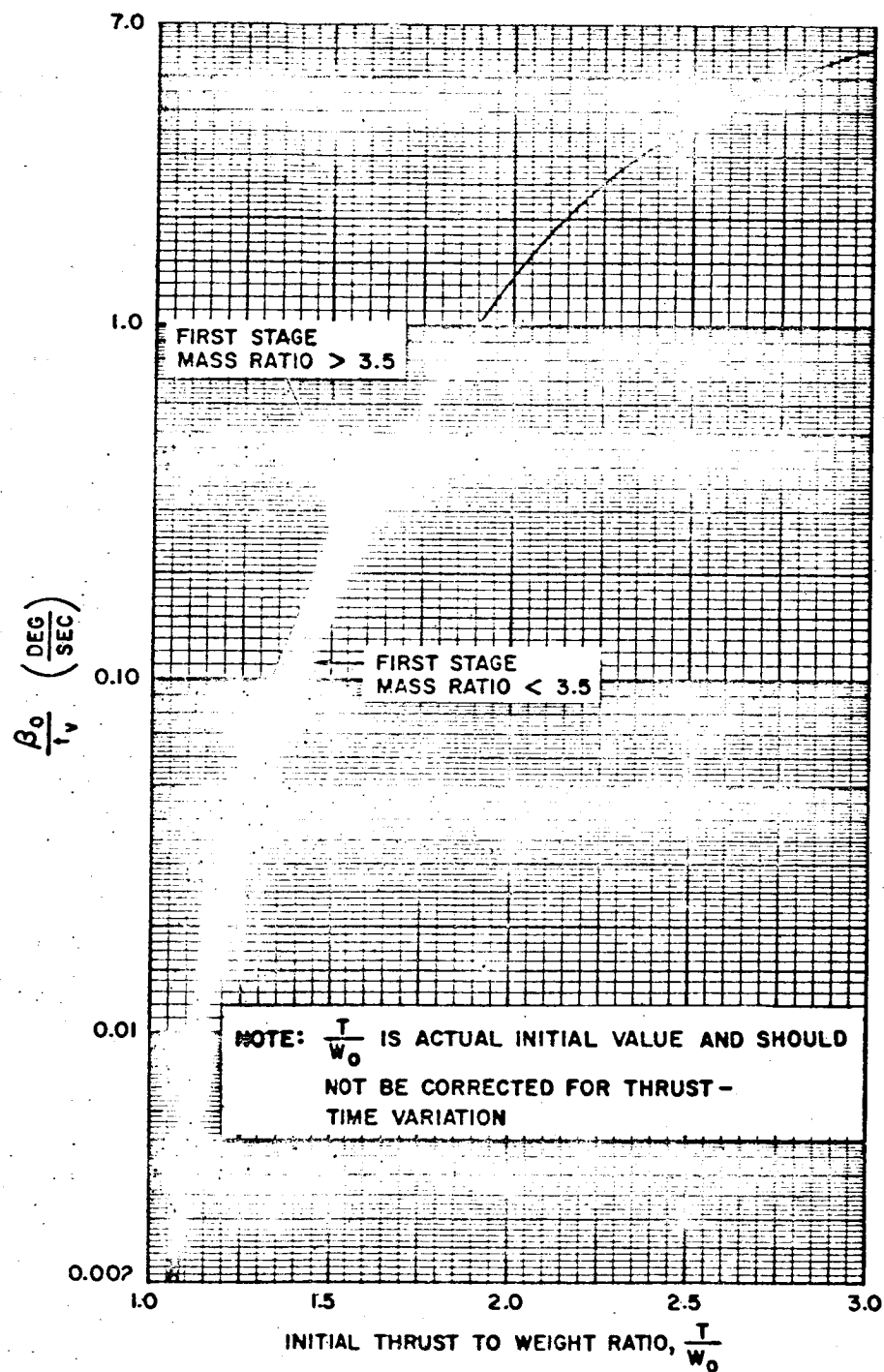


Figure 50. Kick Angle-Vertical Rise Time Ratio (Low Orbit Mission)

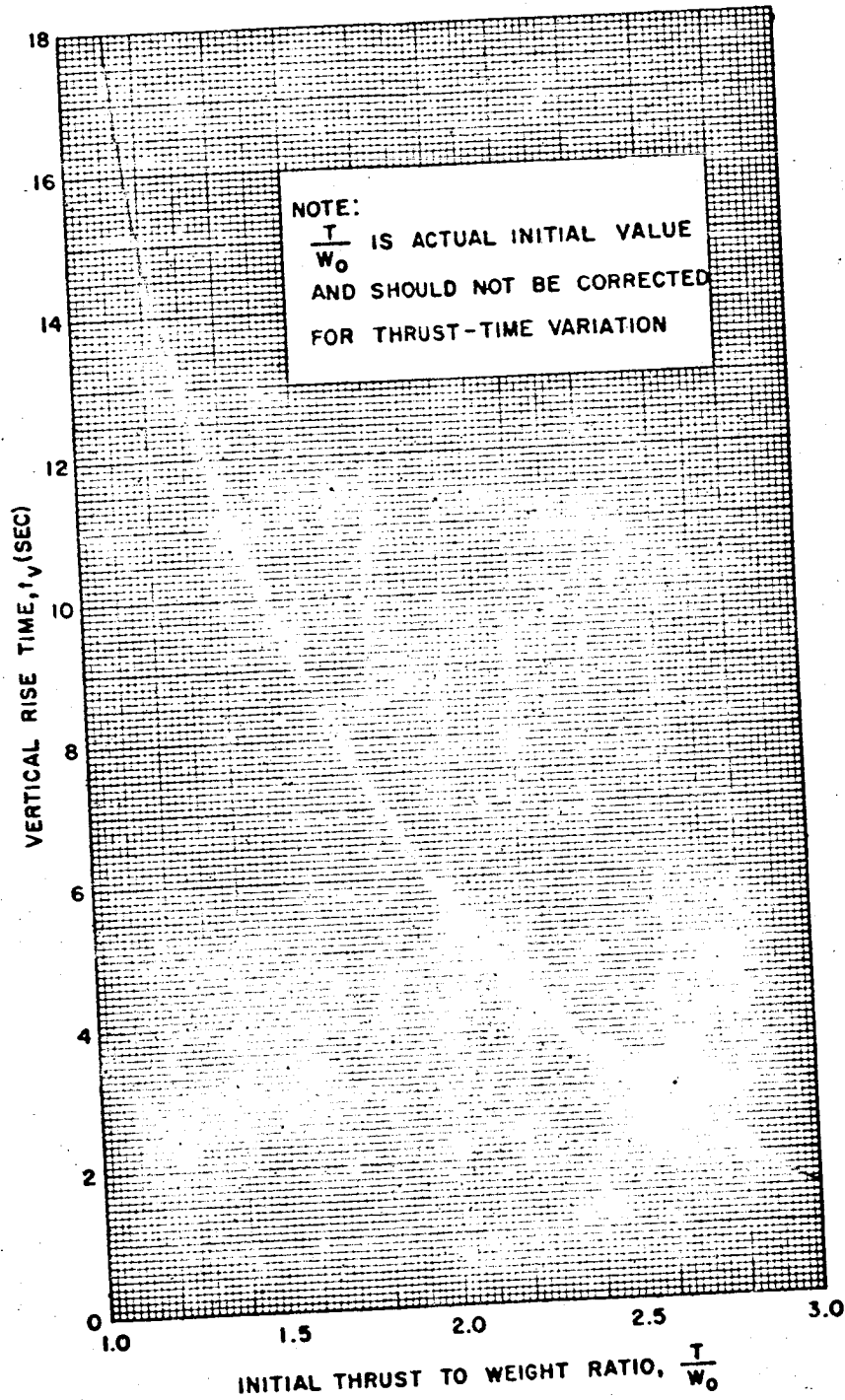


Figure 51. Vehicle Vertical Rise Times

The nomograph shown in Figure 52 presents the first-stage burnout angle as a function of the kick angle, vacuum specific impulse, initial thrust-to-weight ratio, and the first-stage mass ratio. As is shown in the example of Figure 52, the initial thrust-to-weight ratio and vacuum specific impulse are used to construct a horizontal line which intersects a vertical line determined by the initial kick angle at the top of the figure. The intersection of the two line determines the burnout angle. In most cases, the resulting burnout angle will be close to the actual value determined by trajectory calculations.

If the mission of interest is something other than a low altitude orbit, an estimate will have to be made for the burnout angle. Generally, the low orbit mission results in the largest burnout angle and thus other missions would probably require burnout angles somewhat smaller than those given in Figure 52.

2.2.2 Cursory Estimation of Performance

This section provides the designer with a method of estimating the burnout velocity of a vehicle configuration within a short period of time. The method is not sophisticated and thus the results are representative of the first approximation. These data also provide trends for a particular vehicle configuration which can be used to roughly optimize various vehicle characteristics and the trajectory parameters.

Also, there are often times when the total ideal velocity required to perform a particular mission is needed so that a vehicle configuration can be sized to perform the mission. With a minimum of knowledge about the overall configuration and a few estimates, the first approximation for the total velocity loss can be obtained from this section. The sum of total velocity loss and mission velocity gives the required ideal velocity.

This type of analysis applies even if a single stage is being sized to be used with another stage or stages already available.

First-Stage Losses. The ideal or total velocity, V_I , of a stage can be expressed as follows:

$$V_I = g_e \text{Isp}_{\text{vac}} \ln \frac{W_O}{W_{BO}} \quad (1)$$

while the burnout velocity of a stage thrusting in the atmosphere and a gravitational field is

$$V_{BO} = V_I - \Delta V_L \quad (2)$$

The term ΔV_L is defined as the velocity loss due to gravity, drag, and thrust-atmosphere effects. The exact definition of these losses can be found in Appendix A.

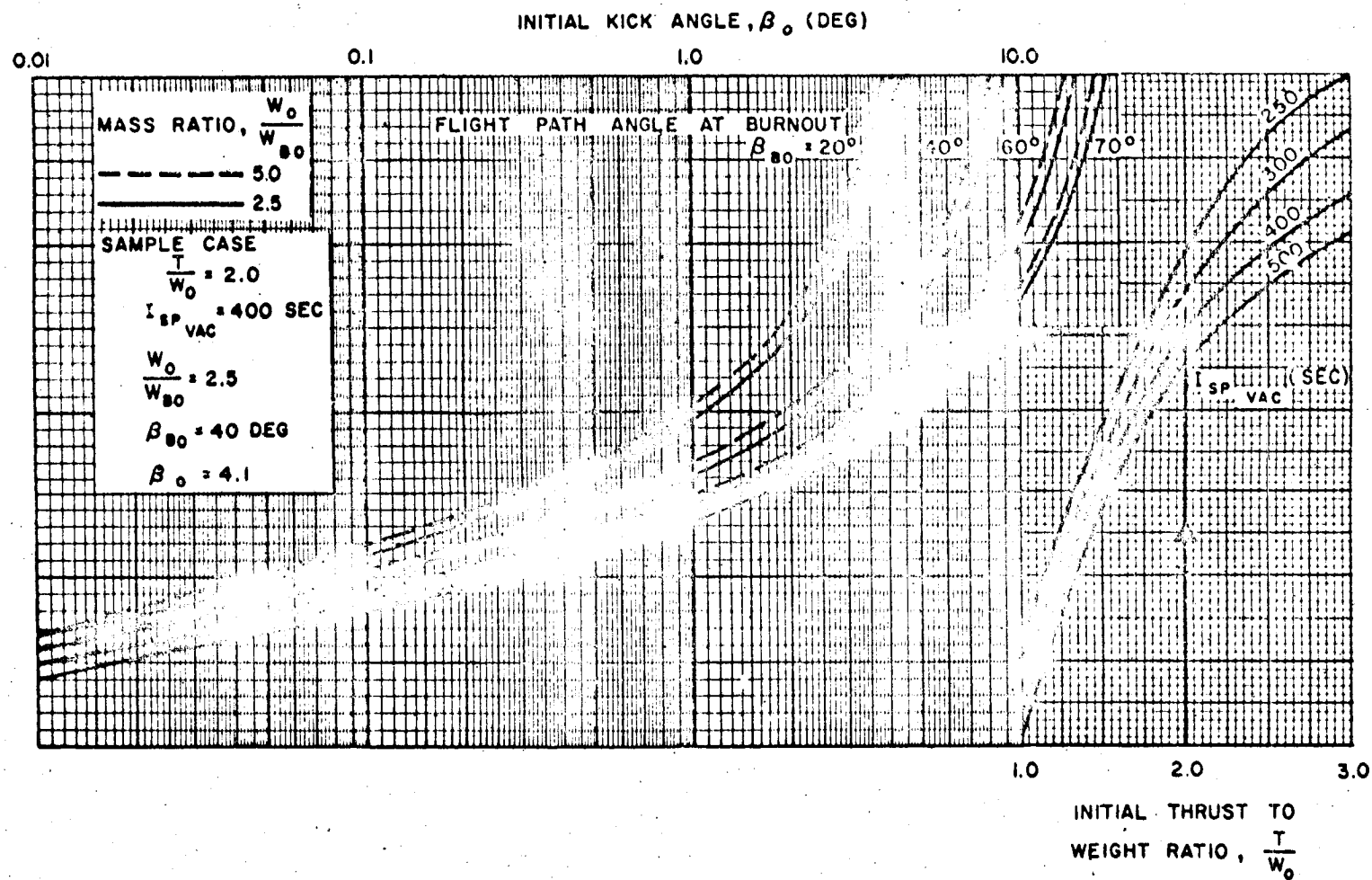
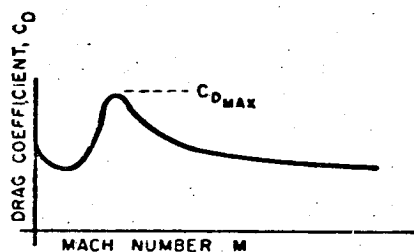


Figure 52. First-Stage Burnout Angle Nomograph

Presented here is an approximate but rapid method for evaluating the first-stage burnout velocity by determining the velocity loss, ΔV_L , during first-stage flight. Figures 53 through 59 present the total velocity loss, ΔV_L , of a single-stage vehicle as a function of the initial thrust-to-weight ratio, vacuum specific impulse, and first-stage burnout flight path angle. These data were generated for a vehicle with the following characteristics:

$$\frac{I_{sp_{sl}}}{I_{sp_{vac}}} = 0.85, \quad \frac{C_{D_{max}} A}{W_O} = 0.0002, \quad \frac{W_O}{W_{BO}} = 4.0$$

The parameter, $C_{D_{max}}$, is the maximum drag coefficient obtained from the drag coefficient versus Mach number variation. This value usually occurs at a Mach number of 1.0. (See diagram.)



If the vehicle of interest has characteristics different from those assumed above, the following relations can be used to adjust the losses obtained from Figures 53 through 59.

$$\Delta(\Delta V_L) = 2 \times 10^6 \left(\frac{C_{D_{max}} A}{W_O} - 0.0002 \right) \quad (3)$$

$$\Delta(\Delta V_L) = 3780 \left(0.85 - \frac{I_{sp_{sl}}}{I_{sp_{vac}}} \right) \quad (4)$$

$$\Delta(\Delta V_L) = 0.85 g_e \frac{T}{W_O} I_{sp_{vac}} \cos \beta_{BO} \left(\frac{1}{4} - \frac{1}{\frac{W_O}{W_{BO}}} \right) \quad (5)$$

After having determined the first-stage burnout velocity, V_{BO} , through the use of Equation (2), the component of the launch site rotational velocity along the assumed launch azimuth is vectorally added to V_{BO} to obtain the inertial burnout velocity $V_{BO_{I1}}$. The proper value of rotational velocity is given in Section 3.1.1 of Chapter 3, while the procedure for the vector addition is given in Section 2.2.3.

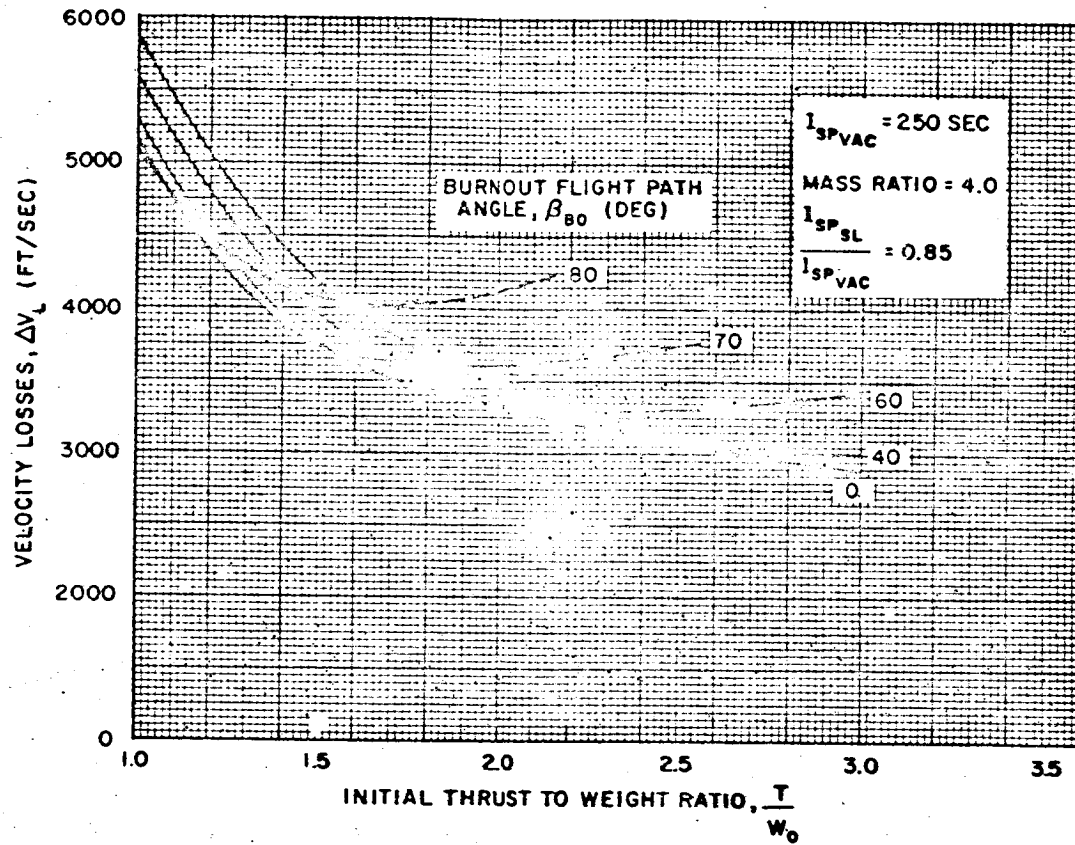


Figure 53. Cursory First-Stage Velocity Losses

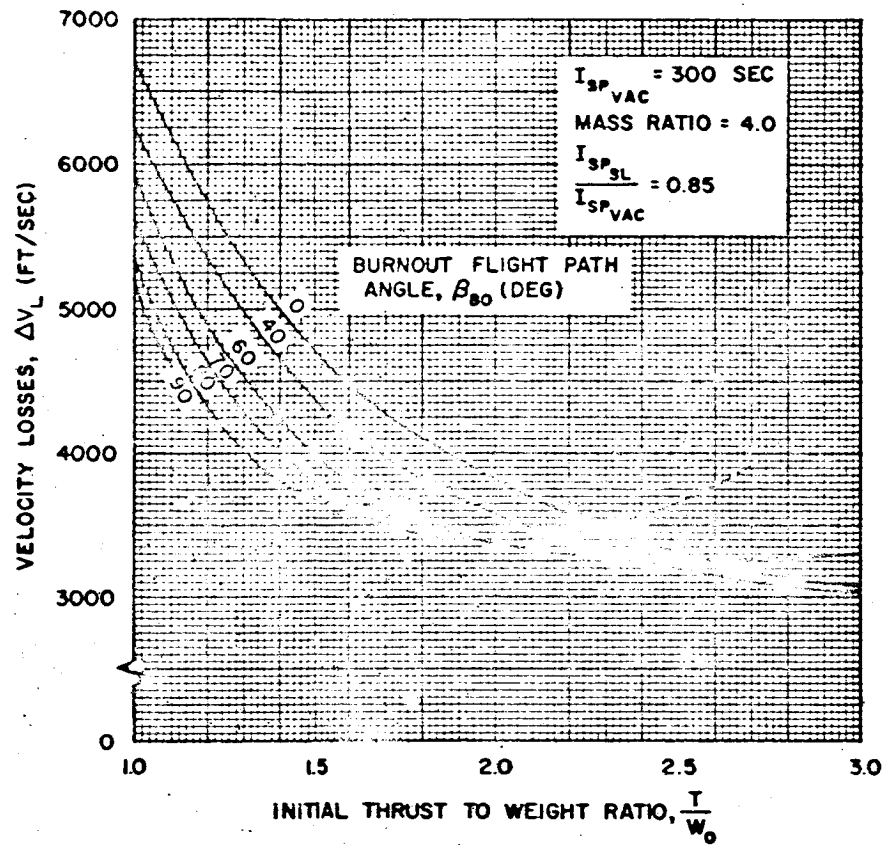


Figure 54. Cursory First-Stage Velocity Losses

Determination of Vehicle Performance

2.73

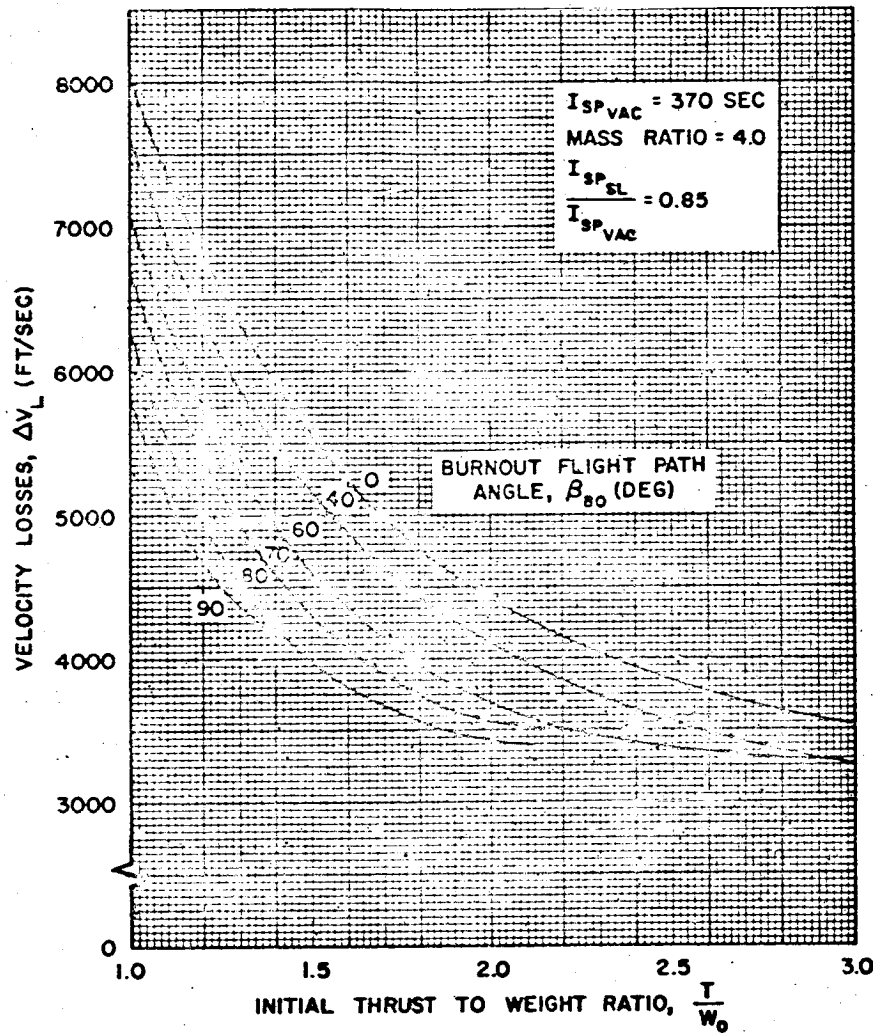


Figure 55. Cursory First-Stage Velocity Losses

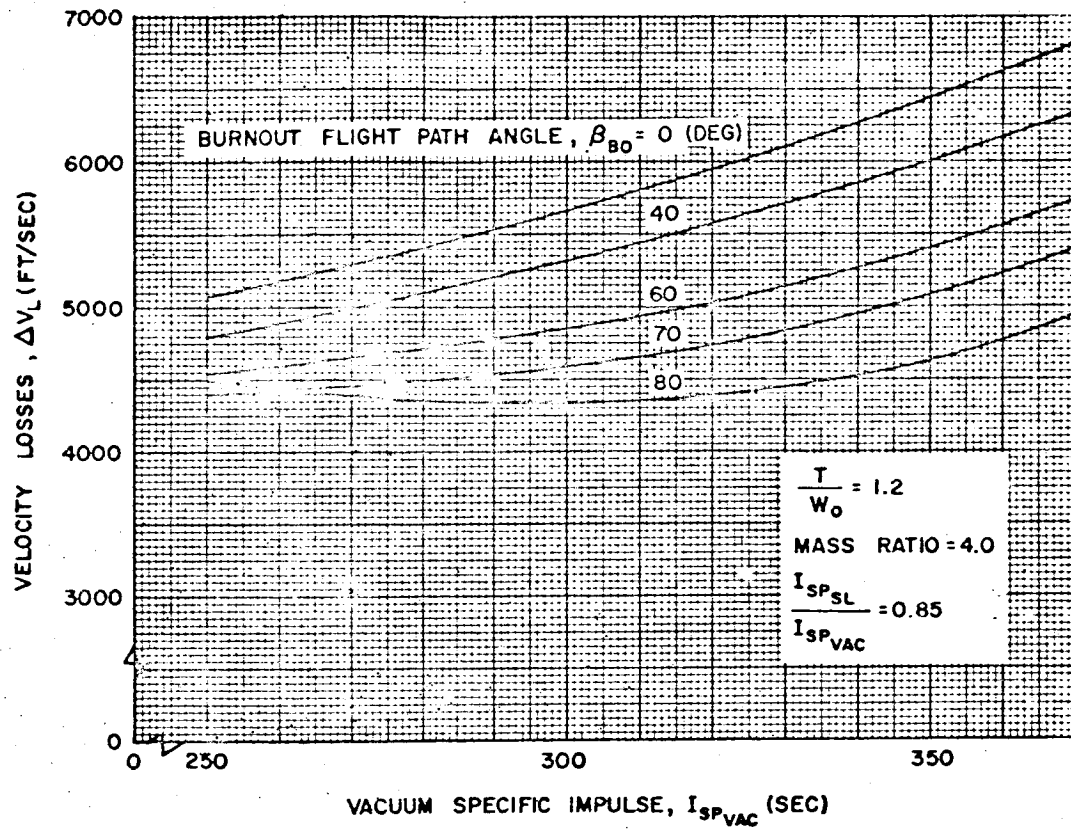


Figure 56. Cursory First-Stage Velocity Losses

Determination of Vehicle Performance

2-75

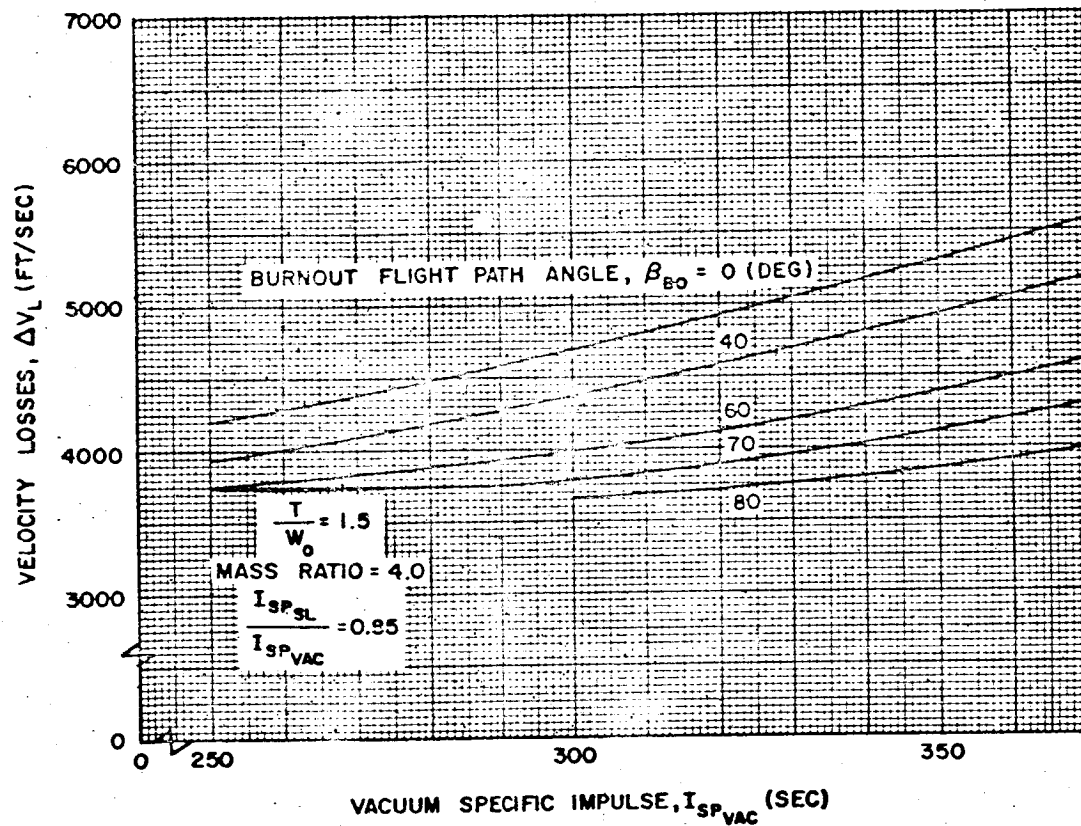


Figure 57. Cursory First-Stage Velocity Losses

2-76

VEHICLE PERFORMANCE ESTIMATION TECHNIQUES

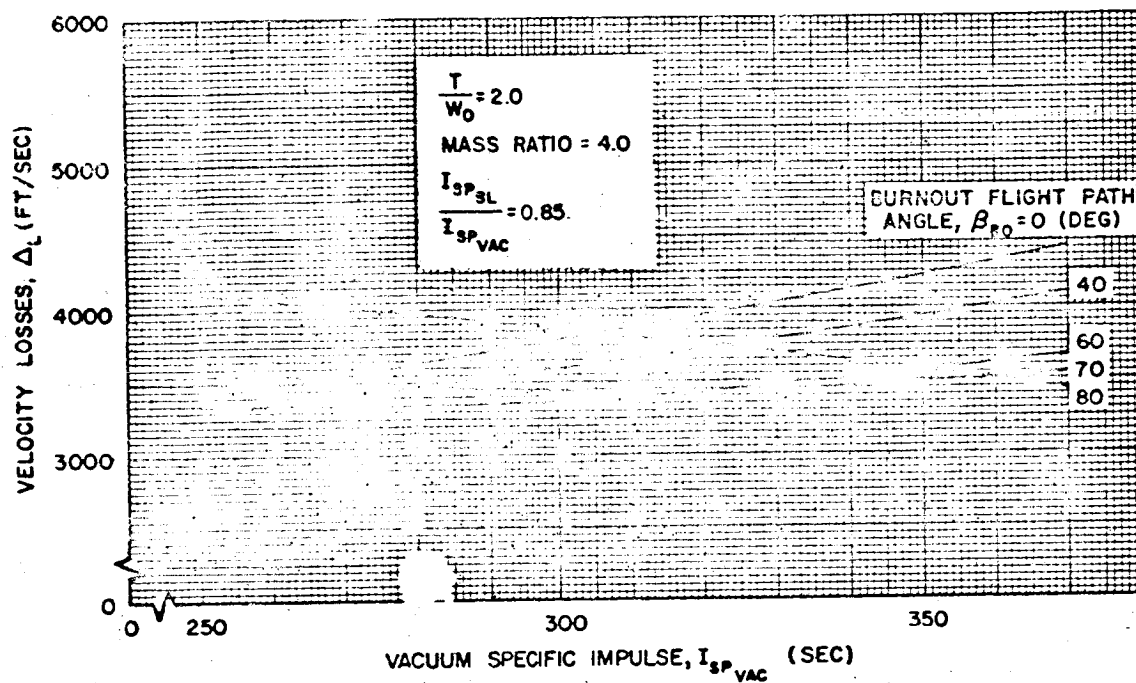


Figure 58. Cursory First-Stage Velocity Losses

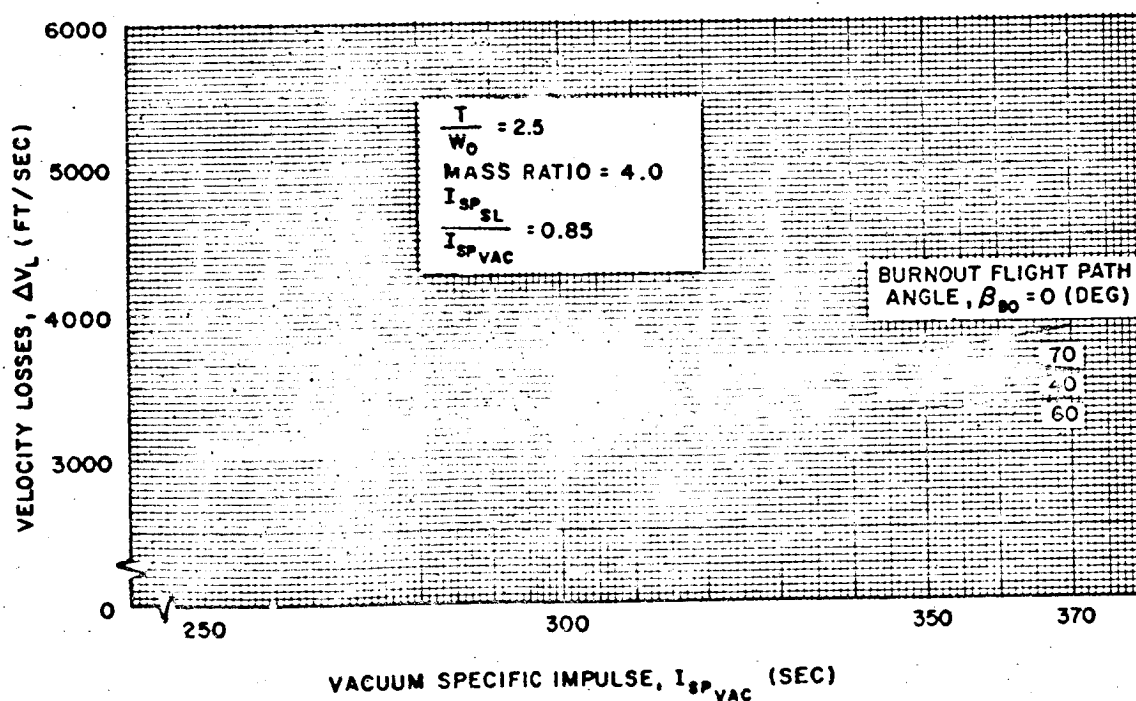


Figure 59. Cursory First-Stage Velocity Losses

Upper-Stage Losses. The burnout velocity of a vehicle's upper stages can be expressed in much the same manner as that shown in Equation (2) for N stages.

$$v_{BO_I}^{(N)} = v_{BO_I} + \sum_{i=2}^N v_I^{(i)} - \sum_{i=2}^N \Delta v_{L_i} \quad (6)$$

where the losses are due to gravity and angle of attack. The gravity loss is the more significant of these, thus the upper stage losses can be expressed as

$$\Delta v_L = g_e t_B \cos \bar{\beta} \quad (7)$$

where $\bar{\beta}$ is an average flight path angle selected between the initial value of the upper stage flight path angle and the burnout value. The average angle, $\bar{\beta}$, is dependent on the thrust-pitch program of the upper stage.

Typical average flight path angles are shown on Figures 60 and 61 for one and two upper stages, respectively. These data, which are a function of the initial flight path angle, were generated from trajectory data for low orbit missions and thus the burnout angle is 90 degrees. Where two upper stages are involved, a dependence on the initial thrust-to-weight ratio is indicated. This is explained by the fact that stages with a low thrust-to-weight ratio ($T_{vac}/W_O < 1.0$) have long burning times and spend a relatively long time near a flight path angle of 90 degrees, which increases the value of $\bar{\beta}$. Stages with a high thrust-to-weight ratio ($T_{vac}/W_O > 1.0$) act much the same as a single upper stage. The data (given in Figures 60 and 61) were determined empirically from several trajectory calculations. Any angle of attack losses due to thrust misalignment were included in the calculations of $\bar{\beta}$. Thus, angle of attack losses have not been neglected.

For missions where the burnout flight path angle is not 90 degrees, the following relation has been determined for an approximation to $\bar{\beta}$ for use in Equation (7),

$$\bar{\beta} = 0.7 (\beta_{BO} - \beta_1) + \beta_1 \quad (8)$$

where β_1 and β_{BO} are the initial and final flight path angles. This relation is at best representative because of the number of variations possible in the upper-stage characteristics and flight profile.

2.2.3 Precise Evaluation of Performance

This section indicates a method of precisely determining the performance characteristics of a given vehicle configuration for a particular mission definition. The

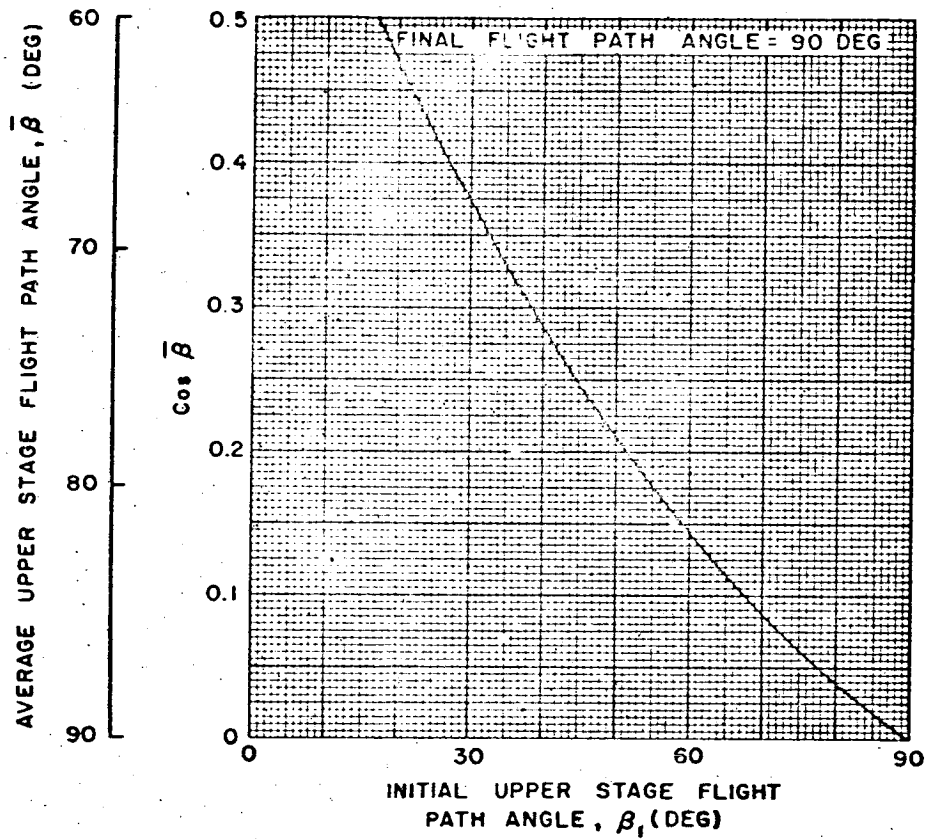


Figure 60. Average Upper-Stage Flight-Path Angle (Single Upper Stage)

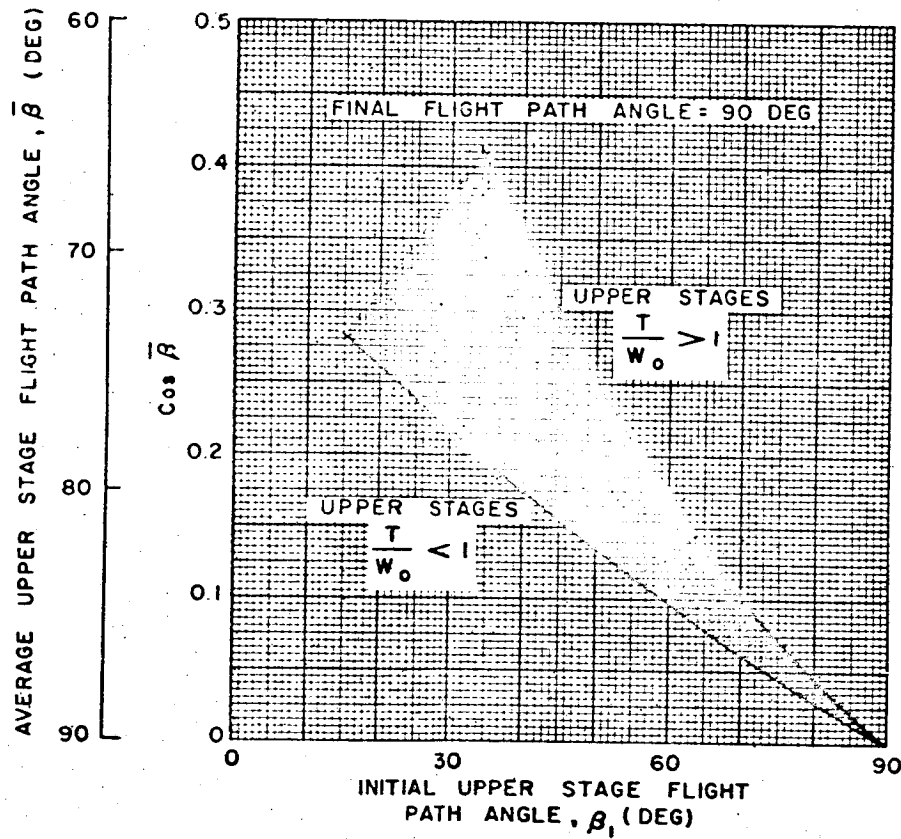


Figure 61. Average Upper-Stage Flight-Path Angle (Two Upper Stages)

REVISED PAGE

3-2
KENTON & SONS CO.
10 X 10 TO THE CM.
3201-140
VOLUME 2
MIDLAND

method can provide essentially a time-history of the trajectory parameters (except during first-stage operation) based on the assumed trajectory mentioned previously. However, a considerable amount of time would be required for the calculation of such a complete description of the trajectory. In most cases, the burnout points of each stage would be sufficient.

As will be explained, an iteration technique is required to obtain the desired mission conditions. The number of iterations performed will be dependent on the accuracy required by the designer. In most cases three or fewer should be sufficient.

The method described below provides not only burnout velocity and angle, but other parameters such as altitude, range angle, and angle of attack. Thus, a general analysis can be made of a vehicle's characteristics. Restrictions such as range safety, heating, loads, and guidance obtained from Chapter 3 can be combined with the performance evaluation to complete the analysis.

First-Stage Performance. The precise determination of first-stage burnout velocity is based on Equation (2) except that gravity, drag, and thrust-atmospheric losses are evaluated separately and more accurately. The total losses of the first stage can be expressed by

$$\Delta V_L = \Delta V_{L_g} + \Delta V_{L_D} + \Delta V_{L_T} \quad (9)$$

where

$$\Delta V_{L_g} = \text{gravitational loss} = (g_e t_B - K_{g5}) \left[1 - K_g \left(1 - \frac{1}{r} \right) \left(\frac{\beta_{BO}}{90^\circ} \right)^2 \right] \quad (10)$$

$$\Delta V_{L_D} = \text{drag loss} = K_D \frac{C_{D_{PD}} A}{W_O} \quad (11)$$

$$\Delta V_{L_T} = \text{thrust-atmospheric loss} = K_a \quad (12)$$

These losses will be discussed individually.

1. Gravitational Loss. The first-stage gravitational loss expressed by Equation (10) is a function of the vehicle design parameters, the burnout angle, and two empirical constants, K_{gg} and K_g . The term $g_e t_B$ in Equation (10), is the gravitational loss expected from vertical flight in a constant gravitational field. However, due to the variation of a gravitational field as the inverse square of the distance from the center of attraction, the constant, K_{gg} , is needed to correct the overestimated loss determined by $g_e t_B$. The value of K_{gg} can be determined from the data shown in Figure 62. The constant, K_g , is a function of the initial thrust-to-weight ratio, vacuum specific impulse, and mass ratio. This constant can be found in Figures 63 and 64 for mass ratios of 2.5 and 5.0, respectively. If the first stage has a mass ratio of some value other than 2.5 or 5.0, the correction factor shown in Figure 65 should be used to adjust the value of K_g for a mass ratio of 2.5 obtained from Figure 63.

2. Drag Losses. The drag losses of a vehicle are shown in Equation (11) to be a function of the ratio, $C_D A/W_O$, where C_D is a representative value of the drag coefficient for the vehicle of interest. In Section 2.2.2, Cursory Estimation of Performance, it was assumed that the maximum drag coefficient was representative of the vehicle drag characteristics. However, for precise calculations, the drag coefficient at maximum drag force during the trajectory, $C_{D_{PD}}$, was found to be more representative. Determining $C_{D_{PD}}$ requires knowledge of the Mach number at maximum drag M_{PD} , in order to pick off the correct value from the curve of drag coefficient versus Mach number. The parameter, M_{PD} , is shown in Figure 66 as a function of the ratio $\sqrt{I_{sp_{vac}}}/(T/W_O)$ and burnout flight path angle. The empirical constant, K_D , was also found to be a function of $\sqrt{I_{sp_{vac}}}/(T/W_O)$ and β_{BO} as is shown in Figure 67.

The drag loss obtained by these relations is representative of a first-stage flight that burns out above the atmosphere. If first-stage burnout occurs in the atmosphere, the drag loss obtained by these relations will essentially include any drag loss encountered during the second-stage flight, thus the second stage can be assumed to be operating in a vacuum.

3. Thrust-Atmospheric Losses. Thrust-atmospheric losses are caused by the reduction of the vacuum thrust level by atmospheric pressure during the portion of flight through the atmosphere. Thus, the ratio of sea level specific impulse to vacuum specific impulse, which is determined by the nozzle and propellant characteristics, is the important parameter determining these losses. Also, the initial thrust-to-weight ratio has a small effect which is included in Figure 68 for the determination of K_a .

It must be pointed out that the values of K_a shown in Figure 68 are representative of conical and DeLaval type nozzles only. Exotic nozzle configurations such as plug (or spike) or expansion-deflection types would have lower losses for the same initial conditions.

VEHICLE PERFORMANCE ESTIMATION TECHNIQUES

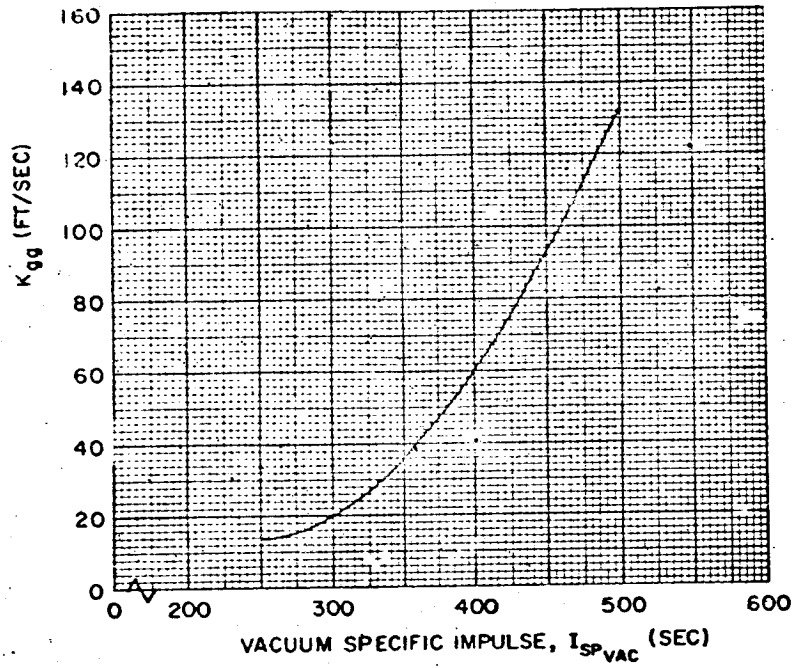


Figure 62. Change in First-Stage Losses Due to Altitude Variation of Gravity

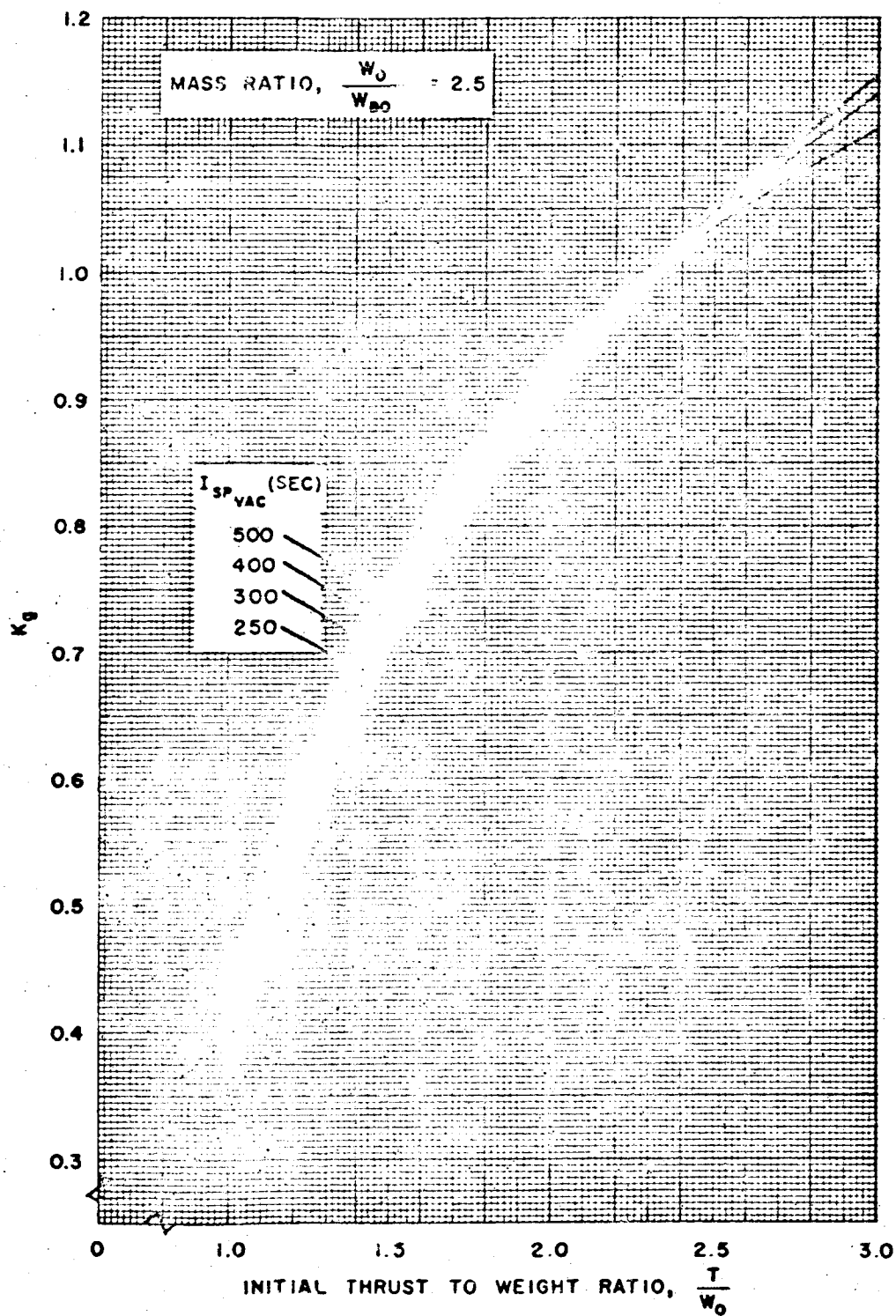


Figure 63. First-Stage Gravity-Loss Constant

2-84

VEHICLE PERFORMANCE ESTIMATION TECHNIQUES

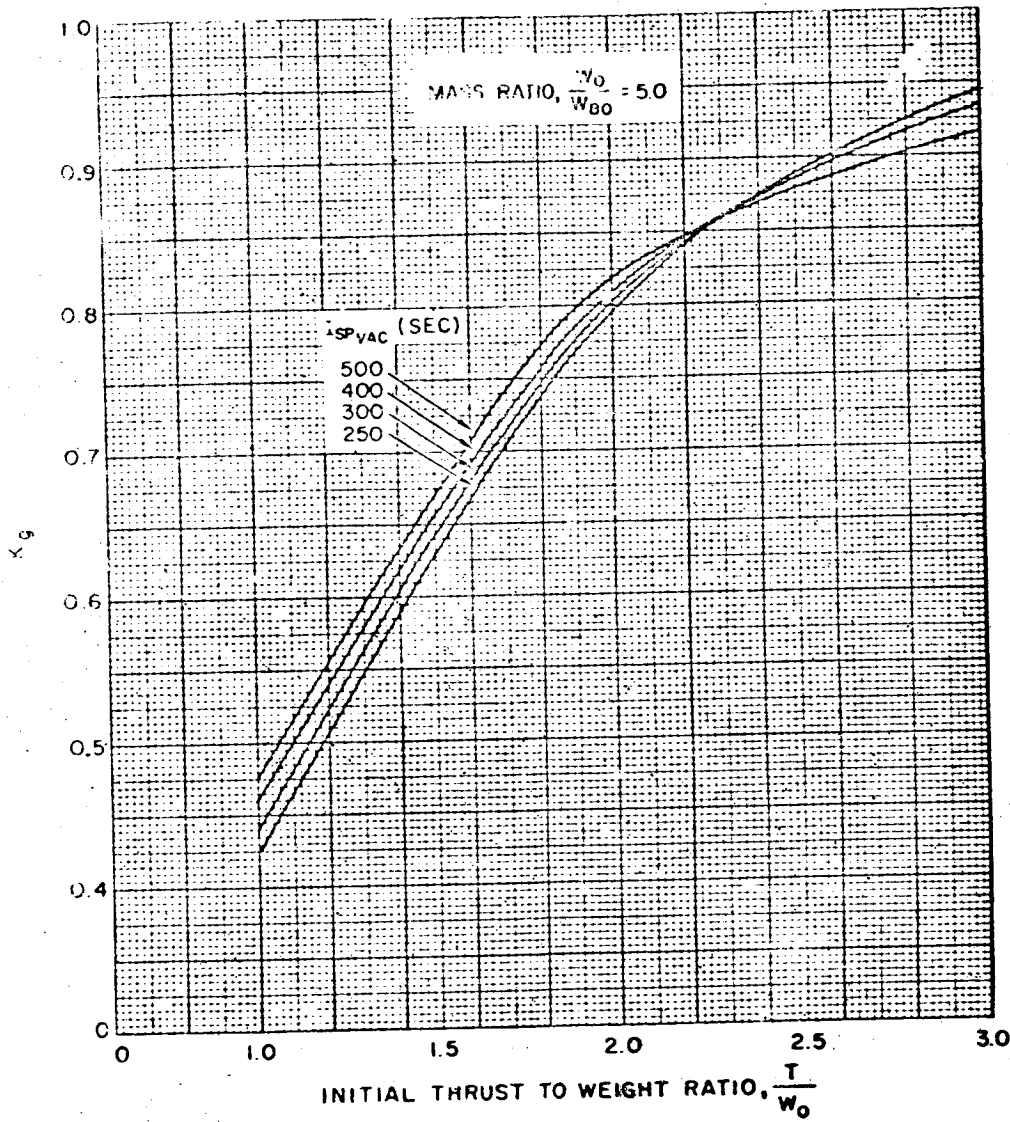


Figure 64. First-Stage Gravity-Loss Constant

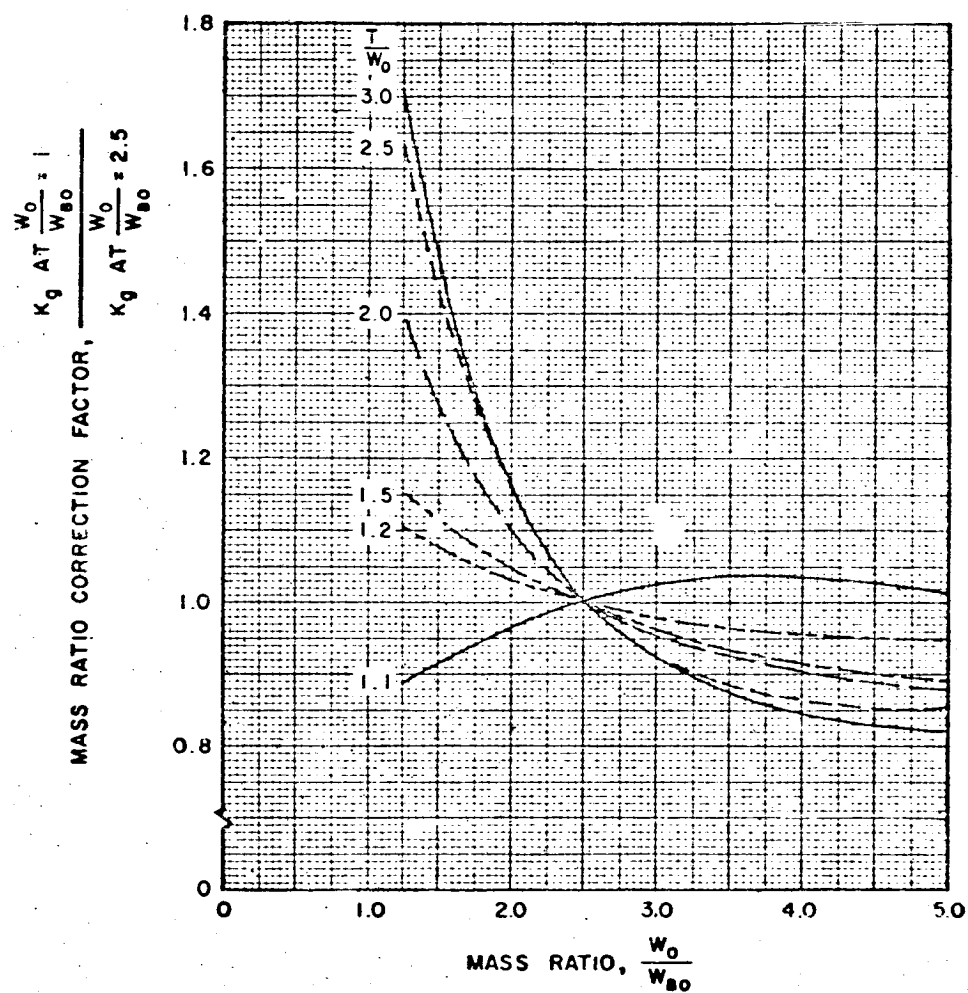


Figure 65. First-Stage Mass Ratio Correction Factor

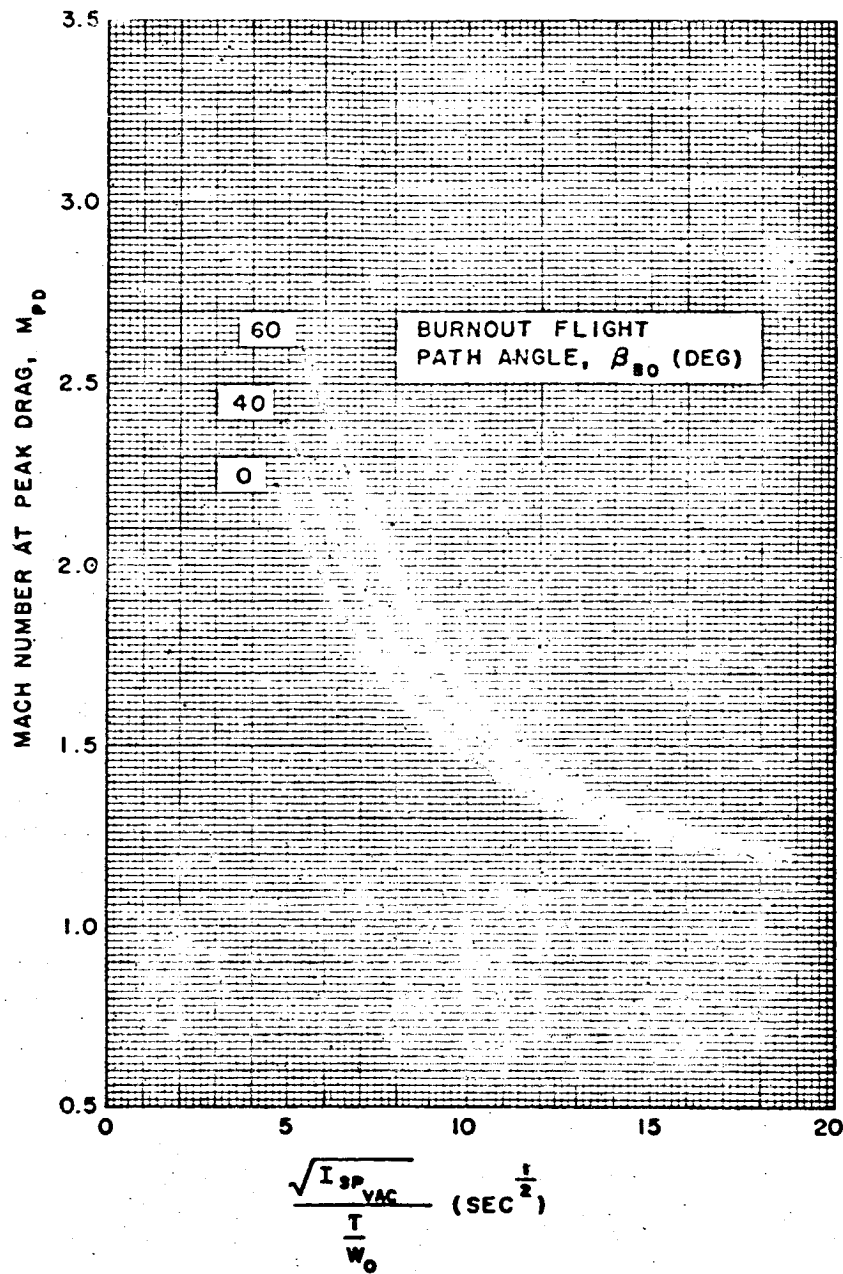


Figure 66. First-Stage Mach Number at Peak Drag

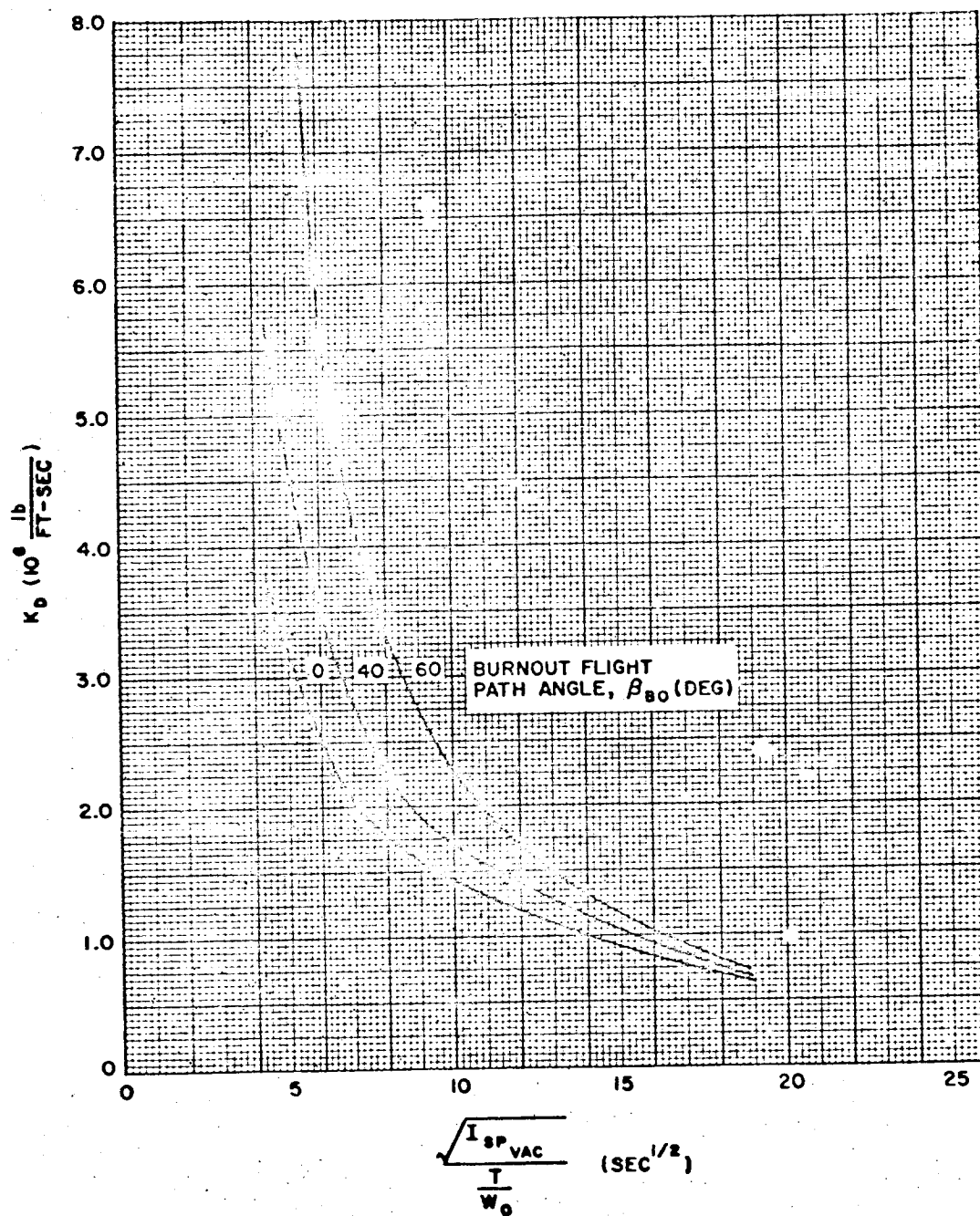


Figure 67. First-Stage Drag-Loss Constant

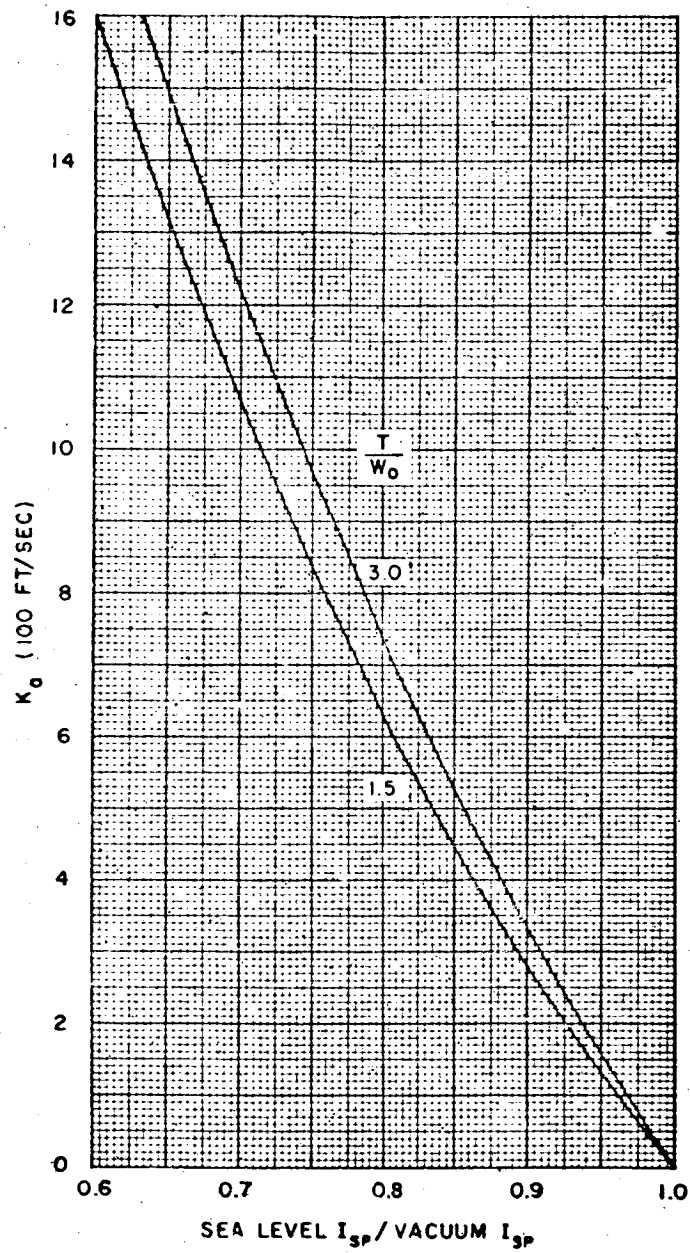


Figure 68. First-Stage Thrust Atmospheric Losses

4. First-Stage Burnout Altitude. Now that the burnout velocity and flight path angle have been determined for the first stage, the calculation of burnout altitude remains to define the first-stage burnout conditions. As developed in Appendix A, the burnout altitude is

$$h_{BO} = \left[h^* - \frac{(\Delta V_{LD} + \Delta V_{LT}) t_B}{2} \right] \left[1 - \left(\frac{\beta_{BO}}{K_h} \right)^2 \right] \quad (13)$$

where h^* is the altitude attainable by the first stage, in nonatmospheric vertical flight.

$$h^* = g_e \text{Isp}_{vac} t_B \left(1 - \frac{\ln \frac{W_O}{W_{BO}}}{\frac{W_O}{W_{BO}} - 1} \right) - \frac{g_e t_B^2}{2} \quad (14)$$

The burnout altitude then is dependent on the vehicle parameters, the atmospheric losses, the burnout flight path angle, and the empirical constant, K_h . The constant, K_h , was found to be a function of initial thrust-to-weight ratio, vacuum specific impulse, and mass ratio. The variation of K_h (in radians) is shown in Figure 69 in nomograph form.

5. First-Stage Range Angle at Burnout. The range angle of the vehicle at first-stage burnout, θ_{BO} , as defined in Figure 49, is necessary to completely define the burnout location. Since the range angle at burnout is small for a vehicle's first stage, an empirical method was used for the representation of range angle. Figure 70 presents a nomograph in terms of the first-stage parameters from which the value of burnout range angle can be obtained. In constructing the nomograph it was assumed that rotation of the earth during first-stage burning was a negligible effect.

6. Effects of Earth's Rotation. In order to use the following methods for analyzing upper stage performance, it is necessary to transform the first-stage burnout conditions into the inertial coordinate system. This requires vectorally adding the rotational velocity of the launch site to the first-stage velocity vector. The magnitude of the rotational velocity in the launch azimuth plane can be determined from Figure 1 in Chapter 3 for the launch site location and launch azimuth of interest. The effect of the component of earth's rotational velocity normal to the launch azimuth plane can be

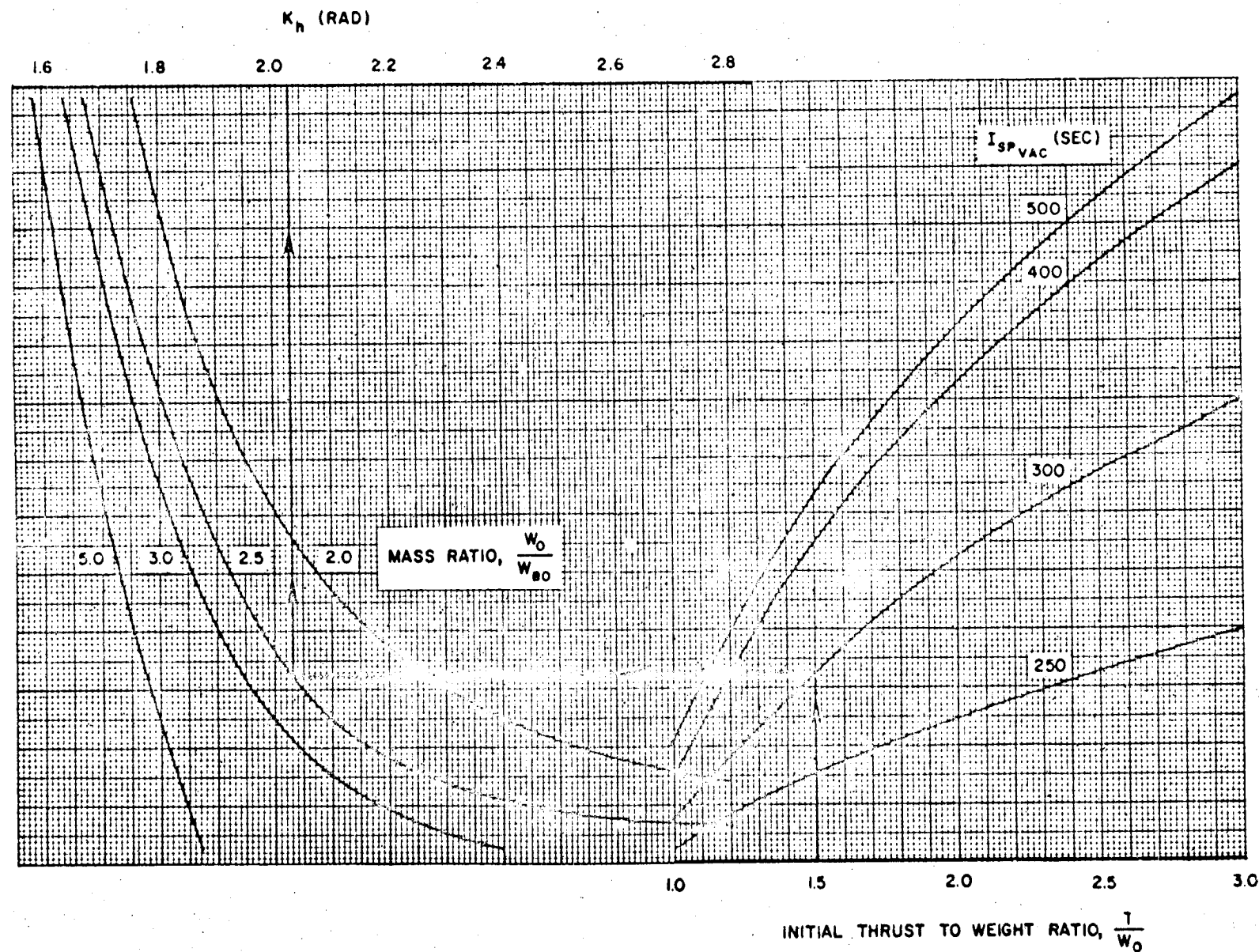


Figure 69. First-Stage Burnout Altitude Constant

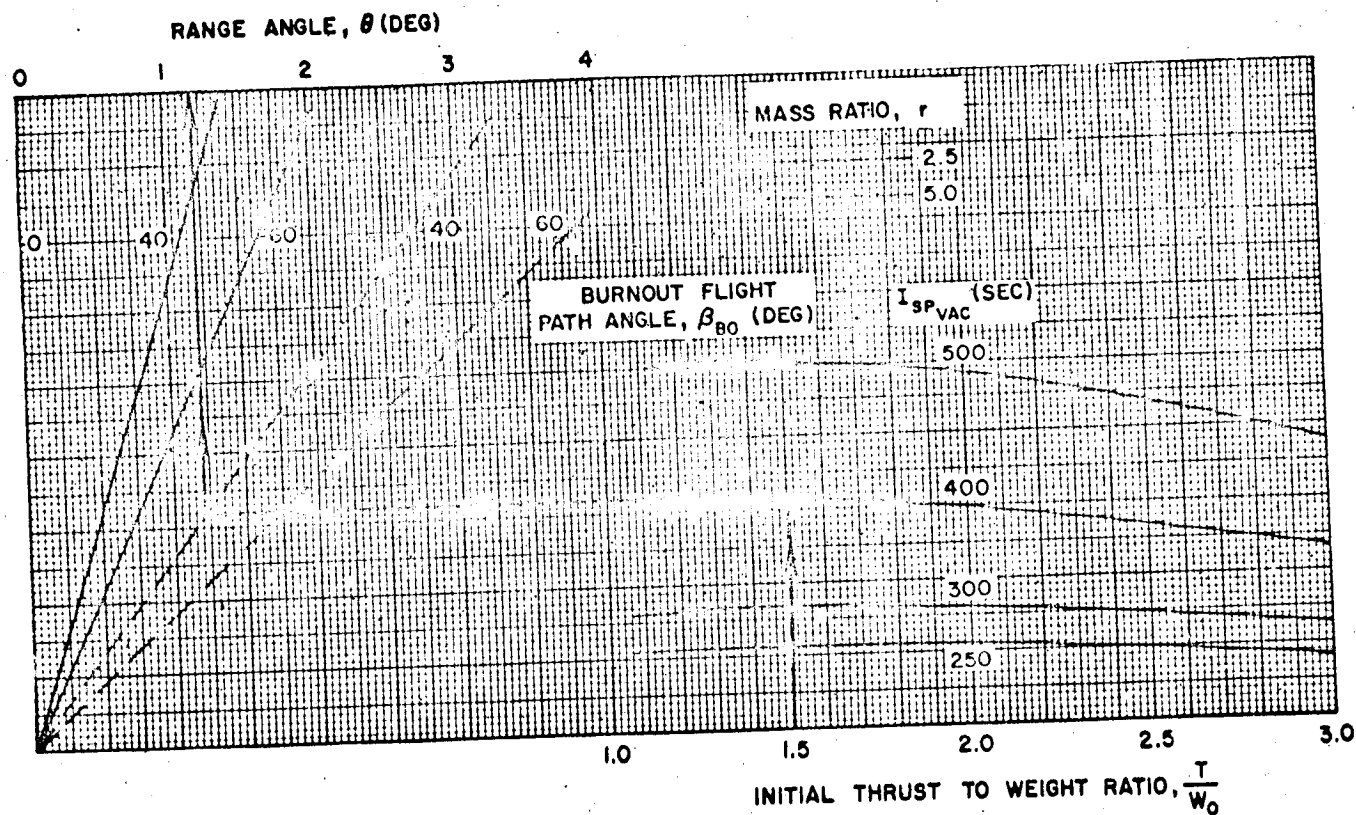
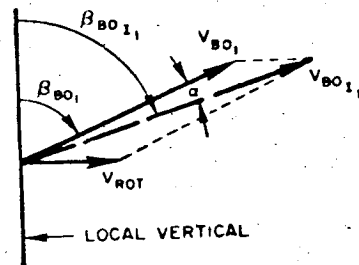


Figure 70. First-Stage Range-Angle Nomograph

considered as simply an effective dog-leg of the trajectory plane and is more fully discussed under the section on Launch Site Limitations in Chapter 3. In using Figure 1 it must be remembered that an eastward launch increases the first-stage velocity while a westward launch decreases the velocity. The schematic indicates the geometry involved while Equations (15) and (16), determined from the laws of cosines and sines respectively, can be used to calculate the values of inertial velocity, V_{BOI} , and inertial flight path angle, β_{BOI} .



$$V_{BOI} = \sqrt{(V_{BO})^2 + (V_{rot})^2 + 2(V_{BO})(V_{rot}) \sin \beta_{BO}} \quad (15)$$

$$\beta_{BOI} = \cos^{-1} \left(\frac{\cos \beta_{BO}}{V_{BOI}} \right) V_{BO} \quad (16)$$

Since the vehicle thrust axis is aligned with the relative velocity vector, V_{BO} , due to the gravity turn, a change in angle of attack, α , results when the transformation is made to the inertial system. This change can be evaluated by Equation (17).

$$\alpha_{BO} = \beta_{BOI} - \beta_{BO} \quad (17)$$

Angle of attack, α , inertial burnout velocity, V_{BOI} , inertial flight path angle at burnout, β_{BOI} , burnout altitude, h_{BO} , and range angle, θ_{BO} , must be known for the performance analysis of succeeding stages. Other data of interest describing trajectory conditions such as elevation angle, look angle, heating, loads, and range safety constraints may be found in Chapter 3.

As mentioned on page 2-62, short coast phases for vernier periods, chill-down, allage control, etc., have significant effects on performance and should be included where necessary. The equations for determining these short-coasting effects along with Kepler's equations for long coast phases are presented later in this chapter.

Precise Computation of Performance Parameters for Nonatmospheric

Powered Flight. After calculation of first-stage performance characteristics for a gravity turn flight within an atmosphere, performance of upper stages in the absence of an atmosphere can be calculated by the methods presented in this section. In addition, performance of the first stage and of subsequent stages can be calculated for lunar launchings.

The discussion of precise computation of nonatmospheric performance is based upon the premise that vehicles will be flown into low-altitude circular orbits. In some cases the circular orbit is the mission of interest and in other cases it serves as a parking orbit from which the vehicle will be injected into trajectories ranging from Hohmann transfer trajectories to escape trajectories. However, the methods presented are valid for other powered flight and first stage operation, such as direct ascent into higher circular orbits or into escape orbits.

Performance for Flight at a Constant Pitch Rate. For trajectories which are flown at a constant pitch rate (constant rate of change of thrust orientation with respect to the launch coordinate system) or at constant thrust attitude (zero pitch rate), the final inertial parameters can be determined for each stage or phase of stage operation by use of the results of Appendix A, if initial inertial parameters are available for that portion of the trajectory. This method is applicable to upper stage operation where atmospheric effects are negligible, and can be used as well for evaluation of first-stage performance during lunar takeoffs.

The results of Appendix A are limited by several assumptions:

- 1) The radial distance from the center of the attracting mass is kept constant at an average effective distance during the burning period, under the assumption that the variation in radial distance during burning is small compared with the initial distance.
- 2) The magnitude of the acceleration due to gravity is assumed constant at its value corresponding to the effective radial distance.
- 3) The stage thrust and propellant flow rate are assumed to be constant with time, consequently requiring that the effective stage specific impulse be constant.
- 4) Thrust orientation varies linearly with time throughout burning, so that the thrust vector is pitched at a constant rate. The analysis is valid for the case of zero pitch rate, where constant attitude is maintained.
- 5) The powered flight motion is planar.

To evaluate the performance over a portion of a trajectory using the method of Appendix A, it is necessary to specify the initial thrust orientation and initial components of velocity in terms of an inertial rectangular coordinate system whose vertical axis lies along the initial local vertical. Thus, where performance is to be computed for more than one stage or phase of stage operation, the reference axes must in each case be rotated about the center of attraction until the vertical axis is the local vertical at that time. Figure 71 illustrates schematically the procedure for a typical trajectory profile. Although it is anticipated that evaluations

will be made for the complete performance of a stage, this need not be the case, as it is possible to execute a series of successive evaluations where each separate phase of analysis provides the initial conditions to succeeding steps. In this way, the time variation of the trajectory elements can be determined for the stages being analyzed.

1. Input Parameters. In terms of the initial conditions (denoted by the subscript i) at the time the analysis is initiated, the initial thrust orientation angle, ϵ_{o_i} , in the new coordinate system is the sum of the initial inertial flight path angle, β_i , and the initial inertial angle of attack, α_i , or

$$\epsilon_{o_i} = \beta_i - \alpha_i = \epsilon_i - \theta_i \quad (18)$$

where ϵ_i and θ_i are respectively the thrust orientation angle and range angle referenced to the launch vertical. The signs of the angles are as shown in Figure 72. In the new coordinate system, components of the initial inertial velocity, V_i , are

$$\left. \begin{aligned} \dot{x}_i &= V_i \sin \beta_i \\ \dot{y}_i &= V_i \cos \beta_i \end{aligned} \right\} \quad (19)$$

Values of β_i , V_i , α_i , θ_i and h_i are those parameters which are available from one of the following sources:

- 1) From the analysis of the first stage given in Section 2.2.3 and corresponding to parameters β_{BO_i} , V_{BO_i} , α_{BO_i} , θ_{BO_i} and h_{BO_i}
- 2) From the analysis at the end of a preceding coast phase
- 3) From an analysis of the immediately preceding portion of the powered flight trajectory by using the methods of this section. The corresponding parameters are β_f , V_f , α_f , θ_f , and h_f [see Equations (38) through (43), this section].

Parameters which must be specified from stage data are: 1) the vacuum specific impulse, $I_{sp_{vac}}$; 2) the initial thrust-to-weight ratio, T_{vac}/W_i ; and 3) the final weight ratio

$$P_f = \frac{W_{final}}{W_{initial}} = \frac{W_f}{W_i} \quad (20)$$

where at any time the weight ratio is defined by

$$p = W/W_i \quad (20a)$$

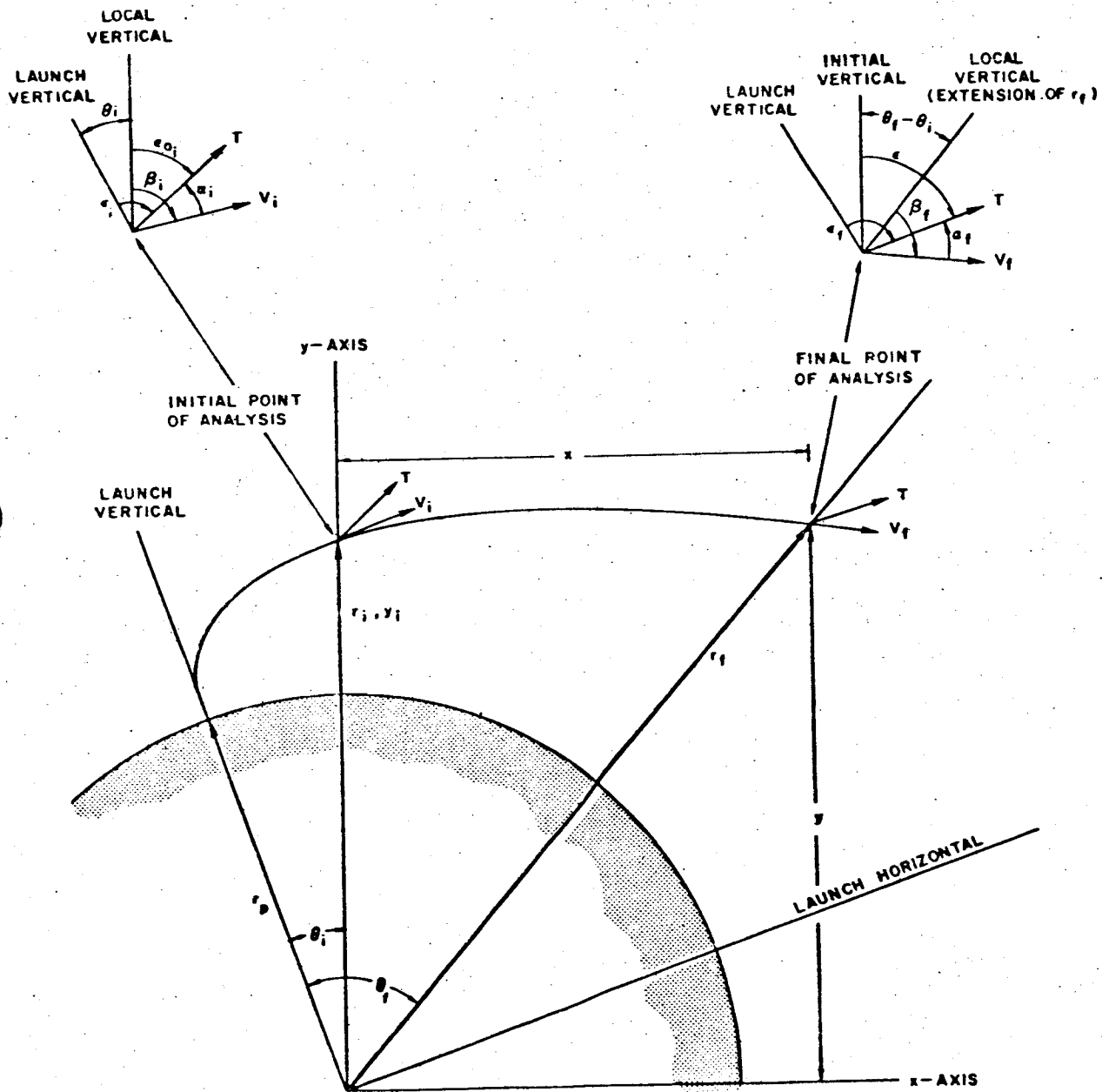


Figure 72. Powered Flight Coordinate System

When the subscripts $i = 0$ and $f = BO$, then $W_f/W_i = W_{BO}/W_0 = 1/r$ where $r =$ the mass ratio.

An initial estimate for the constant pitch rate, $\dot{\epsilon}$, must also be given. Generally, the optimal value of $\dot{\epsilon}$ required to achieve the desired final conditions will lie between $\dot{\epsilon} = 0$ and $\dot{\epsilon} = 0.2$ degree per second. For similar performance by the first stages of vehicles, upper stages with relatively high thrust-to-weight ratios tend to have optimal values of $\dot{\epsilon}$ in the upper part of the range, and values of $\dot{\epsilon}$ for those with relatively low thrust-to-weight ratios will be found in the lower part.

With the altitude at initiation, h_i , given, the value of the radial distance from the center of attraction at that time, r_i (i.e., y_i), can be determined. Then a value of the effective radius, r^* (see assumption 1), may be estimated by the relation

$$r^* = r_i + t_B \left[V_i + g_p \text{Isp}_{vac} \left(1 + \frac{P_f \ln P_f}{1 - P_f} \right) - \frac{g_p t_B}{2} \right] K^* \cos \beta_i \quad (21a)$$

where K^* is a constant for a given vehicle following a given trajectory. For typical vehicles and trajectories, approximate values of K^* have been found by use of the empirical relationship

$$K^* \approx \frac{(0.0163) \frac{T_{vac}}{W_i}}{P_f [1 - P_f (1 - \ln P_f)]} \quad (21b)$$

based on the assumption that the effective altitude for a period of powered flight motion is that altitude at which the average flight path angle is achieved. For classes of vehicles with widely varying physical characteristics which are flown along different trajectories, this empirical relationship will, of course, change somewhat. Generally, the degree of accuracy in r^* as found by this method is acceptable, since the final results of the performance evaluation are relatively insensitive to the small changes in r^* which are a consequence of approximating K^* .

After r^* is computed, the acceleration of gravity at this distance from the attracting body is found by

$$g^* = g_p \left(\frac{r_p}{r^*} \right)^2 \quad (22)$$

for an inverse square field.

2. Computation of Final Trajectory Parameters. The following definitions are now made.

- 1) The effective exhaust velocity is

$$c^* = g_e \text{Isp}_{vac} \quad (23)$$

where g_e is the acceleration due to gravity at the earth's surface.

- 2) The generalized initial thrust-to-weight ratio is

$$\eta = \left(\frac{T_{\text{vac}}}{W_i} \right) \left(\frac{g_e}{g^*} \right) \quad (24)$$

where T_{vac} is constant and W_i is the initial weight.

- 3) The thrust orientation in the new coordinate system is denoted by

$$\epsilon = \nu + \xi p \quad (25)$$

where

$$\left. \begin{aligned} \nu &= \epsilon_{0i} + \frac{c^* \xi}{\eta g^*} \\ \xi &= -\frac{c^* \xi}{\eta g^*} \end{aligned} \right\} \quad (26)$$

- 4) The constants ξ and χ are given by

$$\xi = \frac{(c^*)^2}{\eta g^*} = \frac{g_e I_{sp \text{ vac}}^2}{(T_{\text{vac}}/W_i)} \quad (27)$$

and

$$\chi = \frac{\xi}{c^*} \sqrt{\frac{g^*}{r^*}} = \frac{I_{sp \text{ vac}}}{(T_{\text{vac}}/W_i)} \sqrt{\frac{g^*}{r^*}} \quad (28)$$

for convenience and for the purpose of simplification.

Using these definitions and those given previously, the final rectangular components of position and velocity are given at the end of the trajectory phase by the following equations:

$$y = \frac{L}{\chi} \left[\text{Im}(Z) + \frac{\dot{y}_i}{c^*} \sin \chi (1 - p_f) \right] + r_i \cos \chi (1 - p_f) \quad (29)$$

$$x = \frac{L}{\chi} \left[\text{Im}(\omega) + \frac{k_i}{c^*} \sin \chi (1 - p_f) \right] \quad (30)$$

$$\dot{y} = -c^* \left[R(Z) + \frac{r_i \chi}{\xi} \sin \chi (1 - p_f) \right] + \dot{y}_i \cos \chi (1 - p_f) \quad (31)$$

$$\dot{x} = -c^* R(\omega) + k_i \cos \chi (1 - p_f) \quad (32)$$

where the following additional definitions hold:

$$\begin{cases} \text{Im}(Z) = A \sin \chi p_f - B \cos \chi p_f \\ R(Z) = A \cos \chi p_f + B \sin \chi p_f \end{cases} \quad (33)$$

$$\begin{cases} \text{Im}(\omega) = C \sin \chi p_f - D \cos \chi p_f \\ R(\omega) = C \cos \chi p_f + D \sin \chi p_f \end{cases} \quad (34)$$

and

$$\begin{aligned} A &= \frac{1}{2} (E \cos v - F \sin v) \\ B &= \frac{1}{2} (G \sin v + H \cos v) \\ C &= \frac{1}{2} (E \sin v + F \cos v) \\ D &= \frac{1}{2} (-G \cos v + H \sin v) \end{aligned} \quad (35)$$

$$\begin{aligned} E &= \left\{ \text{Ci} \left[(\xi + \chi) p_f \right] - \text{Ci} (\xi + \chi) \right\} + \left\{ \text{Ci} \left[(\xi - \chi) p_f \right] - \text{Ci} (\xi - \chi) \right\} \\ F &= \left\{ \text{Si} \left[(\xi + \chi) p_f \right] - \text{Si} (\xi + \chi) \right\} + \left\{ \text{Si} \left[(\xi - \chi) p_f \right] - \text{Si} (\xi - \chi) \right\} \\ G &= \left\{ \text{Ci} \left[(\xi + \chi) p_f \right] - \text{Ci} (\xi + \chi) \right\} - \left\{ \text{Ci} \left[(\xi - \chi) p_f \right] - \text{Ci} (\xi - \chi) \right\} \\ H &= \left\{ \text{Si} \left[(\xi + \chi) p_f \right] - \text{Si} (\xi + \chi) \right\} - \left\{ \text{Si} \left[(\xi - \chi) p_f \right] - \text{Si} (\xi - \chi) \right\} \end{aligned} \quad (36)$$

The functions in Equations (36) are the sine and cosine integrals^{9, 10, 11} which are defined symbolically as

$$\begin{aligned} \text{Si}(u) &= \int_0^u \frac{\sin \sigma}{\sigma} d\sigma \\ \text{Ci}(u) &= - \int_u^\infty \frac{\cos \sigma}{\sigma} d\sigma \end{aligned} \quad (37)$$

Upon finding x , y , \dot{x} , and \dot{y} the final values of altitude, h_f , velocity, V_f , and flight path angle, β_f , are determined by

$$h_f = \sqrt{x^2 + y^2} - y_i + h_i = r_f - r_p \quad (38)$$

$$V_f = \sqrt{\dot{x}^2 + \dot{y}^2} \quad (39)$$

$$\beta_f = \cos^{-1} \left(\frac{\dot{x}x + \dot{y}y}{\sqrt{(x^2 + y^2)(\dot{x}^2 + \dot{y}^2)}} \right) = \cos^{-1} \left(\frac{\dot{x}x + \dot{y}y}{V_f r_f} \right) \quad (40)$$

where $y_i = r_i$ at initiation and $r_i = r_p + h_i$.

The incremental value of range angle traversed by the vehicle during the burning phase under analysis is given by

$$(\theta_f - \theta_i) = \cos^{-1} (y/r_f) \quad (41)$$

and the true range angle referenced to the launch vertical is

$$\theta_f = \theta_i + \cos^{-1} (y/r_f) \quad (42)$$

where θ_i is the initial range angle.

Given the initial value, ϵ_{o_i} , for the thrust attitude referenced to the initial vertical, the final attitude, ϵ , with respect to the same reference is

$$\epsilon = \epsilon_{o_i} + \dot{\epsilon} t_B \quad (43)$$

and the thrust attitude referenced to the launch vertical is

$$\epsilon_f = \theta_i + \epsilon \quad (44)$$

The final angle of attack is given by

$$\alpha_f = \beta_f + \theta_f - \epsilon_f \quad (45)$$

with the angles having the algebraic signs indicated in Figure 72.

3. Velocity Loss Computation. The velocity losses for the portion of the trajectory under analysis are assumed to be almost wholly composed of losses due to gravity and angle of attack. Therefore, the losses can be found from the relation

$$\Delta V_{\text{loss}} = g_e \text{ Isp}_{\text{vac}} \ln \left(\frac{W_i}{W_f} \right) + V_i - V_f \quad (46)$$

4. Iteration on Pitch Rate. If the initial estimate of pitch rate, $\dot{\epsilon}$, used in calculating the performance is too low (in the positive sense), the following deviations from the desired mission requirements will result at termination: 1) the final altitude will be too high; 2) the final flight path angle will be too low; and 3) the final velocity will be too low.

If $\dot{\epsilon}$ is too high, the opposite effect upon these parameters will be observed. In either case, the observation of the effect of $\dot{\epsilon}$ upon these three quantities indicates the direction, and to some degree the magnitude, of the change which is required in $\dot{\epsilon}$ in order that the desired final conditions be achieved. If after adjustment of $\dot{\epsilon}$ in the indicated direction the results of the second calculation of parameters do not indicate that this new value is optimal, linear interpolation or short linear extrapolation can be used to closely approximate the optimal value of $\dot{\epsilon}$ to be used in the final iteration. While the relationship between $\dot{\epsilon}$ and the final trajectory parameters is almost linear for small changes in $\dot{\epsilon}$, it may be desirable to obtain a finer approximation for pitch rate; in this case final conditions for three different values of pitch rate can be computed to indicate precisely the value of $\dot{\epsilon}$ which will most nearly achieve the desired orbit conditions simultaneously. Typically, these variations in $\dot{\epsilon}$ will occur within the range mentioned previously, $0 \leq \dot{\epsilon} \leq 0.2$ (although it is possible for vehicles with widely varying characteristics of configuration and powered flight operation to require pitch rates outside this range in accomplishing certain missions).

When evaluating the performance of some vehicles, it is likely that a two-parameter iteration upon $\dot{\epsilon}$ and upon first-stage burnout flight path angle, $(\beta_{BOI})_1$, is required to achieve final conditions that match the required conditions for a given mission. This type of iteration procedure is a necessity for space vehicle launchings other than the low altitude orbit mission considered here as typical, since the analysis for the atmospheric portion of flight provides input conditions to the nonatmospheric analysis only for that case. (Obviously this does not apply to lunar launchings and similar powered flight maneuvers.)

Although the basic evaluation process is suited to manual computation, the solution of the equations for upper-stage performance evaluation given in this section could be greatly facilitated by the use of a small or medium-sized digital computer. Incorporation of any required iteration processes into the computer program would further simplify the application of the method and reduce the time required for an evaluation.

Upper-Stage Operation Out of Orbit. Having once attained a parking orbit, the performance of a stage injection out of this orbit to higher velocities may be calculated in two ways. The precise upper-stage analysis preceding this section can be used to obtain the complete set of final conditions, β_{BO} , V_{BO} , h_{BO} , and θ_{BO} . In the prescribed manner, the pitch rate may be varied to obtain the proper burnout angle, β_{BO} . This method is very accurate but also relatively time consuming.

It has been found that using impulsive velocity calculations to obtain the final velocity provides sufficient accuracy for many applications.

$$V_{BO} = V_{orbit} + g_e I_{sp} \ln r \quad (47)$$

where

$$r = \frac{W_O}{W_{BO}}$$

In particular, injection from an orbit to higher velocities with burnout angles of between 85 and 90 degrees can be simulated in this manner. Typical of this type of simulation is the injection for Hohmann transfer maneuvers. However, this method only gives the magnitude of the burnout velocity and the band in which the burnout angle is contained. The final altitude is assumed to be the same as the initial altitude, which is a relatively accurate assumption except for stages with long burning times. The increment in range angle during burning can be expressed as

$$\theta_{inj} = \frac{V_{orbit} t_B + g_e t_B I_{sp} \left(1 - \frac{\ln r}{r - 1}\right)}{r_e + h_{orbit}} \quad (48)$$

where

V_{orbit} = orbit velocity at ignition

h_{orbit} = orbit altitude at ignition.

If more exact values of the final parameters are required, the first or precise method must be used. When upper stages with long burning times ($t_B > 150$ sec) are used in the injection phase, the impulsive calculation should include a velocity loss of approximately 150 feet per second to account for losses during the injection phase. For missions requiring burnout angles less than 85 degrees, the losses during injection increase for burnout flight path angles of decreasing magnitude and the precise method must be used to maintain a desirable degree of accuracy.

Coasting. In general, there are two reasons for coasting between phases of powered flight. First, a short delay may be necessary to allow reorientation of the vehicle for guidance purposes, completion of the upper-stage ignition cycle, or performance of other similar activities during and after staging. Second, a period of coasting (of varying duration) may be required for achievement of a given mission.

The equations for the evaluation of the performance parameters during a short coast phase (less than 60 seconds) are presented in this section, assuming parabolic motion with constant acceleration. For long periods of coasting, the Keplerian equations of motion along conic sections are presented. The Keplerian equations are valid for the short coast phase also, but the assumption of parabolic flight gives a simple solution with little loss in accuracy over the short time involved.

Performance Evaluation for a Midcourse Correction. The evaluation of performance for a midcourse correction during the coast phase of a lunar or interplanetary trajectory can be calculated assuming ideal conditions; that is, no velocity losses are encountered during the midcourse burning phase. The increment in velocity added during the midcourse correction is given by

$$\Delta V = g_e I_{sp_{vac}} \ln r \quad (49)$$

In most cases, the midcourse velocity increment will be added at some angle with respect to the inertial velocity vector. This changes not only the magnitude of the velocity but also its direction. Thus the increment in velocity must be vectorially added to the inertial velocity vector to determine the total change due to the midcourse correction. A detailed description of the effects of midcourse correction can be found in the companion volume¹ to this handbook.

1. Short Coast Phase. Where the period of coasting is relatively short (less than 60 seconds), the changes in trajectory parameters can be approximated by assuming that the vehicle moves along a parabolic arc, with constant acceleration due to gravity. With the conditions at start of coast given as V_1 , h_1 , β_1 , θ_1 , α_1 , and t_1 , and with the time of coasting, t_c , specified, the velocity at the end of the coast period is

$$V_2 = \sqrt{V_1^2 - 2g_p t_c V_1 \cos \beta_1 + g_p^2 t_c^2} \quad (49)$$

The expression for altitude is

$$h_2 = h_1 + t_c V_1 \cos \beta_1 - \frac{1}{2} g_p t_c^2 \quad (50)$$

The corresponding value of flight path angle is given by

$$\beta_2 = \tan^{-1} \left(\frac{V_1 \sin \beta_1}{V_1 \cos \beta_1 - g_p t_c} \right) \quad (51)$$

where $r_1 = h_1 + r_p$, and r_p is the radius of the attracting planet. (For earth the subscript p will be replaced by e.)

The range angle at the end of coasting in degrees is

$$\theta_2 = \theta_1 + \left(\frac{180}{\pi} \right) \frac{t_c V_1 \sin \beta_1}{r_1} \quad (52)$$

The vehicle angle of attack at the end of coasting, assuming a pitch rate, $\dot{\epsilon}_c$, during coast, is

$$\alpha_2 = \alpha_1 + (\beta_2 - \beta_1) + (\theta_2 - \theta_1) - \dot{\epsilon}_c t_c \quad (53)$$

where β_2 and θ_2 are obtained from Equations (51) and (52) respectively.

If the vehicle thrust axis pitches at the same rate as the velocity vector, the angle of attack will remain constant during coast. The vehicle attitude at the end of coast, with respect to the launch vertical, is

$$\epsilon_2 = \beta_2 + \theta_2 - \alpha_2 \quad (54)$$

2. Long Coast Phase. Whenever there is to be a relatively long (greater than 60 seconds) period of coasting between two phases of powered flight, the trajectory elements at the end of coasting can be approximated on the basis of an assumption that the vehicle moves along a Keplerian ellipse. To determine the other parameters at the end of the coast period, it is necessary that the elements of the burnout point be given, together with either 1) a value of coasting time, or 2) the change in altitude during coasting.

a. Change in Altitude Specified. With $V_1, h_1, \beta_1, t_1, \theta_1, \alpha_1$, and the difference in altitude, $h_2 - h_1$, given, it is required to find the values of V_2, β_2, t_2 , and θ_2 , where the subscripts 1 and 2 refer to the start and end of the coast phase, respectively. With the radius, r_p , of the attracting body known, h_1 and $h_2 - h_1$ give the values of the initial and final radii, r_1 and r_2 .

The length, a , of the semimajor axis of the conic is expressed as

$$a = \frac{r_1 \mu_p}{z \mu_p - v_1^2 r_1} \quad (55)$$

where μ_p is the gravitational constant for the attracting body. The eccentricity is then calculated by solving the equation

$$e = \sqrt{1 - \frac{v_1^2 r_1^2 \sin^2 \beta_1}{a \mu_p}} \quad (56)$$

The values of the eccentric anomaly at the beginning and end of the coast phase can be found from

$$E_1 = \cos^{-1} \left(\frac{a - r_1}{ae} \right) \quad (57)$$

and

$$E_2 = \cos^{-1} \left(\frac{a - r_2}{ae} \right) \quad (58)$$

The time at the end of coasting can now be computed from the equation

$$t_2 = t_1 + \sqrt{\frac{a^3}{\mu_p}} (M_2 - M_1) \quad (59)$$

where the mean anomaly, M_i , is defined as

$$M_i = E_i - e \sin E_i \quad (60)$$

The final time is

$$t_2 = t_1 + \sqrt{\frac{a^3}{\mu_p}} [(E_2 - E_1) + e (\sin E_1 - \sin E_2)] \quad (61)$$

By solving for the length of the semimajor axis at each end of the coast phase and equating the results, the velocity at the end of coasting is found to be

$$v_2 = \sqrt{v_1^2 + 2\mu_p \left(\frac{1}{r_2} - \frac{1}{r_1} \right)} \quad (62)$$

The velocity loss during coasting can be expressed in terms of the given parameters by

$$(V_1 - V_2) = V_1 - \sqrt{V_1^2 + 2\mu_p \left(\frac{1}{r_2} - \frac{1}{r_1} \right)} \quad (63)$$

Since angular momentum is conserved,

$$V_1 r_1 \sin \beta_1 = V_2 r_2 \sin \beta_2$$

and the flight path angle at the end of coasting is

$$\beta_2 = \sin^{-1} \left(\frac{V_1 r_1 \sin \beta_1}{V_2 r_2} \right) \quad (64)$$

The true anomaly at any point on the elliptical path can be expressed in terms of eccentric anomaly as

$$u = \cos^{-1} \left(\frac{\cos E - e}{1 - e \cos E} \right) \quad (65)$$

The change in range angle, $\theta_2 - \theta_1$, during coasting is the same as the change in true anomaly, $u_2 - u_1$, and this quantity can be written as

$$(\theta_2 - \theta_1) = \cos^{-1} \left(\frac{\cos E_2 - e}{1 - e \cos E_2} \right) - \cos^{-1} \left(\frac{\cos E_1 - e}{1 - e \cos E_1} \right)$$

Therefore, the range angle at the end of coasting is

$$\theta_2 = \theta_1 + \cos^{-1} \left(\frac{\cos E_2 - e}{1 - e \cos E_2} \right) - \cos^{-1} \left(\frac{\cos E_1 - e}{1 - e \cos E_1} \right) \quad (66)$$

The vehicle angle of attack at the end of coasting, assuming a pitch rate, $\dot{\epsilon}_c$, during the coast, is

$$\alpha_2 = \alpha_1 + (\beta_2 - \beta_1) + (\theta_2 - \theta_1) - \dot{\epsilon}_c t_c \quad (67)$$

where β_2 and θ_2 are obtained from Equations (64) and (66), respectively. Here again, the angle of attack will remain constant if the vehicle thrust axis pitches at the same rate as the velocity vector. The vehicle attitude at the end of coast, with respect to the launch vector, is

$$\dot{\epsilon}_2 = \beta_2 + \theta_2 - \alpha_2 \quad (68)$$

b. Coasting Time Specified. With V_1 , h_1 , β_1 , t_1 , θ_1 , and the coasting time, $t_2 - t_1$, given, it is required to find the values of V_2 , β_2 , θ_2 , and h_2 . Again h_1 implies knowledge of r_1 . The semimajor axis, a , and eccentricity of the orbit, e , can be found by use of Equations (55) and (56). At the beginning of coasting the eccentric anomaly, E_1 , is computed from Equation (57) and the mean anomaly from

$$M_1 = E_1 - e \sin E_1 \quad (69)$$

An expression for the mean anomaly at the end of coasting is found from Equation (59) to be

$$M_2 = M_1 + (t_2 - t_1) \sqrt{\frac{\mu_p}{a^3}} \quad (70)$$

which can be computed directly. In order to find the eccentric anomaly, E_2 , at the end of coasting, it is necessary to solve the equation

$$M_2 = E_2 - e \sin E_2 \quad (71)$$

for E_2 . The equation is transcendental and an iterative procedure is required for its solution. Applying the Newton-Raphson method, the value of E_2 can be determined by using the root extraction formula

$$(E_2)_{i+1} = (E_2)_i - \frac{f(E_2)_i}{f'(E_2)_i}$$

with $(E_2)_i$ the initial estimate of E_2 and

$$f(E_2) = 0 = E_2 - e \sin E_2 - M_2$$

$$f'(E_2) = 1 - e \cos E_2$$

Thus, E_2 may be found to the desired degree of accuracy by successive use of the equation

$$(E_2)_{i+1} = (E_2)_i - \frac{[(E_2)_i - e \sin (E_2)_i - M_2]}{1 - e \cos (E_2)_i} \quad (72)$$

where the value of M_2 is that found from Equation (70).

Using the value of E_2 found in this manner, the radial distance from the attracting body at the end of coasting is

$$r_2 = a(1 - e \cos E_2) \quad (73)$$

and the altitude is $h_2 = r_2 - r_p$. The velocity is

$$V_2 = \sqrt{V_1^2 + 2\mu_p \left(\frac{1}{r_2} - \frac{1}{r_1} \right)} \quad (74)$$

and the velocity is simply $V_1 - V_2$, as given by Equation (63). At the end of coasting the flight path angle, β_2 , and the range angle, θ_2 , are found by use of Equations (64) and (66), respectively. The final angle of attack, α_2 , and vehicle attitude, ϵ_2 , are found by the use of Equations (67) and (68), respectively.

Example of Performance Estimation. In order to relate the methods for performance estimation given previously in this chapter, an example two-stage, liquid propellant vehicle is analyzed in the following section for a 100 nautical mile circular earth orbit mission. The analysis follows the basic steps shown on page 2-65 for the precise performance evaluation.

1. Vehicle Parameters

a. First Stage

$$\frac{T}{W_O} = 1.30, \quad I_{sp_{vac}} = 295 \text{ sec}, \quad \frac{I_{sp_{sl}}}{I_{sp_{vac}}} = 0.881$$

$$W_O = 2,309,000 \text{ lb}, \quad \frac{W_O}{W_{BO}} = r = 3.06, \quad t_B = 133.6 \text{ sec.}$$

The drag coefficient as a function of Mach number is shown in Figure 73 for a reference area, A , of 452 square feet.

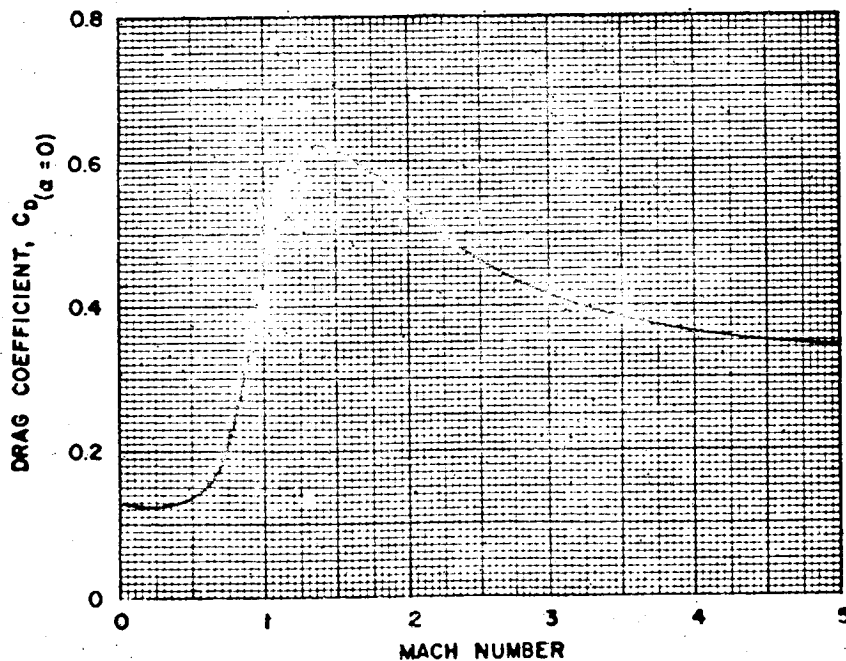


Figure 73. Drag Curve

b. Second Stage

$$\frac{T_{vac}}{W_O} = 0.9205, \text{ } Isp_{vac} = 425 \text{ sec}, \frac{W_O}{W_{BO}} = r = 4.136$$

$$t_B = 350.07 \text{ sec.}$$

The launch is assumed to take place at the Atlantic Missile Range with a launch azimuth of 110 degrees.

2. Determination of First-Stage β_{BO} Referring to Figure 51, the time of vertical rise is found to be 12.8 seconds for a $T/W_O = 1.3$. There is no adjustment required for the initial thrust-to-weight ratio because a liquid propellant vehicle has essentially constant thrust when flown at a constant altitude. Since a low orbit mission is of interest, the ratio of β_O/t_v may be determined from Figure 50. With the first-stage mass ratio of 3.06, the lower portion of the shaded area of Figure 50 is used to obtain $\beta_O/t_v = 0.052 \text{ deg/sec}$, which gives a $\beta_O = 0.67 \text{ degree}$ for $t_v = 12.8 \text{ seconds}$. The burnout angle obtained from Figure 52 for this β_O , with the first stage Isp_{vac} and T/W_O , is 60 degrees.

3. Determination of First Stage Burnout Velocity.

a. Gravity Loss. The first stage gravity loss is found by solving Equation (10).

$$\Delta V_{L_g} = (g_e t_B - K_{gg}) \left[1 - K_g \left(1 - \frac{1}{r} \right) \left(\frac{\beta_{BO}}{90} \right)^2 \right]$$

where K_g and K_{gg} are determined from the data on Figures 63 and 62 respectively. K_{gg} is just a function of Isp_{vac} and found to be 20 feet per second. K_g , as determined from Figure 63, represents a mass ratio of 2.5, and therefore a correction factor obtained from Figure 65 must be used to obtain the proper value for a mass ratio of 3.06.

$$K_{g(3.06)} = (\text{correction factor}) K_{g(2.5)}$$

$$= (0.97)(0.61)$$

$$= (0.59)$$

Therefore, solving Equation (10) with the above values of K_g , K_{gg} , vehicle parameters, and calculated $\beta_{BO} = 60$ degrees gives

$$\Delta V_{L_g} = 3520 \text{ feet per second.}$$

b. Drag Loss. The drag loss as defined by Equation (11),

$$\Delta V_{L_D} = K_D \frac{C_{D_{PD}} A}{W_O}$$

requires the knowledge of the drag coefficient at maximum drag force, $C_{D_{PD}}$, during the trajectory. This is determined by first finding the Mach number at maximum drag, M_{PD} , from Figure 66. M_{PD} depends on β_{BO} and the ratio $\sqrt{I_{sp_{vac}}/(T/W_O)}$.

For

$$\frac{\sqrt{I_{sp_{vac}}}}{\frac{T}{W_O}} = 13.22 \text{ and } \beta_{BO} = 60 \text{ degrees, } M_{PD} = 1.38$$

Referring to the enclosed C_D versus M variation (Figure 73), it is seen that the $C_{D_{PD}} = 0.62$. Thus the drag loss is

$$\Delta V_{L_D} = K_D \frac{(0.62) 452}{W_O} = K_D (121.5 \times 10^{-6})$$

where $K_D = 1.44 \times 10^6$ as obtained from Figure 67. Performing the multiplication gives

$$\Delta V_{L_D} = 175 \text{ ft/sec.}$$

c. Thrust-Atmospheric Effects. The thrust-atmospheric effects are simply obtained from Figure 68 for a value of $I_{sp_{sl}} I_{sp_{vac}} = 0.881$. This result is

$$\Delta V_{L_T} = K_a = 330 \text{ ft/sec.}$$

The first-stage burnout velocity as defined by Equation (2) is

$$V_{BO} = V_I - \Delta V_L$$

where

$$V_I = g_e \text{Isp}_{\text{vac}} \frac{W_O}{W_{BO}}$$

and

$$\Delta V_L = \Delta V_{L_g} + \Delta V_{L_D} + \Delta V_{L_T}$$

For the stage being analyzed

$$V_I = g_e (295) \ln 3.06 = 10,610 \text{ ft/sec}$$

The relative burnout velocity is

$$V_{BO} = 10,610 - 3520 - 175 - 330 = 6,585 \text{ ft/sec}$$

for a relative burnout angle, β_{BO} , of 60.0 degrees.

4. Determination of First-Stage Burnout Altitude. The expression for h_{BO} as given by Equation (13) involves h^* , the burnout altitude for a nonatmospheric vertical ascent.

$$h^* = g_e \text{Isp}_{\text{vac}} t_B \left(1 - \frac{\ln \frac{W_O}{W_{BO}}}{\frac{W_O}{W_{BO}} - 1} \right) - \frac{g_e t_B^2}{2}$$

which gives a value of $h^* = 291,500$ feet for the first stage of interest. The expression for the first stage burnout altitude is

$$h_{BO} = \left[h^* - \frac{(\Delta V_{L_D} + \Delta V_{L_T}) t_B}{2} \right] \left[1 - \left(\frac{\beta_{BO}}{K_h} \right)^2 \right]$$

where the drag and thrust-atmospheric losses are 175 and 330 feet per second, respectively. K_h is the empirical constant obtained from Figure 69:

$$K_h = 2.0 \text{ radians.}$$

Evaluation of h_{BO} gives

$$h_{BO} = \left[291,500 - \frac{(505)(133.6)}{2} \right] \left[1 - \left[\frac{60}{(2)(57.3)} \right]^2 \right] = 187,000 \text{ feet.}$$

5. Determination of Range Angle and Vehicle Attitude at First-Stage Burnout.

It is of interest to determine the range angle from the launch site to first stage burnout, θ , in order to obtain the angular position of the vehicle centerline with respect to the launch vertical. This value can be determined from the nomograph of Figure 70 which gives $\theta = 0.5$ degrees. The expression in Section 3.4.2 gives the vehicle attitude with respect to the launch vertical to be

$$\epsilon_{BO} = \beta_{BO} + \theta_{BO} = 60.5 \text{ degrees.}$$

6. Determination of Earth's Rotational Effects. As previously pointed out, it is necessary to vectorially add the launch azimuth component of the launch site rotational velocity to the first-stage burnout conditions. For a 110-degree launch from AMR, the component of velocity, V_{rot} , is 1262 feet per second as determined from Figure 1 of Chapter 3. The inertial burnout velocity, V_{BO_I} , is shown by Equation (15) to be

$$V_{BO_I} = \sqrt{(V_{BO})^2 + (V_{rot})^2 + 2(V_{BO})(V_{rot}) \sin \beta_{BO}}$$

which gives $V_{BO_I} = 7703$ ft per second.

The inertial burnout angle, β_{BO_I} , is

$$\beta_{BO_I} = \cos^{-1} \left(\frac{\cos \beta_{BO}}{V_{BO_I}} V_{BO} \right)$$

which gives $\beta_{BO_I} = 64.7$ degrees.

Since the velocity vector has been rotated, the vehicle centerline has the following inertial angle of attack:

$$\alpha = \beta_{BO_I} - \beta_{BO} = 4.7 \text{ degrees}$$

which was shown by Equation (17).

No coast phase was assumed for this example so that the second-stage calculations follow directly.

7. Determination of Second-Stage Burnout Conditions. Assuming that the second stage trajectory is essentially nonatmospheric, the stage burnout conditions can be computed by the method described previously. The first-stage inertial burnout conditions required for computation of the final conditions at second-stage burnout are summarized in Table 3.

Table 3. Input Parameters from Results for Stage 1

First-Stage Burnout Parameters	Symbol		Numerical Value
	Stage 1	Stage 2	
Inertial Flight Path Angle (degrees)	β_{BO_I}	β_i	64.7
Inertial Velocity (ft/sec)	V_{BO_I}	V_i	7703
Inertial Angle of Attack (degrees)	α_{BO}	α_i	4.7
Altitude (feet)	h_{BO}	h_i	187,000
Range Angle (degrees)	θ_{BO}	θ_i	0.50

For the purpose of computation it is assumed that these values, as well as those of other input parameters, are exact, as the accuracy of results depends upon the maintenance of several significant digits throughout.

Input Parameters. By use of initial conditions in Table 3, the initial thrust orientation angle and initial components of velocity can be found. From Equation (18), the thrust orientation angle (referenced to the local vertical at the time of second stage ignition) is

$$\begin{aligned}
 \epsilon_{o_i} &= \beta_i - \alpha_i \\
 &= 64.7^\circ - 4.7^\circ \\
 &= 60.0^\circ
 \end{aligned}$$

The initial inertial velocity components are given by Equations (19):

$$\begin{aligned}
 \dot{x}_i &= V_i \sin \beta_i \\
 &= (7703 \text{ ft/sec}) \sin (64.7^\circ) \\
 &= 6964.2 \text{ ft/sec.}
 \end{aligned}$$

$$\begin{aligned}\dot{y}_i &= V_i \cos \beta_i \\ &= (7703 \text{ ft/sec}) \cos (64.7^\circ) \\ &= 3291.9 \text{ ft/sec.}\end{aligned}$$

The second stage characteristics given previously are

$$\begin{aligned}I_{sp_{vac}} &= 425 \text{ sec} \\ T_{vac}/W_i &= T_{vac}/W_O = 0.9205 \\ p_f &= W_f/W_i = W_{BO}/W_O = 0.2418 \\ t_B &= 350.07 \text{ sec.}\end{aligned}$$

Since the second stage thrust-to-weight ratio, T_{vac}/W_i , does not differ markedly from the norm for similar stages and conditions, it is assumed that the desired value of pitch rate, $\dot{\epsilon}$, lies near the middle of the range $0 \leq \dot{\epsilon} \leq 0.2$ degree/second. More explicitly, it is assumed that the constant pitch rate during second-stage burning is

$$\dot{\epsilon} = 0.10 \text{ deg/sec.}$$

The altitude at second stage ignition is $h_i = 187,000$ feet, and the radial distance from the center of the earth at that time is

$$r_i = r_e + h_i = 20,902,900 \text{ ft} + 187,000 \text{ ft} = 21,089,900 \text{ ft}$$

where r_e is the mean radius of the earth.

The effective radial distance during burning is estimated by Equation (21a):

$$r^* = r_i + t_B \left[V_i + g_e I_{sp_{vac}} \left(1 + \frac{p_f \ln p_f}{1 - p_f} \right) - \frac{g_e t_B}{2} \right] K^* \cos \beta_i$$

Through use of Equation (21b),

$$K^* \approx \frac{(0.0163) \frac{T_{vac}}{W_i}}{p_f [1 - p_f (1 - \ln p_f)]}$$

the approximate value of the constant K^* is found to be $K^* = 0.150$ and the gravitational acceleration at the earth's surface, g_e , is taken as 32.174 ft/sec^2 . Using the values of $t_B = 350.07 \text{ sec}$, $I_{sp_{vac}} = 425 \text{ sec}$, $p_f = 0.2418$, $\beta_i = 64.7 \text{ deg}$, $V_i = 7703 \text{ ft/sec}$, and $r_i = 21,089,900 \text{ ft}$ which were given or computed previously, the result is

$$r^* = 21,304,320 \text{ ft.}$$

The acceleration of gravity at a distance of r^* from the earth's center is given by Equation (22) as

$$\begin{aligned} g^* &= g_e \left(\frac{r_e}{r^*} \right)^2 \\ &= (32.174) \left(\frac{20,902,900}{21,304,320} \right)^2 \text{ ft/sec}^2 \\ &= 30.9730 \text{ ft/sec}^2. \end{aligned}$$

The effective exhaust velocity is given by Equation (23) as

$$c^* = g_e \text{Isp}_{\text{vac}} = (32.174) (425) \text{ ft/sec} = 13,674 \text{ ft/sec},$$

and the generalized thrust-to-weight ratio from Equation (24) is

$$\eta = \left(\frac{T_{\text{vac}}}{W_i} \right) \left(\frac{g_e}{g^*} \right) = (0.9205) \left(\frac{32.174}{30.9730} \right) = 0.95619$$

From Equation (25), the thrust orientation referenced to the initial local vertical is given by

$$\epsilon = \nu + \xi p$$

and the components ν and ξ are given by Equation (26) with $\dot{\epsilon} = 0.10$:

$$\nu = \epsilon_{o_i} + \frac{c^* \dot{\epsilon}}{\eta g^*} = (60.0 + 46.1707) \text{ degrees} = 1.85303 \text{ radians}$$

$$\xi = -\frac{c^* \dot{\epsilon}}{\eta g^*} = -0.80583 \text{ radian.}$$

The constants ζ and χ are determined, from Equations (27) and (28), to be

$$\zeta = \frac{(c^*)^2}{\eta g^*} = (6.31334) (10^6) \text{ ft}$$

$$\chi = \frac{\zeta}{c^*} \sqrt{\frac{g^*}{r^*}} = 0.55670 \text{ radian.}$$

It is now desired to find the quantities E, F, G, and H of Equations (36). The evaluation of the sine and cosine integrals involved can be made through use of existing books of tables. The most extensive tables of sine and cosine integrals are those published or sponsored by the National Bureau of Standards^{9, 10, 11} and these are utilized here. The function arguments and function values required in the equations are given in Table 4. In general, it is true that the symbolic relation

$$\text{Si}(-u) = -\text{Si}(u)$$

holds for negative arguments. For real values of the argument only, the following symbolic relationship also holds true:

$$Ci(-u) = Ci(u)$$

Table 4. Tabular Values of the Sine and Cosine Integrals

Function Argument u	Cosine Integral Ci(u)	Sine Integral Si(u)
$(\xi + \chi) = -0.24913$	-0.82805	-0.24827
$(\xi + \chi) p_f = -0.06024$	-2.23313	-0.06023
$(\xi - \chi) = -1.36253$	+0.45689	-1.22959
$(\xi - \chi) p_f = -0.32946$	-0.56011	-0.32748

Use of the results of Table 4 in Equation (36) gives

$$E = \left[Ci \left[(\xi + \chi) p_f \right] - Ci \left(\xi + \chi \right) \right] + \left[Ci \left[(\xi - \chi) p_f \right] - Ci \left(\xi - \chi \right) \right] = -2.42207$$

$$F = \left[Si \left[(\xi + \chi) p_f \right] - Si \left(\xi + \chi \right) \right] + \left[Si \left[(\xi - \chi) p_f \right] - Si \left(\xi - \chi \right) \right] = +1.09015$$

$$G = \left[Ci \left[(\xi + \chi) p_f \right] - Ci \left(\xi + \chi \right) \right] - \left[Ci \left[(\xi - \chi) p_f \right] - Ci \left(\xi - \chi \right) \right] = -0.38807$$

$$H = \left[Si \left[(\xi + \chi) p_f \right] - Si \left(\xi + \chi \right) \right] - \left[Si \left[(\xi - \chi) p_f \right] - Si \left(\xi - \chi \right) \right] = -0.71406$$

The quantities A, B, C, and D given by Equation (35) are now calculated, with $v = 1.85303$. The values are

$$A = 1/2 (E \cos v - F \sin v) = -0.18624$$

$$B = 1/2 (G \sin v + H \cos v) = -0.08693$$

$$C = 1/2 (E \sin v + F \cos v) = -1.31493$$

$$D = 1/2 (-G \cos v + H \sin v) = -0.39695$$

for $\cos v = -0.27850$ and $\sin v = +0.96044$. These values of A, B, C, and D are in turn used to calculate the quantities $Im(Z)$, $R(Z)$, $Im(\omega)$, and $R(\omega)$ from Equations (33) and (34). The value of χp_f is found to be 0.13461 and $\sin \chi p_f = 0.13420$, $\cos \chi p_f = 0.99095$.

$$Im(Z) = A \sin \chi p_f - B \cos \chi p_f = +0.06115$$

$$R(Z) = A \cos \chi p_f + B \sin \chi p_f = -0.19622$$

$$\text{Im}(\omega) = C \sin \chi p_f - D \cos \chi p_f = +0.21689$$

$$R(\omega) = C \cos \chi p_f + D \sin \chi p_f = 1.35630$$

The rectangular coordinates of the second stage burnout position are given by Equations (29) and (30). The angle $\chi(1 - p_f) = 0.42209$ and $\cos \chi(1 - p_f) = +0.91223$ and $\sin \chi(1 - p_f) = +0.40967$, where ℓ , χ , r_i , \dot{y}_i , \dot{x}_i and c^* have the values computed previously.

$$y = \frac{\ell}{\chi} \left[\text{Im}(Z) + \frac{\dot{y}_i}{c^*} \sin \chi(1 - p_f) \right] + r_i \cos \chi(1 - p_f) = 21,050,860 \text{ feet}$$

$$x = \frac{\ell}{\chi} \left[\text{Im}(\omega) + \frac{\dot{x}_i}{c^*} \sin \chi(1 - p_f) \right] = 4,825,780 \text{ feet.}$$

The velocity components at second stage burnout are presented in Equations (31) and (32). These results are

$$\dot{y} = -c^* \left[R(Z) + \frac{r_i \dot{x}}{\ell} \sin \chi(1 - p_f) \right] + \dot{y}_i \cos \chi(1 - p_f) = -4731 \text{ ft/sec}$$

$$\dot{x} = -c^* [R(\omega)] + \dot{x}_i \cos \chi(1 - p_f) = 25,345 \text{ ft/sec}$$

Using the computed values of x , y , \dot{x} , and \dot{y} , the values of the second stage burnout altitude, h_f , burnout velocity, V_f , and burnout flight path angle, β_f , are calculated from Equations (38), (39), and (40):

$$h_f = \sqrt{x^2 + y^2} - y_i + h_i = r_f - r_e = 21,596,910 \text{ feet} - 20,902,900 \text{ feet} = 694,010 \text{ feet}$$

$$V_f = \sqrt{\dot{x}^2 + \dot{y}^2} = 25,345 \text{ ft/sec}$$

$$\beta_f = \cos^{-1} \left(\frac{x\dot{x} + y\dot{y}}{\sqrt{(x^2 + y^2)(\dot{x}^2 + \dot{y}^2)}} \right) = \cos^{-1} (0.03756) = 87.85 \text{ degrees}$$

It is now possible to examine whether the assumed value of pitch rate, $\dot{\epsilon}$, can be changed in such a manner that the final conditions will more nearly approximate the parameters required for achievement of the desired orbit. The corresponding parameters for a 100 nautical mile circular earth orbit are approximately

$$h_c = 607,610 \text{ feet}$$

$$V_c = 25,581 \text{ ft/sec}$$

$$\beta_c = 90.00 \text{ degrees.}$$

By comparison, it is evident that the computed value of burnout altitude is too high, and the values for burnout velocity and flight path angle are too low.

Reference to the criteria given previously on page 2-101 leads to the conclusion that the initial value of $\dot{\epsilon} = 0.10$ deg/sec is too low. However, the parameters obtained through use of this value are sufficiently close to orbital conditions to establish that $\dot{\epsilon}$ is only slightly different from 0.10 deg/sec. Therefore, it is assumed that the difference in pitch rate is $\Delta\dot{\epsilon} = +0.01$ deg/sec and that the new value of pitch rate is $\dot{\epsilon} = 0.11$.

Upon recalculating the components of burnout position and velocity with the new value of $\dot{\epsilon} = 0.11$ and with the other input parameters unchanged, the following results are found:

$$y = 20,987,940 \text{ feet}$$

$$x = 4,835,850 \text{ feet}$$

$$\dot{y} = -5446 \text{ ft/sec}$$

$$\dot{x} = 24,930 \text{ ft/sec}$$

The new burnout elements calculated from these values are

$$h_f = 634,950 \text{ feet}$$

$$V_f = 25,517 \text{ ft/sec}$$

$$\beta_f = 89.35 \text{ degrees}$$

comparison of the new computed trajectory parameters to the desired conditions indicates, in the same manner as before, that the pitch rate is still too low. This fact is further illustrated by Figure 74.

The values of β_f , V_f , and h_f obtained by using the first two estimates of $\dot{\epsilon} = 0.10$ and $\dot{\epsilon} = 0.11$ can be used to find a final value of $\dot{\epsilon}$ which will most nearly satisfy the most critical condition or conditions. By linear extrapolation a value of $\dot{\epsilon}$ can be obtained for each of the three parameters which will result in achievement of that parameter within the error incurred by linear extrapolation. The inability to achieve all orbital conditions simultaneously is largely a result of input inaccuracies from the first-stage analysis, which could be rectified to some extent by iteration upon the flight path angle at first-stage burnout.

Determination of Vehicle Performance

2-119

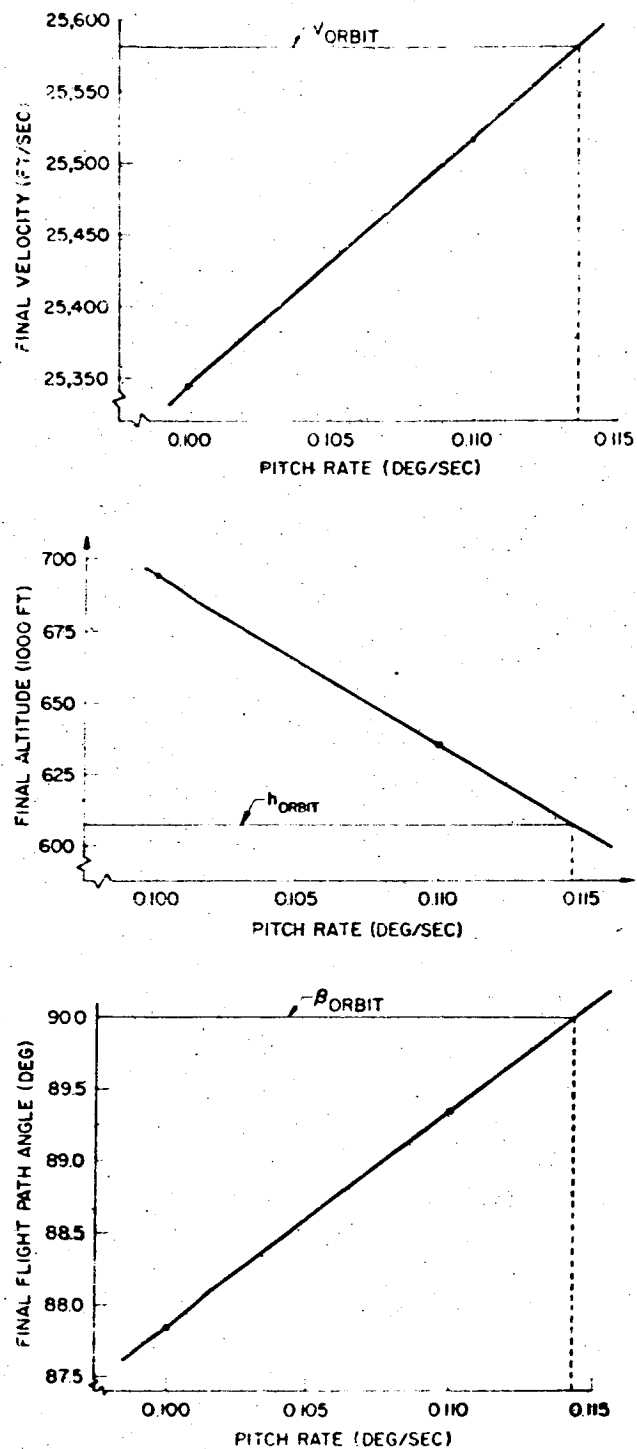


Figure 74 Effect of Pitch Rate Iteration

In order to provide an idea of the accuracy which can be obtained for this particular case without recourse to iteration upon the first-stage burnout angle, a value of pitch rate is chosen by linearly extrapolating to the value $\dot{\epsilon} = 0.1143$, which will give approximately the desired final value of flight path angle (the true relationship between flight path angle and pitch rate is almost linear). Also, this value is intermediate between the extremes of $\dot{\epsilon} = 0.1137$ (required to achieve the desired velocity) and $\dot{\epsilon} = 0.1146$ (required to achieve the desired altitude). The results obtained by the same computational procedure followed previously are:

$$\begin{aligned} y &= 20,960,700 \text{ ft} \\ x &= 4,839,700 \text{ ft} \\ \dot{y} &= -5755 \text{ ft/sec} \\ \dot{x} &= 24,934 \text{ ft/sec} \end{aligned}$$

which in turn are used to compute the final parameters. These are given in Table 5 together with a summary of the values of the burnout trajectory elements computed for the other values of pitch rate.

Table 5. Comparison of Computed Trajectory Parameters

Pitch rate, $\dot{\epsilon}$ (deg/sec)	Altitude, h_f (ft)	Velocity, V_f (ft/sec)	Flight Path Angle, β_f (deg)
0.10	694,010	25,345	87.85
0.11	634,950	25,517	89.35
0.1143	609,220	25,589	89.99
Burnout elements for 100 n mi circular orbit	607,610	25,581	90.00

From Equation (42), the true range angle is

$$\begin{aligned} \theta_f &= \theta_i + \cos^{-1} (y/r_f) = \theta_i + \cos^{-1} \left(\frac{y}{\sqrt{x^2 + y^2}} \right) \\ &= 0.50 + 13.05 \text{ degrees} = 13.55 \text{ degrees} \end{aligned}$$

for

$$\dot{\epsilon} = 0.1143$$

From Equation (43), the thrust orientation angle at second stage burnout is

$$\epsilon = \epsilon_0 + \dot{\epsilon} t_B = 60.0 \text{ degrees} + (0.1143 \text{ deg/sec})(350.07 \text{ sec}) = 100.01 \text{ degrees}$$

where ϵ is referenced to the local vertical at the time of second-stage ignition. The thrust attitude referenced to the launch vertical is given by Equation (44) as

$$\epsilon_f = \theta_i + \epsilon = 0.50 + 100.01 \text{ degrees} = 100.51 \text{ degrees}$$

The final angle of attack, given by Equation (45), is computed by

$$\alpha_f = \beta_f + \theta_f - \epsilon_f = 89.99 + 13.55 - 100.51 \text{ degrees} = 3.53 \text{ degrees}$$

Velocity losses for Stage 2 are given by the relationship of Equation (46):

$$\begin{aligned} \Delta V_L &= g_c \text{ Isp}_{\text{vac}} \ln \frac{W_O}{W_{BO}} + V_i - V_f = c^* \ln 1/p_f + V_i - V_f \\ &= (13,674 \text{ ft/sec}) (1.41964) + 7703 \text{ ft/sec} - 25,589 \text{ ft/sec} \\ &= 1526 \text{ ft/sec.} \end{aligned}$$

Comparison of Results. In order to indicate the validity of the approximate solution and also its accuracy, the trajectory for the example vehicle was simulated with a Two Dimensional Trajectory Program on an IBM 7090 digital computer. Table 6 presents the comparison of results.

Table 6. Comparison of Results

Parameter	Approximate Solution	Computer Simulation
<u>First Stage</u>		
V_{BO_I} (ft/sec)	7,703	7,705
β_{BO_I} (deg)	64.7	64.45
h_{BO} (ft)	187,000	179,410
θ_{BO} (deg)	0.50	0.52
<u>Second Stage</u>		
V_{BO_I} (ft/sec)	25,589	25,581
β_{BO_I} (deg)	89.99	90.00
h_{BO} (ft)	609,220	607,633
θ_{BO} (deg)	13.55	13.52
i (deg/sec)	0.1143	0.1180

Since the function of the method of analysis presently being demonstrated is primarily the computation of vehicle performance rather than simulation by the same method employed in the computer program (although simulation could be effected), it is not expected that the pitch rate for the demonstrative problem will be identical, but it should be comparable. Likewise, occurrence of events along the trajectory are not necessarily expected to coincide, and consequently slightly different results may be produced at intermediate points, as at first-stage burnout in this case. However, the performance results obtained at the final point should be similar.

The accuracy of the approximate solution is within the limits expected for closed form techniques. The largest sources of error are realized from the first-stage analysis and the effect of these deviations is noticeable at final burnout. In the example an iteration involving the first-stage burnout angle could have been performed to make possible the achievement of all final conditions almost simultaneously (with a slightly different pitch rate), but it is probably not necessary for most applications.

However, this type of iteration process will most certainly be necessary for missions where an estimate must be made for the first-stage burnout angle (i. e., for missions other than low altitude orbit missions for which the atmospheric portion of flight has been analyzed in this section).

NOMENCLATURE

A	Reference area for aerodynamic coefficients
a	Semimajor axis of conic section
C_d	Aerodynamic drag coefficient
$C_{D_{max}}$	Maximum drag coefficient
$C_{D_{PD}}$	Drag coefficient at peak drag
c^*	$g_e I_{sp}$ = Effective jet velocity
E	Eccentric anomaly
e	Orbital eccentricity
g^*	Acceleration due to gravity at the distance r^* from the center of attraction
g_e	Acceleration of gravity at earth's surface
g_p	Acceleration of gravity at planet's surface

h^*	Burnout altitude for nonatmospheric vertical ascent
h_a	Apogee altitude
h_{BO}	Altitude at burnout
h_f	Vehicle altitude at end of calculation
h_i	Vehicle altitude at initiation of calculation
h_p	Perigee altitude
$I_{sp_{sl}}$	Sea level specific impulse
$I_{sp_{vac}}$	Vacuum specific impulse
K^*	Upper-stage effective altitude constant
K_a	First-stage thrust - atmospheric loss constant
K_D	First-stage drag loss constant
K_g	First-stage gravity loss constant
K_{gg}	Change in first-stage losses due to altitude variation of gravity
K_h	First-stage burnout altitude constant
M	Mach number or mean anomaly
M_{PD}	Mach number at peak drag
p	Inverse mass ratio
p_f	Inverse mass ratio at the end of calculation
r	$\frac{W_O}{W_{BO}} = \text{Mass ratio}$
r^*	Effective radial distance from attracting body
r_e	Radius of earth
r_f	Radial distance of vehicle from center of attraction at the end of calculation
r_i	Radial distance of vehicle from center of attraction at initiation of calculation
r_p	Radius of planet
T	Transit time for Hohmann transfer or vehicle thrust
T_{vac}	Vacuum thrust
T/W_O	First-stage initial thrust-to-weight ratio

VEHICLE PERFORMANCE ESTIMATION TECHNIQUES

t_B	Stage burning time
t_c	Coast time
t_f	Time of flight
t_v	Vertical rise time
V_{BO}	Relative burnout velocity
V_{BO_I}	Inertial burnout velocity
V_f	Inertial velocity at the end of calculation
V_I	Ideal velocity
V_i	Vehicle velocity at initiation of calculation
V_{rot}	Component of velocity due to earth's rotation
W_{BO}	Burnout weight
W_f	Vehicle weight at the end of calculation
W_i	Vehicle weight at initiation of calculation
W_0	Initial weight
x_f	Horizontal component of vehicle position at the end of calculation
\dot{x}_f	Horizontal component of vehicle inertial velocity at the end of calculation
x_i	Horizontal component of vehicle position at initiation of calculation (equal to zero)
\dot{x}_i	Horizontal component of vehicle inertial velocity at initiation of calculation
y_f	Vertical component of vehicle position at the end of calculation
\dot{y}_f	Vertical component of vehicle inertial velocity at the end of calculation
y_i	Vertical component of vehicle position at initiation of calculation (equal to r_i)
\dot{y}_i	Vertical component of vehicle inertial velocity at initiation of calculation
α	Angle of attack
α_i	Angle of attack at initiation of calculation

Nomenclature

2-125

α_f	Angle of attack at the end of calculation
$\bar{\beta}$	Average flight path angle
β_{BO}	Relative flight path angle
β_{BO_1}	Inertial flight path angle
β_f	Inertial flight path angle at the end of calculation
β_i	Inertial flight path angle at initiation of calculation
β_o	Initial kick angle
ΔV_1	Initial incremental velocity for Hohmann transfer
ΔV_2	Final incremental velocity for Hohmann transfer
ΔV_L	Total velocity loss
ΔV_{L_D}	Velocity loss due to drag
ΔV_{L_g}	Velocity loss due to gravity
ΔV_{L_T}	Velocity loss due to thrust-atmospheric effects
ΔV_T	Total incremental velocity for Hohmann transfer
$\dot{\theta}$	Rate of change of thrust altitude with time: pitch rate
ζ	Defined by Equation (27)
η	$\left(\frac{T_{vac}}{W_i}\right)\left(\frac{g_e}{g^*}\right)$
θ_{BO}	Range angle at burnout
θ_f	Range angle at the end of calculation
θ_i	Range angle at initiation of calculation
μ_p	Gravitational-mass constant for a planet
ν	Defined by Equation (26)
ξ	Defined by Equation (26)
u	Defined by Equation (63)
x	Defined by Equation (28)

REFERENCES

1. Raymond W. Wolverton, ed., Flight Performance Handbook for Orbital Operations, Space Technology Laboratories, Inc., September, 1961. (Prepared for NASA under Contract No. NAS. 8-863).
2. A. B. Mickelwait, E. H. Tompkins, Jr., and R. A. Park, "Interplanetary Navigation," Scientific American, Vol. 203, No. 3, March 1960.
3. A. B. Mickelwait, E. H. Tompkins, Jr., and R. A. Park, "Three-Dimensional Interplanetary Trajectories," IRE Transactions on Military Electronics, Vol. MIL-3, No. 4, October 1959.
4. A. B. Mickelwait and R. C. Booton, Jr., "Analytical and Numerical Studies of Three-Dimensional Trajectories to the Moon," Journal of Aerospace Sciences, Vol. 27, No. 8, August 1960.
5. A. B. Mickelwait, "Lunar Trajectories," Space Technology Laboratories, Inc., STL/TR-59-0000-09898, 1959.
6. W. Hohmann, "The Attainability of Heavenly Bodies," ["Die Erreichbarkeit der Himmelskörper" R. Oldenbourg (Munich, Berlin) 1925] NASA Technical Translation, F-44, November 1960.
7. H. S. Tsien, "Take-Off from Satellite Orbit," Journal of the American Rocket Society, Vol. 23, No. 4, July - August 1953.
8. E. H. Tompkins, "Velocity Requirements for Mars and Venus Missions," Space Technology Laboratories, Inc., Interoffice Correspondence No. 9861.0-12, 9 June 1961.
9. "Table of Sine and Cosine Integrals for Arguments from 10-100." U.S. National Bureau of Standards Applied Mathematics Series 32. U.S. Government Printing Office, Washington, 1954.
10. "Sine, Cosine and Exponential Integrals, Vol. I- Arguments Between Zero and 2 at Intervals of 0.0001." A. N. Lowan, Technical Director. Works Progress Administration (under sponsorship of the National Bureau of Standards) New York, 1940. (Reprinted by Western Periodicals Co., North Hollywood, California, 1956).
11. "Sine, Cosine and Exponential Integrals, Vol. II- Arguments Between 2 and 10 at Intervals of 0.001." A. N. Lowan, Technical Director. Works Progress Administration (under sponsorship of the National Bureau of Standards) New York, 1940. (Reprinted by Western Periodicals Co., North Hollywood, California, 1956).
12. P. Dergarabedian and R. P. TenDyke, "Estimating the Performance Capabilities of Boost Rockets," Space Technology Laboratories, Inc., STL TR-59-0000-00792. 10 September 1959.

CHAPTER 3

SYSTEM CONSIDERATIONS

This chapter of the handbook considers some of the limiting features of space systems and deals with the constraints imposed because of them. Such constraints include launch location, range safety, maximum allowable acceleration, loads, heating, guidance, and performance dispersions. The material presented here is intended to aid the vehicle designer in evaluating various constraining parameters by providing data from which he can, knowing the boost vehicle characteristics, derive the value associated with a constraining parameter. However, no attempt is made to show design modifications or trajectory shaping techniques that will relieve the constraint. Usually at this point in a preliminary design, it is best to design the vehicle to the constraint rather than to shape the trajectory to relieve the constraint. Trajectory shaping should be used only to relieve constraints, such as maximum dynamic pressure or total heat input, when a specific vehicle is being used for a mission for which it was not designed.

3.1 LAUNCH SITE LIMITATIONS

Much work has been done at STL on launch site limitations imposed by geographical location. Of particular interest at STL have been both the "Equatorial Launch Site Study" and the "Astronautics Ship Study." Some of the material presented here has been adapted from unclassified portions of the "Equatorial Launch Site Study."

For preliminary design studies, launch site limitations affecting flight mechanics are functions of latitude, since longitude of launch site only affects the time of launch. Therefore, only the latitude of launch will be considered in this analysis. Also, it is of no concern whether the launch site is in the northern or southern hemisphere.

3.1.1 Earth's Rotation

The computation of vehicle performance should include the velocity vector component in the plane of a trajectory which is associated with the particular launch site location and the azimuth of the trajectory plane. A curve of this velocity component is presented as a function of its two dependent parameters in Figure 1. From the curve it is apparent that the velocity decrement resulting from launch at non-equatorial latitudes is only on the order of 200 ft/sec for the present launch sites.

When estimating a vehicle's payload capability, it is most convenient to assume the velocity component normal to the launch azimuth plane to be merely

3-2

SYSTEM CONSIDERATIONS

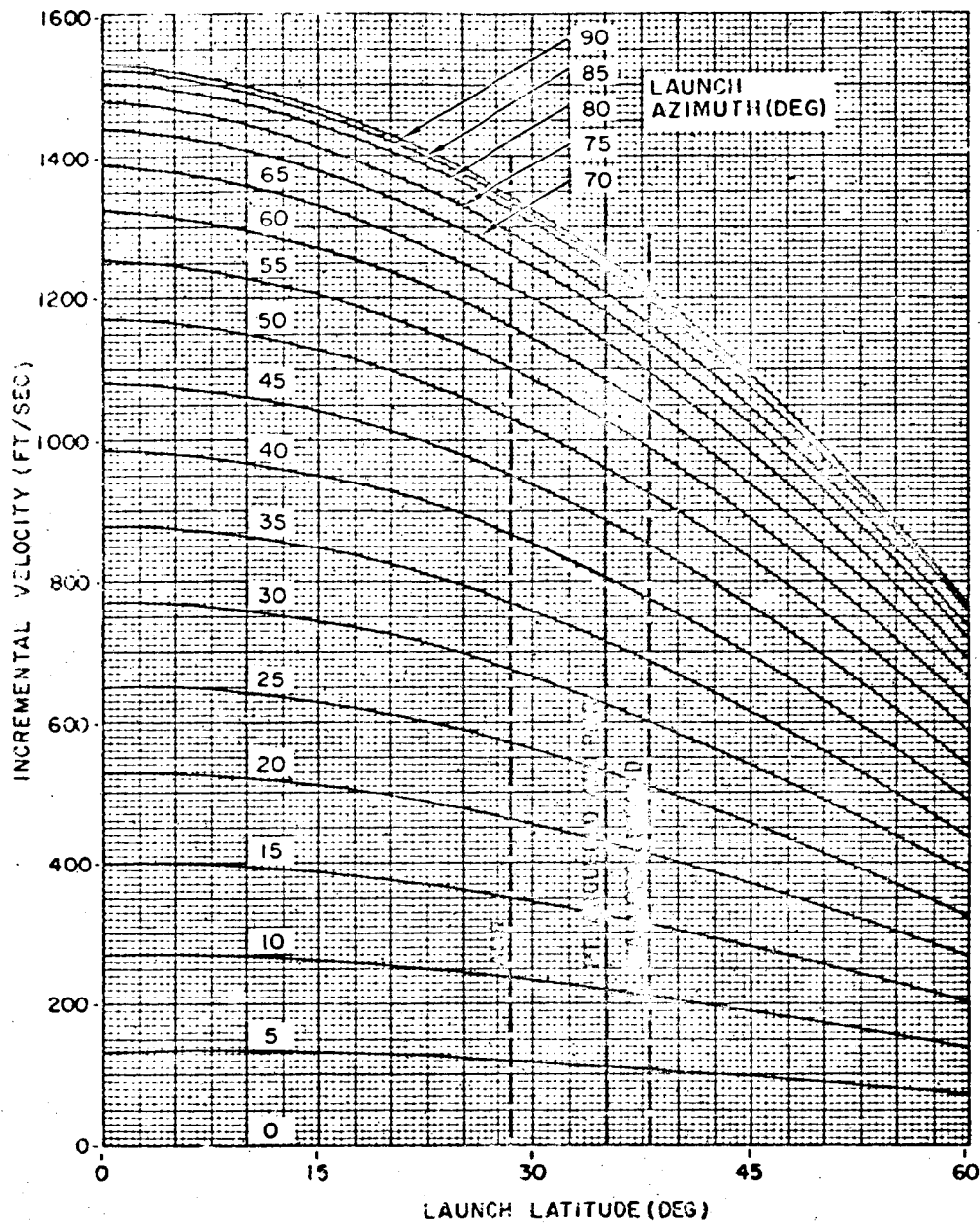


Figure 1. Earth's Rotation Velocity at Launch Site

an effective dog-leg of the trajectory plane. However, to more precisely determine the required launch azimuth, the launch azimuth angle should be perturbed an amount equivalent to the effective dog-leg angle resulting from the earth's rotational velocity component normal to the trajectory plane. This angle is

$$\delta_{dl_{eff}}, \Delta A_z = \frac{87,548 \cos \lambda \cos A_z}{V_{BO} \sin \beta_{BO}} \text{ degrees}$$

where

- A_z = launch azimuth angle
- V_{BO} = inertial burnout velocity in launch azimuth plane (ft/sec)
- β_{BO} = inertial burnout flight path angle in launch azimuth plane
- λ = geocentric latitude of launch site.

Here it is assumed that burnout occurs relatively near the launch location. For operation of upper stages subsequent to a coast period, the effective dog-leg due to the earth's rotation can be ignored because, for a vehicle out of the atmosphere, thrust would probably be directed along the inertial rather than the relative velocity vector.

The maximum effective dog-leg experienced for missions considered in this handbook would be an equatorially launched, low altitude orbit, equivalent to approximately 3.5 degrees.

3.1.2 Trajectory Inclination

The inclination of the trajectory of a space vehicle is a direct function of the launch azimuth and the latitude of launch site. This functional relationship is presented in Figure 2. It is assumed that burnout occurs directly above the launch site and this assumption has a minor effect on the accuracy of the results. From the curve it is evident that the minimum inclination of the trajectory is equal to the latitude of the launch site and requires a 90-degree launch azimuth. For a trajectory of less inclination, a dog-leg maneuver is required.

Orbital Missions. For an orbital mission having an orbit inclination greater than that of the latitude of the launch site, there is a particular azimuth that permits direct injection into a desired trajectory plane provided that the required azimuth does not violate range safety constraints. It is found that the required launch azimuth for a particular orbit inclination becomes more nearly aligned with the earth's tangential velocity with increasing launch latitude, which compensates for the decrease in the earth's tangential velocity resulting from the increase in launch latitude. Therefore, no particular advantage accrues from the use of a launch site location if the desired inclination is greater than the latitude of launch.

3-4

SYSTEM CONSIDERATIONS

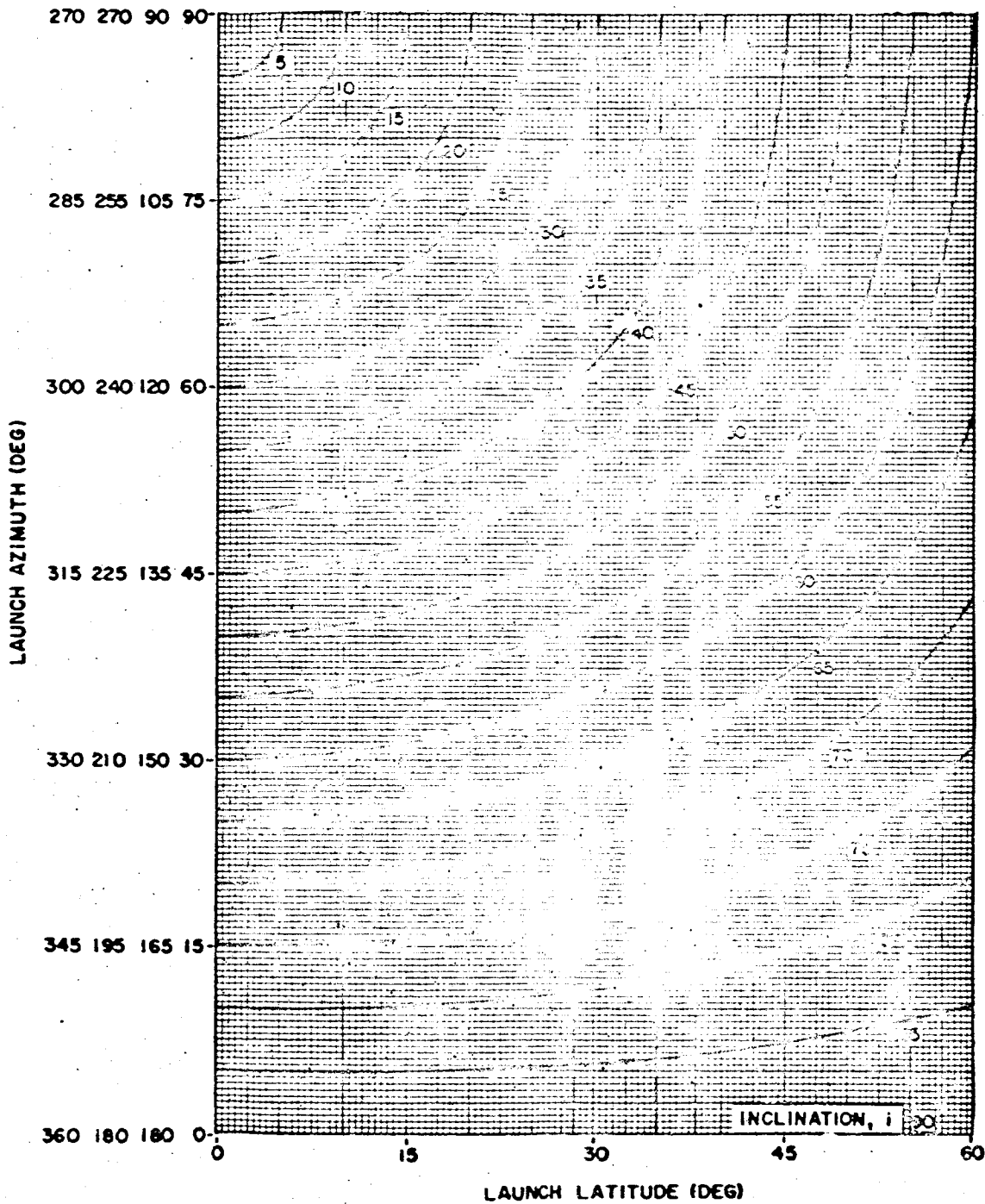


Figure 2. Trajectory Inclination

If the orbit inclination is arbitrary then the optimum launch azimuth is due east, which takes full advantage of earth's rotational effect. The penalty for nonequatorial launch for a due east firing is about 180 ft/sec and 280 ft/sec for AMR and PMR, respectively.

For equatorial orbits it is most desirable to launch due east (corresponding to minimum orbit-inclination) from a site as near to the equator as possible, initiate a Hohmann transfer at an equatorial crossing, and dog-leg at the apogee of the transfer orbit. The penalties for launch into an equatorial orbit from a site at 15 degrees latitude from AMR, and from a site of 45 degrees latitude (representative of sites available in Russia) are shown below on Table 1 for various orbital altitudes.

Table 1. Velocity Penalty for Equatorial Orbits (Ft/Sec)

Orbital Altitude (n mi)	15-Degree Latitude	28.5-Degree Latitude (AMR)	45-Degree Latitude
100	6,800	12,600	19,600
300	6,150	11,700	18,600
1,000	4,500	9,500	15,600
10,000	750	2,300	4,700
20,000	350	1,100	2,500

It is seen that the effect of having a nonequatorial launch site is less severe for the greater orbit altitudes. The table assumes Hohmann transfer dog-leg maneuver from a 100 nautical mile parking orbit executed at an equatorial crossing.

Lunar Missions. The moon travels in a nearly circular orbit with a radius of 207,000 nautical miles and with an inclination with respect to the ecliptic of approximately 5 degrees. This inclination corresponds to an equatorial inclination of 18.5 to 28.5 degrees, depending upon the position of the nodes of the lunar orbit and the ecliptic. From considerations of miss coefficients it is most advantageous to achieve coincidence between the earth-lunar trajectory plane and the lunar orbital plane. However, the rewards for doing this are small, so other considerations may dictate a transfer trajectory inclination resulting in noncoincidence of the two planes. From any launch site having a latitude of less than 18.5 degrees, a vehicle can be launched directly into the moon's orbital plane at two particular times during the day with launch azimuths between 71.5 and 108.5 degrees. At higher latitudes, firing at the proper time of day reduces the extent of the required orbital inclination dog-leg for planar coincidence by about 18.5 to 28.5 degrees. This is roughly

equivalent to an 18.5 to 28.5-degree reduction in the effective launch latitude. Launch from sites at latitudes higher than 18.5 degrees causes only minor performance degradation if noncoincident trajectory-lunar planes are used. Use of noncoincident planes also results in small increases in the error coefficients for the angles required.

Interplanetary Missions. Interplanetary trajectories are complicated by the fact that successively earth, sun, and destination planet, rather than a single mass, exert principal gravitational influence in various regions of the trajectory. Unfortunately, analytic solutions are unavailable for such problems, and it is difficult to provide the sort of broad discussion of the effect of launch latitude that is possible in the study of earth orbits.

A solution to the problem is approximated by dividing the trajectory into three phases and assuming only one effective center of attraction (earth, sun, and destination planet) in the successive phases, but also including the perturbing effects of the other planets during each phase. The relative positions of the earth and destination planet determine the hyperbolic escape velocity vector relative to the earth. For a destination that lies exactly in the ecliptic (earth's orbit) plane, this vector would also lie in the ecliptic plane, that is, at an equatorial inclination between latitude $23^{\circ}27'N$ and latitude $23^{\circ}27'S$, depending on the time of year.

However, for a destination only slightly out of the ecliptic,* the required vehicle velocity vector may be very far out of the ecliptic due to the much stronger influence of the earth's orbital velocity. Thus, it cannot even be said that the required inclination with respect to the earth of the vehicle's trajectory is most likely to lie near the ecliptic, much less near the equator. To somewhat alleviate the problems imposed by the latitude of the launch site, the parking orbit can be used. Therefore, there is little or no advantage to any particular launch latitude (especially the equator) for general interplanetary trajectories. Furthermore, the penalty for nonoptimum latitude appears to be only on the order of the difference between the earth's rotational velocity at the launch site and optimum launch latitude, which is barely significant for launch latitudes of less than 45 degrees. For a more detailed explanation of the required trajectory inclinations for interplanetary trajectories, the reader is directed to References 2 and 3.

Dog-Leg Maneuver. Due to both range safety constraints and launch site locations, it is often necessary to dog-leg in order for the trajectory to have the resulting desired inclination. Dog-legging refers to adding a velocity increment which has a component normal to the trajectory plane. Consequently the effect will be to rotate the plane. For flight path angles near 90 degrees, the dog-leg angle

* Ecliptic inclination of major planetary objectives: Mercury 7.0° , Venus 3.4° , and Mars 1.8° .

and the resulting planar rotation are approximately equal. It is found to be most advantageous to initiate the dog-leg at the lowest velocity along the trajectory which corresponds to apogee of the transfer orbit and at the equatorial crossing. For this analysis it is assumed that the vehicle is parked at 100 nautical miles altitude and coasts to the equator. At the equator the vehicle impulsively injects into a Hohmann transfer orbit. At the apogee of the Hohmann transfer orbit, which also occurs at the equatorial crossing, the satellite is injected by dog-legging the desired amount and circularizing the orbit simultaneously. (See Figure 3 below.)

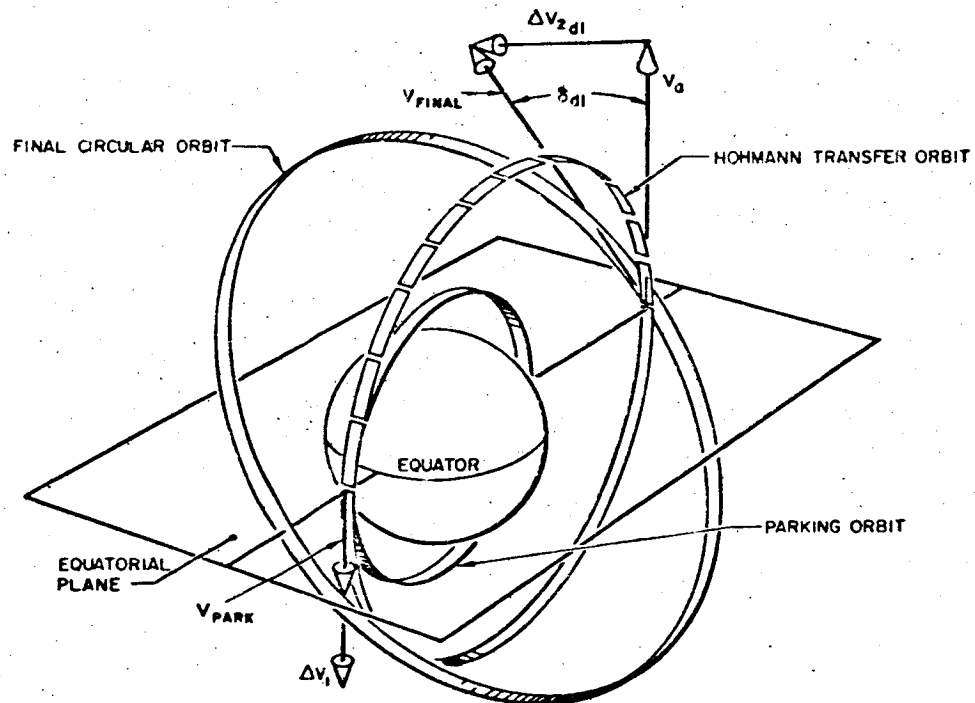


Figure 3. Hohmann Transfer Dog-Leg Maneuver

The required velocity to inject into the transfer orbit, ΔV_1 , as a function of the final orbit altitude is presented in Chapter 2, Figures 17 through 21. The velocity increment, ΔV_{2d1} , to accomplish the dog-leg and circularize the orbit as a function of the desired incremental dog-leg angular change is presented in Figures 4 through 14. The sum of the two velocities, ΔV_1 and ΔV_{2d1} , ΔV_{Tdl} , is also presented as a function of final orbit altitude and desired change in inclination angle in Figures 15 through 22. It should be pointed out that the dog-leg angle and the change in orbital inclination are equivalent for dog-legging at the equatorial crossing. The solution here represents the idealized minimum velocity decrement for dog-legging a circular

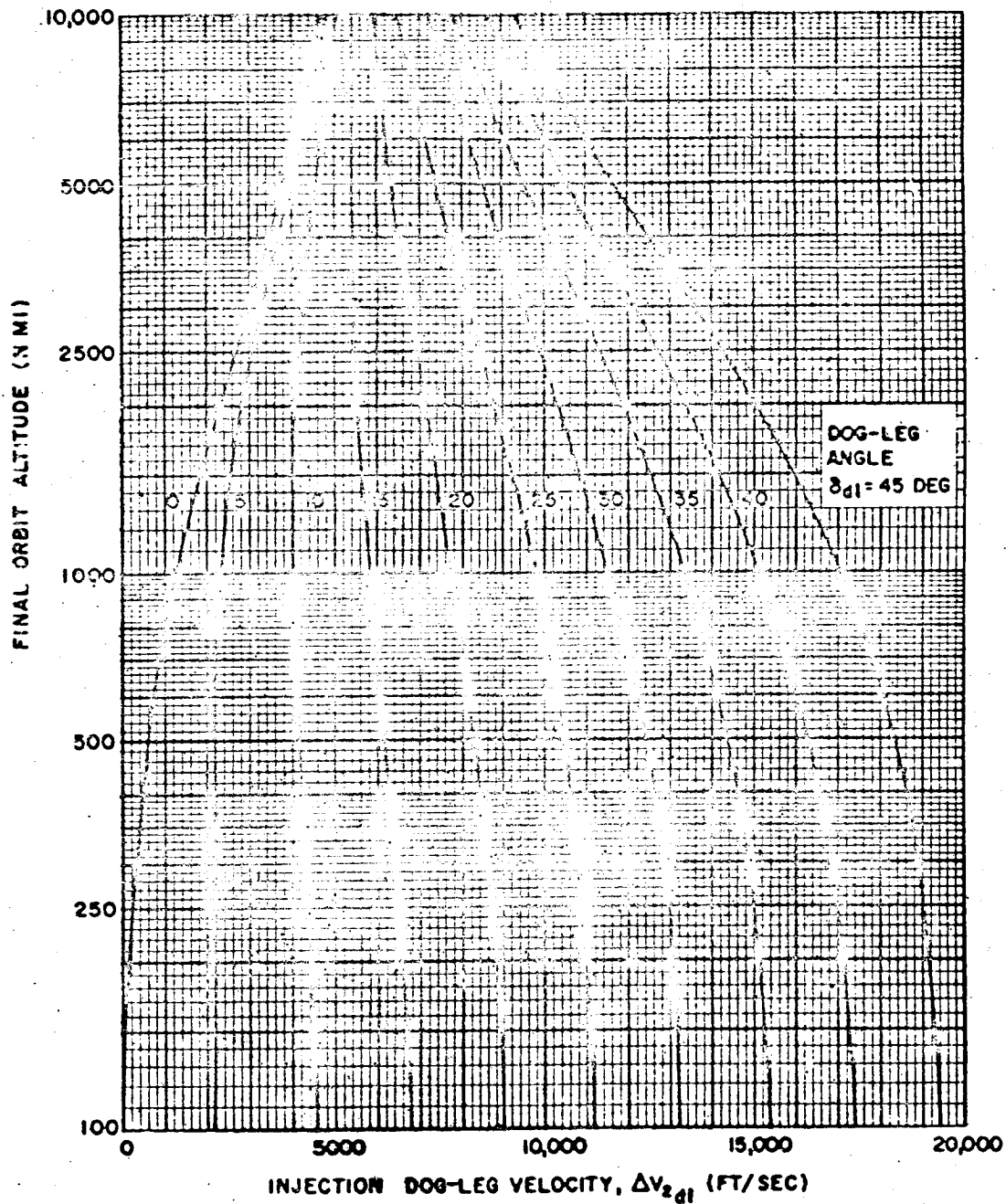


Figure 4. Final Hohmann Transfer Dog-Leg Injection Velocity Requirements (Parking Orbit Altitude = 100 n mi)

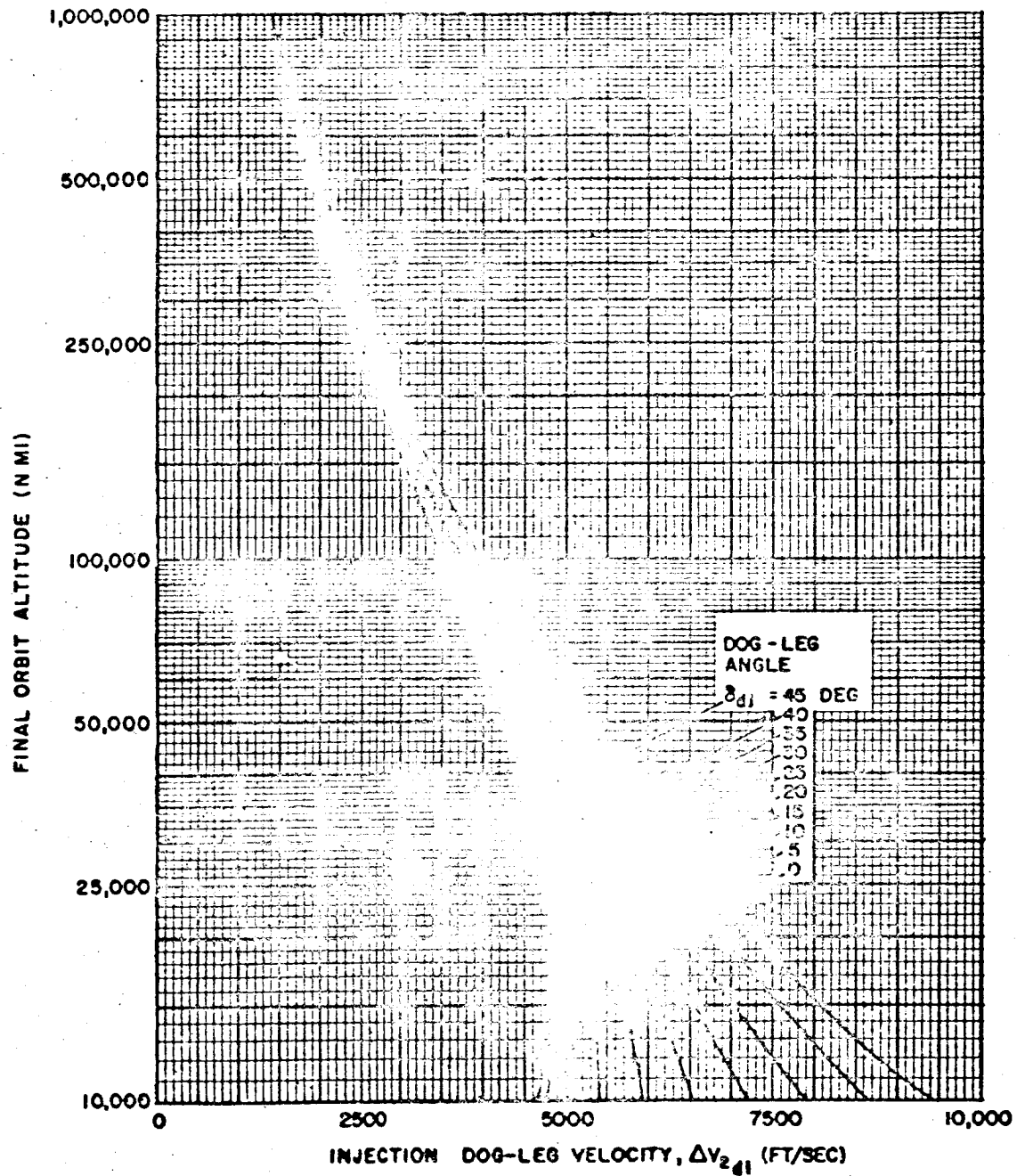


Figure 5. Final Hohmann Transfer Dog-Leg Injection Velocity Requirements
(Parking Orbit Altitude = 100 n mi)

SYSTEM CONSIDERATIONS

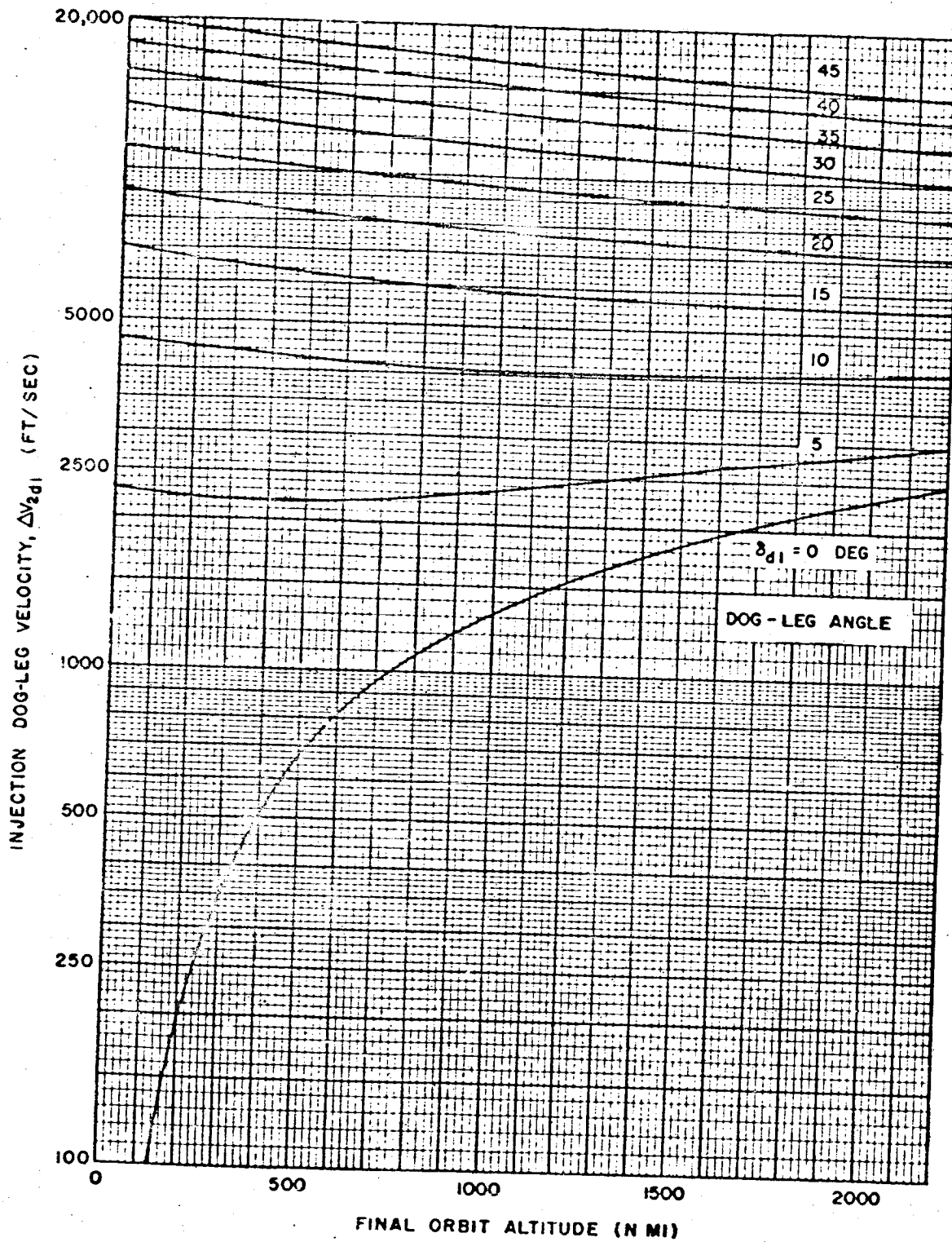


Figure 6. Final Hohmann Transfer Dog-Leg Injection Velocity Requirements
(Parking Orbit Altitude = 100 n mi)

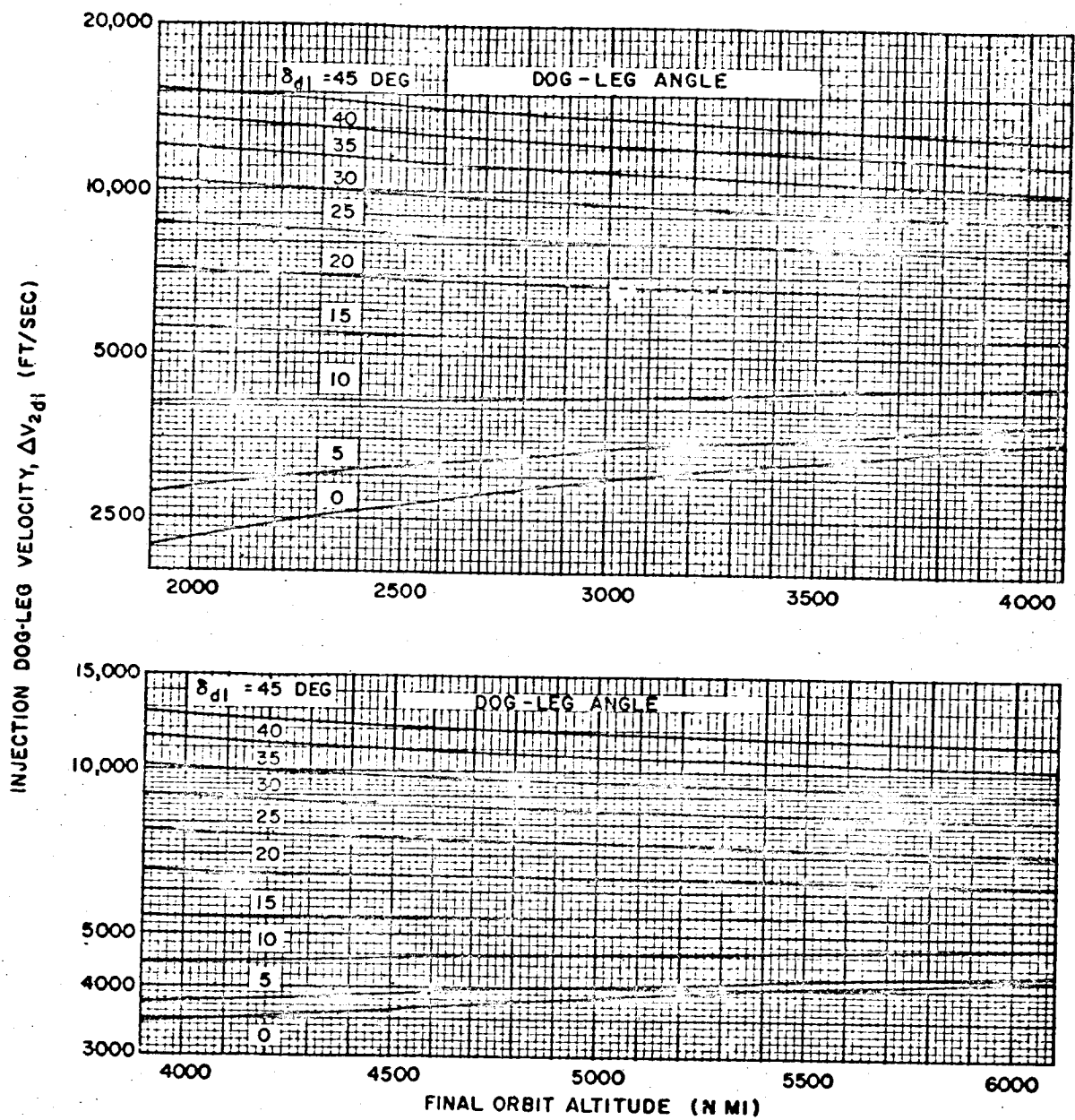


Figure 7. Final Hohmann Transfer Dog-Leg Injection Velocity Requirements
(Parking Orbit Altitude = 100 n mi)

3-12

SYSTEM CONSIDERATIONS

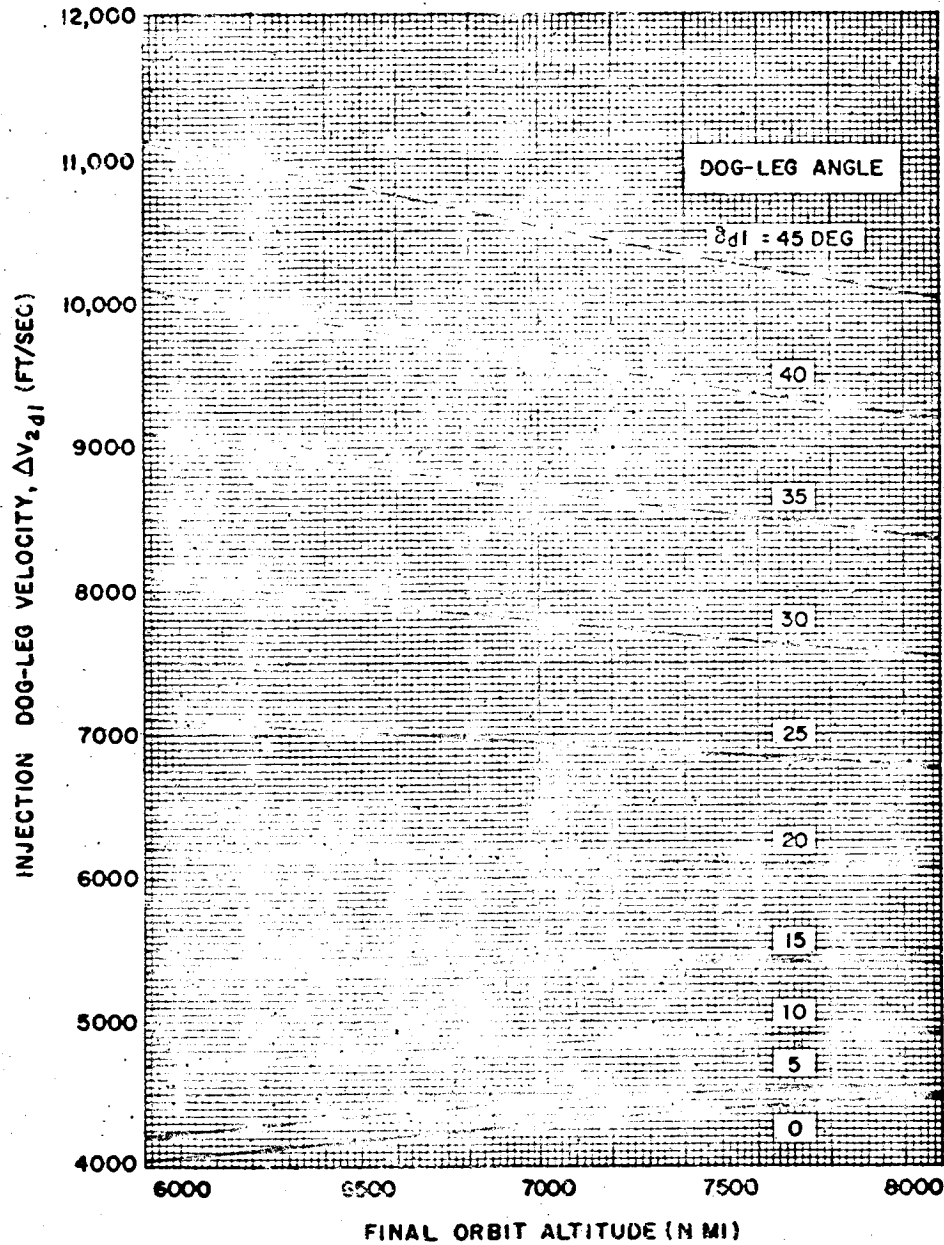


Figure 8. Final Hohmann Transfer Dog-Leg Injection Velocity Requirements (Parking Orbit Altitude = 100 n mi)

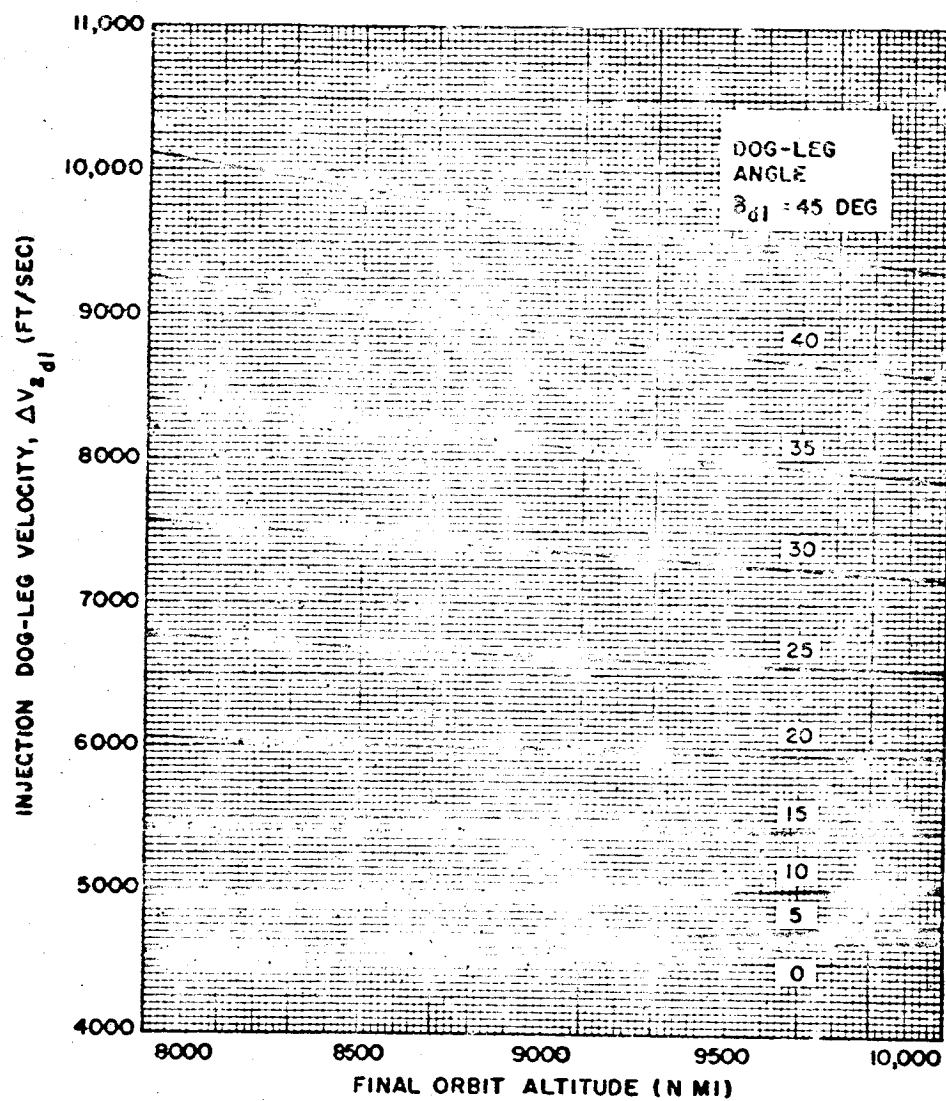


Figure 9. Final Hohmann Transfer Dog-Leg Injection Velocity Requirements (Parking Orbit Altitude = 100 n mi)

SYSTEM CONSIDERATIONS

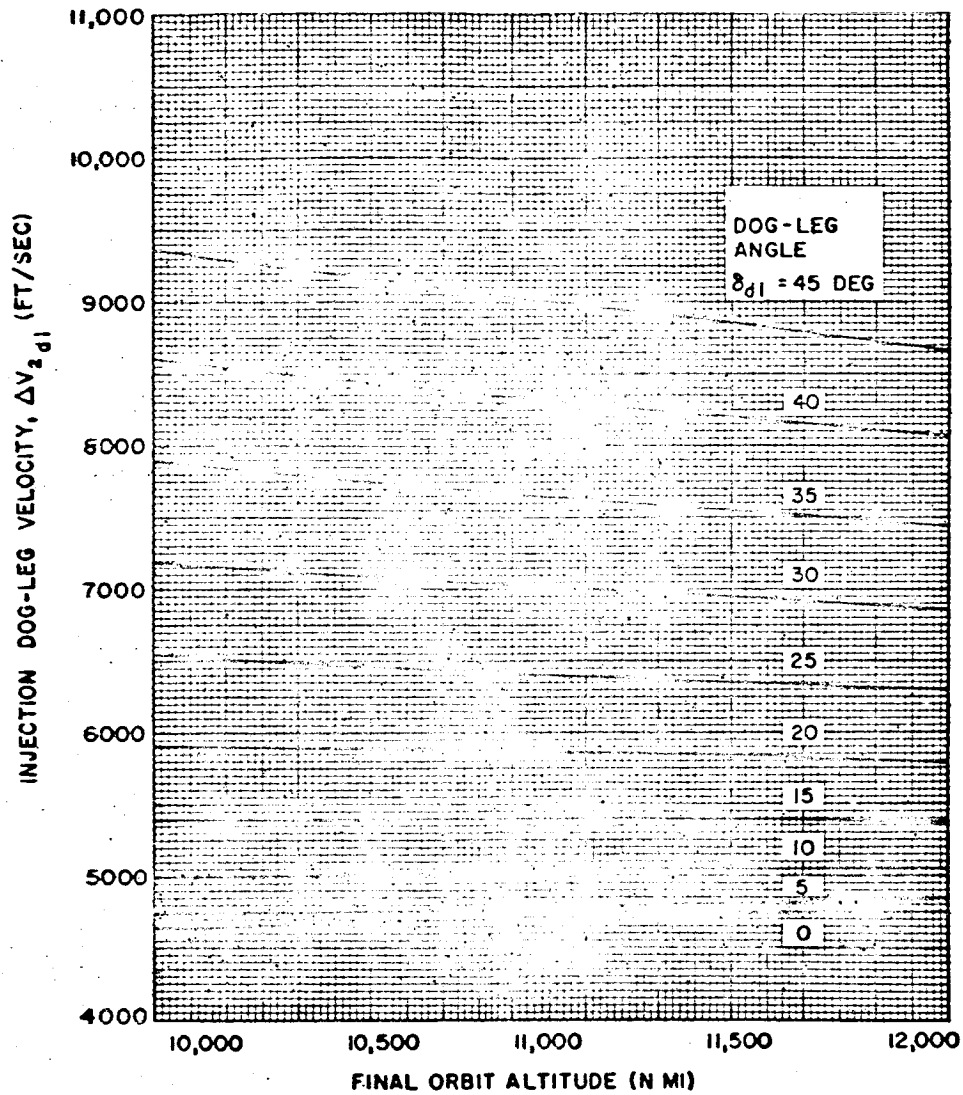


Figure 10. Final Hohmann Transfer Dog-Leg Injection Velocity Requirements
(Parking Orbit Altitude = 100 n mi)

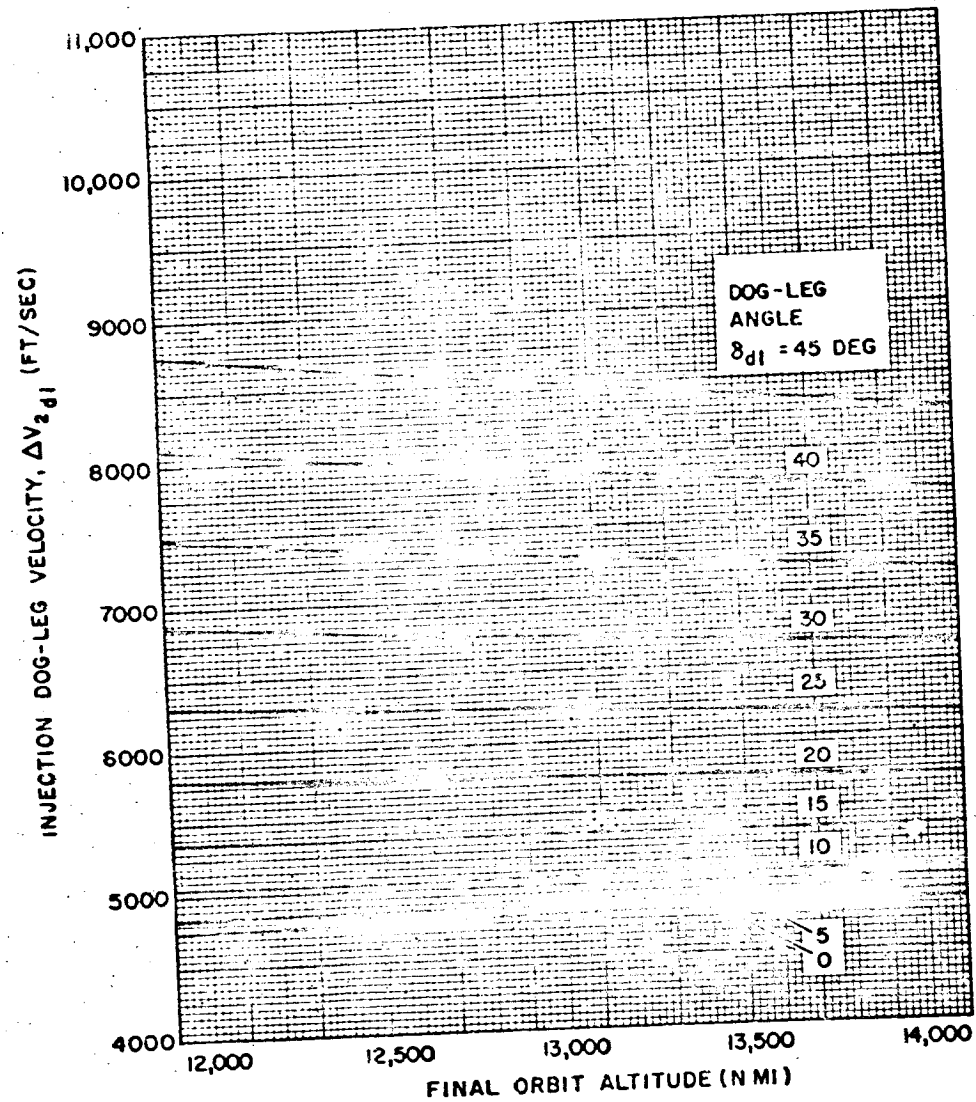


Figure 11. Final Hohmann Transfer Dog-Leg Injection Velocity Requirements
(Parking Orbit Altitude = 100 n mi)

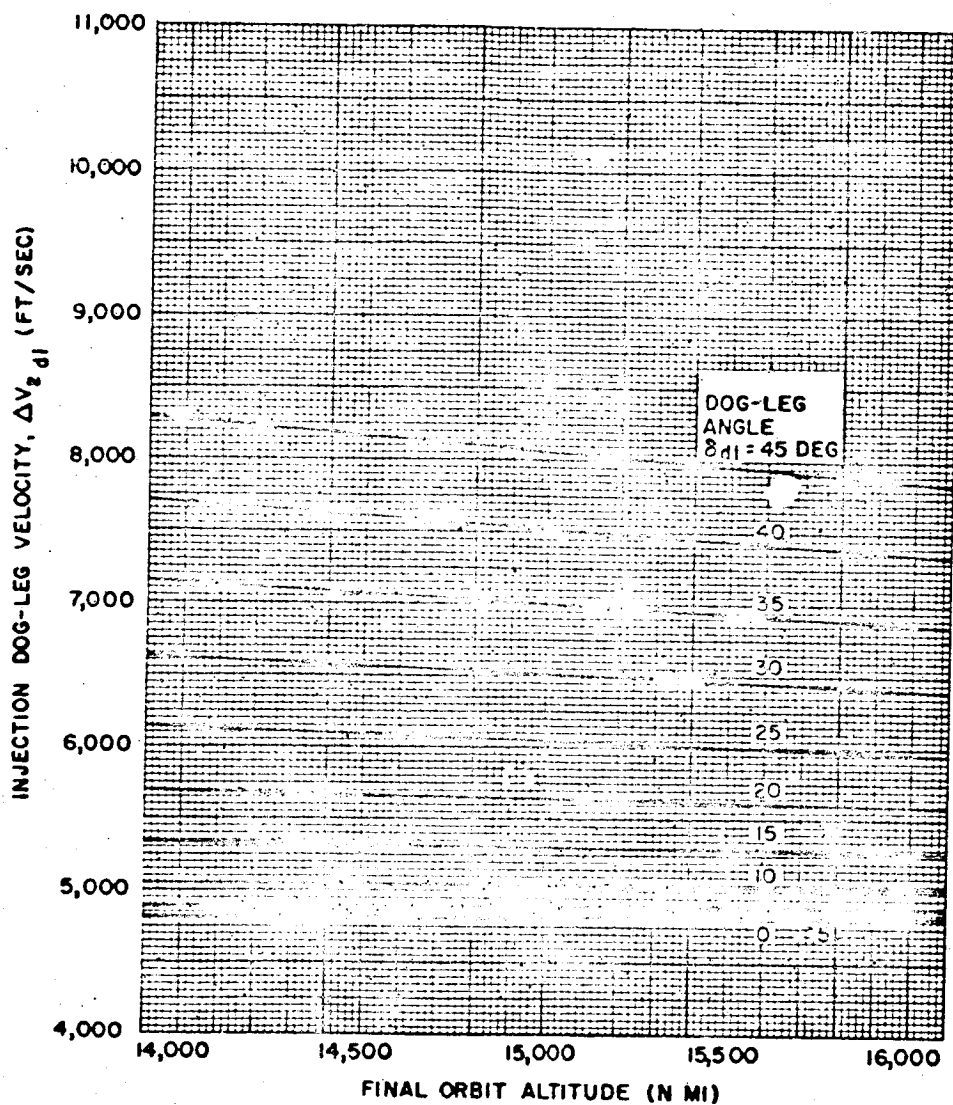


Figure 12. Final Hohmann Transfer Dog-Leg Injection Velocity Requirements
(Parking Orbit Altitude = 100 n mi)

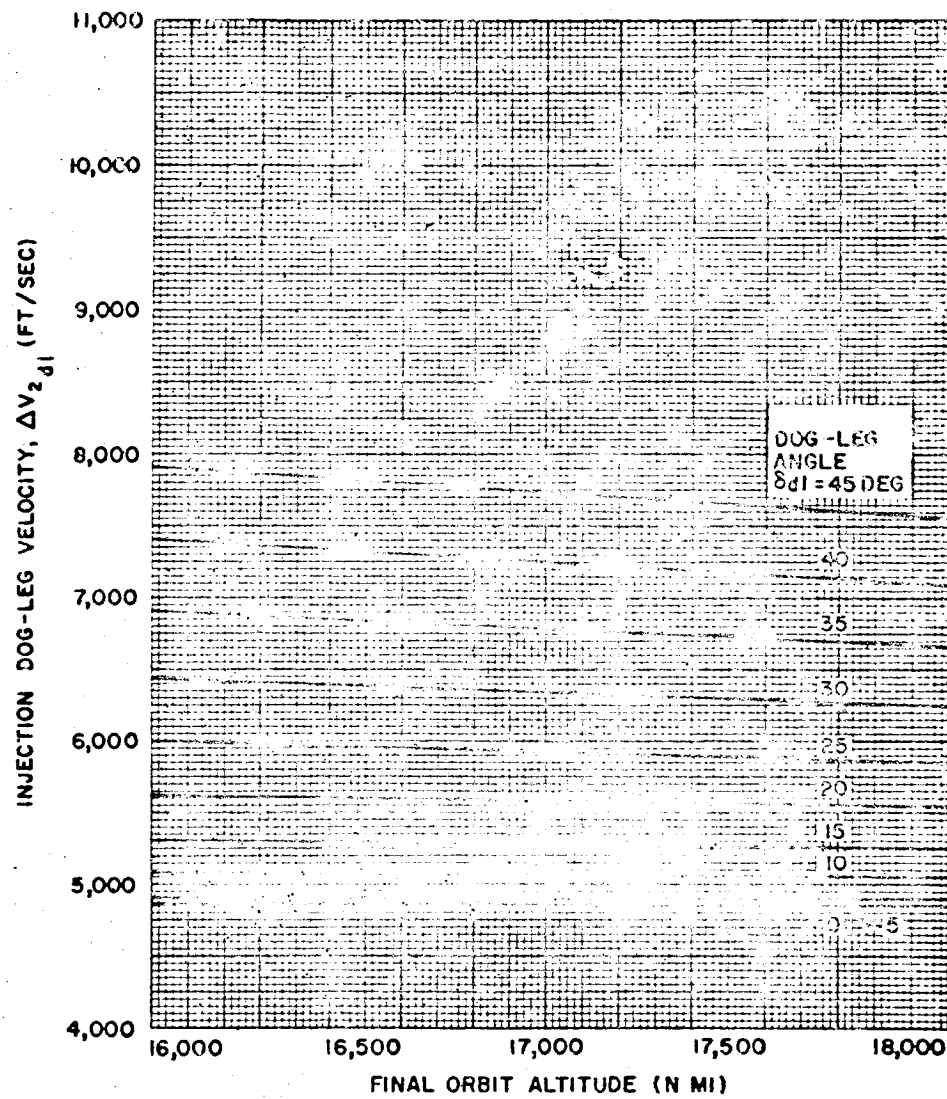


Figure 13. Final Hohmann Transfer Dog-Leg Injection Velocity Requirements
(Parking Orbit Altitude = 100 n mi)

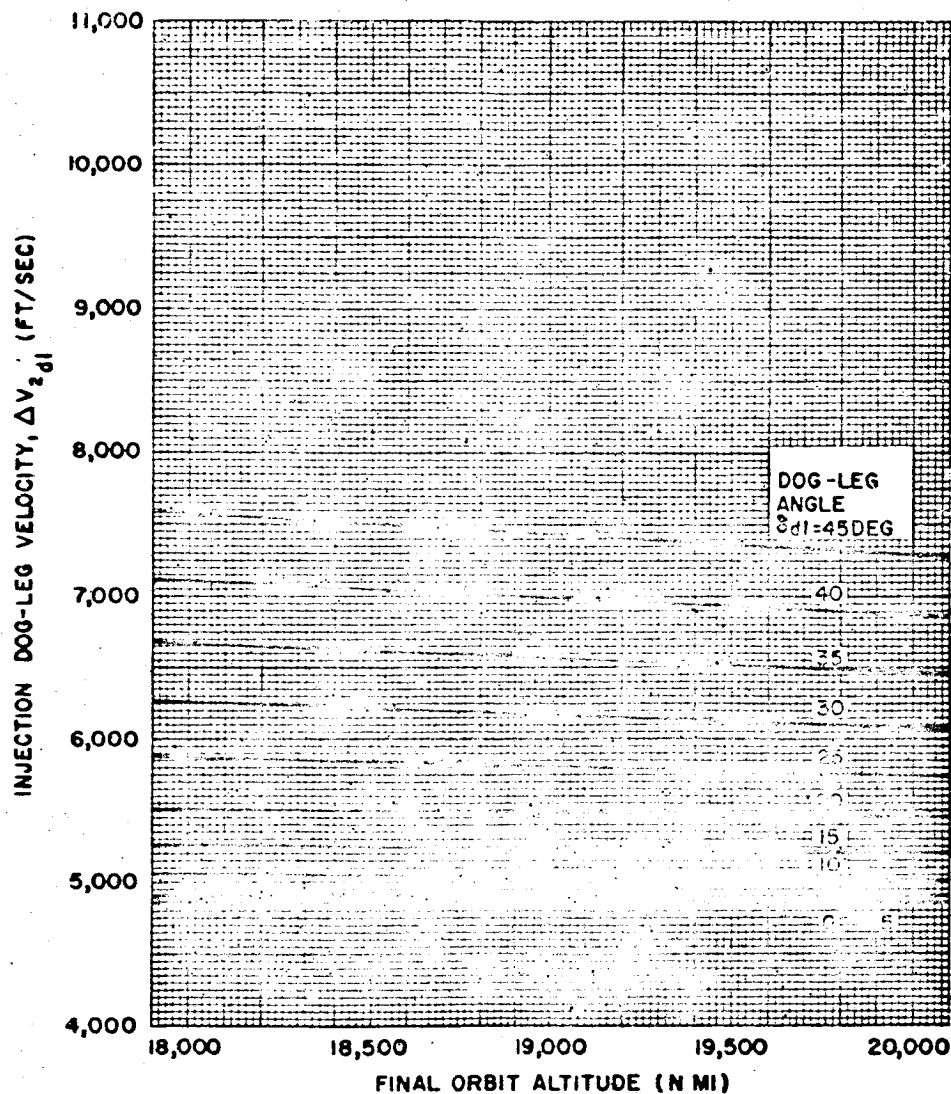


Figure 14. Final Hohmann Transfer Dog-Leg Injection Velocity Requirements
(Parking Orbit Altitude = 100 n mi)

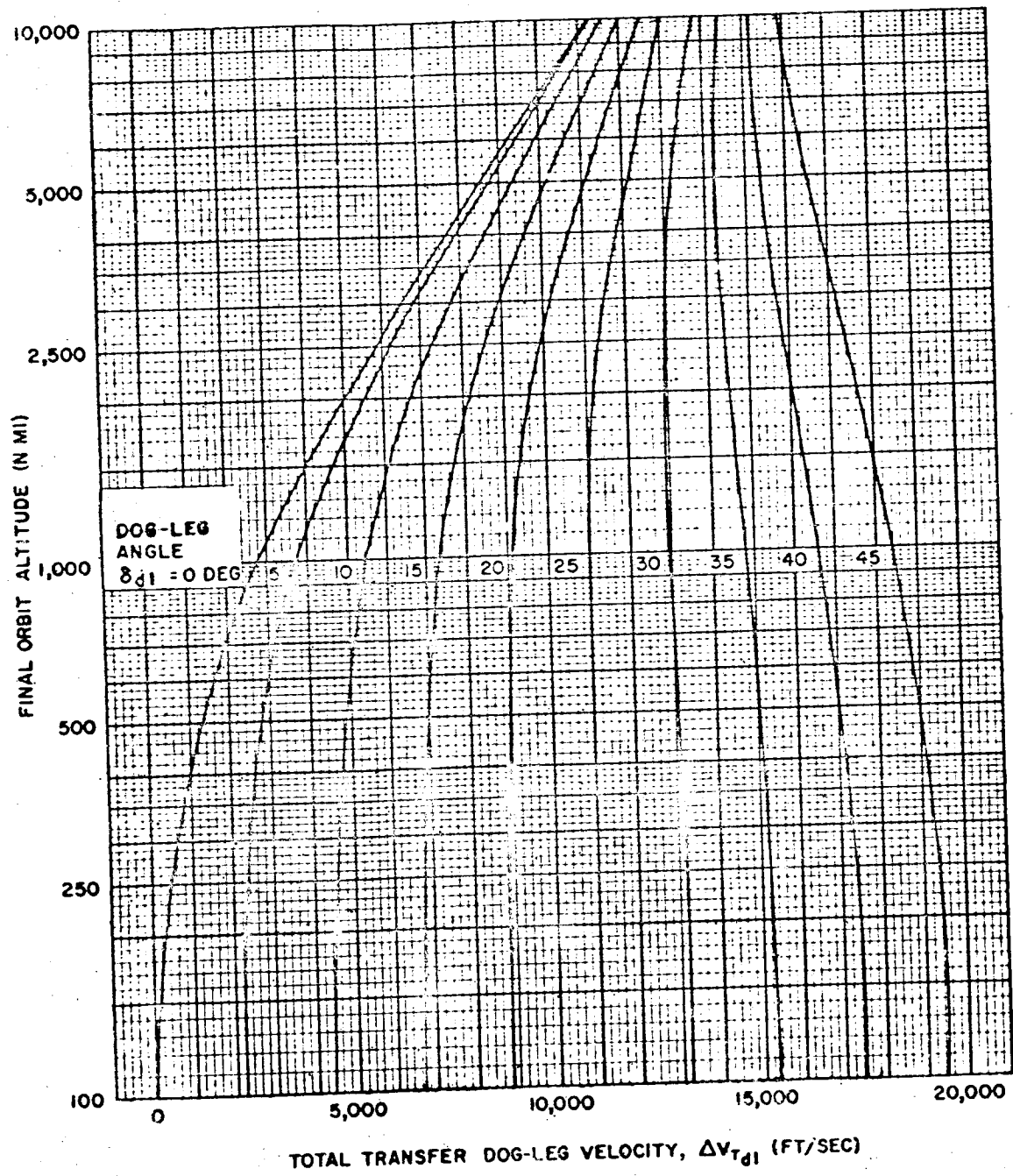


Figure 15. Total Hohmann Transfer Dog-Leg Injection Velocity Requirements
(Parking Orbit Altitude = 100 n mi)

SYSTEM CONSIDERATIONS

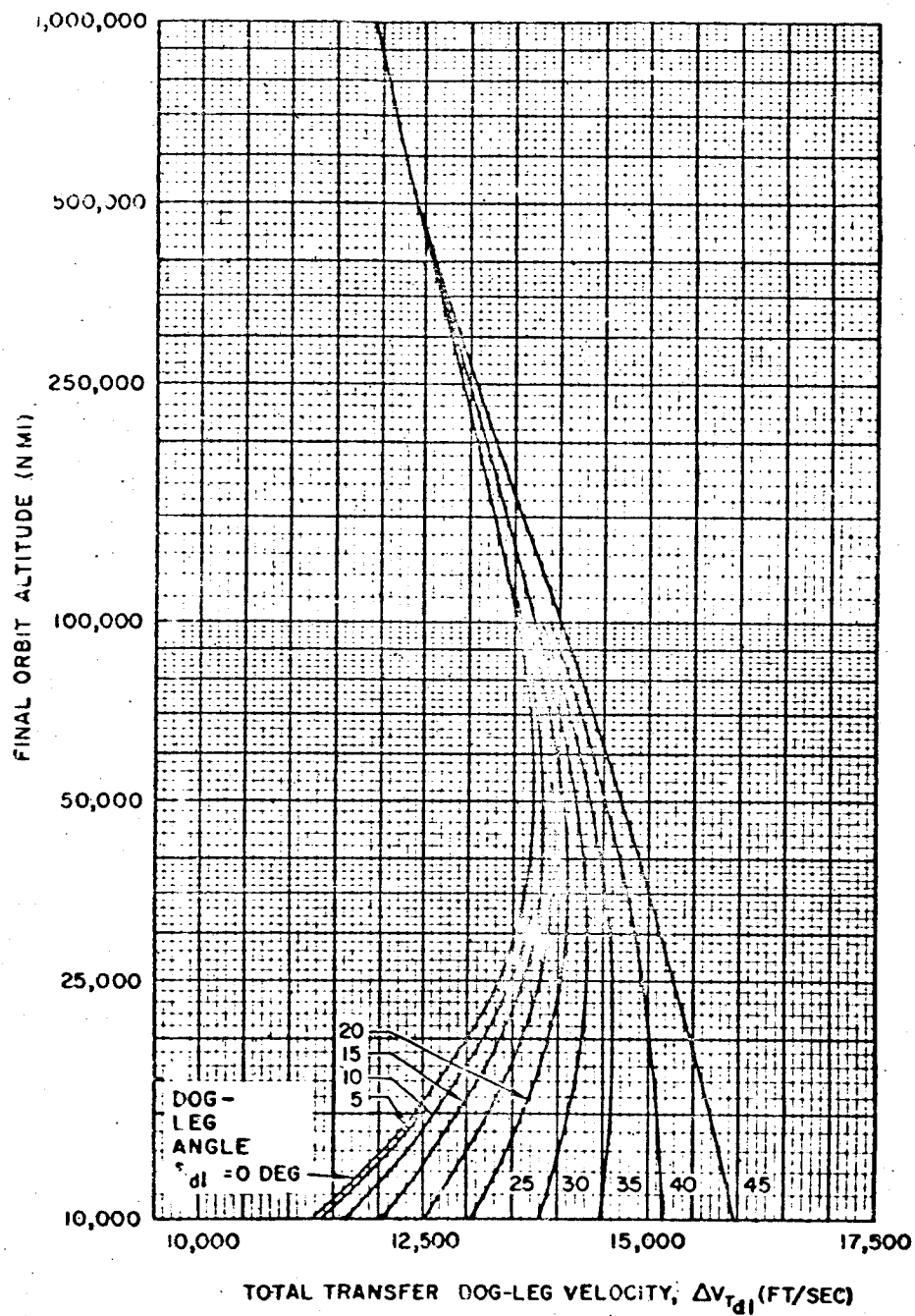


Figure 16. Total Hohmann Transfer Dog-Leg Injection Velocity Requirements
(Parking Orbit Altitude = 100 n mi)

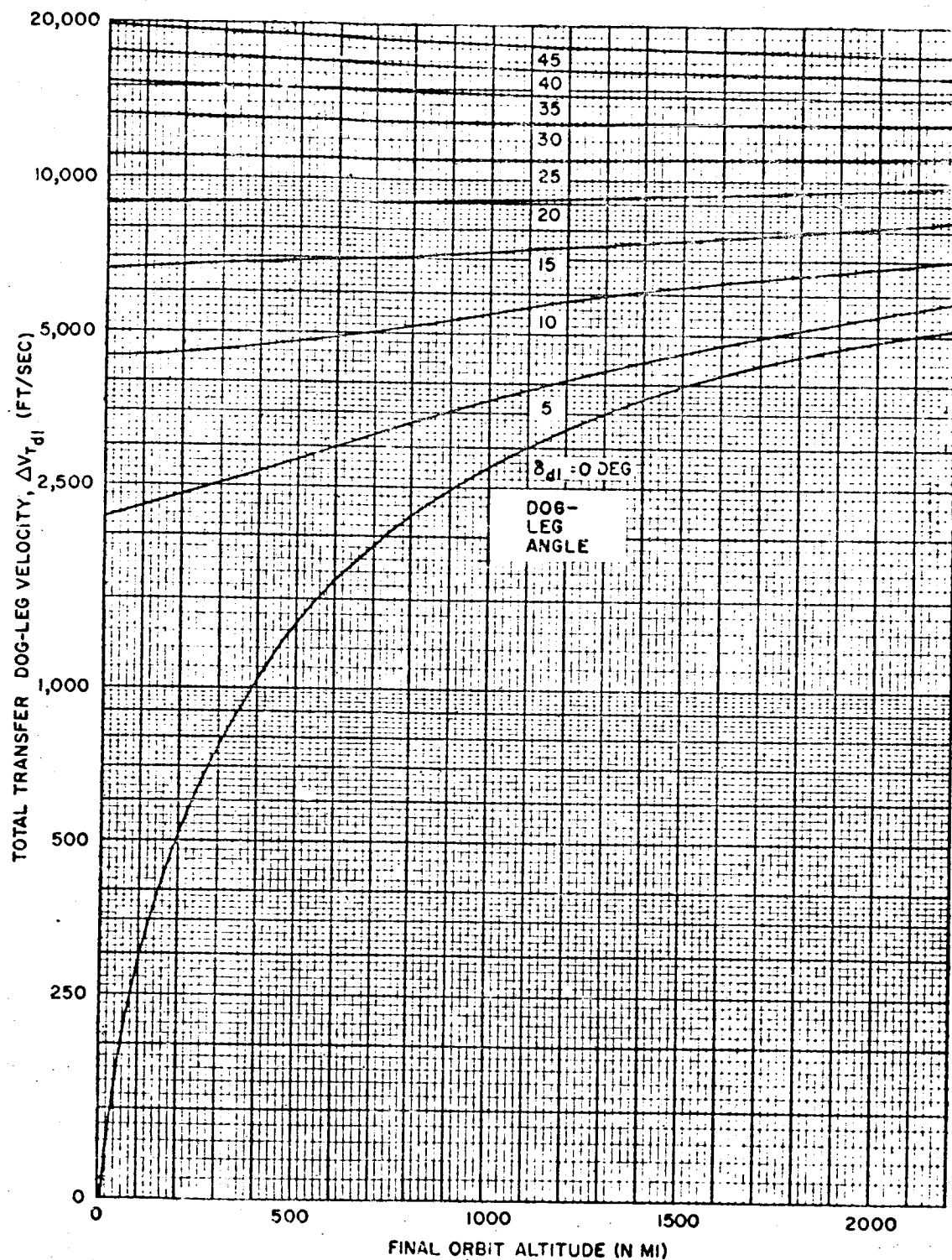


Figure 17. Total Hohmann Transfer Dog-Leg Injection Velocity Requirements
(Parking Orbit Altitude = 100 n mi)

3-22

SYSTEM CONSIDERATIONS

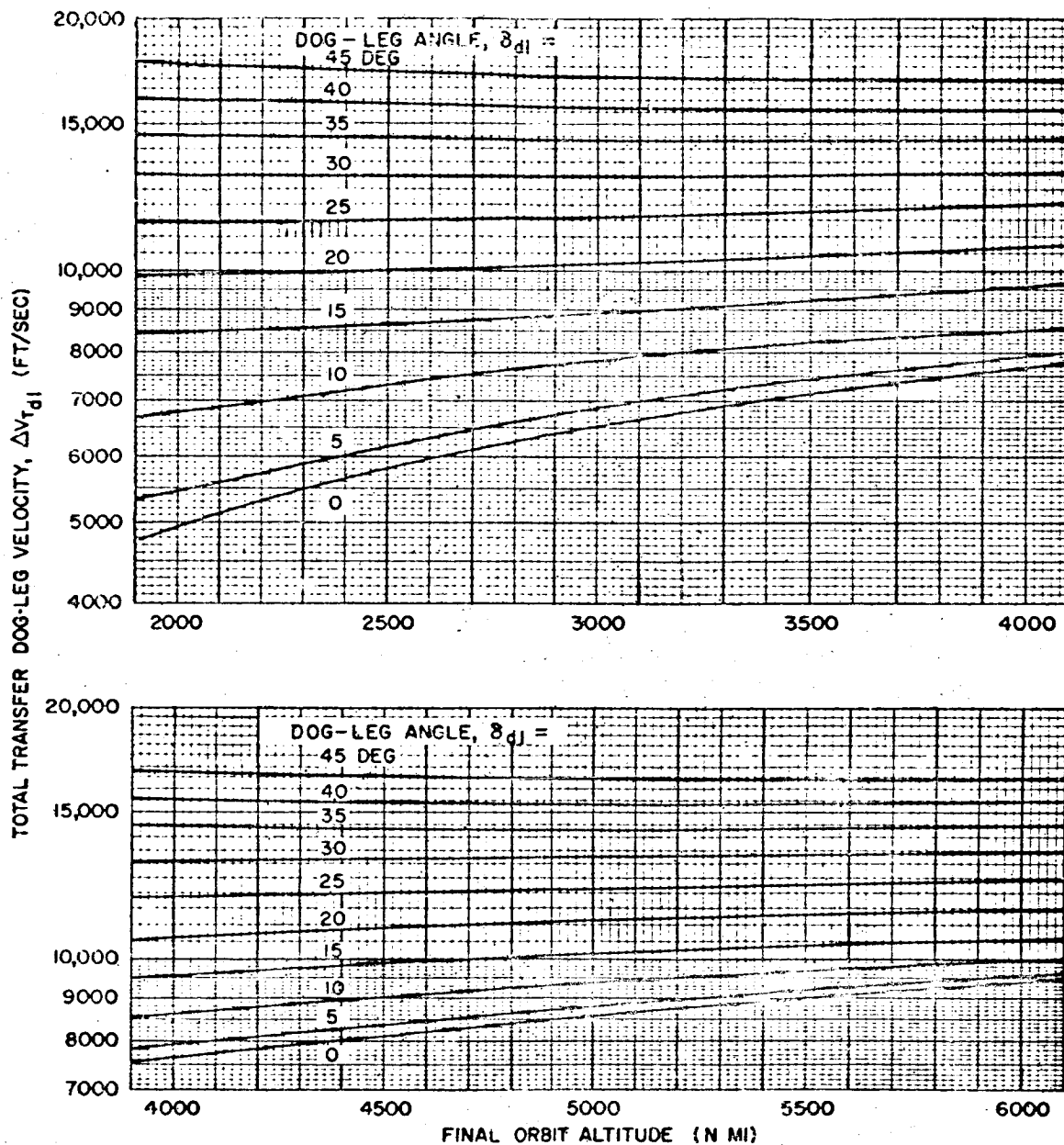


Figure 18. Total Hohmann Transfer Dog-Leg Injection Velocity Requirements
(Parking Orbit Altitude = 100 n mi)

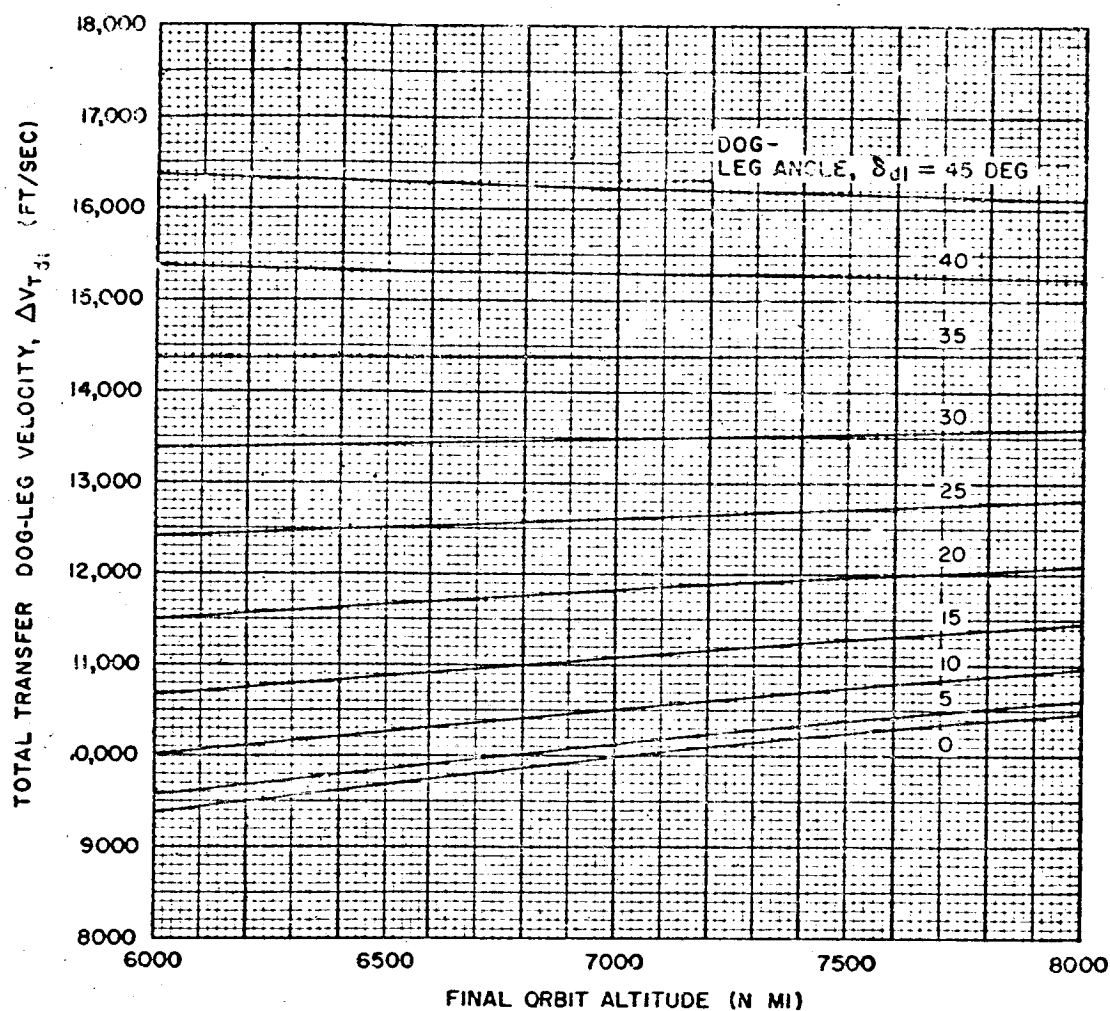


Figure 19. Total Hohmann Transfer Dog-Leg Injection Velocity Requirements
(Parking Orbit Altitude = 100 n mi)

SYSTEM CONSIDERATIONS

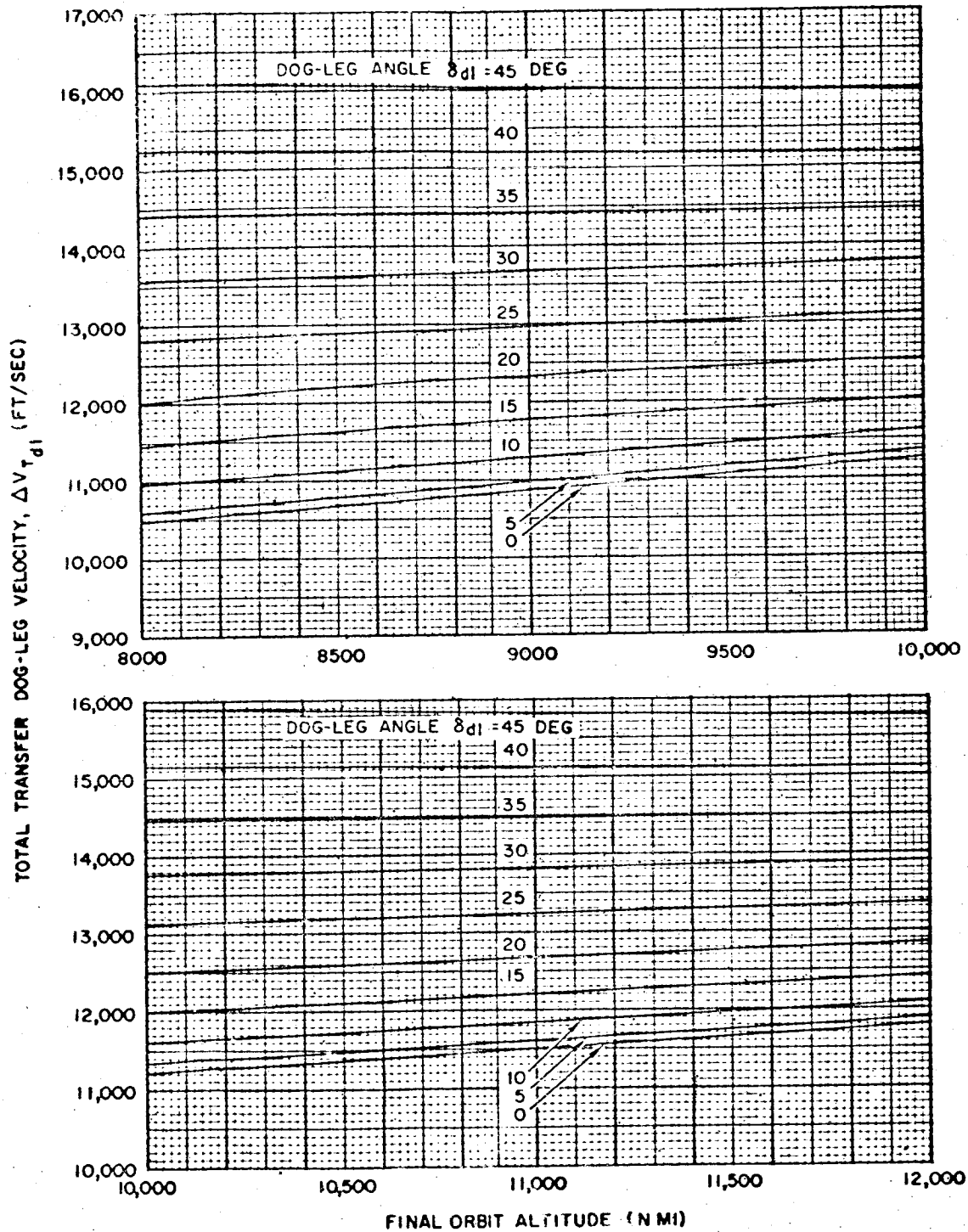


Figure 20. Total Hohmann Transfer Dog-Leg Injection Velocity Requirements
(Parking Orbit Altitude = 100 n mi)

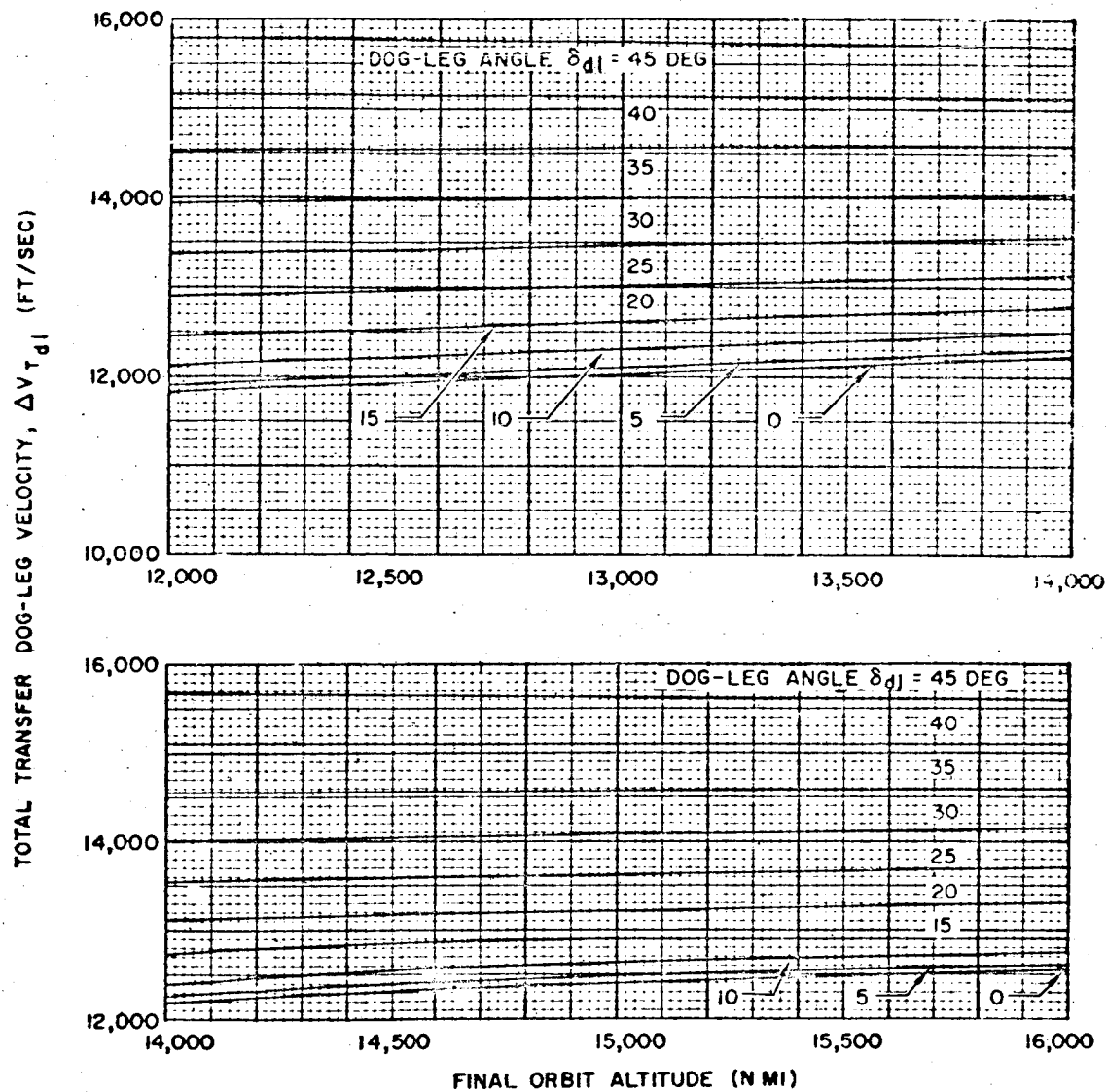


Figure 21. Total Hohmann Transfer Dog-Leg Injection Velocity Requirements
(Parking Orbit Altitude = 100 n mi)

SYSTEM CONSIDERATIONS

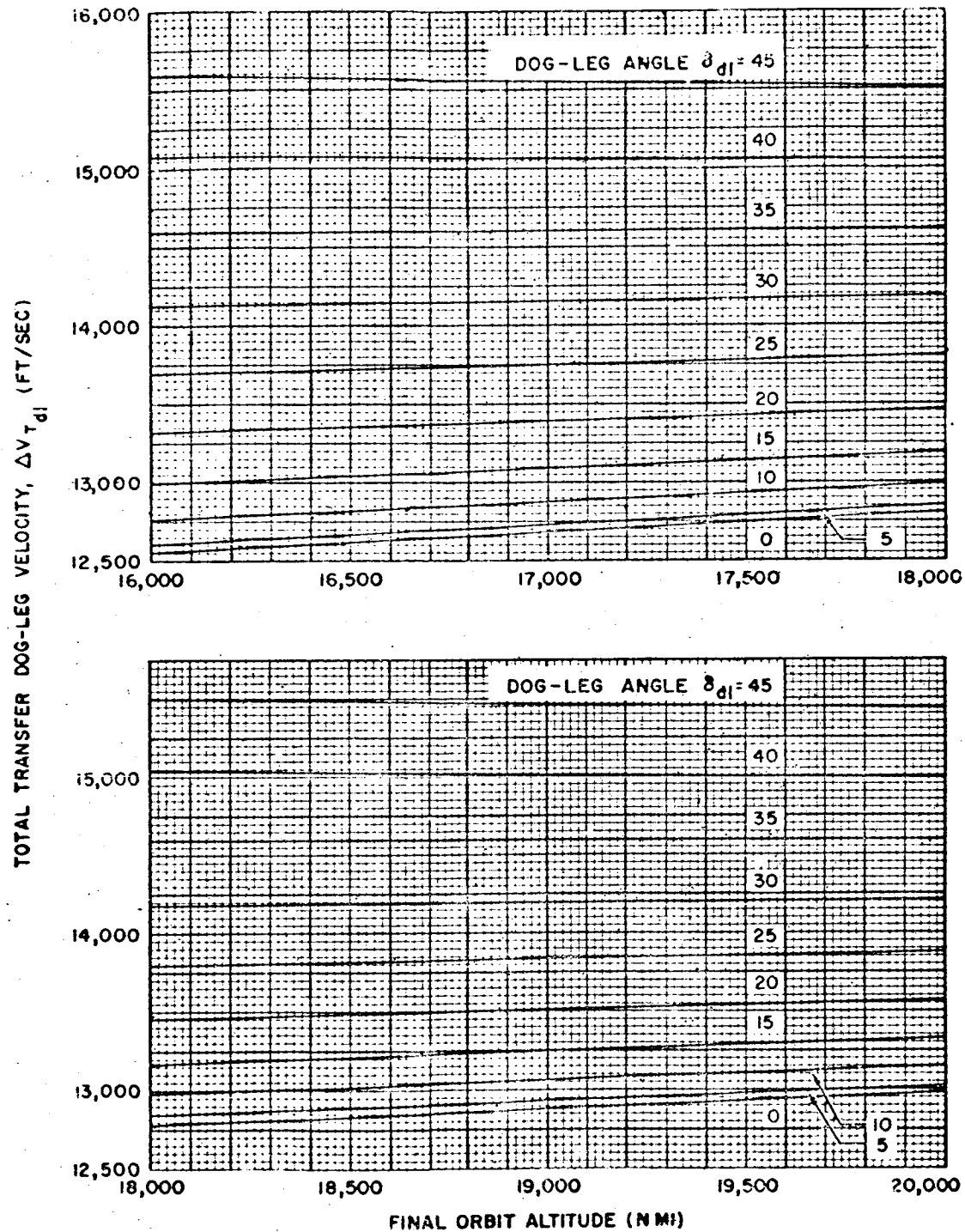


Figure 22. Total Hohmann Transfer Dog-Leg Injection Velocity Requirements (Parking Orbit Altitude = 100 n mi)

Launch Site Limitations

3-21

orbit. Parking at higher initial orbit altitudes, injection at locations other than equatorial crossings, and/or at positions other than apogee and dog-legging after the final orbit has been attained, all result in increased velocity requirements. For dog-legging after the final orbit has been established, the incremental velocity, ΔV_{dl} , required to dog-leg the velocity vector, V , and the trajectory plane by an amount δ_{dl} is approximately

$$\Delta V_{dl} = 2V \sin \left| \frac{\delta_{dl}}{2} \right| \sin \beta$$

The dog-leg angle required for dog-legging other than at equatorial crossings, as a function of the desired orbital inclination (see schematic), is

$$\delta_{dl} = \sin^{-1} \frac{\cos i}{\cos \lambda} - \sin^{-1} \frac{\cos i_{dl}}{\cos \lambda}$$

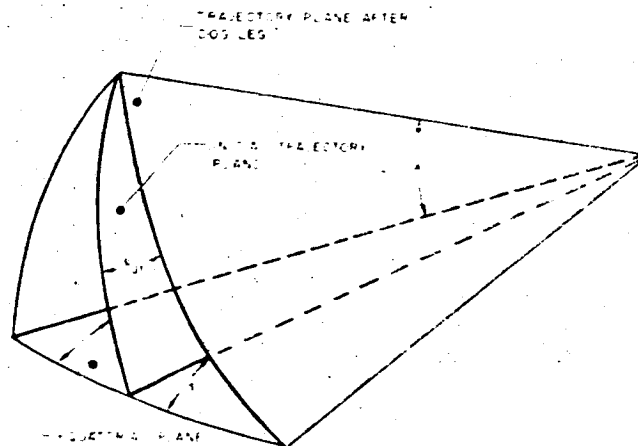
where

i = inclination prior to dog-legging

i_{dl} = desired orbit inclination subsequent to dog-legging

δ_{dl} = dog-leg angle, which is assumed to equal approximately the planar rotation

λ = geocentric latitude at execution of dog-leg.



A case where there will be a decrease in the velocity required to dog-leg and inject is the use of a bi-elliptical transfer maneuver. A reduction can only be realized when the final orbit is of extreme altitude or the dog-leg angle required is extreme. This maneuver consists of 1) injecting into a transfer orbit whose apogee

SYSTEM CONSIDERATIONS

exceeds the desired final orbit, 2) dog-legging and injecting into a transfer orbit of a perigee altitude corresponding to the desired resulting orbit, and 3) deboosting at perigee to circularize the final orbit.

For a circular orbit of 24-hour period, it is seen that no benefit can be realized unless the dog-leg angle required is in excess of about 37.5 degrees.⁴ However, for an inclination change of 60 degrees, a saving on the order of 2000 ft/sec would be realized. For orbital transfer without dog-legging, savings can only be realized when the final orbit is in excess of 41,100 nautical mile radius.

Usually, this method has too many impractical system aspects to warrant its implementation. Such aspects include excessive transfer time and an extra restart requirement.

3.2 RANGE SAFETY

This section of the handbook is devoted to system considerations associated with range safety. Much of the material presented here has been adapted from unclassified portions of Reference 5. The range safety problem is treated in general terms for any launch latitude from which a vehicle might be launched and in more detail with respect to USAF/AMR, USAF/PMR, and NASA/Wallops Island.

There are two basically different aspects to the range safety problems associated with the firing of space vehicles. The first of these is the danger to persons and property in both United States and foreign controlled territories, due to the physical impacting of various portions of the launch vehicle, when the vehicle is fired within the acceptable corridor of exit azimuths and performs satisfactorily. The second class of range safety problems arises from the malfunction of one or more elements of the vehicular and guidance systems. The significant fallout from such malfunctioning shots can be substantially outside the exit azimuth corridor. For example, a runaway control system could create a situation in which maximum thrust is oriented in an undesired direction. The first class of these hazards is that which controls the criteria imposed by the range safety authorities at each launch site.

3.2.1 Range Safety Constraints and Considerations

Whatever may cause the impact point of the various stages to drift outside of the predetermined range safety boundaries, there are a number of range safety hazards which may result, depending upon the nature and timing of possible malfunctions. These may be listed as follows:

- a) The hazard of miscellaneous tanks and missile parts (with no innate explosive capability) landing on U.S. territory or that of either friendly or unfriendly nations
- b) The hazard of single point detonation upon impact of the remaining fuel and oxidizer in the tanks of the given stages. (This may be the result of inadequate destruct energy or improper propellant utilization.)
- c) The spreading of toxic booster fuels (which also usually produces toxic combustion products, for example, H_2-F_2 system) in such a way as to endanger human life or to reduce agricultural property values. Even relatively bland petroleum products, such as RP-1, present a hazard not generally realized in that thorough saturation with a petroleum product generally causes earth to be infertile for years. In addition, three or four lungfuls of air, containing substantial fractions of hydrocarbons in the form of vapor, are generally fatal to humans if immediate prophylactic measures are not put into effect.
- d) In addition, it is assumed that while a deep space probe would not normally carry nuclear weapons aboard, it might be carrying such dangerously radioactive materials as radioisotope energy sources for SNAP-type power generating systems. There might also be nuclear reactors aboard which could be operating in the course of early flight stages for power generation for space work or electrical propulsion, although these are generally considered to be of a type which would be activated only after a successful orbit has been reached. However, in the case of operating nuclear reactors for thermonuclear propulsion, these would be in operation during preorbital flight. The political repercussions of the impact of radioactive material on friendly land areas, as well as the severe problems posed by the same events occurring in countries of Eastern Europe, Africa, or in Cuba, would be severe.

Range hazard considerations are best expressed in terms of the probability of the occurrence of a given event. No matter how low these probabilities, there is reasonable evidence to indicate that certain space shots would be prohibited even on the basis of extremely low probabilities, such as 10^{-6} , of an embarrassing incident occurring.

Table 2 lists the current range safety limitations for the three principal launching sites available in the United States. Naturally, the principal exit azimuth limitations are controlled by the range and trajectory of the specific missiles involved. The exit azimuth values given in Table 2 are approximate extreme limitations for the powered flight phase of orbital and interplanetary missions.

SYSTEM CONSIDERATIONS

Table 2. Range Safety Summary

Launching Site	Location		Permissible Exit Azimuth Limits	
	Latitude	Longitude	Low	High
PAFB/AMR	28° 30'N	80° 50'W	44°	110°
VAFB/PMR	35° 00'N	120° 30'W	170°	301°
NASA/Wallops Island	37° 50'N	75° 30'W	67°*	143°*
<u>Realizable Orbital Inclinations</u>			<u>Satellite Moving</u>	
PAFB/AMR	28.5 to 52.4°		Eastward	
VAFB/PMR	34.7 to 90.0°		Westward	
	81.8 to 90.0°		Eastward	

The latitude and the permissible exit azimuth limits control the realizable orbital inclinations which are possible from the three sites mentioned. Consequently, it is seen that it is not possible, without dog-leg maneuvering, to achieve orbits of less than 28.5 degrees inclination with respect to the equatorial plane. Dog-leg maneuvering at satellite velocities is expensive in terms of energy, and consists of applying a thrust normal to the plane of motion such that the plane of motion will be rotated by the appropriate amount. This velocity increment, of course, has no component in the plane, and hence does nothing other than rotate the plane of orbiting. Clearly, it is impossible to carry out dog-leg maneuvers when a vehicle is already taxed to the limit of its performance capabilities, necessitating a considerable reduction in payload to make such maneuvers possible.

The corridors for the specified azimuth limits are shown in Figures 23 and 24 for AMR and PMR, respectively. No similar plot has been provided for Wallops Island because of lack of firm range safety restrictions on space shots.

3.2.2 Impact Range and Exit Azimuth

The normal impact of ballistic missile stages is not a problem at either AMR or PMR because exit azimuths are selected which will allow stage impacts in remote ocean areas. However, certain satellite and deep space probe launchings require exit azimuths which could bring about stage impact in or near inhabited areas. Consequently, current space boosters present a range safety problem because of their long range. Similarly, future high-thrust boosters, such as the Saturn and

* First-stage limits only.

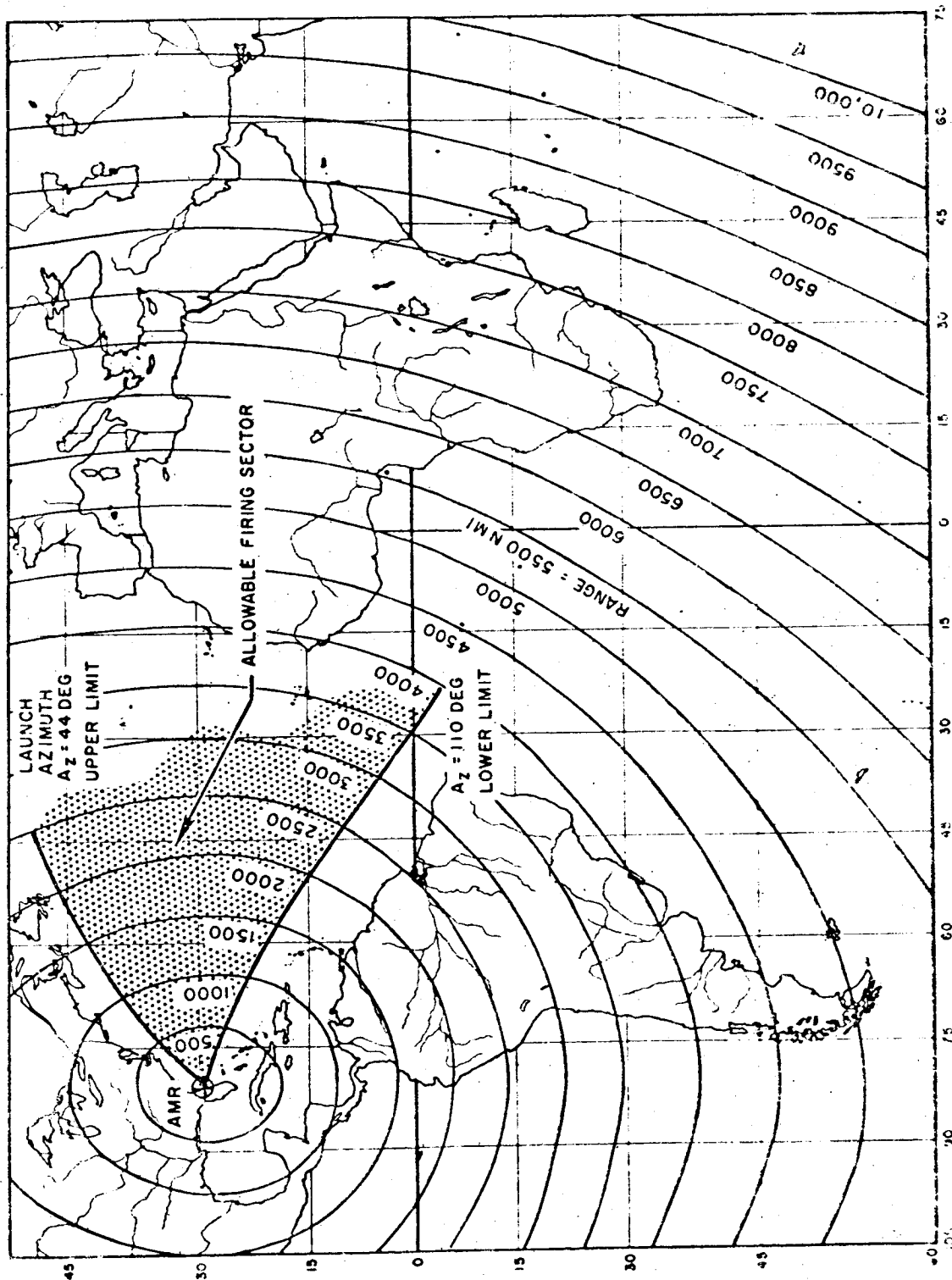


Figure 23. Atlantic Missile Range Firing Sector

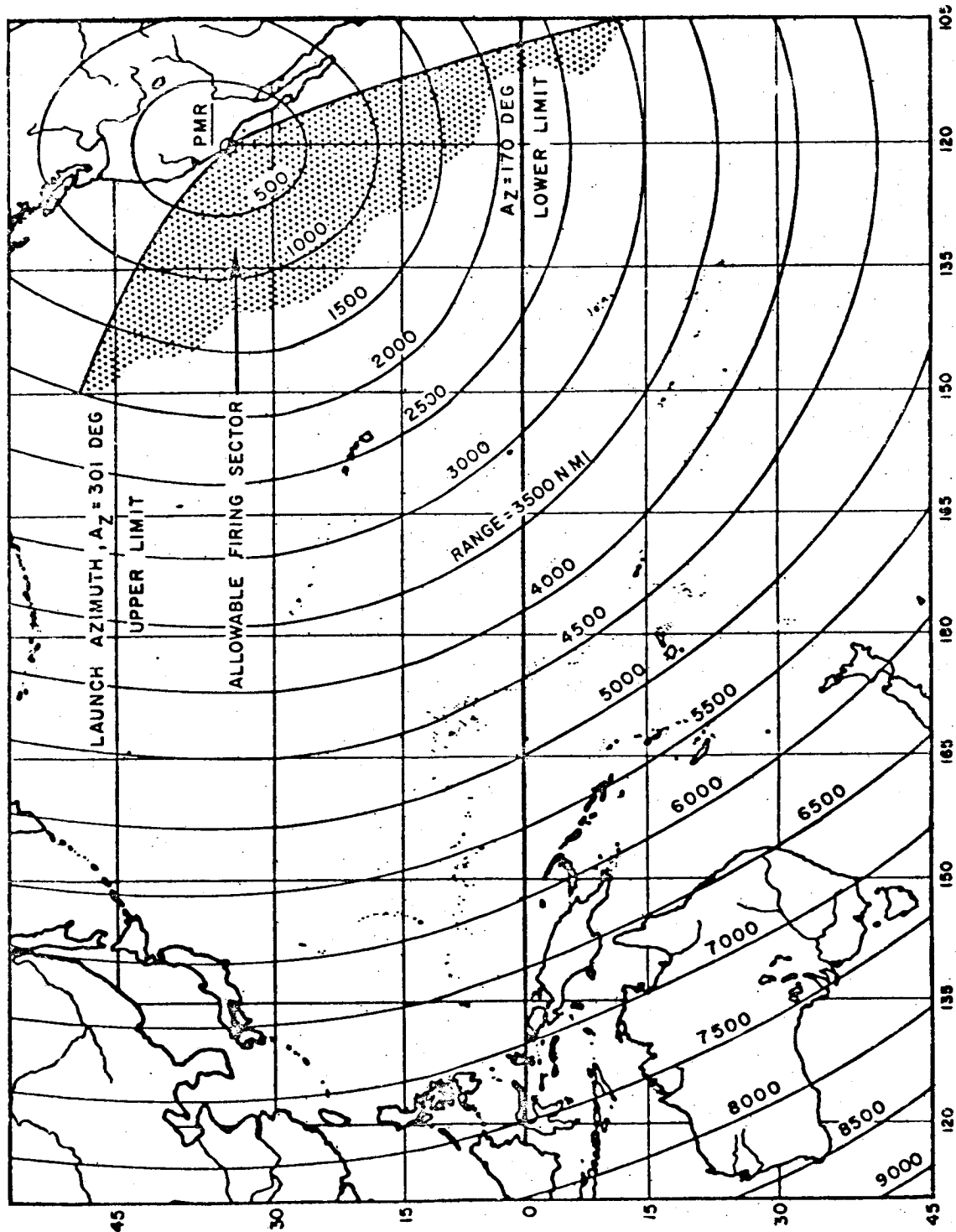


Figure 24. Pacific Missile Range Firing Sector

Nova vehicles, will have the same problem when employed for the same missions. Considerable trade-off between desired exit azimuth and impact of the booster and sustainer vehicles in safe areas is necessarily incurred at AMR, as will be seen in the following section. PMR is suited primarily only for near-polar orbits due to its westward firing restriction, which heavily penalizes payload for missions other than polar.

AMR. Range safety criteria at the Atlantic Missile Range limit available exit azimuths for orbital and deep space probes. Since flight over populated areas by booster vehicles is unacceptable, the exit azimuths are confined to an easterly sector. The upper limit of this sector is about 44 degrees from true North. A typical trace of the IIP (instantaneous impact point) trajectory for a vehicle launched at 44 degrees azimuth comes fairly close to the southern position of Newfoundland and the British Isles (Figure 23). The second-stage impact point and the nominal 3-sigma dispersions of the impact point could quite easily encompass portions of the British Isles and Continental Europe. The sector's southern limit is determined by the proximity of the trace of the IIP to the Bahama Islands. The lower limit is a launch azimuth of about 110 degrees from true North at Cape Canaveral. For a typical shot launched at 110 degrees from Cape Canaveral, the booster dispersion zone is over the ocean area and as such does not present a range safety problem.

A typical example of a range safety constraint controlling the launch azimuth is that in which the second-stage predicted impact location for the sector of allowable launch azimuths covers an area from the Mediterranean Sea southwesterly across northwest Africa and into the South Atlantic Ocean. Since potential stage-impact points on foreign soil are highly undesirable, for this case the choice of a launch azimuth resulting in impact in the Gulf of Guinea might be necessary.

It is clear that at AMR optimum trajectories required to accomplish an orbital injection or a deep space probe are not necessarily compatible with good range safety practices. The limited exit azimuth section (that is, 44 to 110 degrees), plus the potential impact on foreign soil of the first and second stages of research-type vehicles, severely restrict generation of optimum trajectories. For this reason, trajectories requiring dog-leg maneuvers must be used to 1) achieve the necessary trajectory for the accomplishment of certain types of space missions, and 2) minimize the range safety problem.

Impact Location. In order to evaluate properly the range safety problems of multistage vehicles, it is beneficial to construct a template of a typical booster rocket trajectory IIP, its final impact point, and resultant 3-sigma dispersion. Such a template is shown in Figure 25 for launch azimuths out of AMR corresponding to orbit inclinations of 30 to 70 degrees for a typical booster and its Stage I and II impact areas.

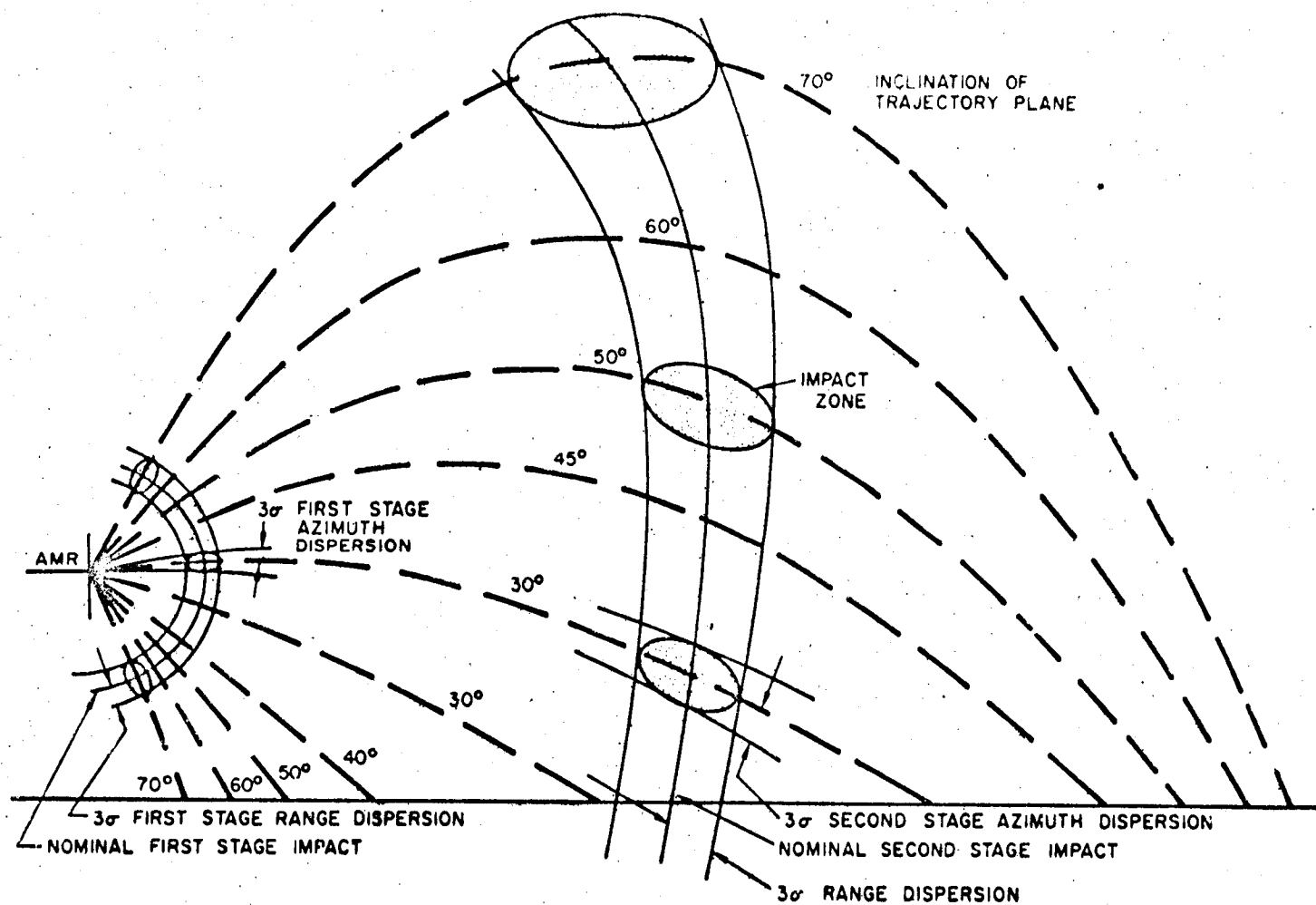


Figure 25. Range Safety Template

The noncircularity of the second-stage dispersion locus is due to the Mercator projection characteristics of the map used to plot these data. Due to the short range involved, the 3-sigma Stage I dispersion curve is, for all practical purposes, a circle around the launch site. It should also be pointed out that the Coriolis effect was neglected in the calculations of the curve because the scale used makes the effect on the shape of this curve negligible. Superimposition of the constructed template onto a map of the same scale and projection will show the Stage I and II impact zones.

Impact points for succeeding stages are not indicated, even though recent studies (References 6 through 9) show that some large mass-to-volume ratio components from these stages will survive re-entry. However, the 3-sigma dispersion zone for these stages is quite large and in many cases uncertain. Also, the lethal area presented by the small number of high mass-to-volume ratio components will contribute almost no kill probability to the overall launch operation.

Range. To construct the template, first draw trajectory traces similar to those in Figure 25. The simplest method is to construct the ground track assuming a non-rotating earth and later make adjustments for the earth's rotation. The trace is generated using the simple trigonometric equation

$$\psi = \psi_L + \sin^{-1} \frac{\tan \lambda}{\tan i} - \sin^{-1} \frac{\tan \lambda_L}{\tan i}$$

$$\text{and } i = \cos^{-1} \cos \lambda_0 \sin A_z$$

where

A_z = launch azimuth

λ_L = latitude of launch site

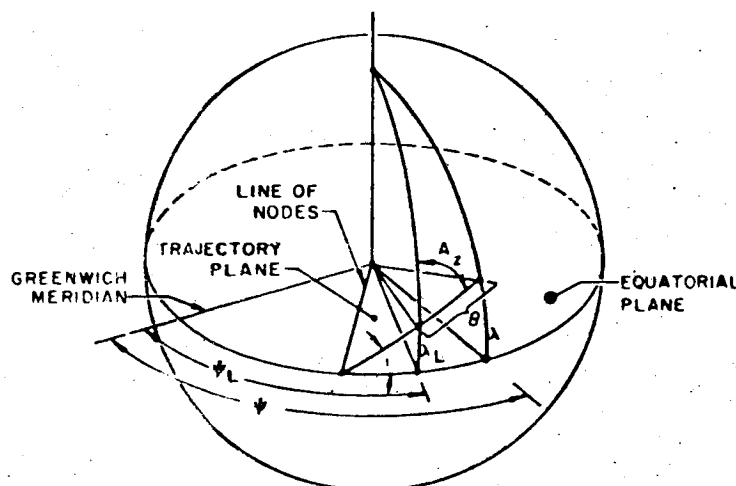
i = trajectory inclination

ψ = longitude of track or impact

λ = latitude of track or impact

ψ_L = longitude of launch site.

The above parameters are illustrated in the following diagram:



SYSTEM CONSIDERATIONS

Next, compute the stages' impact ranges. Using the velocity, flight path angle, altitude, and range of each stage at burnout, computed in Chapter 2, find the non-rotating-earth range from burnout by referring to Figure 26 or 27 and by using V_{BO} and β_{BO} . These figures are based on a burnout altitude of 400,000 feet, which is a realistic average for liquid- and solid-propellant first and second stages. The ranges shown here assume a vacuum re-entry. The change in range due to atmospheric drag is a function of both the entry conditions and the ballistic coefficient, W/C_{DA} , of the entering body. For ranges on the order of 5000 nautical miles, the upper limit of the anticipated range decrement due to drag is about 50 nautical miles for the lowest ballistic coefficient that might be realized (10 to 15 lb/ft²). An entering stage will tumble on entry and may break up depending on its structural characteristics. Liquid propellant stages usually break up near 200,000 feet altitude. Their tanks, in many cases, will "confetti" strewing fragments over a considerable area, the size of which is greatly dependent on the local wind conditions. Solid propellant stages on the other hand, may impact nearly intact. The ballistic coefficient of a tumbling stage is based on 2/3 of the broad side area as the reference area, A , and a value of 2 for the drag coefficient. Since the error incurred by neglecting the atmosphere on entry is small, no method of computation has been included. Also, the impact range curves neglect the effects of the earth's oblateness which results in a range error of the order of 10 nautical miles.¹¹ To correct the impact range for a different burnout altitude, use Figure 28 or 29 to find $\partial R / \partial h_{BO}$ (where the subscript i denotes the number of the stage). Then

$$\Delta R_{h_{BO_i}} = \left(\frac{h_{BO_i} - 400,000}{1000} \right) \frac{\partial R}{\partial h_{BO_i}} \text{ nautical miles.}$$

The nonrotating earth range, R_i , from the launch site to impact is

$$R_i = R_{BO_i} + R_{BO_i \text{ to impact}} + \Delta R_{h_{BO_i}}$$

The range angle $\theta_i = R_i / 60.76$ degrees. The latitude of impact is then found from the following equation (see diagram on page 3-35):

$$\lambda_i = \sin^{-1} \left[\sin i \sin \left(\theta_i + \sin^{-1} \frac{\sin \lambda_L}{\sin i} \right) \right]$$

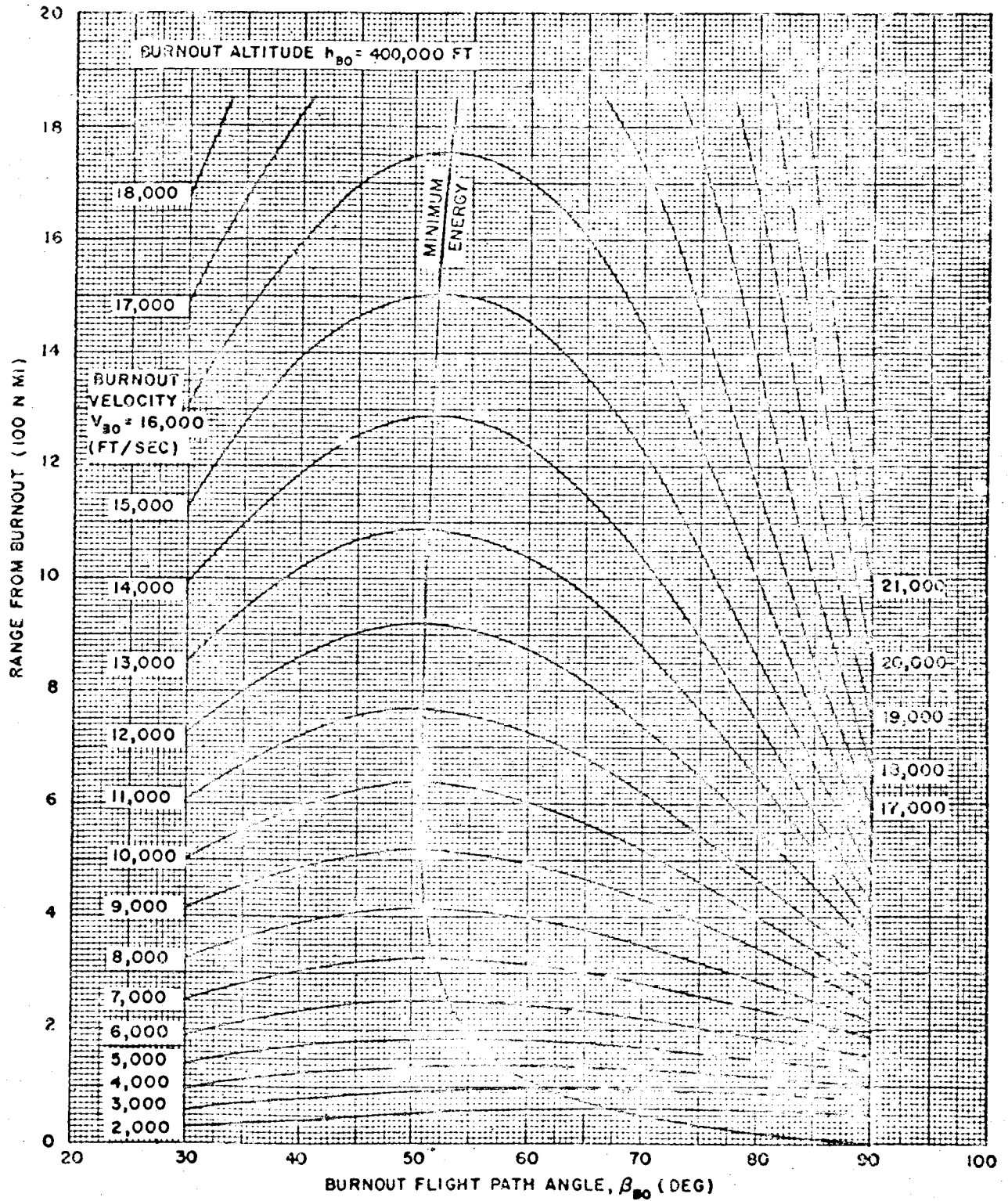


Figure 26. Impact Range from Burnout

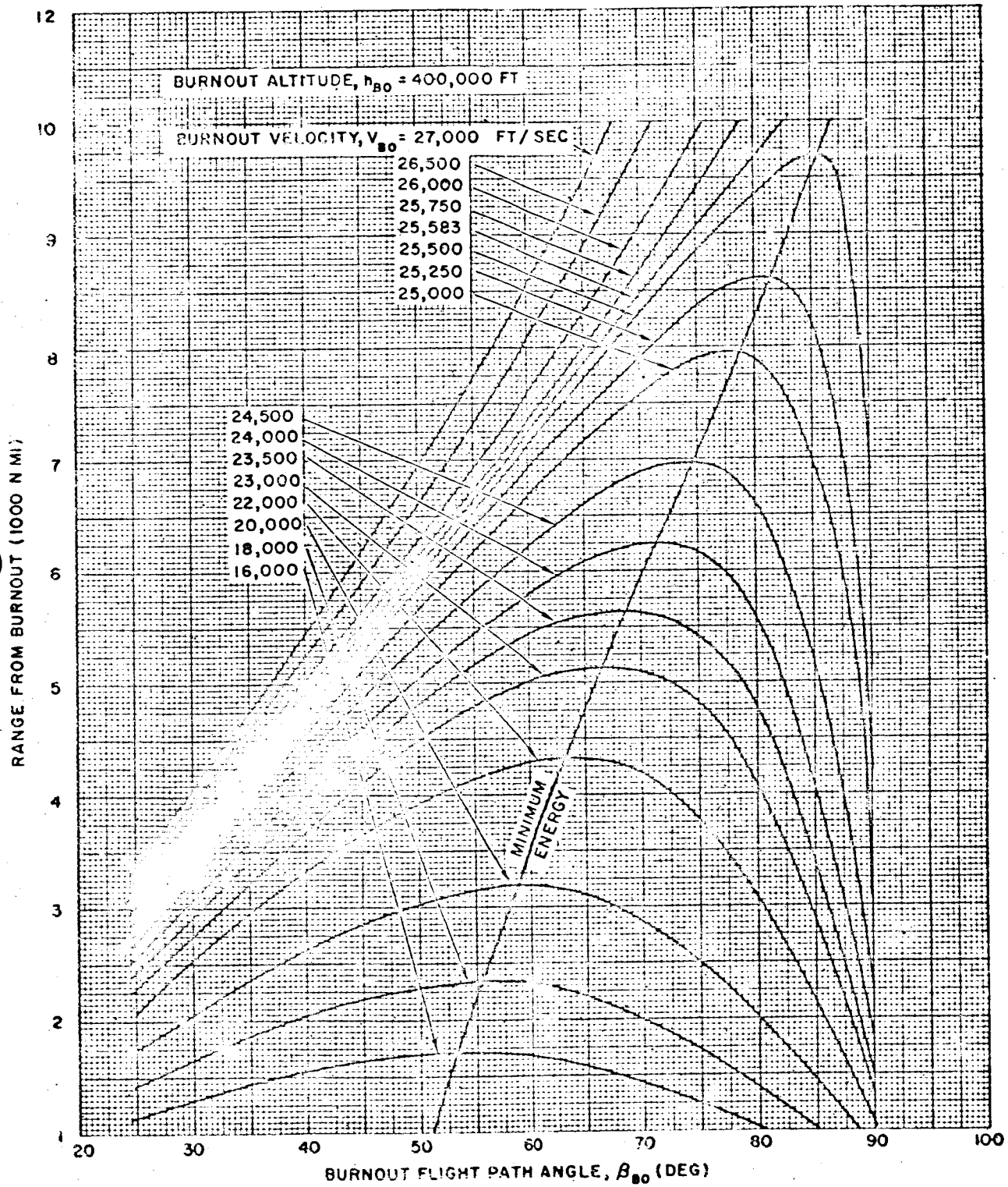


Figure 27. Impact Range from Burnout

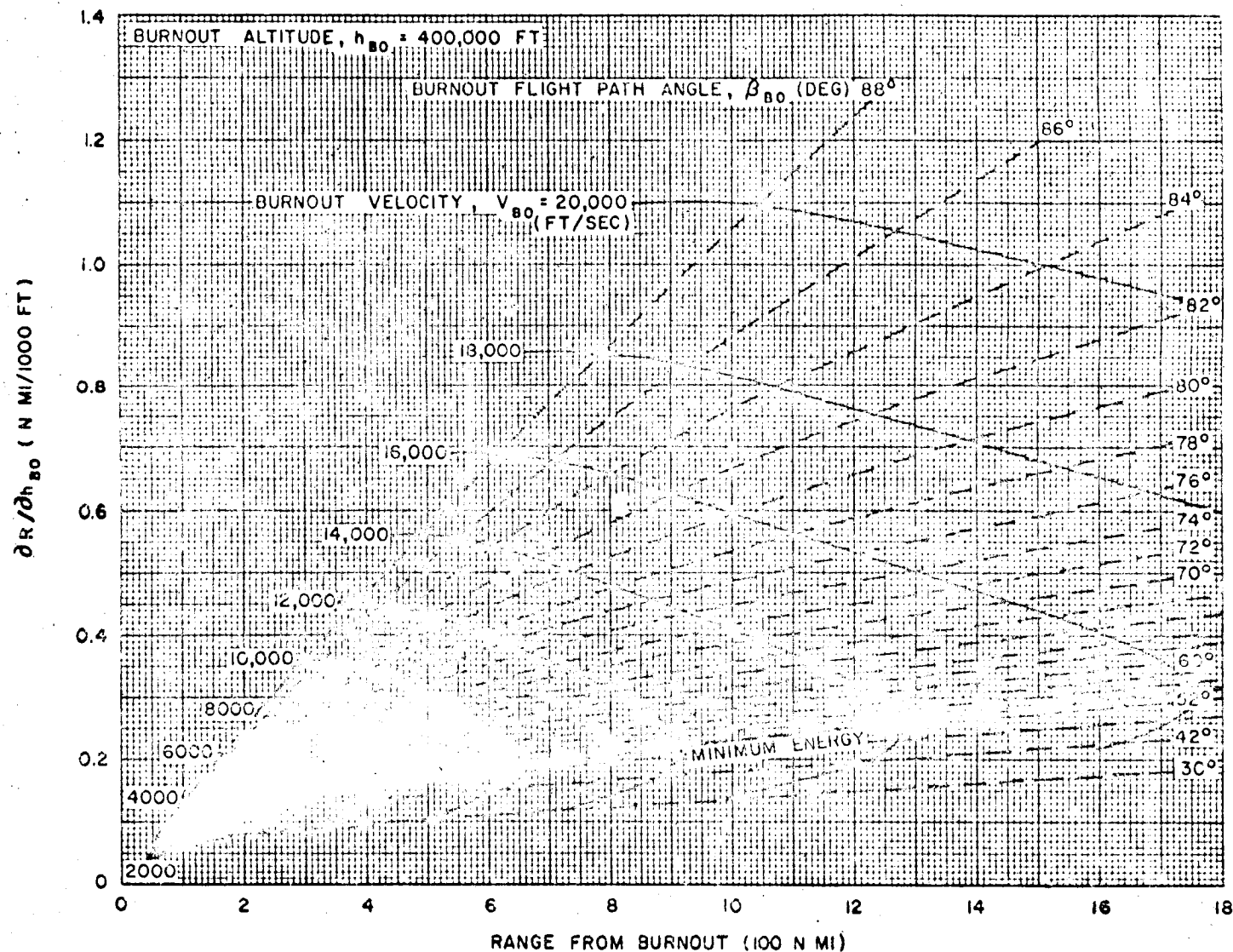


Figure 28. Burnout Altitude-Range Error Coefficient

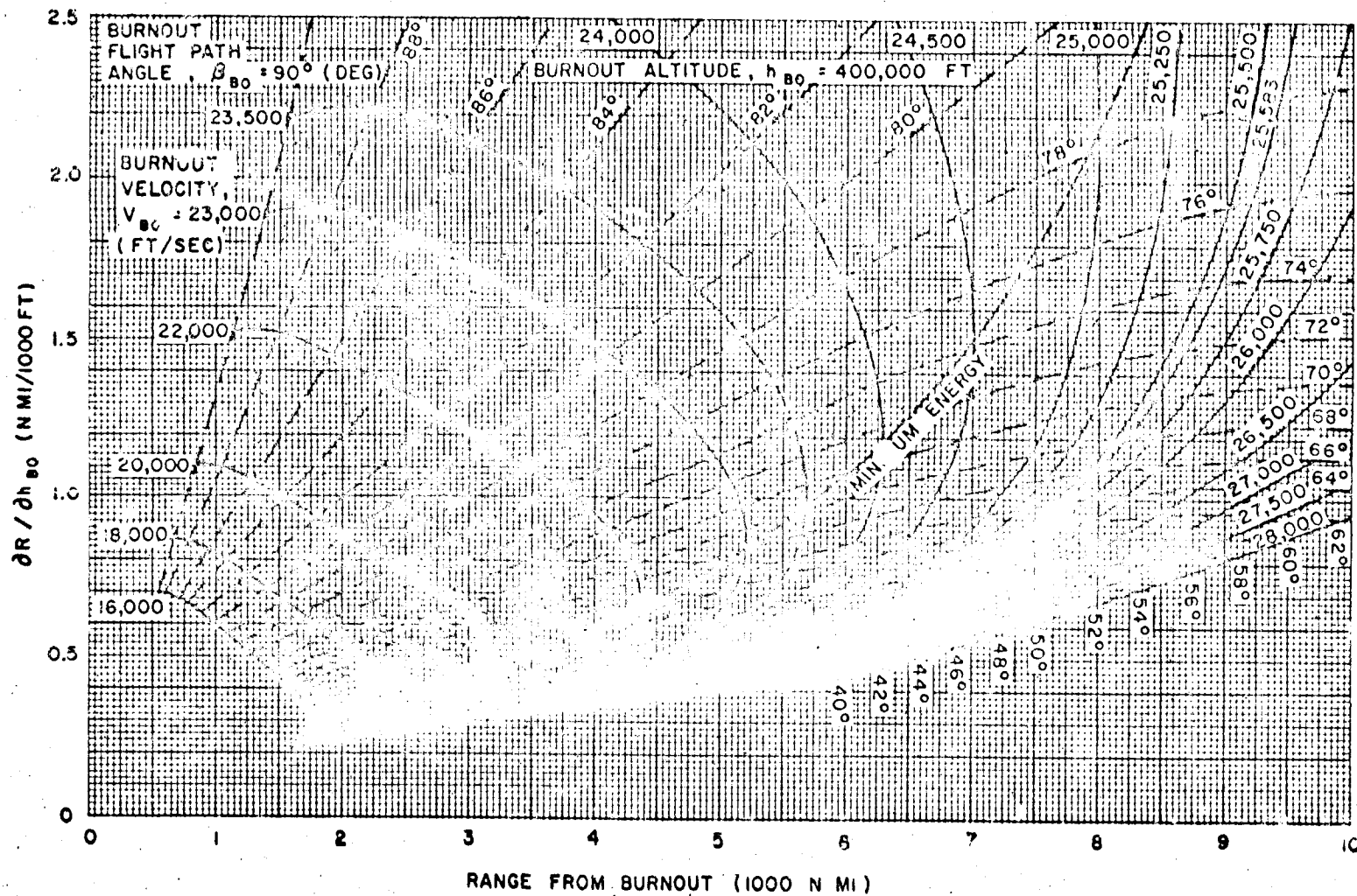


Figure 29. Burnout Altitude-Range Error Coefficient

REORDER IN 62-256

The corresponding longitude of impact can be found by substituting λ_i into the equations for ψ . The impact location can be found for several launch azimuths or trajectory inclinations, and an impact range locus can be plotted. The change in the impact location due to the earth's rotation is realized as a longitudinal shift west for easterly trajectories and the converse for westerly trajectories. There is no latitudinal shift due to the earth's rotation. To adjust for the earth's rotation, it is necessary to find the time from burnout to impact, which has been plotted as a function of the burnout conditions in Figure 30. This plot assumes an average burnout altitude of 400,000 feet. No correction is presented for different altitudes since such a difference would have only a second-order effect on the impact location. Longitudinal shift, $\delta\psi_i$, is equal to

$$\delta\psi_i = \frac{\left[(t_{BO_i} + t_{BO_i \text{ to impact}}) \text{ minutes} \right]}{4} \text{ degrees}$$

where the subscript i denotes the number of the stage.

The impact loci determined by various launch azimuths are then shifted longitudinally the appropriate amount for both first and second stages. The trace on the surface of the earth corresponding to various trajectory inclinations thus can be easily shifted by fairing a new curve through the launch site location and the impact locations of the two stages.

Dispersions. Next, it is desirable to determine the dispersions of the impact locations. The analysis presented here is cursory. Its results should be used only as an indicator. It would be senseless to perform a more elaborate analysis in a preliminary design study, since errors resulting from uncertainty as to vehicle parameters would probably be large compared to those resulting from the following analysis.

It is assumed that the dispersions at burnout associated with the guidance or auto-pilot system and those associated with the vehicle will be available. The velocity dispersion associated with variations in the vehicle's performance parameters can be computed from the analysis presented in Section 3.5 of this chapter. No angular errors as a result of the dispersions of the vehicles' performance parameters are assumed. In most cases it is reasonable to assume the only angular errors will be the result of the autopilot or guidance during the booster operations. The dispersions at burnout to be considered are velocity, flight path angle, azimuth angle, and altitude. Position errors and time at burnout errors can be neglected, since they are of second-order effect for booster stage impact

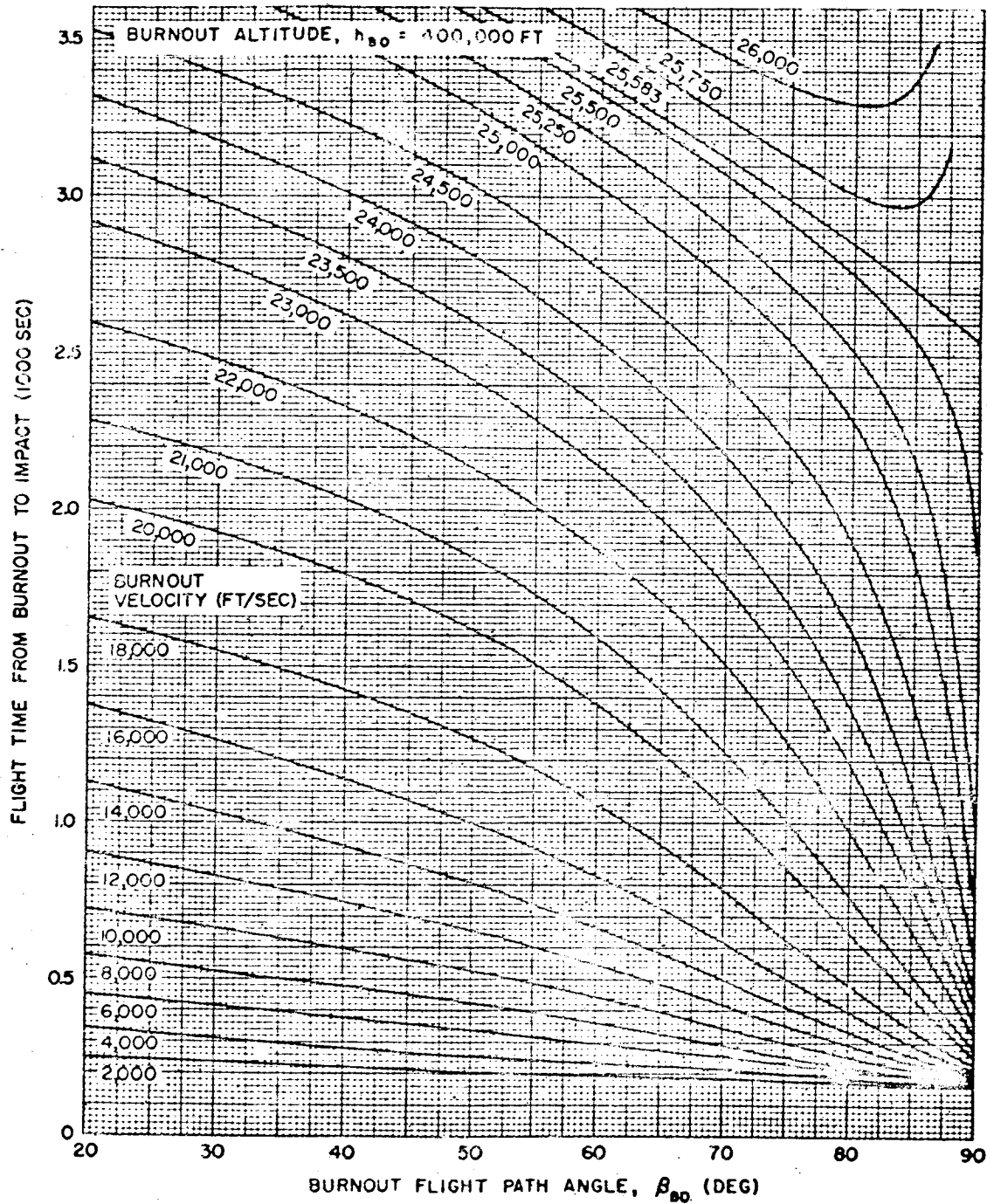


Figure 30. Flight Time from Burnout to Impact

location. Altitude error at burnout can also be neglected if it is not readily available. It is assumed that the errors in velocity, flight path angle, and altitude at burnout result in only downrange dispersions and the azimuth error results in only lateral range dispersions. Downrange errors are assumed to occur along the earth track, whereas crossrange errors are assumed to be normal to the earth track. To be conservative, it is also assumed that correlation of the errors at burnout is unity and that they are normally distributed, whereas the downrange and crossrange errors are assumed to be uncorrelated.

The probability, P , of impact within an elliptical impact zone of equal probability density having semimajor and semiminor axes of dimensions $k\sigma$ is:

$$P = 1 - e^{-\frac{k^2}{2}}$$

For $k = 1, 2$ and 3 , $P \approx 0.39, 0.86$ and 0.99 , respectively. For the template (Figure 30), ± 3 -sigma values were computed for both the downrange and lateral range dispersions and the ellipse was constructed using these as the major and minor axes, respectively. The probability of impact within such an ellipse is approximately 99 percent. The variation in the apparent size of the ellipses for different trajectory inclinations on Figure 25 is caused by the Mercator projection of the map used.

To aid in finding the downrange dispersions Figures 28, 29, and 31 through 34 have been included. The error coefficients shown in the figures, were all computed for a burnout altitude of 400,000 feet. The error resulting from the burnout altitude being different than 400,000 feet is small since such a difference would be small compared to the radius of the earth and since the coefficients are relatively insensitive to small changes in the distance from the center of the earth to the burnout altitude. In computing the error coefficients a spherical nonrotating earth was assumed and the atmospheric entry effects were neglected. The errors incurred from these assumptions are small. ¹¹ The downrange dispersions are

$$(\Delta R)_{V_{BO_i}} = \frac{\partial R}{\partial V_{BO_i}} \delta V_{BO_i}$$

$$(\Delta R)_{\beta_{BO_i}} = \frac{\partial R}{\partial \beta_{BO_i}} \delta \beta_{BO_i}$$

SYSTEM CONSIDERATIONS

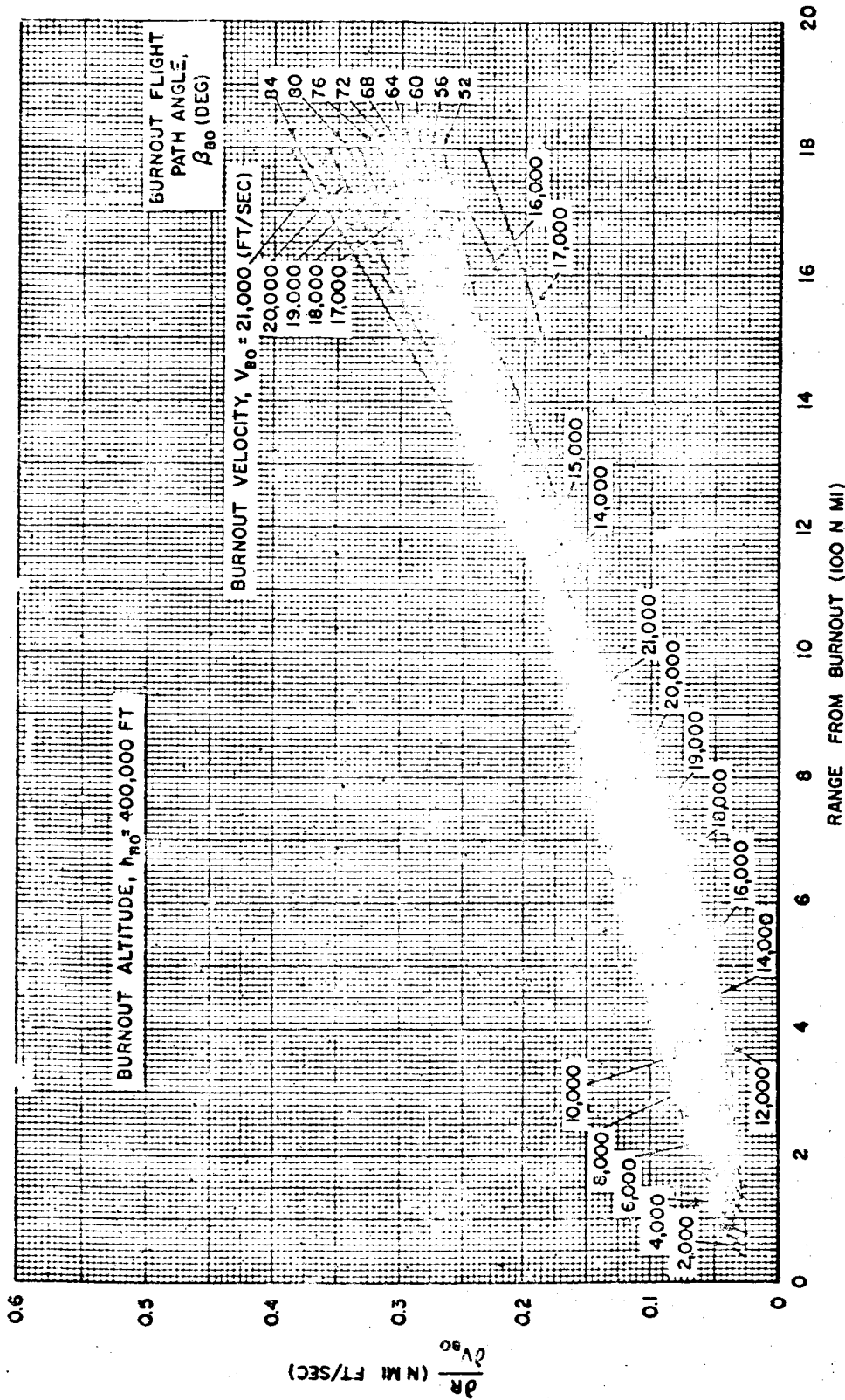


Figure 31. Burnout Velocity-Range Error Coefficient

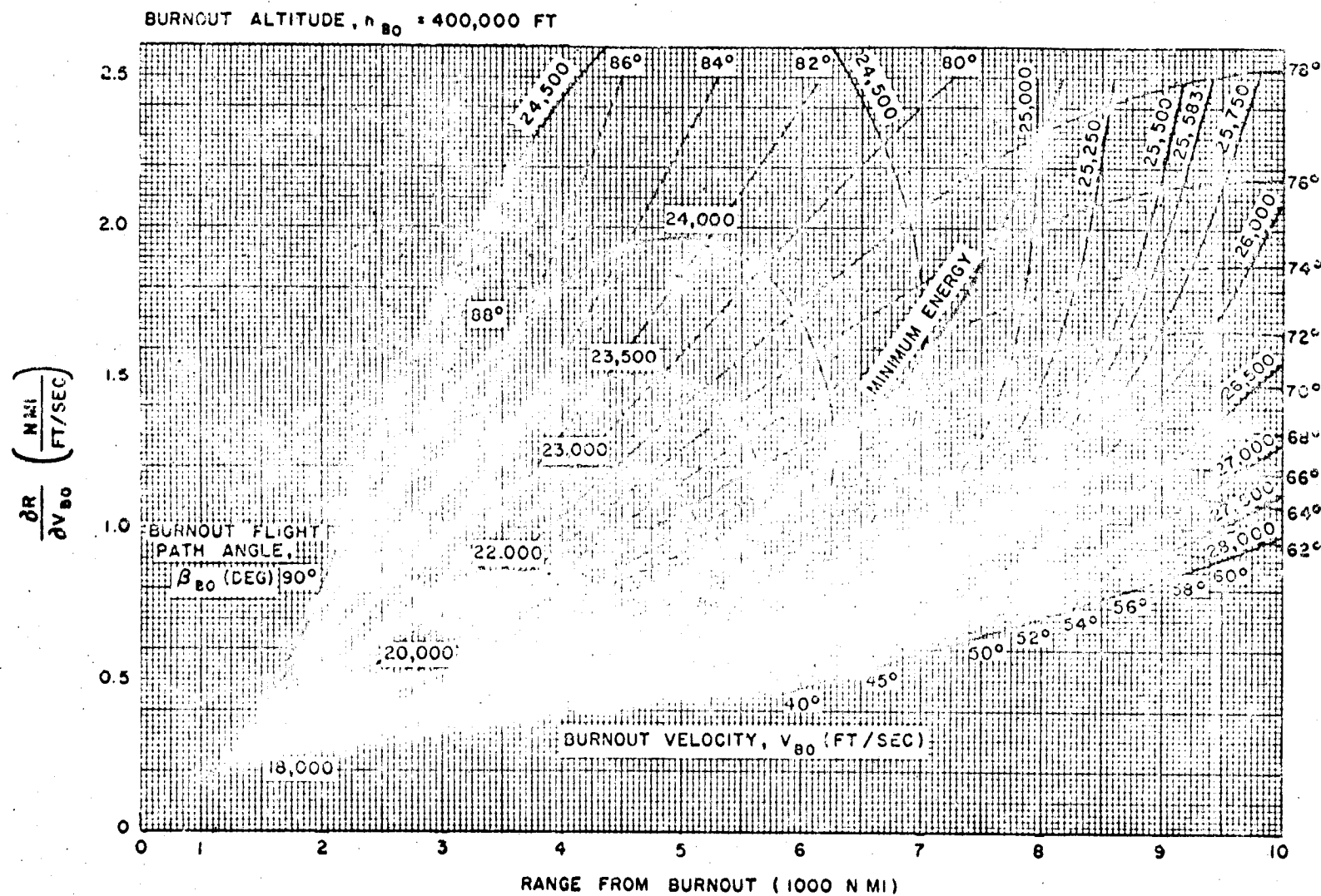


Figure 32. Burnout Velocity-Range Error Coefficient

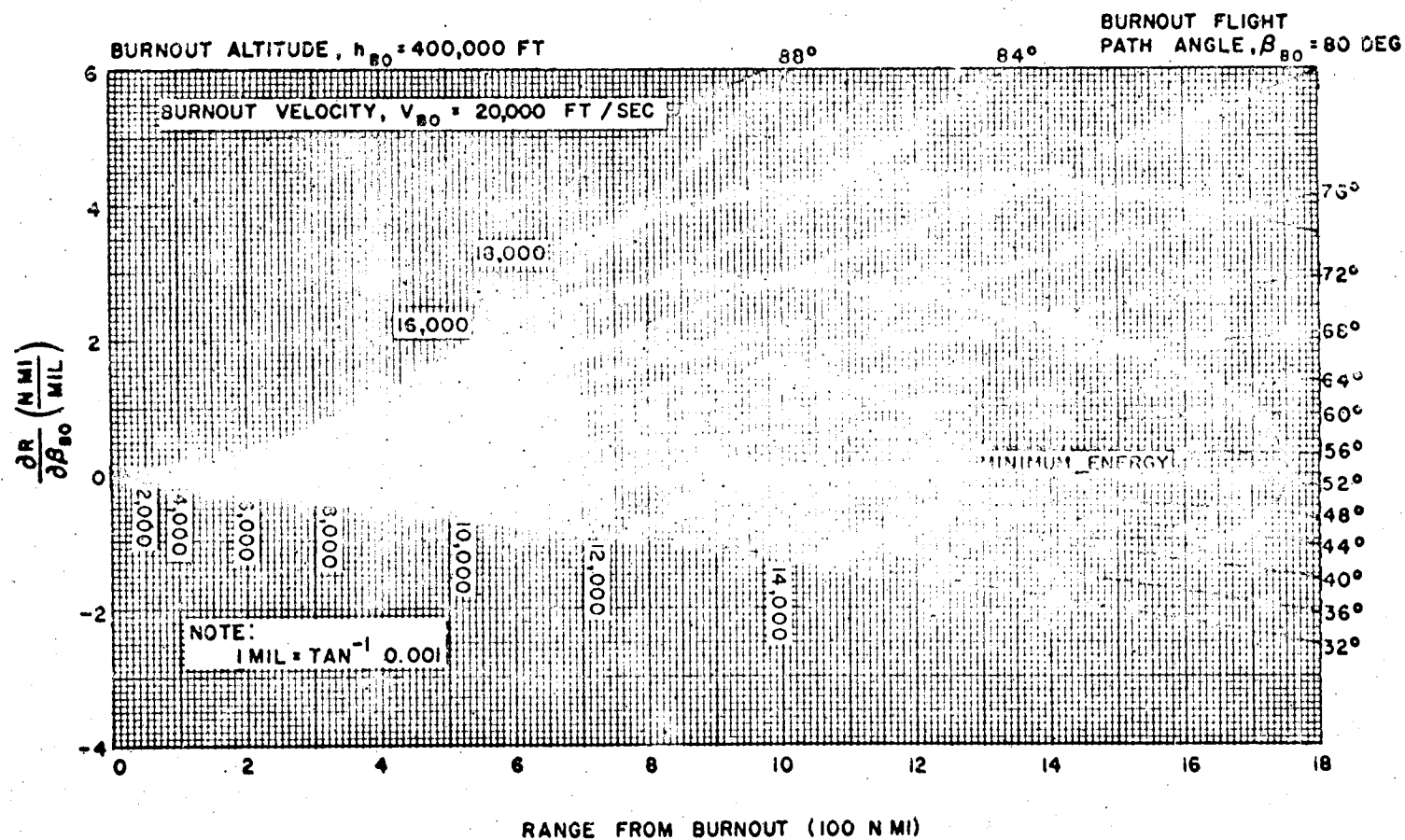


Figure 33. Burnout Flight Path Angle Error Coefficient

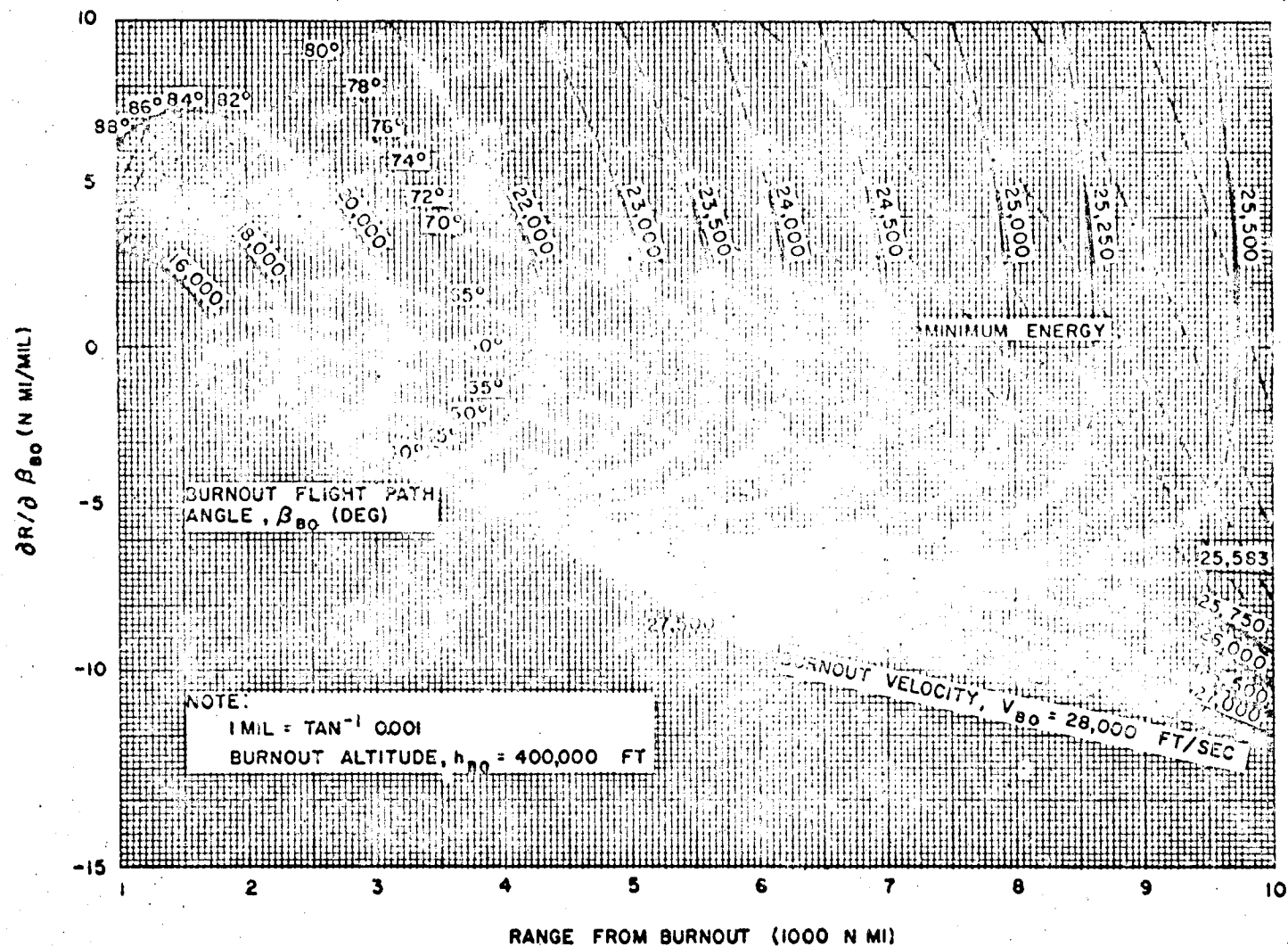


Figure 34. Burnout Flight Path-Angle Error Coefficient

SYSTEM CONSIDERATIONS

$$(\Delta R)_{h_{BO_i}} = \frac{\partial R}{\partial h_{BO_i}} \delta h_{BO_i}$$

and the crossrange dispersion is equal to

$$(\Delta R)_{A_{z_{BO_i}}} = r_e \frac{\sin \theta_{BO_i}}{\sin \beta_{BO_i}} \delta A_{z_{BO_i}}$$

where

$$\delta V_{BO_i}, \delta \beta_{BO_i}, \delta h_{BO_i} \text{ and } \delta A_{z_{BO_i}}$$

are the 3-sigma dispersions (or some other statistical measure of the engineer's own choice) of the burnout conditions.

The total downrange dispersion, assuming positive correlation of unity, is then equal to the sum of the individual downrange dispersions, and the crossrange dispersion is equal to the azimuth dispersion.

$$\pm (\Delta R)_{DR_i} = \pm \left(\left| (\Delta R)_{V_{BO_i}} \right| + \left| (\Delta R)_{\beta_{BO_i}} \right| + \left| (\Delta R)_{h_{BO_i}} \right| \right)$$

$$\pm (\Delta R)_{CR_i} = \pm \left| (\Delta R)_{A_{z_{BO_i}}} \right|$$

The assumption of unity correlation is ultraconservative but is essential since the degree of correlation will most likely be unknown. However, it is assumed that the downrange and crossrange errors are uncorrelated, which gives reasonably accurate results for the coordinate system chosen and since correlation changes only the orientation of the impact zone, not its size. Having computed

$$\pm (\Delta R)_{DR_i} \text{ and } \pm (\Delta R)_{CR_i}$$

these distances can now be laid out along the normal to the ground track at the stages' impact locations for every trajectory inclination, and ellipses can be sketched through the points at each impact location. Then, by overlaying the template on the map, possible range safety hazards are evident and the necessity for further study indicated. Some contemplated launch azimuths might also be eliminated if substantial portions of the impact zone are projected on land masses.

3.3 LOADS AND AERODYNAMIC HEATING

To be considered early in any preliminary design are the maximum anticipated loads and heating parameters. The analysis presented here yields these loads and parameters to a reasonable degree of accuracy so that design criteria can be formulated. Such things as the necessity for aerodynamic heating insulation, structural loads, time to jettison payload shroud, and staging problems would be indicated as a result of the analysis. The reader is referred to Reference 10 for a discussion of the structural aspects of space vehicle design. Dynamic pressure and Mach number at staging are important parameters for dynamic studies of staging. In preliminary design studies, the loads at both maximum acceleration and maximum dynamic pressure are determined by the structural engineer, and each piece of structure is designed with respect to the more critical load. The thermodynamicist is interested in the maximum heat rate and total heat input experienced by the vehicle during powered flight.

3.3.1 Staging

Of interest for structural considerations are axial acceleration and dynamic pressure just prior to staging. Assuming a rectilinear thrust-time curve, maximum acceleration occurs at burnout of each stage. Figure 35 provides data for obtaining the maximum acceleration of upper stages. It is a plot of axial acceleration at burnout as a function of the initial vacuum thrust-to-weight ratio and the mass ratio. To evaluate the maximum acceleration for atmospheric operation, the following equation is applied:

$$a_{BO} = \left\{ \left[1 - (1 - \lambda) \frac{p_{BO}}{p_o} \right] \frac{T_{vac}}{W_o} - \frac{q_{BO}}{W_o/C_{DA}} \right\} r$$

where

$$\frac{T_{vac}}{W_o} = \frac{1}{\lambda} \frac{T_{sl}}{W_o},$$

$$\lambda = \frac{I_{sp_{sl}}}{I_{sp_{vac}}}$$

and the drag coefficient, C_D , is at the hypersonic value.

The dynamic pressure at burnout, q_{BO} , is found from Figure 36 by using the burnout velocity and altitude computed in Chapter 2. The atmospheric pressure ratio at burnout, p_{BO}/p_o , is plotted against burnout altitude, h_{BO} , in Figure 37.

SYSTEM CONSIDERATIONS

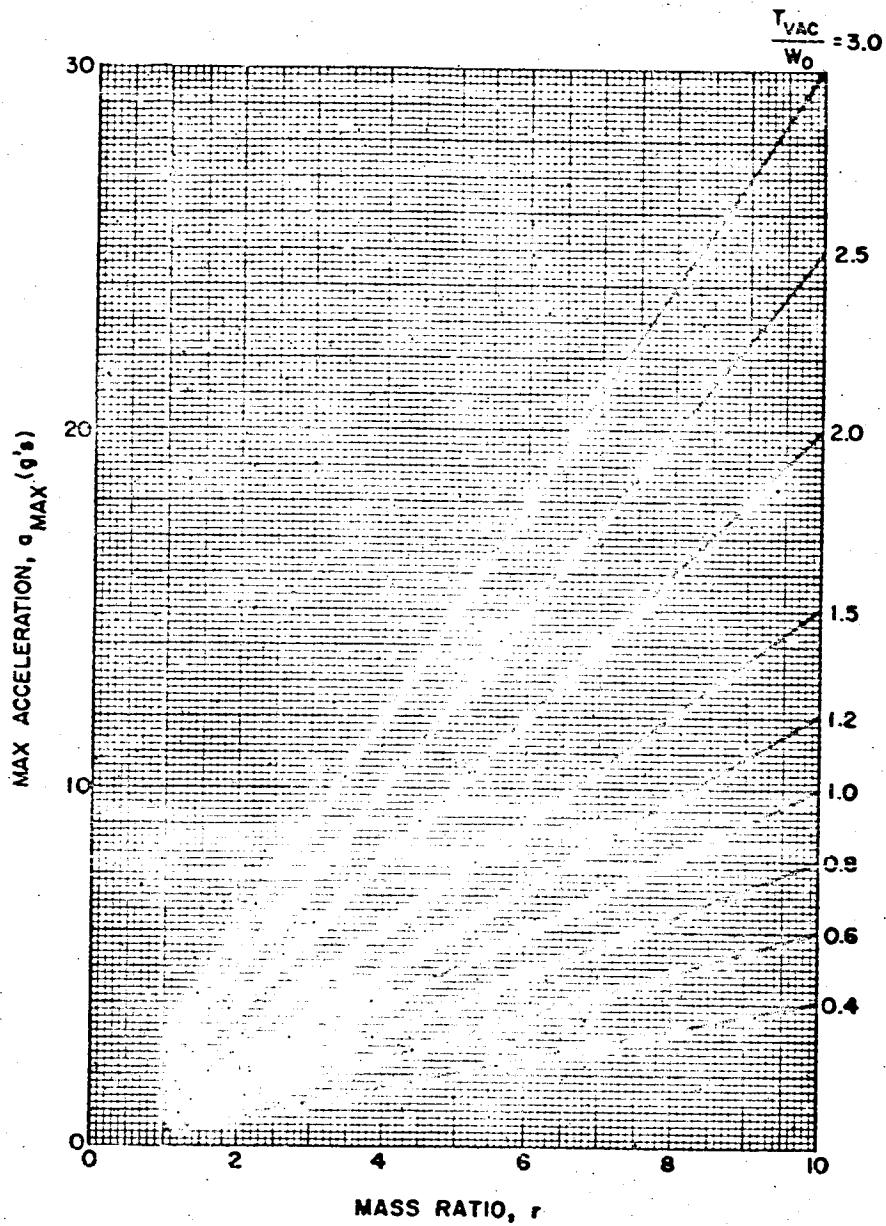


Figure 35. Axial Acceleration at Burnout (Vacuum Conditions)

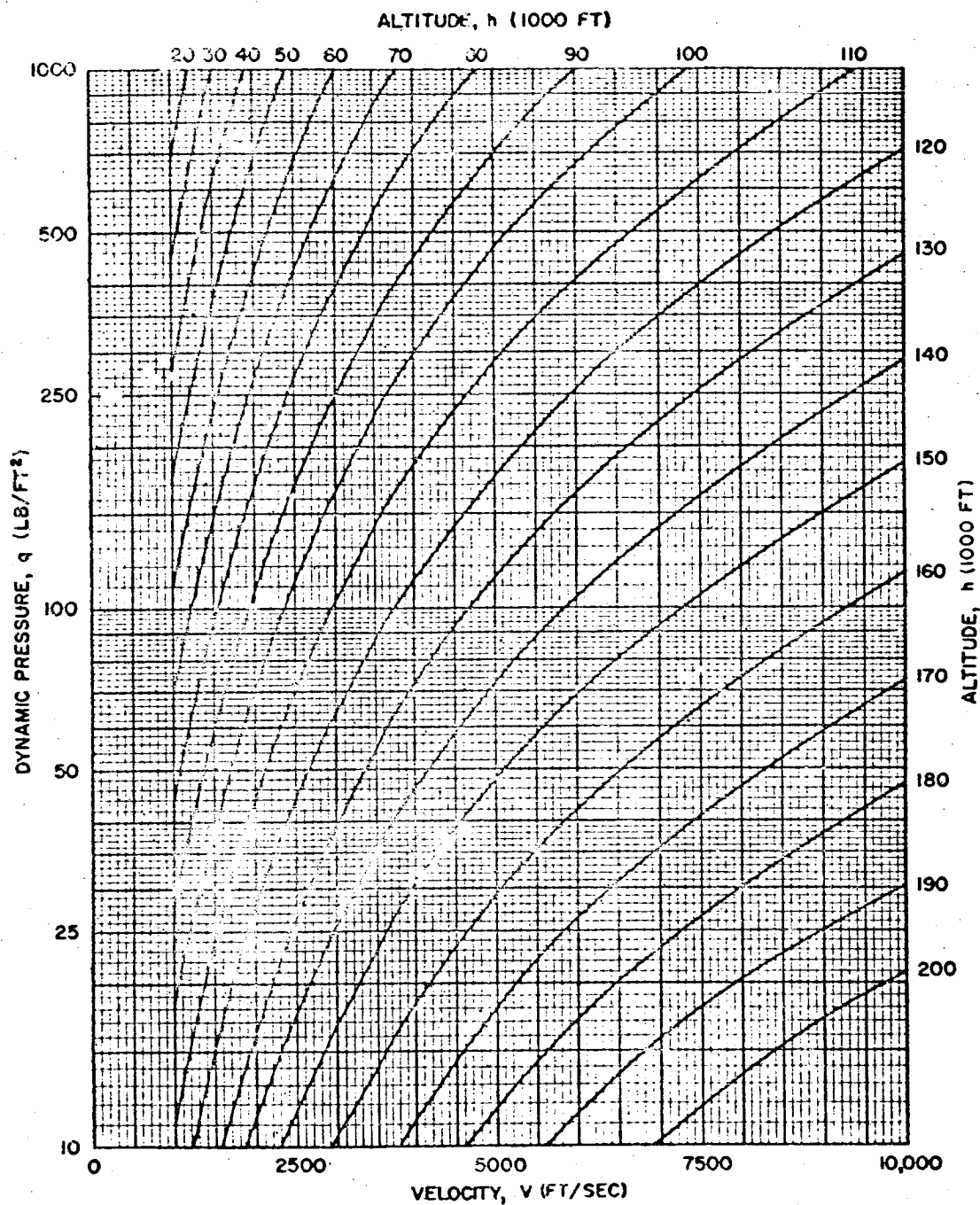


Figure 36. Dynamic Pressure During Stage Operation

NOTES: CONSIDERATIONS

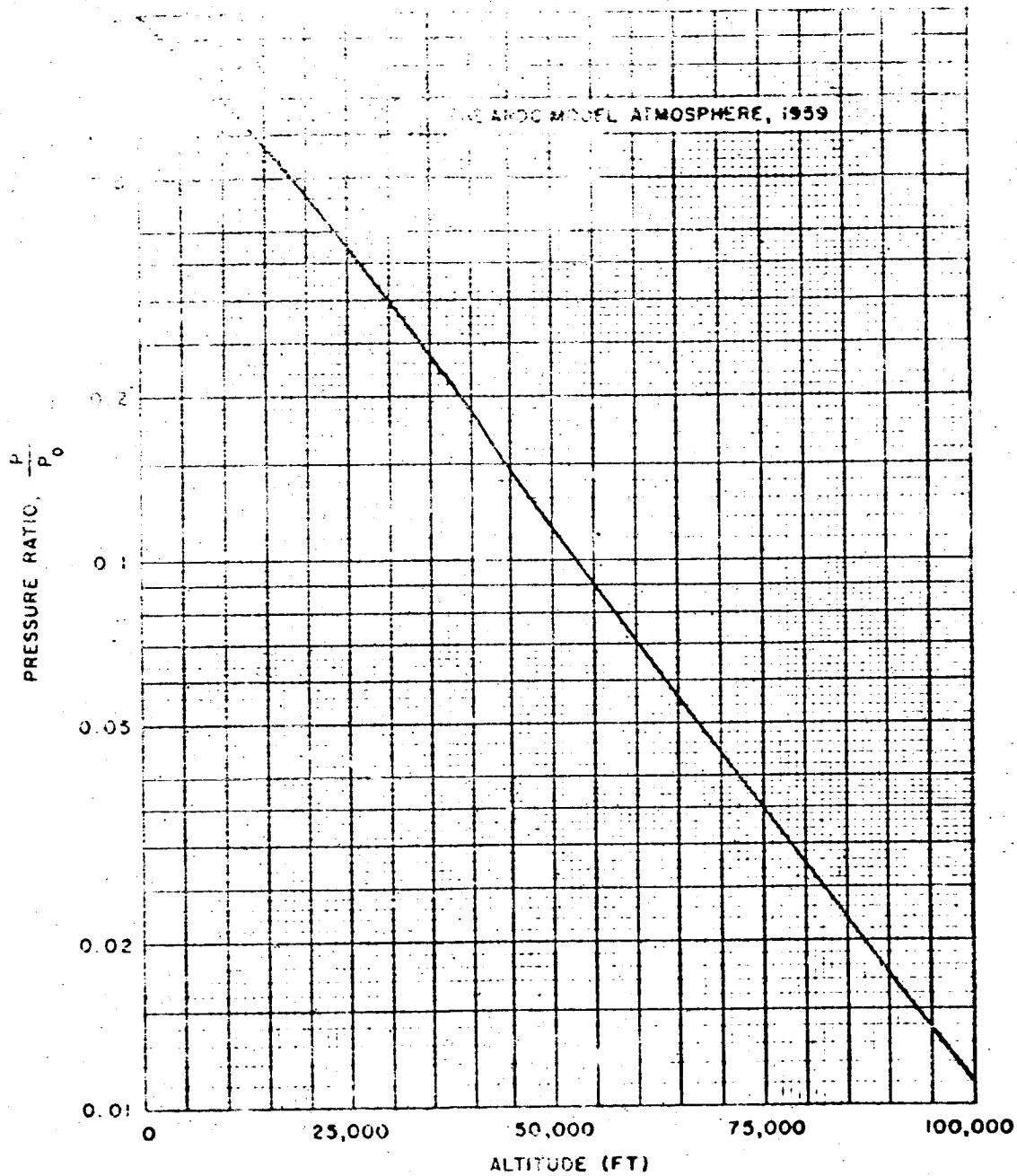


Figure 37. Pressure Ratio for Standard Atmosphere

3.3.2 Maximum Dynamic Pressure

The maximum dynamic pressure and associated axial acceleration during booster operation are of interest to the designer. The nomograph presented in figures 38a and 38b can be used to compute maximum dynamic pressure. This curve was derived empirically and is based on vehicle parameters representative of presently conceived vehicles. In constructing the curve, a rectilinear thrust-time variation was assumed, for other thrust-time variations, an initial thrust-to-weight ratio based on a mean thrust value will give reasonably accurate results.

From experience it has been found that maximum dynamic pressure occurs at altitudes between 30,000 and 35,000 feet. For space shots, maximum dynamic pressure usually occurs at altitudes near the upper limit 35,000 feet. For sounding rockets and highly lofted shots, maximum dynamic pressure occurs nearer the lower limit of 30,000 feet. Also maximum bending loads usually occur in these regions. This is caused by the fact that the greatest wind shears occur at altitudes between 30,000 and 40,000 feet.

To compute the axial acceleration at q_{\max} , the following equation is applied:

$$a_{q_{\max}} = a \left\{ 1 - (1 - \lambda) \frac{P_{q_{\max}}}{P_o} \right\} - \frac{q_{\max}}{\left(\frac{T_{\text{vac}}}{W_o} \right) \left(\frac{W_o}{C_D A} \right)}$$

where

$$\frac{T_{\text{vac}}}{W_o} = \frac{1}{\lambda} \frac{T_{sl}}{W_o}$$

To aid in finding acceleration Figures 39 and 40 are provided. Time of maximum dynamic pressure, $t_{q_{\max}}$, is presented in Figure 39; then, using $t_{q_{\max}}$ for t in Figure 40, the parameter a is found. Since no computation of velocity is made in finding q_{\max} , a curve of Mach number as a function of q_{\max} , Figure 41, is included. It can be used to obtain C_D at q_{\max} for computing $W_o/C_D A$. Mach number has been plotted for both the upper and lower altitude limits for occurrence of maximum dynamic pressure.

3.3.3 Heating

Knowing the maximum heating rate and the total heat input experienced by the vehicle during ascent through the atmosphere, the thermodynamicist can estimate, for instance, the necessity for aerodynamic heating insulation to protect structural elements and also optimize with respect to added insulation weight the boiloff of cryogenic propellants.

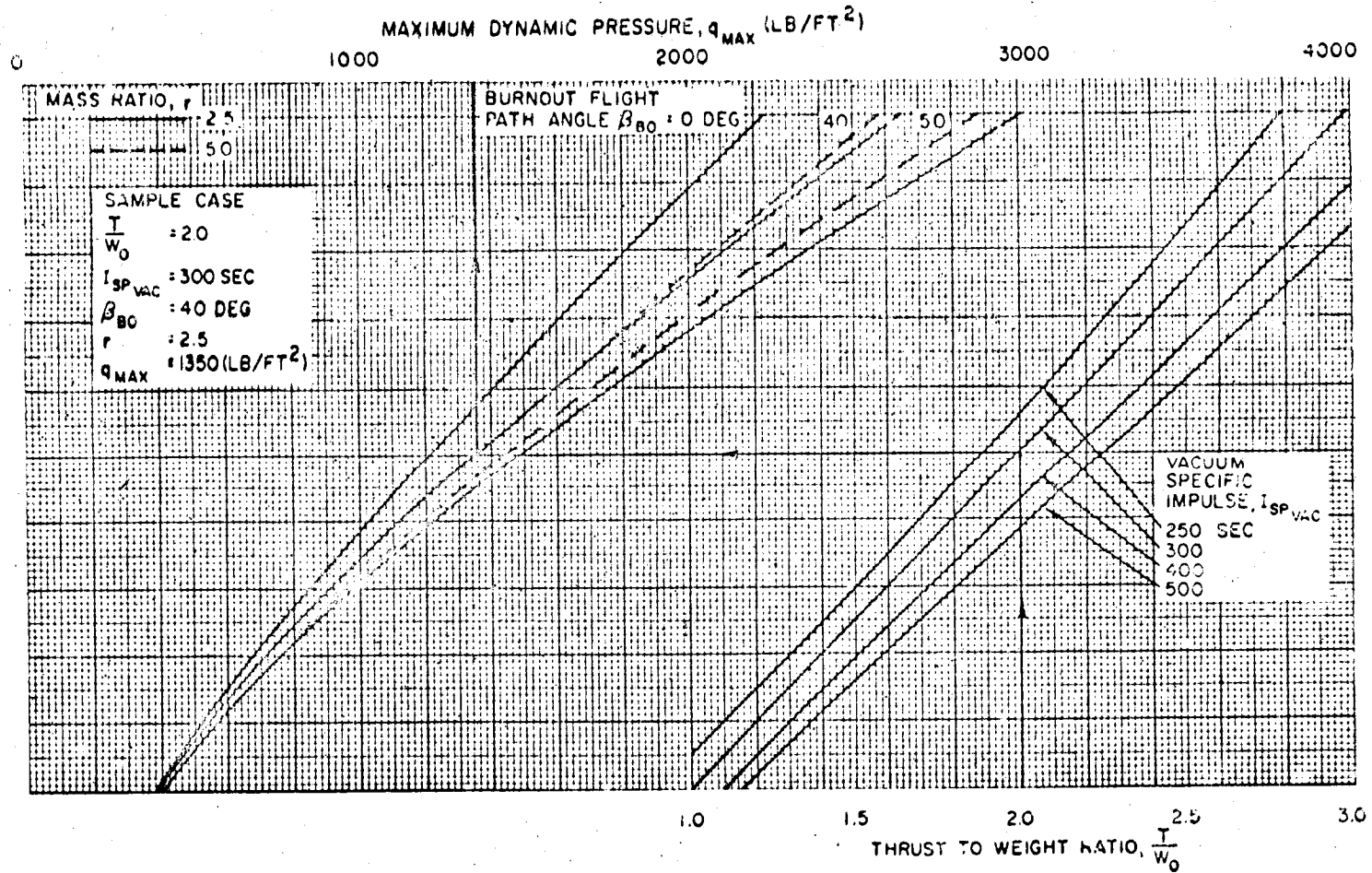


Figure 38a. Maximum Dynamic Pressure Nomograph

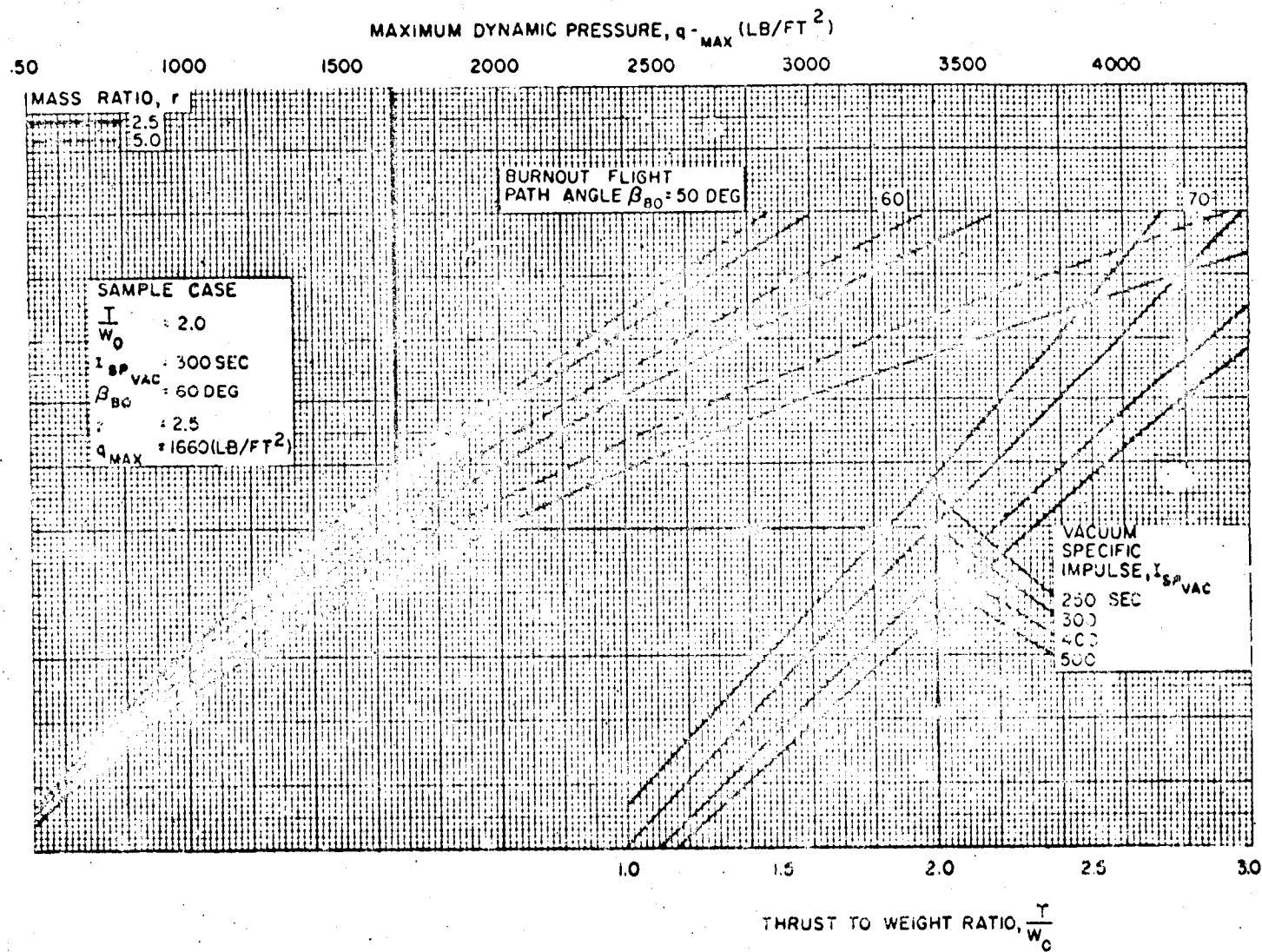


Figure 38b. Maximum Dynamic Pressure Nomograph

SYSTEM CONSIDERATIONS

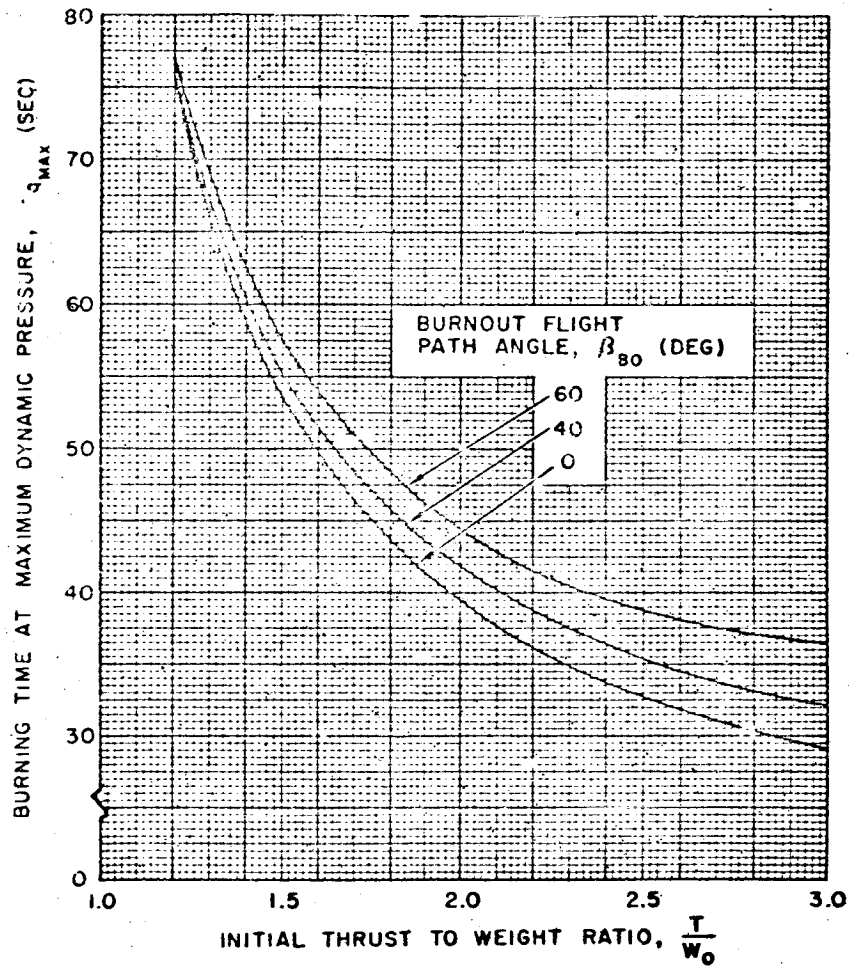


Figure 39. Time at Maximum Dynamic Pressure

Loads and Aerodynamic Heating

3-57

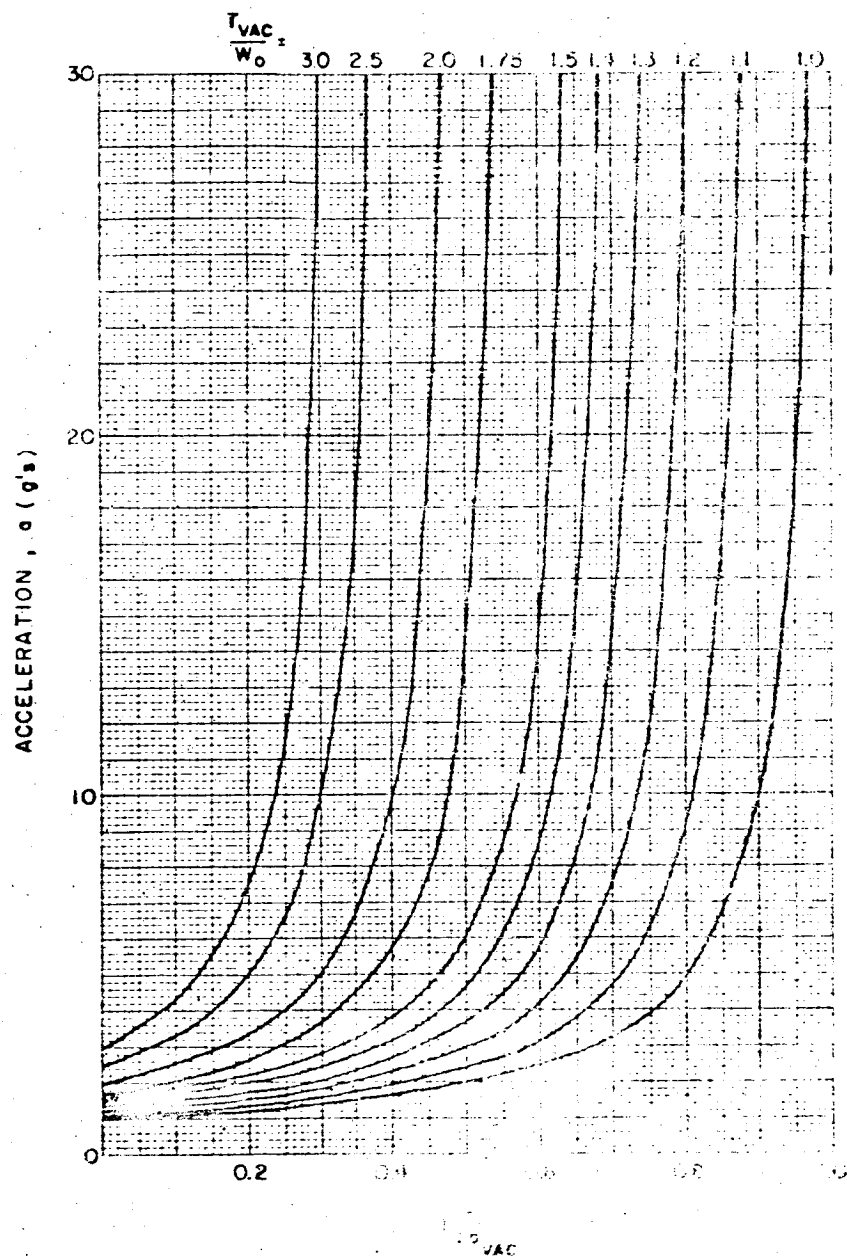


Figure 40. Axial Acceleration During Suez Operation (Vacuum Atmosphere)

3-58

SYSTEM CONSIDERATIONS

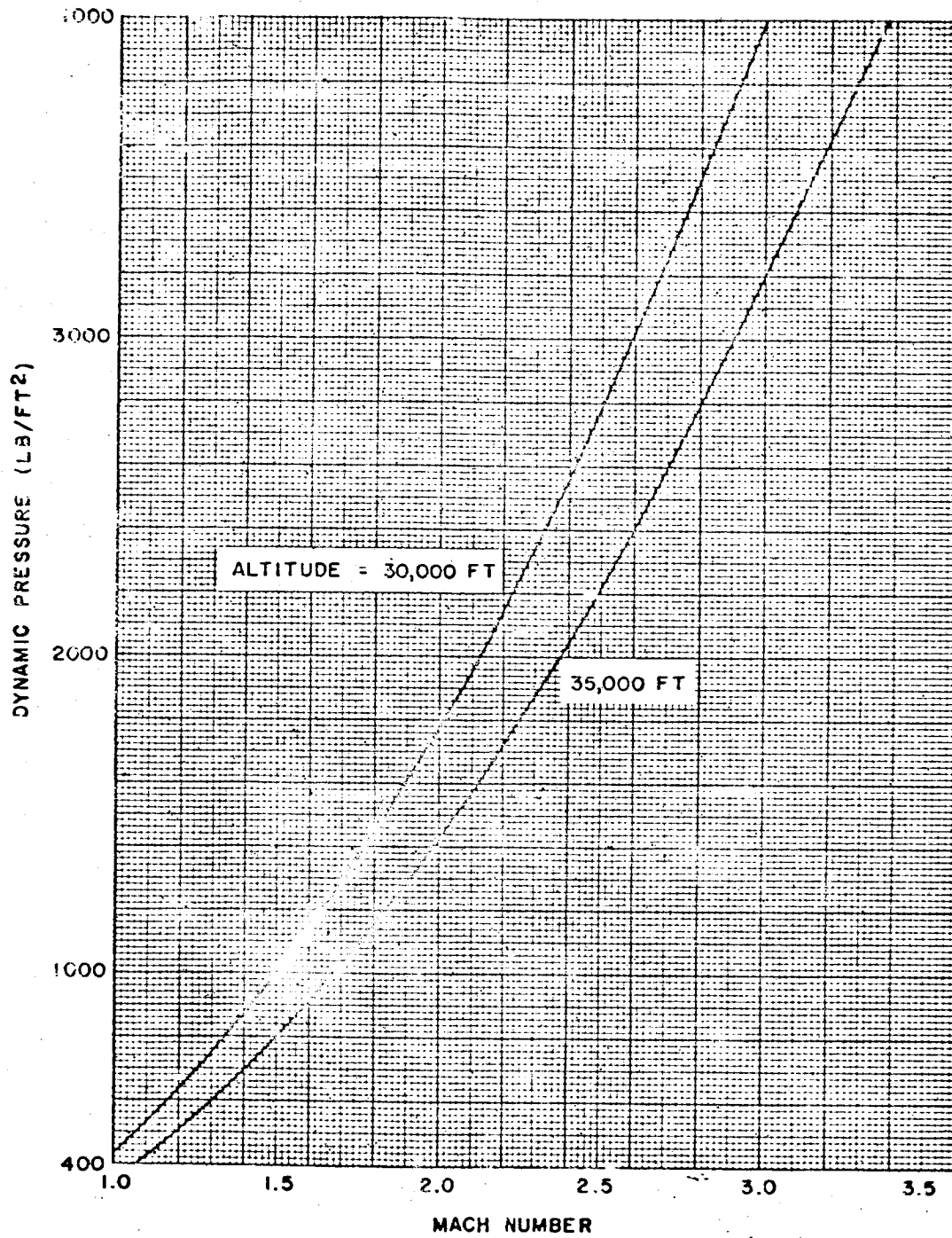


Figure 41. Mach Number at Maximum Dynamic Pressure

Maximum Heating Rate. The maximum value of the parameter, qV , experienced during booster operation is used as a convenient indicator of the maximum heating rate realized by the vehicle. This parameter has been plotted nomographically in Figure 42 as a function of the vehicle parameters.

Total Heat Input. The total heat input during booster operation, is approximated by $\int qV dt$. Although the integrated aerodynamic heat input may be proportional (within the limitations of the assumptions discussed in Appendix B) to $\int qV dt$, it is still necessary to determine if the temperature rise of the missile's external skin is also proportional to this parameter. Obviously, it is the skin temperature and not the aerodynamic heat input which determines when overheating conditions are approached. Numerous factors, in addition to the convective boundary layer input, determine the temperature rise: namely, the thickness and specific heat of the skin, thermal conductivity and emissivity, the presence of insulation, the proximity of heat sinks such as structural members, heat losses to pressurizing gases inside propellant tanks, etc. It has been STL's experience that the total heating indicator, $\int qV dt$, and the maximum heating rate indication, $\int qV_{\max}$, must be calibrated for each booster vehicle by actual skin temperature calculations to establish the maximum safe value. Any trajectory involving this booster may then be quickly evaluated from the standpoint of aerodynamic heating solely on the basis of the heating indicator. Current liquid propellant space boosters have total heating parameters on the order of 0.85 to 1.2×10^8 ft-lb/ft², whereas Saturn and Nova-type vehicles are apt to have total heating parameters on the order of 0.6 and 0.8×10^8 ft-lb/ft². High initial thrust-to-weight ratio, solid-propellant vehicles are apt to have total heating parameters up to 4 to 6×10^8 ft-lb/ft². The total heating parameter has also been presented nomographically as a function of the vehicle first-stage parameters in Figure 43. Though heating is experienced during second-stage operations it is found that the total integral is nearly independent of the second-stage parameters.

3.4 GUIDANCE AND TRACKING

The shaping of a boost phase trajectory is dependent not only on vehicle performance and loads considerations, but also on the effects of the trajectory characteristics on guidance and tracking. It is the object of this section to discuss briefly several parameters that are a function of guidance and tracking characteristics, which in many cases actually dictate the type of trajectory to be used.

Generally speaking, the parameters imposing guidance restrictions are related to radio guidance methods where continuous contact between the ground and vehicle is necessary. The self-contained nature of inertial guidance allows communication contact with the ground to be held to a minimum or eliminated. Tracking, on the

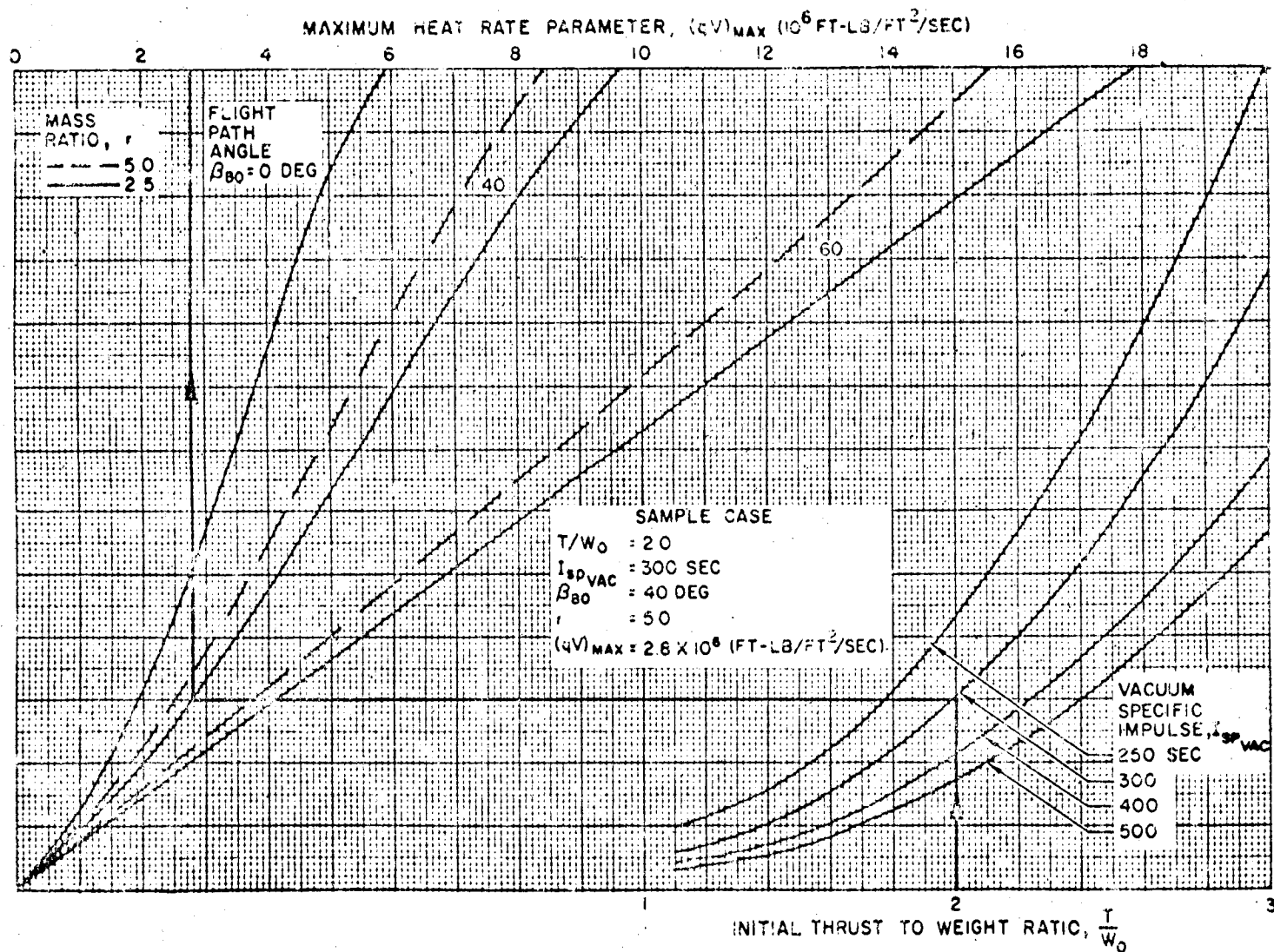


Figure 42. Maximum Heat Rate Parameter Nomograph

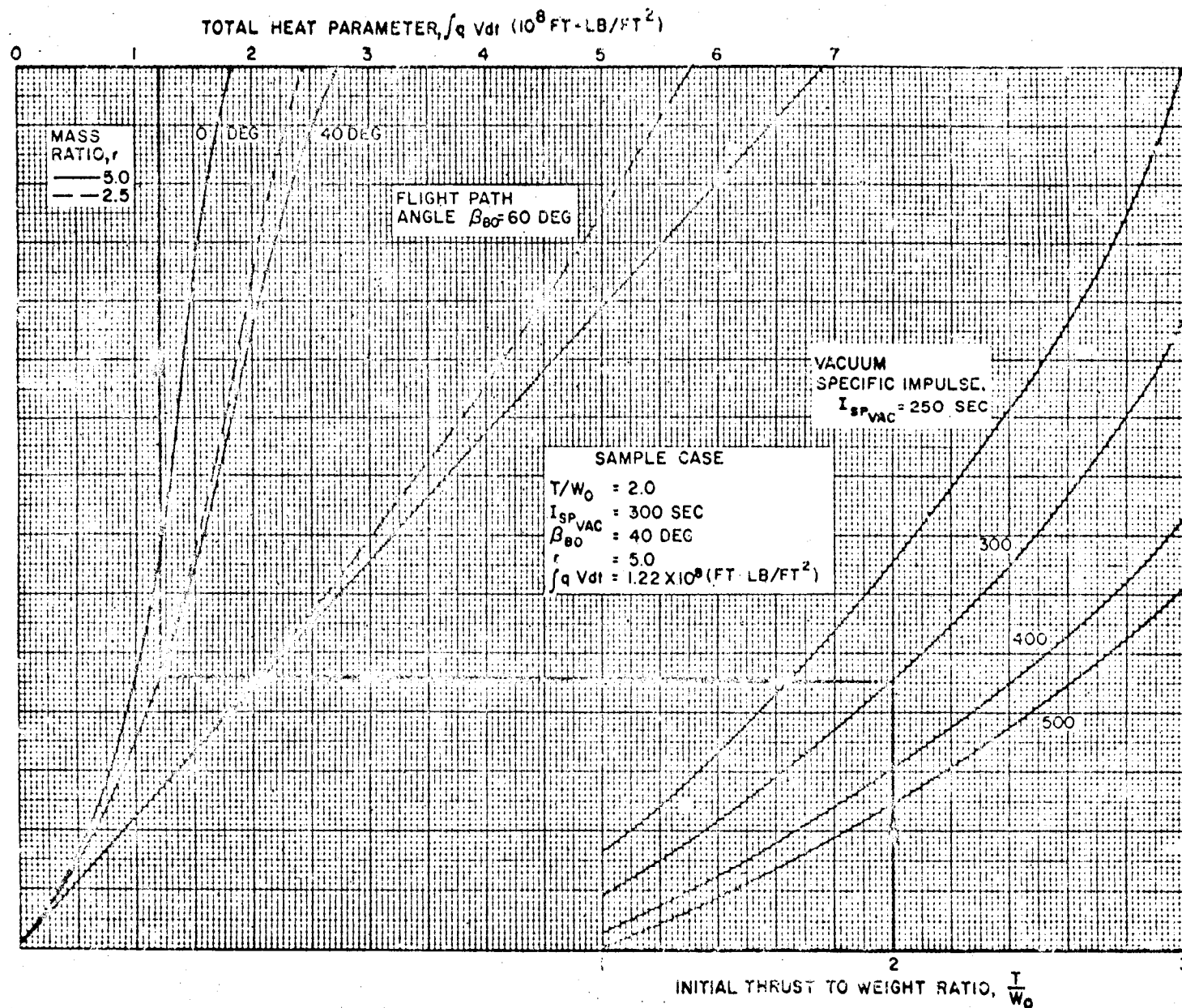


Figure 43. Total Heat Parameter Nomograph

other hand, is required in all systems for range safety. Also, future programs involving manned flight will require essentially continuous tracking and communications.

3.4.1 Elevation Angle

In both radio guidance and tracking, the elevation angle, ζ , is of interest. As shown in Figure 44, ζ is the angle between the line of sight to the vehicle and the horizontal as measured from the location of interest. Typically, the line of sight is the radar beam for the guidance or tracking radar. As the elevation angle approaches values less than 5 degrees, the radar's effectiveness is greatly reduced due to interference from the atmosphere and earth's surface. Keeping this in mind, it is easily seen that a vehicle requiring constant radar contact with a specific location must follow a trajectory with an elevation angle time history that stays above the allowable minimum, usually set between 5 and 10 degrees.

During powered flight, the radar location for radio guidance is usually in or near the vicinity of the launch site and thus

$$\zeta = \cos^{-1} \left[\frac{(r_e + h) \sin \theta}{\bar{R}} \right]$$

where

θ = range angle from launch site

r_e = radius of the earth

h = vehicle altitude

\bar{R} = slant range.

The slant range, \bar{R} , is the range from the radar location to the vehicle measured along the line of sight.

$$\bar{R} = \sqrt{(r_e + h)^2 + r_e^2 - 2r_e(r_e + h) \cos \theta}$$

Figure 45 presents the elevation angle as a function of range angle for various vehicle altitudes. The range angle and altitude are determined from the vehicle performance analysis in Chapter 2 for both first and upper stages.

Several stations used for vehicle tracking are located off the vehicle trajectory. Thus, the equations for elevation angle and slant range are valid only when the range angle, θ , is the value between the vehicle and the station of

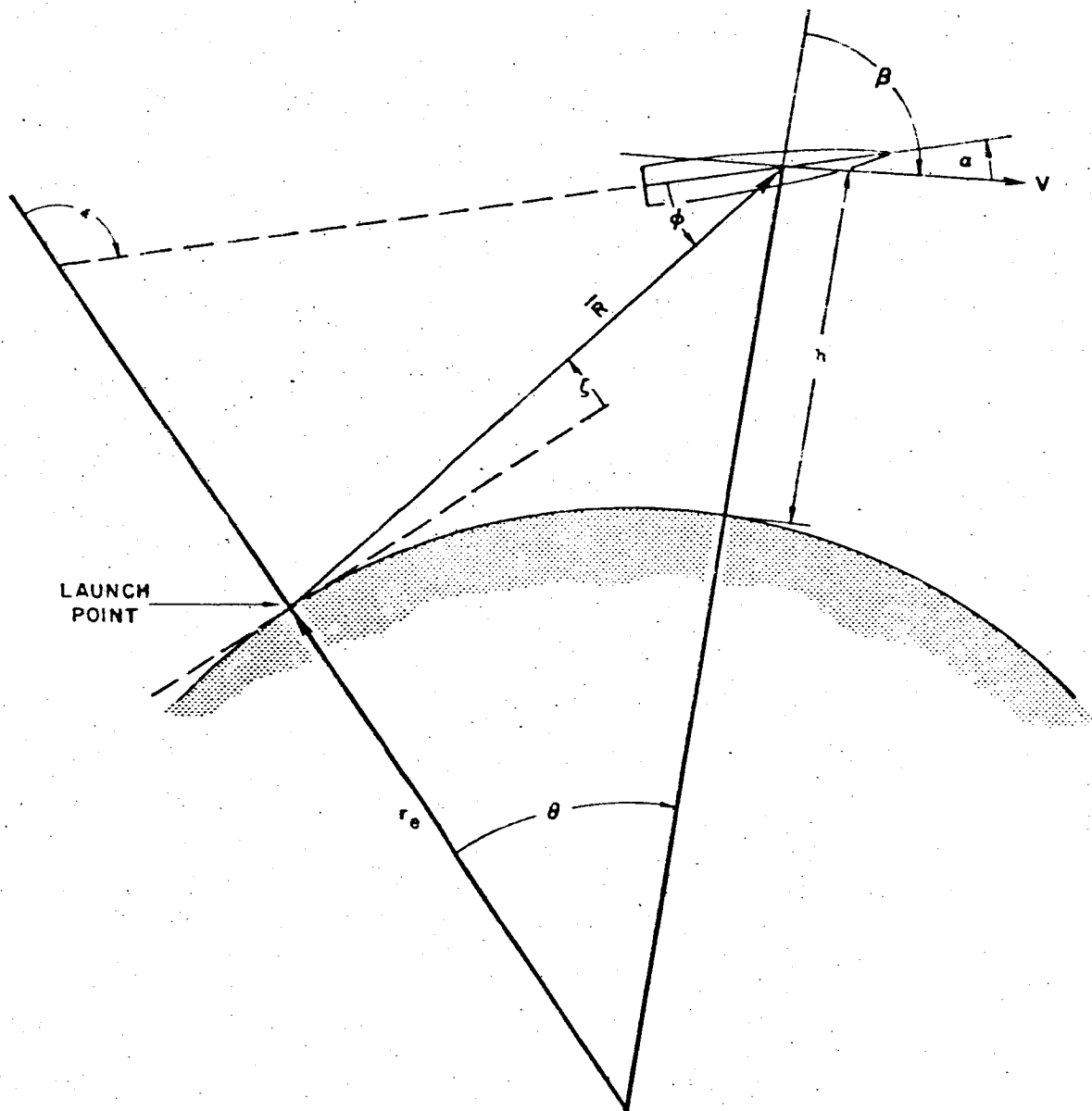


Figure 44. Guidance and Tracking Coordinate System

SYSTEM CONSIDERATIONS

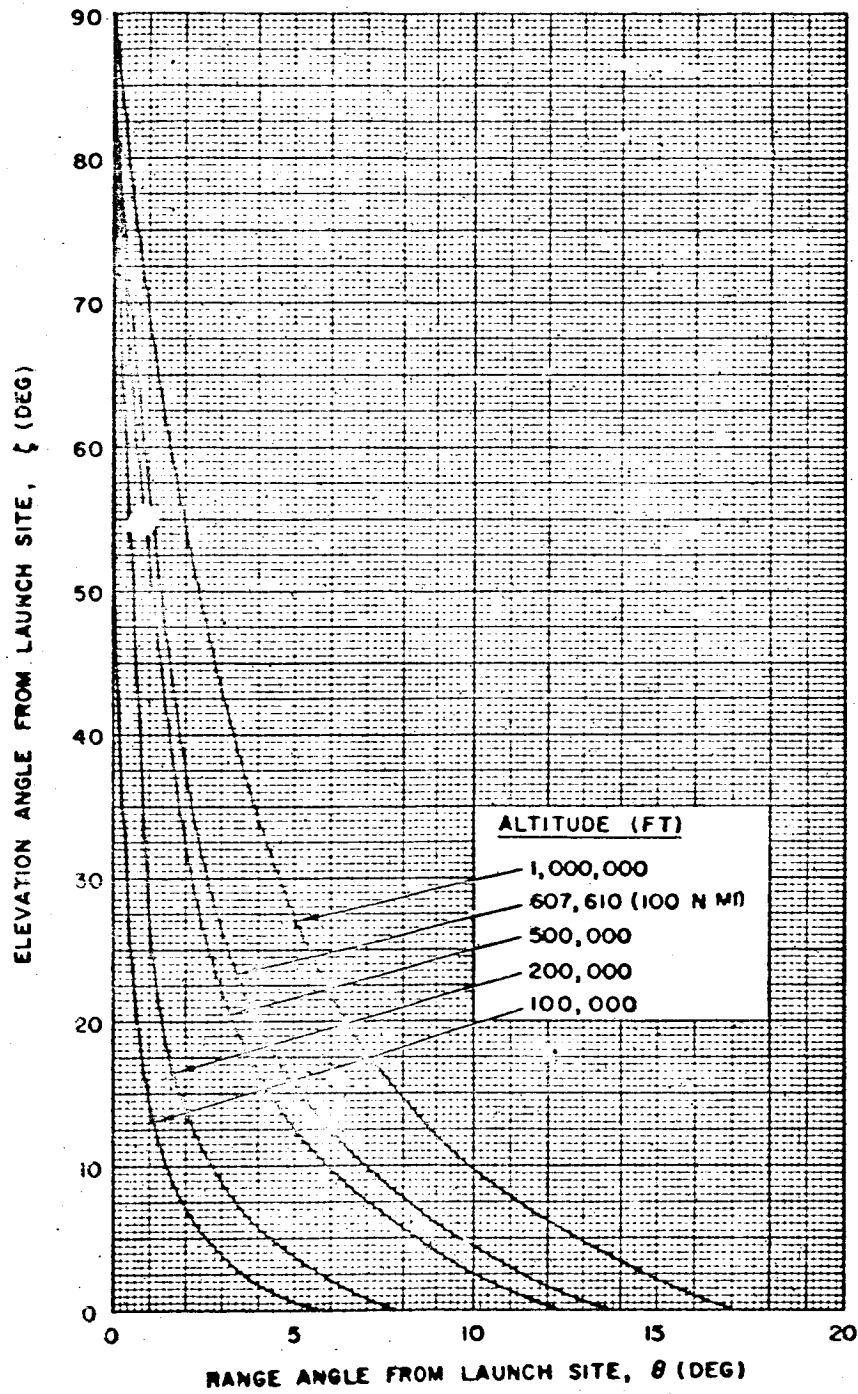


Figure 45. Launch Vehicle Elevation Angle

interest. Referring to the diagram below, the range angle between the launch site and the station location is

$$\theta_{L-S} = \cos^{-1} (\sin \lambda_L \sin \lambda_S + \cos \lambda_L \cos \lambda_S \cos |\phi_L - \phi_S|)$$

where

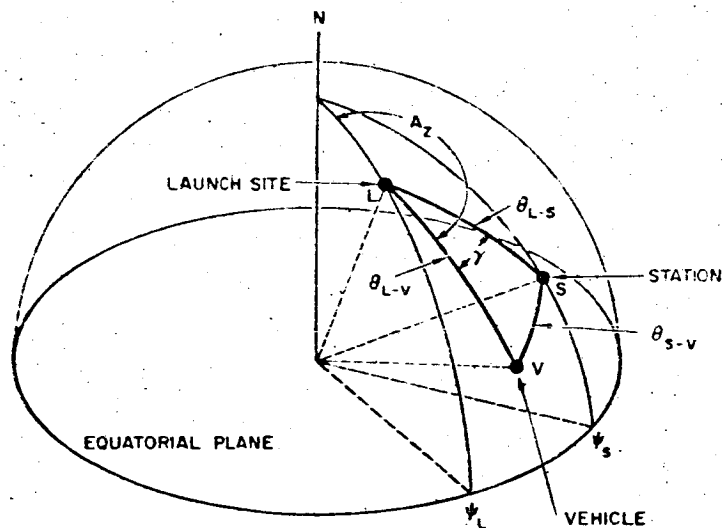
λ_L = launch site latitude (positive north)

λ_S = station latitude (positive north)

ϕ_L = launch site longitude

ϕ_S = station longitude

$| \quad |$ = refers to absolute magnitude.



Given the station location with respect to the launch location, the range angle from the station to the vehicle can be found by the following set of equations. Using θ_{L-S} , the angle between the plane of the trajectory and the plane containing the launch site and station location, γ , can be found from

$$\gamma = \left| A_z - \sin^{-1} \left[\frac{\sin |\phi_L - \phi_S| \sin \theta_{L-S}}{\cos \lambda_S} \right] \right| \text{ for } \phi_L \neq \phi_S$$

or

$$\gamma = \left| A_z - 360^\circ + \sin^{-1} \left[\frac{\sin |\phi_L - \phi_S| \sin \theta_{L-S}}{\cos \lambda_S} \right] \right| \text{ for } \phi_L = \phi_S$$

θ_{S-V} can be found from

$$\theta_{S-V} = \cos^{-1} (\cos \theta_{L-V} \cos \theta_{L-S} + \sin \theta_{L-V} \sin \theta_{L-S} \cos \gamma)$$

where θ_{L-V} is obtained from the vehicle performance analysis in Chapter 2. Having found θ_{S-V} , the plot of elevation angle as a function of range angle (Figure 45) can be used to determine the elevation angle at the station of interest.

3.4.2 Vehicle Angular Displacement

The angular rotation, ϵ , of the vehicle's centerline in the pitch plane is of interest in both guidance and tracking. For guidance systems using gyros, the angular rotation of the gyros with respect to the vehicle during flight is a measure of vehicle attitude. In the case of the inertial guidance system, ϵ is a measure of the angular orientation of the stable platform and the vehicle axis. Generally, gyros have a limit as to the amount of rotation allowed, and thus knowledge of the vehicle attitude is required so that this limit is not exceeded. For the usual vehicle, the limit of gyro rotation is not reached until late in the flight, if at all.

For radio guidance and tracking, the vehicle attitude determines the portion of the vehicle antenna pattern seen by the radar. Vehicle attitude might cause loss of contact due to the interference of the exhaust gases. The parameter determining whether or not interference will result is look angle, ϕ , which is shown to be a function of ϵ in the following section.

The equation for ϵ with respect to the launch vertical (see Figure 44) is

$$\epsilon = \beta + \theta - \alpha$$

where

β = flight path angle

θ = range angle

α = angle of attack

The parameters β , θ , and α are determined in the vehicle performance analysis in Chapter 2.

3.4.3 Look Angle

Look angle ϕ is the parameter that determines the portion of antenna pattern seen by the tracking or guiding radar. Physically, ϕ is the angle between the missile axis and the radar beam or slant range vector, as shown in Figure 44. As the look angle approaches zero, the radar is essentially looking straight into the exhaust plume. Due to the ionized gases in the plume, contact with the antenna is lost.

Experience has shown that if the look angle remains greater than 3 to 5 degrees, contact will not be lost. Since stations not in the plane of the trajectory will not experience loss of contact, the only radar location considered here is at the launch site.

The equation for look angle in terms of known trajectory parameters is

$$\phi = \zeta + \epsilon - 90^\circ$$

where

ζ = elevation angle

ϵ = vehicle attitude angle.

3.5 PERFORMANCE MARGIN CONCEPT

As discussed in Chapter 2, Section 2.1, the performance requirements for a space mission can typically be defined in terms of a required injection velocity at some specified altitude and flight path angle. The determination of booster vehicle payload capability for a mission involves the achievement of the associated specified burnout conditions prior to propellant depletion and without violating certain system constraints. Since most of the variables significantly affecting vehicle performance are random, the statistics of the composite variables must be considered in a quantitative assessment of vehicle payload capabilities.

Several techniques of varying complexity have been derived to treat the statistical aspects of system performance.¹¹ The choice of one over another depends on the objectives of the analysis being performed. A proven technique applicable to most system design studies is to base performance estimates on expected or nominal design parameters and allow a margin for contingencies. This technique is particularly suited for preliminary design analysis, since the margin can be evaluated using best estimates of dispersions of individual system variables and linear exchange ratios which can, in most cases, be estimated analytically.

The performance margin is derived as a velocity margin or "pad" but it can be expressed, if desired, as an equivalent propellant reserve using the appropriate exchange ratio.

3.5.1 Discussion of Performance Margin Analysis

The effect on nominal system performance of perturbation of a single performance variable, say specific impulse of the i th stage, is expressed as an equivalent velocity increment through the use of a linear exchange ratio as follows:

$$\delta V = \left(\frac{\partial V}{\partial I_{sp_{vac,i}}} \right) \delta I_{sp_{vac,i}}$$

SYSTEM CONSIDERATIONS

and the total 1-sigma degradation of system performance due to perturbations of M variables is treated as the root sum square (RSS) of M statistically independent variables

$$\sigma_{\delta V}^2 = \sum_{j=1}^M \left[\left(\frac{\partial V}{\partial X_j} \right) \sigma_{\delta X_j} \right]^2$$

where

$\sigma_{\delta V}$ = 1-sigma velocity margin

$\sigma_{\delta X}$ = 1-sigma perturbation of performance variable X_j

The selection of the actual performance margin will depend upon the exigencies of the particular system being analyzed; however, in most design studies a 3-sigma perturbation of each performance variable is allowed.

The variables to be considered in the evaluation of the margin will again depend upon the particular system being analyzed, although past experience has shown that the margin is primarily a function of a few key variables. For a solid-propellant system these variables would include thrust, specific impulse, inert weight, payload weight, and expendable propellants in each stage. An additional important variable for liquid bipropellant systems is outage (the amount of one propellant remaining above its minimum level for steady operation when the mass of the other propellant has been expended to its minimum level for steady operation). For vehicles utilizing an open-loop flight control system, pitch programmer errors may be a significant variable. The effects of variations of aerodynamic forces and velocity losses due to guidance steering are relatively small and may be neglected in most cases.

The exchange coefficients, or partial derivatives, required to evaluate the performance margin are best determined from digital computer simulations of the system and mission being considered. A nominal trajectory based on the expected or nominal values of all system variables is first synthesized such that all system constraints are satisfied and the required burnout conditions are achieved just prior to propellant depletion. The linearized coefficients are then computed by independently perturbing each performance variable, determining the effect on attainable burnout velocity relative to the nominal trajectory, and forming the ratio representing the partial derivative of velocity with respect to the variable perturbed. In each "perturbed" flight the required burnout conditions are achieved by adjusting the appropriate trajectory constants or preferably by a closed-loop guidance simulation. The magnitude of the perturbation of each variable is generally taken at one or two times its standard deviation.

Alternatively, if less accurate results are acceptable or a computer simulation is not available, most exchange coefficients can be derived analytically from

the expression for theoretical burnout velocity in Appendix B Section 5, analytical expressions are derived which relate perturbations of stage inert weight, propellant weight, burnout weight, specific impulse, and thrust to perturbations of burnout velocity. The results obtained there are summarized in Table 3.

Table 3. Summary of Velocity Exchange Coefficients for Computing Vehicle Performance Margins

Stage Parameter	Coefficients	Units
Inert Weight	$\frac{dV}{dW_{ST_n}} = \sum_{i=1}^n \left(\frac{g \text{ Isp}_{vac}}{W_O} \right)_i (1 - r_i)$	(ft/sec/lb)
Payload Weight	$\frac{dV}{dW_{PL}} = \frac{dV}{dW_{ST_n}}$	(ft/sec/lb)
Burnout Weight	$\frac{dV}{dW_{BO_n}} = \left(\frac{g \text{ Isp}_{vac}}{W_O} \right)_n \left[r_n - \frac{\lambda_n \cos \bar{\beta}_n}{(T/W_O)_n} \right]$	(ft/sec/lb)
Propellant Weight	$\frac{dV}{dW_{P_n}} = \left(\frac{dV}{dW_{ST_n}} - \frac{dV}{dW_{BO_n}} \right)$	(ft/sec/lb)
Specific Impulse	$\frac{dV}{d \text{ Isp}_n} = g \left[\ln r_n - \frac{\lambda_n \cos \bar{\beta}_n}{(T/W_O)_n} \left(1 - \frac{1}{r_n} \right) \right]$	(ft/sec/sec)
Thrust	$\frac{dV}{dT_n} = \frac{\lambda_n g \text{ Isp}_{vacn} \cos \bar{\beta}_n}{100 (T/W_O)_n} \left(1 - \frac{1}{r_n} \right)$	(ft/sec/percent)

To facilitate margin evaluation, the analytical exchange ratios presented in Table 3 are plotted in Figures 46 through 49 for representative values of the performance parameters. In Figure 46 the ratio of burnout velocity to stage inert weight, normalized with respect to stage initial weight, is plotted as a function of stage mass ratio and specific impulse. The data presented are for a single-stage vehicle, but can also be used to evaluate ratios for the upper stages of a multi-stage vehicle by summing the ratio for each lower stage. In Figure 47 the ratio of burnout velocity to stage burnout weight, normalized with respect to stage initial weight, is plotted as a function of stage mass ratio, specific impulse, and parameter, $\frac{\lambda \cos \bar{\beta}}{T/W_O}$. The ratio of burnout velocity to specific impulse is plotted in Figure 48 as a function of stage mass ratio and $\frac{\lambda \cos \bar{\beta}}{T/W_O}$, and the ratio of burnout velocity to thrust is plotted in Figure 49 as a function of stage mass ratio, specific impulse, and $\frac{\lambda \cos \bar{\beta}}{T/W_O}$.

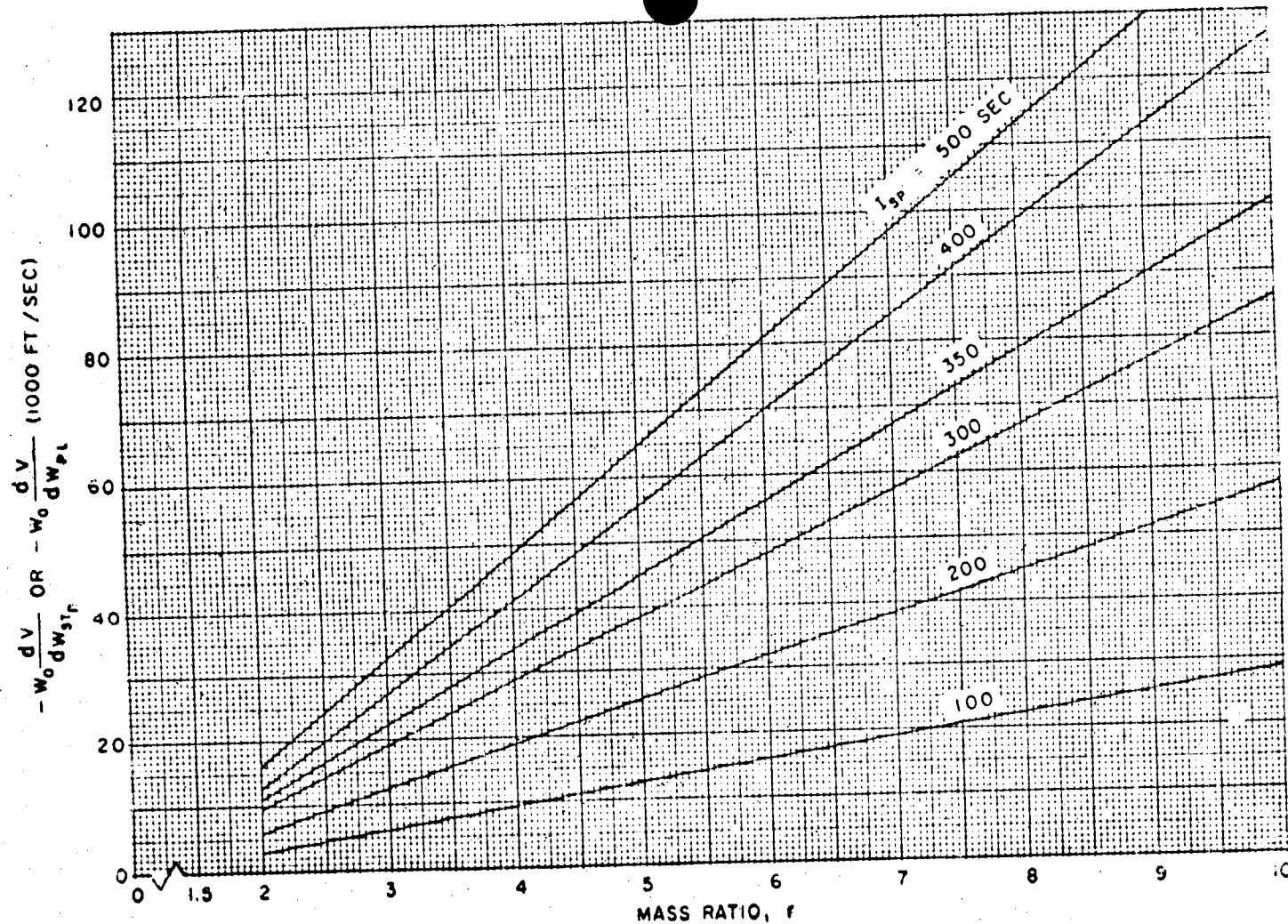


Figure 46. Structural Weight and Payload Weight Velocity Exchange Coefficient (One-Stage)

SYSTEM CONSIDERATIONS

RE-ORDER NO. 62-256

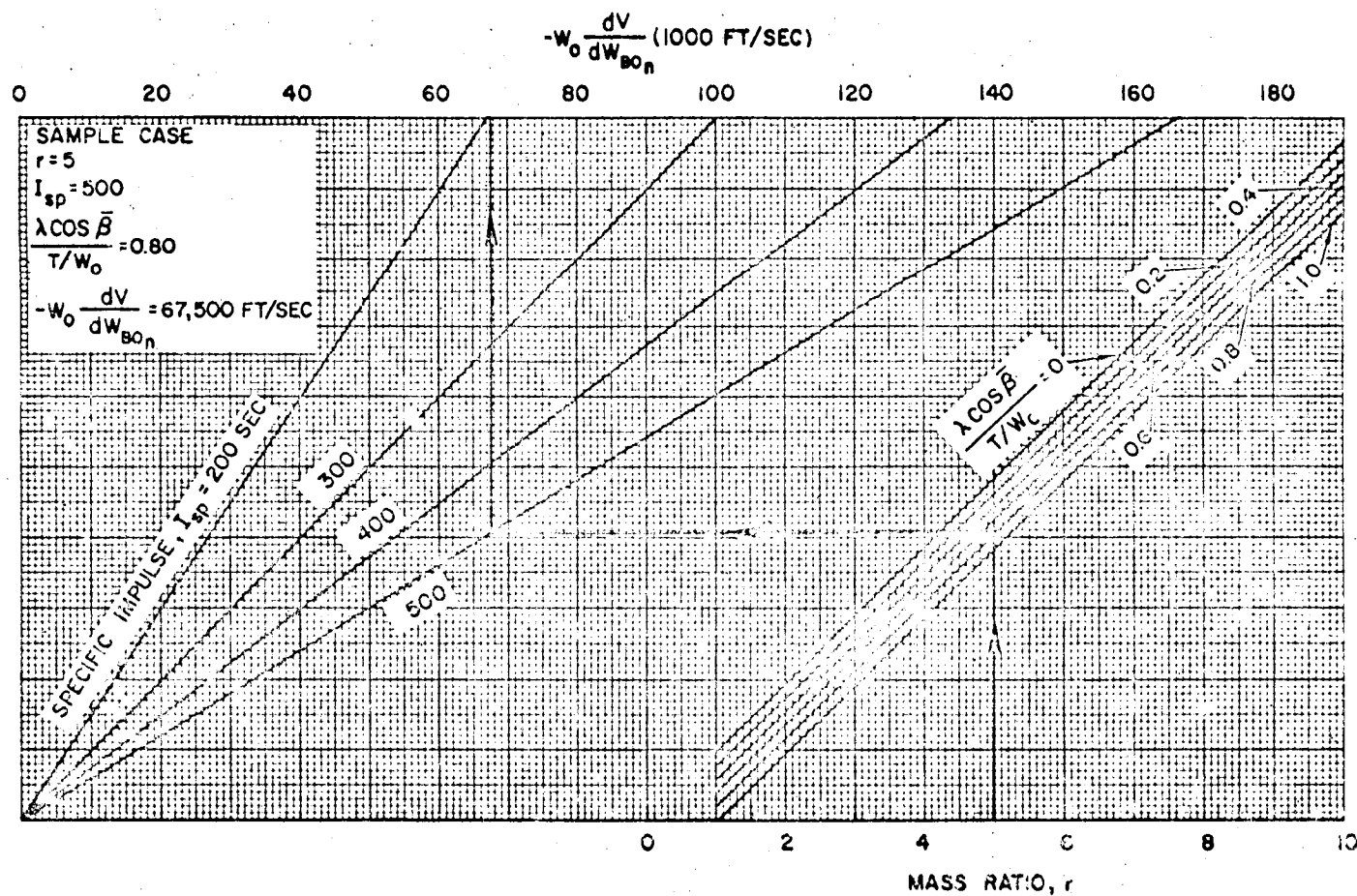


Figure 47. Burnout Weight

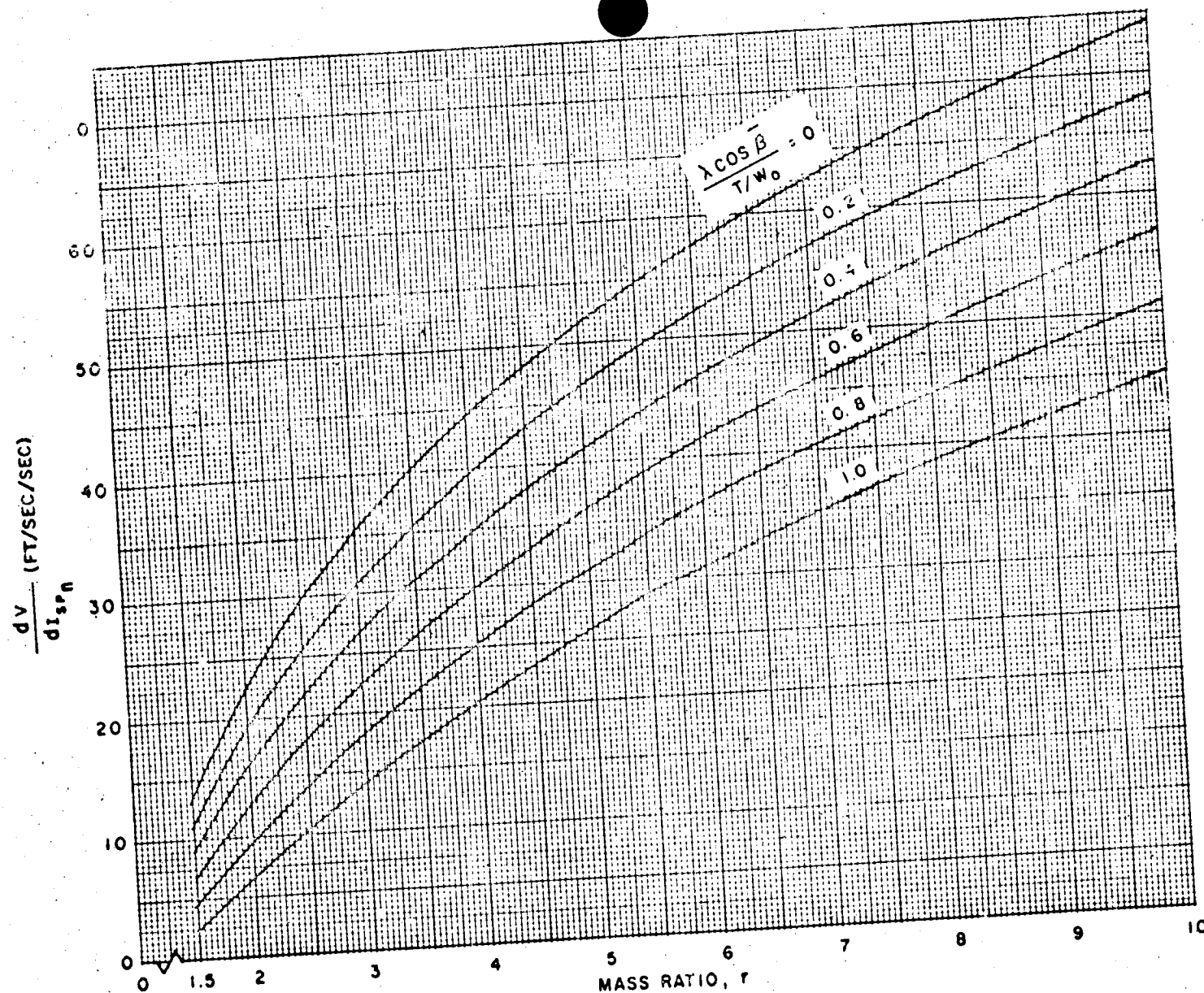


Figure 48. Specific Impulse Velocity Exchange Coefficient

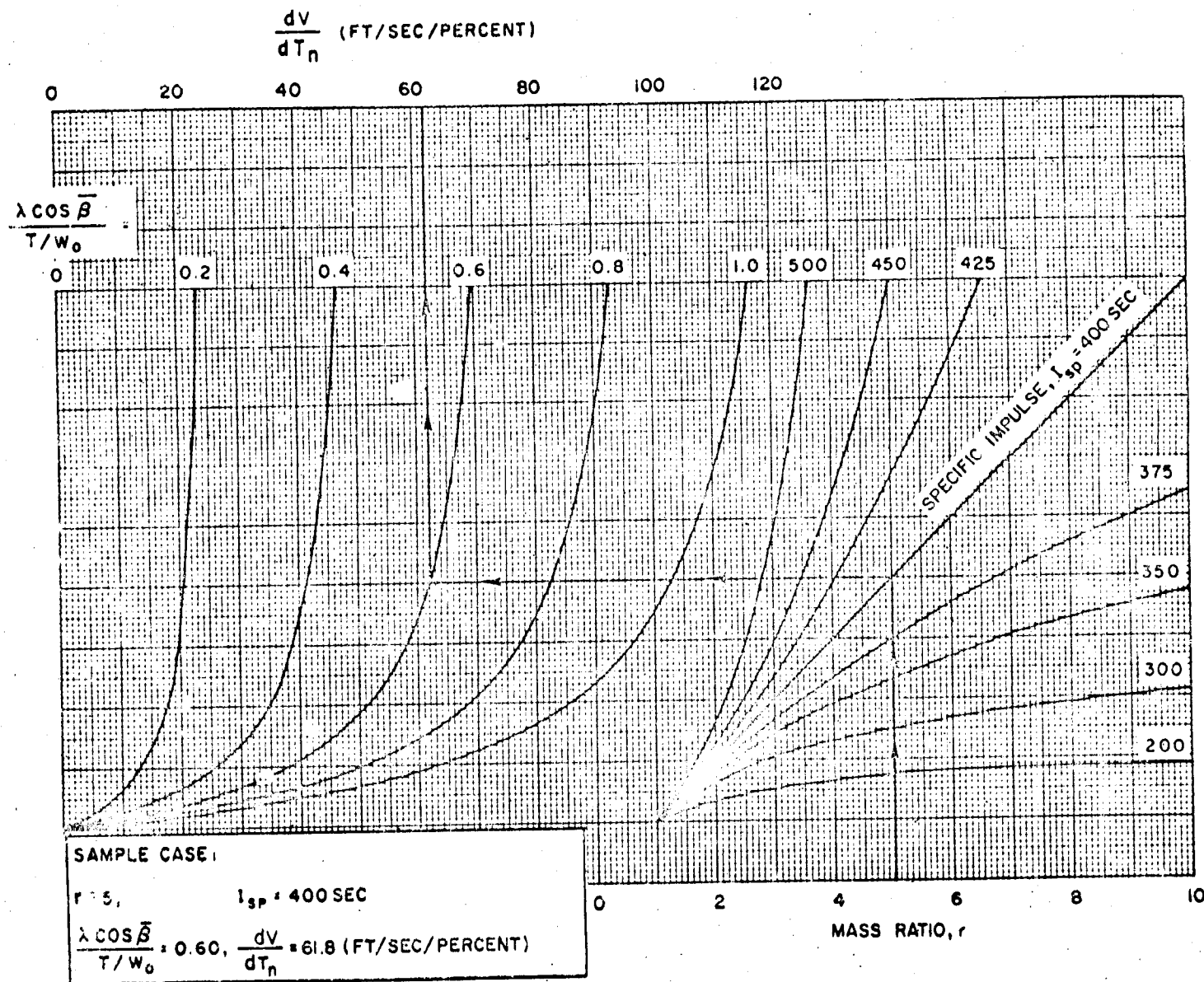


Figure 49. Thrust Velocity Exchange Coefficient

SYSTEM CONSIDERATIONS

In evaluating the parameter $\frac{\lambda \cos \bar{\beta}}{T/W_0}$ which appears in the analytical exchange ratios, it is suggested that a time average of $\cos \bar{\beta}$ be used rather than a time average of $\bar{\beta}$ or arithmetic mean of the initial and burnout angles. Alternatively, use the data presented in paragraph 2.2.2 to estimate "total" velocity losses, ΔV_L , and compute $\cos \bar{\beta}$ from the relation:

$$\cos \bar{\beta} = \frac{\Delta V_L}{g t_B}$$

Use of this procedure is justified since gravity losses make up a major portion of the total losses for most booster vehicles. In computing the parameter, base T/W_0 on sea level thrust and vehicle liftoff weight for first stage, and on vacuum thrust and initial stage weight for upper stages. The ratio of sea level to vacuum specific impulse, λ , is usually assumed to be equal to one for upper stages.

3.5.2 Numerical Example

As an illustration, the performance margin of a hypothetical three-stage booster vehicle will be evaluated. The first stage consists of a cluster of three solid-propellant engines, and the second and third stages use liquid propellants. The assumed nominal vehicle characteristics and dispersions are given in Tables 4 and 5, respectively.

Table 4. Nominal Vehicle Characteristics

Variable	Stage 1	Stage 2	Stage 3
Initial Weight (lb)	2,500,000	600,000	215,000
Burnout Weight (lb)	850,000	245,000	115,000
Sea Level Thrust (lb)	4,500,000	-	-
Vacuum Thrust (lb)	5,000,000	800,000	100,000
Vacuum Specific Impulse (sec)	275	400	400
Average Flight Path Angle (deg)	32	65	85

Table 5. Vehicle Dispersions (1-sigma)

Variable	Stage 1	1 σ Dispersion Stage 2	Stage 3
Inert Weight (lb)	1000/engine	200	100*
Expendable Propellants (lb)	3000/engine	1000	300
Burnout Weight (lb)	-	700	200
Initial Thrust (percent)	1.0/engine**	1.0	1.0
Specific Impulse (sec)	2.0/engine	2.0	2.0

* Includes payload weight dispersion.

** Sea level value.

Using the analytical expressions presented in Table 6, exchange coefficients are computed relating burnout velocity to the following vehicle performance parameters:

<u>Stage 1</u>	<u>Stages 2 and 3</u>
Thrust	Thrust
Specific impulse	Specific impulse
Inert weight	Inert weight
Propellant weight	Propellant weight
	Burnout weight (outage)

These data are summarized in Table 6.

Table 6. Velocity Exchange Coefficients

Variable	Stage 1	Stage 2	Stage 3
Specific Impulse (ft/sec/sec)	25.7	22.8	17.3
Thrust (ft/sec/percent)	+24.8	+24.2	+11.2
Inert Weight (ft/sec/lb)	-0.0069	-0.038	-0.09
Propellant Weight (ft/sec/lb)	+0.003	+0.008	+0.011
Burnout Weight (ft/sec/lb)	-	-0.046	-0.101

Since the first stage is assumed to consist of a cluster of three solid-propellant engines, the total 1-sigma dispersion of each parameter for this stage is treated as a linear combination of statistically independent (uncorrelated) variables.

$$\sigma_{\text{stage}}^2 = \sum_{k=1}^3 \sigma_{k \text{ engine}}^2$$

Then,

$$\begin{aligned} \sigma_T &= \left[(15000)^2 + (15000)^2 + (15000)^2 \right]^{1/2} = 25,980 \text{ lb} \\ &= \frac{25980 \times 100}{4,500,000} = 0.58 \text{ percent of nominal initial thrust} \end{aligned}$$

$$\sigma_{W_P} = \left[(3000)^2 + (3000)^2 + (3000)^2 \right]^{1/2} = 5196 \text{ lb}$$

SYSTEM CONSIDERATIONS

$$\sigma_{isp} = \left[(2)^2 + (2)^2 + (2)^2 \right]^{1/2} = 3.46 \text{ sec}$$

$$\sigma_{WST} = \left[(1000)^2 + (1000)^2 + (1000)^2 \right]^{1/2} = 1732 \text{ lb}$$

The parameter dispersions listed in Table 5 for the second and third stages are assumed to be total dispersions. However, it should be noted that the dispersion of each stage parameter is based on the statistical combination of several error sources, and that the determination of these sources is a major task. For a preliminary design study, however, the dispersions are usually estimates based on experience with similar systems.

Utilizing the parameter dispersions and velocity exchange coefficients for each stage, the performance margin is computed as follows

Stage 1

$$\begin{aligned} (\sigma_{\delta V})_1 &= \left[(24.8 \times 0.58)^2 + (25.7 \times 3.46)^2 + (0.0069 \times 1732)^2 + (0.003 \times 5196)^2 \right]^{1/2} \\ &= \left[(14.31)^2 + (88.92)^2 + (11.9)^2 + (15.59)^2 \right]^{1/2} \\ &= 92.2 \text{ ft/sec.} \end{aligned}$$

Stage 2

$$\begin{aligned} (\sigma_{\delta V})_2 &= \left[(24.2 \times 1)^2 + (22.8 \times 2)^2 + (0.038 \times 200)^2 + (0.008 \times 1000)^2 + (0.046 \times 700)^2 \right]^{1/2} \\ &= \left[(24.2)^2 + (45.6)^2 + (7.6)^2 + (8.0)^2 + (32.2)^2 \right]^{1/2} \\ &= 61.8 \text{ ft/sec.} \end{aligned}$$

Stage 3

$$\begin{aligned} (\sigma_{\delta V})_3 &= \left[(11.2 \times 1)^2 + (17.3 \times 2)^2 + (0.09 \times 100)^2 + (0.011 \times 300)^2 + (0.101 \times 200)^2 \right]^{1/2} \\ &= \left[(11.2)^2 + (34.6)^2 + (9)^2 + (3.3)^2 + (20.2)^2 \right]^{1/2} \\ &= 42.7 \text{ ft/sec.} \end{aligned}$$

The total 1-sigma performance margin is

$$\begin{aligned} (\sigma_{\delta V})_N &= \left[(\sigma_{\delta V})_1^2 + (\sigma_{\delta V})_2^2 + (\sigma_{\delta V})_3^2 \right]^{1/2} \\ &= \left[(154.7)^2 + (87.8)^2 + (54.8)^2 \right]^{1/2} \\ &= 118.9 \text{ ft/sec.} \end{aligned}$$

For most initial design studies, a 3-sigma margin is allowed, so that for the example,

$$\text{performance margin} = 3 \times 118.9 = 357 \text{ ft/sec.}$$

NOMENCLATURE

A	Reference area for aerodynamic coefficients
A_z	Launch azimuth
a_{BO}	Axial acceleration at burnout (in g's)
a_{max}	Maximum axial acceleration (in g's)
C_D	Drag coefficient
h	Altitude
h_{BO}	Altitude at burnout
$I_{sp_{vac}}$	Vacuum specific impulse
i	Orbit inclination or integer corresponding to a particular stage
k	Integer corresponding to a particular stage
n	Integer corresponding to a particular stage
P	Probability
P_{BO}	Atmospheric pressure at burnout altitude
P_o	Atmospheric pressure at sea level
q	Dynamic pressure
q_{BO}	Dynamic pressure at burnout
q_{max}	Maximum dynamic pressure

SYSTEM CONSIDERATIONS

R	Range
R	Slant range
R_{BO}	Range at burnout
r	$\frac{W_O}{W_{BO}} = \text{Mass ratio}$
r_e	Radius of the earth
T or T_{sl}	Sea level thrust
T_{vac}	Vacuum thrust
t_{BO}	Time from liftoff to burnout
$t_{q_{max}}$	Time from liftoff to maximum dynamic pressure
V	Velocity
V_{BO}	Burnout velocity
W_{BO}	Burnout weight
W_O	Gross weight
W_P	Propellant weight
W_{ST}	Structure weight
X	Performance variable
α	Angle of attack
β	Flight path angle
$\bar{\beta}$	Average flight path angle
β_{BO}	Flight path angle at burnout
γ	Defined on Page 3-65
ΔV_1	Initial incremental velocity for Hohmann transfer
ΔV_2	Injection dog-leg velocity
ΔR	Increment in range
ΔR_{DR}	Increment in range for down-range dispersion
ΔR_{CR}	Increment in range for cross-range dispersion
$\Delta V_{T_{dl}}$	Total transfer dog-leg velocity
δ_{dl}	Dog-leg angle
ϵ	Vehicle thrust attitude angle

References

3-79

ζ	Elevation angle
ϑ	Range angle
λ	Geocentric latitude or ratio of sea level specific impulse to vacuum specific impulse
λ_L	Latitude of the launch site
λ_S	Latitude of a tracking station
σ	Standard deviation
ϕ	Look angle
ψ	Geocentric longitude
ψ_L	Longitude of the launch site
ψ_S	Longitude of a tracking station

REFERENCES

1. J. T. Kopecek, A. J. Mallinckrodt, H. P. Roberts, and R. V. Sutton, "Equatorial Launch Site Study," Space Technology Laboratories, Inc., STL/TR-60-0000-02701, 25 March 1960. (S)
2. W. E. Moeckel, "Departure Trajectories for Interplanetary Vehicles," Lewis Research Center, National Aeronautics and Space Administration, J.O. 3c-200R2. (No date)
3. V. C. Clarke, Jr., "Design of Lunar and Interplanetary Ascent Trajectories," Jet Propulsion Laboratory, Technical Report No. 32-30, 26 July 1960.
4. A. H. Milstead, "Bi-elliptical Transfer-Rotation Maneuver to Achieve a 24-Hour Circular Orbit," Space Technology Laboratories, Inc., STL 7720.4-95, 26 April 1960. (C)
5. G. C. Szego, "Contributions to the Astronautics Ship Concept Study Proposal for the Navy," Space Technology Laboratories, Inc., STL 9863-205, 13 March 1961. (C)
6. J. R. Sellars, "Destruction of Able Stages on Re-entry," Space Technology Laboratories, Inc., GM 59-8023-17, 17 April 1959. (S)
7. T. L. Peterson, "Dispersion of Tankage Fragments," Space Technology Laboratories, Inc., TN 59-0000-09340, 31 December 1959. (C)
8. T. L. Peterson, "Dispersion of Atlas Tank Fragments," STL/GM 59-7540-57, 1 December 1959. (C)
9. T. L. Peterson, "Destruction of Re-entrant Fragments," Space Technology Laboratories, Inc., STL/GM 60-7540.4-5, 11 January 1960. (C)
10. P. E. Sandorff, "Structural Considerations in Design of Space Boosters," Journal of American Rocket Society, November 1960.
11. J. E. Brooks, N. E. Friedmann, and E. M. Scheuer, "Statistical Analysis of Performance for Two-Stage Bipropellant Missiles," Space Technology Laboratories, Inc., TR-60-0000-09109, May 1960.

CHAPTER 4

GENERALIZED EXCHANGE RATIO ANALYSIS

During the initial design phases, the problem of estimating the effects of small design changes on vehicle payload performance is a continual one. In other instances, it may be desired to estimate the changes in vehicle characteristics required to maintain some minimum payload capability when a performance parameter is varied. In either case, exchange ratios provide the designer with an expedient and relatively accurate tool for predicting the effects of such changes without resorting to extensive hand calculations or digital computer solutions.

4.1 ANALYTICAL RELATIONSHIPS

The exchange ratios presented herein are derived from the "theoretical" expression for the total velocity gained at burnout by an N stage vehicle.

$$V_{BO} = \sum_{i=1}^N \left(g I_{sp_i} \ln r_i - \Delta V_{g_i} - \Delta V_{L_{a_i}} \right)$$

where

g = gravitational constant = 32.2 ft/sec²

I_{sp_i} = stage i vacuum specific impulse

r_i = stage i mass ratio; initial mass divided by burnout mass

ΔV_{g_i} = velocity losses caused by gravitational effects during stage i

$\Delta V_{L_{a_i}}$ = velocity losses caused by atmospheric effects and thrust vector not acting along the flight path during stage i operation.

In order to facilitate the computation of the exchange ratios, certain simplifying assumptions are made. In general, it is assumed that the perturbation of a single performance parameter will not affect the total velocity losses due to atmospheric effects and thrust vector not acting along the flight path. It is also assumed that the velocity losses due to gravitational effects can be approximated by the following expression:

$$\Delta V_{g_i} = g t_{B_i} \cos \bar{\beta}_i$$

where

t_{B_i} = stage i burning time

$\bar{\beta}_i$ = stage i average flight path angle, a constant.

Other assumptions which are made in the derivation of the ratios are listed with the individual ratios presented below and in Appendix C. The exact effects of these assumptions can only be determined from digital computer simulations of the vehicle and mission being considered. However, the accuracy obtained using the analytical expressions is believed to be adequate for most preliminary design studies.

In Appendix C, Section 1, exchange ratios are derived which relate the effects on vehicle payload capability to perturbations of booster performance parameters; in Appendix C, Section 2, ratios are derived which relate perturbations of booster performance parameters to the amounts that stage gross weight must be varied in order to maintain a fixed payload capability. Booster performance parameters considered include specific impulse, structural weight, initial stage gross weight, propellant weight, and thrust. These particular ratios have been found most useful in vehicle design studies; however, additional ratios can be derived from the equation for the theoretical burnout velocity. The reader is referred to Appendix C for an example of the procedure to be followed in the derivation of other ratios. A summary of the ratios derived in Appendix C follows.

4.1.1 Exchange Ratios for an N-Stage Vehicle

Payload to propellant specific impulse of nth stage is

$$\frac{dW_{PL}}{dI_{sp_n}} = \frac{\ln r_n - \theta_n(1 - 1/r_n)}{\sum_{i=1}^N \left[\left(\frac{I_{sp}}{W_O} \right)_i (r_i - 1) \right]}$$

where

$$\theta = \frac{\lambda \cos \bar{\beta}}{T/W_O}$$

Payload to structural weight of nth stage is

$$\frac{dW_{PL}}{dW_{ST_n}} = - \frac{\sum_{i=1}^n \left[\left(\frac{I_{sp}}{W_O} \right)_i (r_i - 1) \right]}{\sum_{i=1}^N \left[\left(\frac{I_{sp}}{W_O} \right)_i (r_i - 1) \right]}$$

Payload to initial gross weight of nth stage is

$$\frac{dW_{PL}}{dW_{O_n}} = - \frac{\sum_{i=1}^n \left[\left(\frac{I_{sp}}{W_O} \right)_i (1 - r_i) \right] + (1 - \sigma_n) \left(\frac{I_{sp}}{W_O} \right)_n (r_n - \theta_n)}{\sum_{i=n+1}^N \left[\left(\frac{I_{sp}}{W_O} \right)_i (1 - r_i) \right] - (1 - \sigma_n) \left(\frac{I_{sp}}{W_O} \right)_n (r_n - \theta_n)}$$

Payload to propellant loading of nth stage is

$$\left(\frac{dW_{PL}}{dW_{P_n}} \right)_{W_{ST_n}} = \frac{\left(\frac{I_{sp}}{W_O} \right)_n (1 - \theta_n) - \sum_{i=1}^{n-1} \left[\left(\frac{I_{sp}}{W_O} \right)_i (r_i - 1) \right]}{\sum_{i=1}^N \left[\left(\frac{I_{sp}}{W_O} \right)_i (r_i - 1) \right]}$$

Payload to propellant weight, allowing for appropriate structural weight to accommodate the difference in propellant weight (rubber staging), is

$$\frac{dW_{PL}}{dW_{P_n}} = \frac{\left(\frac{I_{sp}}{W_O} \right)_n (r_n - \theta_n) - \frac{1}{1 - \sigma_n} \sum_{i=1}^n \left[\left(\frac{I_{sp}}{W_O} \right)_i (r_i - 1) \right]}{\sum_{i=1}^N \left[\left(\frac{I_{sp}}{W_O} \right)_i (r_i - 1) \right]}$$

Payload to initial thrust (percentage change of nominal thrust) is

$$\frac{dW_{PL}}{dT_n} = \frac{\lambda_n I_{sp_n} \cos \bar{\beta}_n (1 - 1/r_n)}{100 (T/W_O) \sum_{i=1}^N \left[\left(\frac{I_{sp}}{W_O} \right)_i (r_i - 1) \right]}$$

Gross weight of the nth stage to the gross weight of the n + 1 stage, assuming a constant thrust in the nth stage, is

$$\left(\frac{dW_{O_n}}{dW_{O_{n+1}}} \right)_{W_{PL}, T_n} = \frac{(1 - \sigma_n)(r_n - \theta_n)}{1 - \sigma_n r_n - (1 - \sigma_n)\theta_n}$$

Gross weight of the k th stage to the gross weight of the n th stage, assuming a constant thrust-to-weight ratio for each stage below the n th stage, is

$$\left(\frac{dW_{O_k}}{dW_{O_n}} \right)_{W_{PL}, (T/W_{O_i})} = \frac{W_{O_k}}{W_{O_n}} \quad (1 \leq i \leq n-1), (k \leq n)$$

Vehicle liftoff weight to gross weight of the n th stage, assuming a constant thrust-to-weight ratio in each stage, is

$$\left(\frac{dW_{LO}}{dW_{O_n}} \right)_{W_{PL}, (T/W_{O_i})_k} = \frac{1}{W_{O_n}} \sum_{i=1}^n W_{O_i} \quad \begin{matrix} (1 \leq k \leq n-1) \\ (1 \leq i \leq n) \end{matrix}$$

where

$$W_{LO} = W_{O_1}$$

Conversely, the above equations can be used when the payload weight is perturbed to estimate the changes in stage gross weights and vehicle liftoff weight required to achieve a fixed mission velocity requirement. Also, using the above equation in conjunction with those for the stage gross weight presented on page 4-5, one can evaluate the effect on the liftoff weight due to a perturbation of a vehicle parameter in the n th stage.

4.1.2 Exchange Ratios for One-Stage Vehicle

Payload to specific impulse is

$$\frac{dW_{PL}}{dI_{sp}} = \frac{\ln r - \theta(1 - 1/r)}{\frac{I_{sp}}{W_O}(r - 1)}$$

Payload to structural weight is

$$\frac{dW_{PL}}{dW_{ST}} = -1$$

Payload to initial gross weight is

$$\begin{aligned}\frac{dW_{PL}}{dW_O} &= \frac{1 - \sigma r - (1 - \sigma)\theta}{(1 - \sigma)(r - \theta)} \\ &= \frac{W_{PL}}{W_O} \quad (\text{neglecting gravitational and atmospheric effects})\end{aligned}$$

Payload to propellant loading is

$$\left(\frac{dW_{PL}}{dW_P}\right)_{W_{ST}} = \frac{1 - \theta}{r - 1}$$

Payload to propellant weight, allowing the appropriate structural weight to accommodate the difference in propellant weight (rubber staging), is

$$\frac{dW_{PL}}{dW_P} = \frac{1 - \sigma r - (1 - \sigma)\theta}{(1 - \sigma)(r - 1)}$$

Payload to initial thrust (percentage change of nominal thrust) is

$$\frac{dW_{PL}}{dT} = \frac{\lambda W_{BO} \cos \bar{\beta}}{100 T/W_O}$$

Stage gross weight to specific impulse for a fixed payload capability is

$$\left(\frac{dW_O}{dI_{sp}}\right)_{W_{PL}} = - \frac{\ln r - \theta(1 - 1/r)}{\frac{I_{sp}}{W_O} [1 - \sigma r - \theta(1 - \sigma)]}$$

Stage gross weight to inert weight for a fixed payload capability is

$$\left(\frac{dW_O}{dW_{ST}^*}\right)_{W_{PL}} = \frac{(1 - \sigma)(r - \theta)}{1 - \sigma r - (1 - \sigma)\theta}$$

Stage gross weight to initial thrust for a fixed payload capability and percentage change of thrust is

$$\left(\frac{dW_O}{dT}\right)_{W_{PL}} = - \frac{W_O \theta(1 - 1/r)}{100 [1 - \sigma r - (1 - \sigma)\theta]}$$

GENERALIZED EXCHANGE RATIO ANALYSIS

In evaluating the parameter Θ which appears in the analytical exchange ratios, it is suggested that a time average of $\cos \bar{\beta}$ be used rather than a time average of $\bar{\beta}$ or arithmetic mean of the initial and burnout angles. Alternatively, use the data presented in paragraph 2.2.2 to estimate "total" velocity losses, ΔV_L , and compute $\cos \bar{\beta}$ from the relation:

$$\cos \bar{\beta} = \frac{\Delta V_L}{g t_B}$$

Use of this procedure is justified since gravity losses make up a major portion of the total losses for most booster vehicles. In computing the parameter, base T/W_O on sea level thrust and vehicle liftoff weight for first stage, and vacuum thrust and initial stage weight for upper stages. The ratio of sea level to vacuum specific impulse, λ , is usually assumed to be equal to one for upper stages.

4.2 GRAPHICAL PRESENTATION

As an aid to the designer, the above exchange ratios for a single-stage vehicle are plotted in Figures 1 through 8 for representative values of the performance parameters.

In Figure 1, the ratio of payload to specific impulse is plotted as a function of r , Θ , W_O , and I_{sp} . In Figure 2 the ratio of payload to initial gross weight is plotted as a function of r , σ , and Θ . The ratio of payload to propellant weight for a fixed stage structural weight is plotted in Figure 3 as a function of r and Θ , and the ratio of payload to propellant weight for varying stage structural weight is plotted in Figure 4 as a function of r , σ , and Θ .

The ratio of payload to initial thrust is plotted in Figure 5 as a function of r , λ , $\bar{\beta}$, and W_{BO} . The ratio of stage gross weight to specific impulse is plotted in Figure 6 as a function of r , σ , W_O , and I_{sp} for $\Theta = 0$. The ratio of stage gross weight to inert weight is plotted in Figure 7 as a function of r , σ , and Θ . This plot can also be used to determine the resulting perturbation in gross weight of the n th stage of a multistage vehicle due to a perturbation of gross weight of the $n + 1$ stage when a constant thrust is assumed in the n th stage. The ratio of stage gross weight to initial thrust is plotted in Figure 8 as a function of r , σ , Θ , and W_O .

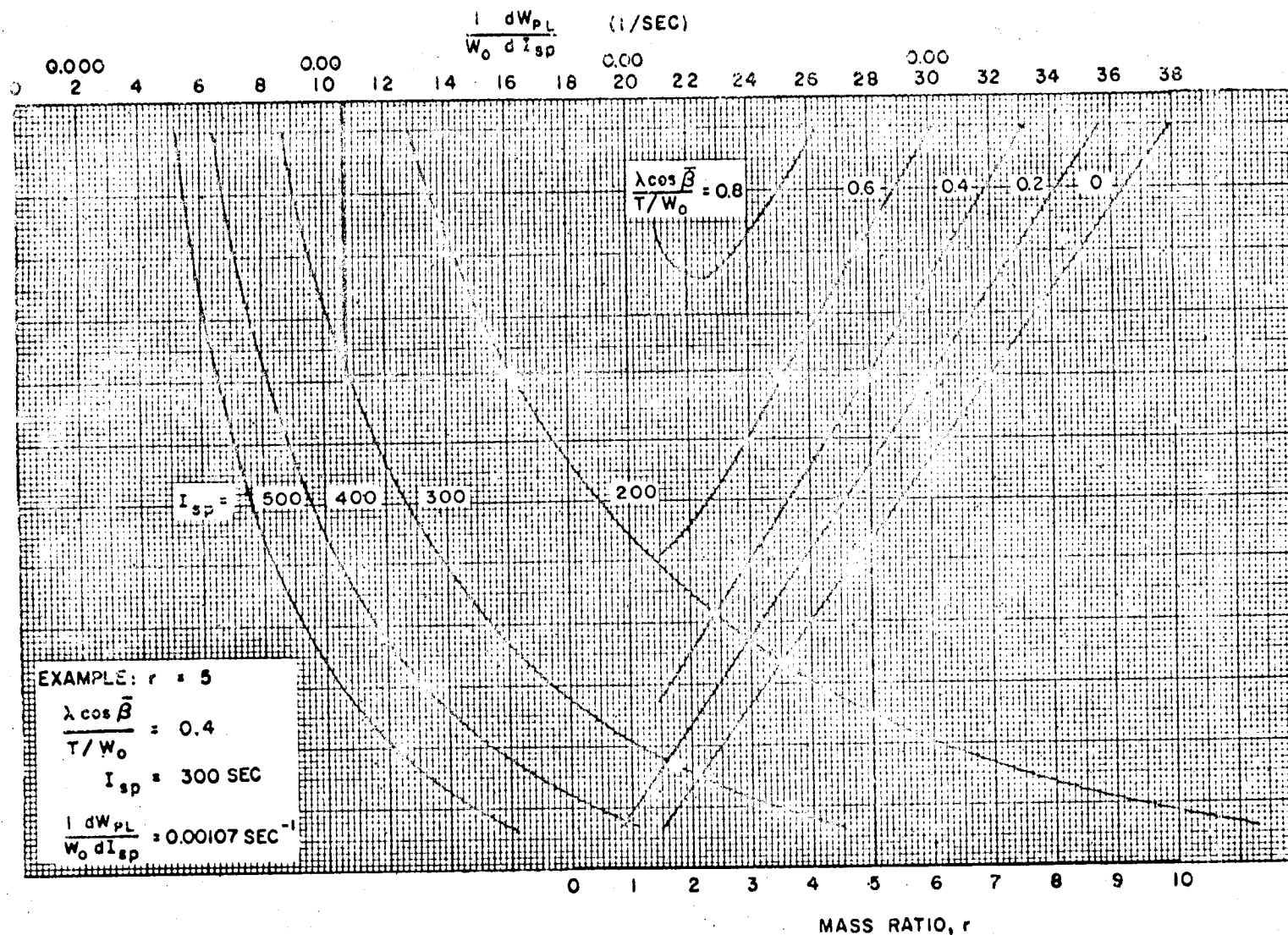


Figure 1. Stage Payload Weight - Specific Impulse Ratio

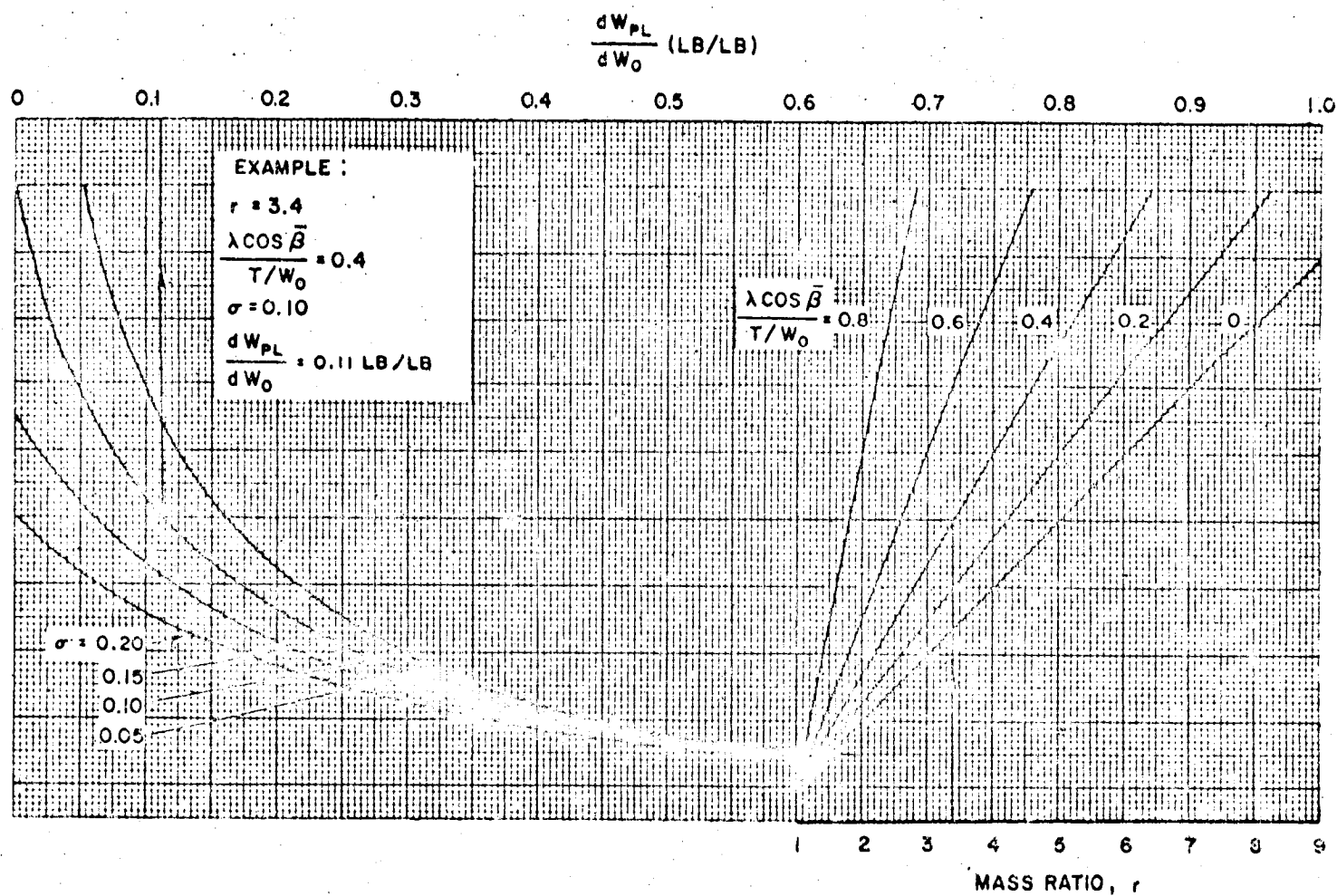


Figure 2. Stage Payload Weight - Stage Initial Gross Weight Exchange Ratio

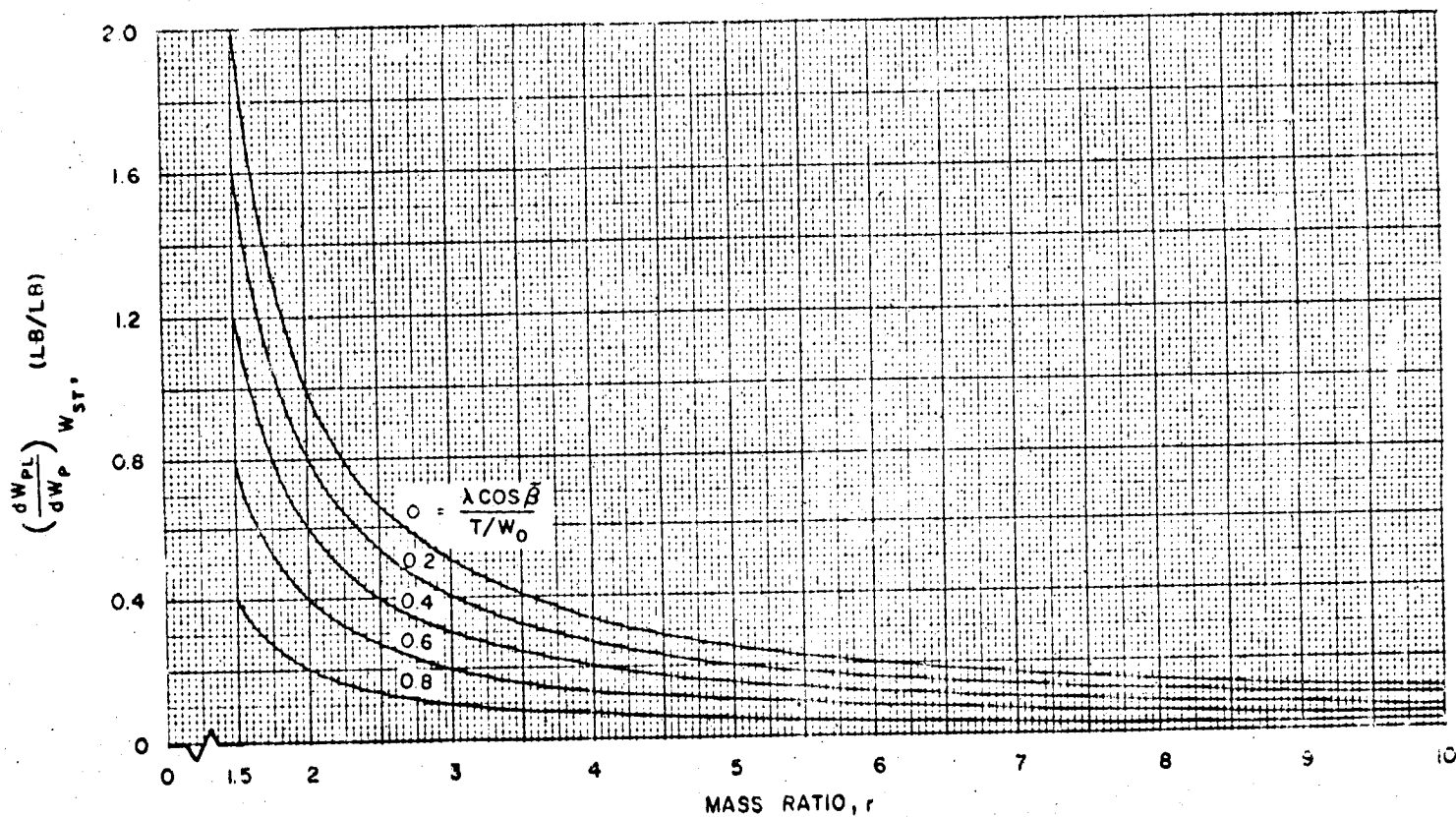
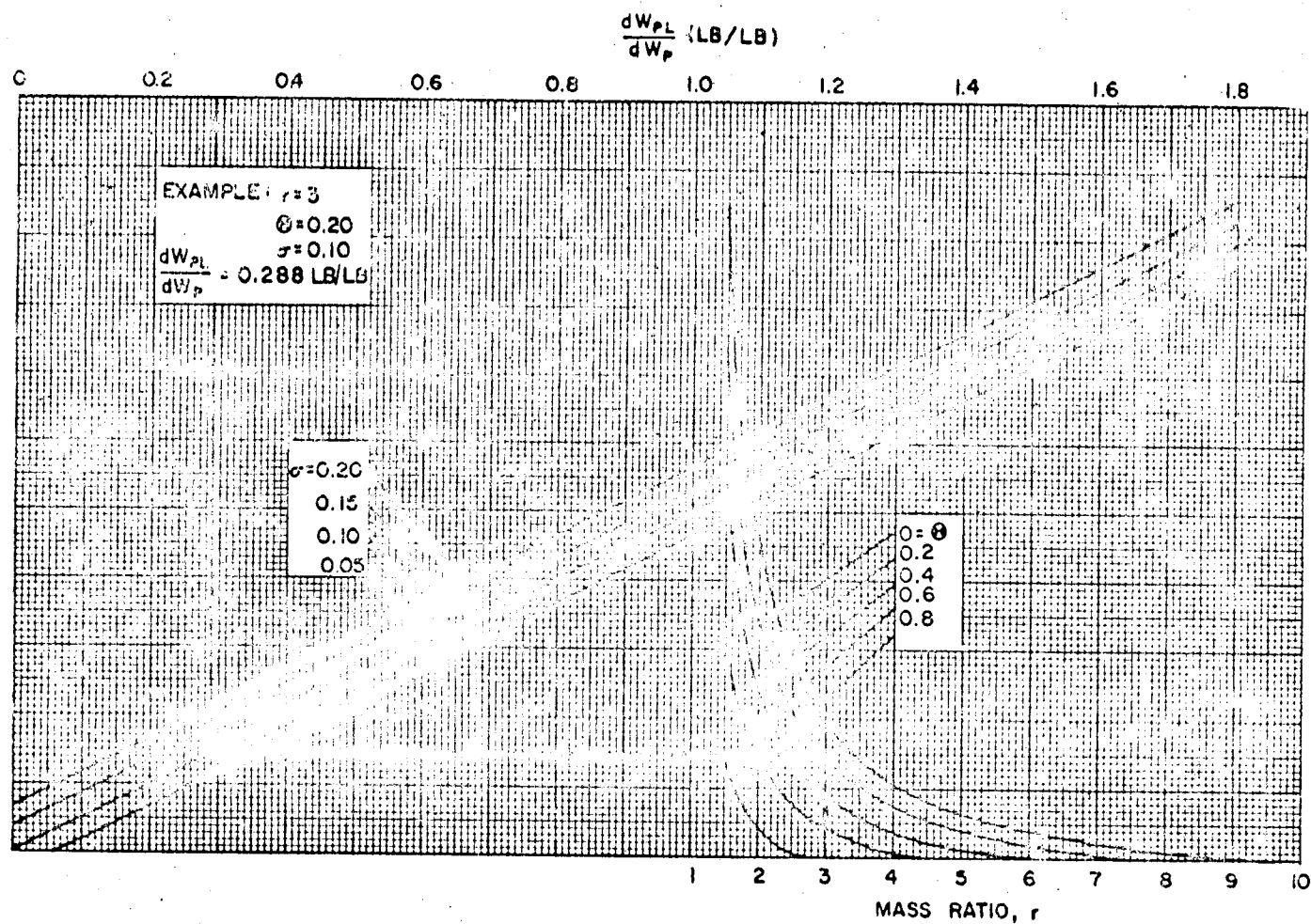


Figure 3. Stage Payload Weight - Propellant Weight Exchange Ratio (Fixed Structural Weight)



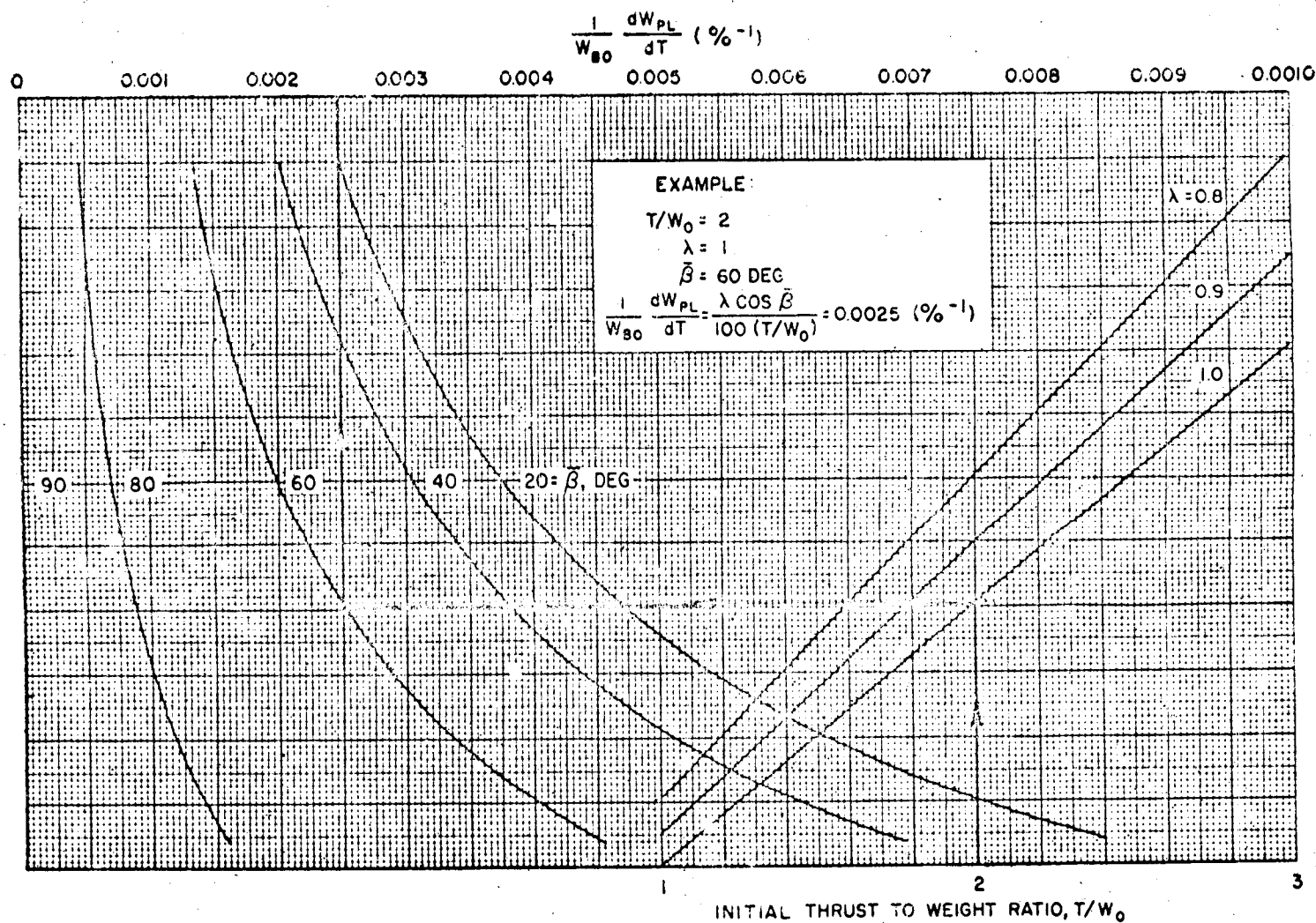


Figure 5. Stage Payload Weight - Thrust Exchange Ratio

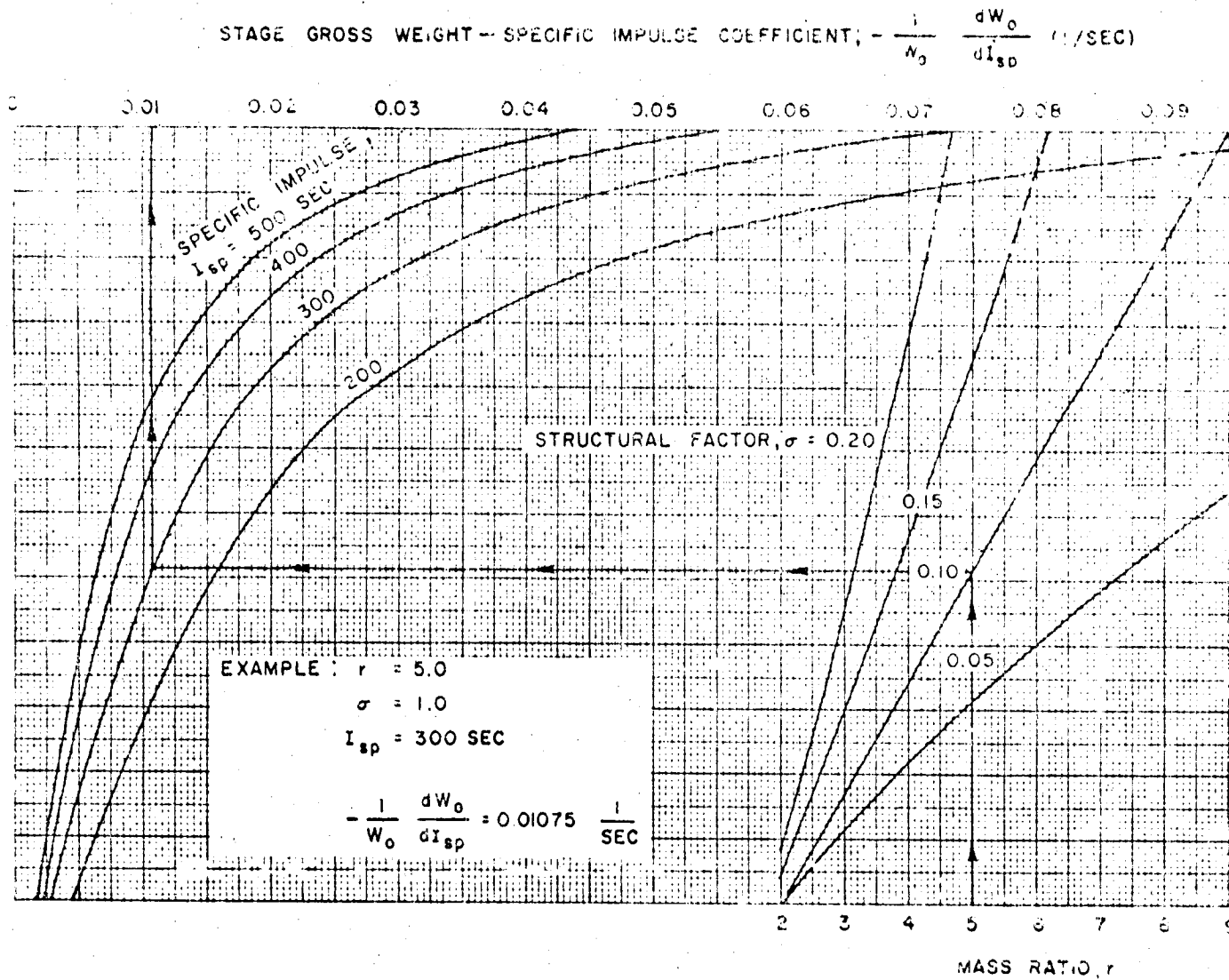


Figure 6. Stage Gross Weight - Specific Impulse Exchange Ratio

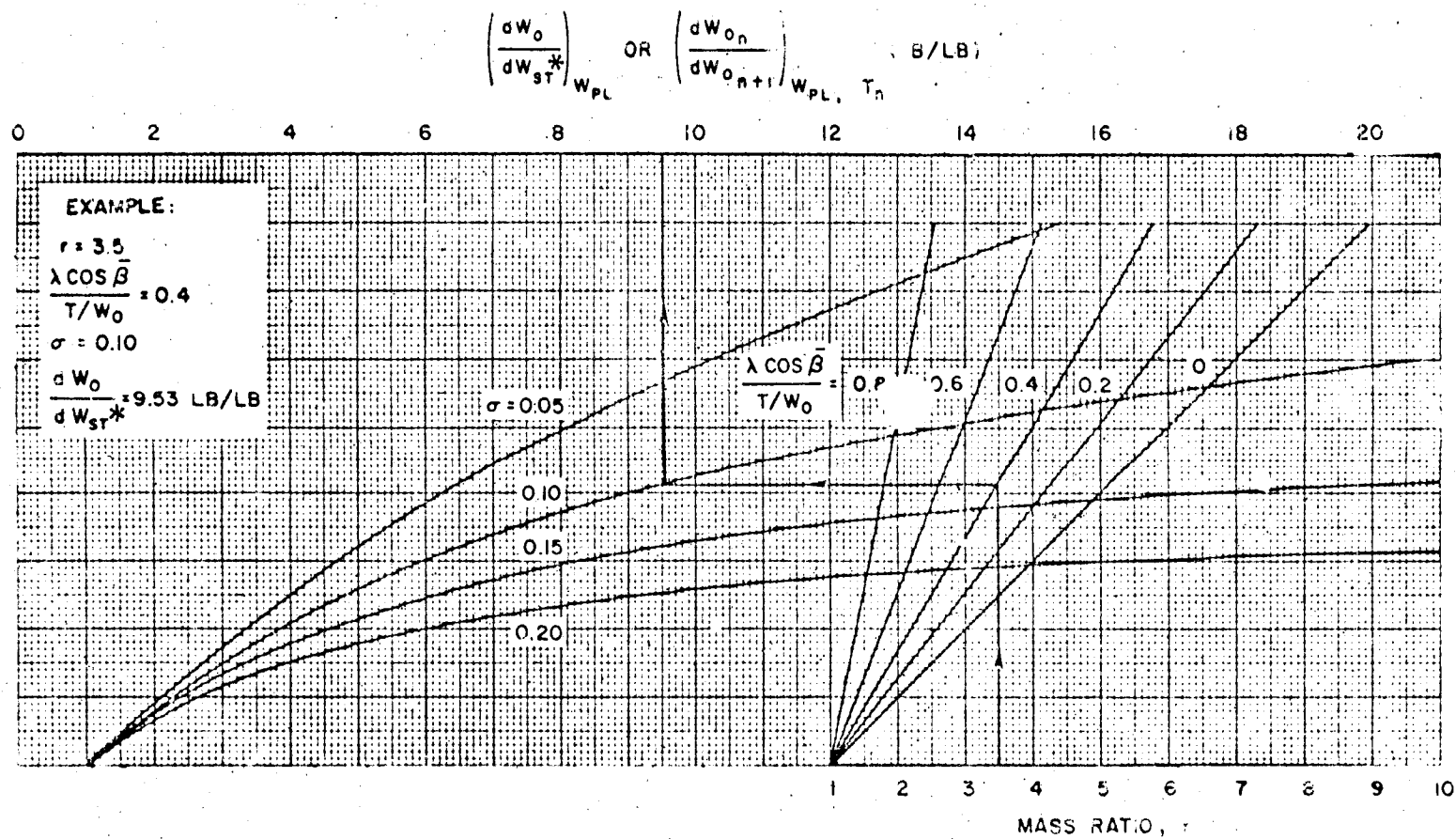


Figure 7. Stage Gross Weight - Inert Weight Exchange Ratio

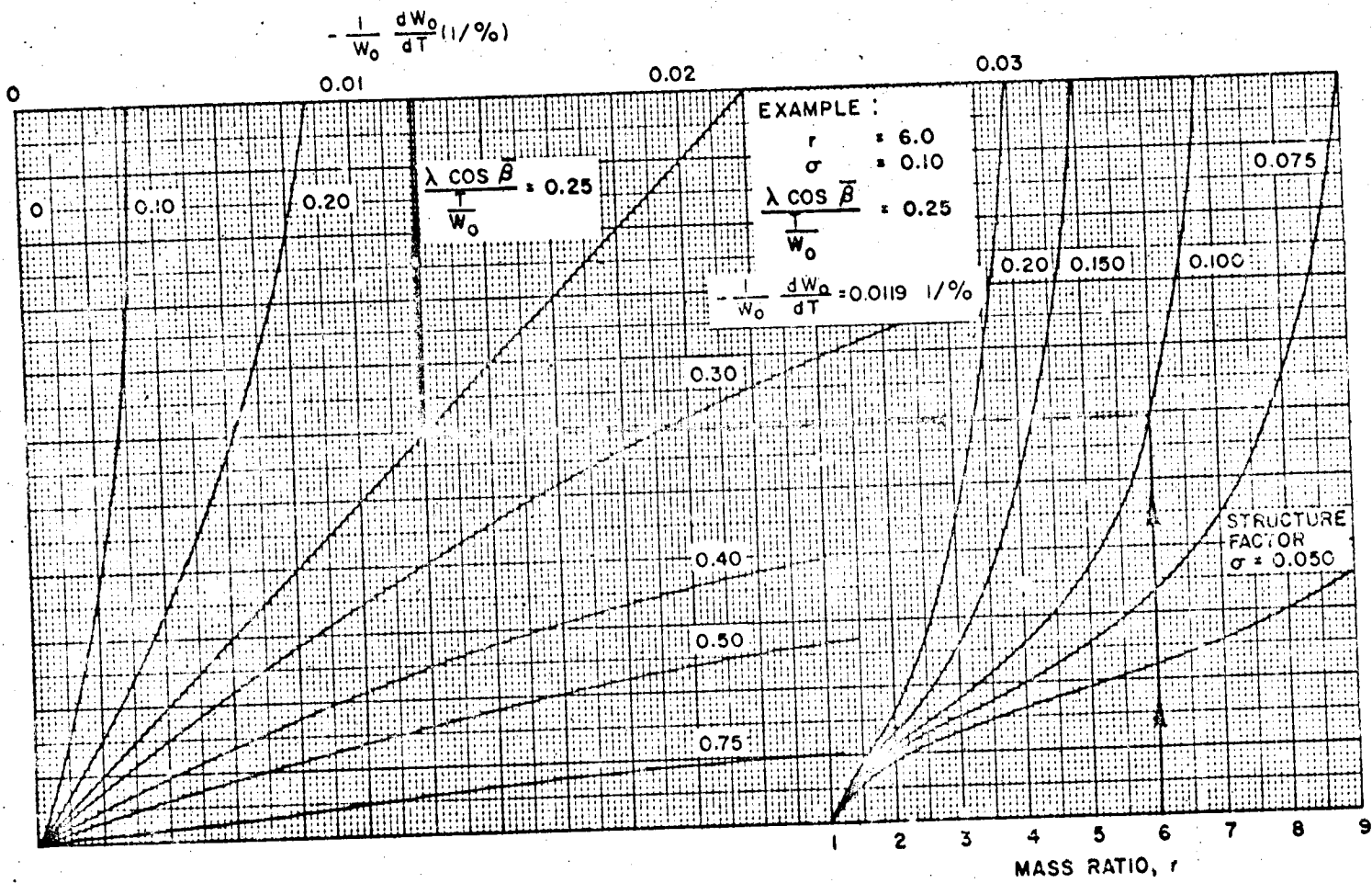


Figure 8. Stage Gross Weight - Thrust Exchange Ratio

REORDER NO. 62-286

4.3 NUMERICAL EXAMPLE

To illustrate the use of exchange ratio analysis, some sample calculations will be presented. It is suggested that the pertinent vehicle data be tabulated in some systematic fashion in order to facilitate the computations and minimize errors. A possible format, to be used in estimating the effect of simultaneously varying several parameters on vehicle payload capability, is shown in Table 1. In the first column the vehicle weights, propulsion, and trajectory parameters required in the computations are listed. In the second column the original or nominal value of each parameter is tabulated, and in the third column the parameter perturbations are given. In the fourth column the exchange ratios corresponding to each parameter are listed. The fifth column lists the change in payload weight caused by each parameter perturbation and the total payload net change.

The exchange ratios presented are computed based on the given configuration data as follows:

$$\begin{aligned} \left(\frac{dw_{PL}}{dw_{P1}} \right)_{w_{ST}} &= \frac{\left(\frac{I_{sp}}{W_O} \right)_1 (1 - \theta_1)}{\sum_{i=1}^3 \left[\left(\frac{I_{sp}}{W_O} \right)_i (r_i - 1) \right]} \\ &= \frac{\frac{275}{2500000} \left[1 - \frac{(4500000)(2500000) \cos 32^\circ}{(5000000)(4500000)} \right]}{\left(\frac{275}{2500000} \right) \left(\frac{2500000}{850000} - 1 \right) + \left(\frac{400}{600000} \right) \left(\frac{600000}{245000} - 1 \right) + \left(\frac{400}{215000} \right) \left(\frac{215000}{115000} - 1 \right)} \\ &= \frac{0.00011 (1 - 0.424)}{0.000213 + 0.000966 + 0.001618} \\ &= \frac{0.000634}{0.002797} = 0.23 \text{ lb/lb} \end{aligned}$$

$$\begin{aligned} \frac{dw_{PL}}{dw_{ST2}} &= \frac{\sum_{i=1}^2 \left[\left(\frac{I_{sp}}{W_O} \right)_i (r_i - 1) \right]}{\sum_{i=1}^3 \left[\left(\frac{I_{sp}}{W_O} \right)_i (r_i - 1) \right]} \\ &= - \frac{0.000213 + 0.000966}{0.002797} \\ &= - 0.422 \text{ lb/lb} \end{aligned}$$

$$\frac{\delta W_{PL}}{\delta I_{ST}} = \frac{\sum_{i=1}^3 \left[\left(\frac{I_{SP}}{W_O} \right)_i (r_i - 1) \right]}{\sum_{i=1}^3 \left[\left(\frac{I_{SP}}{W_O} \right)_i (r_i - 1) \right]}$$

$$= 1.0 \text{ lb/lb}$$

$$\frac{\delta W_{PL}}{\delta I_{SP_3}} = \frac{\ln r_3 - \theta_3 (1 - 1/r_3)}{\sum_{i=1}^3 \left[\left(\frac{I_{SP}}{W_O} \right)_i (r_i - 1) \right]}$$

$$\frac{\ln \frac{215000}{115000} - \frac{215000 \cos 85^\circ}{100000} (1 - \frac{115000}{215000})}{0.002797}$$

$$192.5 \text{ lb/sec}$$

$$\frac{\delta W_{PL}}{\delta I_2} = \frac{N_2 (I_{SP_2} \cos \beta_2) (1 - 1/r_2)}{100 (1/W_O)_2 \sum_{i=1}^3 \left[\left(\frac{I_{SP}}{W_O} \right)_i (r_i - 1) \right]}$$

$$\frac{(1.9) (400) \cos 63^\circ (1 - \frac{245000}{600000})}{(100) (\frac{800000}{600000}) (0.002797)}$$

$$= 269.2 \text{ lb/percent}$$

Utilizing these ratios, payload perturbations are computed for the parameter perturbations. The individual payload perturbations combine algebraically to give the net change in payload capability, as shown at the bottom of Table 1.

Numerical Example

427

Table 1. Example Data Analysis

Parameter	Value	Initial	Final	Exhaust
<u>Trajectory</u>				
$\bar{\theta}_1$	32°			
$\bar{\theta}_2$	5°			
$\bar{\theta}_3$	85°			
<u>Propulsion</u>				
T_1 (sea level)	4,500,000 lb			
T_1 (vacuum)	5,000,000 lb			
Isp_1 (vacuum)	275 sec			
T_2	800,000 lb	1.5 sec	2.5 sec	
Isp_2	400 sec			
T_3	100,000 lb			
Isp_3	400 sec	710 sec	+122.5 lb/sec	+122.5 lb
<u>Weights</u>				
W_{O_1}	2,500,000 lb			
W_{BO_1}	850,000 lb			
W_{P_1}	1,650,000 lb	-50,000 lb	+0.023 lb/lb	+500 lb
W_{ST_1}	250,000 lb			
W_{O_2}	600,000 lb			
W_{BO_2}	245,000 lb			
W_{P_2}	355,000 lb			
W_{ST_2}	10,000 lb	+5,000 lb	+0.422 lb/lb	+2110 lb
W_{O_3}	215,000 lb			
W_{BO_3}	115,000 lb			
W_{P_3}	100,000 lb			
W_{ST_3}	15,000 lb	-1,000 lb	-1.0 lb/lb	-1500 lb
$W_{Pl.}$	100,000 lb			

NOMENCLATURE

g	Acceleration of gravity at sea level
I_{sp}	Vacuum specific impulse
i	Integer corresponding to a particular stage
k	Integer corresponding to a particular stage
N	Integer corresponding to the total number of stages
n	Integer corresponding to a particular stage
r	$\frac{W_O}{W_{BO}} = \text{Mass ratio}$
T	Initial thrust-sea level for the first stage and vacuum for the upper stages
t_B	Stage burning time
V_{BO}	Burnout velocity
W_{BO}	Burnout weight
W_{LO}	Liftoff weight
W_O	Gross weight
W_P	Propellant weight
W_{PL}	Payload weight
W_{ST}	Structure weight
W_{ST}^*	Inert weight including dry weight and trapped propellants below the minimum usable level
$\bar{\beta}$	Average flight path angle
λ	Ratio of sea level specific impulse to vacuum specific impulse
σ	Standard deviation
θ	$\frac{\lambda \cos \bar{\beta}}{\frac{T}{W_O}}$
ΔV_I	Stage ideal velocity
ΔV_g	Velocity losses due to gravitational effects
ΔV_{L_a}	Velocity losses due to atmospheric effects and thrusting at an angle of attack

CHAPTER 5

VEHICLE SIZING

In the field of vehicle preliminary design an engineer requires a knowledge of the basic relationships of the parameters that determine the vehicle physical size and those that define the mission requirements. Relationships of this type range in complexity from the simple equations for a single stage vehicle, to the complicated equations for the optimization of a multistage vehicle in which each stage involves a different design philosophy. It is the object of this chapter to present these relationships in both analytical and graphical form, such that they may be readily adapted to any preliminary design analysis.

The material presented here is intended to aid the designer in determining an optimum vehicle based on design parameters specifying vehicle characteristics. In most cases, the first concern is the minimization of the ratio of vehicle gross weight to payload weight for a specific mission. This type of sizing has been used in the past to determine vehicle sizes for both ballistic missiles and space vehicles. However, other criteria are often used in determining vehicle size. Particular emphasis has recently been placed on the optimization of vehicles for minimum cost. Thus, general optimum sizing, based on any criterion, is included along with the sizing for minimum gross weight - payload weight ratio.

A sizing analysis for any criterion requires that a mission be defined. An examination of the sizing equations indicates that any mission definition is in terms of total ideal velocity, defined as

$$V_{IN} = V_{BOI} - V_{rot} + \Delta V_L \quad (1)$$

where

V_{BOI} = required burnout velocity for the mission of interest

V_{rot} = velocity component due to earth's rotational effects (positive for an eastward launch)

ΔV_L = vehicle velocity losses during flight.

Velocity losses, which are dependent on both the known and unknown vehicle parameters, can be estimated by using the techniques of loss estimation shown in Chapter 2. The unknown parameters, i. e., weights and weight ratios, can usually

be assumed so that the overall loss estimate will be reasonably accurate. In some cases, the velocity losses of vehicles analyzed for the same kind of mission can be used, providing the vehicle characteristics are somewhat the same as for the vehicle being sized.

Before proceeding with the sizing analysis, an important parameter, structure factor, should be discussed. Structure factor, defined as

$$\sigma_n = \frac{W_{O_n} - W_{O_{n+1}} - W_{P_n}}{W_{O_n} - W_{O_{n+1}}} \quad (2)$$

where

W_{O_n} = stage gross weight

W_{P_n} = stage propellant weight,

usually represents that fraction of the stage weight that is not usable propellant and is, therefore, a nondimensional parameter important in vehicle sizing. An examination of vehicle stages presently in use will indicate a range of structure factors from 0.05 to 0.20, or higher. It is apparent that the structure factor is also dependent on such parameters as the type of propellant, the stage thrust level, the weight supported by the stage, and the size of the stage; however, once the design criteria for the stage have been defined to the point that the propellant and thrust level have been chosen, the major contributor to the variation of structure factor is stage size. In almost all cases, an increase in the size of a given type of stage will decrease the stage structure factor (indicating that a more efficient container can be built for increasing propellant weights). In relation to vehicle sizing, the variation of structure factor with stage weight must be included when a sizing analysis is undertaken. It will be pointed out, however, that the use of a constant structure factor with an iterative procedure to include the variation is considerably easier than solving the sizing equations with the variation taken directly into account.

The following relationships for vehicle sizing* are divided into two categories: In the first, expressions, which are relatively simple because of their basic assumptions, are presented to be used in cursory investigations where the assumptions can be tolerated. More complicated, but also more realistic, expressions for vehicle sizing are presented in Section 3.

* The derivation for the equations given in the following sections are found in Appendix D.

5.1 PAYLOAD RATIO

The ratio of vehicle gross weight to payload weight, defined as the payload ratio, is the basic parameter of interest in vehicle sizing. A payload ratio defines an infinite number of vehicle sizes and corresponding payloads that will perform a particular mission, assuming the number of stages, the structure factors, and the velocity losses remain constant. Thus, it becomes an important tool in preliminary design for comparison purposes since it essentially represents the efficiency of the vehicle configuration for the design mission. After having determined the payload ratio, the specific vehicle characteristics, such as propellant and stage weights, can be found for either a specified gross weight or payload weight.

5.1.1 One Stage

The expression for the payload ratio of a one stage vehicle is

$$\frac{W_O}{W_{PL}} = \frac{1 - \sigma}{e^{\frac{V_I}{g \text{Isp}} - \sigma}} \quad (3)$$

where

$$\frac{V_I}{g \text{Isp}} = \text{the nondimensional ideal velocity ratio}$$

The payload ratio is presented in graphical form in Figures 1 and 2 for a range of structure factors from 0.05 to 0.20.

5.1.2 Infinite Staging

The payload ratio for a one stage vehicle represents the maximum value that would ever be required to perform a given mission. On the other hand, the minimum value of payload ratio for the same mission is obtained for a vehicle with an infinite number of stages. Generally the payload ratio of a vehicle with a large number of stages ($N > 10$) of equal structure factor and specific impulse will approach the infinite stage value. The payload for such an infinitely staged vehicle is

$$\frac{W_O}{W_{PL}} = e^{\left(\frac{V_{I_N}}{g \text{Isp} (1 - \sigma)} \right)} \quad (4)$$

The graphical representation of the payload ratio is shown on Figures 3 and 4.

5.1.3 Multiple Staging

When considering vehicles of multiple stages, three different classes come to mind:

- 1) Vehicles with stages of equal structure factor and specific impulse
- 2) Vehicles with stages of equal specific impulse but with different structure factors
- 3) Vehicles with stages of unlike parameters.

The first two classes are considered here, while the third class is analysed later.

Stages of Like Parameters. The probability of constructing a vehicle with stages of equal parameters is unlikely. However, analysis of such a vehicle provides information on the effect of increasing the number of stages of a vehicle, as well as providing a rapid method of sizing a multi-stage vehicle for preliminary design investigation. The optimum sizing equation developed in this section indicates that a vehicle of like parameters should have equal stage payload ratios for optimum sizing.

$$\frac{W_{O1}}{W_{O2}} = \frac{W_{O2}}{W_{O3}} = \dots = \frac{W_{Oi}}{W_{Oi+1}} = \dots = \frac{W_{ON}}{W_{PL}} \quad (5)$$

implying equal ideal velocities per stage such that

$$V_{I_N} = NV_{I_n} \quad (6)$$

where

N = number of stages

V_{I_n} = ideal velocity of one stage.

The payload ratio for a vehicle with like parameters is

$$\frac{W_O}{W_{PL}} = \left(\frac{1 - \sigma}{\frac{V_{I_N}}{e^{NgIsp} - \sigma}} \right)^N \quad (7)$$

This equation is graphically represented in Figures 5 through 36 for vehicles with one to five stages and with structure factors ranging from 0.05 to 0.20.

Unlike Structure Factors. The assumption of stages with like specific impulses but unlike structure factors approaches reality when the clustering of solid propellant engines is considered. In such a case, the specific impulse of each stage would remain constant while the structure factor would vary slightly from stage to stage due to the effect of clustering engines.

The direct solution of the optimization equation of Section 5.3.1 for unlike structure factors becomes involved for vehicles of more than two stages; thus, this analysis will be presented for a two stage vehicle. As developed in Appendix D, the equation for payload ratio of a two stage vehicle with like specific impulses but unlike structure factors is

$$\frac{W_O}{W_{PL}} = \frac{(1-\sigma_1)(1-\sigma_2)}{\left(\frac{V_{IN}}{e^{2gisp} - \sqrt{\sigma_1\sigma_2}} \right)^2} \quad (8)$$

The payload ratio is shown graphically in Figures 37 through 52. The payload ratio of each individual stage can be determined by the use of the payload ratio distribution factor shown in Figure 53. For vehicles of three or more stages with unlike structure factors, the figure can be used by optimally sizing the first stage with respect to the second, the second with respect to the third and so on.

5.2 STAGE MASS RATIO

In order to define characteristics of stages after having sized a vehicle, analytical and graphical expressions for stage mass ratio are included for the classes of vehicles considered in the preceding subsection.

5.2.1 One Stage

The analytical expression for the mass ratio of a single stage is

$$r = e^{\frac{V_I}{gisp}} = \frac{\frac{W_O}{W_{PL}}}{\sigma \frac{W_O}{W_{PL}} + (1-\sigma)} \quad (9)$$

where

$$r = \frac{W_O}{W_{BO}}$$

Equation (9), as a function of the ideal velocity ratio, is shown in graphical form in Figure 54.

5.2.2 Infinite Staging

The vehicle mass ratio for an infinitely staged vehicle is simply equal to the payload ratio.

$$r = \frac{W_O}{W_{PL}} \quad (N = \infty)$$

5.2.3 Multiple Staging

Like Parameters. Equation (6) indicated that the total ideal velocity, V_{IN} , of an optimally sized vehicle with like parameters was divided equally among the stages. Thus the mass ratio of each stage is

$$r_n = e^{\frac{V_{IN}}{N g I_{sp}}} \quad (10)$$

shown in Figure 54 as a function of the ideal velocity ratio.

Two-Stage Vehicle with Unlike Structure Factors. The mass ratio of any stage is shown by Equation (9) to be

$$\frac{W_{O_n}}{W_{BO_n}} = \frac{\frac{W_{O_n}}{W_{O_{n+1}}}}{\sigma_n \frac{W_{O_n}}{W_{O_{n+1}}} + (1 - \sigma_n)} \quad (11)$$

Since the individual stage payload ratios for the vehicle of interest have been determined by Equation (8) and Figure 53, the individual mass ratios can be determined from Equation (11). Graphically, Equation (11) is presented in Figures 55 through 57. These figures can also be used for a single-stage vehicle where

$$\frac{W_{O_n}}{W_{O_{n+1}}} = \frac{W_O}{W_{PL}}$$

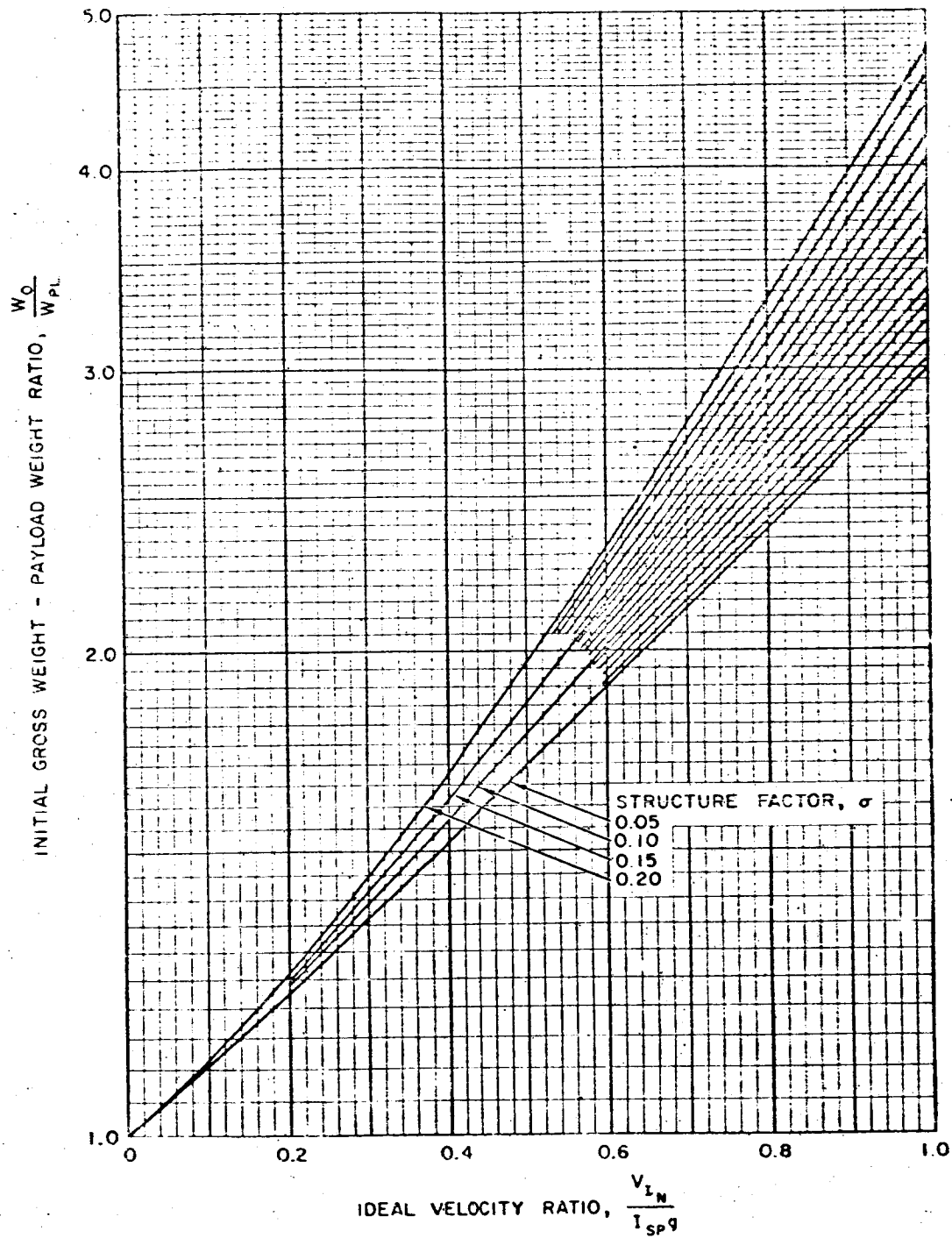


Figure 1. Payload Ratio (Single-Stage Vehicle)

VEHICLE SIZING

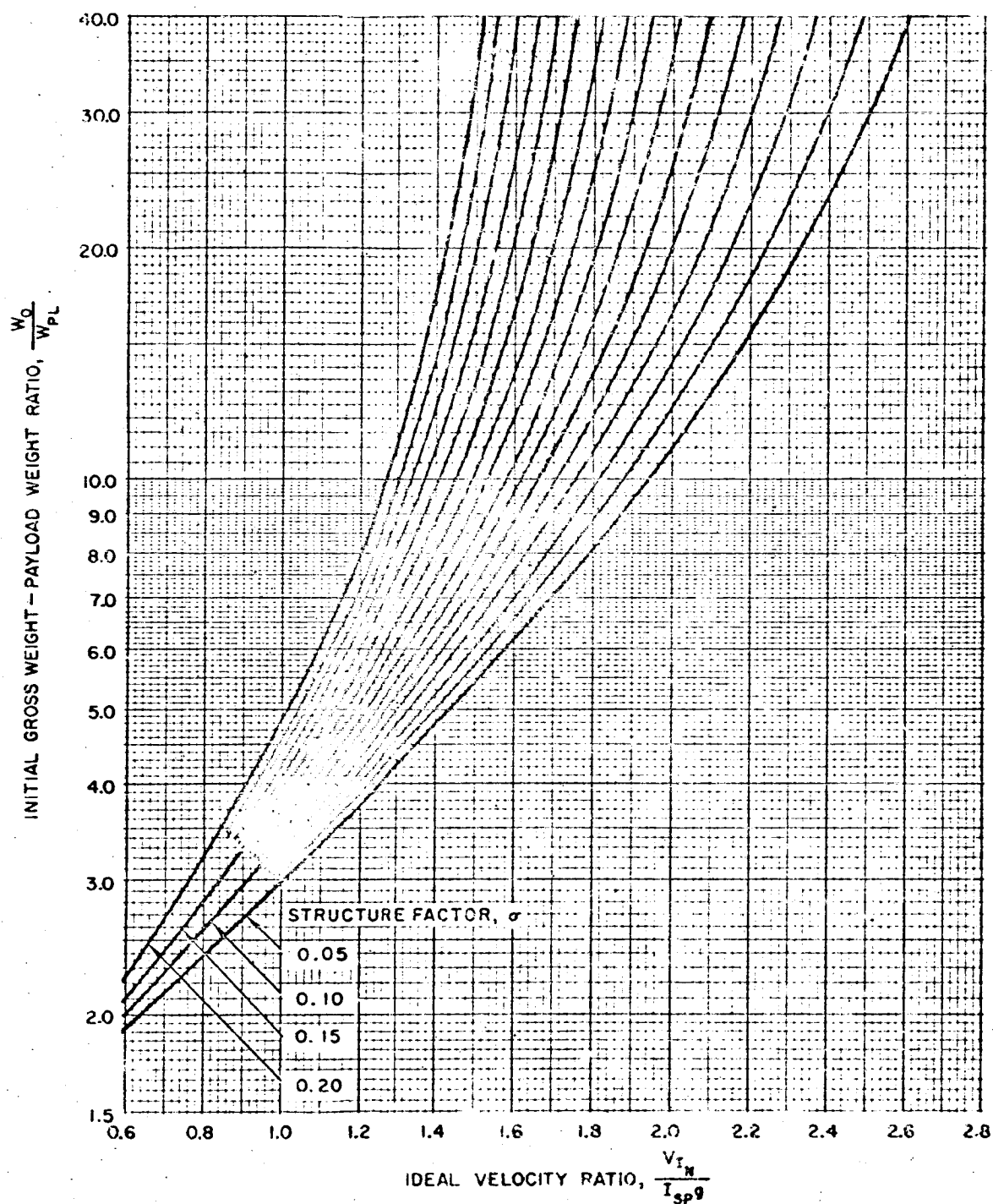


Figure 2. Payload Ratio (Single-Stage Vehicle)

Payload Ratio

5-9

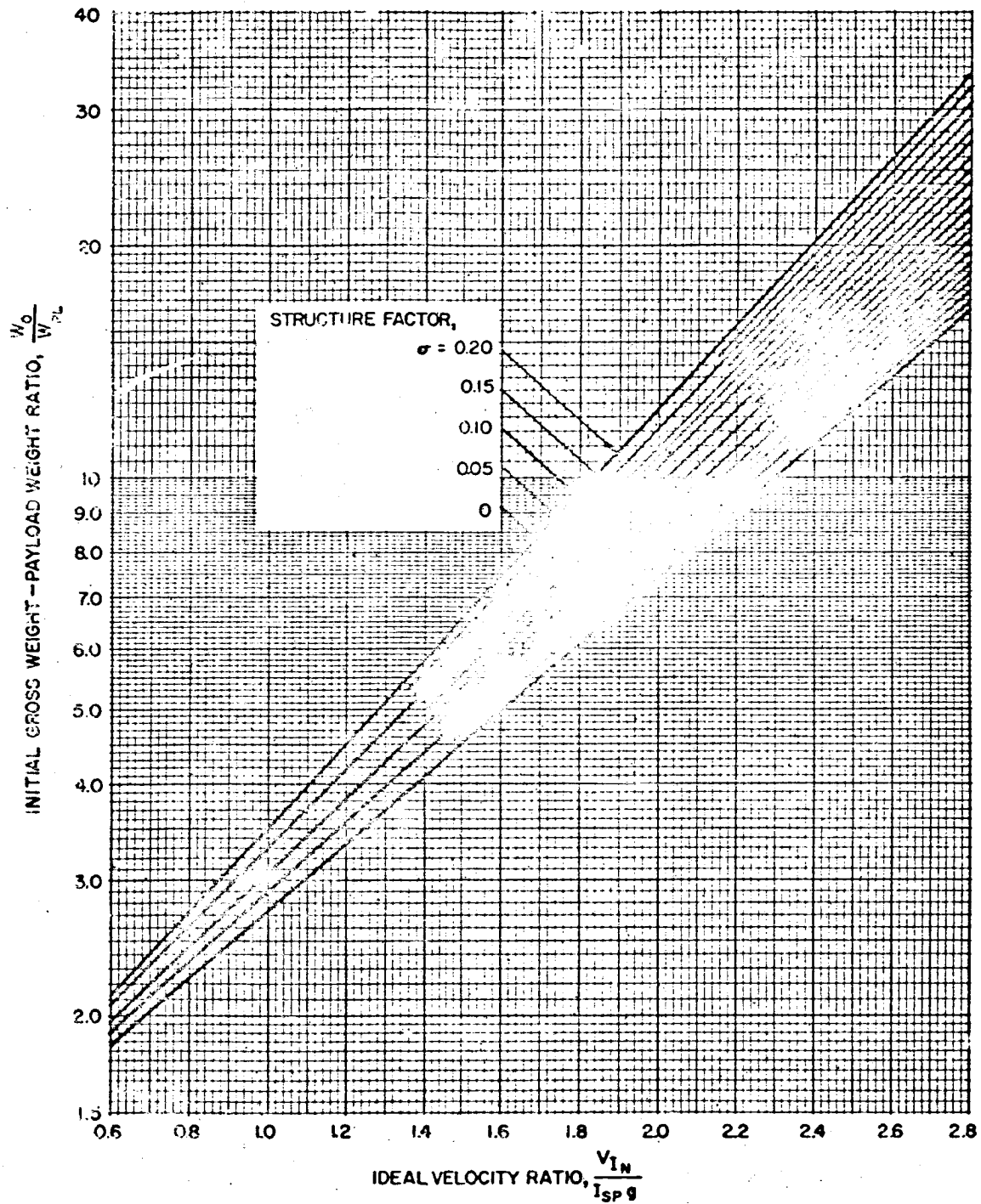


Figure 3. Payload Ratio (Infinite Staging)

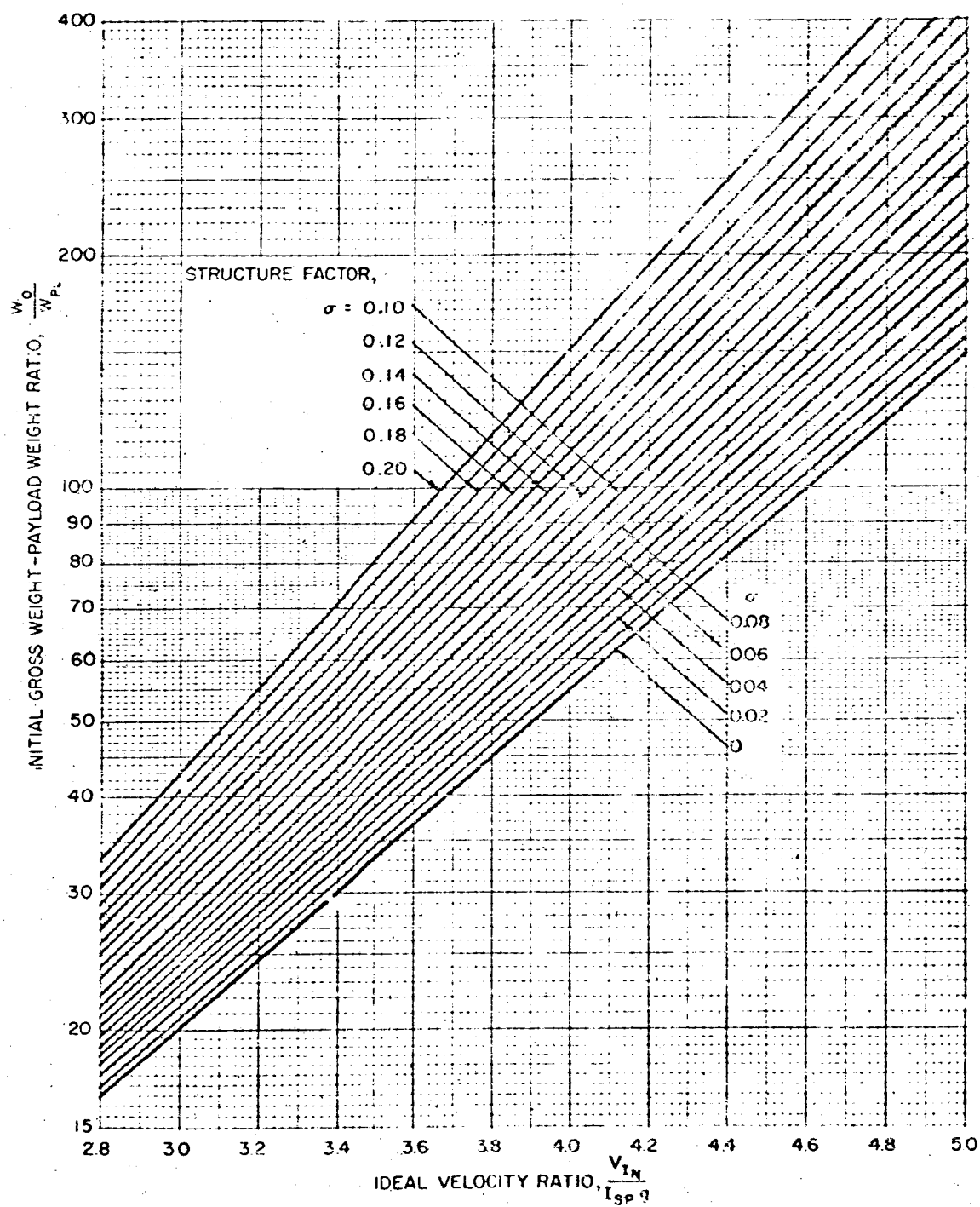


Figure 4. Payload Ratio (Infinite Staging)

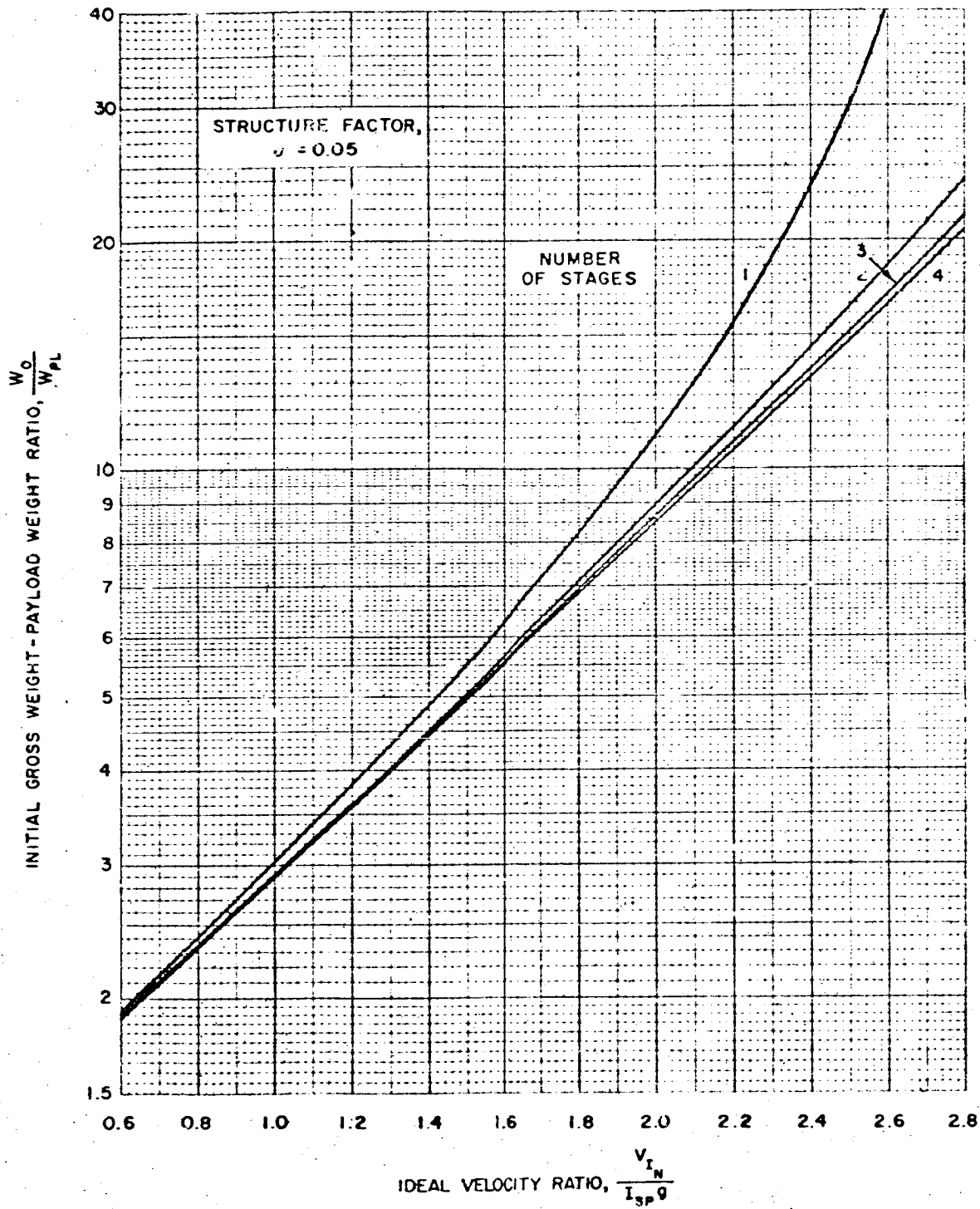


Figure 5. Payload Ratio for Like Parameters (Multiple Stage)

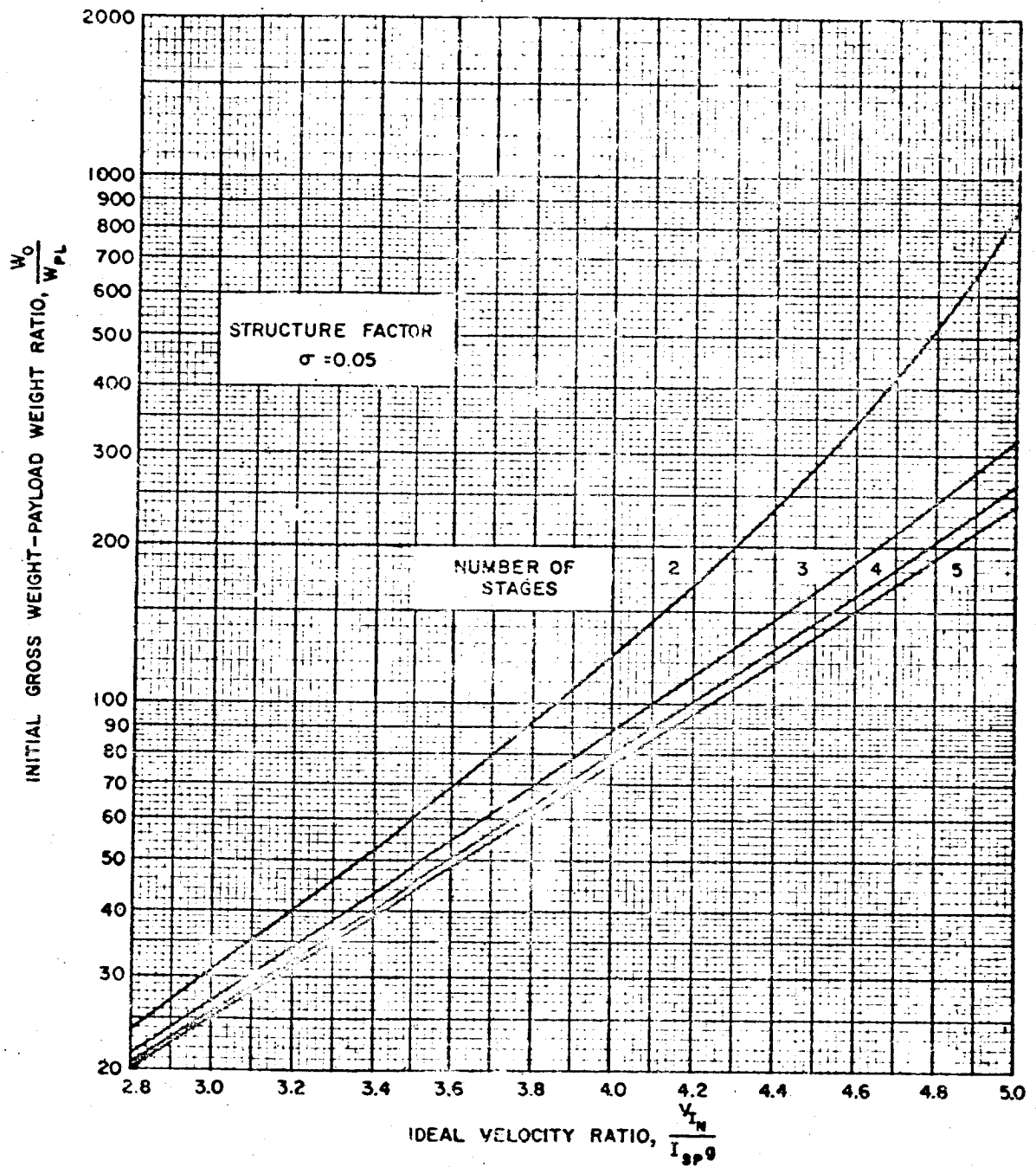


Figure 6. Payload Ratio for Like Parameters (Multiple Stage)

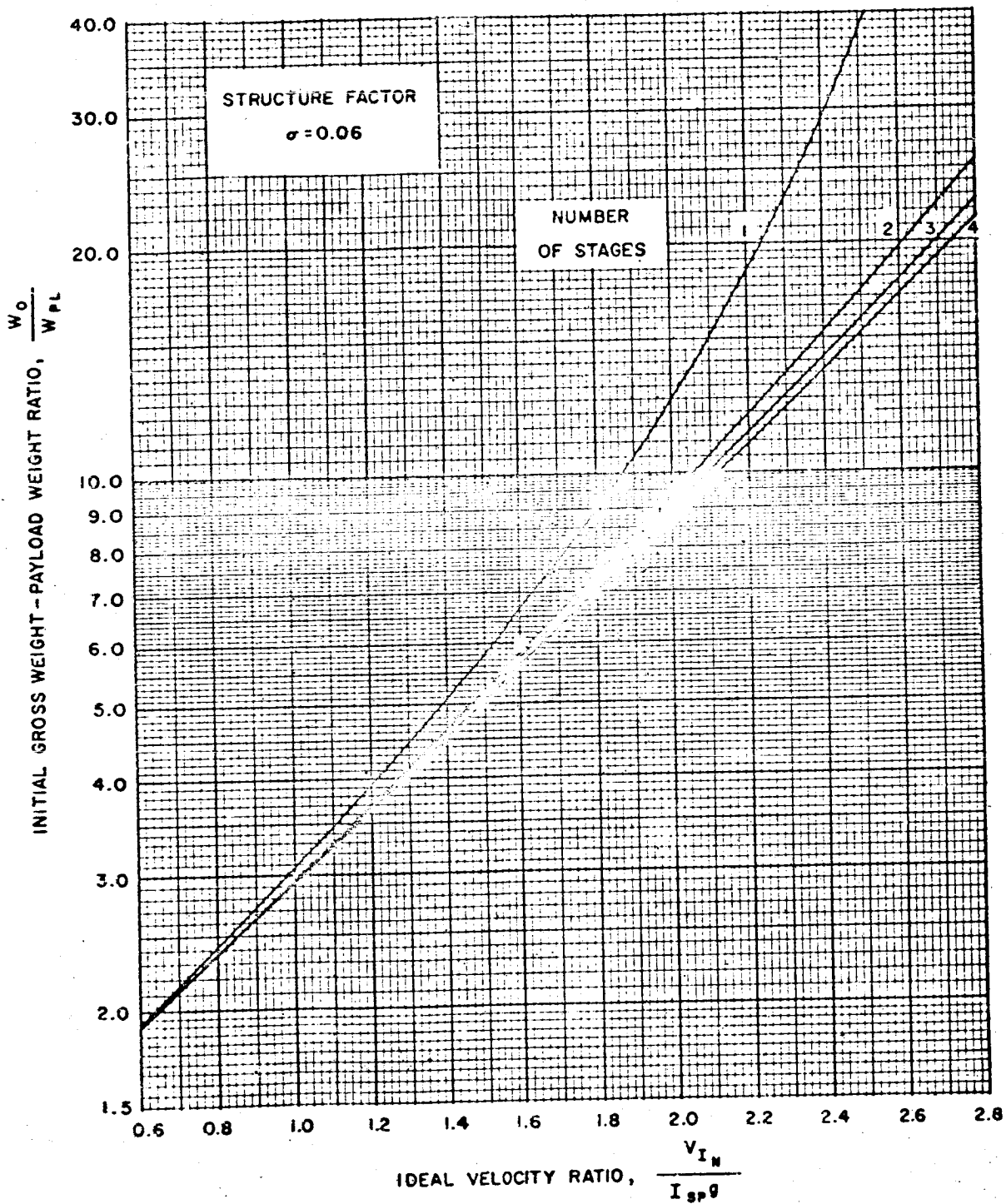


Figure 7. Payload Ratio for Like Parameters (Multiple Stage)

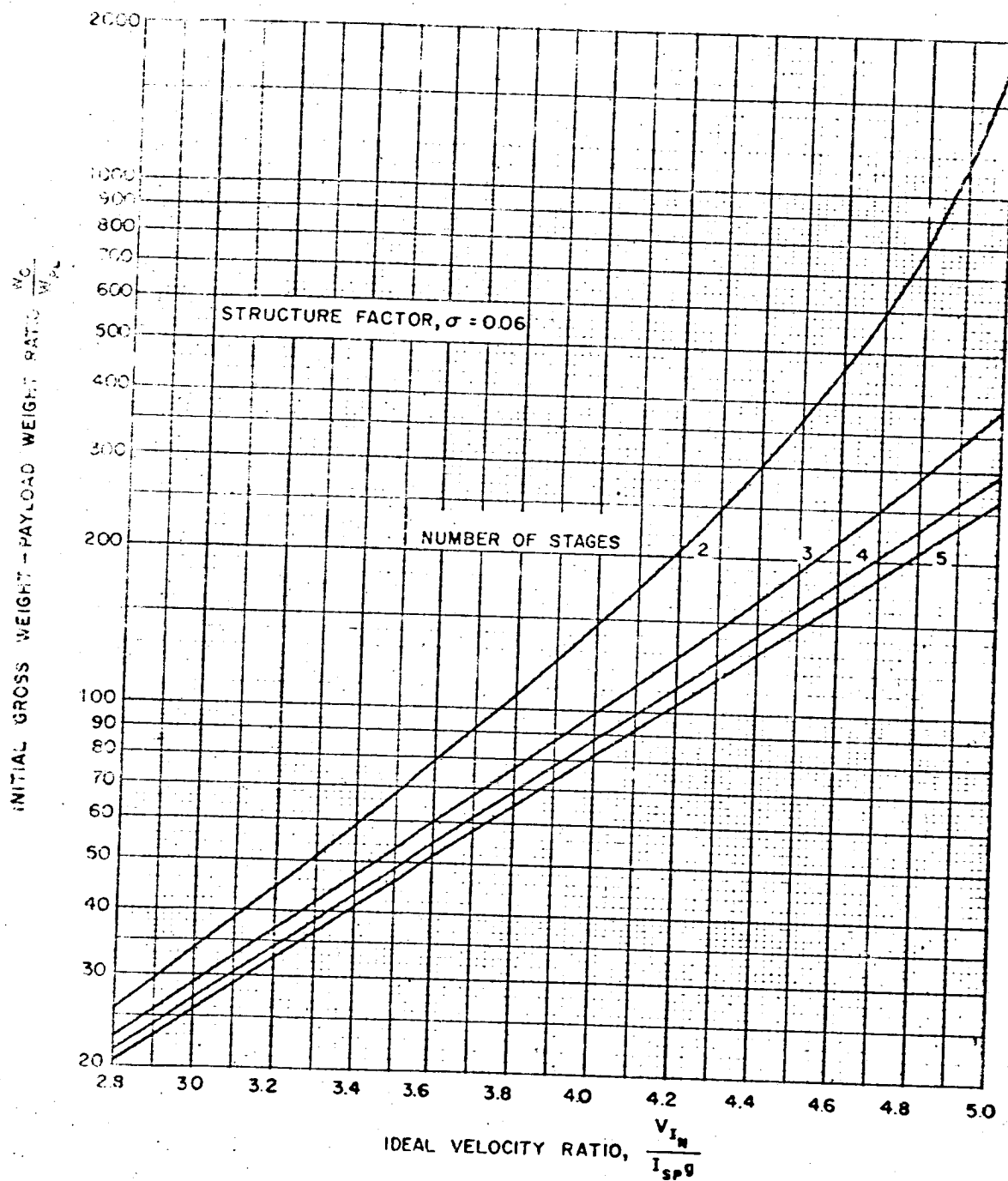


Figure 8. Payload Ratio for Like Parameters (Multiple Stage)

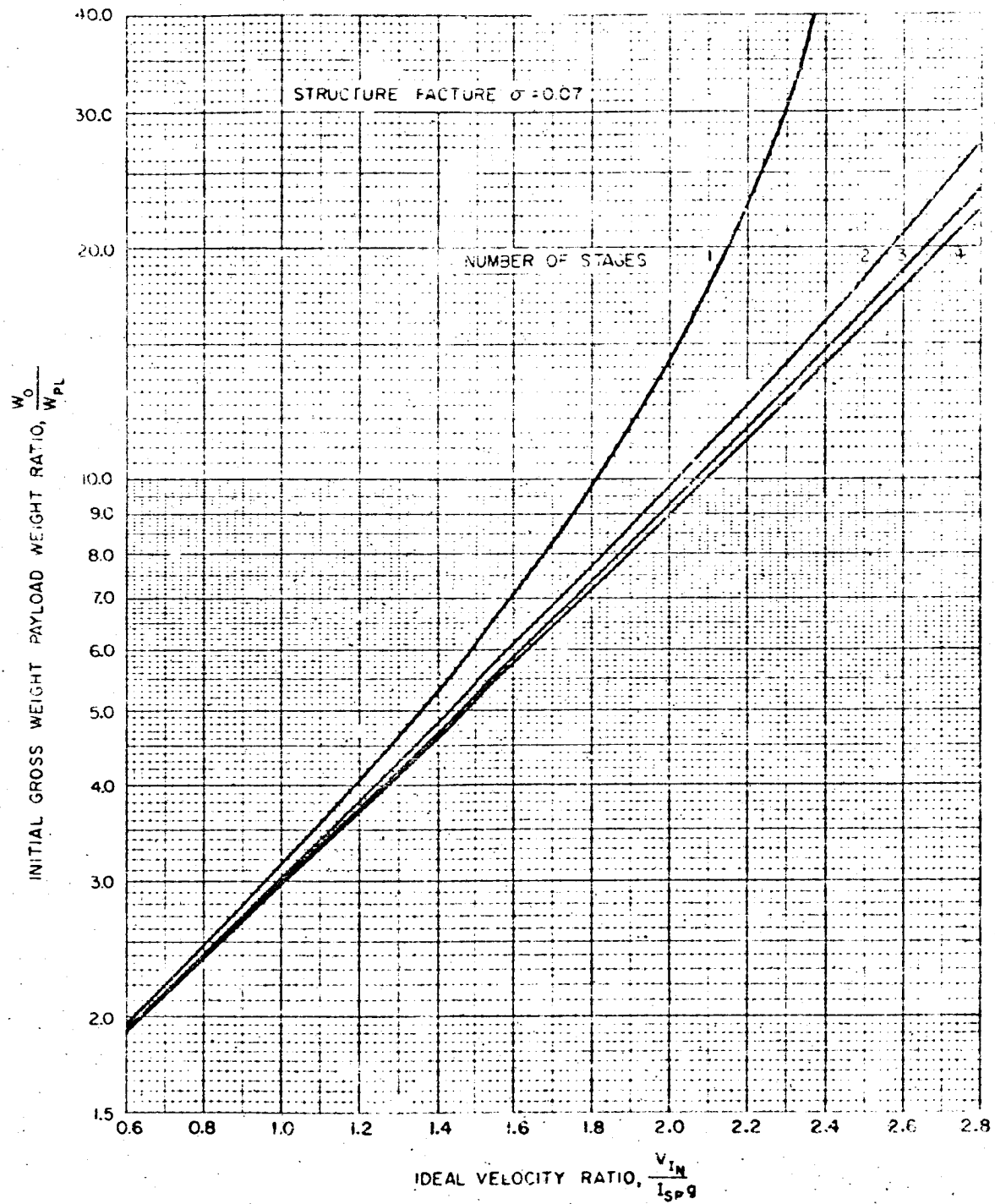


Figure 9. Payload Ratio for Like Parameters (Multiple Stage)

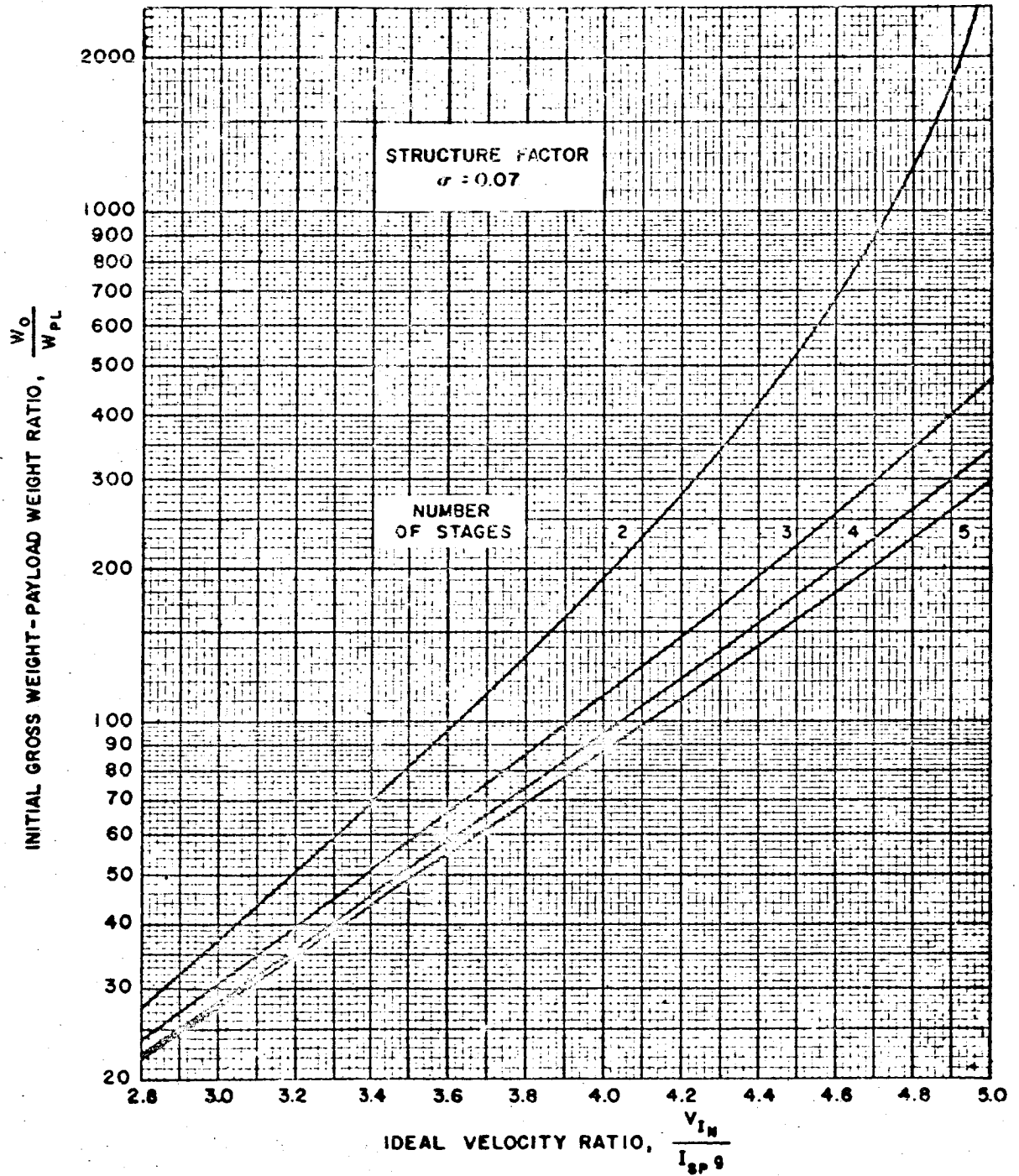


Figure 10. Payload Ratio for Like Parameters (Multiple Stage)

Payload Ratio

5-17

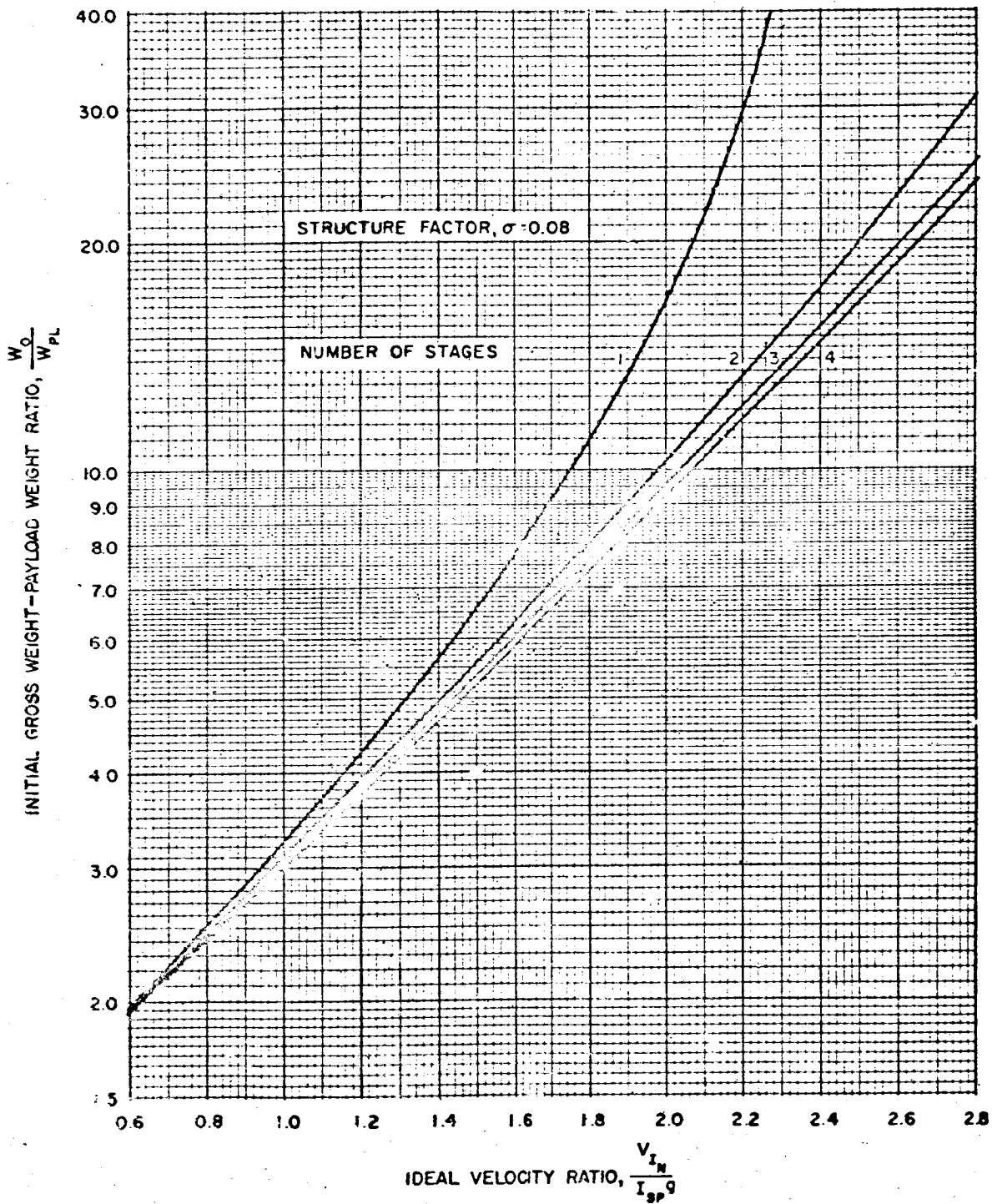


Figure 11. Payload Ratio for Like Parameters (Multiple Stage)

5-18

VEHICLE SIZING

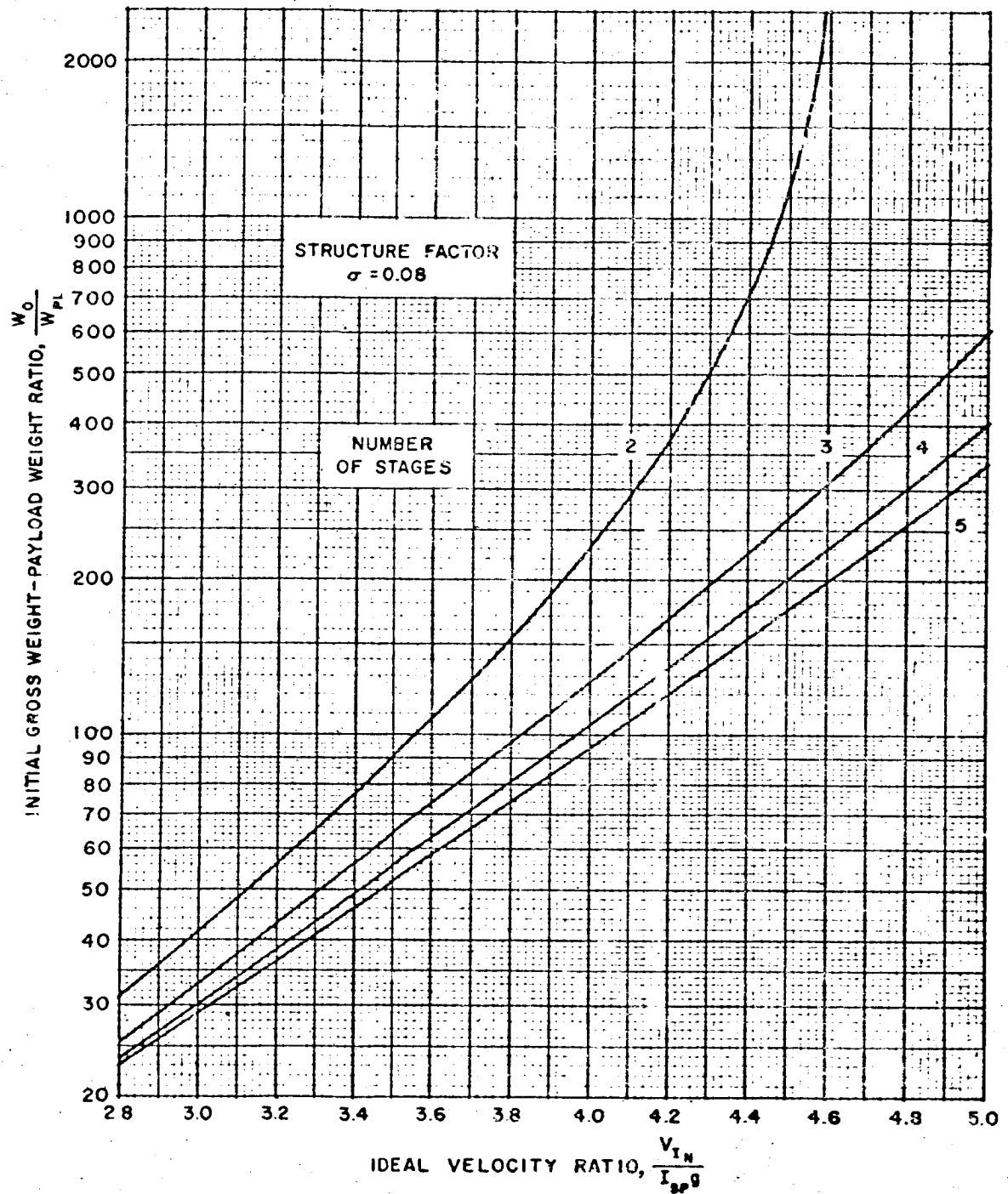


Figure 12. Payload Ratio for Like Parameters (Multiple Stage)

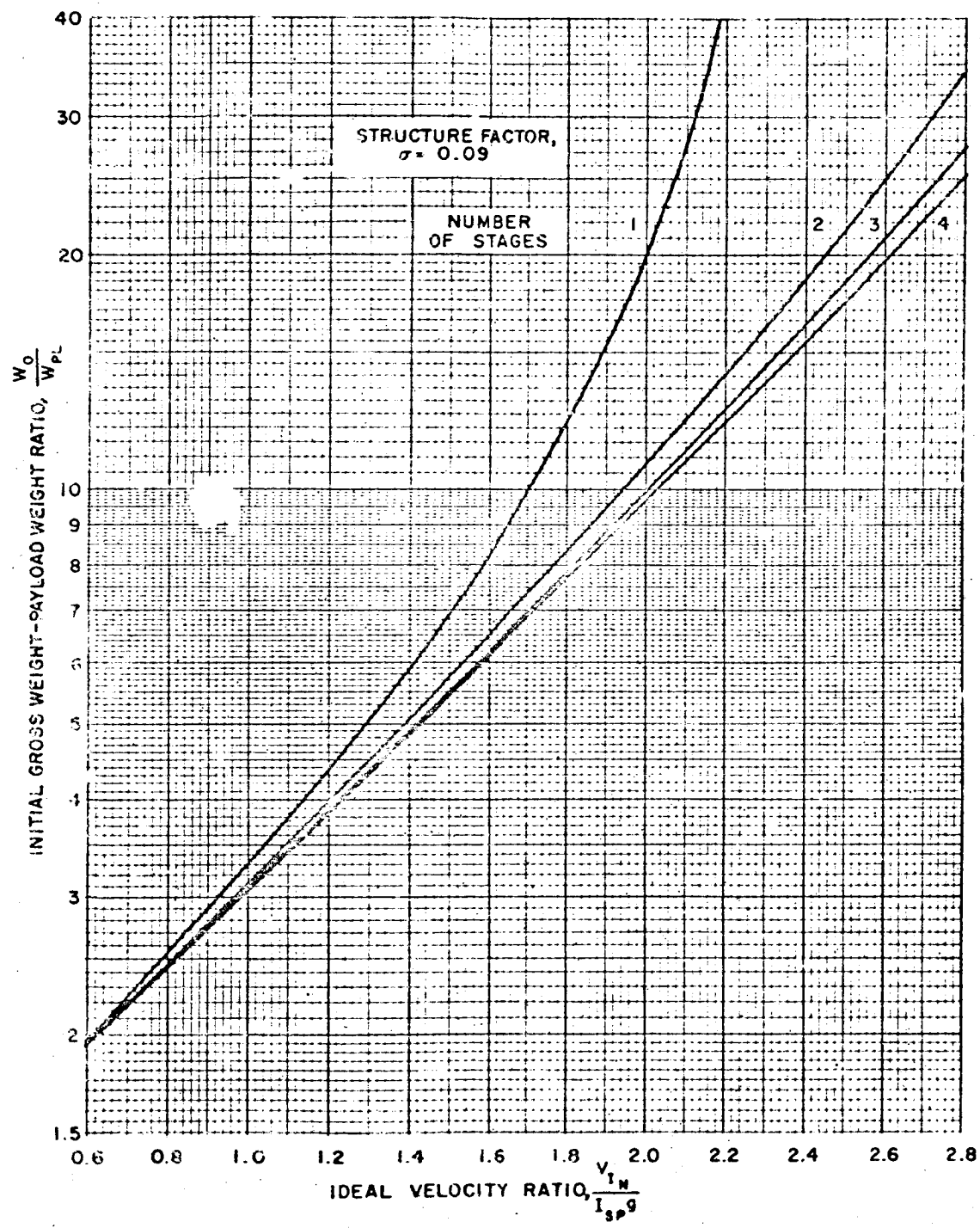


Figure 13. Payload Ratio for Like Parameters (Multiple Stage)

S-20

VEHICLE SIZING

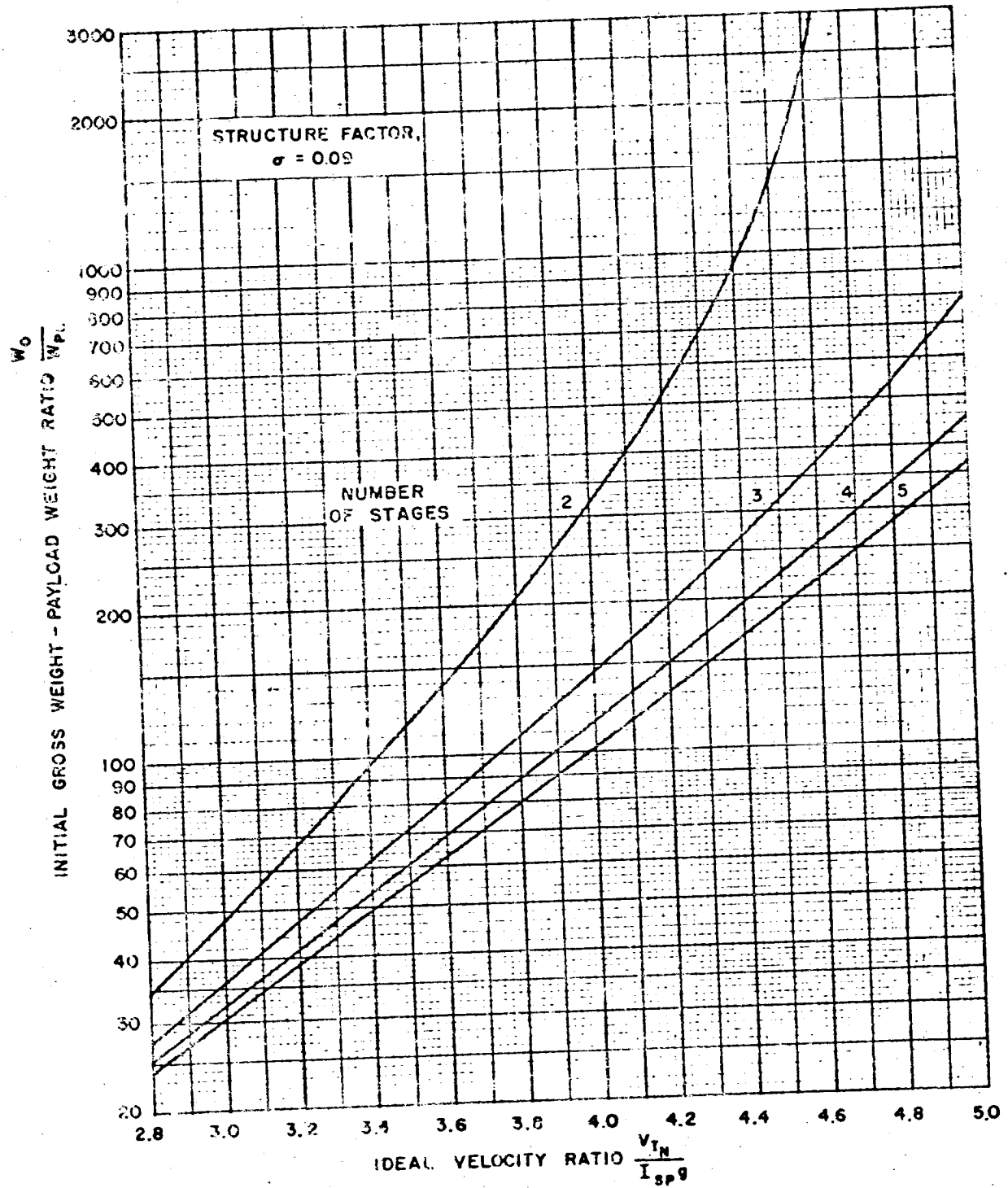


Figure 14. Payload Ratio for Like Parameters (Multiple Stage)

Payload Ratio

5-21

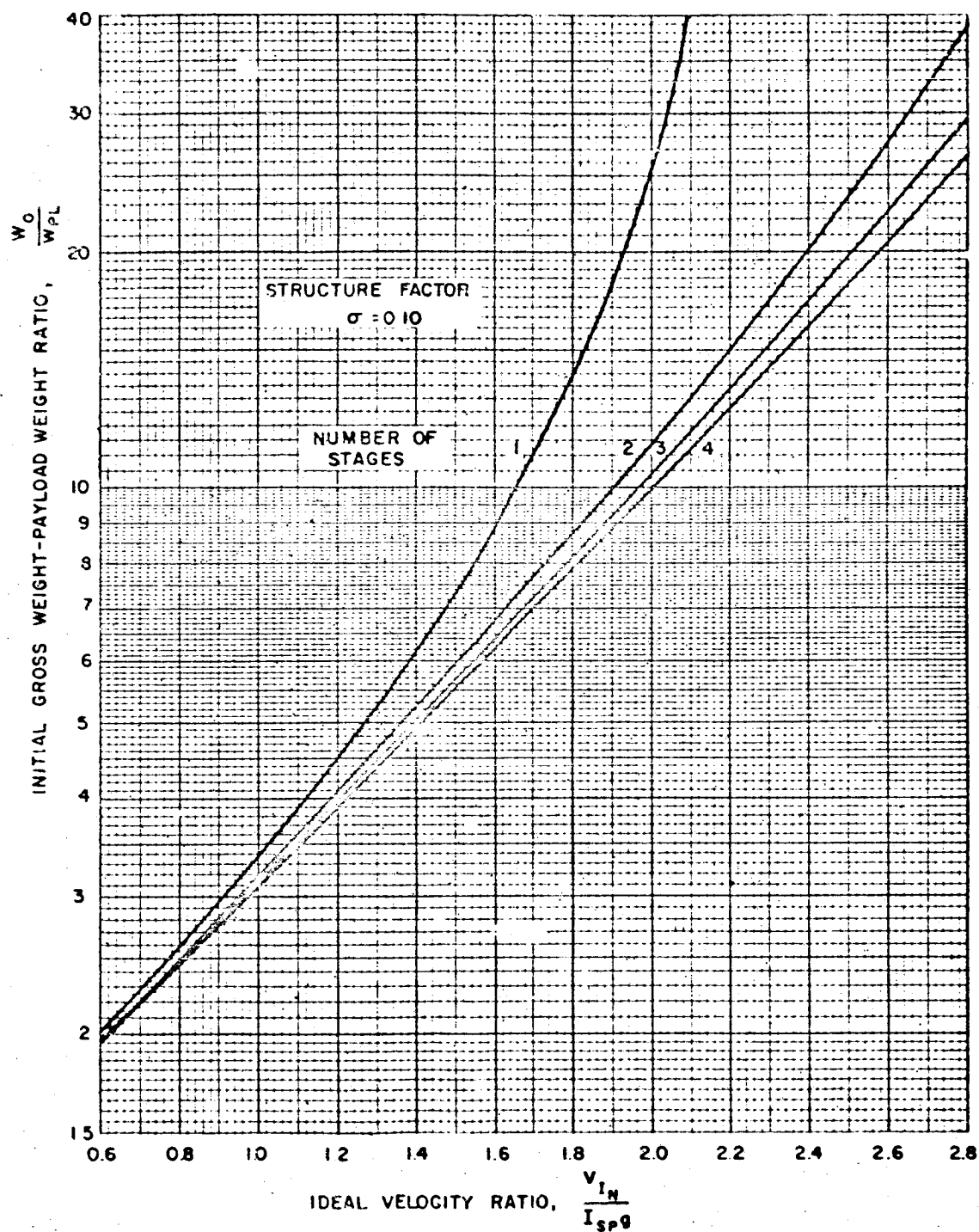


Figure 15. Payload Ratio for Like Parameters (Multiple Stage)

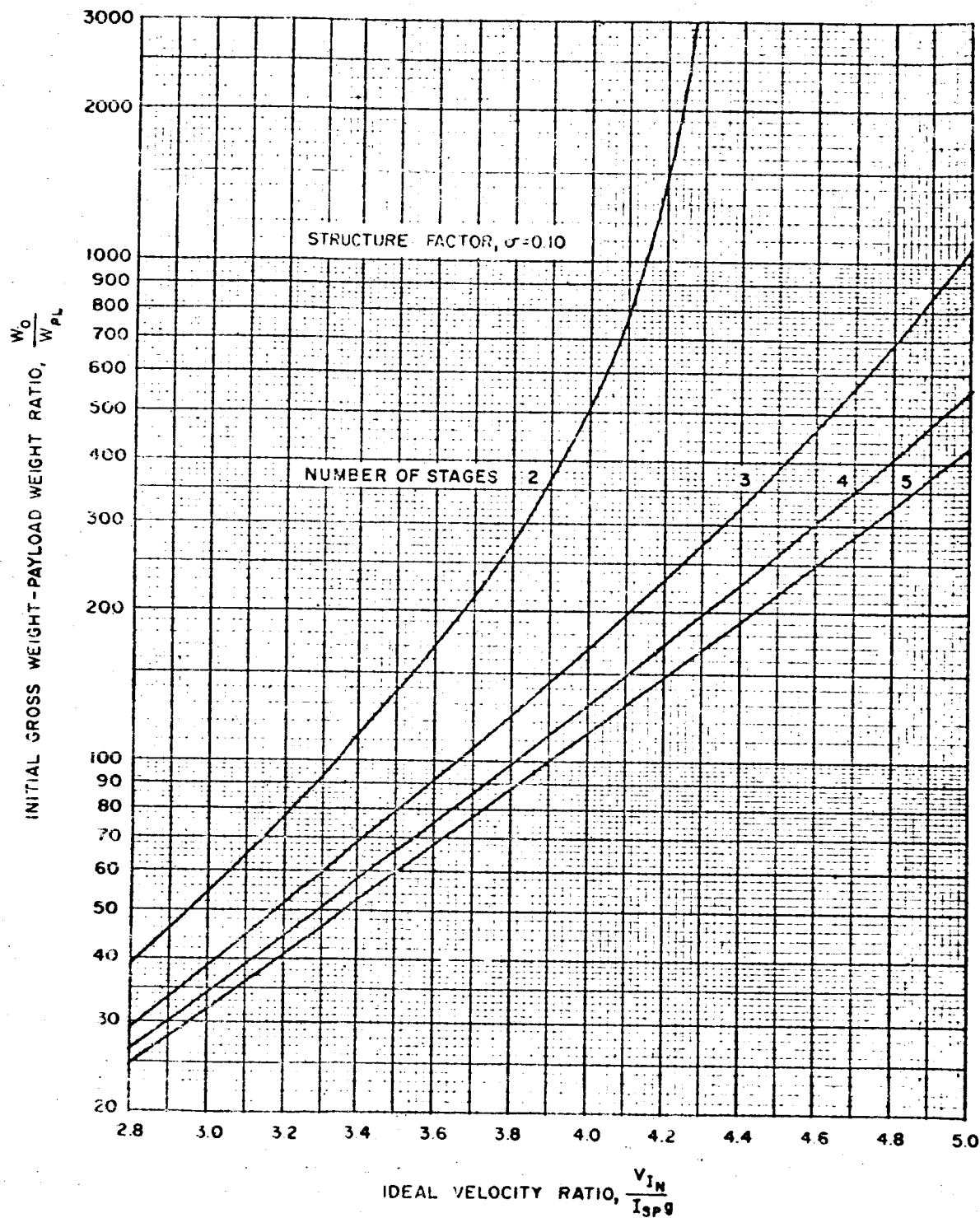


Figure 16. Payload Ratio for Like Parameters (Multiple Stage)

Payload Ratio

5-23

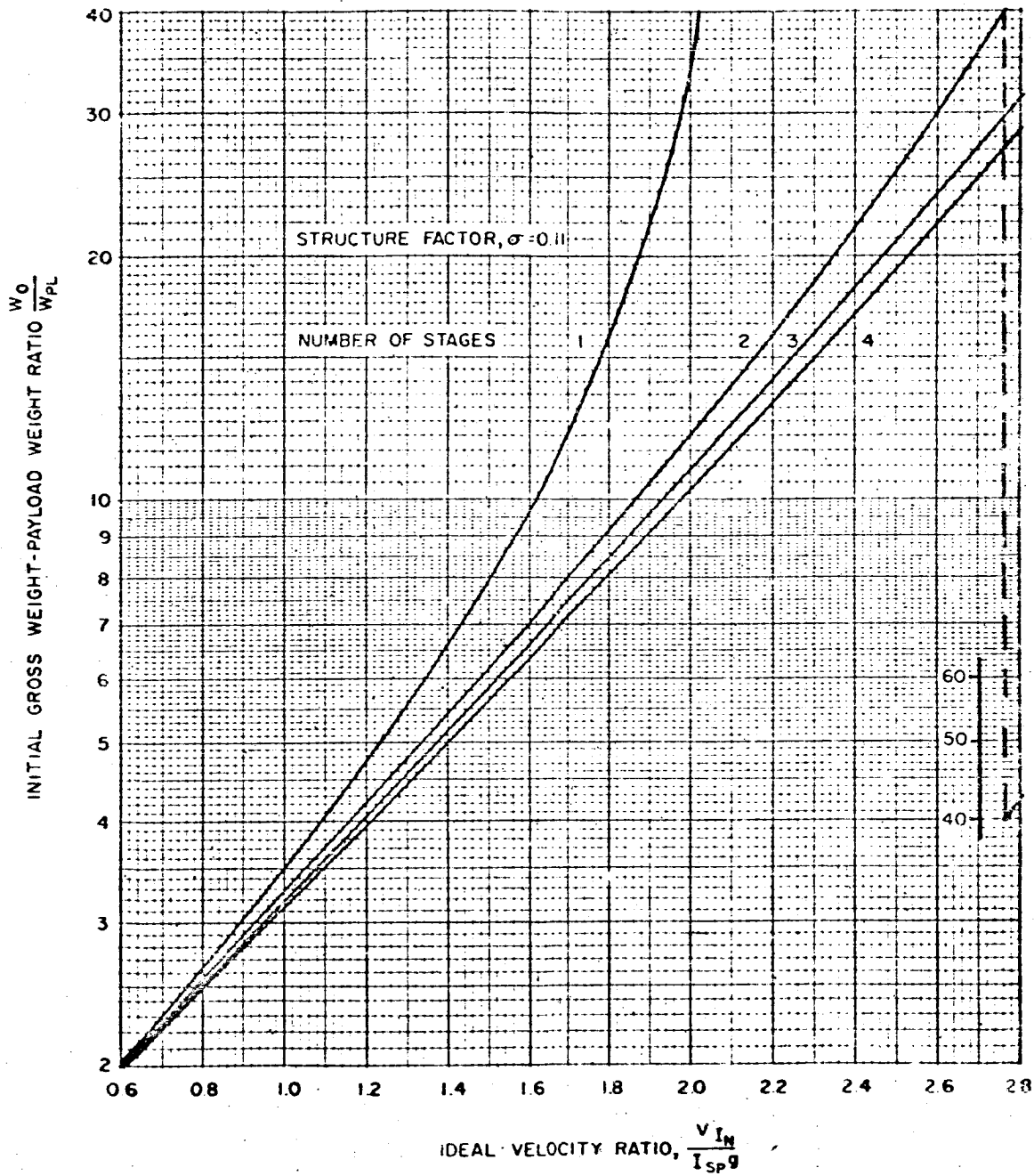


Figure 17. Payload Ratio for Like Parameters (Multiple Stage)

5-24

VEHICLE SIZING

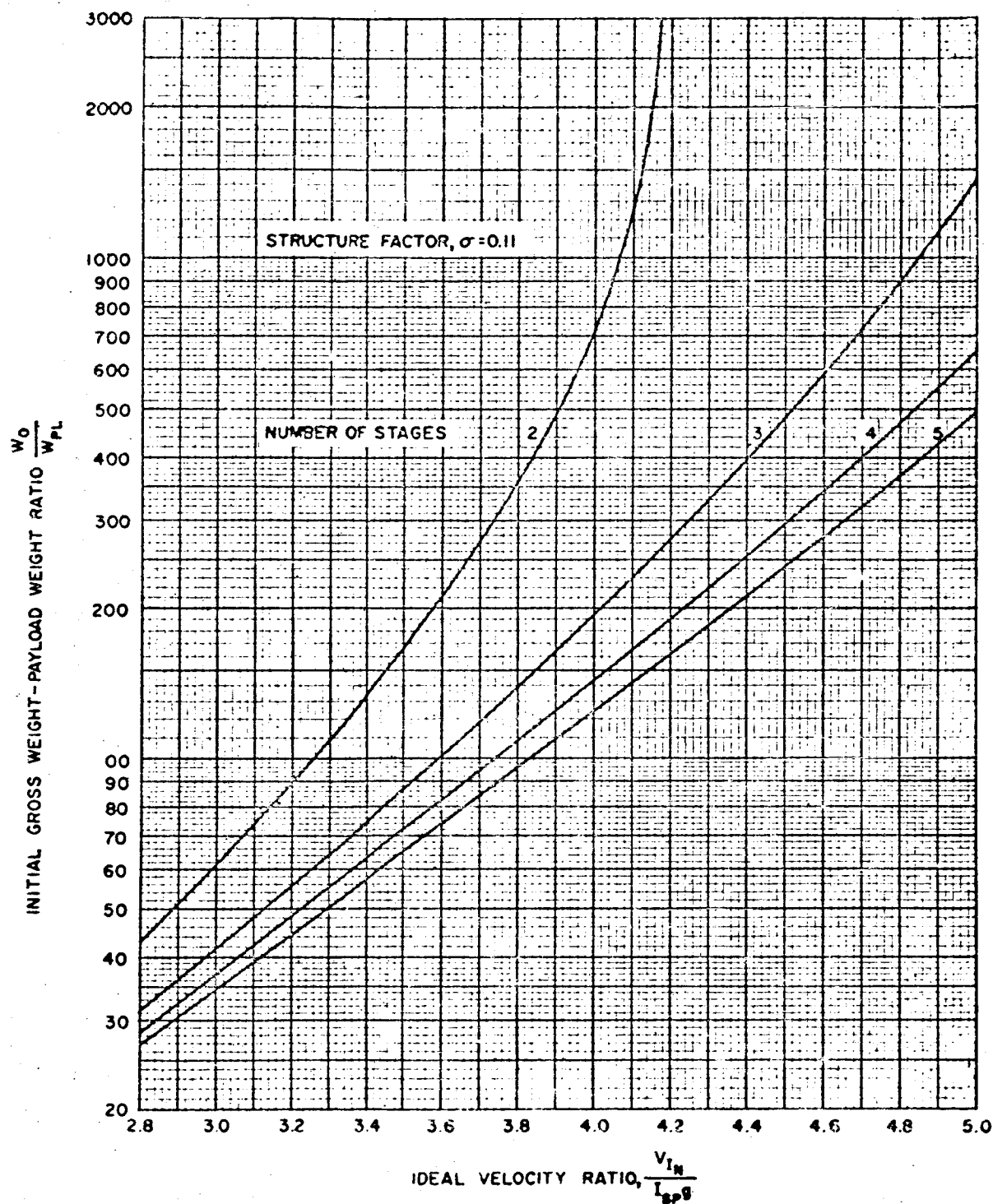


Figure 18. Payload Ratio for Like Parameters (Multiple Stage)

Payload Ratio

5-25

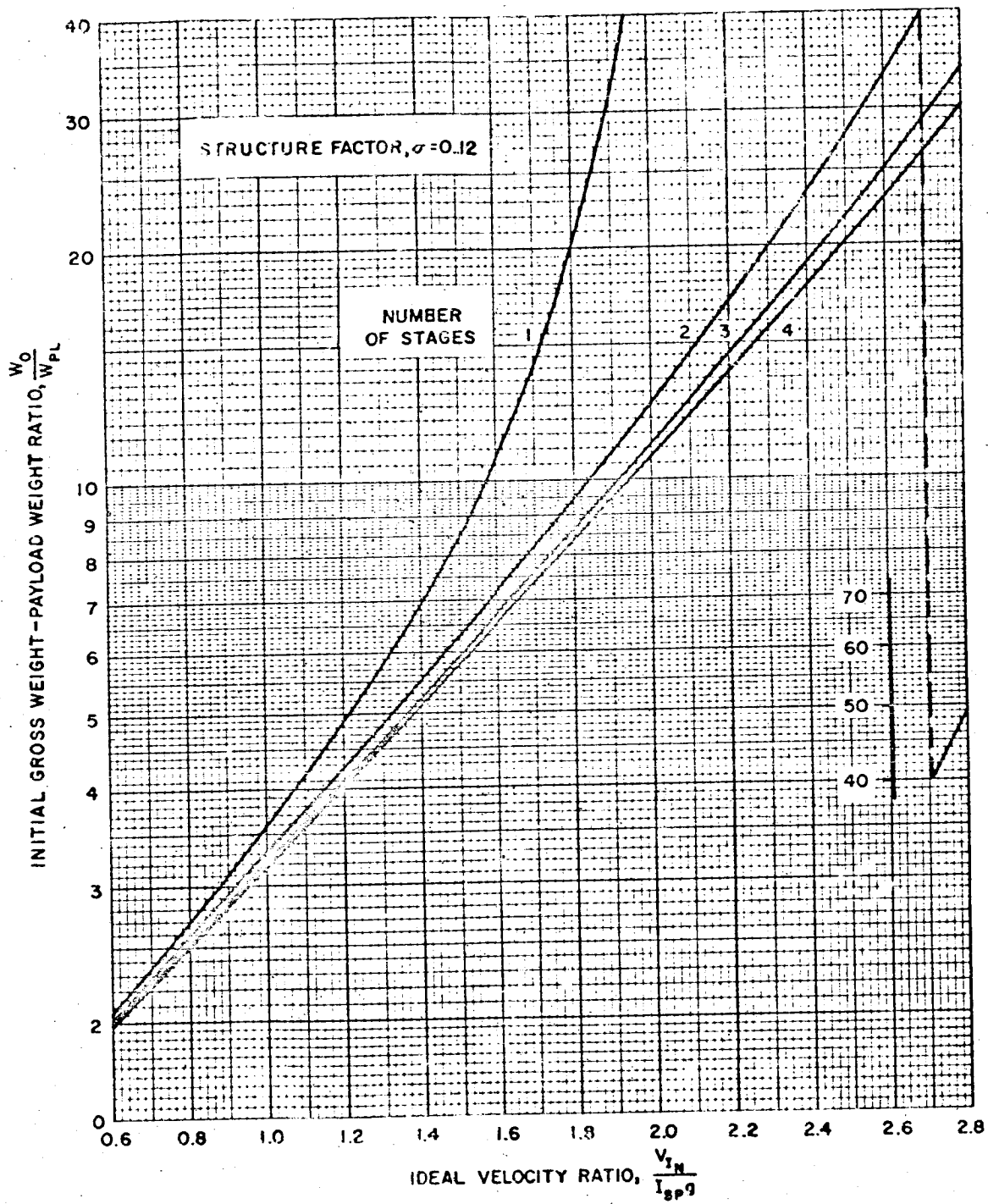


Figure 19. Payload Ratio for Like Parameters (Multiple Stage)

5-26

VEHICLE SIZING

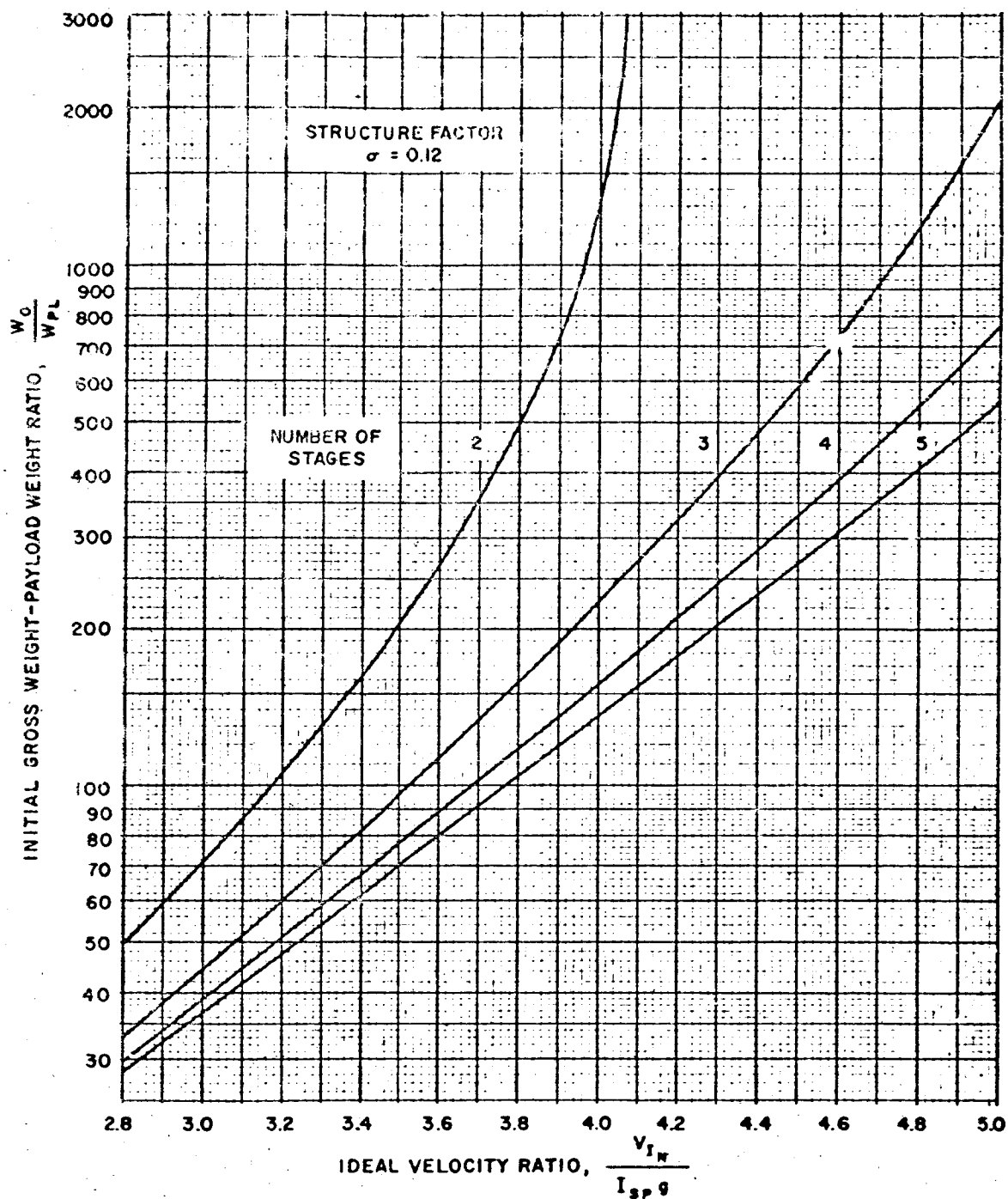


Figure 20. Payload Ratio for Like Parameters (Multiple Stage)

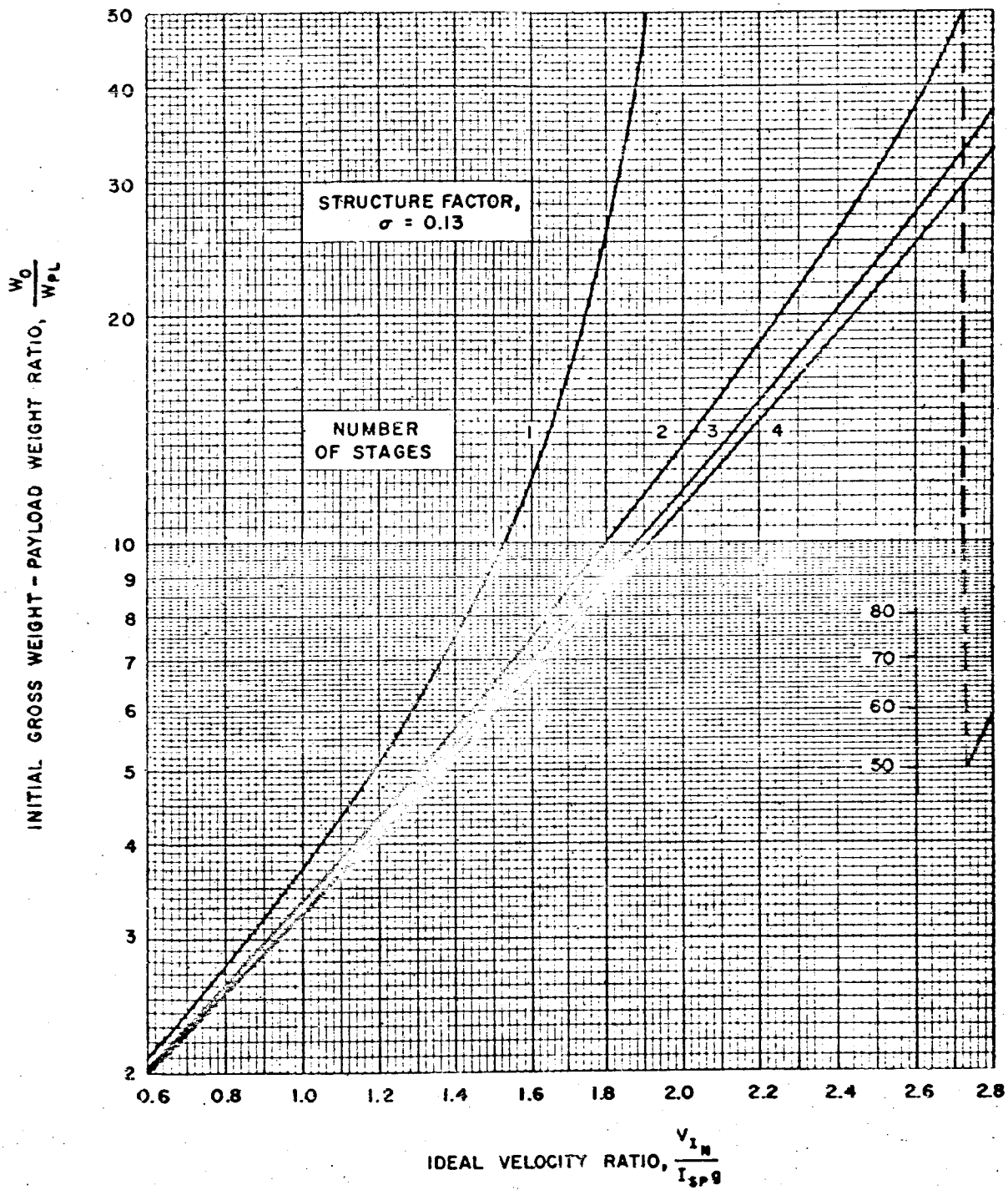


Figure 21. Payload Ratio for Like Parameters (Multiple Stage)

5-28

VEHICLE SIZING

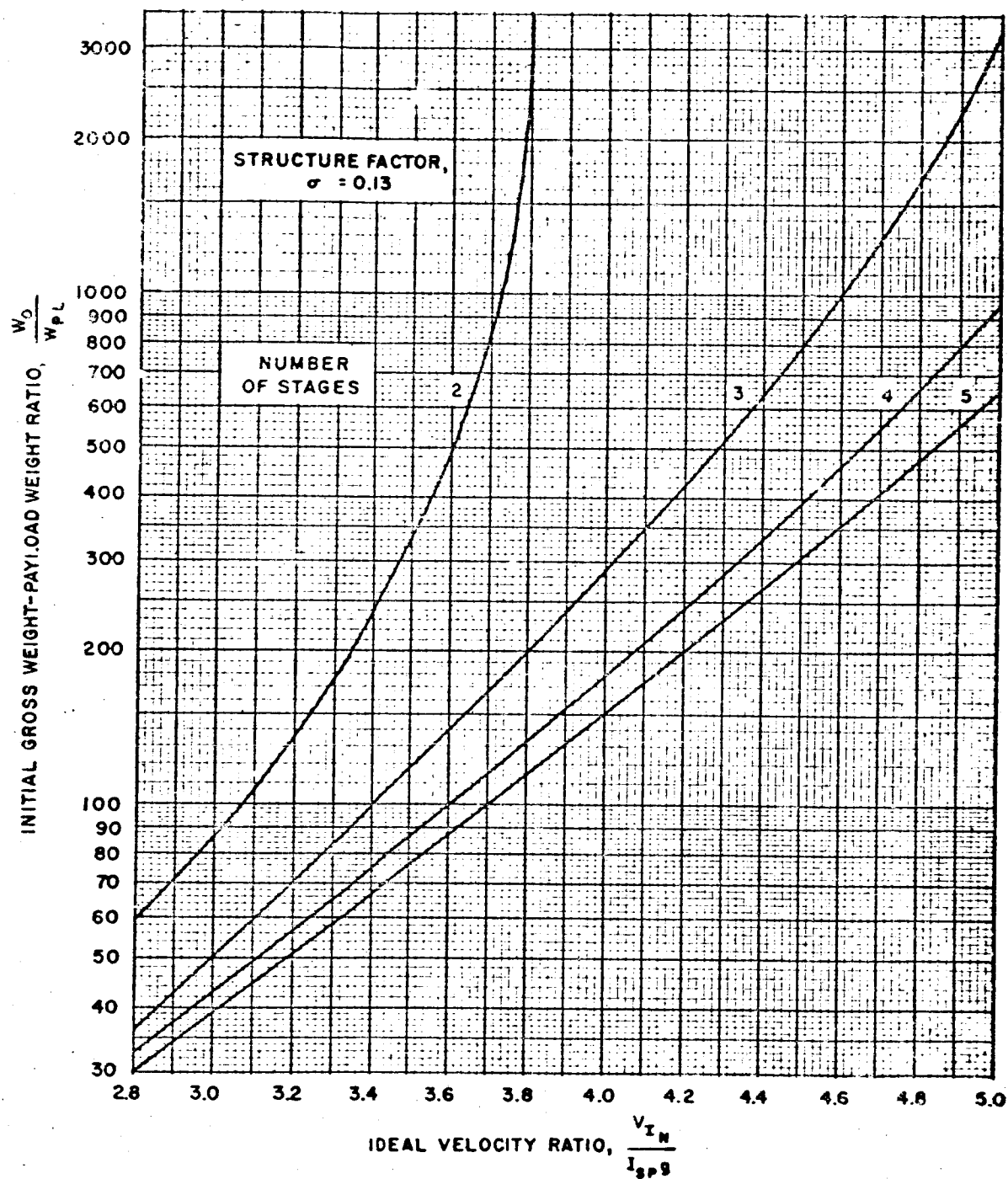


Figure 22. Payload Ratio for Like Parameters (Multiple Stage)

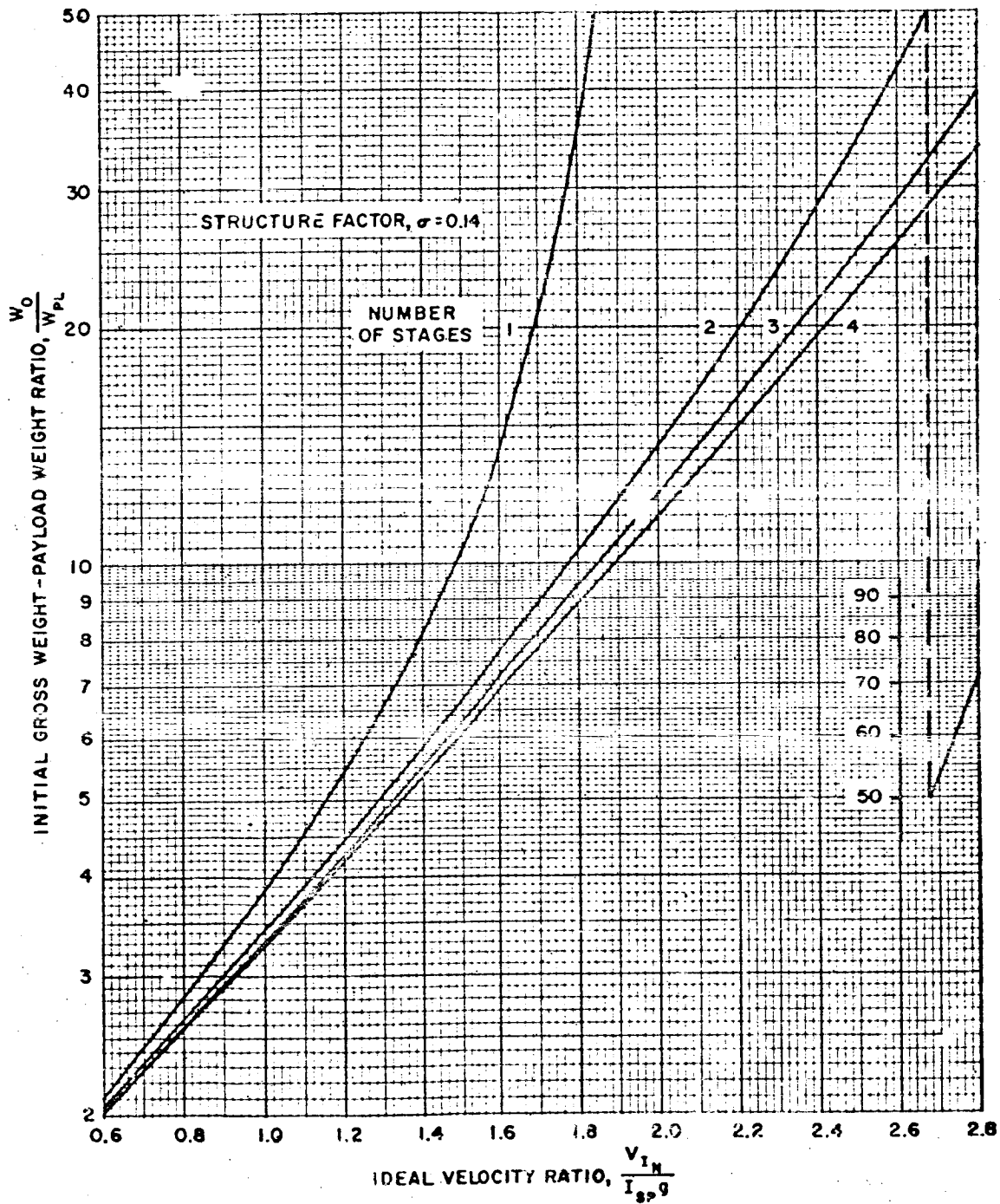


Figure 23. Payload Ratio for Like Parameters (Multiple Stage)

5-30

VEHICLE SIZING

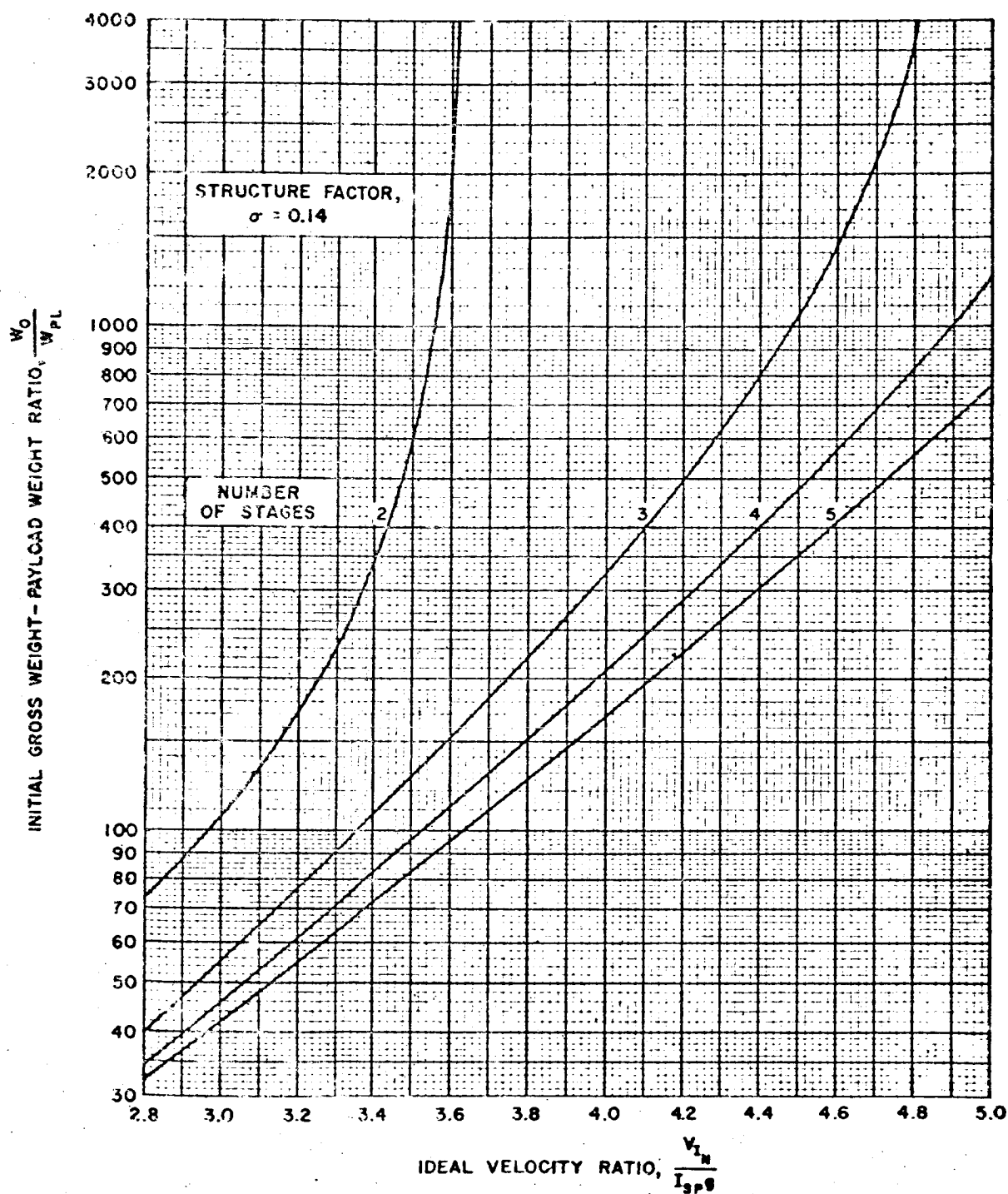


Figure 24 Payload Ratio for Like Parameters (Multiple Stage)

Payload Ratio

5-31

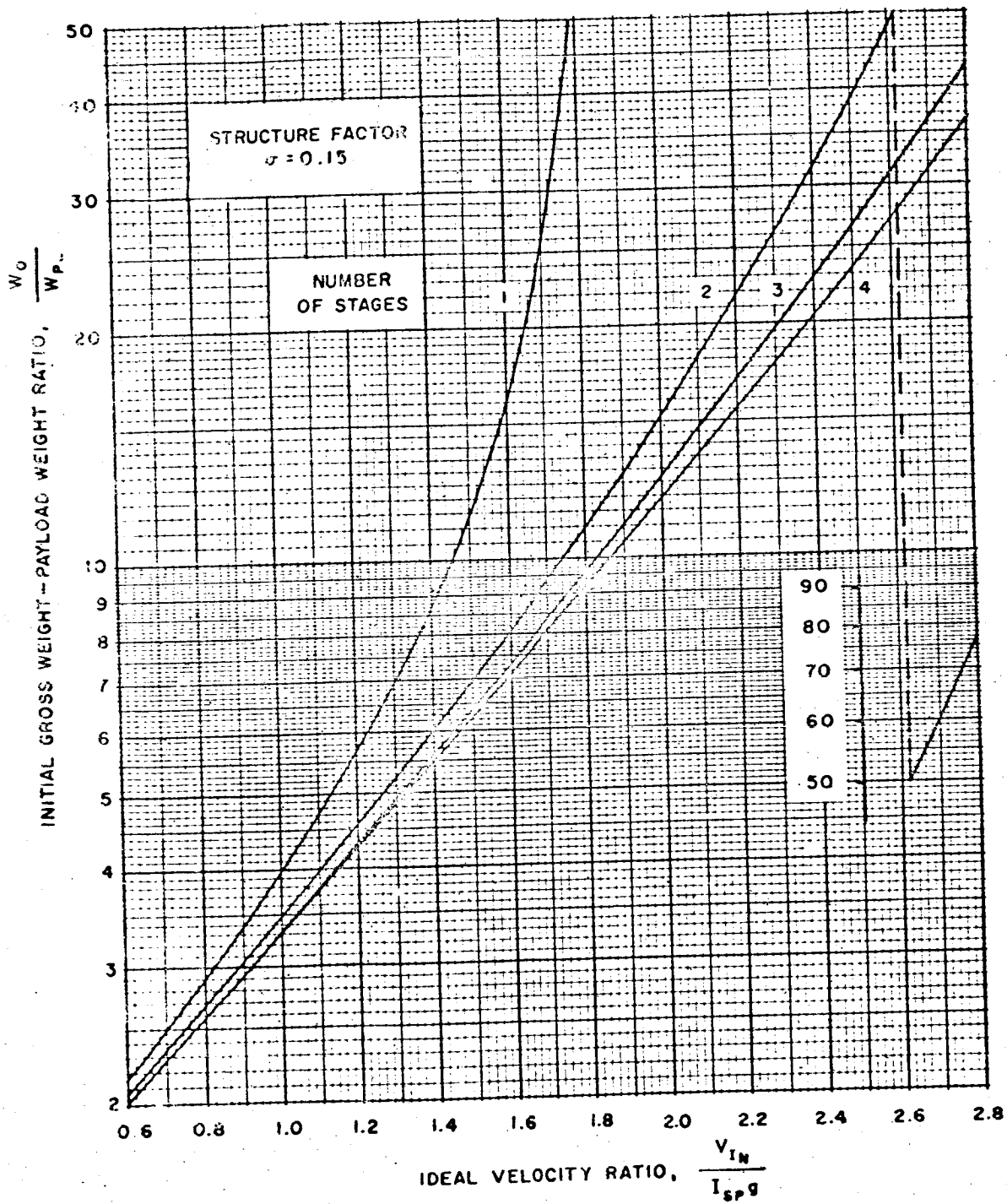


Figure 25. Payload Ratio for Like Parameters (Multiple Stage)

5-32

VEHICLE SIZING

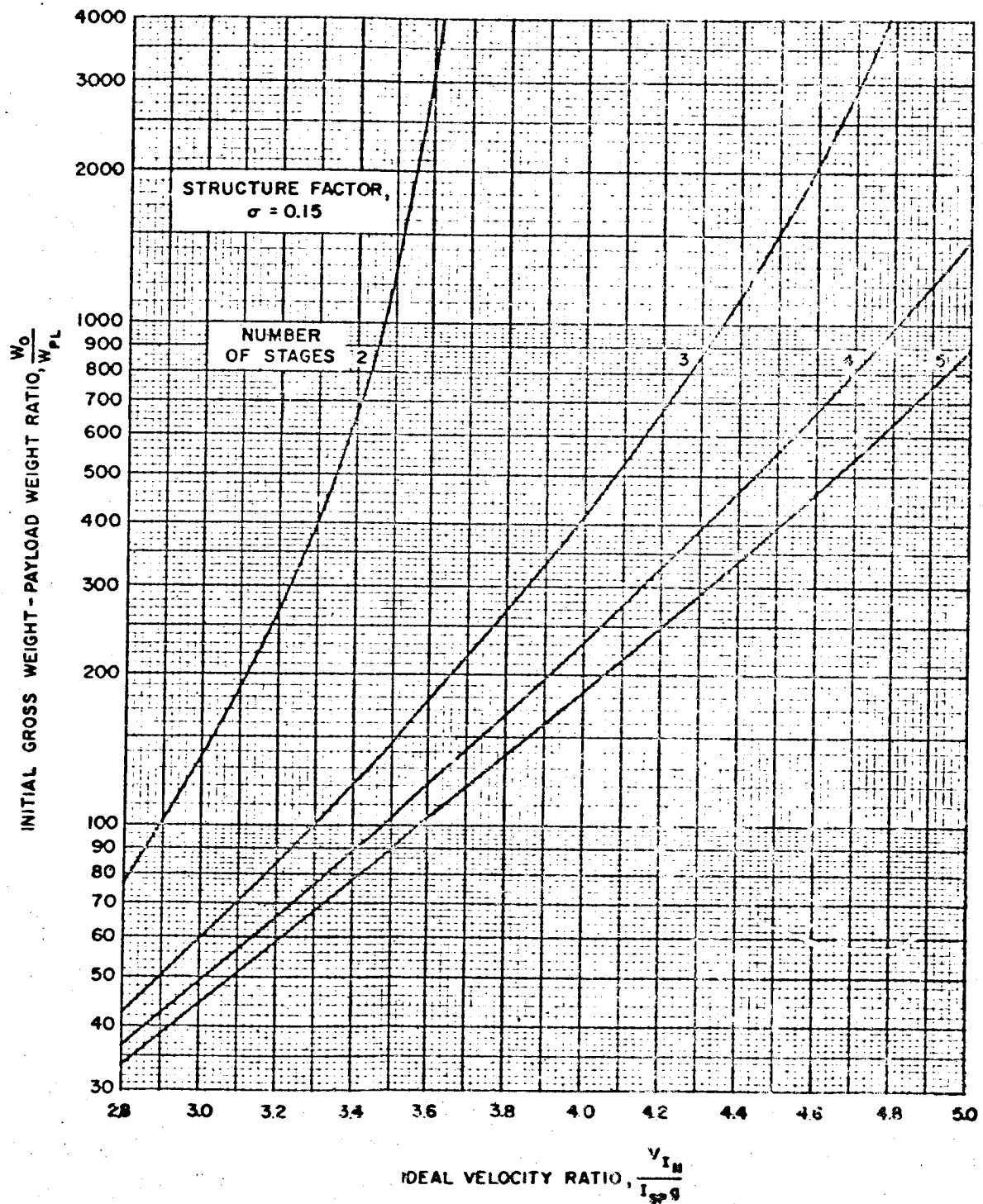


Figure 26. Payload Ratio for Like Parameters (Multiple Stage)

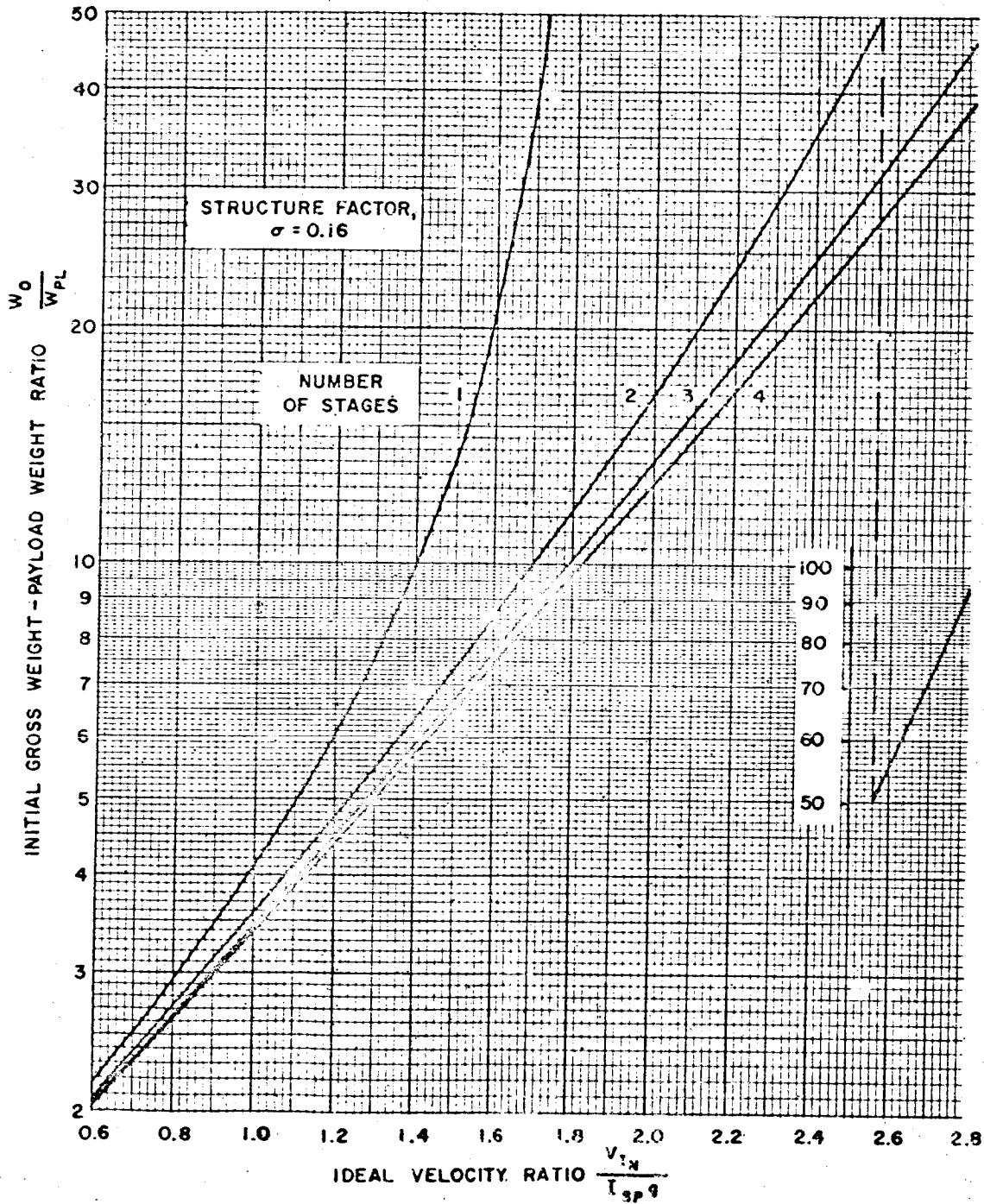


Figure 27. Payload Ratio for Like Parameters (Multiple Stage)

5-34

VEHICLE SIZING

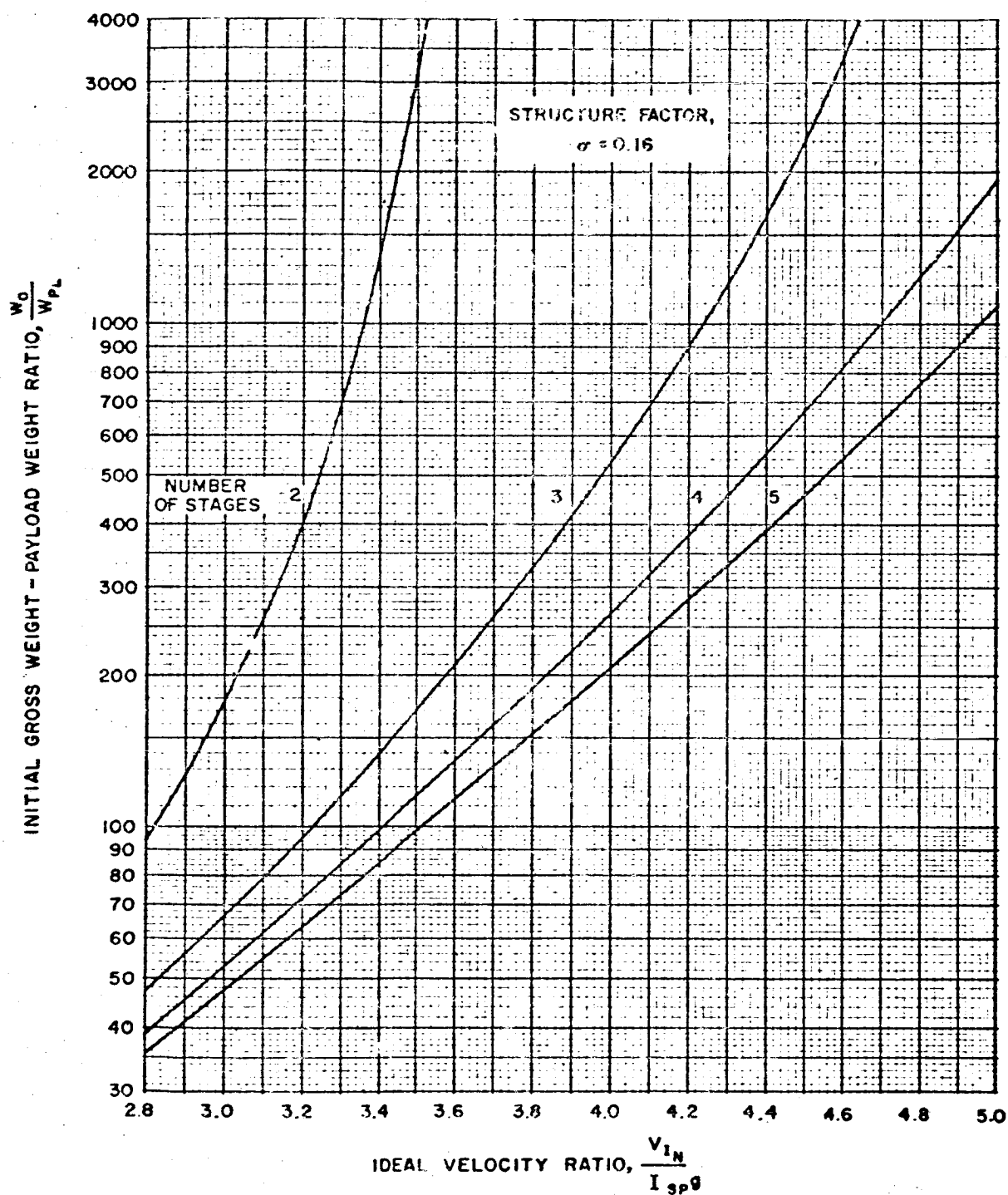


Figure 28. Payload Ratio for Like Parameters (Multiple Stage)

Payload Ratio

5-35

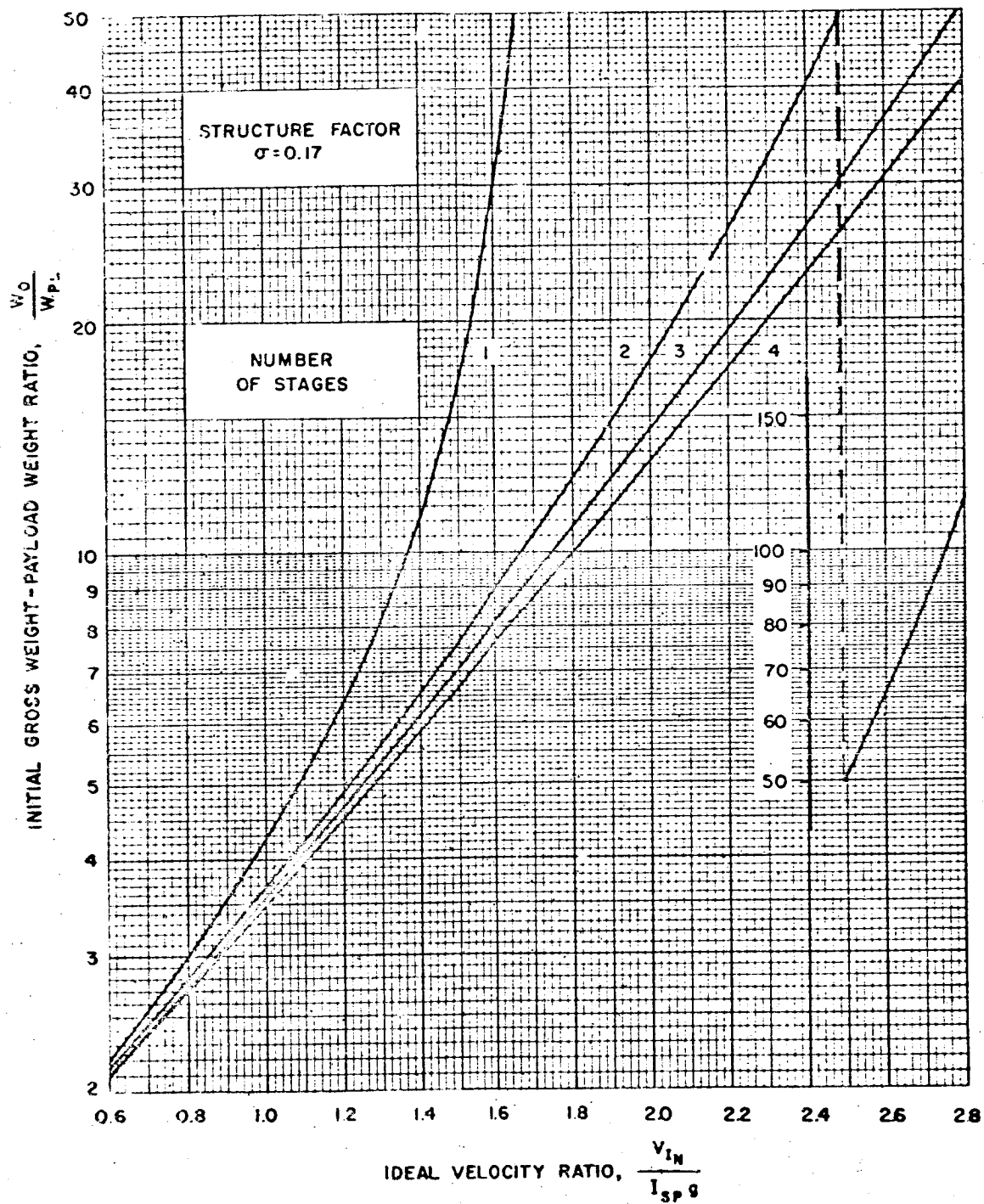


Figure 29. Payload Ratio for Like Parameters (Multiple Stage)

5-36

VEHICLE SIZING

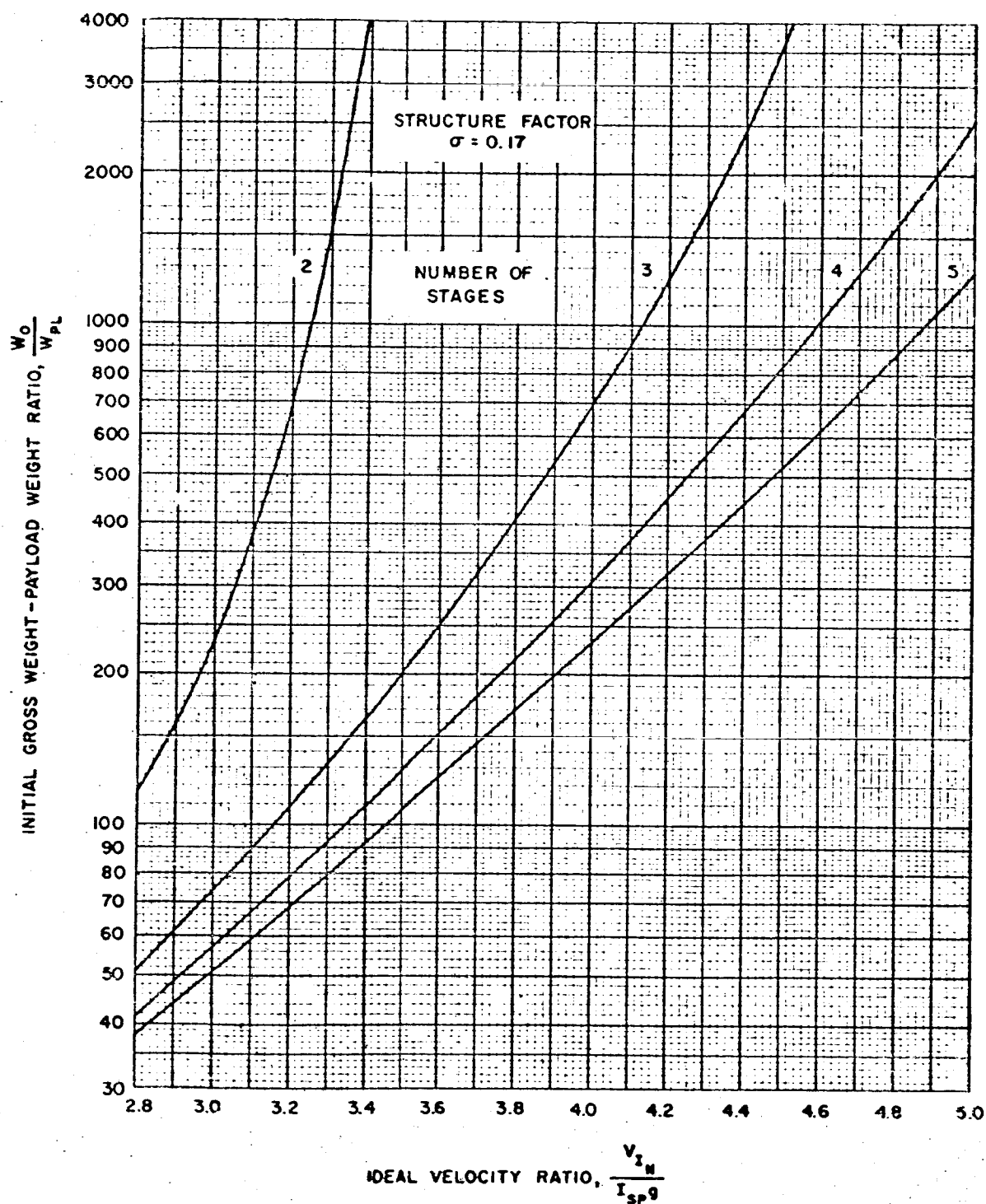


Figure 30. Payload Ratio for Like Parameters (Multiple Stage)

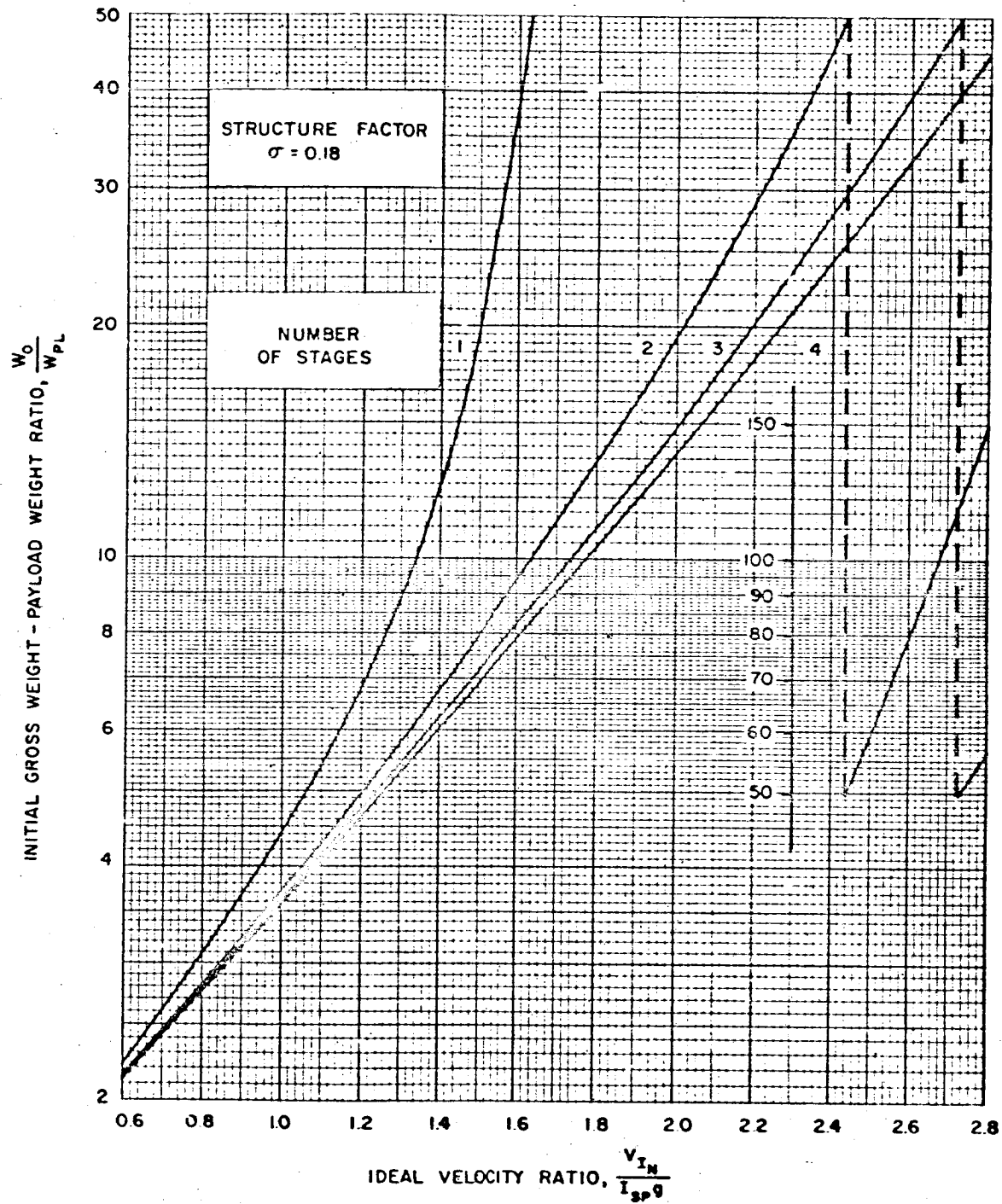


Figure 31. Payload Ratio for Like Parameters (Multiple Stage)

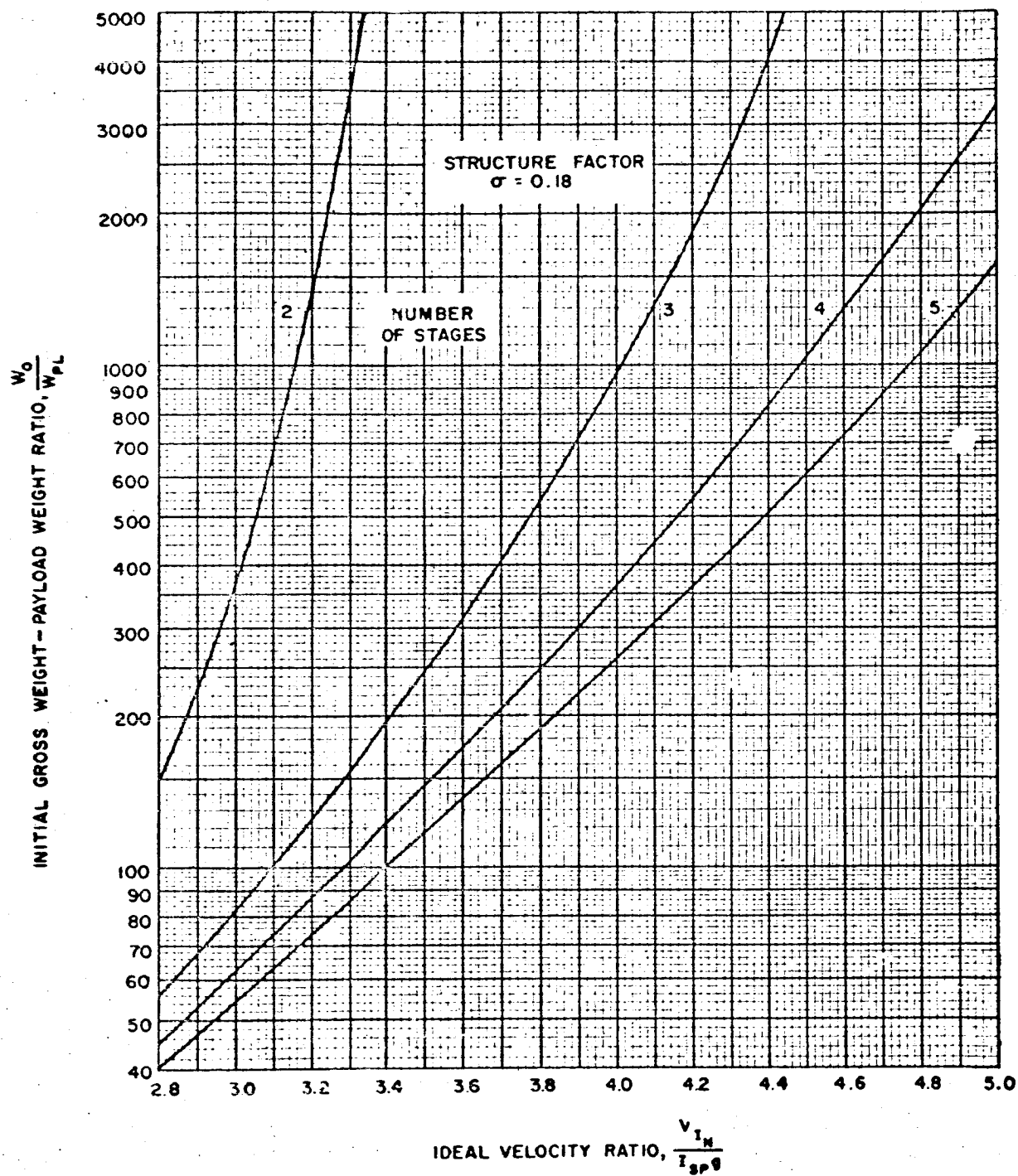


Figure 32. Payload Ratio for Like Parameters (Multiple Stage)

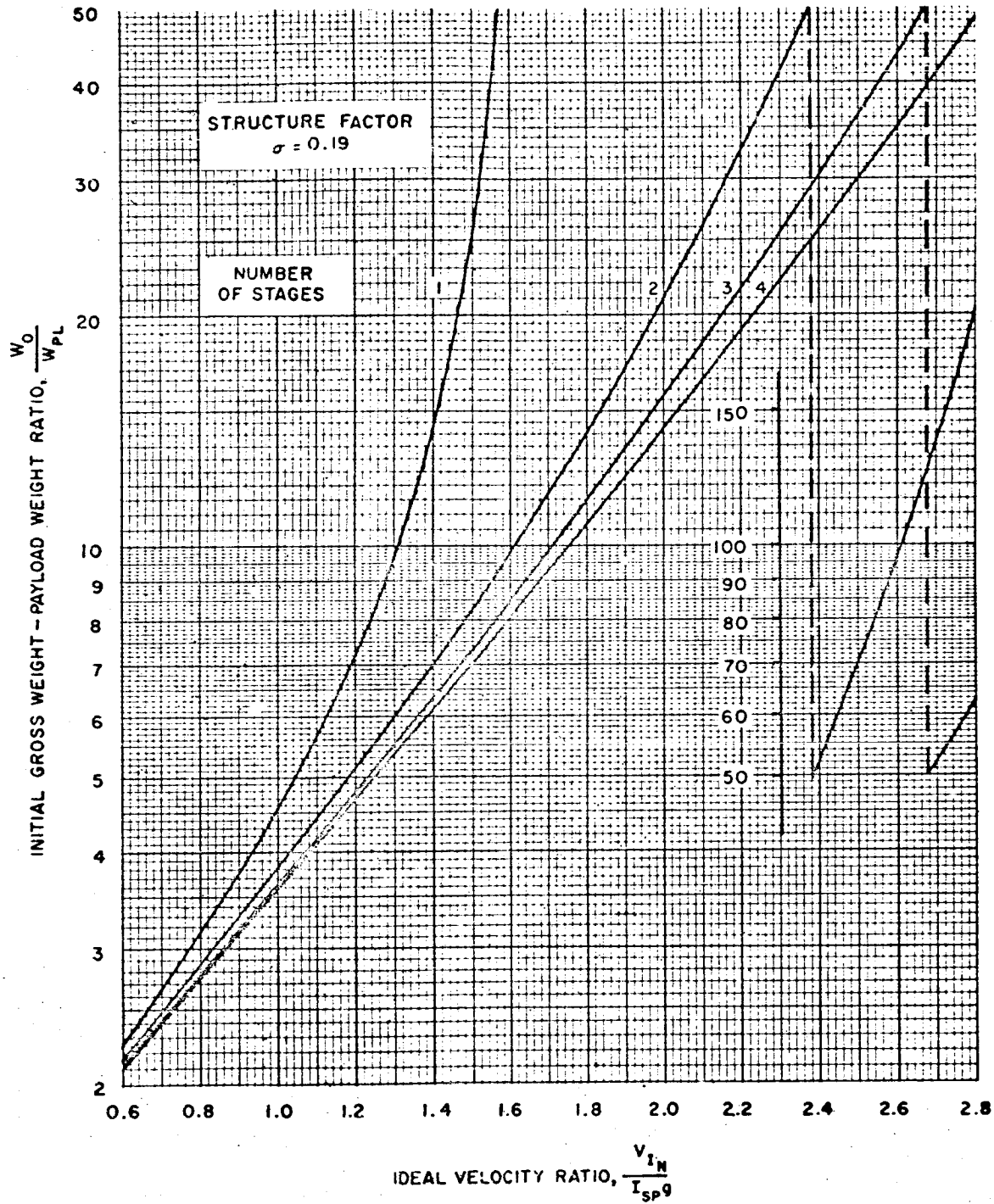


Figure 33. Payload Ratio for Like Parameters (Multiple Stage)

5-40

VEHICLE SIZING

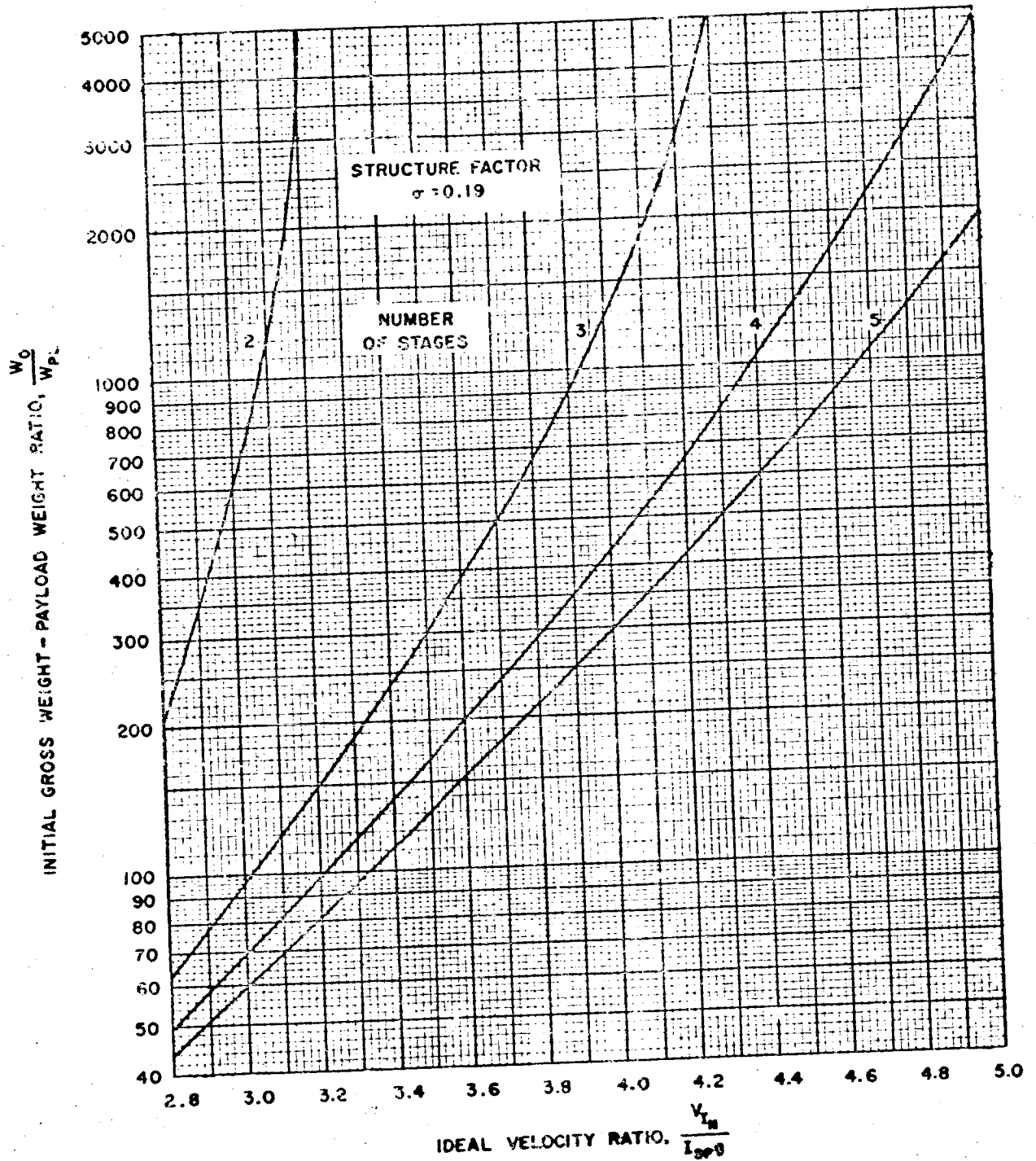


Figure 34. Payload Ratio for Like Parameters (Multiple Stage)

Payload Ratio

5-41

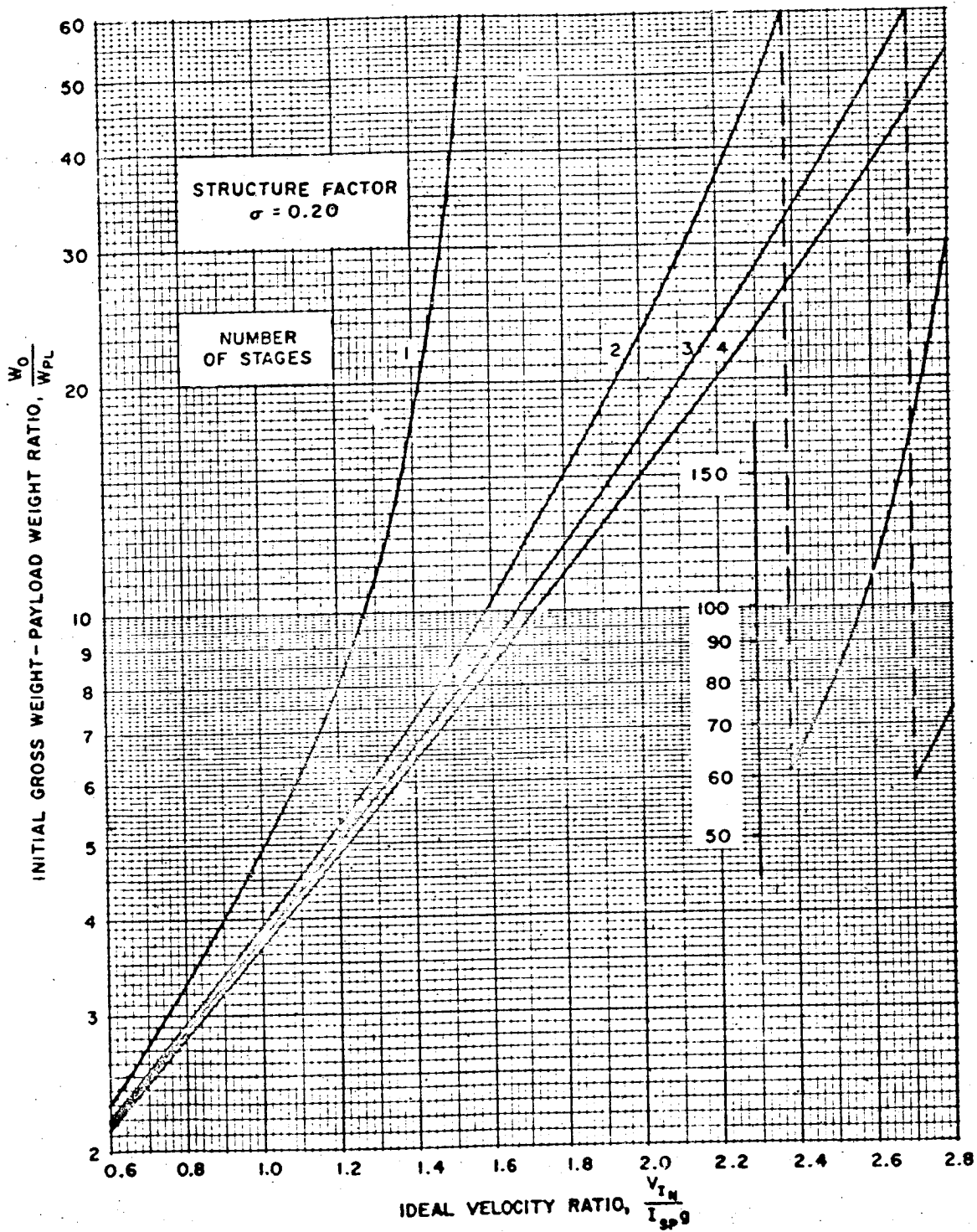


Figure 35. Payload Ratio for Like Parameters (Multiple Stage)

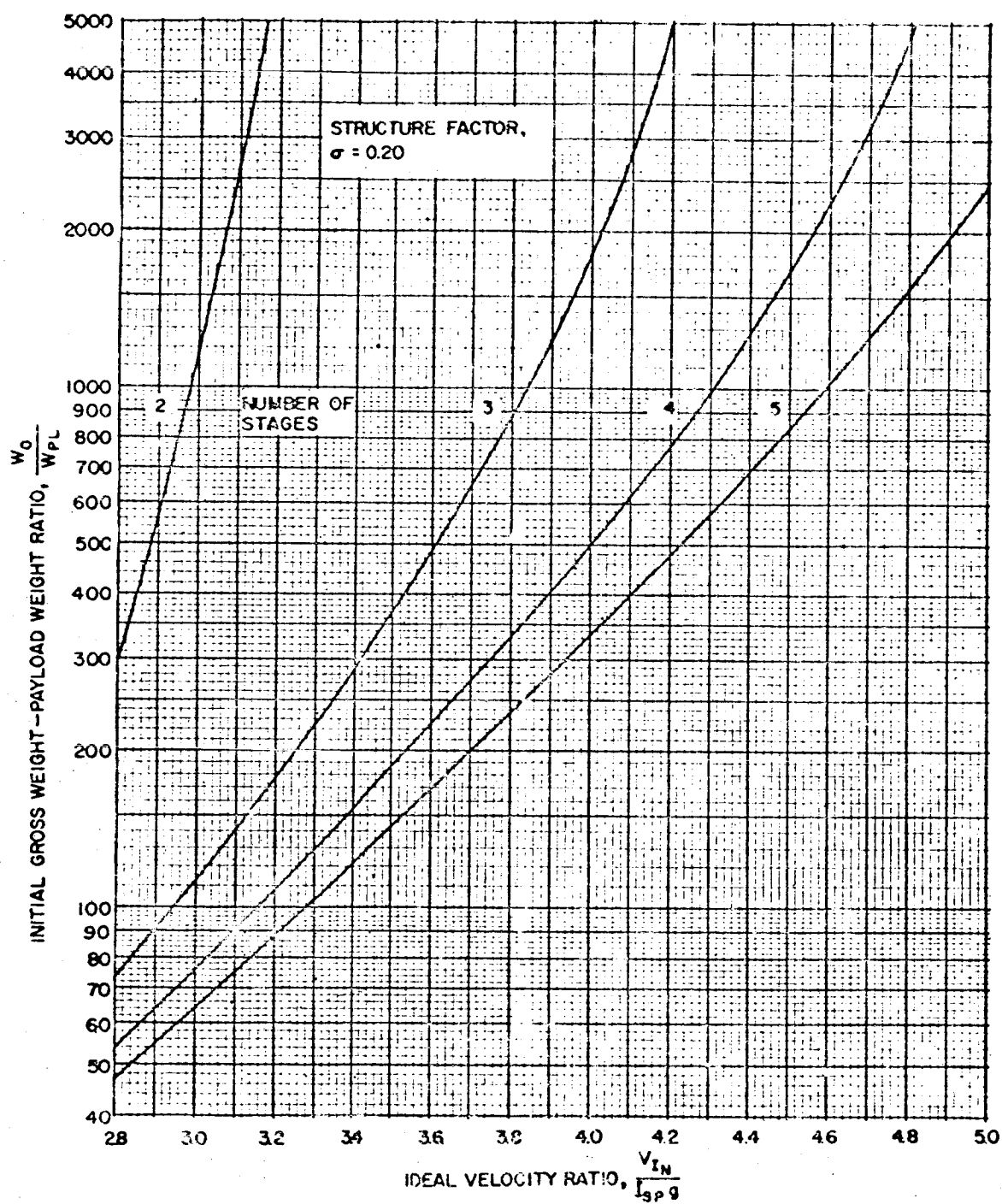


Figure 36. Payload Ratio for Like Parameters (Multiple Stage)

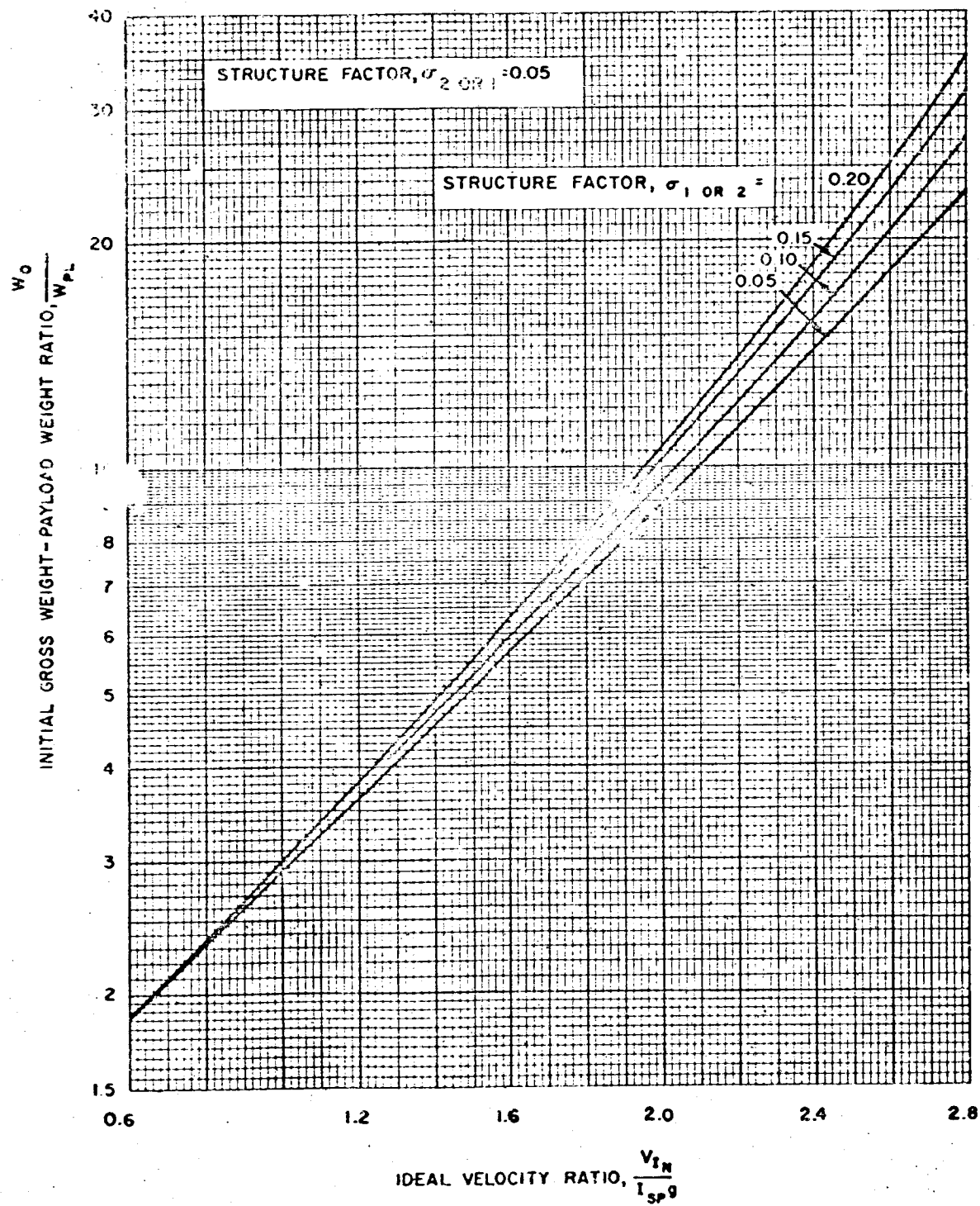


Figure 37. Payload Ratio for Unlike Structure Factors (Two-Stage Vehicles)

5-44

VEHICLE SIZING

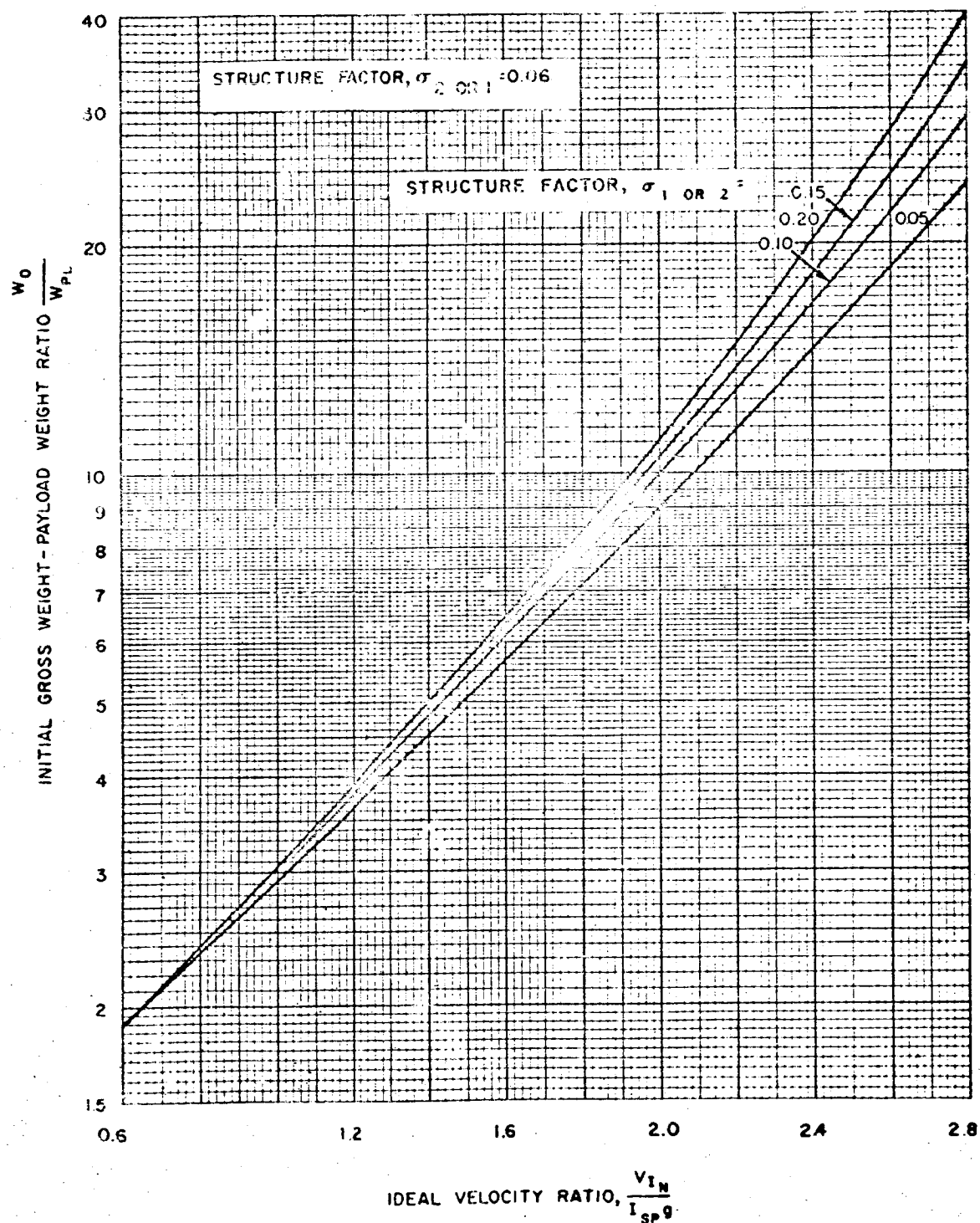


Figure 38. Payload Ratio for Unlike Structure Factors (Two-Stage Vehicles)

Payload Ratio

5-45

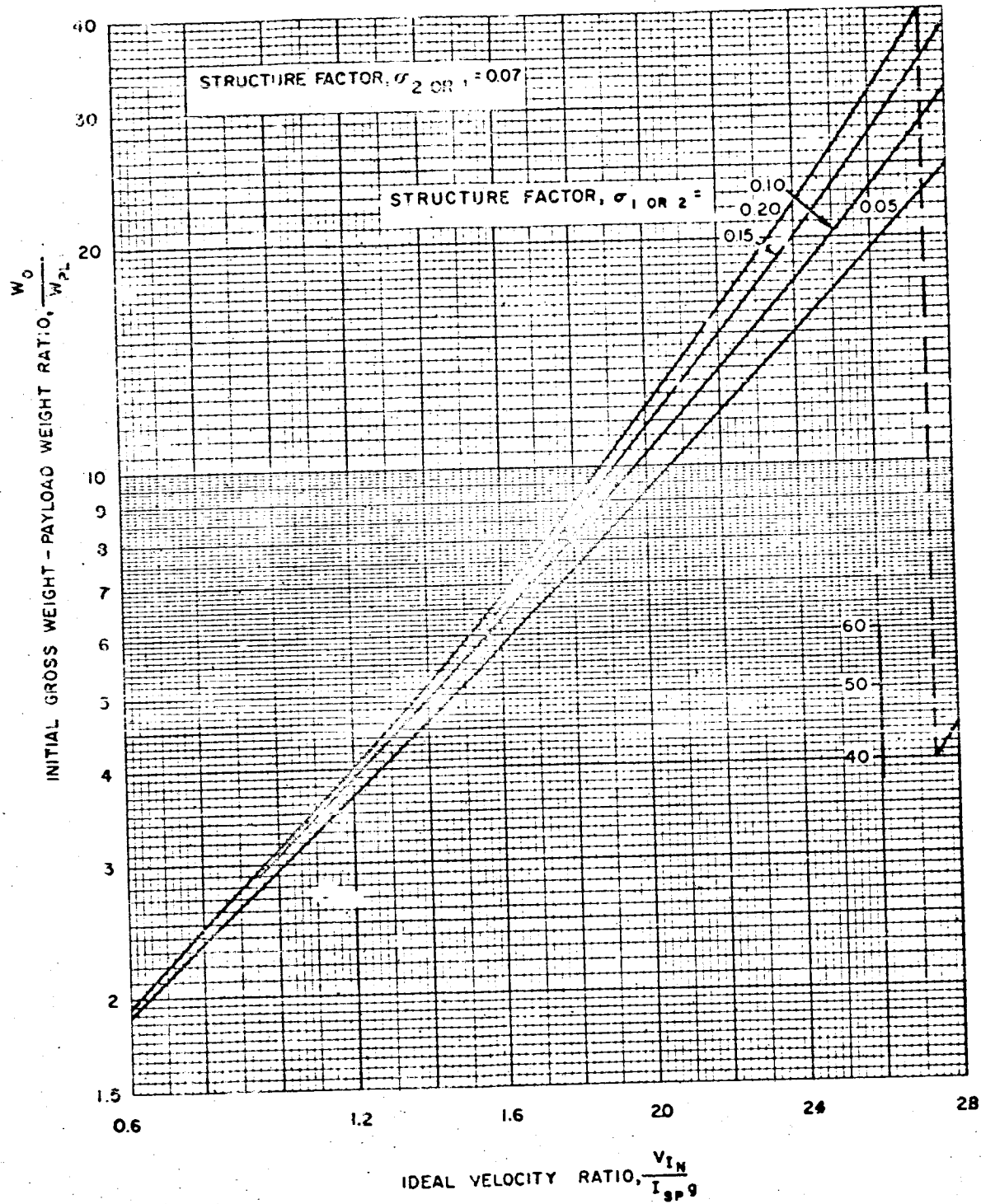


Figure 39. Payload Ratio for Unlike Structure Factors (Two-Stage Vehicles)

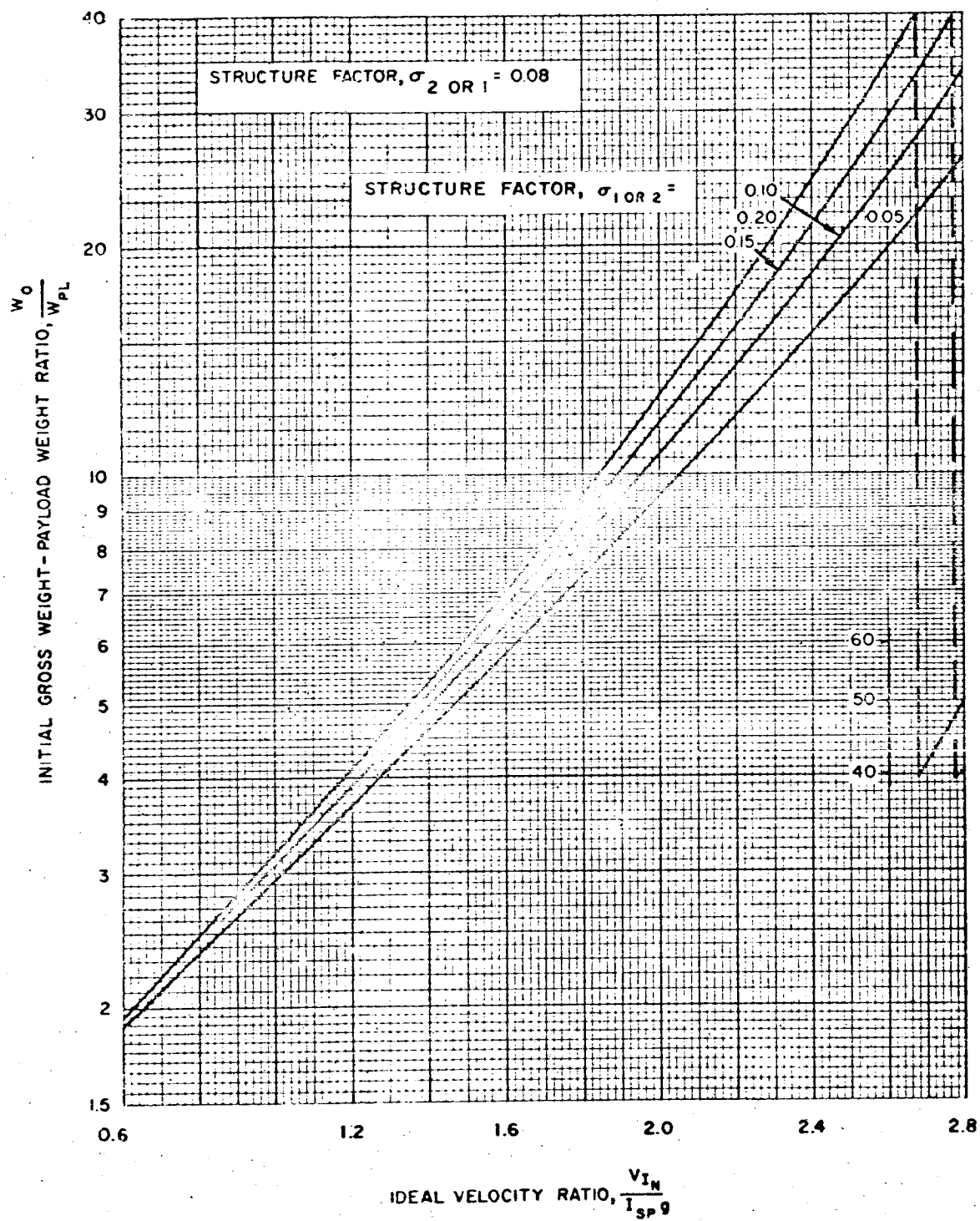


Figure 40. Payload Ratio for Unlike Structure Factors (Two-Stage Vehicles)

Payload Ratio

5-47

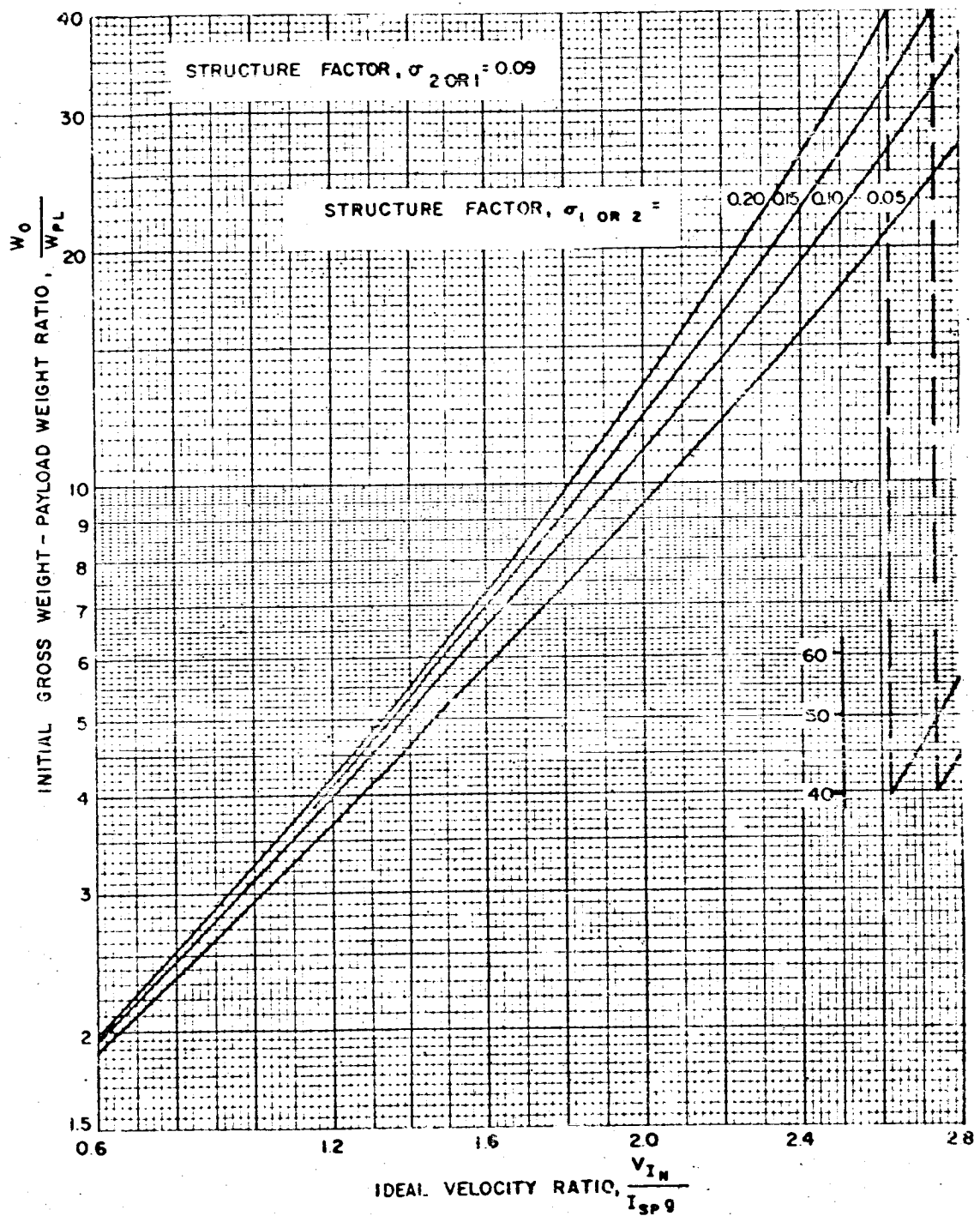


Figure 41. Payload Ratio for Unlike Structure Factors (Two-Stage Vehicles)

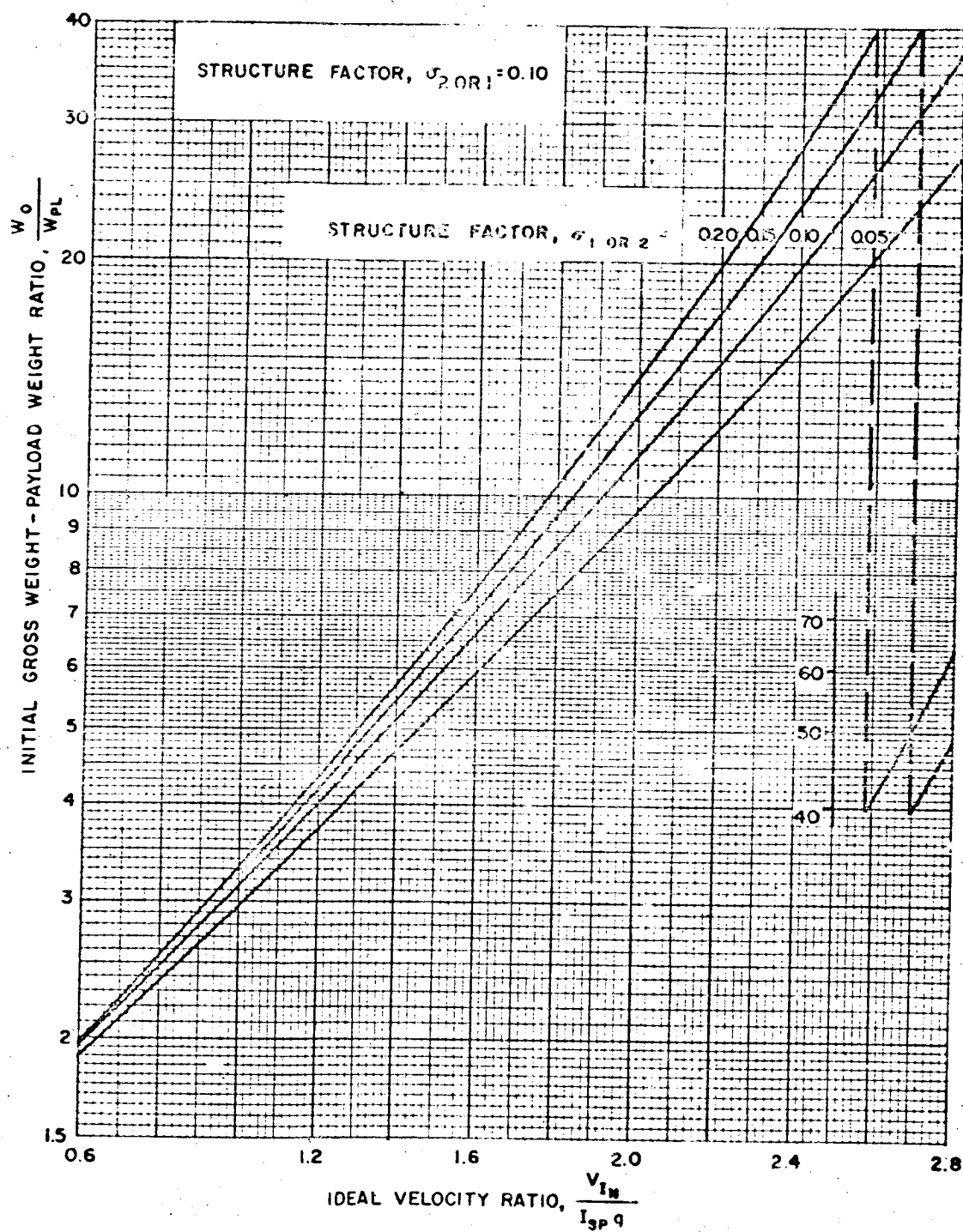


Figure 42. Payload Ratio for Unlike Structure Factors (Two-Stage Vehicles)

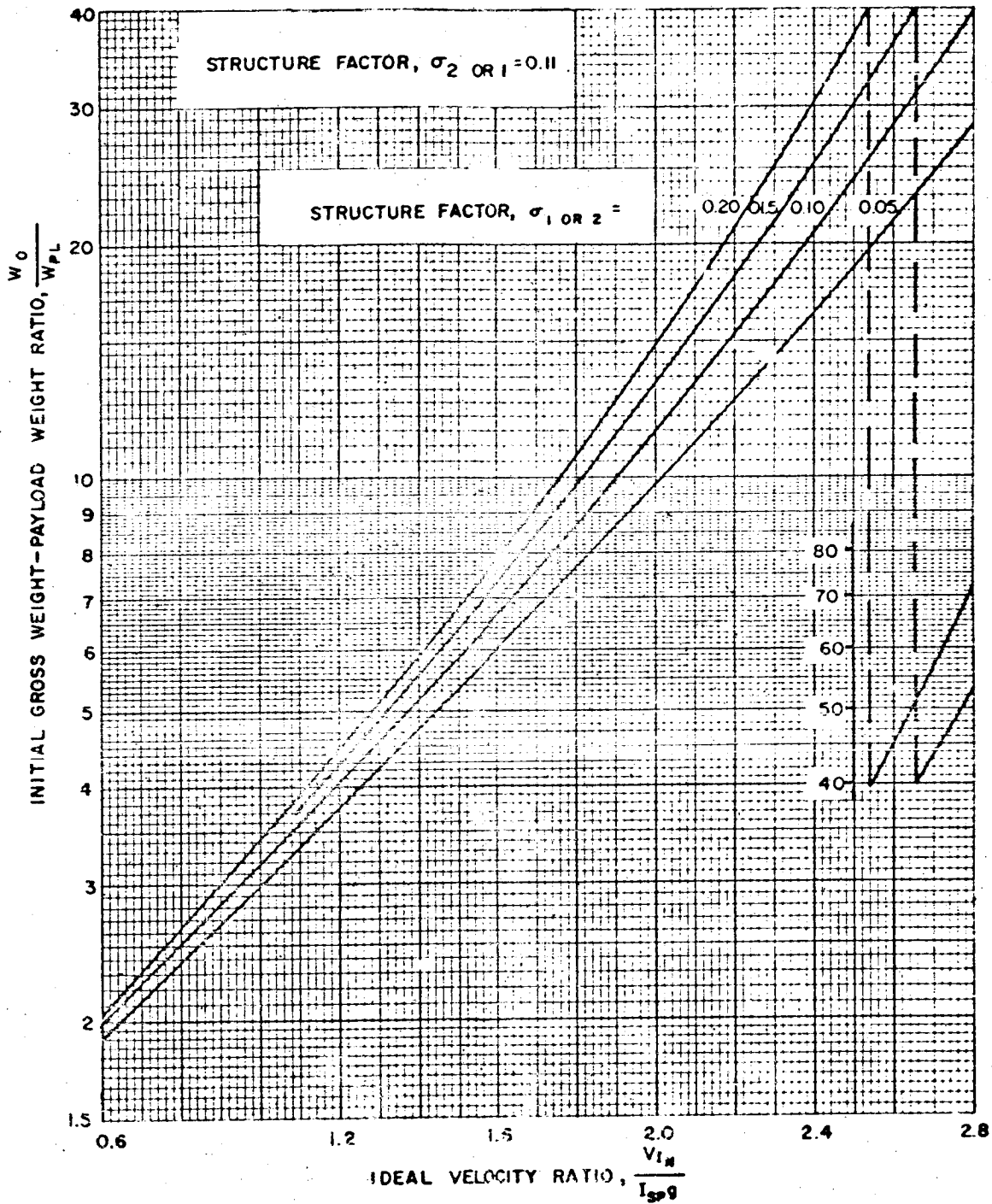


Figure 43. Payload Ratio for Unlike Structure Factors (Two-Stage Vehicles)

5-50

VEHICLE SIZING

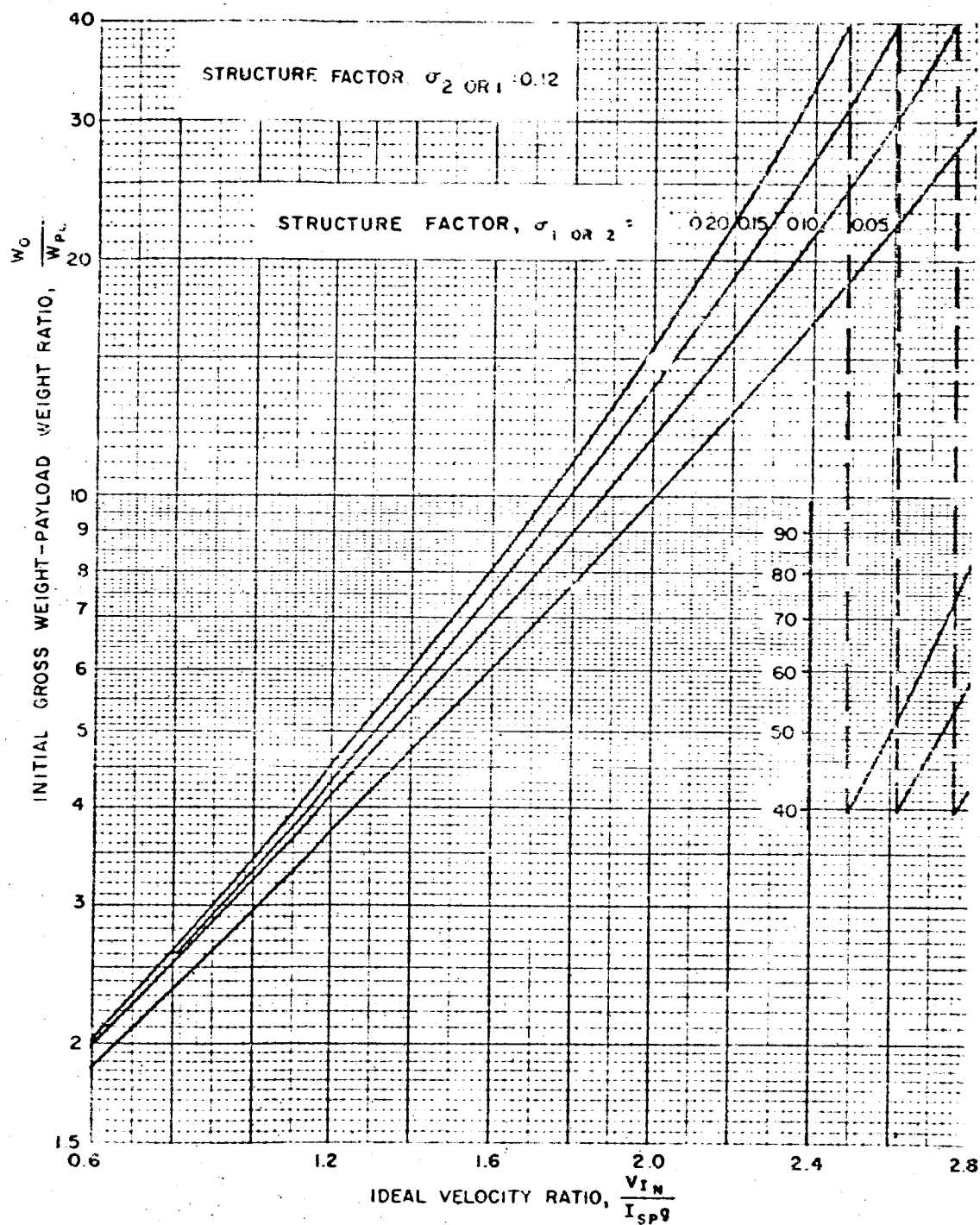


Figure 44. Payload Ratio for Unlike Structure Factors (Two-Stage Vehicles)

Payload Ratio

5-51

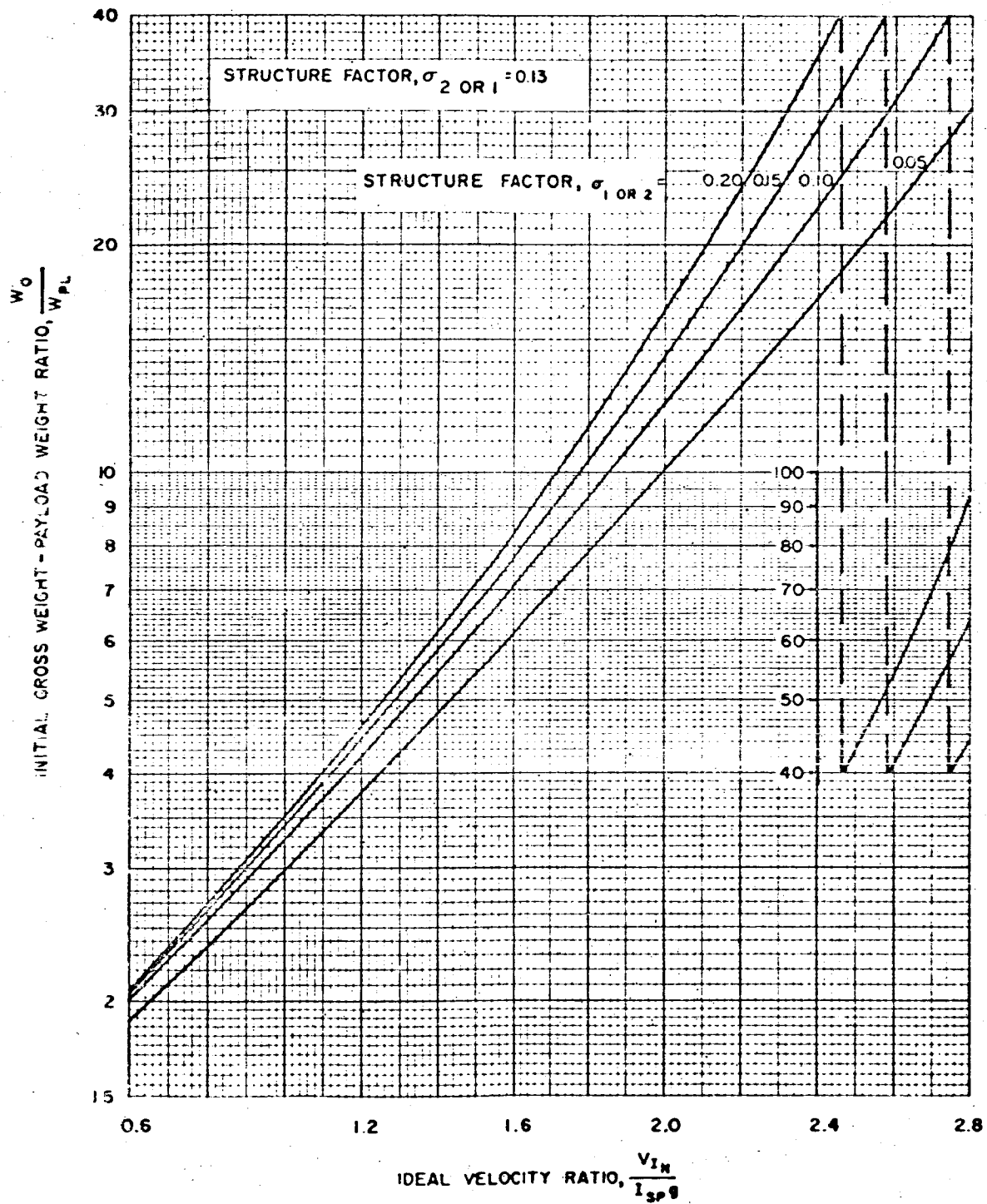


Figure 45. Payload Ratio for Unlike Structure Factors (Two-Stage Vehicles)

5-52

VEHICLE SIZING

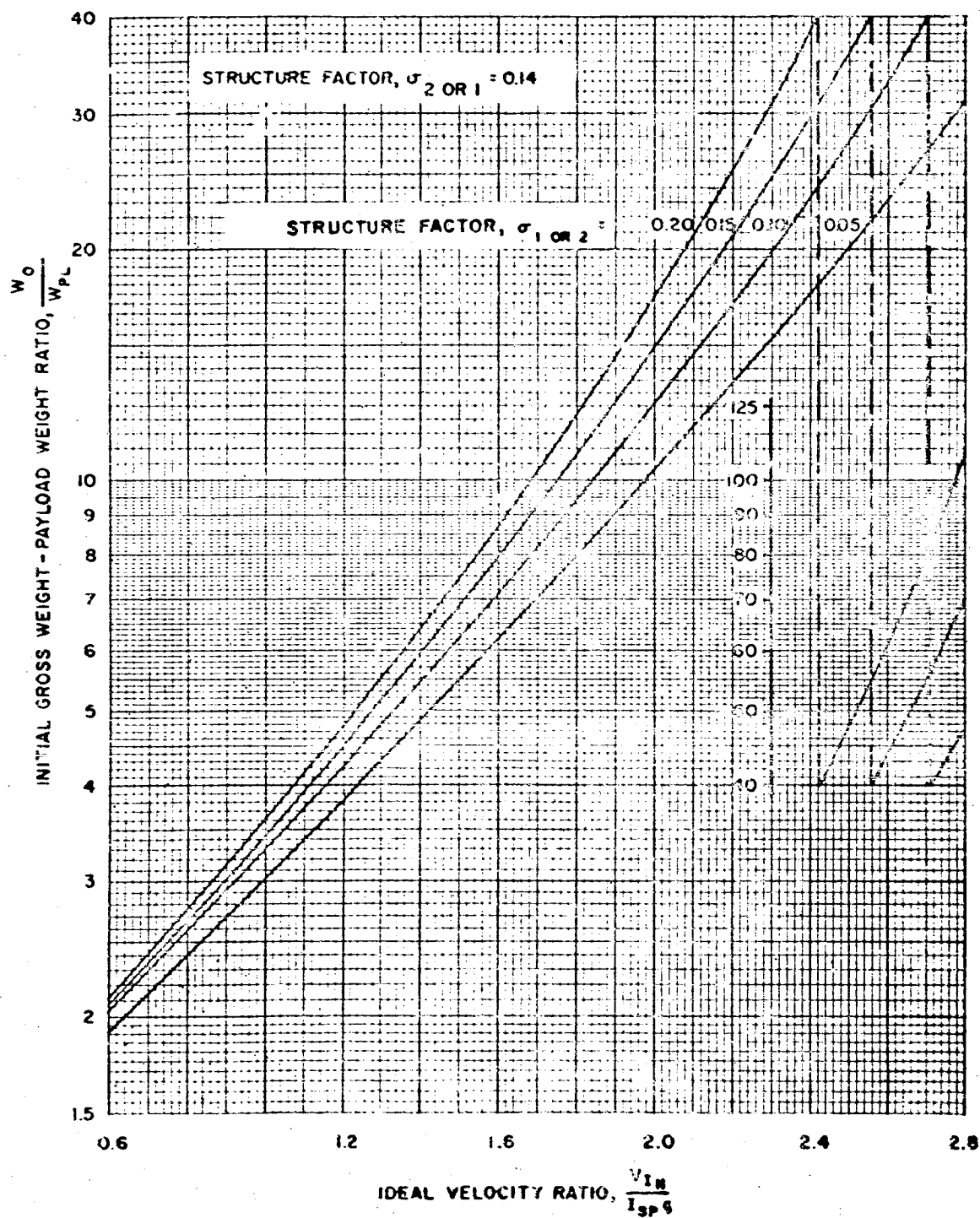


Figure 46. Payload Ratio for Unlike Structure Factors (Two-Stage Vehicles)

Payload Ratio

5-53

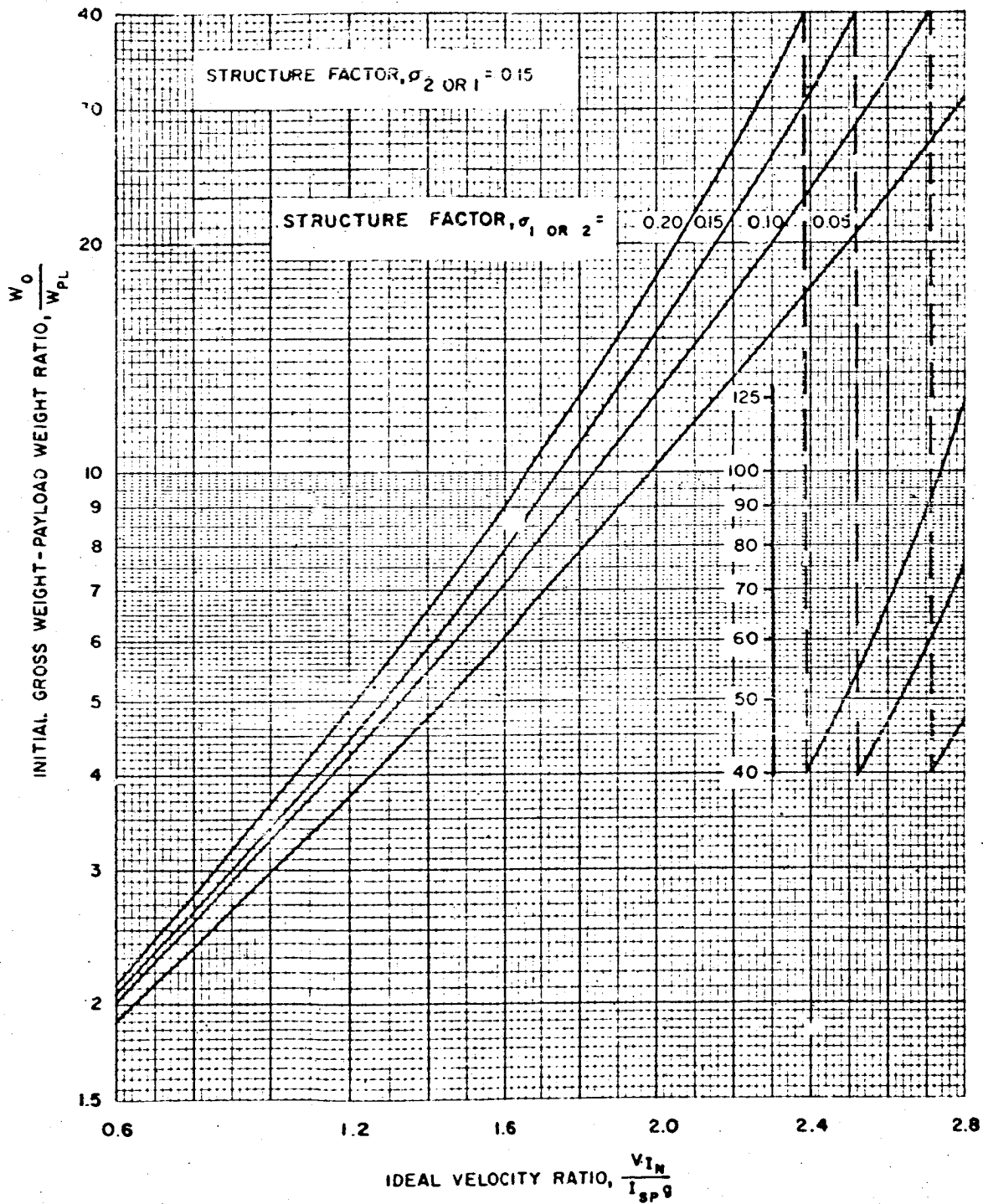


Figure 47. Payload Ratio for Unlike Structure Factors (Two-Stage Vehicles)

5-54

VEHICLE SIZING

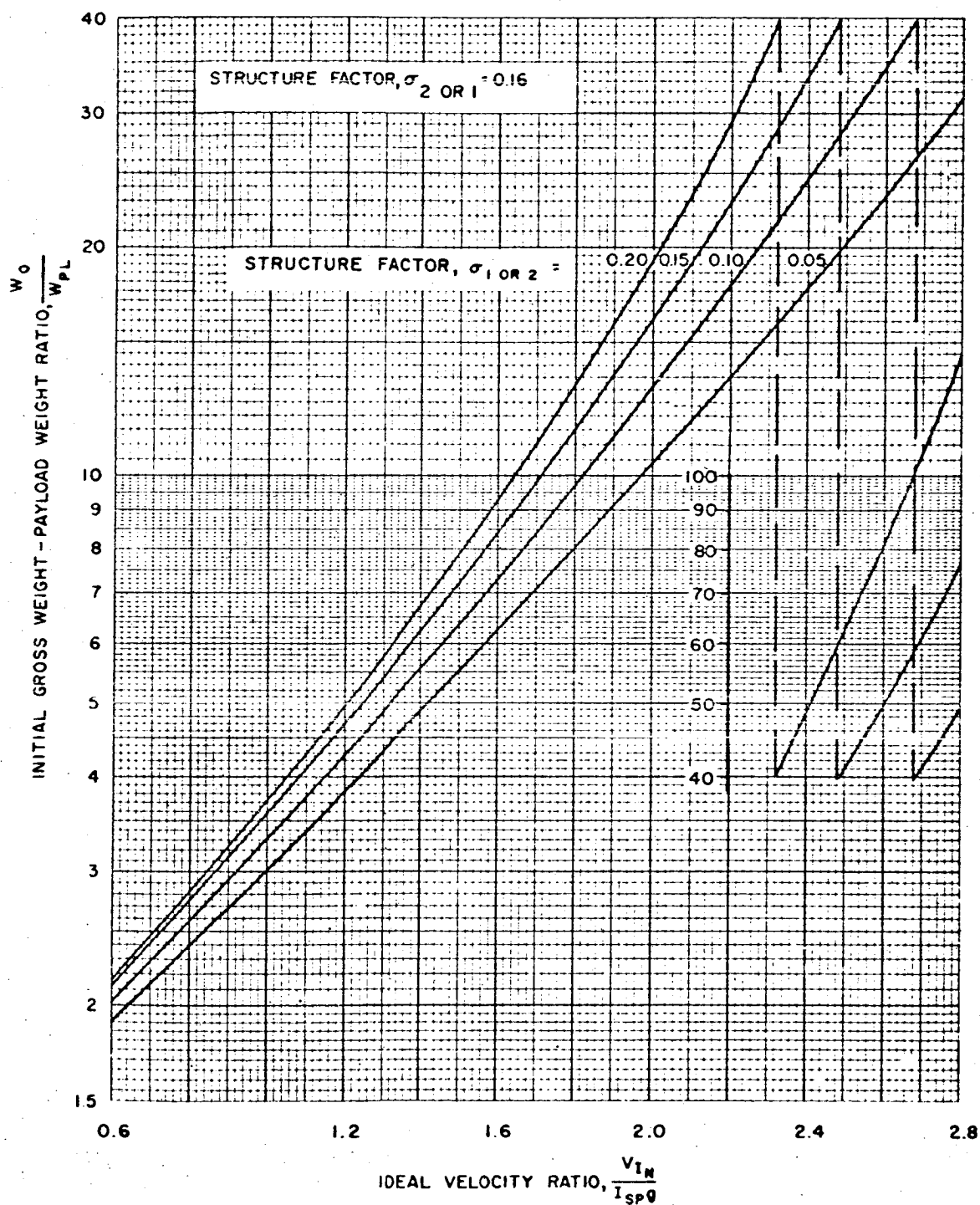


Figure 48. Payload Ratio for Unlike Structure Factors (Two-Stage Vehicles)

Payload Ratio

5-55

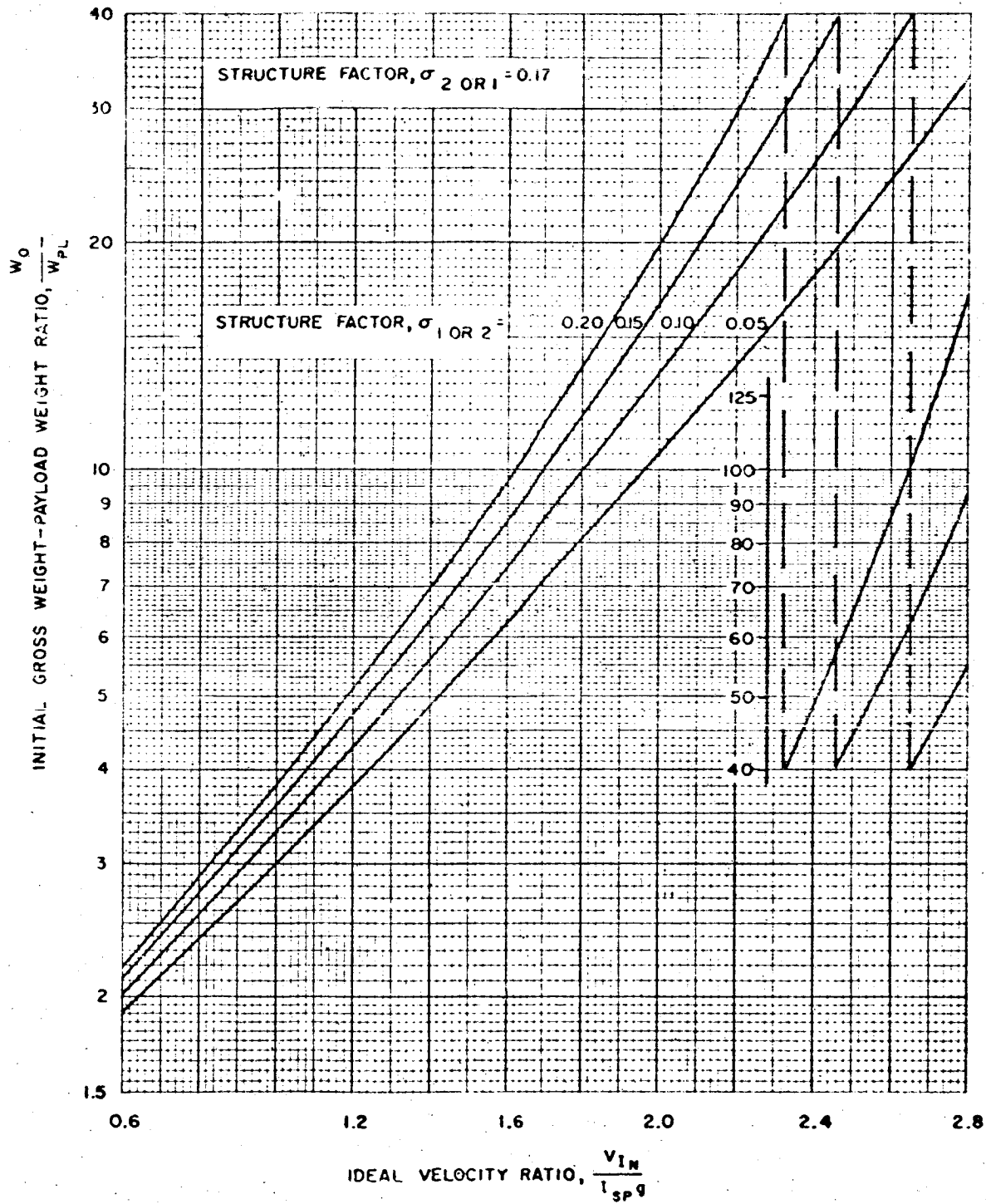


Figure 49. Payload Ratio for Unlike Structure Factors (Two-Stage Vehicles)

5-56

VEHICLE SIZING

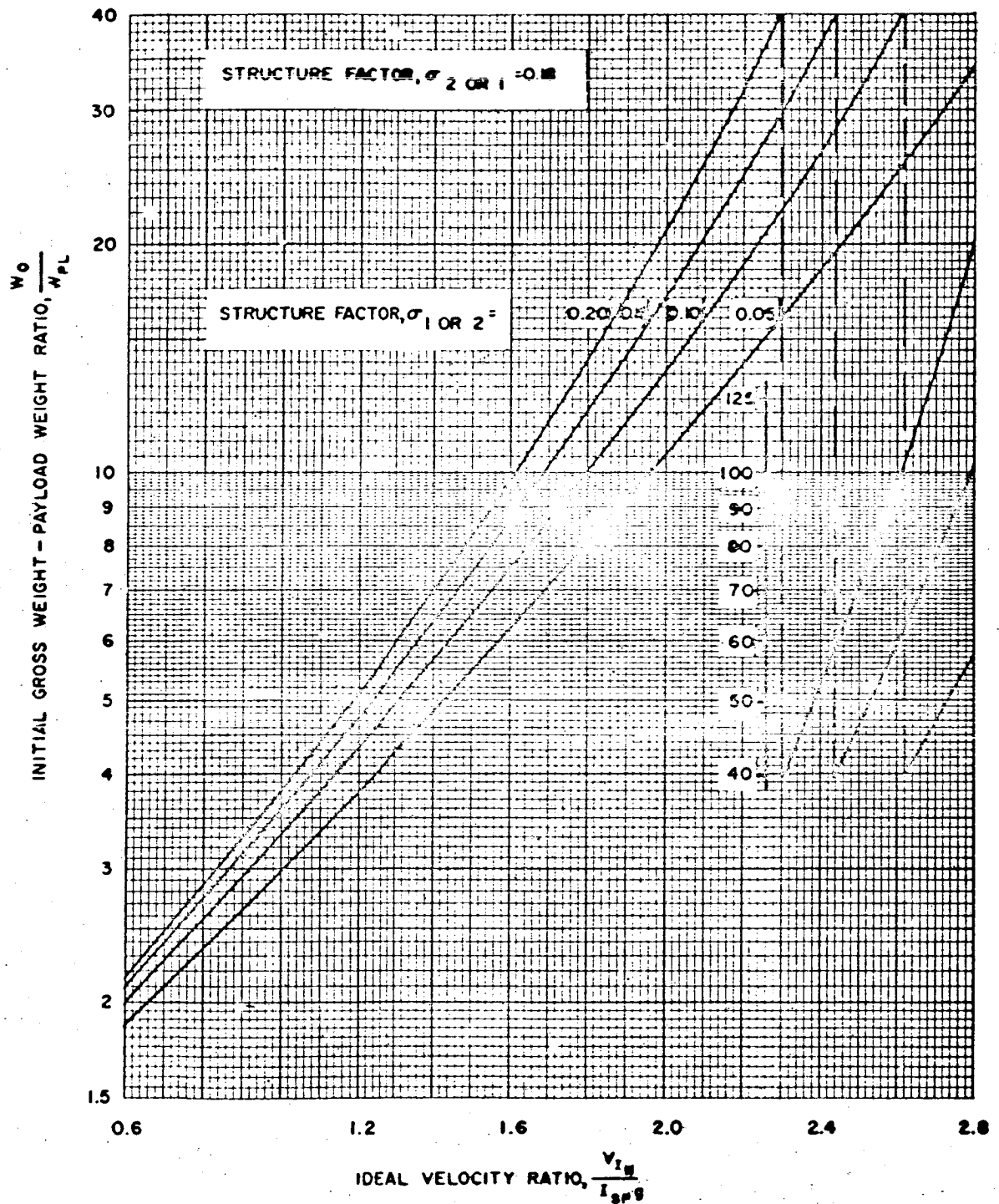


Figure 50. Payload Ratio for Unlike Structure Factors (Two-Stage Vehicles)

Payload Ratio

S-57

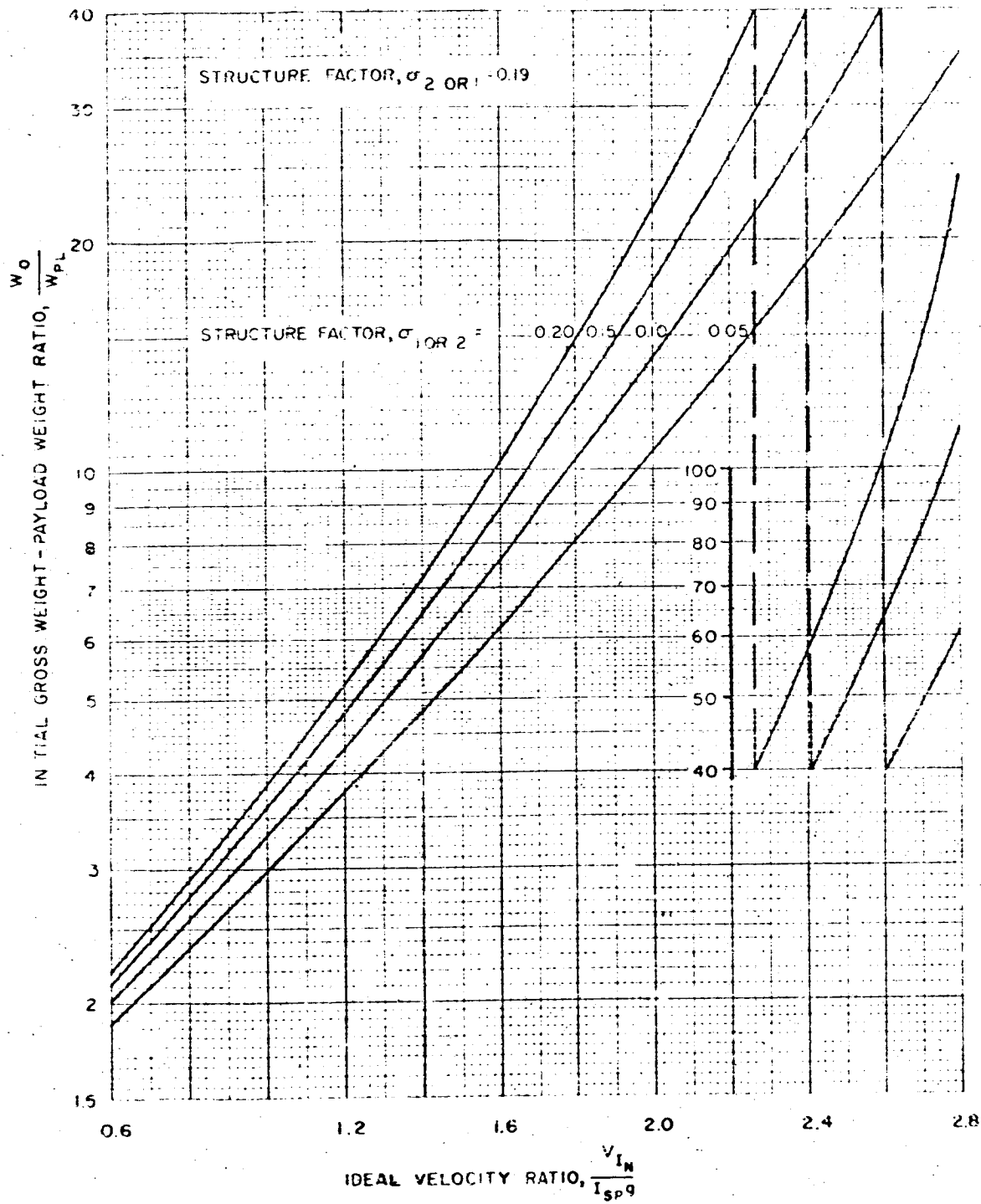


Figure 51. Payload Ratio for Unlike Structure Factors (Two-Stage Vehicles)

5-58

VEHICLE SIZING

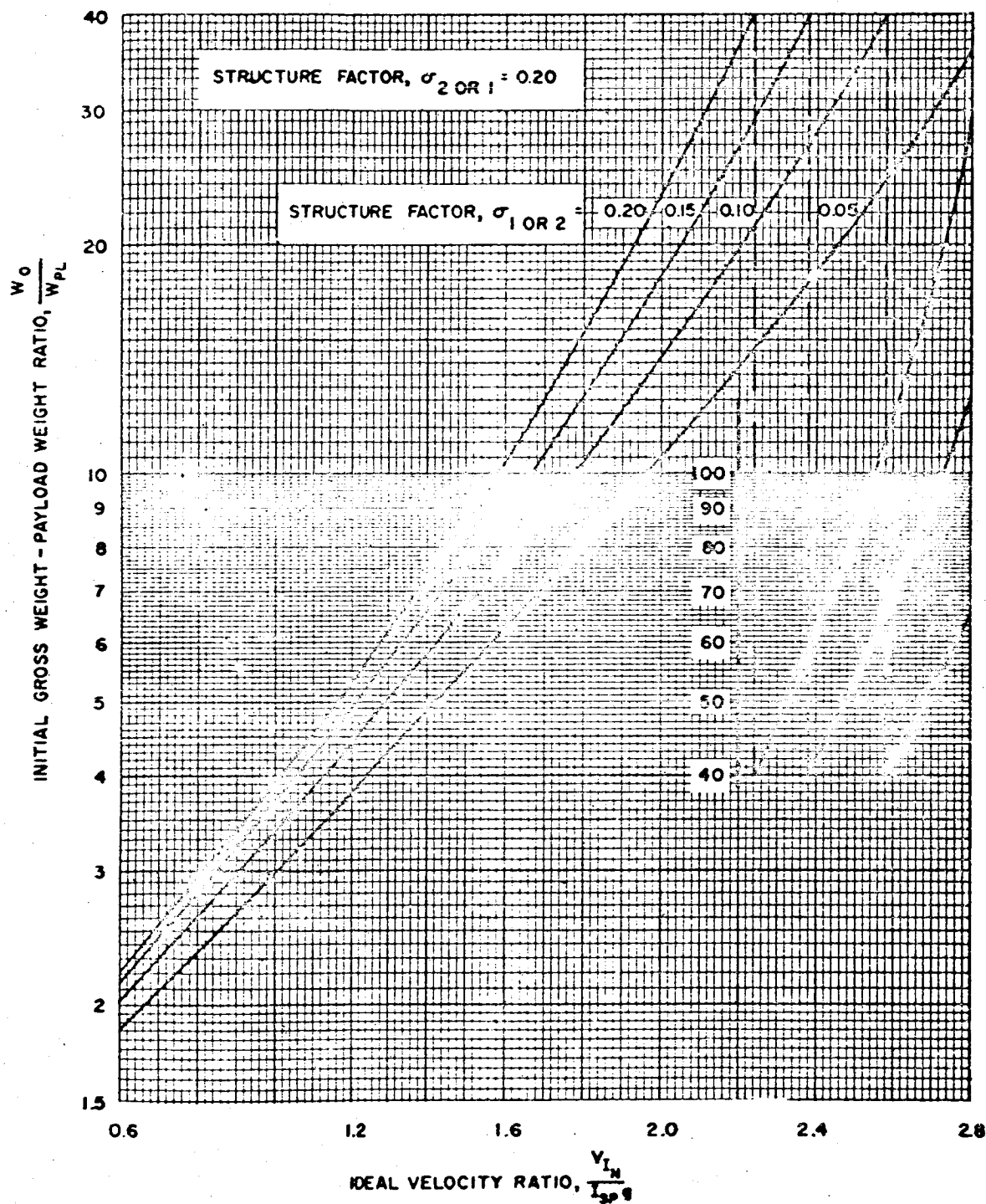


Figure 52. Payload Ratio for Unlike Structure Factors (Two-Stage Vehicles)

Payload Ratio

5-59

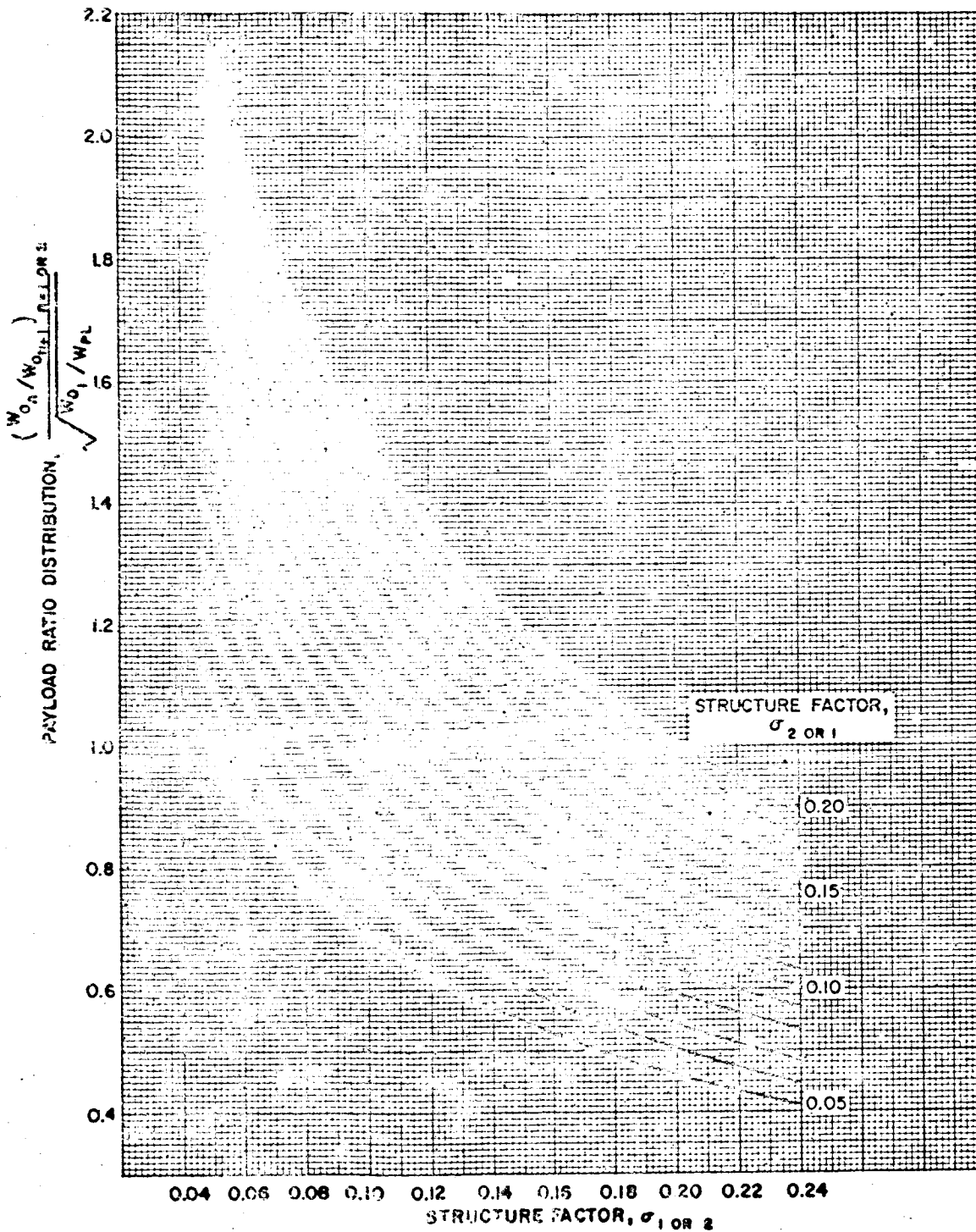


Figure 53. Stage Payload Ratio for Unlike Structure Factors (Two Stage Vehicles)

5-60

VEHICLE SIZING

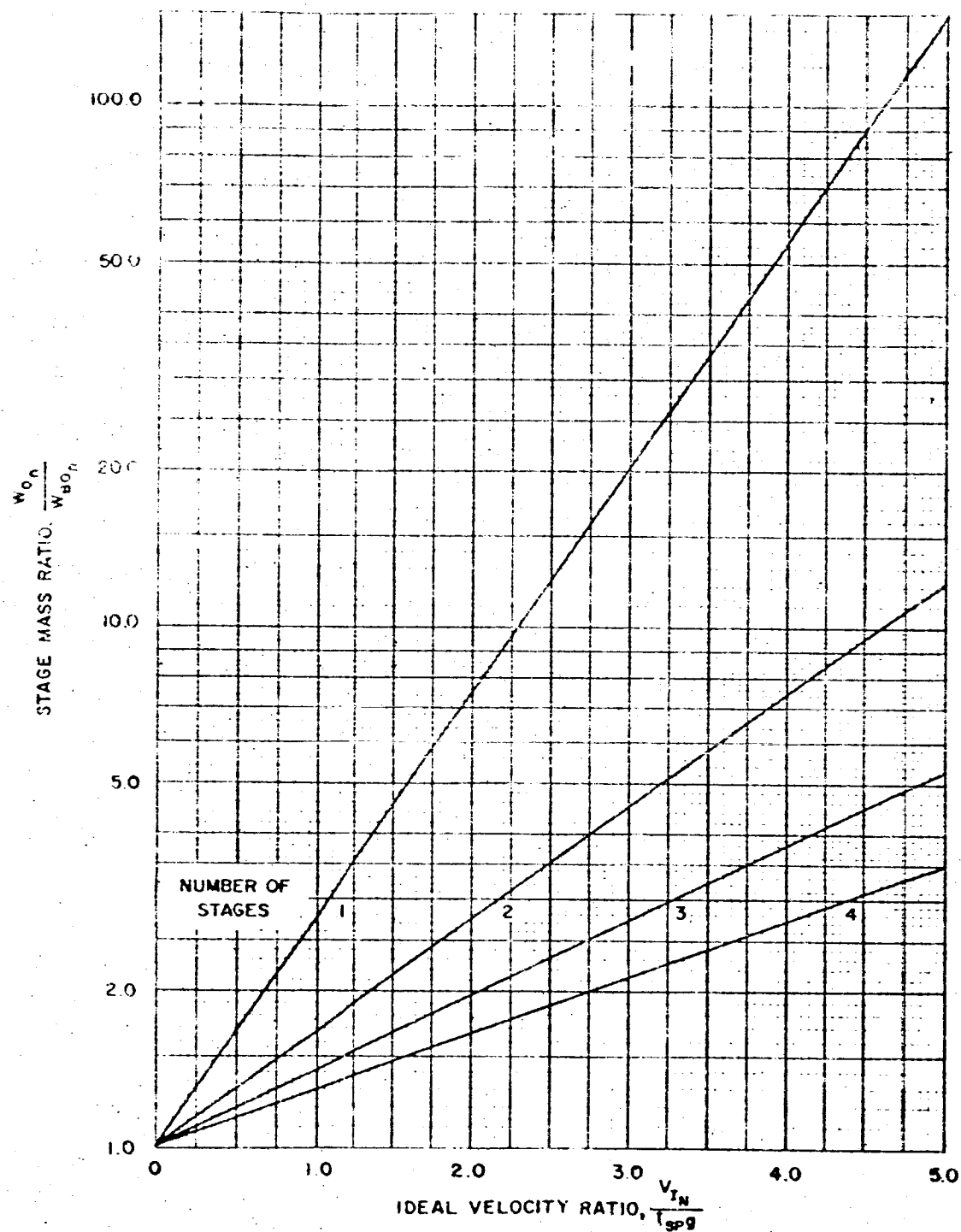


Figure 54. Stage Mass Ratio for Like Parameters (Multiple-Stage Vehicles)

Stage Mass Ratio

5-61

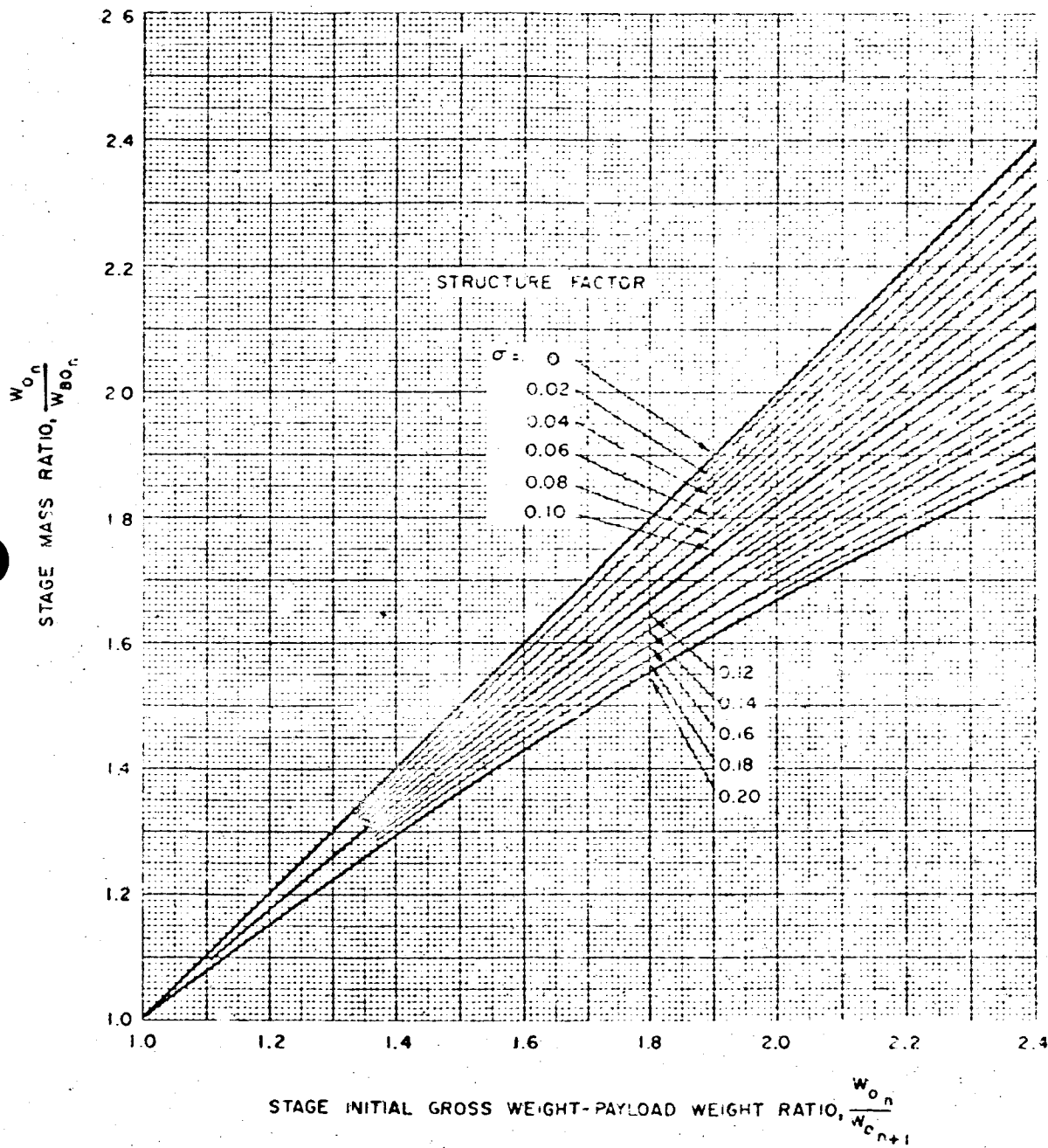


Figure 55. Stage Mass Ratio (Single-Stage Vehicle)

5-62

VEHICLE SIZING

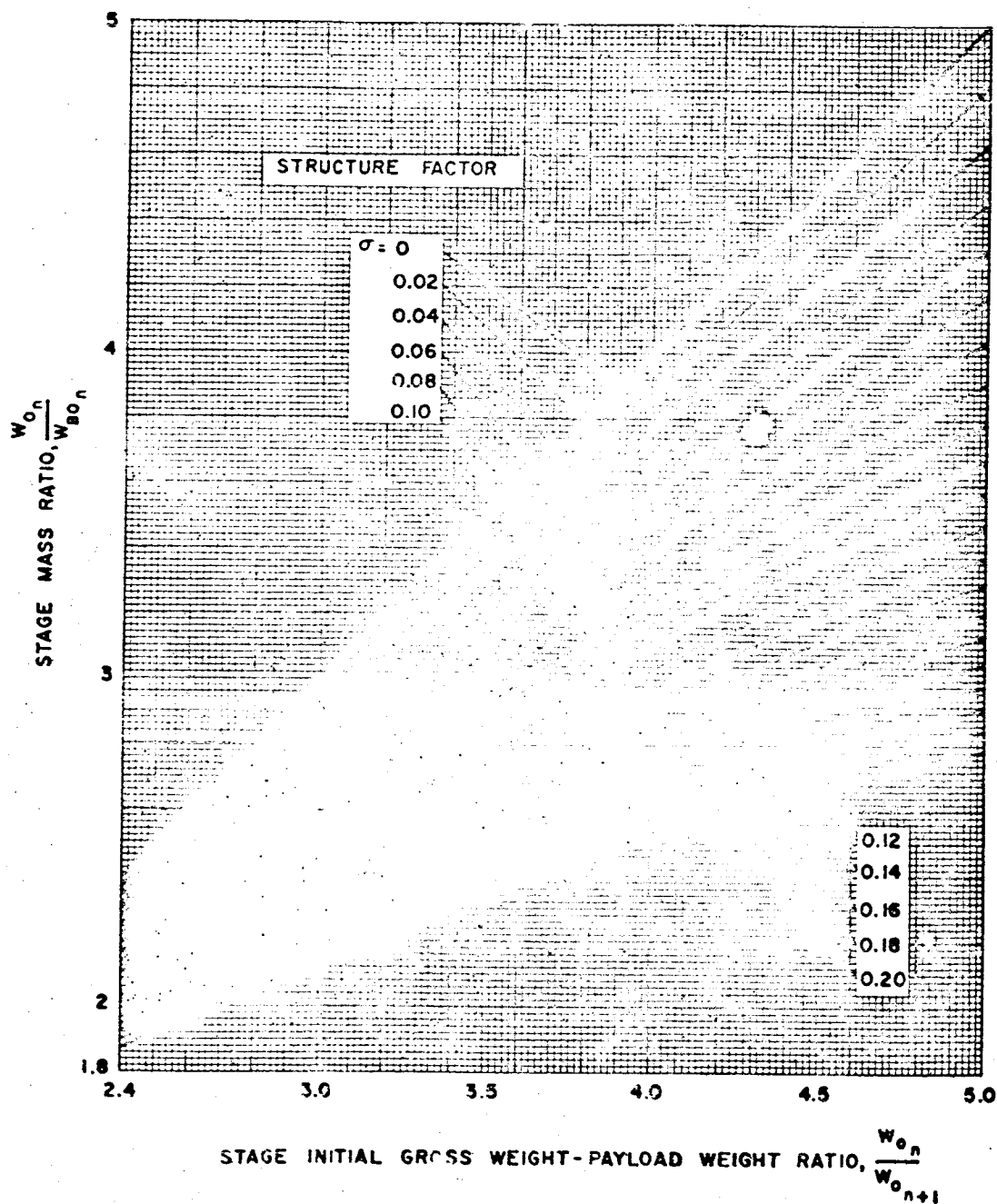


Figure 56. Stage Mass Ratio (Single-Stage Vehicle)

Stage Mass Ratio

5-63

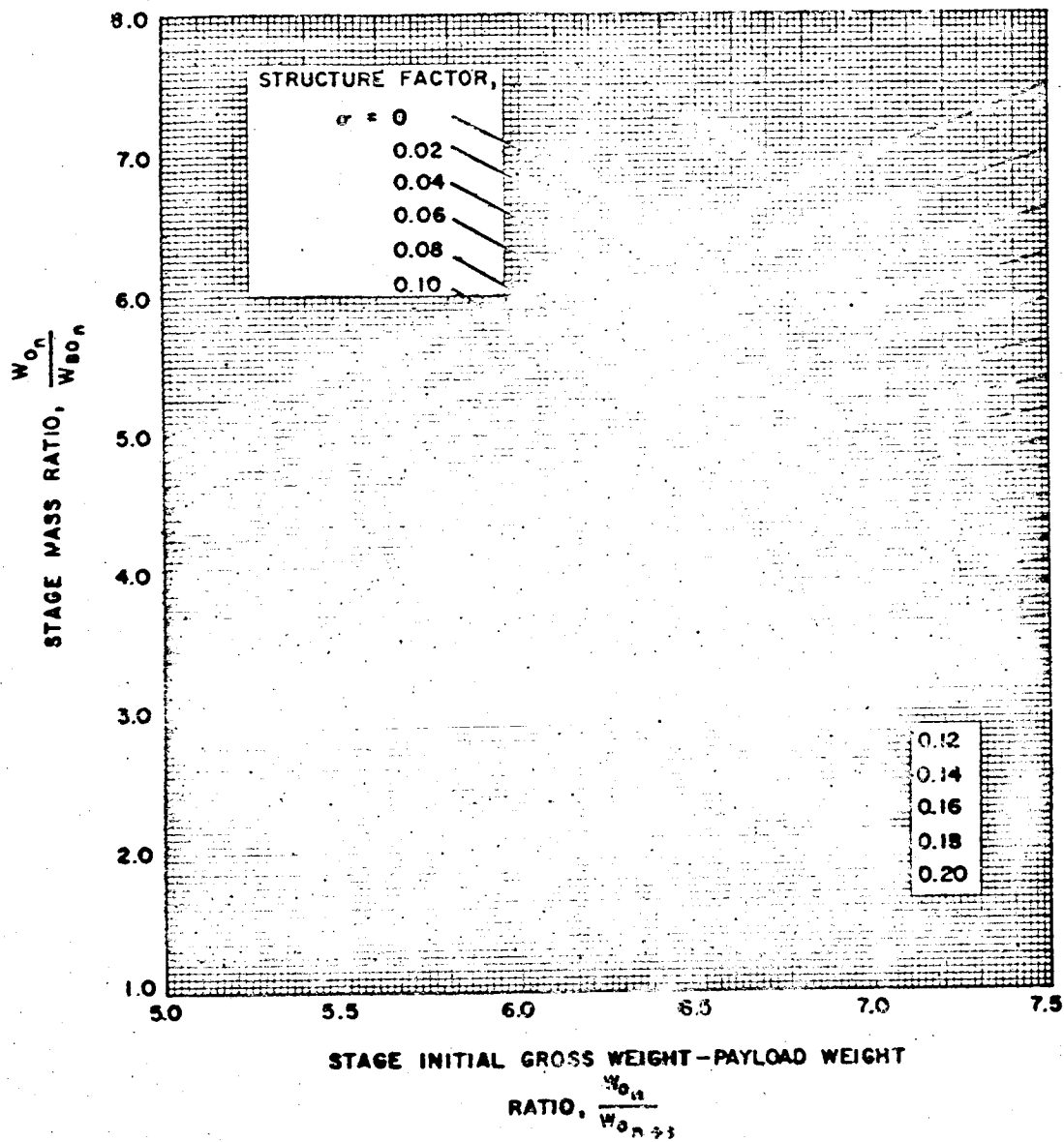


Figure 57. Stage Mass Ratio (Single-Stage Vehicle)

5.3 OPTIMUM SIZING FOR MINIMUM GROSS WEIGHT—PAYLOAD WEIGHT RATIO

The commonly used approximation to optimum sizing of a vehicle with respect to the overall system is sizing for maximum payload or, if the payload weight is given, sizing for minimum gross weight (corresponding to a minimum gross weight-payload weight ratio in both cases). Sizing for maximum payload weight is discussed in this section; sizing for criteria other than maximum payload is discussed later in Chapter 5. For background on the subject of optimum sizing, the reader is referred to the thorough and annotated bibliography of Reference 1; other pertinent sources (some included in the bibliography) are found in References 2 through 6.

All the solutions presented here assume that a given fixed total impulsive velocity means constant gravitational and atmospheric losses. A solution including variable losses could be developed using portions of the analyses presented in Chapter 2, but the increased accuracy would not warrant the increased complexity. Three different solutions for optimum sizing for maximum payload and minimum initial gross weight are presented; the difference in these solutions is in the approximation to the representation of the structure factor-stage size relationship, where structure factor, σ_i , is defined as

$$\sigma_i \equiv \frac{w_{ST_i}}{w_{O_i} - w_{O_{i+1}}}$$

The first and most commonly used approximation assumes the structure factor to be constant with respect to stage weight; in other words, structure weight is linearly proportional to stage weight. The second solution assumes that the structure factor is linearly proportional to stage weight. This solution was adapted from that presented in Reference 11; however, in the reference the structure factor was assumed to be linearly proportional to the propellant weight. The third and most accurate solution assumes the structure factor curve to be fitted by the higher order approximation

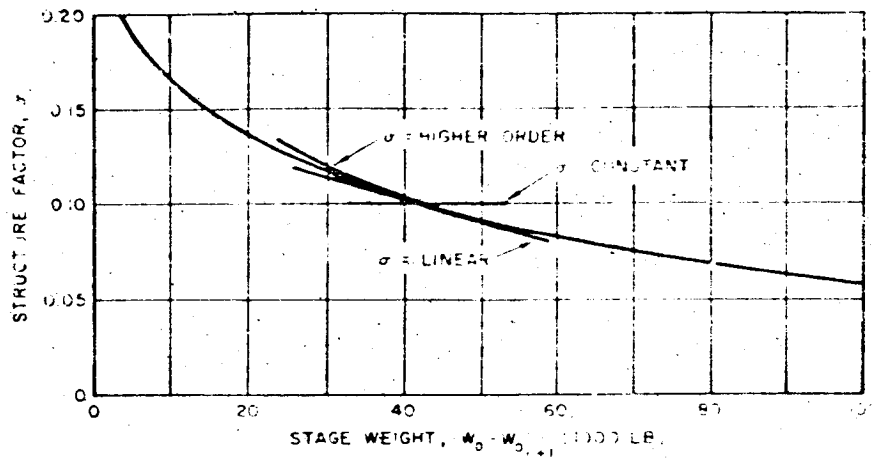
$$C_1 \left(w_{O_i} - w_{O_{i+1}} \right)^{a_1 - 1}$$

This solution was adapted directly from Reference 10. The fit of each approximation for a typical structure factor curve is illustrated in Figure 58.

Let the reader be cautioned that the last two solutions are too complex for solution in reasonable time without the aid of a small digital computer. The first solution, which assumes constant structure factor, is readily computed either by hand or with a small computer, such as the Burrough's E 102. The easiest method of computation is the use of the nomograph presented and discussed in Section 3.3. The constant structure factor assumption is found to be a reasonable approximation for

Optimum Sizing for Minimum Gross Weight - Payload Weight Ratio

565



APPROXIMATIONS

$$\text{CONSTANT} = \sigma_i = 0.10$$

$$\text{LINEAR} = \sigma_i = A_i (w_0 - w_{0,i+1}) + B_i = -0.0017 \left(\frac{w_0 + w_{0,i+1}}{1000} \right) + 0.015$$

$$\text{HIGHER ORDER} = \sigma_i = C_i (w_0 - w_{0,i+1})^{\alpha_i} = 0.95 (w_0 - w_{0,i+1})^{0.634}$$

$$\text{WHERE } \sigma_i = \frac{w_{ST_i}}{w_0 - w_{0,i+1}}$$

Figure 58. Curve Fits for the Approximation of the Structure Factor Variation

vehicles of gross weights in excess of the 1,000- to 10,000-pound class, and, by using an iterative procedure, a variation of structure factor with stage weight can be simulated to improve the accuracy of the solution. The variable structure factor solutions, if programmed on a digital computer, facilitate the computation; however, the increased accuracy results in only a small increase in performance capability, since the optima are rather flat. If only large digital computers like the IBM 7090 are available, it is recommended that a solution be programmed similar to that presented in Reference 13, where the vehicle is sized and the trajectory simulated simultaneously on the computer.* This kind of method can make use of the exact structure factor stage weight curve in the sizing procedure. It has been found most profitable when using a sizing-trajectory program, to use the nomographical solution for initial estimates. This procedure has been found to reduce the computing time by a factor of three or four. Such large programs have the facility to simulate real life "constraints" and to incorporate the characteristics of actual vehicle components, such as engines, stages, and structural weight or structure factor curves of individual elements of the vehicle structure (e. g., tank, thrust, interstage, intrastage, payload fairing, and shroud structures). Similarly, sizing-trajectory programs that size with respect to minimum cost are also feasible, and have been developed and used in the industry.

The proper ultimate in sizing-trajectory programs is the General Design-Sizing Trajectory Program, presently under consideration at STL, which will be feasible when larger (in terms of storage capacity), higher-speed digital computers are available. The program would consist of many subprograms, representing all the disciplines associated with a vehicle system design. The subprograms would be continually updated to incorporate improvements in the technology. Characteristics of particular "off the shelf" hardware components would also be stored in the program. The program would have a build in decision making capability to aid in achieving the optimum system. Such a program would be designed to require a minimum of input, much of which would be qualitative. The usefulness of this type of program is reflected by how little input is required.

However, it is found that an engineer experienced in vehicle design, using the material presented in this handbook and, in particular, using the nomograph and evaluating the vehicle performance per the analyses presented in Chapter 2, can design a realistically optimum vehicle system in a relatively short time (without the engineer having to use a digital computer). However, it is desirable, but not necessary, to check the vehicle performance with a two-dimensional trajectory program, which provides much additional information.

* Such programs exist and are used at STL; however, they are not presented here because of the intended scope of the handbook and their proprietary nature.

5.3.1 Constant Structure Factor

Assuming a constant structure factor $\sigma_i = \text{constant}$, the analytical equations for sizing, where

$$\sigma_i = \frac{W_{ST_i}}{W_{O_i} - W_{O_{i+1}}} \quad (12)$$

are essentially the same whether the sizing is for minimum gross weight or maximum payload. One first needs an estimation of the total ideal velocity, readily approximated from the cursory analysis presented in Chapter 2. The solution is iterative with respect to the ideal velocity; therefore, it is best to plot the optimum distribution as a function of the ideal velocity and iterate, calculating the exact velocity losses for the optimally distribution vehicles per Chapter 2 until the estimated ideal velocity is found that matches the computed value.

To optimally size a vehicle, it is necessary to assume a stage size: if the vehicle is being sized for minimum vehicle gross weight, a stage gross weight-payload weight ratio is assumed for the first stage; if sizing is for maximum payload, a stage gross weight-payload weight ratio is assumed for the last stage. In either case, if a variable structure factor is not being simulated, it does not matter whether one starts at the first stage or the last. Using the equation below,* the succeeding or preceding stage weight ratio is found:

$$x_{n+1} = \frac{\frac{I_{sp_{n+1}}}{I_{sp_n}} (1 - \sigma_{n+1}) [x_n \sigma_n + (1 - \sigma_n)] - (1 - \sigma_{n+1}) (1 - \sigma_n)}{\sigma_{n+1} (1 - \sigma_n)} \quad (1 \leq n \leq N - 1) \quad (13)$$

where

$$x_n = W_{O_n} / W_{O_{n+1}} \quad , \quad W_{C_{N+1}} = W_{PL}$$

To approximate a variable structure factor-stage weight curve, first assume an approximate structure factor of the stage being optimized and, having determined its optimum size, compare the assumed structure factor with the actual structure factor; then iterate until they coincide. Next compute all succeeding (or preceding) stage gross weight-payload weight ratios, using the previously computed ratio. (It may be desirable, with respect to minimizing the effort for programming the solution,

* When starting at the top of the vehicle, all $n + 1$ and n subscripts are interchanged.

to size all the stages with respect to either the first or last stage gross weight-payload weight ratio, this is possible by simply manipulating the subscripts in the above equation.) Having found all the ratios, compute the total ideal velocity.

$$V_{1_N} = \sum_{i=1}^N I_{sp_i} g \ln \frac{x_i}{x_i \sigma_i + (1 - \sigma_i)} \quad (14)$$

Iterate on the initial assumed stage gross weight-payload weight ratio, and compute the others until the resulting ideal velocity corresponds to that estimated to be required. Then compute the exact ideal velocity required, compare with the vehicle's actual capability, and iterate again. If necessary assume a new value for the total ideal velocity required. The vehicle gross weight-payload-weight ratio is then computed from,

$$X_N = \prod_{i=1}^N x_i \quad (15)$$

The solution sounds tedious; however, with experience and the aid of the nomograph presented in Section 3.3 or a small computer, it becomes very fast.

Should a stage, such as a booster, be specified and should maximum payload be desired, sizing proceeds in exactly the same manner as for the upper unspecified stages; however, several gross weights of the upper stages would be assumed and the optimum propellant distribution as a function of the total ideal velocity capability of the upper stages determined. The burnout velocity capability of the booster would also be determined as a function of its payload weight (gross weight of upper stages). The velocity losses associated with the upper stage operation would be calculated for each upper stage gross weight-booster combination and payload corresponding to the desired mission requirements determined. The payload capability would then be plotted as a function of the upper stage gross weight, and the maximum payload found. This result, corresponding to maximum payload capability for a specified booster which is different than minimum gross weight-payload weight ratio, is in most cases more desirable. Minimum gross weight-payload weight ratio for a vehicle having a specified stage is found in the same manner as for a vehicle of all unspecified stages, except that the stage weight of the specified stage is held constant.

5.3.2 Variable Structure Factor

The procedure for sizing, assuming a variable structure, is the same as for constant structure factor, except there is no necessity to perform an iteration on structure factor if the curve fit is good at the point of optimization. There are two solutions presented here for approximations to the representation to be used for the fit to the structure factor curve. Which solution is used is dependent upon the type of digital computer to be employed.

Linear Approximation. The stage structure factor curve is assumed to have the form,

$$r_i = A_i (W_{O_i} - W_{O_{i+1}}) + B_i \quad (16)$$

where

$$\sigma_i = \frac{W_{ST_i}}{W_{O_i} - W_{O_{i+1}}} \quad (16a)$$

One has to be careful to fit the portion of the structure factor curve where the optimum size is anticipated to exist to insure good accuracy. There are two different sets of equations dependent upon whether the payload or vehicle gross weight is given.

1. Given Initial Gross Weight

a. Stage Gross Weight-Payload Weight Ratio

$$\begin{aligned} Isp_n & \left\{ (1 - B_n) + \frac{A_n W_{O_1}}{\prod_{k=1}^n x_k} \left[2x_n (x_n - 1) \right] \right\} \\ & \frac{A_n W_{O_1}}{\prod_{k=1}^n x_k} (x_n - 1)^2 \\ & = \frac{Isp_{n-1} \left\{ (1 - B_{n-1}) + \frac{A_{n-1} W_{O_1}}{\prod_{k=1}^{n-1} x_k} \left[2x_{n-1} (x_{n-1} - 1) \right] \right\}}{x_{n-1} - (1 - B_{n-1})(x_{n-1} - 1) - \frac{A_{n-1} W_{O_1}}{\prod_{k=1}^{n-1} x_k} (x_{n-1} - 1)^2} \quad (2 \leq n \leq N) \end{aligned} \quad (17)$$

To solve for x_1, x_2, \dots, x_N it is easiest to assume a value for x_1 and iterate on x_2 until the above equation is fulfilled. Having found x_2 , iterate on x_3 , etc.

b. Total Ideal Velocity

$$V_{I_N} = \sum_{i=1}^N Isp_i g \ln \frac{x_i}{x_i - (1 - B_i)(x_i - 1) - \frac{A_i W_{O_1}}{\prod_{k=1}^i x_k} (x_i - 1)^2} \quad (18)$$

c. Vehicle Gross Weight-Payload Weight Ratio

$$X_N = \prod_{i=1}^N x_i \quad (19)$$

2. Given Payload Weighta. Stage Gross Weight-Payload Weight Ratio

$$\begin{aligned} & \frac{I_{sp_n} \left[(1 - B_n) + A_n W_{PL} (x_n^2 - 1) \prod_{k=n+1}^{N+1} x_k \right]}{x_n - (1 - B_n)(x_n - 1) - A_n W_{PL} (x_n - 1)^2 \prod_{k=n+1}^{N+1} x_k} \\ &= \frac{I_{sp_{n-1}} \left[(1 - B_{n-1}) + A_{n-1} W_{PL} (x_{n-1}^2 - 1) \prod_{k=n}^{N+1} x_k \right]}{x_{n-1} - (1 - B_{n-1})(x_{n-1} - 1) - A_{n-1} W_{PL} (x_{n-1} - 1)^2 \prod_{k=n}^{N+1} x_k} \quad (2 \leq n \leq N) \end{aligned} \quad (20)$$

where

$$x_{k=N+1} = \frac{W_{PL}}{W_{PL}} = 1 \quad (20a)$$

To solve for x_1, x_2, \dots, x_n first assume a value for x_n and iterate on x_{n-1} until the above equation is fulfilled. Having found x_{n-1} , iterate on x_{n-2} , etc.

b. Total Ideal Velocity

$$V_{I_N} = \sum_{i=1}^N I_{sp_i} g \ln \frac{x_i}{x_i - (1 - B_i)(x_i - 1) - \frac{A_i W_{O_i}}{\prod_{k=1}^i x_k} (x_i - 1)^2} \quad (21)$$

c. Vehicle Gross Weight-Payload Weight Ratio

$$X_N = \prod_{i=1}^N x_i \quad (22)$$

High-Order Approximation. The structure factor curve is assumed to have the form

$$\sigma_i = C_i (W_{O_i} - W_{O_{i+1}})^{a_i-1} \quad (23)$$

where

$$\sigma_i = \frac{W_{ST_i}}{W_{O_i} - W_{O_{i+1}}} \quad (24)$$

Again, there are two sets of equations dependent upon whether the payload or the vehicle gross weight is given. This type of approximation results in a much better fit.

1. Given Initial Gross Weight

a. Stage Gross Weight-Payload Weight Ratio

$$\frac{Isp_n \left\{ 1 + C_n a_n \left(\frac{W_{O_i}}{\prod_{k=1}^n x_k} \right)^{a_n-1} \left[(x_n - 1)^{a_n} - x_n (x_n - 1)^{a_n-1} \right] \right\}}{x_n \left[1 + C_n \left(\frac{W_{O_i}}{\prod_{k=1}^n x_k} \right)^{a_n-1} (x_n - 1)^{a_n} \right]} \\ \frac{Isp_{n-1} \left\{ 1 + C_{n-1} a_{n-1} \left(\frac{W_{O_i}}{\prod_{k=1}^{n-1} x_k} \right)^{a_{n-1}-1} \left[(x_{n-1} - 1)^{a_{n-1}} - x_{n-1} (x_{n-1} - 1)^{a_{n-1}-1} \right] \right\}}{x_{n-1} \left[1 + C_{n-1} \left(\frac{W_{O_i}}{\prod_{k=1}^{n-1} x_k} \right)^{a_{n-1}-1} (x_{n-1} - 1)^{a_{n-1}} \right]} \quad (2 \leq n \leq N) \quad (25)$$

As before, it is necessary to iterate in order to find each value of x_1 .

b. Total Ideal Velocity

$$V_{I_N} = \sum_{i=1}^N I_{sp_i} g \ln \frac{x_i}{1 + C_i \left(\frac{W_{O_i}}{\prod_{k=1}^i x_k} \right)^{a_i - 1} (x_i - 1)^{a_i}} \quad (26)$$

c. Vehicle Gross Weight-Payload Ratio

$$X_N = \prod_{i=1}^N x_i \quad (27)$$

2. Given Payload Weight

a. Stage Gross Weight-Payload Weight Ratio

$$\begin{aligned} I_{sp_n} \left\{ 1 + C_n \left(W_{PL} \prod_{k=n+1}^{N+1} x_k \right)^{a_n - 1} \left[(x_{n-1})^{a_n} - a_n x_n (x_{n-1})^{a_n - 1} \right] \right\} \\ \left[1 + C_n \left(W_{PL} \prod_{k=n+1}^{N+1} x_k \right)^{a_n - 1} (x_{n-1})^{a_n} \right] \\ = \frac{I_{sp_{n-1}} \left\{ 1 + C_{n-1} \left(W_{PL} \prod_{k=n}^{N+1} x_k \right)^{a_{n-1} - 1} \left[(x_{n-1} - 1)^{a_{n-1}} - a_{n-1} x_{n-1} (x_{n-1} - 1)^{a_{n-1} - 1} \right] \right\}}{\left[1 + C_{n-1} \left(W_{PL} \prod_{k=n}^{N+1} x_k \right)^{a_{n-1} - 1} (x_{n-1} - 1)^{a_{n-1}} \right]} \end{aligned} \quad (2 \leq n \leq N) \quad (28)$$

where

$$x_{k=N+1} = W_{PL} / W_{PL} = 1 \quad (29)$$

Again, it is necessary to iterate to find each value of x_i .

b. Total Ideal Velocity

$$V_{I_N} = \sum_{i=1}^N I_{sp} g \ln \frac{x_i}{1 + C_i \left(W_{PL} \prod_{k=1}^{N+1} x_k \right)^{a_i - 1} (x_i - 1)^{a_i}} \quad (30)$$

c. Vehicle Gross Weight-Payload Weight Ratio

$$X_N = \prod_{i=1}^N x_i \quad (31)$$

5.3.3 Optimum Sizing Nomograph

The equations for the optimum sizing of a vehicle for a given mission have been developed in the two preceding subsections. These equations are relatively complicated and require an iterative method for solution. In order to relieve the time-consuming task of straight-forward solution of these equations, a graphic means of solution, in the form of a nomograph, has been developed.¹⁷

As indicated in Section 3 of Appendix D, the equation representing optimum sizing of a multiple stage vehicle shown in Section 5.3.1 can be rewritten as

$$Isp_1 (1 - r_1 \sigma_1) = \dots = Isp_n (1 - r_n \sigma_n) = Isp_{n+1} (1 - r_{n+1} \sigma_{n+1}) = \dots = Isp_N (1 - r_N \sigma_N) \quad (32)$$

where

$$r = \frac{W_O}{W_{BO}}$$

This equation relates the parameters of each stage of a vehicle, to facilitate optimum sizing when different constant structure factors, σ , and different specific impulses, Isp , are assumed in each stage. The assumption of a constant structure factor in a stage simplifies the sizing equations (cf., the equations in Sections 5.3.1 and 5.3.2). Even though the solution itself allows no variations of a stage structure factor, an iterative procedure can be used to include a variation where necessary.

Equation (32) in itself does not provide the complete relationship for vehicle sizing. Since a mission requirement must be met in terms of a total ideal velocity, the following equations must be considered with Equation (32):

$$V_{I_N} = g \sum_{i=1}^N Isp_i \ln r_i \quad (33)$$

As mentioned previously, the total ideal velocity is the sum of the mission burnout velocity, the velocity losses incurred by the vehicle during flight, and the earth's

rotational effects. Generally, the velocity losses can be estimated with reasonable accuracy (see Section 2.2) without knowing the size and shape of the vehicle. During the sizing of a vehicle, the payload ratio of each stage,

$$\frac{W_{O_n}}{W_{O_{n+1}}}$$

is of interest to determine the overall vehicle payload ratio, W_O/W_{PL} .

The payload ratio of any stage is

$$\frac{W_{O_n}}{W_{O_{n+1}}} = \frac{n(1 - \sigma_n)}{1 - r_n \sigma_n} \quad (34)$$

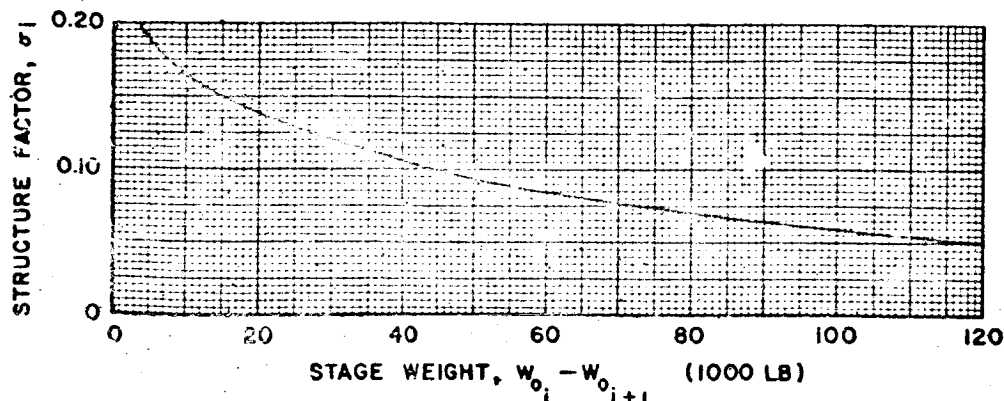
while the overall vehicle payload ratio is

$$\frac{W_O}{W_{PL}} = \prod_{i=1}^N \frac{W_{O_i}}{W_{O_{i+1}}} \quad (35)$$

Since Equations (32), (33) and (34) are a function of the mass ratio of the stages, a nomograph based on that parameter was easily constructed. Examination of Equation (32) indicates that the sizing of all the stages of a vehicle can be referred to the parameters of one particular stage, thus reducing the time required for the analysis.

The Optimum Sizing Nomograph will be found inside the back cover. In order to clearly explain its use, an example sizing problem will be illustrated.

Problem. Determine the optimum weight ratio distribution required to put a 4,000 pound payload into a 100-nautical mile circular orbit with a three stage vehicle, assuming an eastward launch from AMR. The specific impulses of the first three stages are 250, 300, and 350 lb-sec/lb respectively. The following variation of structure factor with stage weight is assumed valid for all three stages.



The ideal velocity for which the vehicle will be sized is

$$V_{I_N} = V_{BO} - V_{rot} + \Delta V_L \quad (36)$$

where

- V_{BO} = mission burnout velocity
 V_{rot} = earth's rotational component
 ΔV_L = vehicle velocity losses (assumed to be 5000 ft/sec for illustration of the problem)

which gives

$$V_{I_N} = 25,581 - 1,342 + 5,000 = 29,239 \text{ ft/sec.}$$

Having once obtained the necessary input parameters, the sizing analysis requires the following steps for solution:

- 1) Assume a structure factor for each stage.

<u>Stage</u>	<u>Structure Factor</u>
1	0.07
2	0.10
3	0.15

- 2) Assume an initial mass ratio for the first stage ($r_1 = 3.00$).
- 3) Enter the nomograph at the "start" position at the above mass ratio.
- 4) Move vertically upward to the first stage structure factor ($\sigma_1 = 0.07$).
- 5) Extend a horizontal line right to the first stage specific impulse ($I_{sp1} = 250 \text{ sec}$).
- 6) Construct a vertical line downward to the second and third stage specific impulses ($I_{sp2} = 300 \text{ sec}$ and $I_{sp3} = 350 \text{ sec}$).
- 7) From the second stage specific impulse move right horizontally to the second stage structure factor ($\sigma_2 = 0.10$).
- 8) Extend a vertical line upward and read the second stage mass ratio ($r_2 = 3.35$).

- 9) Repeat Steps 7) and 8), using the third stage specific impulse and structure factor ($\sigma_3 = 0.15$ gives $r_3 = 2.85$).
- 10) Using the specific impulse and mass ratio obtained above for each stage, determine the stage ideal velocity from the curve in the lower left hand side of the nomograph. The following velocities were obtained for the example stages:

Stage	Mass Ratio	Ideal Velocity (ft/sec)
1	3.00	8,850
2	3.35	11,650
3	2.85	11,800

The sum of the stage ideal velocities, 32,300 ft/sec, is considerably above that required.

- 11) Repeat Steps 1) through 10) with a different assumption for the initial mass ratio until the desired velocity is reached. For the example, the desired velocity is reached with first, second, and third stage mass ratios of 2.48, 3.07, and 2.68 respectively.
- 12) For the mass ratios and structural factors, find the stage payload ratios from the plot in the upper right hand corner of the nomograph. Note that the value on the ordinate is the inverse of the payload ratio. For the example, the payload ratios are given below:

Stage	Mass Ratio	Structure Factor	Payload Ratio
1	2.48	0.07	2.79
2	3.07	0.10	3.98
3	2.68	0.15	3.81

- 13) The total vehicle payload ratio is found by Equation (35) which gives

$$\frac{W_O}{W_{PL}} = \prod_{i=1}^N \frac{W_{O_i}}{W_{O_{i+1}}} = (2.79)(3.98)(3.81) = 42.3$$

Thus the vehicle gross weight required to put the 4,000-pound payload in orbit is

$$W_O = (42.3)(4000) = 169,000 \text{ lb}$$

- 14) It must be remembered that the structure factors for each stage were assumed values, and thus the respective stage weights must be computed to obtain the correct values of σ from the plot of structure factor versus stage weight. The weight of a particular stage of a vehicle is

$$W_{S_n} = W_{O_n} \left[\frac{r_n - 1}{r_n (1 - \sigma_n)} \right] \quad (37)$$

where

$$W_{O_n} = W_{O_{n+1}} + W_{S_n}$$

For the example, the stage weights and proper structure factors are:

Stage	Assumed σ	Stage Weight (lb)	Actual σ
1	0.07	108,500	0.055
2	0.10	45,400	0.100
3	0.15	11,200	0.163

After a comparison of structure factors, it is seen that the vehicle previously sized is now in error, and a new analysis must be performed. (One could compute the actual structure factor after computing each optimum stage ratio and iterate until the assumed value matches that desired.)

- 15) Recalculate Steps 1) through 14) until the assumed structure factors approach the actual values with the desired accuracy. The actual structure factors obtained in Step 14) can be used as the assumed values for the next iteration. In the case of the example, the second iteration is seen to have considerably reduced the difference in structure factors which gives the following:

Stage	Assumed σ	Stage Weight (lb)	Actual σ
1	0.055	119,200	0.050
2	0.100	38,200	0.105
3	0.163	9,600	0.168

Using the above, a 171,000-pound vehicle is required to perform the mission of interest.

After experience in the use of the nomograph, an engineer can optimally size a vehicle in a relatively short time.

5.4 GENERAL OPTIMUM SIZING

All the sizing criteria developed up to now have considered only sizing with respect to minimum initial gross weight. However, often problems arise where a criterion other than minimum gross weight is desired. Such a criterion might be minimum system cost, minimum volume, minimum length, or maximum probable payload. Each of these design criteria have been investigated at STL with respect to a particular vehicle design.

The general solution presented here requires that parameters involved be representable as functions of the vehicle's weight. This constraint, however, usually does not limit the scope of application since time dependent parameters (as might be found in a reliability problem) can be related to the weight, and weight is a time dependent function. A similar analysis can be found in Reference 9.

5.4.1 Development of Solution

Given a set of weight dependent vehicle parameters, the criterion to be optimized, C , can be represented as

$$C = F(x_1, x_2, x_3, \dots, x_{i=N}) \quad (38)$$

where

$$x_i = \frac{W_{O_i}}{W_{O_{i+1}}}$$

It is desired to find the extremum of C . However, imposed on the solution is the constraint that a given total ideal velocity must be achieved. The ideal velocity, V_{I_N} , is the sum of the burnout velocity and the velocity losses, and is defined by the particular mission. This constraint is represented by the equation

$$V_{I_N} = G(x_1, x_2, x_3, \dots, x_{i=N}) = \text{const.} \quad (39)$$

Using the solution devised by Lagrange¹⁸ for constrained maxima and minima problems, the solution is

$$F'(x_1) + \phi G'(x_1) = 0 \quad (40)_1$$

$$F'(x_2) + \phi G'(x_2) = 0 \quad (40)_2$$

$$F'(x_3) + \phi G'(x_3) = 0 \quad (40)_3$$

⋮

⋮

⋮

$$F'(x_{i=N}) + \phi G'(x_{i=N}) = 0 \quad (40)_N$$

$$V_{I_N} = G(x_1, x_2, x_3, \dots, x_{i=N}) \quad (40)_{N+1}$$

where

$$F'(x_i) = \frac{\partial F(x_1, x_2, x_3, \dots, x_{i=N})}{\partial x_i} \quad (40a)$$

$$G'(x_i) = \frac{\partial G(x_1, x_2, x_3, \dots, x_{i=N})}{\partial x_i} \quad (40b)$$

ϕ is an undetermined multiplier known as the "Lagrangian multiplier." Equations (40)₁ through (40)_N have N+1 unknowns, the (N+1)th unknown being ϕ . The (N+1)th equation used in the solution is Equation (40)_{N+1}; however, this equation is logarithmic in nature, making it impossible to solve implicitly for x_i . However, it is possible to solve Equations (40)₁ through (40)_N by iteration such that the constraint is fulfilled. Other problems might arise where other constraints are imposed on the solution such as burnout altitude or burnout flight path angle. A similar solution exists where M defines the total number of constraints. This is

$$F'(x_1) + \sum_{m=1}^M \phi_m G'_m(x_1) = 0 \quad (41a)_1$$

$$F'(x_2) + \sum_{m=1}^M \phi_m G'_m(x_2) = 0 \quad (41a)_2$$

$$F'(x_3) + \sum_{m=1}^M \phi_m G'_m(x_3) = 0 \quad (41a)_3$$

$$F'(x_{i=N}) + \sum_{m=1}^M \phi_m G'_m(x_{i=N}) = 0 \quad (41a)_N$$

$$G_1(x_1, x_2, x_3, \dots, x_{i=N}) = \text{constant} \quad (41b)_1$$

$$G_2(x_1, x_2, x_3, \dots, x_{i=N}) = \text{constant} \quad (41b)_2$$

$$G_3(x_1, x_2, x_3, \dots, x_{i=N}) = \text{constant} \quad (41b)_3$$

$$G_{m=M}(x_1, x_2, x_3, \dots, x_{i=N}) = \text{constant} \quad (41b)_M$$

$$F'(x_i) = \frac{\partial F(x_1, x_2, x_3, \dots, x_i = N)}{\partial x_i} \quad (41c)$$

$$G'_m(x_i) = \frac{\partial G(x_1, x_2, x_3, \dots, x_i = N)}{\partial x_i} \quad (41d)$$

Usually the solutions resulting for $m > 1$ are so complex that it is desirable to use a high speed computer unless $G_m(x_1, x_2, x_3, \dots, x_{i=N})$ is a trivial function, such as maximum allowable acceleration for a particular stage.

5.4.2 Examples

Sample Problem for Parallel Staging.¹⁹ Parallel staging is defined as staging a vehicle such that upper stage engines are also used during the lower stage operation. This usually results in the stages being placed alongside one another; hence, the name "parallel staging." The conventional method of staging by "stacking" one stage on top of another is referred to as "tandem staging."

Often parallel staging is proposed in order to achieve better performance than is obtainable with tandem staging. However, little has been written on the effects of parallel staging on vehicle design. It is the purpose of this section to solve the parallel boost problem for minimum initial total gross weight as an example of the use of the solution developed for general optimum sizing.

The problem was solved assuming a system of only two stages, staged parallel. It is doubtful that it would ever be desirable to stage any more than two stages in parallel. It is also assumed that during first-stage burning, the second-stage engine burns propellant from the first-stage tank only. However, provision is made for a propellant of different specific impulse in the second-stage tank. Whether an engine will be available that will burn different propellants is not part of this problem.

1. Derivation and Solution of the Parallel Staging Equations for Minimum Gross Weight. It is desired to minimize the initial gross weight of a two-stage, parallel staged vehicle having a given payload and a required total velocity. This can be achieved by minimizing the total initial gross weight-payload weight ratio for the required total velocity. The total payload ratio is simply the product of the ratio of the individual stage gross weights to their payloads (x_1 and x_2).

$$X_N = x_1 \cdot x_2 \quad (42)$$

where

$$x_1 = \frac{W_{O_1}}{W_{O_2}} \quad (42a)$$

$$x_2 = \frac{W_{O_2}}{W_{PL}} \quad (42b)$$

Imposed on the solution is the constraint that a given ideal velocity, V_I , must be achieved. It is easily shown that the ideal velocity equals

$$V_{I_N} = Isp_1 g \ln \frac{W_{O_1}}{W_{BO_1}} + Isp_2 g \ln \frac{W_{O_2}}{W_{BO_2}} \quad (43)$$

where

$$\frac{W_{O_1}}{W_{BO_1}} = \frac{W_{O_1}}{W_{O_1} - W_{P_1}} \quad (43a)$$

$$\frac{W_{O_2}}{W_{BO_2}} = \frac{W_{O_2}}{W_{O_2} - W_{P_2}} \quad (43b)$$

Now

$$X_N = F(x_1, x_2)$$

It is, therefore, necessary to find $V_{I_N} = G(x_1, x_2)$.

The weight of the first-stage engine may be expressed as

$$\begin{aligned} W_{ENG_1} &= \left[\left(\frac{T}{W_{O_1}} \right) - \frac{1}{x_2} \left(\frac{T}{W_{O_2}} \right) \right] \sigma_{ENG_1} W_{O_1} \\ &= \left[\left(\frac{T}{W_{O_1}} \right) - \frac{1}{x_1} \left(\frac{T}{W_{O_2}} \right) \right] \sigma_{ENG_1} W_{O_1} \end{aligned} \quad (44)$$

Similarly, for the second-stage engine

$$W_{ENG_2} = \left(\frac{T}{W_{O_2}} \right) \sigma_{ENG_2} W_{O_2} \quad (45)$$

It is assumed that the tank and accessory weights are directly proportional to the propellant weight. Therefore,

$$(w_{T\&A})_1 = \sigma_{T\&A_1} w_{P_1} \quad (46)$$

$$(w_{T\&A})_2 = \sigma_{T\&A_2} w_{P_2} \quad (47)$$

The initial gross weights of the first and second stages are

$$w_{O_1} = w_{ENG_1} + w_{P_1} + (w_{T\&A})_1 + w_{O_2} \quad (48)$$

$$w_{O_2} = w_{ENG_2} + w_{P_2} + (w_{T\&A})_2 + w_{PL} \quad (49)$$

Substituting Equations (44) and (48) and Equations (45) and (47) into Equations (48) and (49) respectively and solving for the propellant weight,

$$w_{P_1} = \frac{w_{O_1} - w_{O_2} - \left[\left(\frac{T}{w_{O_1}} \right) - \frac{1}{x_1} \left(\frac{T}{w_{O_2}} \right) \right] \sigma_{ENG_1} w_{O_1}}{(1 + \sigma_{T\&A_1})} \quad (50)$$

$$w_{P_2} = \frac{w_{O_2} - w_{PL} - \left(\frac{T}{w_{O_2}} \right) \sigma_{ENG_2} w_{O_2}}{(1 + \sigma_{T\&A_2})} \quad (51)$$

Substituting Equations (50) and (51) into Equation (43) and solving for $V_I = G(x_1, x_2)$,

$$V_{I_N} = Isp_1 g \ln \frac{x_1 (1 + \sigma_{T\&A_1})}{x_1 \left[\sigma_{T\&A_1} + \sigma_{ENG_1} \left(\frac{T}{w_{O_1}} \right) \right] + \left[1 - \left(\frac{T}{w_{O_2}} \right) \sigma_{ENG_1} \right]} + Isp_2 g \ln \frac{x_2 (1 + \sigma_{T\&A_2})}{x_2 \left[\sigma_{T\&A_2} + \sigma_{ENG_2} \left(\frac{T}{w_{O_2}} \right) \right] + 1} \quad (52)$$

Applying the solution developed for $F(x_1, x_2)$ constrained by $G(x_1, x_2)$.

$$F'(x_1) + \phi G'(x_1) = 0 \quad (53)_1$$

$$F'(x_2) + \phi G'(x_2) = 0 \quad (53)_2$$

$$V_{LN} = G(x_1, x_2) \quad (53)_3$$

where

$$F'(x_i) = \frac{\partial F(x_1, x_2)}{\partial x_i} \quad (53a)$$

$$G'(x_i) = \frac{\partial G(x_1, x_2)}{\partial x_i} \quad (53b)$$

Solving Equation (42) for $F'(x_1)$ and $F'(x_2)$,

$$F'(x_1) = x_2 \quad (54)$$

$$F'(x_2) = x_1 \quad (55)$$

Similarly, solving Equation (52) for $G'(x_1)$ and $G'(x_2)$,

$$G'(x_1) = \frac{Isp_1 g}{x_1 \left\{ x_1 \left[\frac{\sigma_{T \& A_1} + \sigma_{ENG_1} \left(\frac{T}{W_{O_1}} \right)}{1 - \left(\frac{T}{W_{O_2}} \right) \sigma_{ENG_1}} \right] + 1 \right\}} \quad (56)$$

$$G'(x_2) = \frac{Isp_2 g}{x_2 \left\{ x_2 \left[\sigma_{T \& A_2} + \sigma_{ENG_2} \left(\frac{T}{W_{O_2}} \right) \right] + 1 \right\}} \quad (57)$$

Substituting Equations (54) and (56) and Equations (55) and (57) into Equations (23)_{1, 2, 3}, respectively, and solving simultaneously for x_1 .

$$x_1 = \frac{\left[x_2 \left[\sigma_{T\&A_2} + \sigma_{ENG_2} \left(\frac{T}{W_O} \right)_2 \right] + 1 \right] \frac{isp_1}{isp_2} - 1}{\left[\frac{\sigma_{T\&A_1} + \sigma_{ENG_1} \left(\frac{T}{W_O} \right)_1}{1 - \sigma_{ENG_1} \left(\frac{T}{W_O} \right)_2} \right]} \quad (58)$$

To solve a particular problem, one should assume a value for x_2 and solve for x_1 . Then substitute x_1 and x_2 into Equation (52) and determine V_{IN} . If a given V_{IN} is desired then it is necessary to iterate by varying x_2 .

2. Discussion. Since the solution is algebraic and simple in nature, the problem can be easily solved on "desk size" computers or nomographically. By analyzing the solution, it can be shown that the weight saved by parallel staging, as compared to tandem staging, is equal to $\sigma_{ENG_1} (T/W_O)_1$ (which is equivalent to the engine weight saved), if all the vehicle parameters remain constant. This is about 0.5 to 3 percent of the total gross weight. If additional structure is required, the weight saving is even less. Should it be desired to design a multistage (more than two stages) vehicle with the first two stages in parallel and the rest in tandem, the upper stages should be staged for minimum gross weight with respect to the second stage by using the method described in Section 5.3.1. Then the first and second stages should be staged for minimum gross weight with respect to the first stage, using the method described herein.

The results show that parallel staging saves little weight (if any). However, reliability is greatly increased (5 to 20 percent) and there is a substantial cost saving (10 to 20 percent of total vehicle cost). These latter features, which result from reducing the required number of engines, make parallel staging an important design consideration.

If it were desired to design a two-stage parallel staged vehicle for minimum vehicle cost as opposed to minimum gross weight this would be feasible by altering the method discussed in Reference 19. It is felt that the cost saving by staging for minimum vehicle cost, as opposed to minimum gross weight, will be less for parallel staging than that for tandem. For a two-stage vehicle, the saving would be negligible. However, for a multistage parallel-tandem configuration, the saving could be substantial.

3. Summary. A method for staging two-stage parallel staged vehicles for minimum gross weight has been developed. It has been indicated, while the weight

saving can be small, the reliability improvement and cost saving warrant consideration of parallel staging as a design criterion. Designing a two-stage parallel staged vehicle for minimum initial gross weight approximates the solution of designing for minimum vehicle cost. However, for a multistage parallel-tandem staged vehicle, designing for minimum initial gross weight is not equivalent to designing for minimum vehicle cost.

Sample Problem Where Criterion is Cost.¹² Recently, the emphasis on vehicle sizing has been shifted from seeking minimum initial gross to minimum overall system cost. Minimum initial gross weight-to-payload weight ratio is often construed as being the minimum cost vehicle. This, however, is not the case. Vehicles in the past have been extremely sensitive to propellant distribution because of their low performance parameters, and sizing for other criteria has resulted in approximately the same propellant distribution. However, as the attainable propellant specific impulse has improved, so have engines and structures, thus lessening sensitivity to propellant distribution. A need for costing equations is indicated. Hence, the derivation of the equations for minimum systems costs, assuming linear cost and weight relationships, is presented here. The solution found by using these assumptions can be programmed and solved on a desk-size digital computer. A computer is required due to the complexity of the solution and necessity for an iterative procedure.

For the case when the cost and weight relationships are nonlinear and discontinuous, a large digital computer is required to solve for optimal cost. However, the equations for the solutions would differ from those for the sample problem presented here. Use of the large computer also makes possible the simultaneous computation of the trajectory.

1. Propellant Cost. Total propellant cost,

$$K_P = \sum_{i=1}^N \beta_{P_i} W_{P_i} \quad (59)$$

Propellant cost per pound of payload,

$$K_P = \sum_{i=1}^N \beta_{P_i} \left(\frac{W_{P_i}}{W_{O_i}} \right) \frac{W_{O_i}}{W_{PL}} \quad (60)$$

The term $\frac{W_{O_i}}{W_{PL}}$ is

$$\frac{W_{O_i}}{W_{PL}} = \prod_{i=1}^N \frac{W_{O_i}}{W_{O_{i+1}}} \quad (61)$$

5-86

VEHICLE SIZING

where

$$W_{O_{N+1}} = W_{PL} \quad (61a)$$

The propellant weight is

$$W_{P_i} = W_{O_i} - W_{O_{i+1}} - W_{ST_i} \quad (62)$$

The structural weight is

$$W_{ST_i} = W_{ENG_i} + W_{TS_i} + W_{INT_i} + W_{TK_i} + W_{ACC_i} \quad (63)$$

where

$$W_{ENG_i} \equiv \sigma_{ENG_i} T_i \quad (63a)$$

$$W_{TS_i} \equiv \sigma_{TS_i} W_{O_i} \quad (63b)$$

$$W_{INT_i} \equiv \sigma_{INT_i} W_{O_i} \quad (63c)$$

$$W_{TK_i} \equiv \sigma_{TK_i} W_{P_i} \quad (63d)$$

Substituting Equation (63) into Equation (62), the expression for (W_P/W_O) equals

$$\left(\frac{W_P}{W_O}\right)_i = \left(\frac{1}{1 + \sigma_{TK_i}}\right) \left(1 - \sigma_{j_i} - \frac{1}{x_i}\right) \quad (64)$$

where

$$\sigma_{j_i} \equiv \sigma_{ENG_i} \left(\frac{T}{W_O}\right)_i + \sigma_{TS_i} + \sigma_{INT_i} + \left(\frac{W_{ACC}}{W_O}\right)_i \quad (64a)$$

$$x_i = \frac{W_{O_i}}{W_{O_{i+1}}} \quad (64b)$$

Substituting Equations (61) and (64) into Equation (60), the propellant cost per pound of payload equals

$$K_P = \sum_{i=1}^N \left[\frac{\beta_{P_i}}{(1 + \sigma_{TK_i})} \left(1 - \sigma_{j_i} - \frac{1}{x_i}\right) \prod_{k=i}^N x_k \right] \quad (65)$$

2. Engine Cost. Total engine cost,

$$\kappa_{ENG} = \sum_{i=1}^N \beta_{ENG_i} T_i \quad (66)$$

Engine cost per pound of payload,

$$\kappa_{ENG} = \sum_{i=1}^N \beta_{ENG_i} \left(\frac{T}{W_O} \right)_i \frac{W_{O_i}}{W_{PL}} \quad (67)$$

By substituting Equation (57),

$$\kappa_{ENG} = \sum_{i=1}^N \left[\beta_{ENG_i} \left(\frac{T}{W_O} \right)_i \prod_{k=i}^N x_k \right] \quad (68)$$

3. Thrust Structure Cost. Total thrust structure cost,

(69)

$$\kappa_{TS} = \sum_{i=1}^N \beta_{TS_i} W_{TS_i} \quad (32)$$

Thrust structure cost per pound of payload,

$$\kappa_{TS} = \sum_{i=1}^N \beta_{TS_i} \left(\frac{W_{TS}}{W_O} \right)_i \frac{W_{O_i}}{W_{PL}} \quad (70)$$

By substituting Equations (61) and (63b),

$$\kappa_{TS} = \sum_{i=1}^N \left(\beta_{TS_i} \sigma_{TS_i} \prod_{k=i}^N x_k \right) \quad (71)$$

4. Interstage Structure Cost. Total interstage structure cost,

$$\kappa_{INT} = \sum_{i=1}^N \beta_{INT_i} W_{INT_i} \quad (72)$$

Interstage structure cost per pound of payload,

$$\kappa_{INT} = \sum_{i=1}^N \beta_{INT_i} \left(\frac{W_{INT}}{W_O} \right)_i \frac{W_{O_i}}{W_{PL}} \quad (73)$$

By substituting Equations (61) and (63c),

$$K_{INT} = \sum_{i=1}^N \left(\beta_{INT_i} \sigma_{INT_i} \prod_{k=i}^N x_k \right) \quad (74)$$

5. Tank Structure Cost. Total tank structure cost,

$$K_{TK} = \sum_{i=1}^N \beta_{TK_i} w_{TK_i} \quad (75)$$

Tank structure cost per pound of payload,

$$K_{TK} = \sum_{i=1}^N \beta_{TK_i} \sigma_{TK_i} \left(\frac{w_P}{w_{O_i}} \right) \frac{w_{O_i}}{w_{PL}} \quad (76)$$

By substituting Equations (61) and (63d),

$$K_{TK} = \sum_{i=1}^N \left[\frac{\beta_{TK_i} \sigma_{TK_i}}{(1 + \sigma_{TK_i})} \left(1 - \sigma_{j_i} - \frac{1}{x_i} \right) \prod_{k=i}^N x_k \right] \quad (77)$$

6. Accessory Cost. Total accessory cost,

$$K_{ACC} = \sum_{i=1}^N K_{ACC_i} \quad (78)$$

Accessory cost per pound of payload,

$$K_{ACC} = \frac{\sum_{i=1}^N K_{ACC_i}}{w_{PL}} \quad (79)$$

7. Total Fixed Nonvehicle Costs. Total fixed nonvehicle cost equals K_{NV} .

General Optimum Sizing

5-89

Fixed nonvehicle costs per pound of payload,

$$K_{NV} = \frac{K_{NV}}{W_{PL}} \quad (80)$$

8. Total Cost. Total cost equals the sum of all the vehicle costs and the non-vehicle costs. Cost per pound of payload,

$$K_N = K_P + K_{TS} + K_{INT} + K_{TK} + K_{ACC} + K_{NV} \quad (81)$$

a. Optimization of Vehicle Sizing for Minimum Cost. Given a set of vehicle parameters and cost parameters from the previously developed equations, the total cost can be represented as

$$K_N = F(x_1, x_2, x_3, \dots, x_{i=N}) \quad (82)$$

It is desired to minimize the total cost per pound of payload, K_N .

Associated with the particular mission is an ideal impulsive velocity, V_{I_N} , which can be represented as

$$V_{I_N} = G(x_1, x_2, x_3, \dots, x_{i=N}) \quad (83)$$

From the solution developed early in this section, the equations for the optimum are

$$F'(x_1) + \phi G'(x_1) = 0 \quad (83)_1$$

$$F'(x_2) + \phi G'(x_2) = 0 \quad (84)_2$$

$$F'(x_3) + \phi G'(x_3) = 0 \quad (85)_3$$

$$F'(x_{i=N}) + \phi G'(x_{i=N}) = 0 \quad (85)_{i=N}$$

$$V_{I_N} = G(x_1, x_2, x_3, \dots, x_i) - \text{const.} \quad (85)_{N+1}$$

The equation for K_N , by substituting Equations (65), (67), (71), (79), and (80) into Equation (81), is

$$K_N = \left(\frac{K_{NV} + K_{ACC}}{W_{O_1}} \right) \prod_{i=1}^N x_i + \sum_{i=1}^N \left(A_i + \frac{B_i}{x_i} \right) \prod_{k=i}^N x_k \quad (86)$$

where

$$A_i = \left(\frac{\beta_{P_i} + \beta_{TK_i} \sigma_{TK_i}}{1 + \sigma_{TK_i}} \right) (1 - \sigma_{j_i}) + \beta_{ENG_i} \left(\frac{T}{W_{O_i}} \right) + (\beta_{TS_i} \sigma_{TS_i}) + (\beta_{INT_i} \sigma_{INT_i}) \quad (86a)$$

$$B_i = - \left(\frac{\beta_{P_i} + \beta_{TK_i} \sigma_{TK_i}}{1 + \sigma_{TK_i}} \right) \quad (86b)$$

This solution assumes the total vehicle gross weight to remain constant. Another similar solution can be derived assuming the payload weight to remain constant.

The total ideal velocity equation constraining the solution is

$$V_{I_N} = \sum_{i=1}^N Isp_i g \ln \frac{i}{1 - \left(\frac{W_P}{W_{O_i}} \right)} \quad (87)$$

Substituting Equation (27),

$$V_{I_N} = \sum_{i=1}^N Isp_i g \ln \frac{x_i^{(1 + \sigma_{TK_i})}}{x_i^{(\sigma_{TK_i} + \sigma_{j_i})} + 1} \quad (88)$$

where as before,

$$\sigma_{j_i} \equiv \sigma_{ENG_i} \left(\frac{T}{W_{O_i}} \right) + \sigma_{TS_i} + \sigma_{INT_i} + \left(\frac{W_{ACC}}{W_{O_i}} \right) \quad (88a)$$

Solving Equation (45) for $F'(x_1)$, $F'(x_2)$, ... $F'(x_n)$... $F'(x_{i=N})$,

$$F'(x_1) = \left(\frac{K_{NV} + K_{ACC}}{w_{O_1}} \right) \frac{1}{x_1} \prod_{i=1}^N x_i + \frac{A_1}{x_1} \prod_{k=1}^N x_k \quad (89)_1$$

$$F'(x_2) = \left(\frac{K_{NV} + K_{ACC}}{w_{O_1}} \right) \frac{1}{x_2} \prod_{i=1}^N x_i + \frac{A_1}{x_2} \prod_{k=1}^N x_k + \frac{B_1}{x_1 x_2} \prod_{k=1}^N x_k + \frac{A_2}{x_2} \prod_{k=2}^N x_k \quad (89)_2$$

$$F'(x_n) = \left(\frac{K_{NV} + K_{ACC}}{w_{O_1}} \right) \frac{1}{x_n} \prod_{i=1}^N x_i + \frac{1}{x_n} \left(\sum_{i=1}^n A_i \prod_{k=i}^N x_k + \sum_{i=1}^{n-1} \frac{B_i}{x_i} \prod_{k=i}^N x_k \right), \quad (n \neq 1) \quad (89)_n$$

$$F'(x_N) = \left(\frac{K_{NV} + K_{ACC}}{w_{O_1}} \right) \frac{1}{x_N} \prod_{i=1}^N x_i + \frac{1}{x_N} \left(\sum_{i=1}^N A_i \prod_{k=i}^N x_k + \sum_{i=1}^{N-1} \frac{B_i}{x_i} \prod_{k=i}^N x_k \right) \quad (89)_N$$

Solving Equation (53) for $G'(x_i)$,

$$G'(x_i) = \frac{Isp_i g}{x_i \left[x_i (\sigma_{TK_i} + \sigma_{j_i}) + 1 \right]} \quad (90)_i$$

Substituting Equations (54)₁ and (55)₁ into Equation (50)₁, Equations (54)₂ and (55)₂ into Equation (50)₂, and solving simultaneously for x_2 ,

$$x_2 = \frac{1}{(\sigma_{TK_2} + \sigma_{j_2})} \left\{ \frac{\left(\frac{K_{NV} + K_{ACC}}{w_{O_1}} + A_1 \right) x_1 \left[x_1 (\sigma_{TK_1} + \sigma_{j_1}) + 1 \right]^{\frac{Isp_2}{Isp_1}}}{\left(\frac{K_{NV} + K_{ACC}}{w_{O_1}} + A_1 \right) x_1 + A_2 + B_1} - 1 \right\} \quad (91)_1$$

Similarly solving for x_3 ,

$$x_3 = \frac{1}{(\sigma_{TK_3} + \sigma_{j_3})} \left\{ \frac{\left[\left(\frac{K_{NV} + K_{ACC}}{w_{O_1}} + A_1 \right) x_1 + A_2 + B_1 \right] x_2 \left[x_2 (\sigma_{TK_2} + \sigma_{j_2}) + 1 \right]^{\frac{Isp_3}{Isp_2}}}{\left[\left(\frac{K_{NV} + K_{ACC}}{w_{O_1}} + A_1 \right) x_1 x_2 + A_2 x_2 + A_3 + B_1 x_2 + B_2 \right]} - 1 \right\} \quad (91)_2$$

$$x_n = \frac{1}{(\sigma_{TK_n} + \sigma_{J_n})} \left\{ \frac{\left[\left(\frac{K_{NV} + K_{ACC}}{W_{O_1}} \right) \prod_{i=1}^{n-2} x_k + \frac{1}{x_{n-1}} \left(\sum_{i=1}^{n-1} A_i \prod_{k=i}^n x_k + \sum_{i=1}^{n-2} \frac{B_i}{x_i} \prod_{k=i+1}^n x_k \right) \right] (x_{n-1})^{(\sigma_{TK_{n-1}} + \sigma_{J_{n-1}} + 1)} \frac{Isp_n}{Isp_{n-1}}}{\left[\left(\frac{K_{NV} + K_{ACC}}{W_{O_1}} \right) \prod_{i=1}^{n-1} x_k + \frac{1}{x_n} \sum_{i=1}^n A_i \prod_{k=i}^n x_k + \sum_{i=1}^{n-1} \frac{B_i}{x_i} \prod_{k=i+1}^n x_k \right]} - 1 \right\} \quad (n > 2) \quad (92)_n$$

From Equations (91), it is evident that, for the criterion of minimum cost, a stage's design is affected only by itself and the stages below it. Therefore, in order to solve the problem, a value of x_1 needs to be assumed; the x_2 corresponding to minimum cost can then be determined. Knowing x_1 and x_2 , x_3 can be determined. Similarly the other x_i 's can be found. Substituting the determined x_i values into Equation (53), the constraint can be tested. Then x_1 is iterated upon until this constraint is fulfilled. Having determined the optimum distribution, the actual cost, and the cost per pound of payload of each item considered, and the aggregate costs can be found.

2. Discussion. The solution for parallel staging, like the solution for minimum system costs, is algebraic and not complex. Sizing for minimum system cost tends to decrease the size of upper stages compared to sizes obtained when sizing for minimum initial gross weight. As nonvehicle and accessory costs increase with respect to vehicle cost, the solution shifts towards the solution for the minimum initial gross weight; sizing for optimum system cost also indicates the optimal number of stages.

The particular weight and cost relationships assumed are subjected to conjecture. However, those assumed serve to illustrate the method of solution. Other more appropriate relationships can be substituted into the solution indicated by merely substituting the desired relationships for the constants, A_i and B_i . The inclusion of higher order and discontinuous relationships complicates the solution such that only large digital computers can be used. When this is the case, there are other more appropriate solutions.

Not included were nonvehicle costs that are vehicle dependent. Such factors as reliability, maintenance, and transportation can be included if desired.

3. Summary. The use of the general equations for optimally sizing a vehicle where system cost is the criterion for the optimization has been illustrated. The solution developed is readily solvable on desk-size computers. The results are applicable to preliminary design studies as an engineering aid.

Nomenclature

5-93

NOMENCLATURE

A	}	Coefficients for structure factor curve fit
B		
C		
g		Acceleration of gravity
I_{sp}		Vacuum specific impulse
i		Integer corresponding to a particular stage
K_{ACC}		Total vehicle accessory cost per pound of payload
K_N		Total system cost per pound of payload
K_{NV}		Total nonvehicle cost per pound of payload
k		Integer corresponding to a particular stage
N		Integer corresponding to the total number of stages
n		Integer corresponding to a particular stage
r		$\frac{W_C}{W_{BO}}$ = stage mass ratio
T		Thrust
V_{BO_I}		Inertial burnout velocity
$\frac{V_I}{gI_{sp}}$		Ideal velocity ratio
V_{I_N}		Total ideal velocity for all N stages
V_{rot}		Rotational velocity component of the earth
W_{ACC}		Accessory weight
W_{BO}		Burnout weight
W_{ENG}		Engine weight
W_{INT}		Interstage weight
W_O		Gross weight
$\frac{W_O}{W_{PL}}$		Gross weight-to-payload weight ratio

VEHICLE SIZING

W_P	Propellant weight
W_{PL}	Payload weight
W_{ST}	Structural weight
W_{TK}	Tank weight
$W_{T\&A}$	Tank and accessory weight
W_{TS}	Thrust structure weight
X_N	Total vehicle gross weight-to-payload weight ratio
x	Stage gross weight-to-stage payload weight ratio
α	Exponent for structure factor curve fit
β_{ENG}	Engine cost per pound of thrust
β_{INT}	Interstage cost per pound
β_P	Propellant cost per pound
β_{TK}	Tank cost per pound
β_{TS}	Thrust structure cost per pound
ΔV_L	Total velocity losses
σ	Structure factor - structure weight-to-stage weight ratio
σ_{ENG}	Engine weight per pound of thrust
σ_{INT}	Interstage weight-to-stage gross weight ratio
σ_{TK}	Tank weight-to-stage gross weight ratio
$\sigma_{T\&A}$	Tank and accessory weight-to-stage gross weight ratio
σ_{TS}	Thrust structure weight-to-stage gross weight ratio
κ_{ACC}	Total vehicle accessory cost per pound of payload
κ_{ENG}	Total vehicle engine cost per pound of payload
κ_{INT}	Total vehicle interstage cost per pound of payload
κ_N	Total system cost per pound of payload

References

5-95

κ_{NV}	Total nonvehicle cost per pound of payload
κ_P	Total vehicle propellant cost per pound of payload
κ_{TK}	Total vehicle thrust structure cost per pound of payload
ϕ	Lagrangian multiplier

REFERENCES

1. Björn Bergqvist, "The Optimization Problem for Rocket Vehicles Subjected to Medium and High Accelerations: A Literature Survey" Astronautik 1 (1959).
2. M. Goldsmith, "On the Optimization of Two-Stage Rockets," Jet Propulsion, Vol. 27, 1957.
3. L. Weisbord, "A Generalized Optimization Procedure of N-Staged Missiles," Jet Propulsion, March 1958.
4. M. Vertregt, "A Method for Calculating the Mass Ratios of Step Rockets," Journal of the British Interplanetary Society, vol. 15, 1956.
5. F. J. Malina and M. Summerfield, "The Problem of Escape from the Earth by Rockets," Journal of Aeronautical Sciences, vol. 14, August 1947.
6. E. E. H. Schurmann, "Optimum Staging Technique for Multi-Staged Rocket Vehicles," Jet Propulsion, vol. 27, 1957.
7. M. Subotowricz, "The Optimization of the N-Step Rocket with Different Construction Parameters and Propellant Specific Impulses in Each Stage," Jet Propulsion, vol. 28, July 1958.
8. H. H. Hall and E. D. Zambelle, "On the Optimization of Multistage Rockets," Jet Propulsion, vol. 28, July 1958.
9. C. H. Builder, "General Solution for Optimization of Staging of Multistage Boost Vehicles," American Rocket Society Journal, July 1959.
10. J. J. Coleman, "Optimum Stage-Weight Distribution of Multistage Rockets," American Rocket Society Journal, February 1961.
11. J. J. Coleman, "Optimization of Stage Weight for Linear Structural Weight Dependence on Propellant Weight," Space Technology Laboratories Document Number SDA 60-4, 25 February 1960.

12. G. C. Goldbaum and J. F. White, "Effects of Vehicle Cost on Design and Sizing of Multi-Stage Rockets," Missiles and Space Systems Department Douglas Aircraft Company, Inc., Santa Monica, California, Engineering Paper No. 801, 1 August 1959; presented at the Fourth Symposium on Ballistic Missiles and Space Technology, University of California at Los Angeles, California.
13. R. L. Chase, "Multistage Rocket Staging Optimization," presented at the American Astronautical Society 6th National Annual Meeting, 18-21 January 1960, New York City, New York, Preprint No. 60-41.
14. C. J. Wang, G. W. Anthony and H. R. Lawrence, "Thrust Optimization of a Nuclear Rocket of Variable Specific Impulse," American Rocket Society Journal, May 1959.
15. A. Schnitt, "Cost Optimization of Large Booster Systems," Space Technology Laboratories, STL-TN-59-0000-00333, 13 November 1959.
16. H. H. Koelle,* "On the Optimum Size of Orbital Carrier Vehicles Based on Overall Economy," submitted for presentation to the 11th International Astronautical Congress of the International Astronautical Federation, Stockholm, Sweden, 15-30 August 1960.
17. J. T. Wintler, "An Approximate Method to Determine the Optimum Weight Distribution of a Multistage Rocket Vehicle," Space Technology Laboratories, Inc. Document No. 7720.4-100, 3 June 1960.
18. I. S. and F. S. Sokolnikoff, Higher Mathematics for Engineers and Physicists, McGraw Hill Book Co., Inc., 1949, pp. 163-167.
19. J. F. White, "Method for Staging Parallel Boosters for Minimum Gross Weight," Space Technology Laboratories, TM-59-0000-00399, 16 September 1959.

* National Aeronautics and Space Administration. George C. Marshall, Space Flight Center, Huntsville, Alabama.

CHAPTER 6

LUNAR/PLANETARY DEBOOST AND LUNAR LANDING

This chapter presents a simple analysis of the phase of powered flight during deboost in the vicinity of the moon or planet. Data have been included for deboost only in the vicinity of Earth, Moon, Venus, and Mars, but the analysis is applicable to other planets.

Descent from interplanetary and earth-lunar trajectories or planetary and lunar orbits may be analyzed in two phases. For interplanetary deboost these phases are: 1) transfer from initial trajectory to the edge of the planet's sensible atmosphere, and 2) atmospheric entry. For orbital deboost the phases are: 1) transfer from initial lunar trajectory to a new trajectory from which the terminal deboost maneuver is performed, and 2) the terminal deboost phase. For some missions it may be found that the first phase of both interplanetary and orbital deboost is eliminated.

To facilitate computations of the first phase, impulsive burning is assumed. The equations for this phase are presented so that the engineer can readily adapt them to his particular study. No attempt has been made to present the equations in parametric form for the range of parameters and number of planets to be considered since this would constitute a sizable study effort.

The exchange ratio and the vehicle sizing analyses for the first phase, presented in Chapters 4 and 5 respectively, are applicable to analyzing the deboost vehicle.

The planetary second phase is covered in detail in Chapter 7, assuming a ballistic entry. A cursory analysis of the lunar second phase for a vertical descending terminal deboost maneuver is presented in this chapter.

6.1 LUNAR/PLANETARY DEBOOST

Deboost may be desired from a circular or elliptical orbit about the planet under consideration, or from a hyperbolic trajectory followed by a vehicle approaching from another planet. By use of a single velocity impulse applied to the vehicle, a new orbit, usually but not necessarily an ellipse, is achieved to bring the vehicle to atmospheric entry or to the point of initiation of terminal deboost in the case of the moon. The end point of the vacuum deboost trajectory in the vicinity of a planet is an arbitrary altitude defining the beginning of the sensible atmosphere. The initial orbit and deboost orbit are assumed to be coplanar, the motion in each described by Kepler's laws. This is illustrated in Figure 1.

6-2

LUNAR/PLANETARY DEBOOST AND LUNAR LANDING

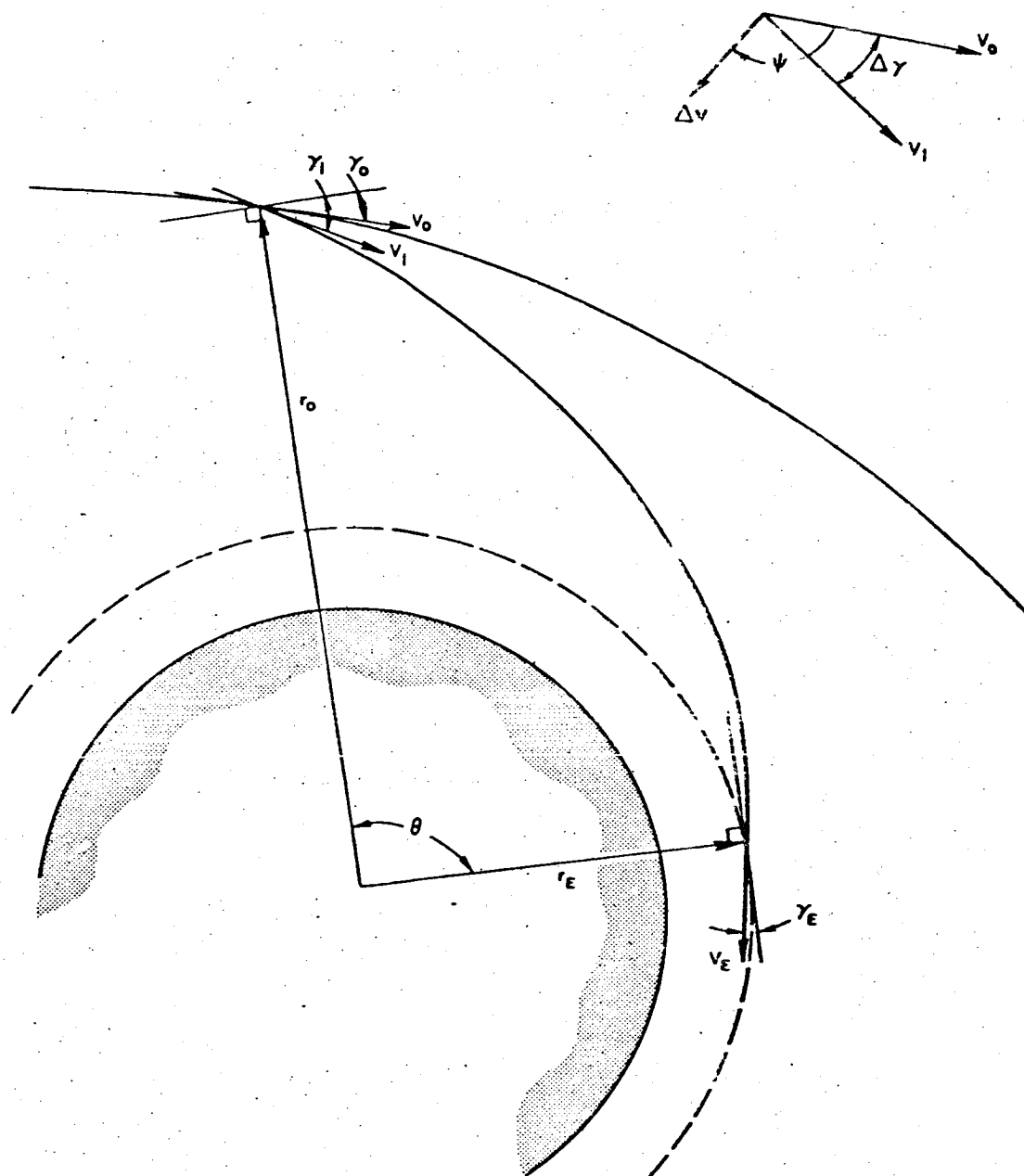


Figure 1. Lunar/Interplanetary Deboost Coordinate System

Two approaches are possible in a deboost problem. In each it is assumed that the velocity, altitude, and flight path angle of the initial orbit are known at the time retro impulse is applied. For the first approach, the velocity impulse, ΔV , and thrust angle, ψ , may be specified. Simple, closed form solutions are available for the velocity and flight path angle at atmospheric entry or initiation of terminal deboost near the moon. If the entry velocity and entry angle are specified, however, an iterative method is required to obtain velocity impulse and thrust angle. References 1, 2, and 3 provide additional material for lunar/planetary deboost.

6.2 EQUATIONS FOR IMPULSIVE VACUUM DEBOOST

Presented here are the equations required for the closed form solution of entry velocity, entry angle, planet range angle, and time of flight. Equations are also presented for the errors in entry velocity, entry angle, and range angle due to thrust misalignment or an error in magnitude of velocity impulse. The iterative method is discussed, as is the method of determining thrust angle to minimize velocity impulse required.

6.2.1 Equations for Specified Deboost Conditions

The following equations, in nondimensional form, indicate the method of solution for entry velocity, V_E , entry angle, γ_E , range angle, θ , time of flight, Δt , and the error equations, assuming ΔV and ψ are known. It is assumed that ΔV is less than V_o .

$$\left(\frac{V_1}{V_o}\right)^2 = \left[1 + \left(\frac{\Delta V}{V_o}\right)^2 + 2\left(\frac{\Delta V}{V_o}\right)\cos\psi\right] \quad (1)$$

$$\left(\frac{V_E}{V_o}\right)^2 = \frac{2\mu_p}{V_o^2} \left(\frac{1}{r_E} - \frac{1}{r_o}\right) + \left(\frac{V_1}{V_o}\right)^2 \quad (2)$$

$$\gamma_1 = \gamma_o + \Delta\gamma = \gamma_o + \tan^{-1} \frac{\frac{\Delta V}{V_o} \sin\psi}{1 + \frac{\Delta V}{V_o} \cos\psi} \quad (3)$$

$$\left(-\frac{\pi}{2} \leq \Delta\gamma \leq \frac{\pi}{2}\right)$$

$$\gamma_E = \cos^{-1} \left[\left(\frac{v_1}{v_o} \right) \left(\frac{v_o}{v_E} \right) \left(\frac{r_o}{r_E} \right) \cos \gamma_1 \right]$$

$$= \cos^{-1} \left[\left(\frac{v_1}{v_o} \right) \left(\frac{v_o}{v_E} \right) \left(\frac{r_o}{r_E} \right) (\cos \gamma_o \cos \Delta \gamma - \sin \gamma_o \sin \Delta \gamma) \right] \quad (4)$$

$$\frac{\partial v_E}{\partial (\Delta V)} = \left(\frac{v_o}{v_E} \right) \left(\frac{\Delta V}{v_o} + \cos \psi \right) \quad (5)$$

$$\frac{\partial v_E}{\partial \psi} = - \left(\frac{v_o}{v_E} \right) \left(\frac{\Delta V}{v_o} \right) v_o \sin \psi \quad (6)$$

$$\frac{\partial \gamma_E}{\partial (\Delta V)} = - \csc \gamma_E \left(\frac{r_o}{r_E} \right) \left\{ \frac{\cos \gamma_o \cos \psi - \sin \gamma_o \sin \psi}{v_o \left(\frac{v_E}{v_o} \right)} \right.$$

$$\left. \frac{\left[\left(1 + \frac{\Delta V}{v_o} \cos \psi \right) (\cos \gamma_o) - \frac{\Delta V}{v_o} \sin \psi \sin \gamma_o \right] \left(\frac{\Delta V}{v_o} + \cos \psi \right)}{v_o \left(\frac{v_E}{v_o} \right)^3} \right\} \quad (7)$$

$$\frac{\partial \gamma_E}{\partial \psi} = - \csc \gamma_E \left(\frac{r_o}{r_E} \right) \left\{ \frac{\frac{\Delta V}{v_o} (\sin \psi \cos \gamma_o + \cos \psi \sin \gamma_o)}{\frac{v_E}{v_o}} \right.$$

$$\left. \frac{\left[\left(1 + \frac{\Delta V}{v_o} \cos \psi \right) \cos \gamma_o - \frac{\Delta V}{v_o} \sin \psi \sin \gamma_o \right] \frac{\Delta V}{v_o} \sin \psi}{\left(\frac{v_E}{v_o} \right)^3} \right\} \quad (8)$$

The computation of various elements of the deboost orbit (\bar{h} , a , e , v , E) is not actually necessary. However, the relative simplicity of the equations for planet range angle, θ , time of flight, $t_{1 \rightarrow E}$, and their derivatives makes it advantageous to compute these elements to aid in understanding the later equations or finding errors in calculations.

$$\bar{h} = \left(\frac{v_1}{v_o} \right) v_o r_o \cos \gamma_1 \quad (9)$$

Equations for Impulsive Vacuum Deboost

6-5

$$a = \left[\frac{2}{r_o} - \left(\frac{v_1}{v_o} \right)^2 \frac{v_o^2}{\mu_p} \right]^{-1} \quad (10)$$

$$e = \left(1 - \frac{\bar{h}^2}{\mu_p a} \right)^{1/2} \quad (11)$$

$$v_1 = \cos^{-1} \left(\frac{\frac{\bar{h}^2}{\mu_p} - r_o}{er_o} \right) \quad (12)$$

$$v_E = \cos^{-1} \left(\frac{\frac{\bar{h}^2}{\mu_p} - r_E}{er_E} \right) \quad (13)$$

$$\theta = v_1 - v_E \quad (14)$$

$$E_1 = \cos^{-1} \left[\frac{1}{e} \left(1 - \frac{r_o}{a} \right) \right] \quad (e \leq 1) \quad (15)$$

$$E_1' = iE_1 = \cosh^{-1} \left[\frac{1}{e} \left(1 + \frac{r_o}{a} \right) \right] \quad (e > 1) \quad (15')$$

$$E_E = \cos^{-1} \left[\frac{1}{e} \left(1 - \frac{r_E}{a} \right) \right] \quad (e \leq 1) \quad (16)$$

$$E_E' = iE_E = \cosh^{-1} \left[\frac{1}{e} \left(1 + \frac{r_E}{a} \right) \right] \quad (e > 1) \quad (16')$$

$$t_1 = \sqrt{\frac{a^3}{\mu_p}} (E_1 - e \sin E_1) \quad (e \leq 1) \quad (17)$$

$$t_1' = \sqrt{\frac{a^3}{\mu_p}} (e \sinh E_1' - E_1') \quad (e > 1) \quad (17')$$

$$t_E = \sqrt{\frac{a^3}{\mu_p}} (E_E - e \sin E_E) \quad (e \leq 1) \quad (18)$$

$$t_E' = \sqrt{\frac{a^3}{\mu_p}} (e \sinh E_E' - E_E') \quad (e > 1) \quad (18')$$

If the deboost trajectory is a hyperbola, the semimajor axis, a , will be negative and the eccentricity, e , greater than one. This will cause no trouble until calculation of the time of flight. For this calculation, Equations (15') through (18') are substituted for Equations (15) through (18).

$$t_{1 \rightarrow E} = t_1 - t_E \quad (19)$$

$$\frac{\partial \gamma_1}{\partial \psi} = \frac{\frac{\Delta V}{V_o} \left(\frac{\Delta V}{V_o} + \cos \psi \right)}{\left(\frac{V_1}{V_o} \right)^2} \quad (20)$$

$$\frac{\partial \gamma_1}{\partial (\Delta V)} = \frac{\sin \psi}{V_o \left(\frac{V_1}{V_o} \right)^2} \quad (21)$$

$$\frac{\partial \bar{h}}{\partial \psi} = -V_o r_o \left[\left(\frac{V_1}{V_o} \right) \sin \gamma_1 \frac{\partial \gamma_1}{\partial \psi} + \frac{\left(\frac{\Delta V}{V_o} \right) \sin \psi \cos \gamma_1}{\left(\frac{V_1}{V_o} \right)} \right] \quad (22)$$

$$\frac{\partial \bar{h}}{\partial (\Delta V)} = V_o r_o \left[\frac{\left(\frac{\Delta V}{V_o} + \cos \psi \right) \cos \gamma_1}{V_o \left(\frac{V_1}{V_o} \right)} - \left(\frac{V_1}{V_o} \right) \sin \gamma_1 \frac{\partial \gamma_1}{\partial (\Delta V)} \right] \quad (23)$$

$$\frac{\partial \theta}{\partial \psi} = \frac{\bar{h} \cos^2 \gamma_1}{\mu_p} \left[\frac{\left(\frac{\bar{h}^2}{\mu_p} - r_o \right) \left(2 \tan \gamma_1 \frac{\partial \bar{h}}{\partial \psi} + \bar{h} \sec^2 \gamma_1 \frac{\partial \gamma_1}{\partial \psi} \right) - 2 \frac{\bar{h}^2}{\mu_p} \tan \gamma_1 \frac{\partial \bar{h}}{\partial \psi}}{\left(\frac{\bar{h}^2}{\mu_p} - r_o \right)^2} \right]$$

$$- \frac{\bar{h} \cos^2 \gamma_E}{\mu_p} \left[\frac{\left(\frac{\bar{h}^2}{\mu_p} - r_E \right) \left(2 \tan \gamma_E \frac{\partial \bar{h}}{\partial \psi} + \bar{h} \sec^2 \gamma_E \frac{\partial \gamma_E}{\partial \psi} \right) - 2 \frac{\bar{h}^2}{\mu_p} \tan \gamma_E \frac{\partial \bar{h}}{\partial \psi}}{\left(\frac{\bar{h}^2}{\mu_p} - r_E \right)^2} \right] \quad (24)$$

$$\frac{\partial \theta}{\partial (\Delta V)} = \frac{\bar{h} \cos^2 \gamma_1}{\mu_p} \left[\frac{\left(\frac{\bar{h}^2}{\mu_p} - r_o \right) \left(2 \tan \gamma_1 \frac{\partial \bar{h}}{\partial (\Delta V)} + \bar{h} \sec^2 \gamma_1 \frac{\partial \gamma_1}{\partial (\Delta V)} \right) - 2 \frac{\bar{h}^2}{\mu_p} \tan \gamma_1 \frac{\partial \bar{h}}{\partial (\Delta V)}}{\left(\frac{\bar{h}^2}{\mu_p} - r_o \right)^2} \right] - \frac{\bar{h} \cos^2 \gamma_E}{\mu_p} \left[\frac{\left(\frac{\bar{h}^2}{\mu_p} - r_E \right) \left(2 \tan \gamma_E \frac{\partial \bar{h}}{\partial (\Delta V)} + \bar{h} \sec^2 \gamma_E \frac{\partial \gamma_E}{\partial (\Delta V)} \right) - 2 \frac{\bar{h}^2}{\mu_p} \tan \gamma_E \frac{\partial \bar{h}}{\partial (\Delta V)}}{\left(\frac{\bar{h}^2}{\mu_p} - r_E \right)^2} \right] \quad (25)$$

Use of a value of ΔV or ψ which gives an ellipse with a perigee higher than r_E will manifest itself in Equation (4), yielding a cosine larger than one.

The initial trajectory may be such that the vehicle is on an impact course with the planet, but will enter the atmosphere at too high a velocity or entry angle. The above equations can be applied in this case by using values of ψ greater than 180 degrees to slow the vehicle and/or flatten the entry.

If for some reason a value of ψ greater than 180 degrees is used, care should be taken in computing θ . The true anomaly after velocity impulse application, v_1 , may be greater than 180 degrees. This would not be apparent in computing the cosine of this angle. An additional equation,

$$v_1 = \sin^{-1} \left(\frac{\bar{h}^2}{e r_o \mu_p} \tan \gamma_1 \right) \quad (26)$$

will indicate the quadrant in which v_1 lies.

6.2.2 Equations for Specified Entry Conditions

Assuming now that entry velocity and entry angle are specified, the above equations can still be used. Equations (1) and (2) can be solved simultaneously for arbitrary values of ψ to find ΔV , or vice versa. Equations (3) and (4) are then solved to find γ_E . The value found is compared with the desired value of γ_E and a new estimate of ψ or ΔV is made. The partial derivatives, $\partial \gamma_E / \partial \psi$ and $\partial \gamma_E / \partial (\Delta V)$, can be used to estimate the new value of ψ or ΔV .

If only the entry angle is constrained, so that entry velocity is not of primary importance, a value of ψ can be found for which ΔV is a minimum. Since, if only entry angle is specified, there are an infinite number of ellipses which will give this angle, a ΔV exists for each value of ψ . Simultaneous solution of Equations (4) and (27) will provide an optimum value of ψ .

$$\frac{\Delta V}{V_o} = \frac{-[\cos \psi \sin(\psi + \gamma_o) + \sin \gamma_o] \pm \sqrt{S}}{2 \sin(\psi + \gamma_o)} \quad (27)$$

$$S = \sin^2 \psi [\cos(\psi - \gamma_o) \cos(\psi + \gamma_o)] - \cos \gamma_o \sin \gamma_o \cos \psi \sin \psi (1 + 2 \sin^2 \psi)$$

$$-4 \sin^2(\psi + \gamma_o) \left[\frac{2\mu_p}{V_o^2} \left(\frac{1}{r_E} - \frac{1}{r_o} \right) \right]$$

This equation is best solved by selecting a value of ψ (at or near 180 degrees as a first estimate) and solving for $\Delta V/V_o$ and γ_E . The derivative, $\partial \gamma_E / \partial \psi$, can then be employed to get a second estimate of ψ , assuming a linear relationship in the neighborhood of the initial point.

$$\Delta \psi = \frac{\gamma_{E \text{ desired}} - \gamma_{E \text{ computed}}}{\frac{\partial \gamma_E}{\partial \psi}} \quad (28)$$

Succeeding iterations are made in the same manner. For small changes in γ and ψ , it will probably not be necessary to recompute the derivative for each iteration.

If the entry velocity is constrained but no restrictions are placed on entry angle, the optimum ψ for minimum ΔV is 180 degrees, and ΔV can be found from the following equation:

$$\frac{\Delta V}{V_o} = 1 - \left[\left(\frac{V_E}{V_o} \right)^2 - \frac{2\mu_p}{V_o^2} \left(\frac{1}{r_E} - \frac{1}{r_o} \right) \right]^{1/2} \quad (29)$$

Equation (29) shows that for a given V_o the velocity impulse required, ΔV , is lower for small values of r_o . However, in most cases V_o will also be higher at points nearer the planet, so this possibility should be investigated for the particular problem to determine the optimum point at which the velocity increment should be added.

6.2.3 Planetary Data for Deboost Equations

Values for μ_p and suggested values for r_E for each planet are shown in Table 1. The radius of Venus given is not that of the planet itself but of its atmospheric cloud "shell." This value is known much more accurately than the radius of the body and the altitude of sensible atmosphere is given with respect to this cloud layer.

Velocity Requirements for a Vertical Descent Lunar Landing

6-9

Table 1. Planetary Constants

Body	Earth	Moon	Venus	Mars
Radius (ft)	2.09029×10^7	0.5702×10^7	2.001×10^7	1.120×10^7
μ_p (ft ³ /sec ²)	1.40766×10^{16}	0.01727×10^{16}	1.145×10^{16}	0.1515×10^{16}
Altitude of sensible atmosphere (ft)	300,000	0	250,000	500,000
r_E (ft)	2.12029×10^7	0.5702×10^7	2.026×10^7	1.270×10^7

The altitude of sensible atmosphere is that altitude where any appreciable effect is realized for a ballistic entry. Should a lifting entry be considered then the altitude of sensible atmosphere would be greater (400,000 feet for earth).

6.3 VELOCITY REQUIREMENTS FOR A VERTICAL DESCENT LUNAR LANDING

The total velocity requirements and corresponding vehicle sizing for landing on the lunar surface with near zero velocity is of importance for almost all future lunar programs. An exact analysis of the problem involves the usual digital simulation which is costly and time consuming. For preliminary design purposes, however, the assumption of a purely vertical descent during the retrophase allows the estimation of the upper limits of the vehicle design requirements for the landing maneuver. Thus, in order to indicate the general velocity and vehicle size requirements, a vertical descent with a single burning phase is assumed for this analysis.

The development of the equations pertaining to this analysis is given in Appendix E. The equation describing the vehicle characteristics is

$$\frac{V_{IMP}}{g_e I_{sp}} = \sqrt{\left(\ln \frac{W_O}{W_{BO}}\right)^2 - \frac{2g_m}{g_e \frac{T_{vac}}{W_O}} \left(\frac{\frac{W_O}{W_{BO}} - 1 - \ln \frac{W_O}{W_{BO}}}{\frac{W_O}{W_{BO}}}\right)} \quad (30)$$

where V_{IMP} is the impact velocity for the nominal trajectory with no retrophase. When the approach trajectory to impact the surface is hyperbolic the impact velocity is defined as

$$V_{IMP} = \sqrt{\frac{2\mu_m}{r_m} + (V_\infty)^2} \quad (31)$$

where

μ_m = lunar gravitational constant

r_m = radius of the moon

V_∞ = approach velocity at an infinite distance from the lunar surface.

A typical variation of the impact velocity as a function of earth-lunar time of flight is shown on Figure 2. The approach trajectory need not be hyperbolic, however, to estimate the vehicle characteristics with Equation (30). The retrolanding phase after a deboost from a lunar orbit can be approximated providing the nonretro impact velocity is known.

Equation (30) gives the vehicle mass ratio required to land the vehicle with zero velocity on the lunar surface for a specific approach trajectory which is defined by V_{IMP} . The variation of the required mass ratio with the nondimensional velocity term is shown in Figure 3 for various initial thrust-to-weight ratios measured in earth standards.

The total ideal velocity required for the landing maneuver is shown in Figures 4, 5 and 6 for specific impulses of 270, 300, and 420 seconds, respectively. These values of specific impulse were chosen to represent solid, storable liquid, and cryogenic propellants which might be used for landing systems. The ideal velocity is shown as a function of the nonretro impact velocity, typical values of which are indicated for the 50, 66, and 90-hour earth-to-moon trajectories discussed in Chapter 2.

The magnitude of the initial thrust-to-weight ratio is seen in Figure 7 to have a large effect on the velocity requirement for the landing maneuver. As the thrust-to-weight ratio increases, the velocity requirement decreases, but the rate of decrease diminishes as T_{vac}/W_0 approaches 1.5. Thus a definite optimum exists when structure requirements and velocity requirements are considered together.

This type of cursory analysis, when combined with the earth boost-phase estimation techniques, allows the preliminary development of a complete launch system from earth takeoff to lunar landing. Also, it is possible to extend the analysis to the terminal phase of landing on other planets by the use of appropriate constants providing the nonatmospheric assumption holds, or if velocity increments or specific impulse degradations are included to account for the atmospheric effects. A further analysis into the problem of a soft lunar landing is shown in Joseph's report on propellant consumption during soft landing.⁴

Velocity Requirements for a Vertical Descent Lunar Landing

6-11

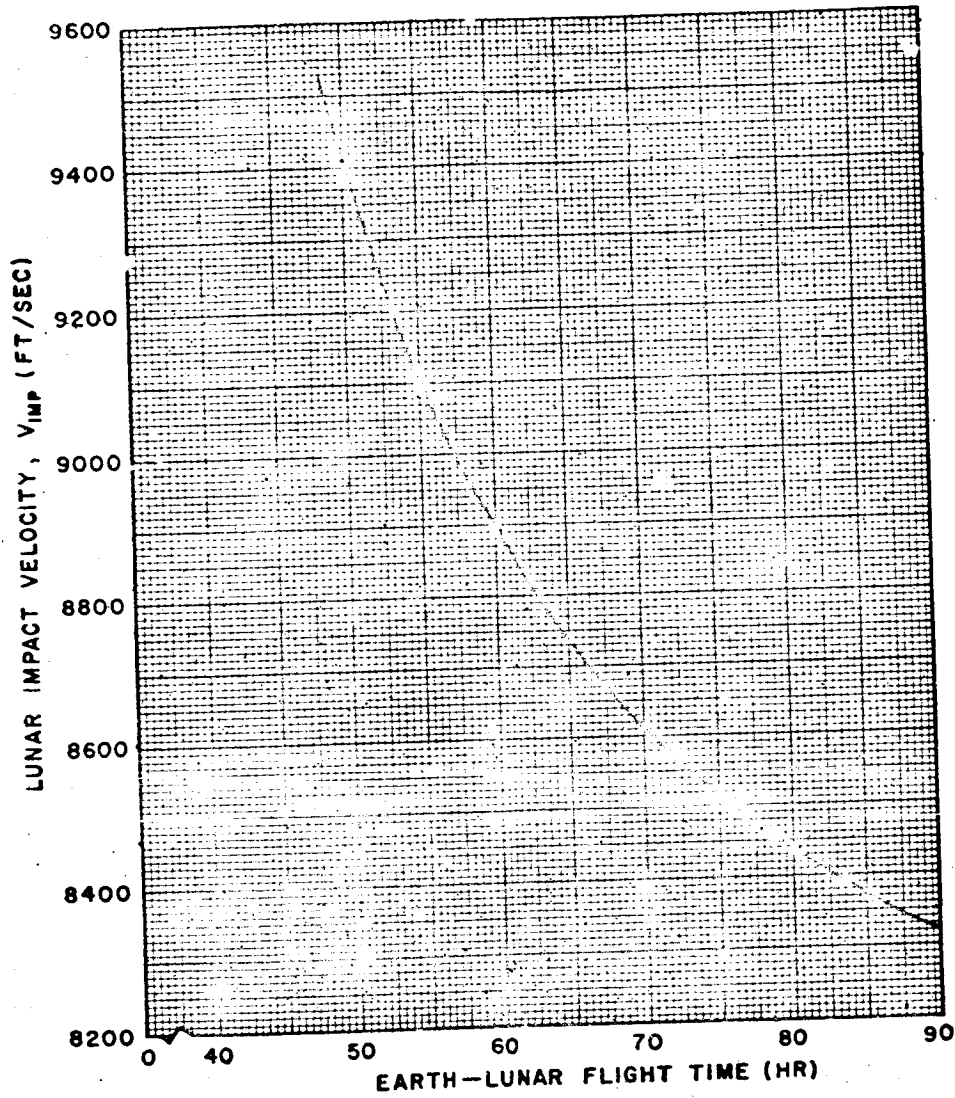


Figure 2. Approximate Nonretro Lunar Impact Velocity

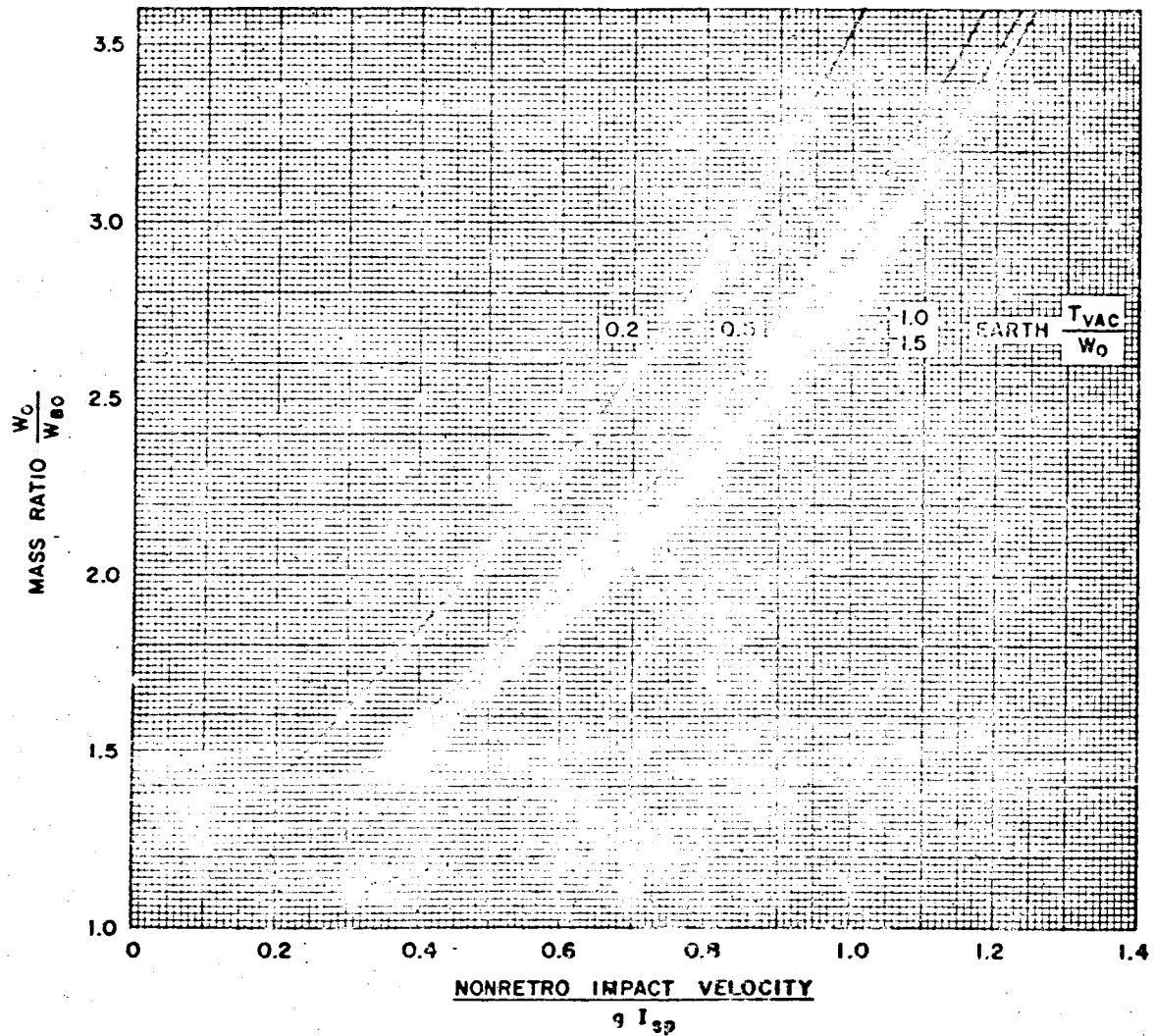


Figure 3. Lunar Landing Mass Ratio (Single-Burning Phase, Vertical Descent)

Velocity Requirements for a Vertical Descent Lunar Landing

6-13

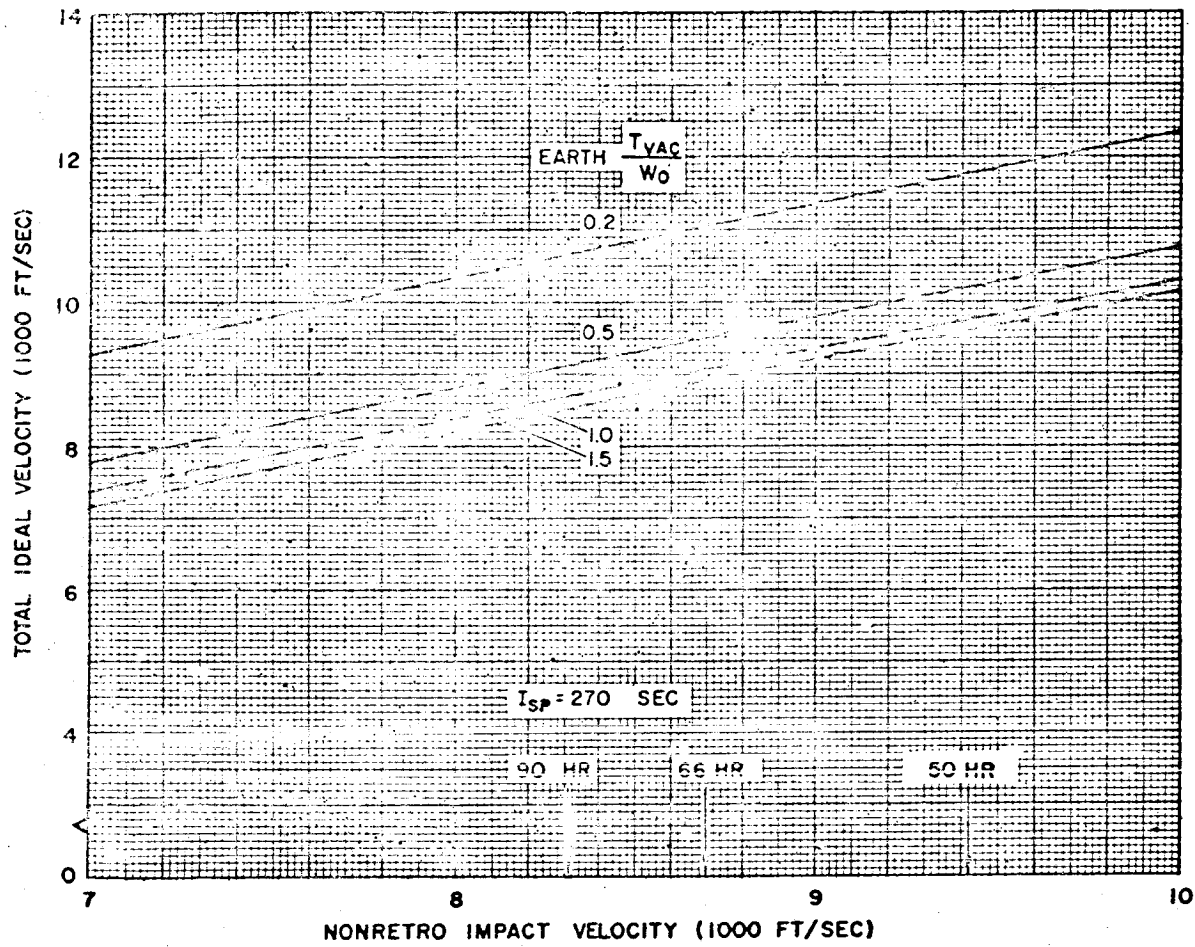


Figure 4. Total Ideal Velocity for Lunar Landing (Single-Burning Phase, Vertical Descent)

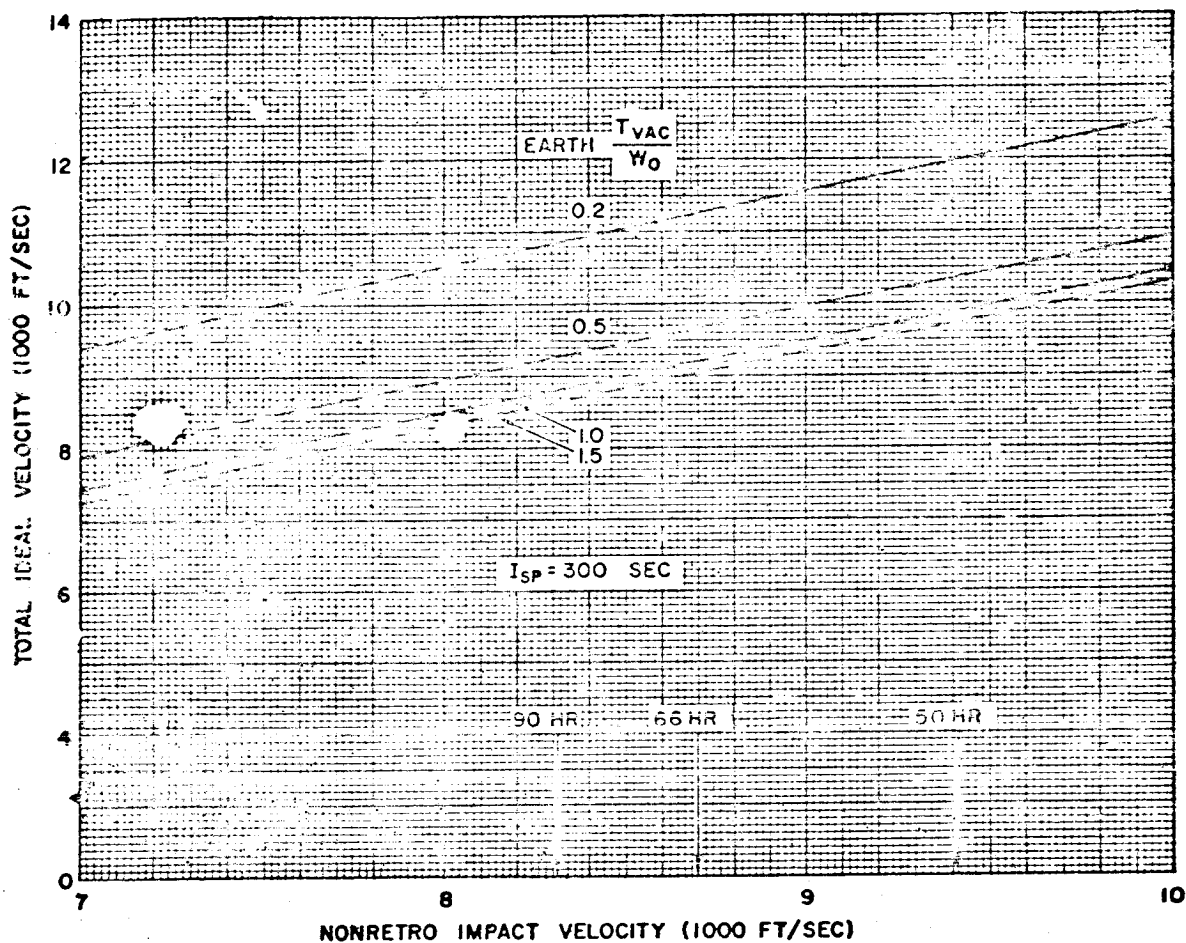


Figure 5. Total Ideal Velocity for Lunar Landing (Single-Burning Phase, Vertical Descent)

6-16

LUNAR/PLANETARY DEBOOST AND LUNAR LANDING

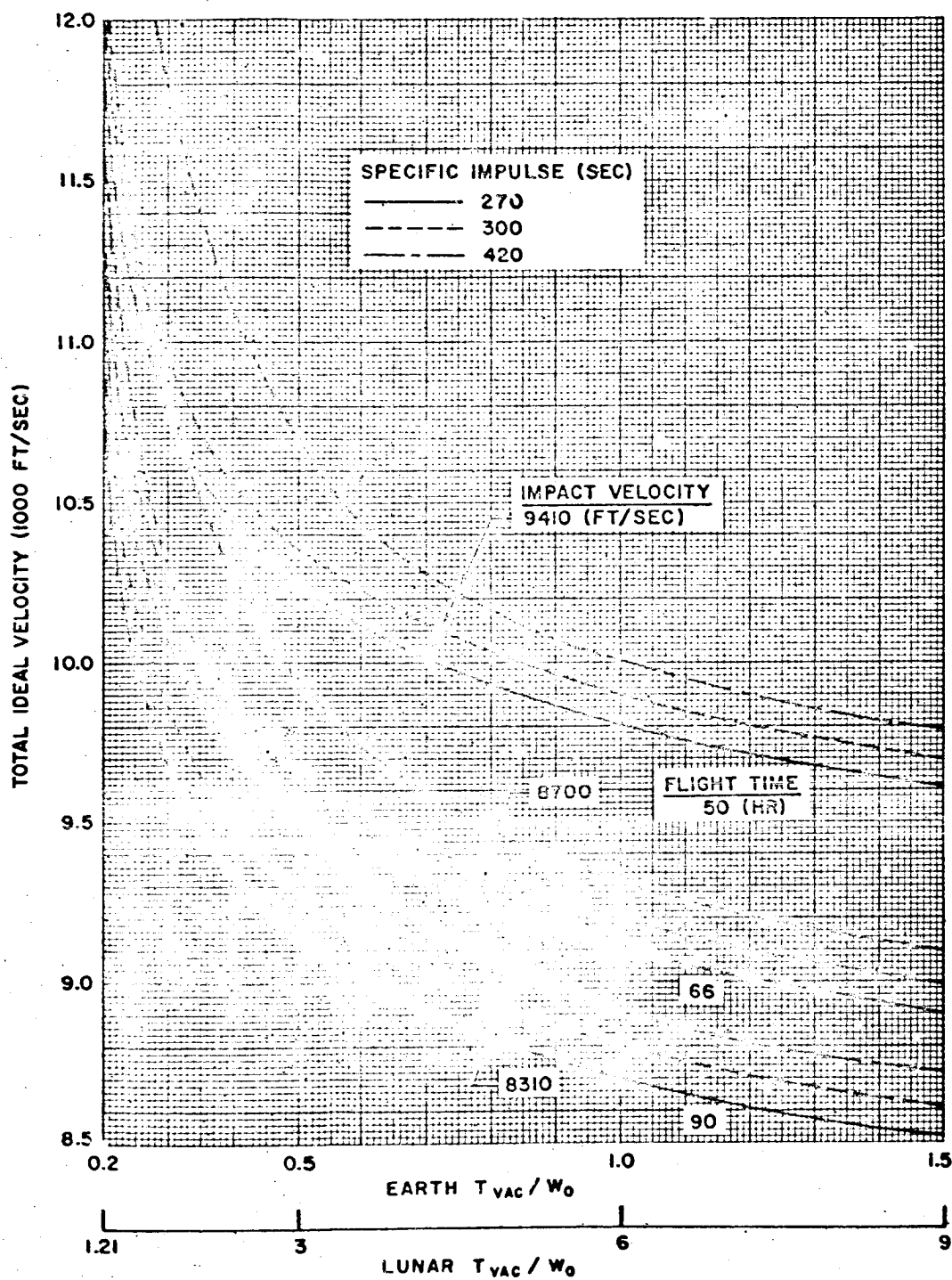


Figure 7. Effect of Thrust-to-Weight Ratio for Lunar Landing (Single-Burning Phase, Vertical Descent)

Nomenclature

6-17

NOMENCLATURE

a	Semimajor axis of deboost orbit
E_1	Eccentric anomaly after impulse application
E_E	Eccentric anomaly at atmospheric entry
e	Eccentricity of deboost orbit
g_e	Earth gravitational acceleration
g_m	Lunar gravitational acceleration
\bar{h}	Angular momentum of deboost orbit
I_{sp}	Vacuum specific impulse
r_E	Radius from planet center to outer edge of atmosphere
r_m	Radius of the moon
r_o	Radius from planet center to deboost impulse application point
T_{vac}	Vacuum thrust
V_1	Velocity immediately after impulse application
V_E	Velocity at atmospheric entry
V_{imp}	Impact velocity with no retrophase
V_o	Velocity in initial orbit at impulse application point
V_∞	Velocity at an infinite distance
W_{BO}	Vehicle burnout weight
W_o	Vehicle initial weight
γ_1	Flight path angle immediately after impulse application
γ_E	Flight path angle at atmospheric entry
γ_o	Flight path angle in initial orbit at impulse application point
ΔV	Velocity impulse applied for deboost
$\Delta \gamma$	Change in flight path angle due to velocity impulse application

θ	Planet range angle tranversed during deboost trajectory
μ_m	Lunar gravitational constant
μ_p	Planet gravitational constant
ψ	Angle between initial orbit velocity vector and velocity impulse vector (see Figure 1).
v_1	True anomaly after impulse application
v_E	True anomaly at atmosphere entry

REFERENCES

1. R. L. Phillips, "Descent Trajectories for Manned Space Vehicles," Space Technology Laboratories, GM-TR-0165-0041⁶, 20 June 1958.
2. George Low, "Nearly Circular Transfer Trajectories for Descending Satellites," NASA TR R3, 1959.
3. Alan L. Friedlander and David P. Harry III, "Requirements of Trajectory Corrective Impulses During the Approach Phase of an Interplanetary Mission," NASA TN D-255, January 1960.
4. P. Joseph, "Minimization of Propellant Consumption During Soft Landing," Space Technology Laboratories, Inc., 9321 4-186, 30 October 1961.

CHAPTER 7

PLANETARY ENTRY

7.1 VEHICLE DESIGN CONSIDERATIONS FOR ATMOSPHERIC ENTRY

The design of an entry vehicle requires numerous compromises and is subject to a number of considerations and requirements. The major considerations and requirements are imposed by 1) the payload, 2) the thermal environment and the thermal protection system, 3) the structural system and the loading due to the trajectory and the dynamic motion, 4) the stability and dynamic motion of the entry vehicle, and 5) the required accuracy of impact point prediction.

7.1.1 Payload Considerations

The payload may restrict entry vehicle design by imposing limitations on allowable forces and temperatures. Alleviation of axial force or deceleration is achieved by decreasing the entry angle (as measured downward from the local horizontal) or, if this method becomes too restrictive, by drag modulation. To a certain extent, both methods increase vehicle weight. Drag modulation also reduces reliability because of the added complexity of the entry vehicle, whereas decreased entry angle increases impact point dispersion. The use of lift decreases maximum deceleration to a much greater extent than the two methods mentioned above; however, the design of a lifting vehicle is an order of magnitude more complex than that of a zero lift ballistic vehicle.

Alleviation of normal force or side loads is accomplished for a ballistic vehicle by either an increased static stability margin or an attitude control system. Both of these methods add weight to the vehicle. Also, the attitude control system decreases reliability, and increasing the stability margin may increase the overall vehicle length.

Two general methods of controlling attitude are available. The first operates prior to entry so that the entry angle of attack is small. The second method begins control during entry and is initiated by some small magnitude of deceleration, say 0.3 or 3.0 ft/sec². Essentially this method is used to rapidly dampen the oscillation of the vehicle so that the angle of attack becomes very small early in the entry trajectory. If the entry angle of attack of the vehicle is random, the attitude control system must be designed to handle the case of the backward entry.

To utilize the lift properly, a lifting vehicle must be designed with an attitude control system. As a consequence, the allowable normal force now specifies a band of trajectories in which the vehicle must fly.

The payload will undoubtedly have temperature limitations that must be considered in the entry vehicle design. These limitations may or may not be critical to the design. If they are, the thickness of the insulation portion of the heat protection system and the insulation material choice will be governed to a large extent by these maximum allowable payload temperatures. Often, to avoid large insulation weights, it is possible to thermally isolate the payload from the external thermal protection system by using small-area, low-conductivity supports and internal radiation shields and/or superinsulation. These cannot be used in the external protection system for strength reasons. A much more sophisticated method of thermal protection for the payload is the use of an internal refrigeration system. This method is probably worth investigating if large payloads are under consideration.

7.1.2 Thermal Protection System

Two modes of heat transfer to an entry vehicle exist during the entry phase of flight. These are the laminar and turbulent aerodynamic boundary layer heat transfer and the transfer of radiant energy to the vehicle surface from the hot gas between the shock wave and the vehicle. The relative magnitudes of these two modes of heat transfer are functions of vehicle shape, entry velocity, and atmosphere (scale height and components). In general, the blunter the vehicle and the higher the entry velocity the greater the radiation heat transfer rate relative to the aerodynamic rate. The radiation heat transfer rate is the first to reach its maximum during the entry trajectory; next is the turbulent rate, and finally the laminar rate. As the entry angle is decreased both the rate and total radiant heat transfer decrease, whereas for aerodynamic heat transfer only the rate decreases while the total increases.

Protection against this thermal environment may be accomplished in a number of ways, and the methods chosen are dependent primarily upon the magnitudes of both the rate and the total of heat transfer. If both rate and total are sufficiently low, a simple heat sink made of copper or beryllium may be adequate. The simple heat sink is heat rate limited only to prevent the outer surface from melting. However, if the total heat that must be absorbed is large, the weight of the heat sink becomes excessive. For rates that are relatively low, it is possible to absorb the heat in a thin skin and reradiate it to the external environment. For example, if a thin skin can withstand a temperature of 5000°R , it can reradiate up to $300 \text{ Btu/ft}^2 \text{ sec}$ so that the heat protection system now becomes a matter of insulating the remainder of the vehicle from this high-temperature skin. On the other hand, at low heat rates it is also possible to use low-temperature ablating materials for heat absorption. This alleviates the insulation problem, but weight is now required as ablating material rather than insulation. At high heat transfer rates and high total heating, the use of high-surface-temperature ablating materials is required.

35

7.1.3 Loading of the Structural System

The external loading on the entry vehicle is due to the air pressure caused by the motion of the vehicle through the atmosphere. Because the vehicle is in free flight, this pressure varies directly with both deceleration and ballistic coefficient. The deceleration varies as the square of the entry velocity, the inverse of the scale height of the atmosphere, and almost directly with the sine of the entry angle. At entry angles of less than 10 degrees, variation of deceleration with sine of the entry angle becomes too conservative.

During that portion of the flight when the vehicle is oscillating, the pressure around the vehicle is unsymmetrical and consequently the loading is also unsymmetrical. In general, the maximum unsymmetrical load occurs earlier than the maximum symmetrical load. Although maximum loads occur after maximum heat rates so that the heat does have some time to flow into the structure, generally the structural temperature rise is insignificant and room-temperature modulus of elasticity and yield strength may be used. It is well to check this point for each specific design. The other point on the trajectory at which the structure may be critical is at impact. At this point structural temperatures are at or near their maximum, and high-temperature properties must be used.

7.1.4 Stability and Dynamic Motion

During entry the dynamic motion of an entry vehicle is similar to a system that has a variable spring constant; that is, both the frequency and amplitude vary with time. Initially, the static stability coefficient determines the dynamic motion of the vehicle. If the dynamic stability of the vehicle were zero, the amplitude of the angle of attack would decrease continually until maximum dynamic pressure is reached, after which the amplitude would increase to some value between the minimum value and the entry angle of attack. The frequency would increase from zero to a maximum at maximum dynamic pressure and would then decrease.

For a vehicle with a positive dynamic stability, the frequency pattern remains essentially the same; however, the amplitude differs in that at some altitude the dynamic damping begins to dominate so that the amplitude may not increase at all or may increase only slightly before it again decreases due to the dynamic damping. For high ballistic coefficient vehicles the angle of attack amplitude at maximum dynamic pressure is much less than that which would be computed if only the static stability coefficient were considered, whereas for low ballistic coefficient vehicles the dynamic stability of the vehicle is not important until the vehicle is below the maximum dynamic pressure altitude.

7.1.5 Accuracy of Impact Point Prediction

For ballistic entry vehicles that do not have terminal guidance, errors in impact point prediction are caused by uncertainties in 1) atmospheric density, 2) wind velocity and direction, 3) external shape of vehicle, 4) lateral center-of-gravity location, 5) angle-of-attack history, and 6) uncertainty in drag coefficient. In addition to the contributors to error listed above, there are errors in impact point prediction accumulated prior to entry into the atmosphere that are due to the guidance and propulsion system.

Of the errors listed above, 3), 4), and 5) are or can be made negligible as compared to wind and density errors by spinning the vehicle slowly about its longitudinal axis. Care must be taken in specifying the spin rate because a high spin rate becomes detrimental in that the angle-of-attack convergence is reduced. Even for very low ballistic coefficient vehicles, the wind and density errors will also be negligible as compared to the overall accuracy unless the system accuracy is less than about 30 nautical miles. The uncertainty of pressure at the Mach 1 altitude and the cotangent of the entry angle may be used to estimate impact-point uncertainty due to density. The variation of pressure gives the variation of altitude at which Mach 1 is reached, and the range error caused thereby is equal to the vertical error times the cotangent of the flight path angle. The uncertainty due to wind may be estimated from the time of fall from Mach 1 to impact. If the entry contribution to uncertainty of impact point becomes important and it is desirable to reduce this portion of the uncertainty, it can be accomplished by increasing the ballistic coefficient and/or increasing the entry angle. Increasing the ballistic coefficient lowers the Mach 1 altitude so that the time of fall for that portion of the trajectory is reduced and thus reduces the effect of winds. Increasing the entry angle directly reduces the effect of density uncertainty by the change in the cotangent of the angle and also lowers the Mach 1 altitude which then reduces the effect of winds. The entry velocity also affects the Mach 1 altitude; however, for a given mission very little change can be made in this velocity.

7.2 ATMOSPHERES OF THE PLANETS

For the study of entry into the atmospheres of the planets, it is necessary to assume values for some of the physical characteristics of the atmospheres. Since the desired values are only approximately known for the planets being considered here, namely Mars and Venus, it is desirable to consider a range of values in some cases. This is especially necessary if estimates are to be made for such purposes as preliminary design.

7.2.1 Earth

The atmosphere of the earth is approximated by the exponential variation of density

$$\rho = \rho_0 e^{-\beta h}$$

where ρ_0 is 0.0027 slug/ft³ and the scale height, β^{-1} or H , is 23,500 feet. Figure 1 shows the comparison of this approximation and the ARDC 1959¹ atmosphere. This is the same atmosphere as that used by Chapman.²

7.2.2 Mars

The atmosphere of Mars is approximated by three models which are here called the low-, medium-, and high-temperature cases. These will be explained more fully below. The densities for these atmospheres are given by

$$\rho = 0.00071 e^{-\frac{h}{30,000}} \text{ slugs/ft}^3 \text{ (low temperature)}$$

$$\rho = 0.00035 e^{-\frac{h}{45,500}} \text{ slugs/ft}^3 \text{ (medium temperature)}$$

$$\rho = 0.00016 e^{-\frac{h}{61,000}} \text{ slugs/ft}^3 \text{ (high temperature)}$$

where h is the altitude in feet above the surface of the planet.

These formulas for the atmosphere of Mars were derived from the data of Reference 3. Values are listed as High, Low, and Middle to give a possible range. The following table lists independently determined quantities.

	<u>Low</u>	<u>Middle</u>	<u>High</u>
Acceleration of surface gravity, g_c (ft/sec ²)	11.8	12.3	12.8
Surface mass pressure, M_m (slugs/ft ²)	9.5	16	22
Stratosphere temperature, T (°R)	230	320	410
Surface temperature, T_o (°R)	380	410	470

7-6

PLANETARY ENTRY

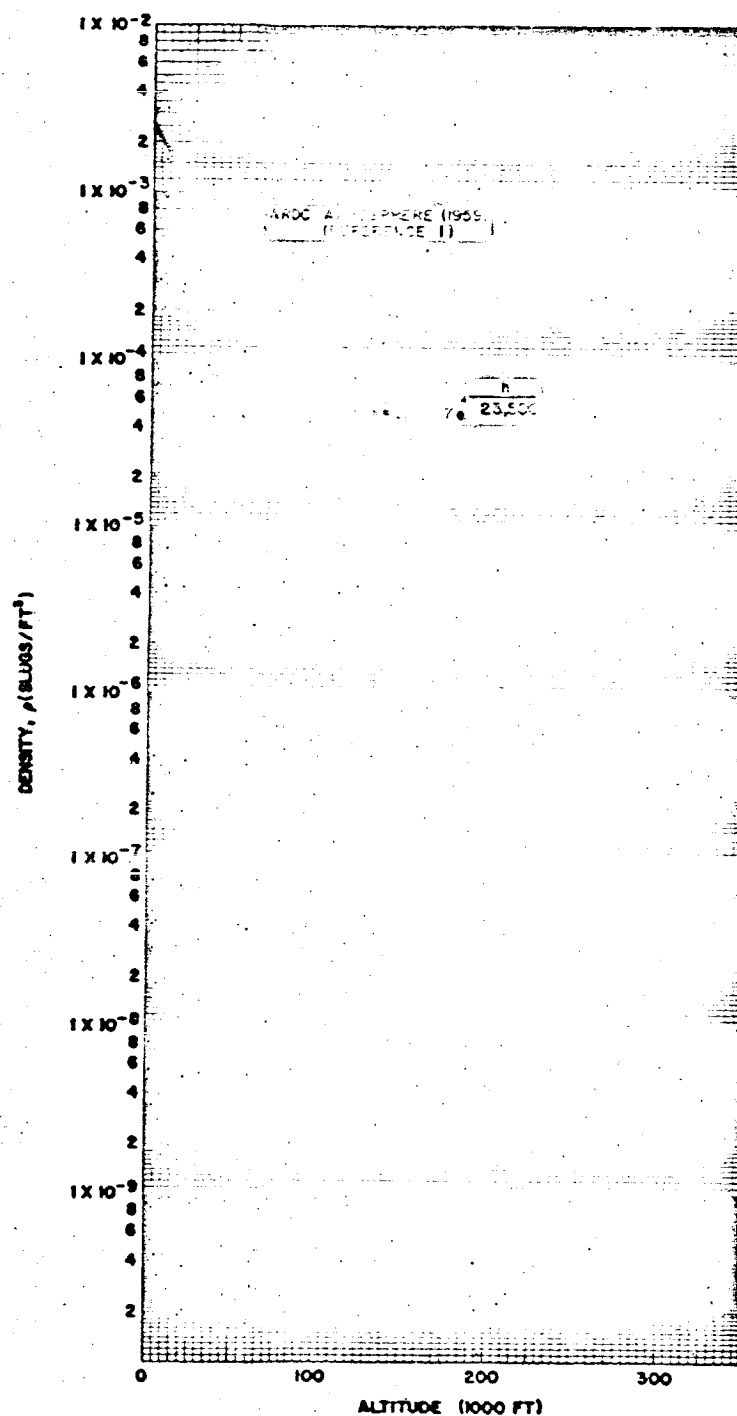


Figure 1. Comparison of Exponential Atmosphere with ARDC Atmosphere of 1959

From these values of M_m and g_o a surface pressure can be then computed.

	Low ← ($M_m \cdot g_o$) → High		
Surface pressure, p_o (lb/ft ²)	113	196	284

The concentrations leading to the molecular weights to go with these values are:

Concentration of constituents by volume (percent)			
CO ₂	7.2	1.9	0.7
A	6.0		0.6
O ₂ *			
N ₂	86.8		98.7
Average molecular weight, M	29.9	28.4	28.2

A surface density can then be computed where the low value of surface pressure is combined with the high value of surface temperature and vice versa.

	High ← (T_o) → Low		
	Low ← ($M_m \cdot g_o$) → High		
Surface density, ρ_s (slugs/ft ³)	1.4×10^{-4}	2.7×10^{-4}	4.3×10^{-4}

Then surface densities are adjusted to stratosphere temperatures in order to match the stratosphere with an exponential atmosphere.

$$p = p_o e^{-\beta h}$$

Values of the scale height, $H = \beta^{-1}$, are computed from

$$H = \frac{RT}{Mg}$$

where R is the universal gas constant (ft-lb/mole °R).

* Believed to be present in negligible amount.

	<u>High</u>	<u>Middle</u>	<u>Low</u>
	High ←	(T_o, T) →	Low
	Low ←	(M_{in}, g_o) →	High
Scale height, H, β^{-1} (ft)	61,000	45,500	30,000
Surface density, ρ_o (slugs/ft ³)	0.00016	0.00035	0.00071

7.2.3 Venus

The atmosphere of Venus is approximated by three models for which the density may be expressed in exponential form

$$\rho = \rho_o e^{-\beta h}$$

or

$$\rho = 0.0037 e^{-\frac{h}{18,000}}$$

$$\rho = 0.00095 e^{-\frac{h}{20,000}}$$

$$\rho = 0.00030 e^{-\frac{h}{22,000}}$$

The scale heights, $H = \beta^{-1}$, used are based on the measurements made on the occultation of Regulus.⁴ The variation in scale height was taken as a variation of 20 percent below the value measured at the basic altitude of the measurement, which was 70 kilometers or 230,000 feet above the cloud layer. This was the variation over the range of measurements of 50 to 70 kilometers above the cloud layer, and temperature considerations indicate the variation would not be much greater. It was assumed that the flight phenomena of interest would be below this 70-kilometer altitude. Since the location of the surface of the planet Venus is extremely uncertain and since its location is not necessary for such phenomena as maximum deceleration and heating rates, the altitude, h , is measured from the surface of the cloud layer. The radius of this spherical surface is 6100 kilometers or 3290 nautical miles.

Since the pressure was measured by the measurements of Reference 4 at 70 kilometers above the cloud layer, the density can be calculated for an isothermal atmosphere from

$$\rho = \frac{P}{Hg}$$

The acceleration of gravity, g , at this altitude is 28.2 ft/sec^2 and the pressure is 0.0054 lb/ft^2 .

Since a variation in scale heights is assumed for three different isothermal atmospheres, the resulting values of ρ_0 for the different values of H are considerably different. This is not a serious problem, however, for the purposes of this section of the handbook, since ρ_0 is merely the density at some arbitrary altitude.

The composition of the atmosphere is considered here to be most probably 90 percent CO_2 and 10 percent N_2 , all undissociated in the altitude range of interest. However, it is possible that there is much more N_2 than this.⁵ Therefore, as an extreme it can be assumed that there is 10 percent CO_2 and 90 percent N_2 . As an intermediate case the relative concentration of 50 percent CO_2 and 50 percent N_2 is assumed. These values do not affect the estimated density since it was calculated on pressure and scale height measurements. They will, however, have an effect on heating.

7.3 GENERAL ENTRY FUNCTION

Many phenomena that occur during atmospheric entry of a ballistic vehicle may be quantitatively expressed as

$$f = K \rho^i V^j \quad (1)$$

where f is the quantity of interest, ρ is atmospheric density, V is velocity of the vehicle, and K , i , and j are constants. Table 1 contains some of the phenomena of interest and the corresponding values of K , i , and j for entry into an atmosphere of air. R_N is the vehicle nose radius and Δ is the ballistic coefficient.

Table 1. Constants Associated with f Function

f	K^*	i	j	i/j
Deceleration (g 's)	$\frac{1}{2\Delta}$	1	2	0.5
Stagnation aerodynamic heat rate, q_s	$1.48 \times 10^{-8} (R_N)^{-1/2}$	0.5	3	0.167
Laminar heat rate, q_L	$K_{q_s} f_L$ (configuration, body point)	0.5	3	0.167
Turbulent heat rate, q_T	$K_{q_s} f_T$ (configuration, body point)	0.8	3.39	0.236
Stagnation radiant heat rate, q_R	$0.814 \times 10^{-84} R_N$	1.7	21.2	0.08

* K_{q_s} is the K for the stagnation aerodynamic heat rate.

The properties of the function f , with respect to the vehicle trajectory are easily determined with the aid of trajectory characteristics. This approach has been given by Ambrosio.⁶

If a static isothermal atmosphere is assumed and if the entry angle is sufficiently steep (greater than about 10 degrees) so that the path angle measured from the local horizontal may be assumed constant, the velocity equation in the set of trajectory equations is readily integrated. As discussed in the section on deceleration, this yields

$$\frac{V}{V_E} = \exp \left(\frac{g_c}{g_p} \frac{p}{2\Delta \sin \gamma_E} \right) = \exp \left(\frac{g_c \rho}{2\beta \Delta \sin \gamma_E} \right) \quad (2)$$

where

V = velocity (ft/sec)

p = atmospheric pressure (lb/ft²)

$\Delta = W/C_D A$, ballistic coefficient (lb/ft²)

γ = flight path angle measured positive up from the local horizontal

g = acceleration of gravity (ft/sec²)

g_c = gravitational conversion constant (ft/sec²)

and subscripts p and E refer to planet and entry, respectively.

In the pressure form of the equation the approximation is made that $g = g_p$, a constant within the planetary atmosphere, so that $p\beta_p = g_p \rho$. The density form of the equation uses the exponential atmosphere discussed in the section on atmospheres. The elapsed time for a vehicle to fall from pressure p_1 to pressure p_2 is obtained by integrating the equation

$$\frac{dh}{dt} = V \sin \gamma_E \quad (3)$$

with the aid of Equation (2) and the previously stated assumptions. This results in

$$t_{1 \rightarrow 2} = \frac{1}{\beta_p V_E \sin(-\gamma_E)} \left[\bar{E}_i \left[\frac{g_c}{g_p} \frac{p_2}{2\Delta \sin(-\gamma_E)} \right] - \bar{E}_i \left[\frac{g_c}{g_p} \frac{p_1}{2\Delta \sin(-\gamma_E)} \right] \right] \quad (4)$$

where

$t_{1 \rightarrow 2}$ = the time from pressure p_1 to pressure p_2 (sec)

β_p = the reciprocal of the scale height of the atmosphere (ft⁻¹)

and

$\overline{\text{Ei}}(\xi)$ = the exponential integral defined by

$$\overline{\text{Ei}}(\xi) = \int_{-\infty}^{\xi} \frac{e^t}{t} dt$$

which is tabulated in References 7 and 8 and plotted in Figure 2.

The atmospheric pressure at which the function, f , is maximum is

$$(p)_{f \max} = -2 \frac{i}{j} \frac{g_p}{g_c} \Delta \sin \gamma_E \quad (5)$$

If x is defined by

$$x = -\frac{g_c}{g_p} \frac{j p}{2 \Delta \sin \gamma_E} \quad (6)$$

then

$$(x)_{f \max} = i \quad (7)$$

The velocity at which the function is maximum is obtained from Equation (2).

$$\left(\frac{v}{v_E} \right)_{f \max} = e^{-i/j} \quad (8)$$

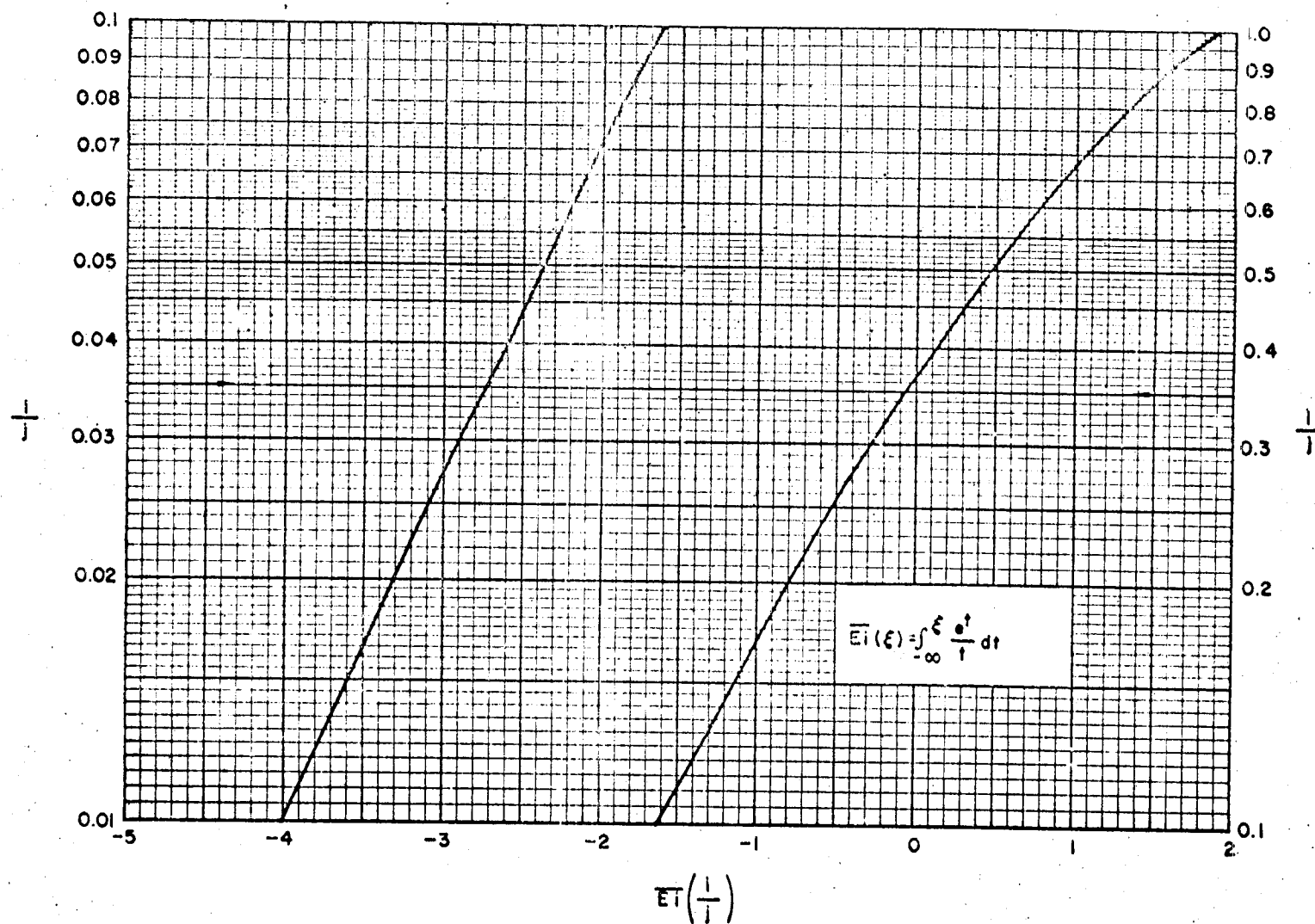
Figure 3 contains a graphical presentation of Equation (8) with the velocity ratio at maximum f plotted as a function of i/j .

Equations (5) and (8) and the relationship between atmospheric pressure and density for a static isothermal atmosphere $\rho \beta_p = g_p \rho$ are substituted into Equation (1) to obtain the maximum value of f .

$$f_{\max} = K \left[\frac{2 \beta_p}{e g_c} \frac{i}{j} \Delta \sin(-\gamma_E) \right]^i v_E^j \quad (9)$$

The ratio of f to its maximum value is now readily obtained.

$$\frac{f}{f_{\max}} = \left(\frac{x}{i} \right)^i e^{(i-x)} \quad (10)$$

Figure 2. The Function $Ei(\xi i)$

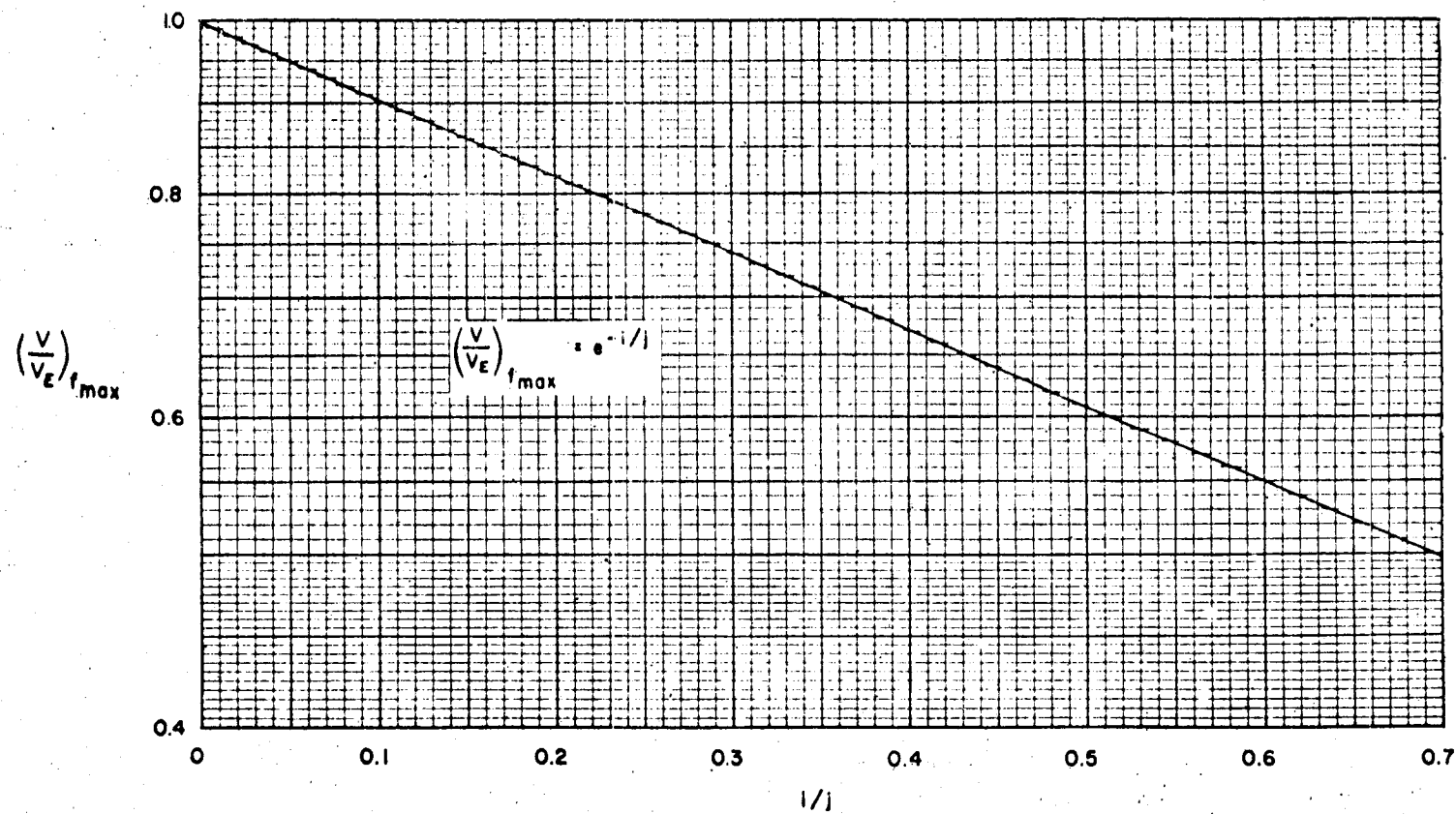


Figure 3. Ratio of Velocity to Entry Velocity at f_{max} as a Function of $1/j$

Equation (10) is presented graphically in Figures 4a and 4b, where f/f_{\max} is plotted as a function of x for values of i equal to 0, 0.5, 0.8, 1.0, and 1.7.

For some of the phenomena the integrated value of f is of interest. This integral is

$$F = \int_0^t f \, d\tau \quad (11)$$

The equation for F , with the aid of Equations (2) and (3), transforms into

$$F = K \left[\frac{2\Delta}{g_c (j-1)} \right]^i \left[\beta_p \sin(-\gamma_E) \right]^{i-1} V_E^{j-1} \int_0^{(j-1) \ln(V_E/V)} t^{i-1} e^{-t} dt$$

The integral in this equation is the incomplete gamma function if i is greater than zero, so that this equation may be written as

$$F = K \left[\frac{2\Delta}{g_c (j-1)} \right]^i \left[\beta_p \sin(-\gamma_E) \right]^{i-1} V_E^{j-1} \Gamma \left[i, (j-1) \ln \frac{V_E}{V} \right], \quad i > 0 \quad (12)$$

If the impact velocity is low enough and/or j is large enough so that $(j-1) \ln(V_E/V)$ is greater than about 6, the incomplete gamma function is very closely approximated by the complete gamma function. The total integrated value (i.e., from entry to impact) of f then becomes

$$F_{\text{total}} = K \left[\frac{2\Delta}{g_c (j-1)} \right]^i \left[\beta_p \sin(-\gamma_E) \right]^{i-1} V_E^{j-1} \Gamma(i) \quad (13)$$

This is true for all vehicles with a ballistic coefficient, Δ , in thousands of pounds per square foot or less. From an examination of Equations (7) and (13), one deduces that if i is less than one (as is true for both laminar and turbulent heating), steeper entry angles give large values of the function f but smaller integrated values of F ; whereas, if i is greater than one, both the function and its integral increase with steeper entry angles.

A convenient relationship between F_{total} and f_{\max} is obtained by dividing Equation (13) by Equation (9)

$$\frac{F_{\text{total}}}{f_{\max}} = \left(\frac{e}{i} \frac{j}{j-1} \right)^i \frac{\Gamma(i)}{\beta_p V_E \sin(-\gamma_E)} = \frac{G(i, j)}{\beta_p V_E \sin(-\gamma_E)} \quad (14)$$

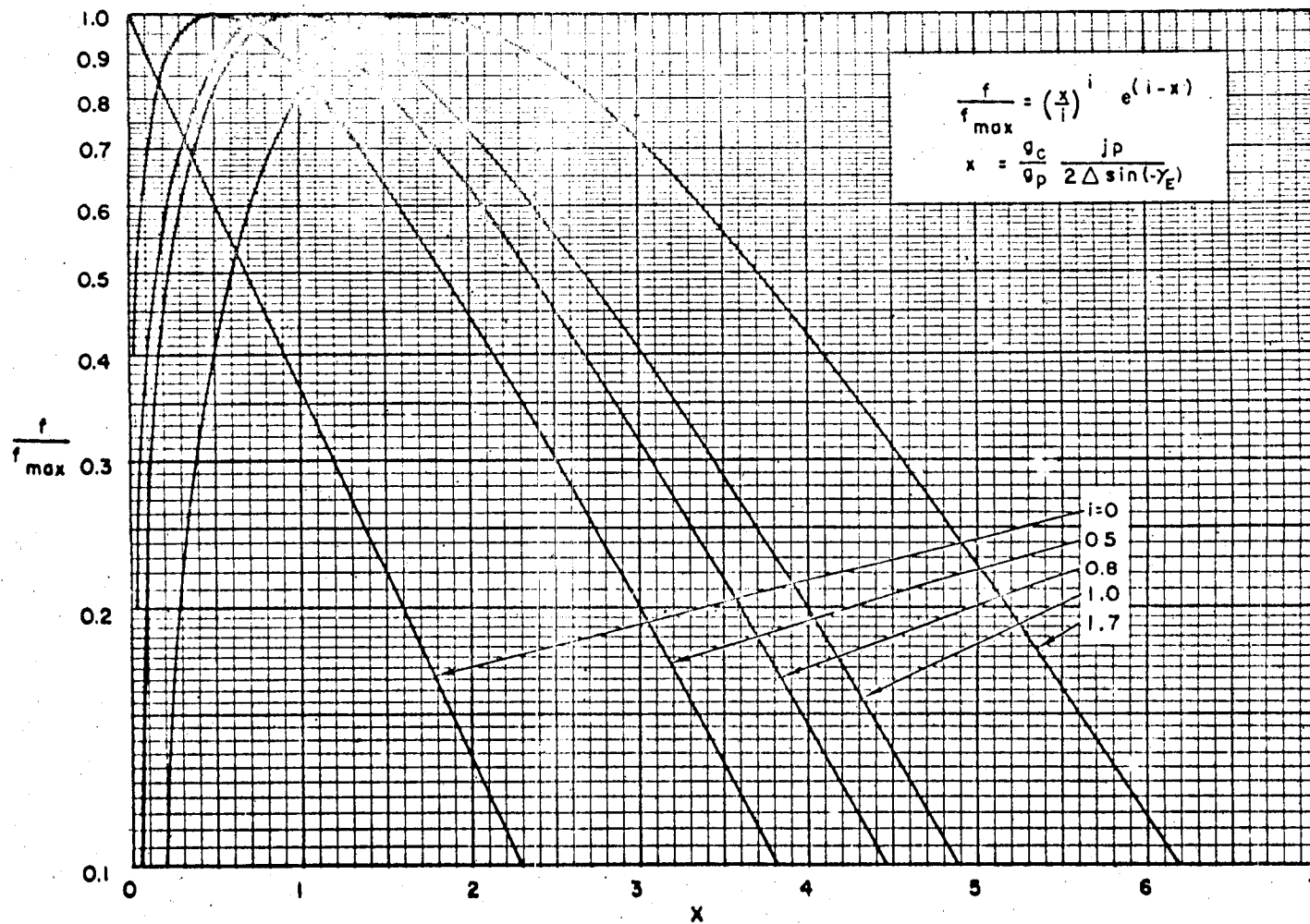


Figure 4a. Variation of f/f_{\max} with Pressure

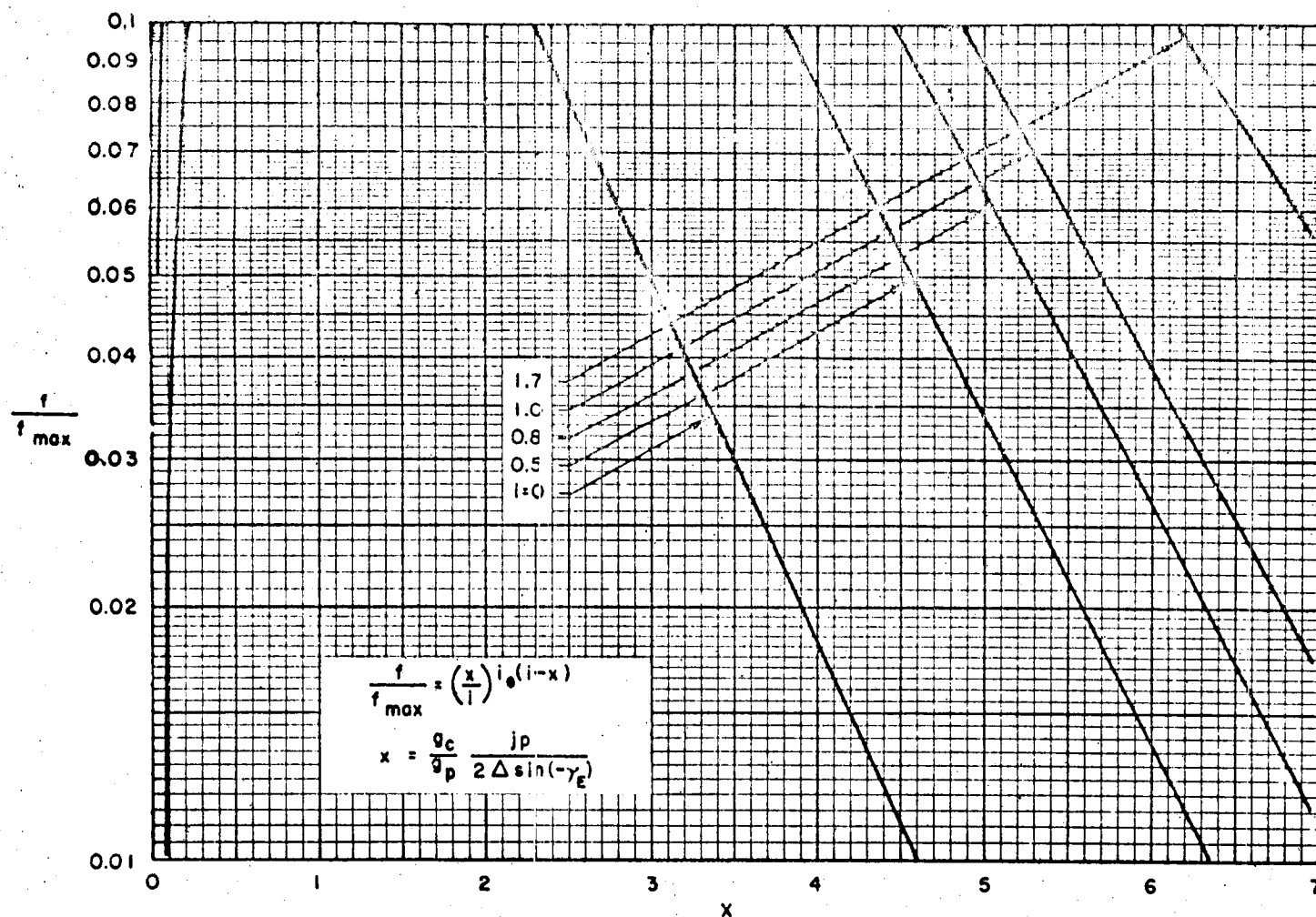
Figure 4b. Variation of f/f_{\max} with Pressure

Figure 5 presents

$$G(i, j) = \beta_p V_E \sin(-\gamma_E) \frac{F_{\text{total}}}{f_{\text{max}}}$$

as a function of i with j as a parameter, and Figure 6a presents the same information with j as the independent variable and i as a parameter. Figure 6b presents an enlargement of the left-hand side of Figure 6a.

The time for f/f_{max} to go from a small value to one and from one to a small value may be determined from Equations (4), (5), and (6).

$$t_{1 \rightarrow f_{\text{max}}} = \frac{1}{\beta_p V_E \sin(-\gamma_E)} \left[\bar{Ei}\left(\frac{i}{j}\right) - \bar{Ei}\left(\frac{x}{j}\right)_1 \right] = \frac{\Delta T_1}{\beta_p V_E \sin(-\gamma_E)} \quad (15)$$

$$t_{f_{\text{max}} \rightarrow 2} = \frac{1}{\beta_p V_E \sin(-\gamma_E)} \left[\bar{Ei}\left(\frac{x}{j}\right)_2 - \bar{Ei}\left(\frac{i}{j}\right) \right] = \frac{\Delta T_2}{\beta_p V_E \sin(-\gamma_E)} \quad (16)$$

where $(x/j)_1$ and $(x/j)_2$ are the two values of x/j for the desired small value of f/f_{max} as determined from Equation (6) and a specified value of j .

Figures 7 and 8 present the information in Equation (15) in graphical form to aid in computing time for f/f_{max} to increase from one-hundredth to one and from one-tenth to one, respectively. Figures 9 and 10 aid in computing time for f/f_{max} to decrease from one to one-hundredth and from one to one-tenth, respectively.

From Equations (4) and (5) the time interval between the maximum values of phenomenon one and phenomenon two is

$$t_{1 \rightarrow 2} = \frac{1}{\beta_p V_E \sin(-\gamma_E)} \left[\bar{Ei}\left(\frac{i}{j}\right)_2 - \bar{Ei}\left(\frac{i}{j}\right)_1 \right] \quad (17)$$

Figure 2 presents the exponential integral, \bar{Ei} , as a function of i/j as an aid in computations applied to Equation (17).

Example:

As an example of the use of the foregoing equations and curves, consider a 1-foot-nose-radius ballistic vehicle whose ballistic coefficient is 10 lb/ft² entering the earth's atmosphere at an angle, γ_E , of -30 degrees and a velocity, V_E , of 36,000 ft/sec. A scale height of 23,500 feet for the earth's atmosphere and the quantities given in Table 1 will be used.

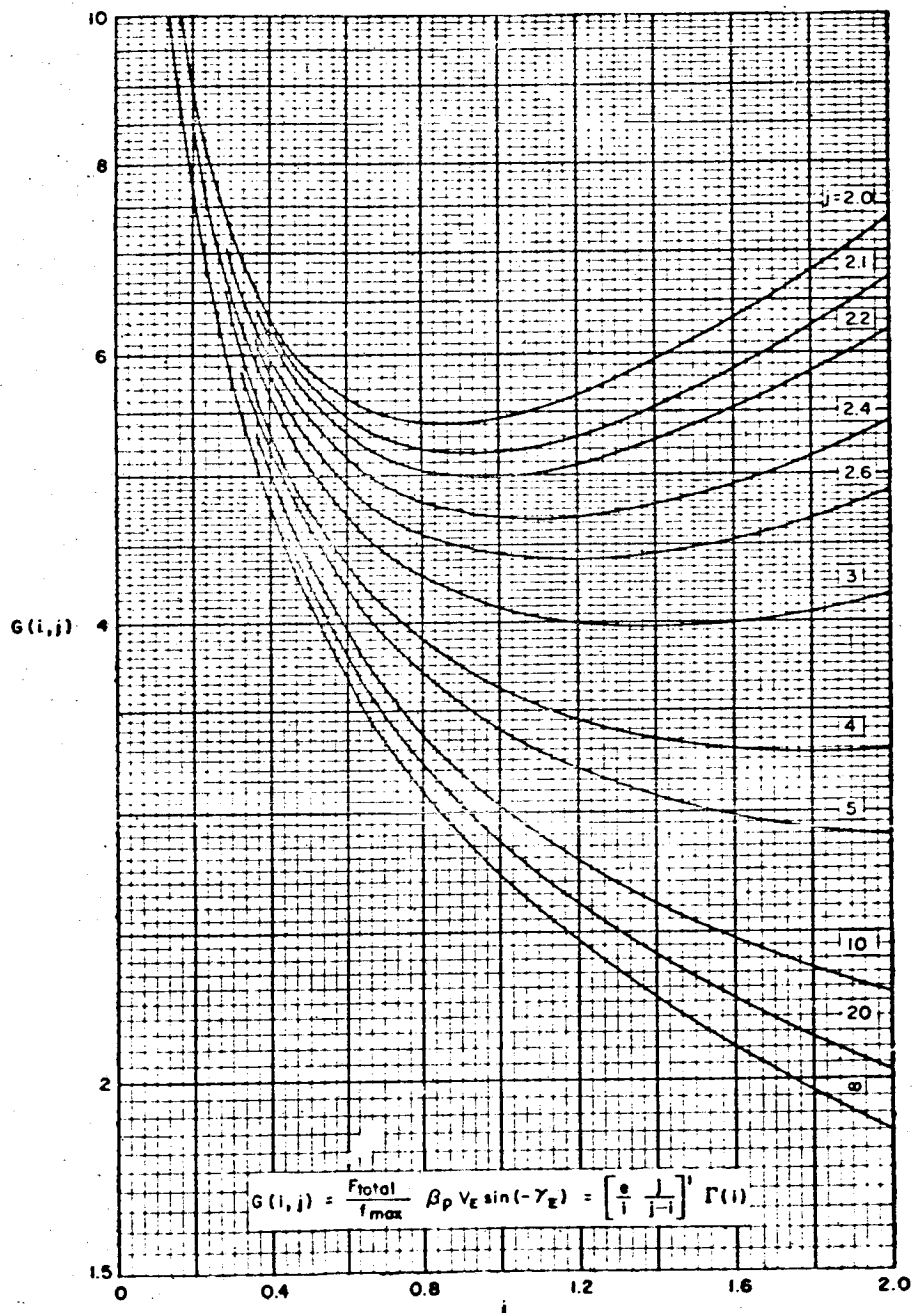


Figure 5. Function $G(i, j)$ as a Function of i for Various j 's

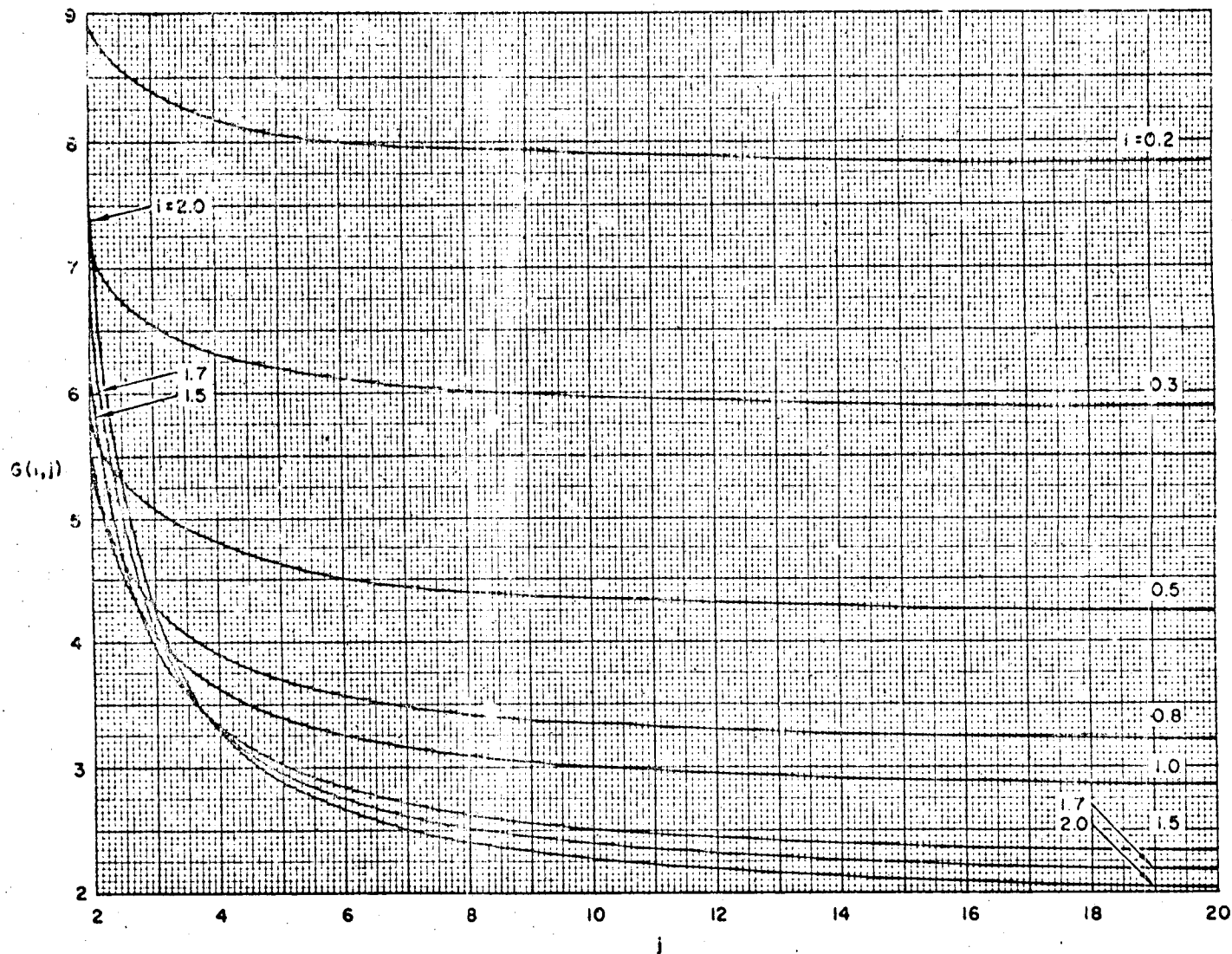


Figure 6a. Function $G(i, j)$ as a Function of j for Various i 's

PLANETARY ENTRY

7-20

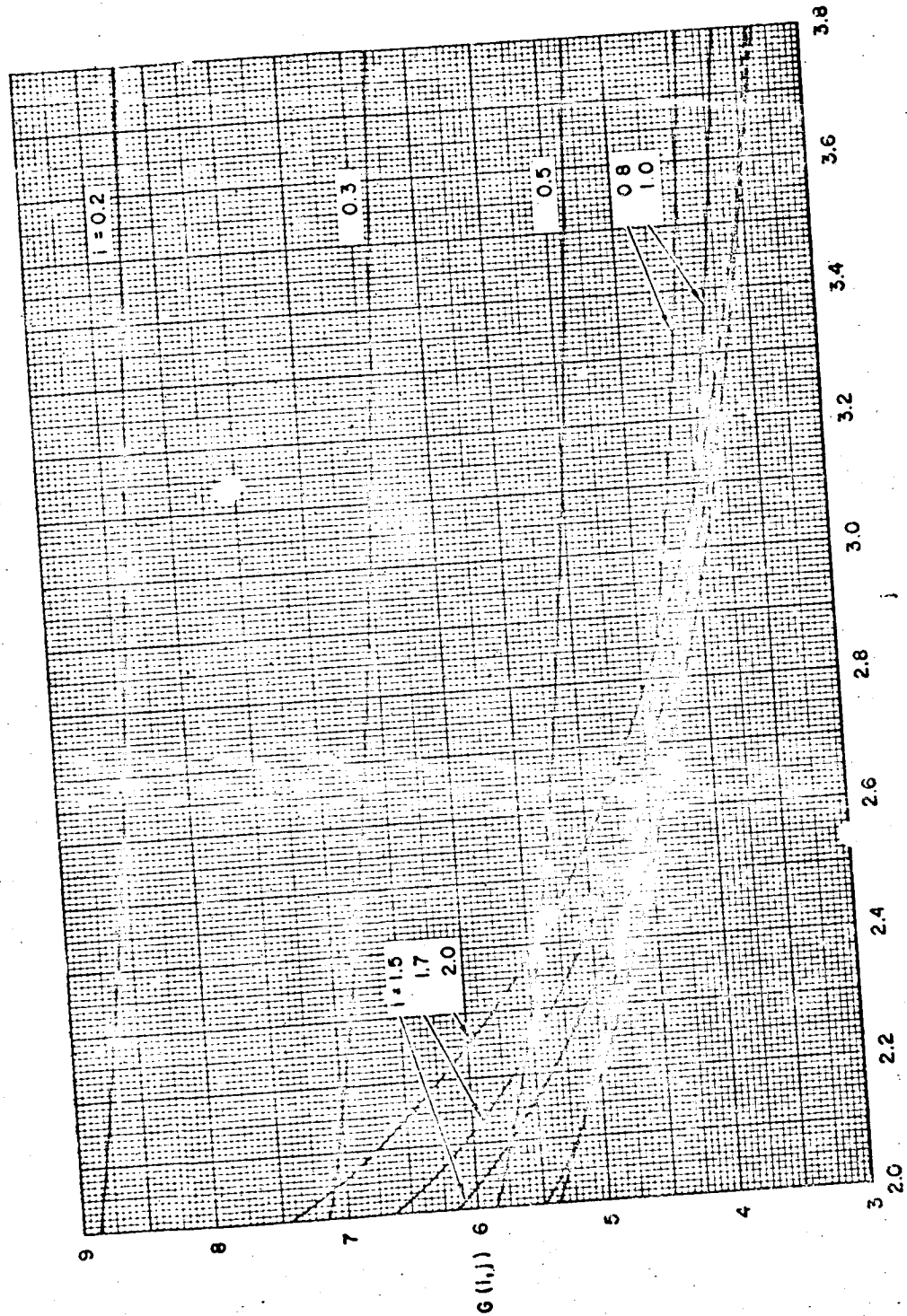


Figure 6b. Function $G(i,j)$ as a Function of j for Various i 's

General Entry Function

7-21

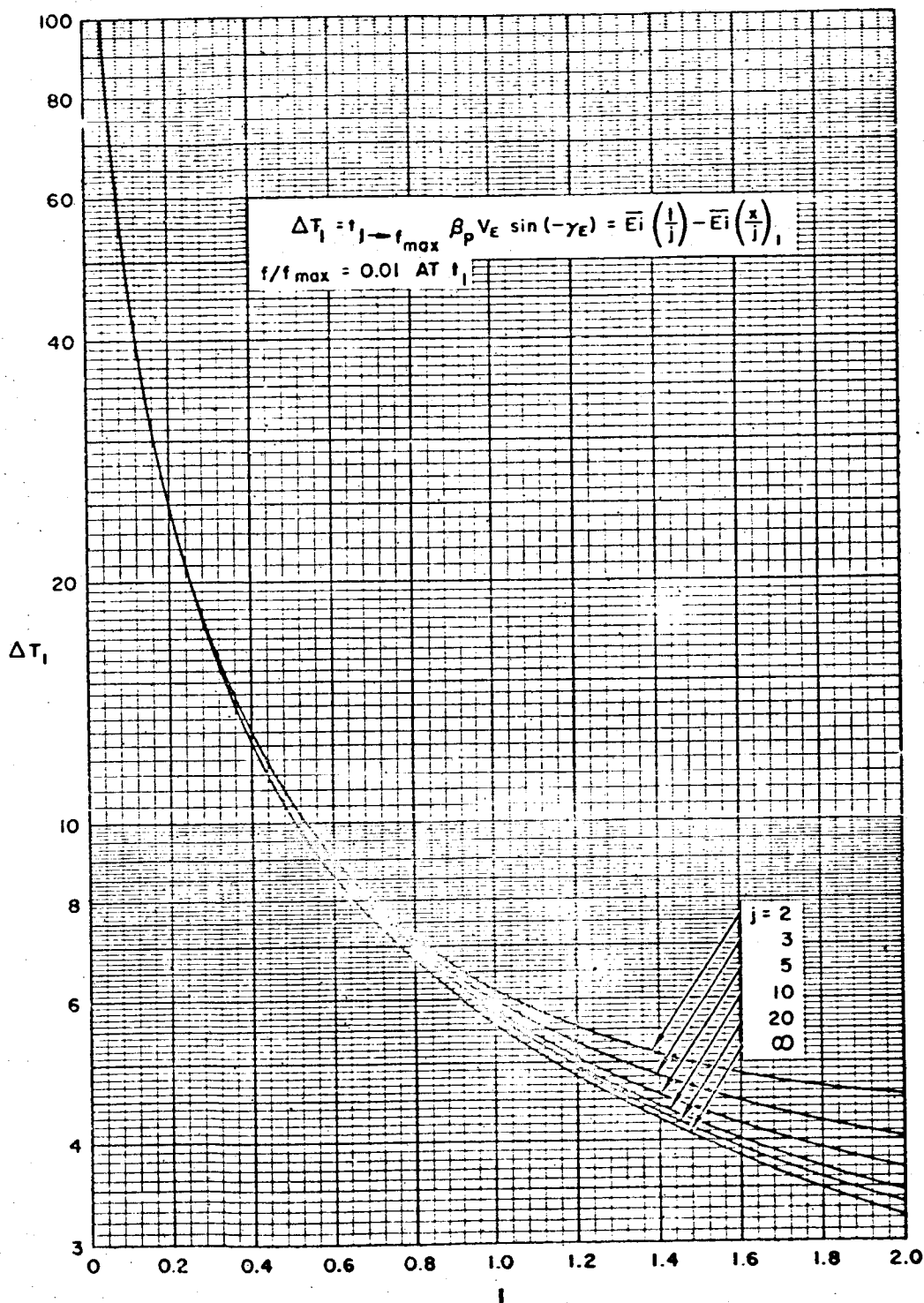


Figure 7. Function for Elapsed Time from $f/f_{\max} = 0.01$ to $f/f_{\max} = 1.0$ as a Function of i and j

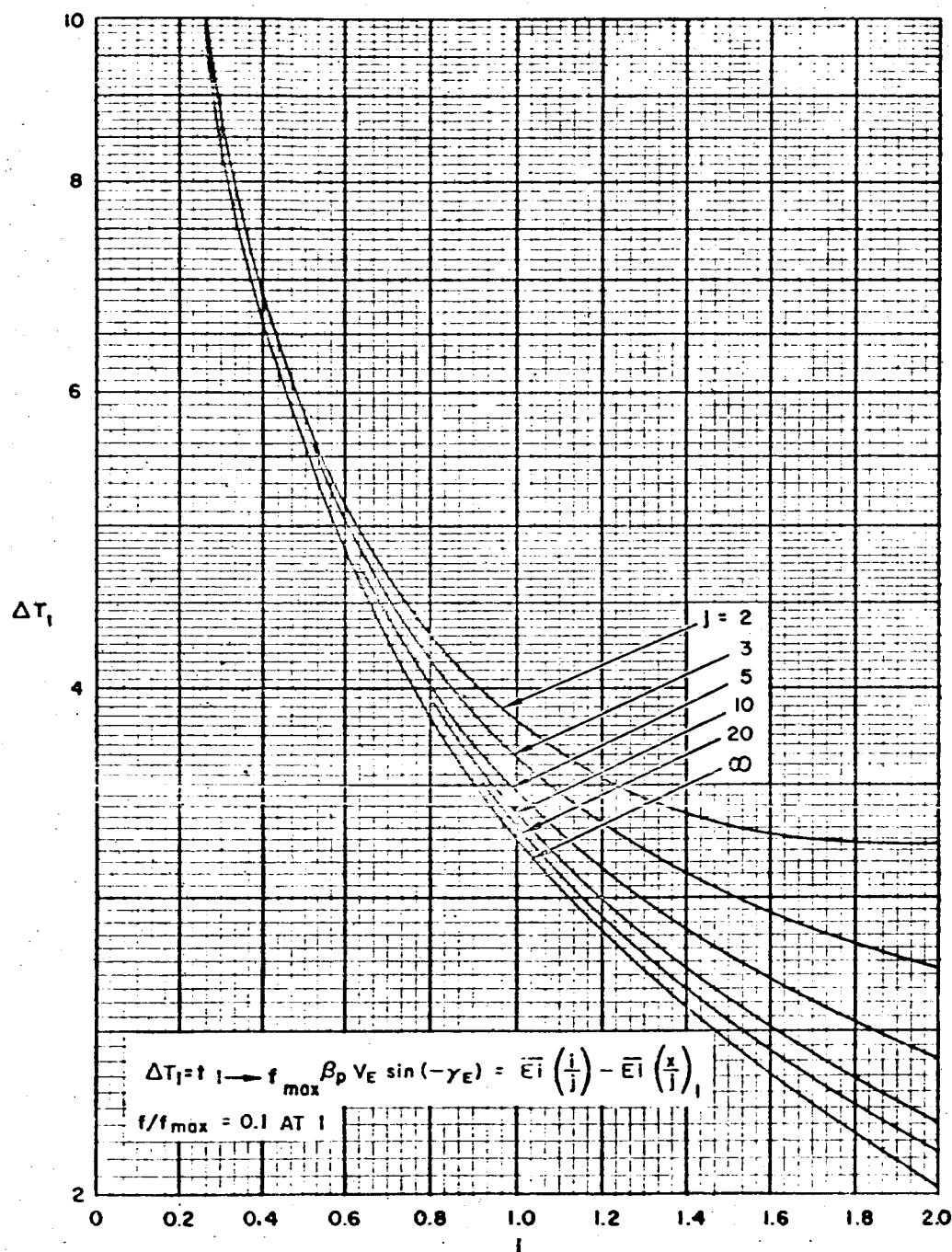


Figure 8. Function for Elapsed Time from $f/f_{\max} = 0.1$ to $f/f_{\max} = 1.0$ as a Function of i and j

General Entry Function

7-23

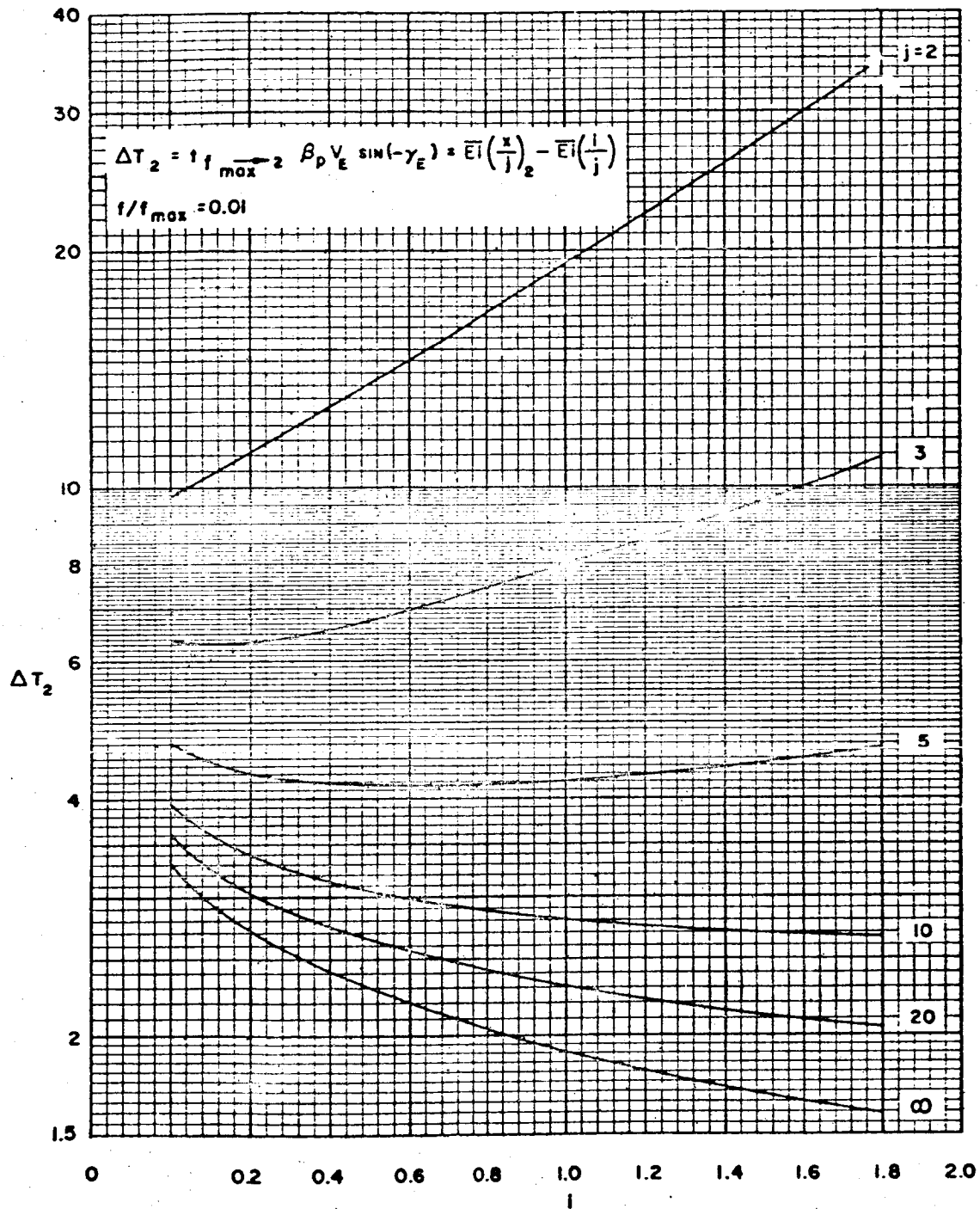


Figure 9. Function for Elapsed Time from $i/f_{\max} = 1.0$ to $i/f_{\max} = 0.01$ as a Function of i and j

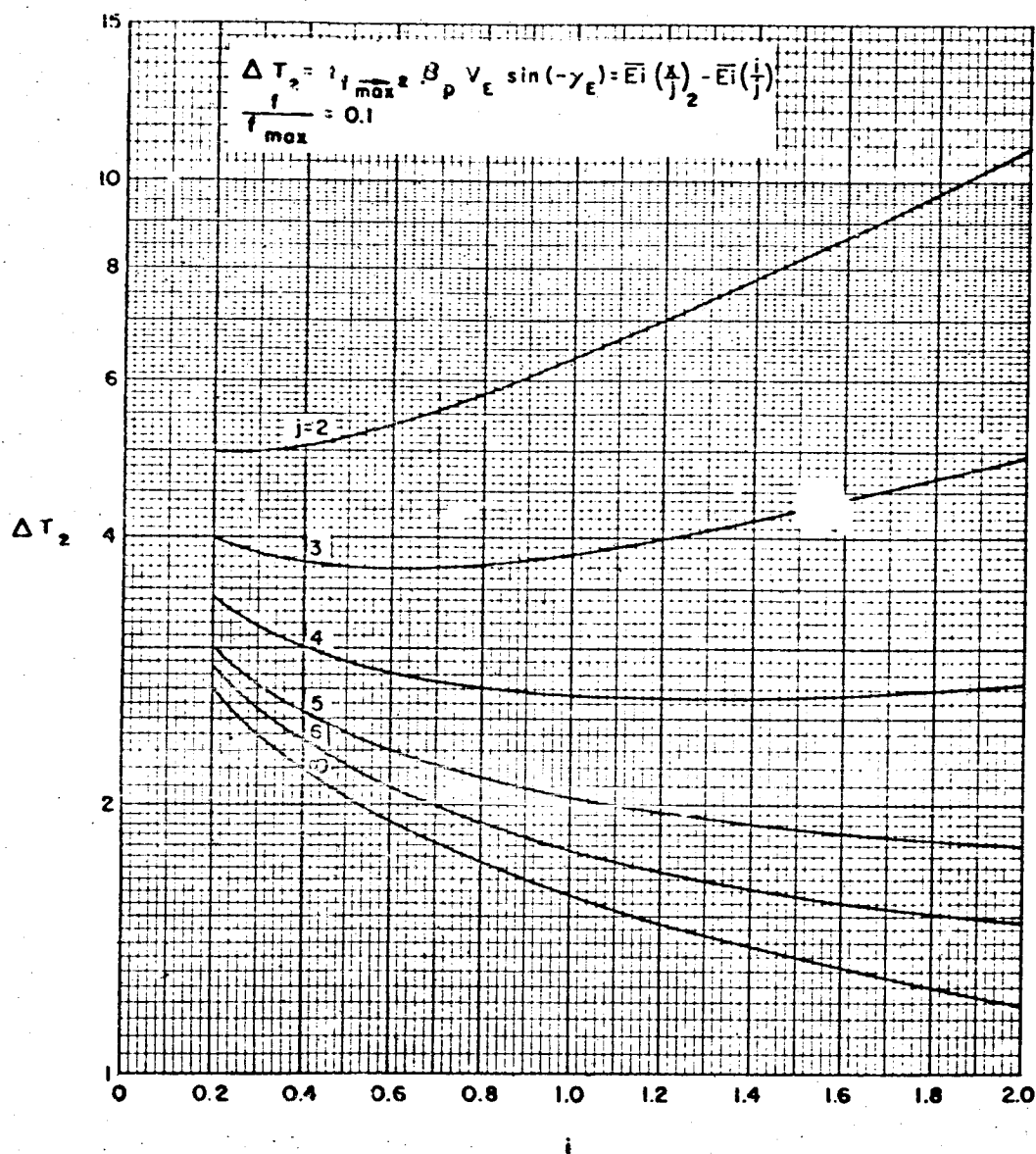


Figure 10. Function for Elapsed Time from $f/f_{\max} = 1.0$ to $f/f_{\max} = 0.1$ as a Function of i and j

From Figure 3, the velocity ratio at maximum stagnation radiant heat rate is 0.92 so that the velocity is 33,120 ft/sec. The altitude for maximum stagnation radiant heat rate is determined from Equation (5) and either an altitude-pressure table or the exponential atmosphere equation

$$p = p_{po} e^{-\beta_p h} = \frac{g_p}{\beta_p} p_{po} e^{-\beta_p h} \quad (18)$$

For entry into the earth's atmosphere, it is more convenient to use an altitude-pressure table. From Equation (5),

$$(p)_{f_{max}} = 2 \times 0.08 \times 1 \times 10 \times \sin 30^\circ = 0.8 \text{ lb/ft}^2 \quad (19)$$

Thus, using the 1959 ARDC model atmosphere tables,¹ the altitude for maximum stagnation radiant heat rate is between 186,000 and 187,000 feet. The magnitude of this maximum is obtained from Equation (9).

$$f_{max} = 0.814 \times 10^{-84} \left(\frac{2 \times 0.08 \times 10 \times \sin 30^\circ}{2.718 \times 23,500 \times 32.174} \right)^{1.7} (36,000)^{21.2} = 40.5 \text{ Btu/ft}^2 \text{ sec} \quad (20)$$

The altitudes between which radiant heat rate is greater than 10 percent of maximum are determined with the aid of Figure 4. The corresponding x values obtained from the figure are 0.2 and 6.2, and the corresponding free stream pressures computed from Equation (6) and the values of x are 0.095 and 2.93 lb/ft². From the atmosphere tables, the desired altitudes are 235,000 and 151,000 feet. The total amount of stagnation radiant heating is computed from Equation (14) and either Figure 5 or 6. The quantity $\beta_p V_E \sin(-\gamma_E)$ is required not only for this computation but also in the determination of time intervals

$$\beta_p V_E \sin(-\gamma_E) = \frac{36,000 \sin 30^\circ}{23,000} = 0.766 \quad (21)$$

From Figure 6, $G(1.7, 21.2) = 2.17$. Thus,

$$F_{total} = \frac{2.17}{0.766} 40.5 = 115 \text{ Btu/ft}^2 \quad (22)$$

The time intervals for radiant heating to go from 1 percent of maximum to maximum and from maximum back to 1 percent are obtained from Figures 7 and 9 and the value of $\beta_p V_E \sin(-\gamma_E)$ computed above.

$$t_{1 \rightarrow f_{\max}} = \frac{\Delta T_1}{\beta_p V_E \sin(-\gamma_E)} = \frac{3.78}{0.766} = 4.95 \text{ sec} \quad (23)$$

and

$$t_{f_{\max} \rightarrow 2} = \frac{\Delta T_2}{\beta_p V_E \sin(-\gamma_E)} = \frac{2.07}{0.766} = 2.72 \text{ sec} \quad (24)$$

A quantity that is of particular interest in the preliminary design of the primary structure of an entry vehicle is the time interval from maximum heating to maximum deceleration. This time interval as well as others may be determined from Figure 2 and Equation (17). For the radiant heating case,

$$t_{1 \rightarrow 2} = \frac{\overline{Ei}(0.5) - \overline{Ei}(0.08)}{0.766} = \frac{0.47 - (-1.87)}{0.766} = 3.06 \text{ sec} \quad (25)$$

If this time of 3.06 seconds is small compared to the thermal time constant of the shell of the vehicle, preliminary design of the structure can be based on ambient temperature properties.

7.4 DECELERATION FOR BALLISTIC TRAJECTORIES

For the purpose of analyzing the motion of a vehicle entering planetary atmospheres along a ballistic path (nonlifting), it is convenient to use the approach established by Allen and Eggers.⁹ The equation of motion in the direction of flight is

$$\frac{dV}{dt} = -\frac{1}{2} \rho V^2 g_c \frac{C_{DA}}{W} - g \sin \gamma \quad (26)$$

in which g_c is the gravitational conversion constant. The flight path angle is at an angle $-\gamma$ with respect to the local horizontal when the altitude is decreasing. For a large class of entries the gravity term can be neglected, since the deceleration due to drag is much higher than the acceleration due to the gravity component. This approximation is good down to velocities and altitudes where the deceleration due to drag has decreased to values of the order of the acceleration of gravity. Involved in the same approximation is the neglect of the equation for acceleration perpendicular to the direction of flight. This approximation is not good for small entry angles of less than about 10 degrees.

The approximation to the atmospheric variation of density with altitude is used:

$$\rho = \rho_0 e^{-\beta h} \quad (27)$$

where ρ_0 and β are given in Section 7.2 on planetary atmospheres and h is the altitude above some reference surface.

The following relations for this simplified ballistic trajectory can be given by

$$\begin{aligned}
 V &= V_E \exp\left(\frac{\rho_0 g_c e^{-\beta h}}{2\beta\Delta \sin \gamma_E}\right) = V_E \exp\left(\frac{g_c}{g_p} \frac{p}{2\Delta \sin \gamma_E}\right) \\
 \frac{dV}{dt} &= -\frac{\rho_0 g_c e^{-\beta h}}{2\Delta} V_E^2 \exp\left(\frac{\rho_0 g_c e^{-\beta h}}{\beta\Delta \sin \gamma_E}\right) = -\frac{\beta p}{2\Delta} \frac{g_c}{g_p} V_E^2 \exp\left(\frac{g_c}{g_p} \frac{p}{\Delta \sin \gamma_E}\right) \\
 &= \beta V_E^2 \sin \gamma_E \left(\frac{V}{V_E}\right)^2 \ln\left(\frac{V_E}{V}\right) \quad (28)
 \end{aligned}$$

where the ballistic parameter is $\Delta = W/C_D A$ in lb/ft^2 , and V_E and γ_E are values at some nominal atmospheric entry altitude, which is often taken as 300,000 feet for the earth. The terms involving p are derived by using $g_p dp = \beta dh$ and the very close approximation $g = g_p$, a constant. It should be noted that dV/dt can be given as a function of only β , V_E , and V/V_E . The maximum value of deceleration is given by

$$\left(\frac{dV}{dt}\right)_{\max} = \frac{\beta V_E^2 \sin \gamma_E}{2e} \quad (29)$$

which occurs at the altitude

$$h = \frac{1}{\beta} \ln\left(\frac{\rho_0 g_c}{\beta\Delta \sin \gamma_E}\right) \quad (30)$$

and the velocity at this point is

$$V = V_E e^{-1/2} \approx 0.61 V_E \quad (31)$$

Values of maximum deceleration for the earth, Mars, and Venus are given in Figure 11 as a function of entry angle and entry velocity.

It is to be noted that the maximum deceleration according to the above equation is independent of Δ . It has been shown, however, by Phillips and Cohen¹⁰ that the maximum deceleration can be decreased by modulating or varying the drag during

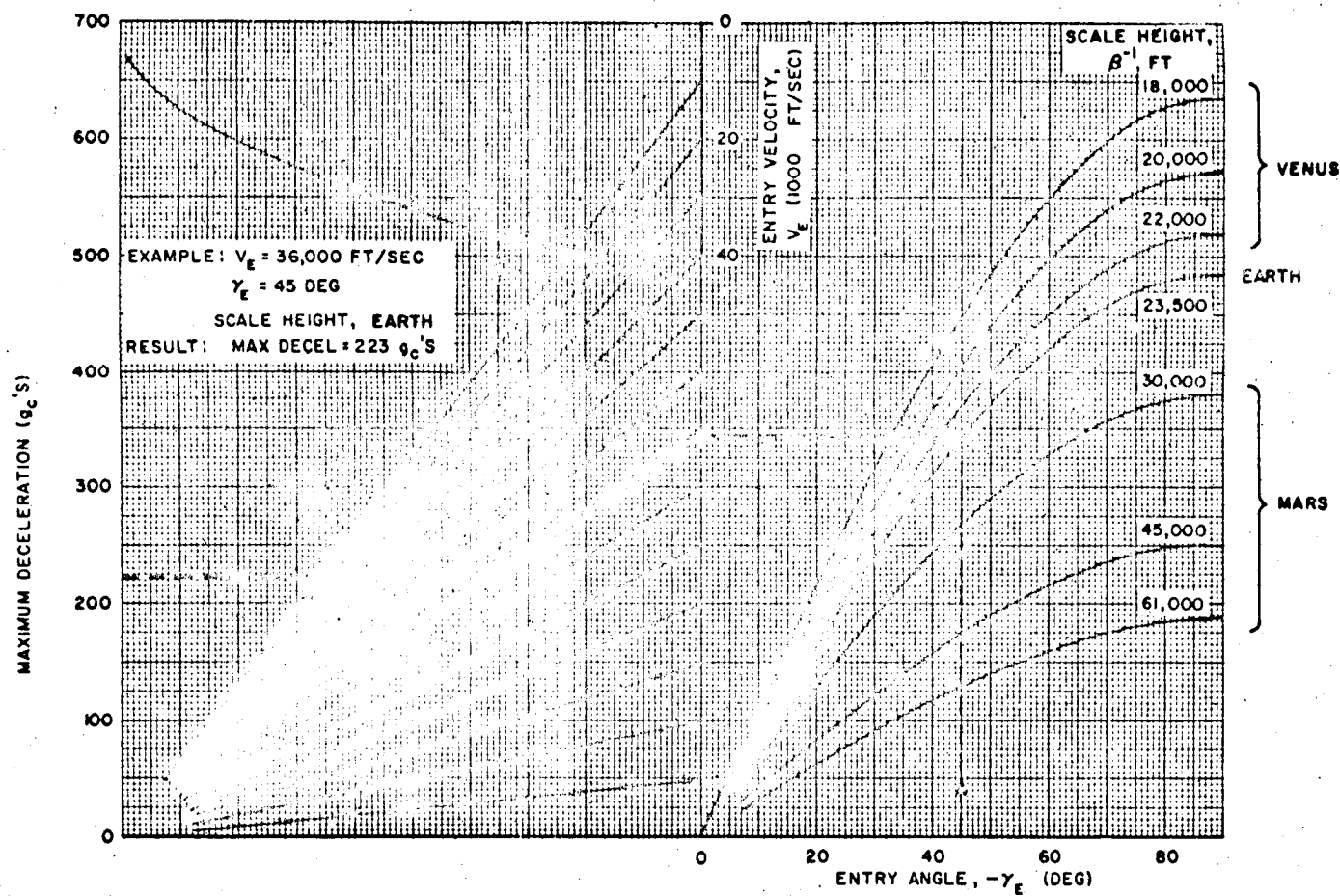


Figure 11. Maximum Deceleration in Earth g 's as a Function of Entry Velocity and Angle for Earth, Venus and Mars

entry. If this is done in one step from a ballistic coefficient of Δ_0 to Δ_1 , a reduction in maximum deceleration expressed by the ratio D_1/D_0 is possible. Here D_1 is the lowest maximum deceleration possible depending on the time of change from Δ_0 to Δ_1 , and D_0 is the maximum deceleration experienced with a constant $\Delta = \Delta_0$. This ratio of D_1/D_0 as a function of Δ_1/Δ_0 , where $D_1/D_0 = \exp \left[\lambda_1 \left(1 - \frac{\Delta_1}{\Delta_0} \right) \right]$ is shown in Figure 12. The value λ_1 in this figure gives the density ρ^* , or altitude, h^* , at which Δ changes from Δ_0 to Δ_1 by the relation

$$\lambda_1 = - \frac{g_c \rho^*}{\Delta_1^\beta \sin \gamma_E} = - \frac{g_c \rho_0 e^{-\beta h^*}}{\Delta_1^\beta \sin \gamma_E} \quad (32)$$

The relation between λ_1 and Δ_1/Δ_0 is

$$\frac{\Delta_1}{\Delta_0} = \frac{1}{\lambda_1} \exp (\lambda_1 - 1) \quad (33)$$

If a variable or continuous change from Δ_0 to Δ_1 is used, it is possible to attain a greater reduction in deceleration. The values of D_1/D_0 attainable as a function of Δ_1/Δ_0 are given in Figure 13. Here $D_1/D_0 = \lambda_0 \exp (1 - \lambda_0)$. The λ_0 value in this figure gives the density, ρ^* , or altitude, h^* , at which drag modulation begins by the relation

$$\lambda_0 = - \frac{g_c \rho^*}{\Delta_0^\beta \sin \gamma_E} = - \frac{g_c \rho_0 e^{-\beta h^*}}{\Delta_0^\beta \sin \gamma_E} \quad (34)$$

The relation between λ_0 and Δ_1/Δ_0 is

$$\frac{\Delta_1}{\Delta_0} = \lambda_0 \exp \left(\frac{1}{\lambda_0} - 1 \right) \quad (35)$$

These figures were obtained from Reference 10 which also contains the analytical background. It should be noted that, although a single step change in drag does not decrease maximum deceleration as much as a continuous modulation, the implementation of such a change would probably be much simpler.

This subject of drag modulation has also recently been treated analytically by Levy¹¹ with a different approach. His results agree with the above results for continuous modulation for earth entry from parabolic velocity at an entry angle of 6 degrees.

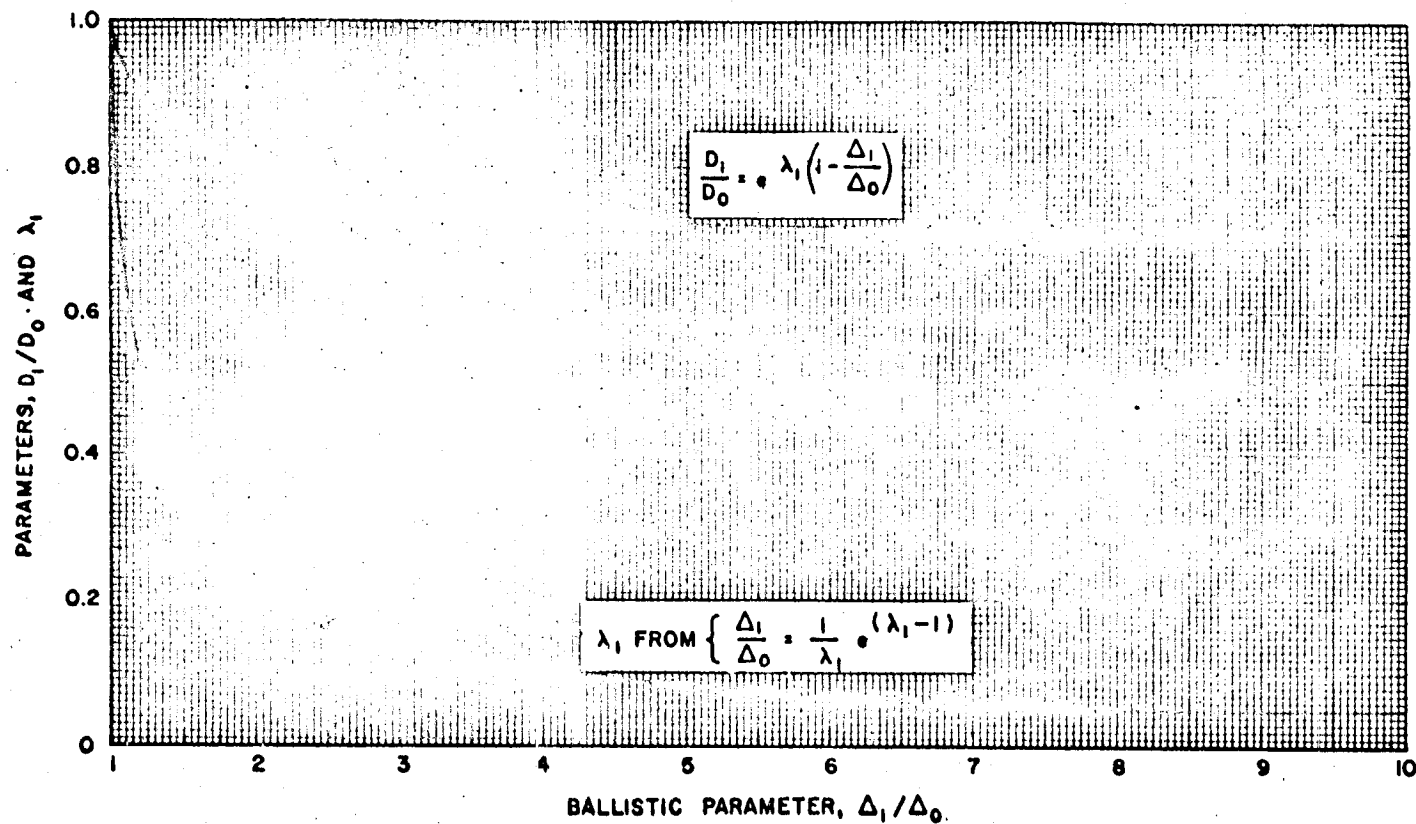


Figure 12. Parameters for Discrete Modulation (Single Step)

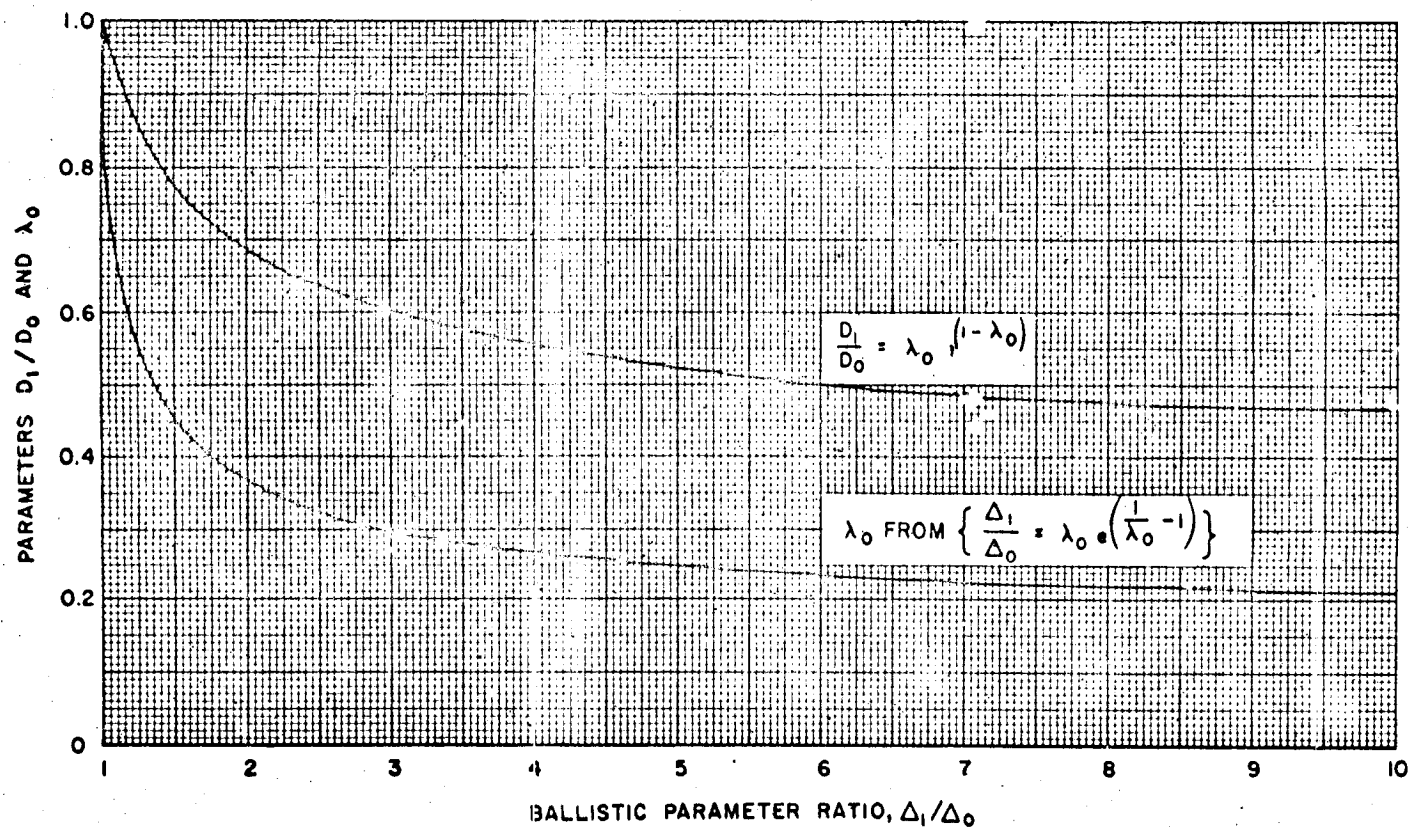


Figure 13. Parameters for Variable Modulation (Continuous)

An example of a vehicle returning to earth from the moon using a drag modulation is shown in Figure 14. This is the result of machine calculations. It can be seen that a decrease in maximum deceleration due to drag modulation allows a steeper entry angle if there is a maximum deceleration criterion imposed by human tolerance.

A more sophisticated method for reducing deceleration is to use a vehicle with lifting capability. This was initially shown by Lees, Hartwig, and Cohen.¹² The application of lift to entry into planetary atmospheres is treated extensively by Chapman.^{2,13}

7.5 HEATING FOR PLANETARY ENTRY

In order to find the amount of material necessary for the heat protection of a vehicle entering a planetary atmosphere, certain approximate formulas will be given for the heating rate and the total heat pulse. These can then be combined with the material properties to give the amount of material required. For the information in this handbook it is assumed that ballistic or nonlifting vehicles are used and that they are relatively blunt, since the missions envisioned do not require high velocities down to sea level. This obviously alleviates the heating problem. The stagnation point heating rate is given, and its applicability to the overall heating problem is then discussed.

7.5.1 Stagnation Point Heating

The cold wall laminar convective heating rate at the stagnation point of a blunt body is given by Lees¹⁴ as

$$q_s = \frac{0.707}{778} \sigma^{-2/3} \frac{1}{\sqrt{R_N}} \sqrt{\frac{R_N \left(\frac{du_e}{dx} \right)_s}{u_\infty}} \sqrt{\rho_{es} \mu_{es}} \sqrt{u_\infty} H_e \quad \text{Btu/ft}^2\text{-sec} \quad (36)$$

where

q_s = stagnation point heat rate (Btu/ft²-sec)

σ = Prandtl number

R_N = nose radius (ft)

$\left(\frac{du_e}{dx} \right)_s$ = stagnation point velocity gradient (1/sec)

u_∞ = free stream velocity (ft/sec)

ρ_∞ = free stream density (slugs/ft³)

ρ_{es} = stagnation point density (slugs/ft³)

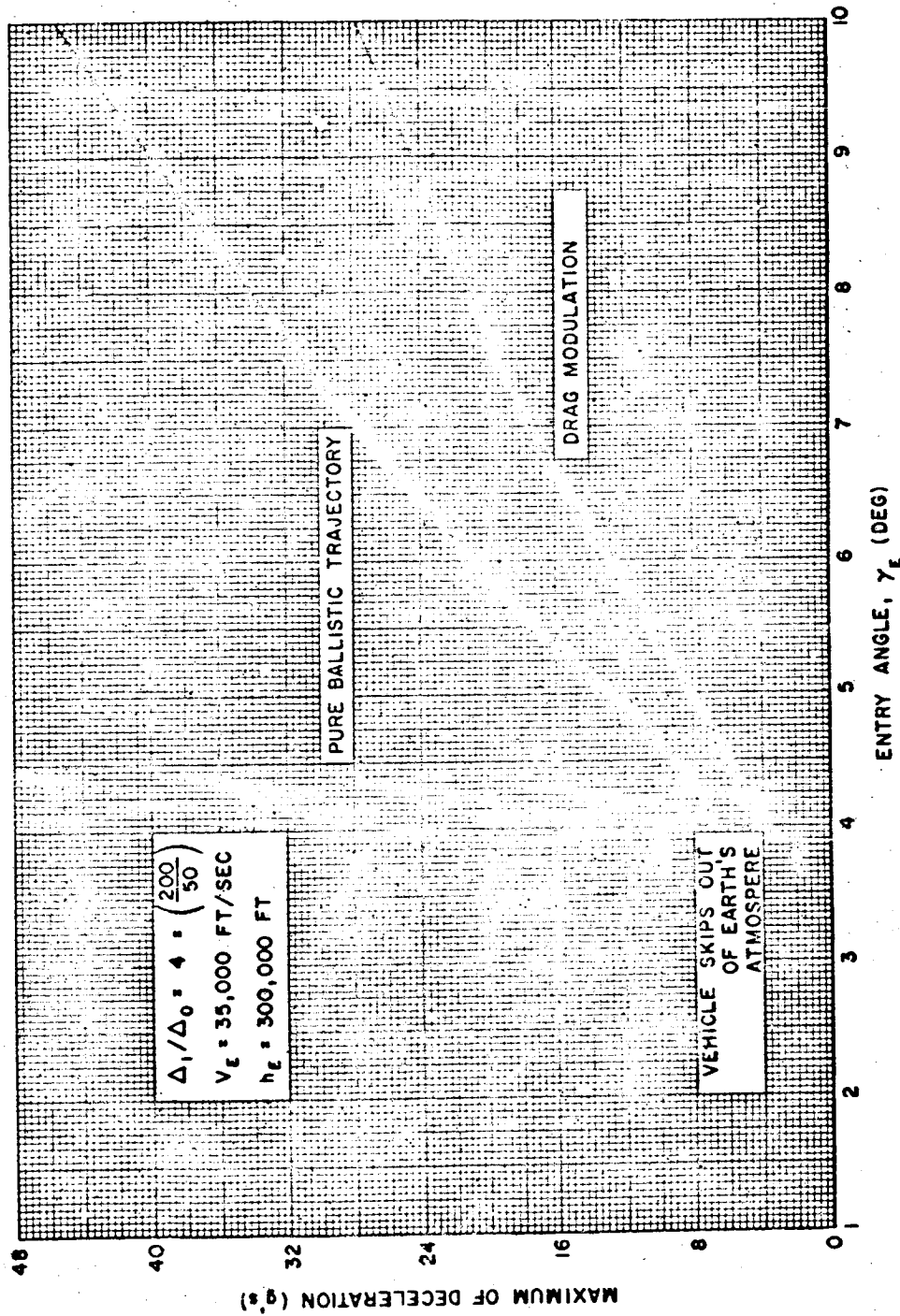


Figure 14. Maximum Deceleration Experienced by a Vehicle Returning from the Moon

μ_{es} = stagnation point viscosity (slugs/ft-sec)

H_e = stagnation enthalpy (ft-lb/slug)

The above system of units is used throughout this section except on the graphs of the gas properties where the units are given.

In the units given after Equation (36), the equation of state for air or nitrogen at the enthalpy levels of interest can be written as

$$\frac{p}{p} = 0.037h^{-0.725} \quad \text{slugs/ft-lb} \quad (37)$$

and the viscosity can be given by

$$\frac{\mu}{p} = 0.922 \times 10^{-10} h^{-0.358} \quad \text{slugs}^2/\text{ft}^2\text{-lb-sec} \quad (38)$$

These properties have been obtained as curve fits to theoretical equilibrium calculations (see Figures 15, 16, 17, and 18). The references from which these properties were obtained are given below.

Gas	Temperature < 3000°K		3000°K ≤ Temperature ≤ 15,000°K	
	Thermodynamic Properties	Viscosity	Thermodynamic Properties	Viscosity
Air	Reference 15	Reference 15	Reference 16	Reference 17
N ₂	Reference 15	Reference 15	Reference 18	
CO ₂	Reference 15	Reference 15	Reference 19	Reference 20

Values of high-temperature viscosity for nitrogen were not located. However, since the molecular weight of nitrogen is nearly that of air, it is assumed that the viscosity of high-temperature nitrogen is the same as for air.²¹ This assumption is supported by the low-temperature values of the viscosity of nitrogen, as shown in Figure 17.

The following approximation for hypersonic flow can be used:

$$H_e = \frac{u_{\infty}^2}{2} \quad \text{ft-lb/slugs} \quad (39)$$

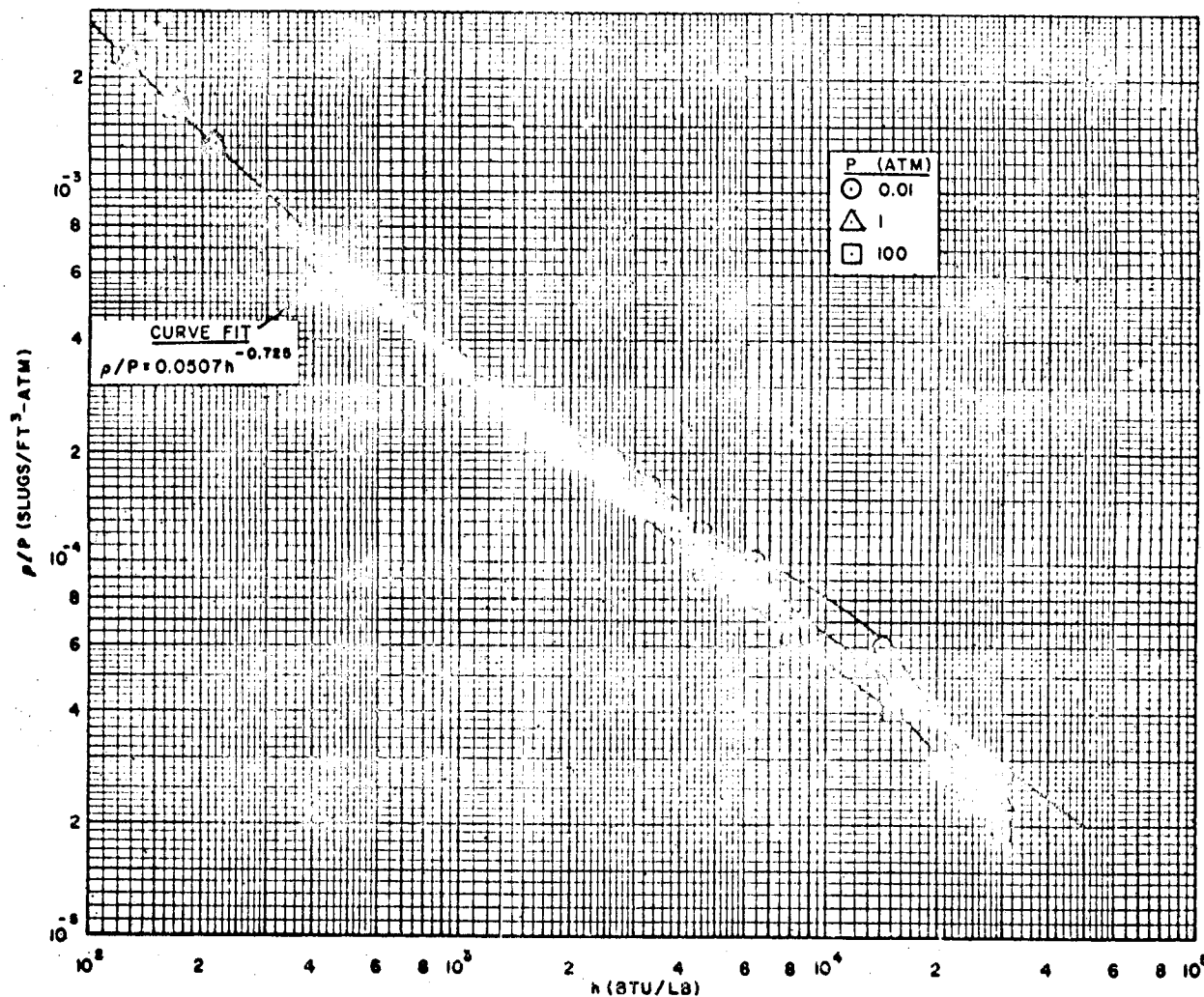


Figure 15. Equation of State for Air

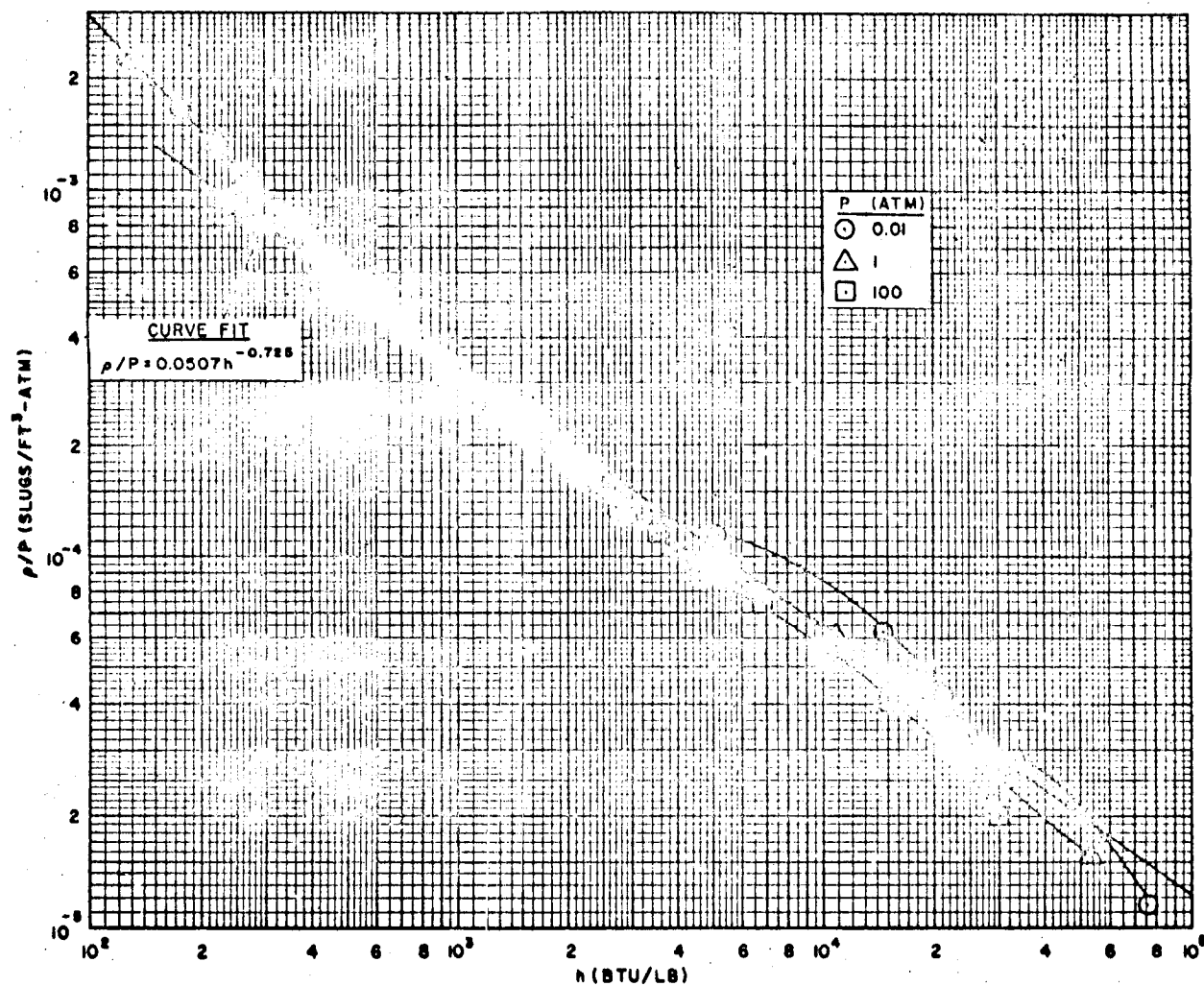


Figure 1.6. Equation of State for Nitrogen

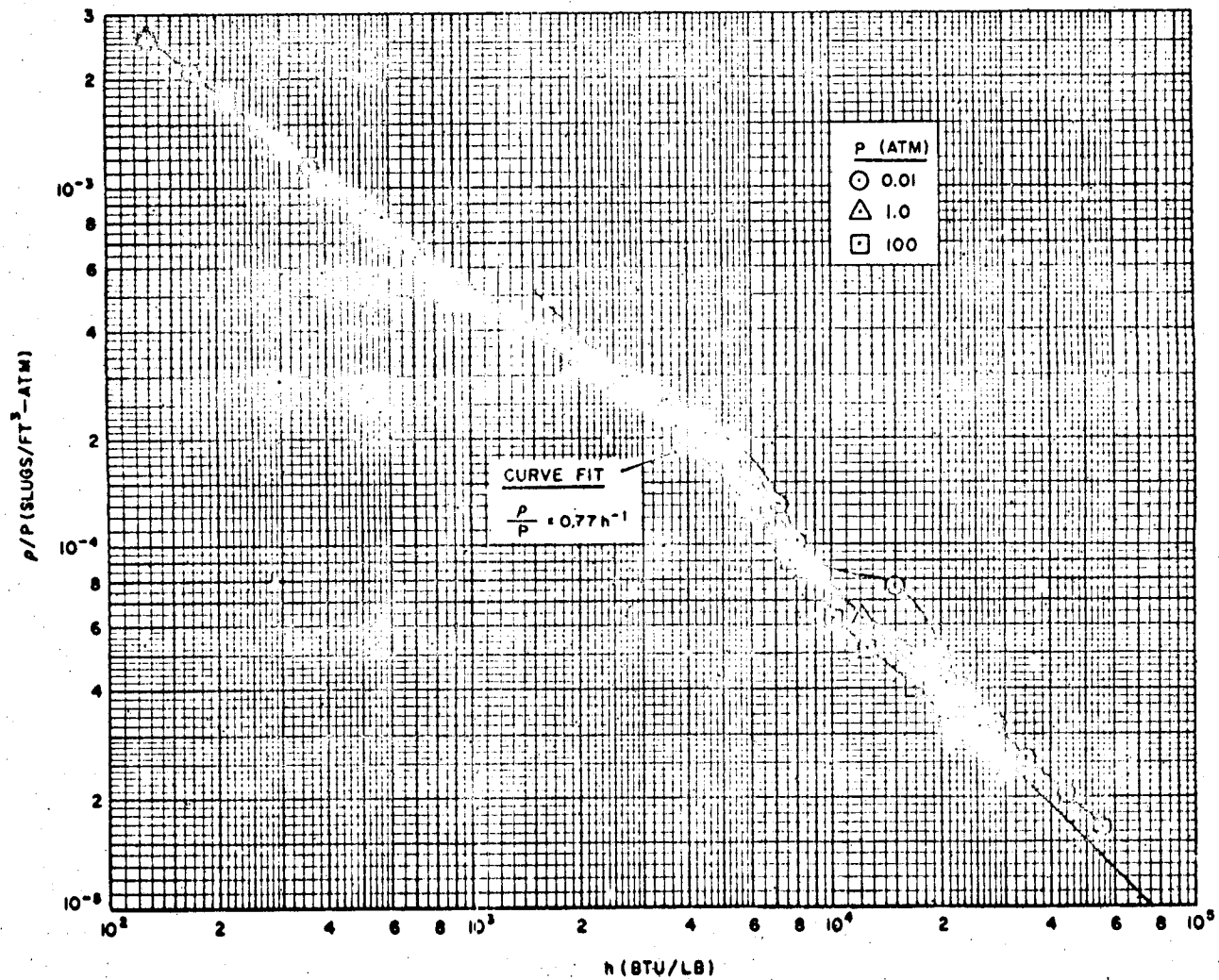


Figure 17. Equation of State for Carbon Dioxide

Heating for Planetary Entry

7-37

RE-ORDER NO. 62-286

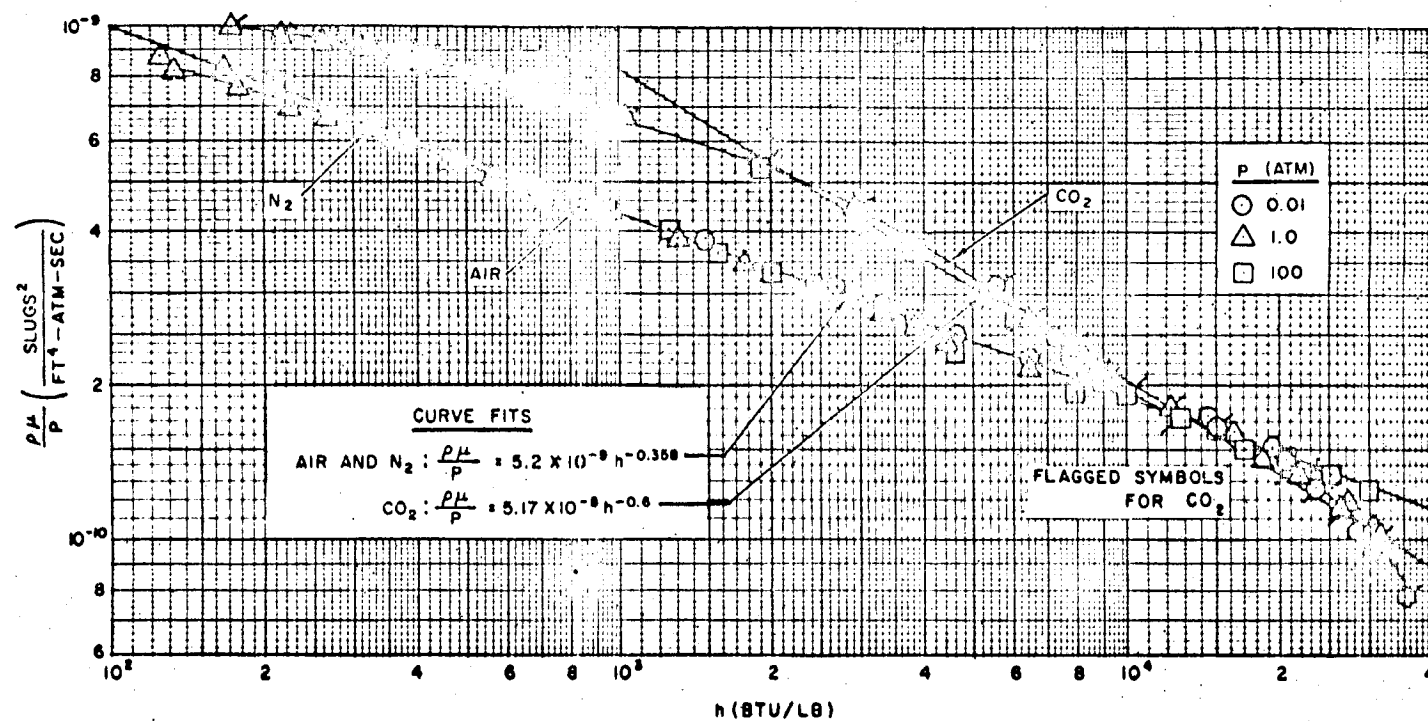


Figure 18. Viscosity of Air, Nitrogen, and Carbon Dioxide

$$p_{es} = \rho_{\infty} u_{\infty}^2 \quad \text{lb/ft}^2 \quad (40)$$

$$R_N \left(\frac{du_c}{u_{\infty}^2} \right)_s = \frac{\sqrt{2}}{u_{\infty}} \sqrt{\frac{p_{es}}{\rho_{es}}} \quad (\text{hemisphere}) \quad (41)$$

Equations (37) through (41) can be applied to Equation (36), assuming $\sigma = 0.71$, to give

$$q_s = \frac{1.48 \times 10^{-8}}{\sqrt{R_N}} \rho_{\infty}^{1/2} u_{\infty}^3 \quad \text{Btu/ft}^2\text{-sec}$$

or in terms of the notation of the previous section where ρ and V are free-stream density and velocity, respectively

$$q_s = \frac{1.48 \times 10^{-8}}{\sqrt{R_N}} \rho^{1/2} V^3 \quad \text{Btu/ft}^2 \text{ sec (air and N}_2\text{)} \quad (42)$$

For a carbon dioxide atmosphere where

$$\frac{\rho}{p} = 9.13 \text{ h}^{-1} \quad \text{slugs/ft-lb} \quad (43)$$

and

$$\frac{\rho \mu}{p} = 1.069 \times 10^{-8} \text{ h}^{-0.6} \quad \text{slugs}^2/\text{ft}^2\text{-lb-sec} \quad (44)$$

the stagnation point heat rate is

$$q_s = \frac{4.19 \times 10^{-8}}{\sqrt{R_N}} \rho^{1/2} V^{2.9} \quad \text{Btu/ft}^2\text{sec (CO}_2\text{)} \quad (45)$$

Since these values are cold wall heat rates, it should be noted that a correction factor may be applied for hot wall heat rates if the wall temperatures are high enough. The correction for an ablation temperature of 1000°R is small, but the correction for an ablation temperature of 5000°R might require a 15 or 20 percent correction at the highest heating rates.

It has been found that the stagnation point heating rate can be used to estimate heating over the entire frontal surface of a blunt entry vehicle. This assumes laminar flow, a factor which will be discussed later. If \bar{q} is the average heating rate

in $\text{Btu/ft}^2/\text{sec}$ and A_s is the surface area of the forward facing surface over which this heating takes place, then, in terms of the stagnation point heating rate, q_s , and the projected frontal area, A_c , the heating can be expressed as

$$\bar{q}A_s = Kq_s A_c \sqrt{\frac{R_N}{R_B}}$$

Here R_N is nose radius and R_B is base radius (base of forward facing part). This treatment is due to Gazley,²² although expressed here in a different form, and is an approximation for the heating on the forward-facing surface of a class of blunt bodies including a hemisphere, sphere-cones, and elliptical shapes. Using References 13 and 23, the value of K was 0.80 for a hemisphere and was accurate within ± 10 percent for a class of bodies including sphere-cones with half cone angles of 15, 20, and 25 degrees, R_N/R_B of 1/3, and an ellipsoid of revolution with a ratio of major to minor axis of 2 or R_N/R_B of 1/2.

Total cold wall convective heating at the stagnation point for air and nitrogen as obtained from Equation (42) is

$$Q = \frac{4.62 \times 10^{-9}}{\sqrt{\beta R_N}} \sqrt{\frac{W}{C_D A}} \frac{V_E^2}{\sqrt{\sin(-\gamma_E)}} \text{ Btu/ft}^2 \text{ (air and N}_2\text{)} \quad (47)$$

and for carbon dioxide as obtained from Equation (45) is

$$Q = \frac{1.345 \times 10^{-8}}{\sqrt{\beta R_N}} \sqrt{\frac{W}{C_D A}} \frac{V_E^{1.9}}{\sqrt{\sin(-\gamma_E)}} \text{ Btu/ft}^2 \text{ (CO}_2\text{)} \quad (48)$$

To use Equations (42), (45), (47), and (48) for the planetary atmospheres given in Section 7.2, it is recommended that the nitrogen formulas be used for atmospheres that are approximately 90 percent nitrogen, and that the carbon dioxide formulas be used for the atmosphere that is approximately 90 percent carbon dioxide. For one of the assumed cases for Venus of half nitrogen and half carbon dioxide, a formula is not available.

7.5.2 Boundary Layer Transition

Since the above formulas for estimating heat rates have been based on a laminar boundary layer, it is of interest to consider the range of flight and configuration parameters where this is valid.

The Reynolds number Re_x , based on conditions at the edge of the boundary layer and distance from the stagnation point along the surface, is

$$Re_x = \frac{\rho_e u_e x}{\mu_e} \quad (49)$$

Using the previously given relations for ρ , p , and μ for air and

$$h_e = H_e - \frac{u_e^2}{2} = \frac{u_\infty^2}{2} \left(\frac{p_e}{p_{es}} \right)^{\frac{\bar{\gamma}-1}{\bar{\gamma}}} \quad (50)$$

where $\bar{\gamma} \approx 1.2$

$$Re_x = 3.17 (10^7) \rho V^{0.816} \left(\frac{p_e}{p_{es}} \right)^{0.816} \left[1 - \left(\frac{p_e}{p_{es}} \right)^{1/6} \right]^{1/2} x \quad (51)$$

This is of the form $f = K\rho^i V^j$ for a given position (p_e/p_{es} , x) on the body which is of a class of general entry functions discussed in Section 7.3. It is therefore possible to give immediately the maximum Reynolds number for a particular entry trajectory (V_E , γ_E) and configuration (W/C_{DA} , R_N). For a hemisphere the maximum Reynolds number with $p_e/p_{es} = \sin^2 \theta_b$ is at about $\theta_b = 40$ or 50 degrees from the nose, and

$$\left\{ \left(\frac{p_e}{p_{es}} \right)^{0.816} \left[1 - \left(\frac{p_e}{p_{es}} \right)^{1/6} \right]^{1/2} x \right\}_{\max} = 0.138 R_N \quad (52)$$

where R_N is the nose radius in feet. For this case the maximum Reynolds number is then

$$Re_{x_{\max}} = 5.2 (W/C_{DA}) \sin(-\gamma_E) V_E^{0.816} R_N \quad (53)$$

A transition Reynolds number of 5×10^5 can be used. Thus, for an earth entry at escape velocity the condition for maintaining a Reynolds number below this transition value is

$$W/C_D A \sin(-\gamma_E) R_N < 18.4 \quad (54)$$

Thus, for a 45-degree entry with a nose of 2 feet and a $W/C_D A$ of 13 lb/ft², the boundary layer would be laminar all the way. This is somewhat conservative since maximum Reynolds number is not attained until the heating rate has passed its maximum and has decreased to about 25 percent of its maximum. This can be seen from Figure 2 of Section 7.3. That is to say, that at maximum heating the maximum Reynolds number on the body is about one-half of what it will be when the heating rate is decreased to 25 percent of its maximum.

7.5.3 Radiation Heating

Heating due to radiation from the hot gas behind the shock wave cannot be calculated with accuracy even for the earth's atmosphere. However, it is of interest to consider it since its dependence on configuration and entry conditions for planetary atmospheres will be functionally similar.

Fitting the data of Yoshikawa and Wick,²⁴ which is dependent on the Av data of Reference 25, the following expression for equilibrium radiant heat is obtained:

$$q_R = 0.814 \times 10^{-84} R_N^{1.7} v^{21.2} \text{ Btu/ft}^2 \text{ sec} \quad (55)$$

This equation depends on fitting the above data for velocities from 29,000 to 36,000 ft/sec which is the range in which most of the radiant heat pulse takes place at escape velocity. A similar expression is given in Reference 26. This then gives a total heating of

$$Q_R = 0.34 \times 10^{-91} R_N (W/C_D A)^{1.7} \sin^{0.7}(-\gamma_E) V_E^{20.2} \text{ Btu/ft}^2 \quad (56)$$

In Figure 19 the total radiation heating of Equation (56) is compared with the total stagnation point convective heating of Equation (47) for an entry velocity of 35,000 ft/sec. The dependence of the relative magnitude of these values on the vehicle configuration (R_N , $W/C_D A$) and entry conditions (γ_E , V_E) can be seen. It should be noted that this was done for the earth's atmosphere. However, it can be seen that radiation heating becomes relatively more important as R_N and $W/C_D A$ increase. The strong dependence on velocity is, of course, significant.

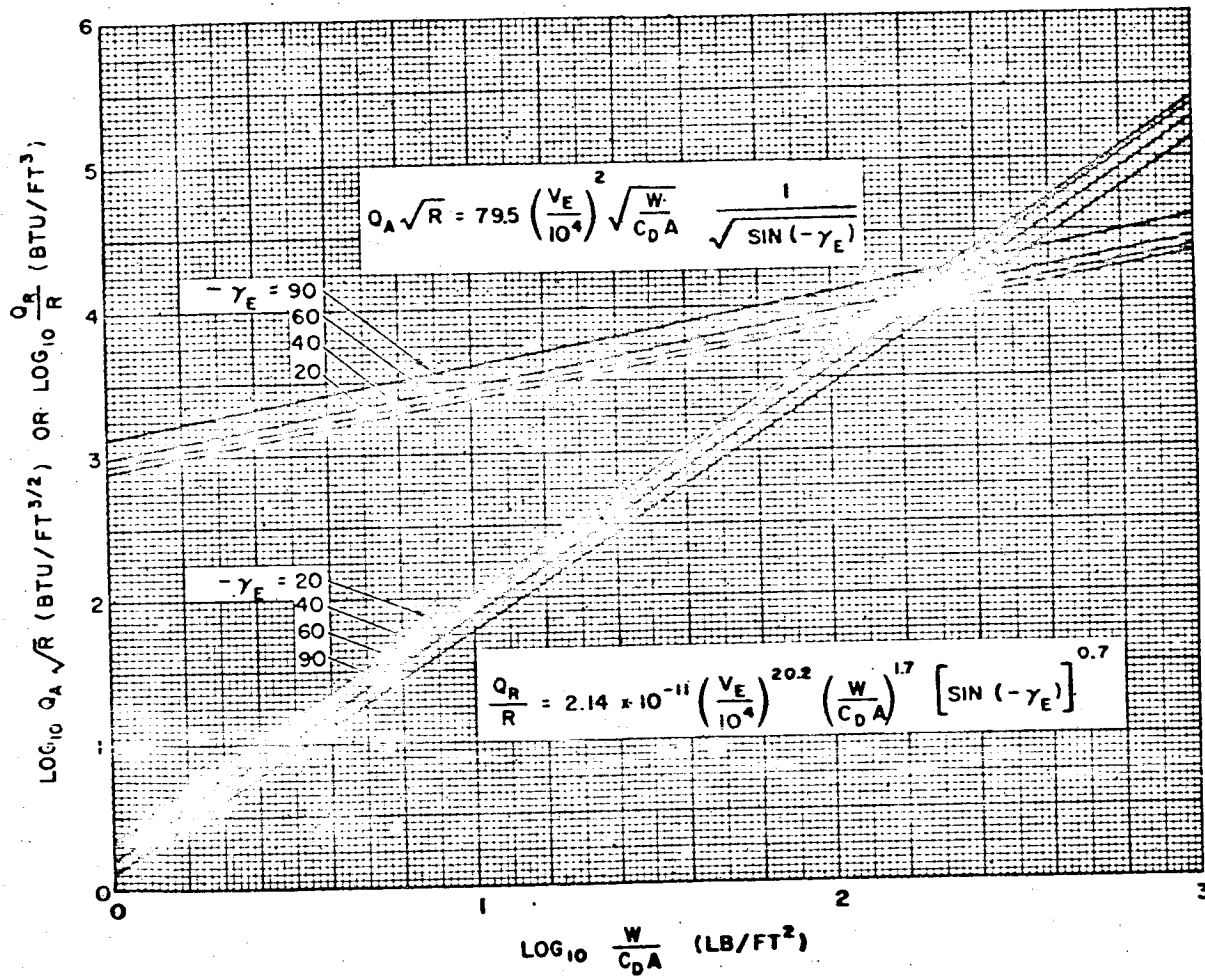


Figure 19. Stagnation Point, Total Heating (Radiation and Aerodynamic)

NOMENCLATURE

A	Reference area for aerodynamic coefficients, ft^2
A_c	Projected frontal area, ft^2
A_s	Surface area of forward facing surface, ft^2
C_D	Drag coefficient, $D/\frac{1}{2}\rho V^2 A$, dimensionless
F	Integral of general entry function, Equation (11)
F_{total}	Integral of general entry function from entry to impact, Equation (13)
f	General entry function, Equation (1)
$G(i, j)$	Function relating F_{total} and f_{max} , Figure 5, $\left(\frac{e}{i} \frac{j}{j-1}\right)^i \Gamma(i)$
g	Local acceleration of gravity, ft/sec^2
g_c	Gravitational conversion constant, $32.174 \text{ ft}/\text{sec}^2$
g_o	Acceleration of gravity at surface of planet, ft/sec^2
g_p	Acceleration of gravity for planet, ft/sec^2
H	Scale height of atmosphere, β^{-1} , ft
H_e	Stagnation enthalpy at edge of boundary layer, $\text{ft-lb}/\text{slug}$
h	Static enthalpy, $\text{ft-lb}/\text{slug}$; altitude above reference surface, ft
h_e	Static enthalpy at edge of boundary layer, $\text{ft-lb}/\text{slug}$
i	Exponent of ρ in the general entry function, Equation (1)
j	Exponent of V in the general entry function, Equation (1)
K	Constant in the general entry function, Equation (1)
	Constant relating stagnation heat rate to total heat rate, Equation (46)
M_m	Surface mass pressure, slugs/ft^2
M	Average molecular weight
p	Static pressure, free stream value in trajectory equations, lb/ft^2
p_e	Static pressure at edge of boundary layer, lb/ft^2
p_{es}	Total pressure at edge of boundary layer, lb/ft^2
p_o	Pressure at surface of planet, lb/ft^2
Q	Total convective heating over trajectory, Btu/ft^2
Q_R	Total radiation heating over trajectory, Btu/ft^2

Nomenclature

7-45

q	Heating rate, Btu/ft ² sec
\bar{q}	Average heating rate over frontal surface, Btu/ft ² sec
q_s	Convective heating rate at stagnation point, Btu/ft ² sec
q_R	Radiative heating rate at stagnation point, Btu/ft ² sec
R	Universal gas constant, ft-lb/mole °R
R_B	Radius of base of front-facing part of vehicle, i. e., radius of maximum cross-sectional area, ft
Re_x	Reynolds number based on distance from stagnation point, dimensionless
R_N	Nose radius, ft
T	Temperature, °R
T_o	Temperature at surface of planet, °R
t	Time, sec
t_{1-2}	Elapsed time from 1 to 2, sec
u_e	Flow velocity at edge of boundary layer, ft/sec
u_∞	Free stream velocity, ft/sec
V	Velocity of vehicle, therefore free stream velocity, ft/sec
V_E	Entry velocity, ft/sec
W	Weight of vehicle, lb
x	Parameter in general entry function analysis, Equation (6)
$\left(\frac{du_c}{dx}\right)_s$	Stagnation point velocity gradient, 1/sec
β	Reciprocal of scale height of atmosphere, 1/ft
$\Gamma(i)$	Gamma function
γ	Flight path angle, positive up from local horizontal, deg or radians
γ_E	Entry flight path angle, deg or radians
$\bar{\gamma}$	Effective ratio of specific heats
Δ	Ballistic parameter, $W/C_D A$, lb/ft ²
Δ_o	Ballistic parameter before modulation, lb/ft ²
Δ_1	Ballistic parameter after modulation, lb/ft ²
Δ_T	Elapsed time function, dimensionless, Figures 7 to 10

λ_0, λ_1	Parameters in drag modulation
μ	Gas viscosity, slugs/ft sec
μ_{es}	Stagnation point viscosity, slugs/ft sec
ρ	Gas density, slugs/ft ³
ρ_{es}	Stagnation point density, slugs/ft ³
ρ_0	Density of atmosphere at reference surface, slugs/ft ³
ρ_s	Density of atmosphere at surface of planet, slugs/ft ³
ρ_∞	Free stream density, slugs/ft ³
σ	Prandtl number

REFERENCES

1. R.A. Minzner, K.S.W. Champion and H.L. Pond, "The ARDC Model Atmosphere, 1959," AFCRC-TR-59-267, Air Force Surveys in Geophysics No. 115, August 1959.
2. Dean R. Chapman, "An Approximate Analytical Method for Studying Entry into Planetary Atmospheres," NASA TR R-11, 1959.
3. Data on Martian Atmosphere Supplied by the Jet Propulsion Laboratory.
4. G. deVaucouleurs and D. Menzel, "Results of the Occultation of Regulus by Venus," Nature, Vol. 188, No. 4744, October 1, 1960, pp. 28-33.
5. Lewis D. Kaplan, "A New Interpretation of the Structure and CO₂ Content of the Venus Atmosphere," RAND Corporation P-2213, February 2, 1961, Revised May 2, 1961.
6. A. Ambrosio, "A General Atmospheric Entry Function and its Characteristics," Space Technology Laboratories, Inc., 8989-0001-NU-000, August 4, 1961.
7. E. Jahnke and F. Emde, Tables of Functions, Dover Publications, 1945.
8. "Sine, Cosine, and Exponential Integrals," Arguments Between Zero and 2 at Intervals of 0.0001, Vol. I. A.N. Lowan, Technical Director, Works Progress Administration, New York, 1940; Reprinted by Western Periodicals Co., North Hollywood, California, 1956.
9. H. Julian Allen and A. J. Eggers, Jr., "A Study of the Motion and Aerodynamic Heating of Ballistic Missiles Entering the Earth's Atmosphere at High Supersonic Speeds," NACA Report 1381, 1958.
10. Richard L. Phillips and Clarence B. Cohen, "Use of Drag Modulation to Reduce Deceleration Loads During Atmospheric Entry," GM-TR-0165-00352, Space Technology Laboratories, Inc., April 9, 1958; also, American Rocket Society Journal, Vol. 29, No. 6, June 1959, pp. 414-422.

References

7-47

REFERENCES (Continued)

11. Lionel L. Levy, "An Approximate Analytical Method for Studying Atmosphere Entry of Vehicles with Modulated Aerodynamic Forces," NASA TN D-319, October 1960.
12. Lester Lees, Frederic W. Hartwig, and Clarence B. Cohen, "The Use of Aerodynamic Lift During Entry into the Earth's Atmosphere," GM-TR-0165-00519, Space Technology Laboratories, Inc., November 20, 1958; or ARS Reprint 785-59, ARS Controllable Satellites Conference, M.I.T., April 30 - May 1, 1959.
13. Dean R. Chapman, "An Analysis of the Corridor and Guidance Requirements for Supercircular Entry into Planetary Atmospheres," NASA TR-55, 1959.
14. Lester Lees, "Laminar Heat Transfer over Blunt-Nosed Bodies at Hypersonic Flight Speeds," Jet Propulsion, Vol. 27, No. 4, April 1956, pp. 259-269.
15. J. Hilsenrath and C. W. Becket, etc., "Tables of Thermal Properties of Gases," NBS Circular 564, November 1955.
16. W. E. Moeckel and K. C. Weston, "Composition and Thermodynamic Properties of Air in Chemical Equilibrium," NACA TN 4265, April 1958.
17. C. F. Hansen, "Approximations for the Thermodynamic and Transport Properties of High-Temperature Air," NACA TN 4150, March 1958.
18. R. L. Humphrey, W. J. Little and L. A. Seeley, "Mollier Diagram for Nitrogen," AEDC-TN-60-83, May 1960.
19. J. L. Raymond, "Thermodynamic Properties of the Atmosphere of Venus," RAND RM-2292, November 1958.
20. M. Thomas, "Transport Properties of High Temperature Gases," Douglas Aircraft Company, Engineering Paper No. 1161, March 1961.
21. S. Chapman and T. G. Cowling, The Mathematical Theory of Non-uniform Gases, Cambridge at the University Press, 1960, pp. 230-233.
22. Carl Gazley, Jr., "Atmospheric Entry of Manned Vehicles," Proceedings of the Manned Space Stations Symposium, Los Angeles, California, April 20-22, 1960, pp. 14-25.
23. R. W. Detra and H. Hidalgo, "Generalized Heat Transfer Formulae and Graphs," Research Report 72, Avco Research Laboratory, March 1960. (First published as Research Note 72, May, 1958.)
24. K. K. Yoshikawa and B. H. Wick, "Radiative Heat Transfer During Parabolic Atmospheric Entry Velocity," NASA Technical Note, D-1074, November 1961.
25. B. Kivel and K. Bailey, "Tables of Radiation from High Temperature Air," Research Report 21, Avco Research Laboratory, December 1957.
26. Uriel M. Lovelace, "Charts Reporting Kinematic and Heating Parameters for a Ballistic Re-entry at Speeds of 26,000 and 45,000 feet per second," NASA TN D-968, October 1961

APPENDIX A

VEHICLE PERFORMANCE ESTIMATION TECHNIQUES

1 ORBITAL MISSION REQUIREMENTS

The equations used in the development of the data presented in this section are derived from Kepler's equations. For coplanar orbital transfer, a Hohmann transfer was assumed (see Figure A-1). The effects of having finite burning times are assumed to be negligible since all powered flight occurs at angles very nearly equal to 90 degrees.

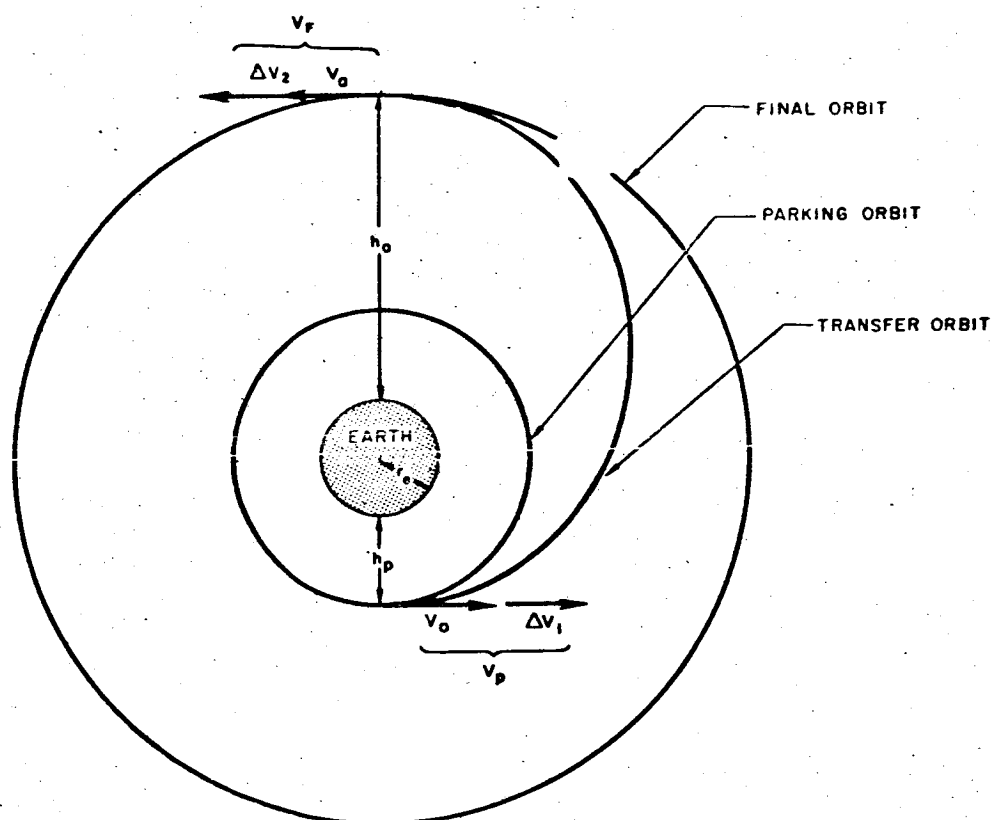


Figure A-1. Hohmann Transfer Maneuver

1.1 Velocity Versus Altitude

Perigee velocity as a function of perigee altitude and orbital eccentricity is

$$v_p = \sqrt{\frac{\mu_e(1+e)}{h_p + r_e}} \quad (\text{A.1})$$

VEHICLE PERFORMANCE ESTIMATION TECHNIQUES

1.2 Orbital Period Versus Altitude

Orbital period as a function of perigee altitude and orbital eccentricity is

$$P = 2\pi \sqrt{\frac{(r_e + h_p)^3}{\mu_e (1 - e)^3}} \quad (A.2)$$

1.3 Hohmann Transfer

For the Hohmann transfer maneuver (see Figure A-1), an impulsive incremental velocity, ΔV_1 , is added tangentially while in a circular parking orbit. The point of execution corresponds to the perigee of the transfer orbit. At apogee of the transfer orbit a second incremental impulsive velocity, ΔV_2 , of sufficient magnitude to circularize the orbit, is added.

ΔV_1 ,

$$\Delta V_1 = \sqrt{\frac{2\mu_e}{h_p + r_e} \left(\frac{h_a + r_e}{h_a + h_p + 2r_e} \right)} - \sqrt{\frac{\mu_e}{h_p + r_e}} \quad (A.3)$$

ΔV_2 ,

$$\Delta V_2 = \sqrt{\frac{\mu_e}{h_a + r_e}} - \sqrt{\frac{2\mu_e}{h_a + r_e} \left(\frac{h_p + r_e}{h_a + h_p + 2r_e} \right)} \quad (A.4)$$

ΔV_T ,

$$\Delta V_T = \Delta V_1 + \Delta V_2 \quad (A.5)$$

The time required to accomplish the maneuver (transit time from perigee to apogee of transfer orbit), T , is

$$T = \frac{\pi}{2\sqrt{2\mu_e}} (h_a + h_p + 2r_e)^{3/2} \quad (A.6)$$

2 VELOCITY LOSS ESTIMATION

This section presents the analytical and empirical analysis used to determine expressions representing vehicle velocity losses which in turn are used to determine vehicle performance characteristics.

An analysis of the equations of motion of a vehicle thrusting in the atmosphere will indicate a complicated set of differential equations which require a digital computer for exact solutions. However, investigation of each term of the equations

Velocity Loss Estimation

A-3

will provide information indicating the effects of gravity and atmospheric losses on the overall vehicle performance. This type of examination usually leads to expressions representing empirical data generated in past studies.

On the other hand, the equations of motion of stages that operate out of the atmosphere can be integrated in closed form after certain simplifying assumptions have been made. Thus, the precise upper stage performance estimation is based on a purely analytical technique.

The equations of motion of a vehicle thrusting in the earth's atmosphere are

$$m\dot{V} = T_h \cos \alpha - mg_e \left(\frac{r_e}{r_h} \right)^2 \cos \beta - D \quad (A.7)$$

$$mV\dot{\beta} = mg_e \left(\frac{r_e}{r_h} \right)^2 \sin \beta - T_h \sin \alpha - m \frac{V^2 \sin \beta}{r_h} \quad (A.8)$$

It is assumed that a vehicle thrusting in the atmosphere will have a pitch program that follows a gravity turn (zero angle of attack). Thus, Equations (A.7) and (A.8) become

$$m\dot{V} = T_h - mg_e \left(\frac{r_e}{r_h} \right)^2 \cos \beta - D \quad (A.9)$$

$$mV\dot{\beta} = mg_e \left(\frac{r_e}{r_h} \right)^2 \sin \beta - \frac{mV^2 \sin \beta}{r_h} \quad (A.10)$$

Realizing that

$$T_h = T_{vac} \left[1 - \frac{P_h}{P_{sl}} (1 - \lambda) \right] \quad (A.11)$$

$$\lambda = \frac{I_{sp_{sl}}}{I_{sp_{vac}}}$$

$$mg_e = W_O - \dot{W}_t \quad (A.12)$$

$$D = C_D \frac{1}{2} \rho_h V^2 A \quad (A.13)$$

Equation (A. 9) can be rewritten as

$$\frac{\dot{V}}{g_e} = \frac{T_{vac}}{W_O - W_t} - \frac{T_{vac}}{W_O - W_t} \left[\frac{p_h}{p_{sl}} (1 - \lambda) \right] - \left(\frac{r_e}{r_h} \right)^2 \cos \beta - \frac{C_D \rho_h V^2 A}{2(W_O - W_t)} \quad (A. 14)$$

Rearranging Equation (A. 14) and integrating,

$$\begin{aligned} \frac{V_{BO}}{g_e} = & I_{sp_{vac}} \ln \frac{W_O}{W_{BO}} - \int_0^{t_B} \frac{\frac{T}{W_O} \left(\frac{1}{\lambda} - 1 \right) \frac{p_h}{p_{sl}}}{\left[1 - \frac{\left(\frac{T}{W_O} \right)}{I_{sp_{sl}}} t \right]} dt \\ & - \int_0^{t_B} \left(\frac{r_e}{r} \right)^2 \cos \beta dt - \int_0^{t_B} \frac{\frac{1}{2} \rho_h V^2 C_D A}{W_O \left[1 - \frac{\left(\frac{T}{W_O} \right)}{I_{sp_{sl}}} t \right]} dt \end{aligned} \quad (A. 15)$$

The velocity losses due to gravitation, drag, and thrust-atmosphere effects are respectively defined by the following integrals:

$$\Delta V_{L_g} = g_e \int_0^{t_B} \left(\frac{r_e}{r} \right)^2 \cos \beta dt \quad (A. 16)$$

$$\Delta V_{L_D} = g_e \int_0^{t_B} \frac{\frac{1}{2} \rho_h V^2 C_D A}{W_O \left[1 - \frac{\left(\frac{T}{W_O} \right)}{I_{sp_{sl}}} t \right]} dt \quad (A. 17)$$

$$\Delta V_{L_T} = g_e \int_0^{t_B} \frac{\frac{T}{W_O} \left(\frac{1}{\lambda} - 1 \right) \frac{p_h}{p_{sl}}}{\left[1 - \frac{\left(\frac{T}{W_O} \right)}{I_{sp_{sl}}} t \right]} dt \quad (A. 18)$$

Velocity Loss Estimation

A-5

The ideal or total velocity of a particular stage is

$$V_I = g_e I_{sp_{vac}} \ln \frac{W_O}{W_{BO}} \quad (A. 19)$$

such that the burnout velocity of the stage operating in the atmosphere is

$$V_{BO} = V_I - \Delta V_{L_g} - \Delta V_{L_D} - \Delta V_{L_T} \quad (A. 20)$$

The above equation defines the losses to be investigated in the following section.

2.1 Cursory Gravity, Drag, and Thrust-Atmospheric Losses

2.1.1 First Stage Losses

In order to facilitate a rapid but cursory method for vehicle performance evaluation, total first stage losses were determined empirically, assuming a vehicle with the following typical design parameters:

$\lambda = 0.85$ = Ratio of sea level specific impulse to vacuum specific impulse

$\frac{C_{D_{max}} A}{W_O} = 0.0002$ = Ratio of maximum drag coefficient and reference area to the initial gross weight (ft²/lb)

$\frac{W_O}{W_{BO}} = 4.0$ = Mass ratio.

These design parameters were held constant and the total losses were obtained as a function of first-stage burnout angle and initial thrust-to-weight ratio for vacuum specific impulses of 250, 300, and 370(lb-sec)/lb. These data were determined from gravity turn trajectory simulations computed on an IBM 7090 digital computer assuming a spherical, nonrotating earth. The results are shown in Figures 53 through 59 in Chapter 2.

In order to account for the change in total losses due to variance in the vehicle design parameters, the following relations were derived.

Change in Mass Ratio. The effect of changing the mass ratio essentially changes only the gravity loss of the vehicle. It may be assumed that the change in mass ratio is essentially an increment in burning time which occurs at the nominal burnout conditions. Thus the change in losses, $\Delta(\Delta V_L)$, can be expressed as

A-5

VEHICLE PERFORMANCE ESTIMATION TECHNIQUES

$$\Delta(\Delta V_L) = g_e \Delta t \cos \beta_{BO} \quad (A.21)$$

where

$$\Delta t = t_{\text{nominal}} \left(\frac{\Delta W_P}{W_P} \right) \quad (A.22)$$

and ΔW_P is the change in propellant weight burned which is equivalent to the ΔW_{BO} .

Thus,

$$\Delta(\Delta V_L) = g_e \cos \beta_{BO} t_{\text{nominal}} \left(\frac{\Delta W_{BO}}{W_O} \right) \frac{W_O}{W_P} \quad (A.23)$$

Realizing that

$$\frac{t_{\text{nominal}} W_O}{W_P} = \frac{W_O}{\dot{W}} = \frac{I_{sp} s_l}{\left(\frac{T}{W_O} \right)} \quad (A.24)$$

Equation (A.23) can be rearranged into the form:

$$\Delta(\Delta V_L) = g_e \lambda \frac{I_{sp} \text{vac}}{\left(\frac{T}{W_O} \right)} \cos \beta_{BO} \left(\frac{W_{BO} \text{nominal}}{W_O} - \frac{W_{BO} \text{new}}{W_O} \right) \quad (A.25)$$

where

$$\lambda = 0.85 \text{ and } \frac{W_{BO} \text{nominal}}{W_O} = \frac{1}{4}$$

Thus,

$$\Delta(\Delta V_L) = 0.85 g_e \frac{I_{sp} \text{vac}}{\left(\frac{T}{W_O} \right)} \cos \beta_{BO} \left[\frac{1}{4} - \frac{1}{\left(\frac{W_O}{W_{BO}} \right)_{\text{new}}} \right] \quad (A.26)$$

Change in λ . The change in losses due to a variation in the specific impulse ratio can simply be expressed as

$$\Delta(\Delta V_L) = \frac{d\Delta V_L}{d\lambda} \Delta \lambda \quad (A.27)$$

Velocity Loss Estimation

A-7

where $d\Delta V_L/d\lambda$ is the slope of the thrust loss variation with respect to the specific impulse ratio as obtained in Section 2.2.1, presenting the precise computation of losses.

Change in Drag Characteristics. A change in the vehicle drag parameter, $C_{D_{max}} A/W_O$, will effectively change the losses in the following manner:

$$\Delta(\Delta V_L) = K_D \left[\left(\frac{C_{D_{max}} A}{W_O} \right)_{new} - \left(\frac{C_{D_{max}} A}{W_O} \right)_{assumed} \right] \quad (A. 28)$$

where K_D is an empirical constant obtained from Section 2.2.1, presenting the precise computation of losses. A typical value of this constant is 2.0×10^6 lb/(ft-sec). Thus, a change in the drag parameter can be expressed as

$$\Delta(\Delta V_L) = 2.0 \times 10^6 \left[\left(\frac{C_{D_{max}} A}{W_O} \right)_{new} - 0.0002 \right] \quad (A. 29)$$

These variations in losses should be added to or subtracted from the nominal losses presented in Figures 53 through 59 (Chapter 2) to account for changes in the nominal vehicle parameters.

2.1.2 Velocity Losses for Upper Stages

Certain assumptions were made to determine a cursory expression for the upper-stage velocity losses: 1) that the upper-stage flight takes place entirely beyond the effects of the atmosphere (there are no drag or thrust losses); and 2) that the major contributor to the upper-stage losses is the gravity effect (implying the angle of attack is small). The upper-stage(s) losses can then be expressed as

$$\Delta V_L = g_e \int_{t_1}^{t_2} \cos \beta \, dt \quad (A. 30)$$

It is assumed that the time-varying $\cos \beta$ is replaced by an average value ($\cos \bar{\beta}$) selected between the initial value of the upper-stage flight path angle and the value at stage burnout. Then, Equation (A. 30) becomes

$$\Delta V_L = g_e t_B \cos \bar{\beta} \quad (A. 31)$$

which, expressed in terms of the upper stage(s) initial condition, is

$$\Delta V_L = g_e \frac{I_{sp_{vac}}}{\left(\frac{T_{vac}}{W_O}\right)} \left[1 - \left(\frac{W_O}{W_{BO}}\right) \right] \cos \bar{\beta} \quad (A.32)$$

2.2 Precise Computation of Losses

2.2.1 First Stage Losses

Gravity Losses. As previously defined by Equation (A.16), the gravity losses of a stage are

$$\Delta V_{L_g} = g_e \int_0^{t_B} \left(\frac{r_e}{r_h}\right)^2 \cos \beta \, dt$$

which requires numerical integration for solution. Thus, the results of machine trajectory calculations generated in various studies here at STL were combined into an empirical relationship representative of vehicles with a wide range of design parameters.

An insight into the behavior of the gravity losses can be gained by examining vertical flight. In vertical flight, the gravitational losses are easily obtained by the relation

$$\Delta V_{L_g} = g_e t_B \quad (A.33)$$

For a vehicle that pitches over to some burnout angle, β_{BO} , other than zero, the gravity losses will be some fraction of that lost in pure vertical flight. Also, it would be expected that the fraction depends on the initial thrust-to-weight ratio and stage mass ratio.

The following empirical equation has been based on the above mentioned interactions. This relation assumes the first stage to follow a gravity turn over a spherical earth.

$$\Delta V_{L_g} = (g_e t_B - K_{gg}) \left\{ 1 - K_g \left[1 - \left(\frac{W_O}{W_{BO}}\right) \right] \left(\frac{\beta_{BO}}{90^\circ}\right)^2 \right\} \quad (A.34)$$

The term gt_B represents the losses from a vertical flight in a constant gravitational field. However, since the earth's gravitational field varies as the inverse square of the distance from the earth's center, the term gt_B actually overestimates this loss. In order to account for this, the constant K_{gg} has been included as a function of vacuum specific impulse. The form of Equation (A.34) was found to fit the actual results better than the more obvious choice of $K \cos \beta_{BO}$.

Drag Losses. The drag losses as previously defined by Equation (A.17) are represented by

$$\Delta V_{L_D} = g \int_0^{t_B} \frac{\frac{1}{2} \rho_h v^2 C_D A}{W_O \left[1 - \frac{\left(\frac{T}{W_O} \right) t}{I_{sp_{sl}}} \right]} dt$$

This again requires numerical integration for solution.

Examination of the drag integral indicates the losses to be a function of the ballistic parameter, $W_O/C_D A$, which is time varying. It was found that from vehicle to vehicle, the drag losses could be represented by the relation

$$\Delta V_{L_D} = K_D \frac{C_D A}{W_O} \quad (A.35)$$

where the drag coefficient, C_D , is taken at some appropriate value. Initial investigations considered the maximum, C_D , which occurs approximately at a Mach number of 1.0, to be the appropriate value for use in Equation (A.35). However, a study of drag curves of several vehicles indicated the maximum value to be inconsistent for vehicles of like configurations. Thus, a better representation was found by using the drag coefficient at the time of maximum drag force during the trajectory. This requires knowledge of the time when peak drag occurs. From the data available, it was determined that the Mach number at peak drag, which is a function of burnout flight path angle, vacuum specific impulse, and initial thrust-to-weight ratio, could be presented in graphical form with reasonable accuracy. The resulting variation with these parameters is shown in Figure 66 (Chapter 2). With the knowledge of the Mach number

at peak drag, the drag coefficient for use in Equation (A.35) can be readily obtained. This, of course, assumes a knowledge of the drag coefficient variation with Mach number for the vehicle of interest. However, even in preliminary vehicle design, the usual advance knowledge of the basic vehicle shape allows a good approximation to the drag coefficient variation.

The empirical constant, K_D , was found to be a function of burnout flight path angle, vacuum specific impulse, and initial thrust-to-weight ratio. The burnout angle, β_{BO} , is a measure of the portion of the first-stage trajectory that is contained in the atmosphere. As the burnout angle increases, the density associated with each velocity is increased, and the resulting drag loss is increased. The ratio

$$\frac{\sqrt{I_{sp_{vac}}}}{\left(\frac{T}{W_O}\right)}$$

was found to group the constant, K_D , for the different specific impulses and thrust-to-weight ratios considered. This ratio accounts for the change in vehicle weight with time. The lower the value of this quantity, the lower the vehicle weight will be at peak drag, resulting in increased drag losses.

Thrust-Atmospheric Losses. The effect of atmospheric pressure reducing the thrust of a vehicle results in losses defined by Equation (A.18).

$$\Delta V_{L_T} = g_e \int_0^{t_B} \frac{\left(\frac{T}{W_O}\right) \left(\frac{1}{\lambda} - 1\right) \frac{P_h}{P_{sl}}}{\left[1 - \left(\frac{T}{W_O}\right) \frac{t}{I_{sp_{sl}}}\right]} dt$$

Because of the time variance of atmospheric pressure along the trajectory, numerical integration is necessary for solution. However, representation of this loss can again be made by the following relation based on empirical data.

$$\Delta V_{L_T} = K_a \quad (A.36)$$

Examination of Equation (A.18) indicates the thrust losses to be dependent on the ratio of sea level to vacuum specific impulse, along with the initial thrust-to-weight ratio. The effect of initial thrust-to-weight ratio is relatively small due to canceling conditions. For increasing thrust-to-weight ratios, the difference in the sea level

vacuum thrust increases, contributing to larger losses. However, the larger thrust-to-weight ratios reduce the amount of flight time in the atmosphere, reducing the losses and counteracting the above effect.

The empirical data studies to obtain the variation of K_a were based on a conical De Laval type thrust nozzle. Other exotic nozzle types, such as a plug or expansion-deflection nozzle, could be represented in the same manner, but would require further analysis for empirical representation.

First-Stage Burnout Altitude. In order to totally define the first-stage burnout conditions, knowledge of the burnout altitude is required. Referring again to vertical flight assuming no atmosphere and constant g , Equation (A.15) becomes

$$V_{BO} = g_e \text{Isp}_{vac} \ln \frac{W_O}{W_{BO}} - g_e t_B \quad (\text{A. 37})$$

Integrating once gives vertical ascent burnout altitude, h^* :

$$h^* = g_e \text{Isp}_{vac} t_B \left(1 - \frac{\ln \frac{W_O}{W_{BO}}}{\frac{W_O}{W_{BO}} - 1} \right) - \frac{g_e t_B^2}{2} \quad (\text{A. 38})$$

Assuming the drag and thrust-atmosphere losses are averaged over the burning time, and the effect of pitching to some burnout angle, β_{BO} , other than vertical is represented by

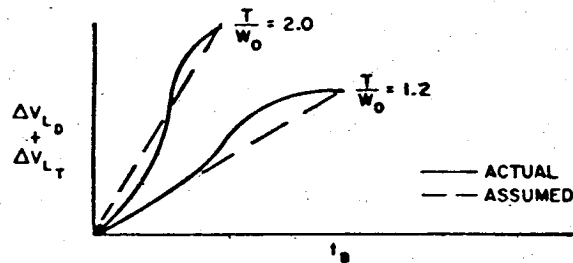
$$\left[1 - \left(\frac{\beta_{BO}}{K_h} \right)^2 \right]$$

the burnout altitude, h_{BO} , can be represented as

$$h_{BO} = \left[h^* - \frac{(\Delta V_{L_D} + \Delta V_{L_T}) t_B}{2} \right] \left[1 - \left(\frac{\beta_{BO}}{K_h} \right)^2 \right] \quad (\text{A. 39})$$

where K_h is an empirical constant determined from trajectory calculations. The validity of averaging the losses over the total burning time is shown in the following schematic for two representative vehicles. The sum of the drag and thrust-atmospheric losses is shown as a function of burning time for stages of low and high initial thrust-to-weight ratios.

As is shown, the vehicle with the low initial thrust-to-weight ratio reached the maximum sum of the losses before burnout; thus, the time average over the whole burning time overestimates the effect of losses on burnout altitude. However, the overall error resulting from this overestimation is generally less than 4 percent of the total altitude.



The constant, K_h , was found to be a function of vacuum specific impulse, initial thrust-to-weight ratio, and first-stage mass ratio.

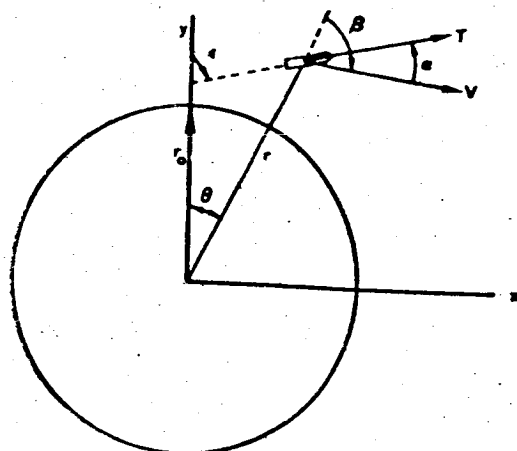
3 UPPER STAGES—POWERED FLIGHT EQUATIONS OF MOTION FOR NONATMOSPHERIC FLIGHT AT A CONSTANT PITCH RATE

3.1 Introduction and Discussion

The following section presents a set of powered flight equations of motion for a thrusting point mass in the absence of an atmosphere. (The solution derived here was adapted from that presented in Reference 1.) The following limiting assumptions are made:

- 1) The magnitude of the acceleration due to gravity is a constant during the burning period.
- 2) The variation in radial distance during burning is small compared with the initial distance from the attracting mass.
- 3) Thrust and propellant flow rate are constant with time.
- 4) Motion occurs in a plane.
- 5) Thrust attitude varies linearly with time (if it varies).

To write the equations of plane motion of the point mass under the above assumptions, consider a planet-centered orthogonal inertial coordinate system with the y-axis in the direction of the local vertical at the time the analysis is initiated.



From Figure A-2, the differential equations of motion are

$$\ddot{y} = \left(\frac{T}{m}\right) \cos \epsilon - g^* \cos \theta \quad (\text{A.40})$$

$$\ddot{x} = \left(\frac{T}{m}\right) \sin \epsilon - g^* \sin \theta \quad (\text{A.41})$$

where g^* is the acceleration due to gravity which is representative of the burning period.

Figure A-2. Coordinate System

To find solutions for these differential equations, it is convenient to change their form, and necessary to use certain of the assumptions outlined previously. First, consider that

$$\cos \theta = y/r \quad (\text{A.42})$$

$$\sin \theta = x/r \quad (\text{A.43})$$

Under assumption 2,

$$g^* \cos \theta = \frac{g^* y}{r} = \frac{g^* y}{r^* \left(1 + \frac{\delta r}{r^*}\right)} \approx (g^*/r^*) y \quad (\text{A.44})$$

and similarly

$$g^* \sin \theta \approx (g^*/r^*) x \quad (\text{A.45})$$

where r^* is the effective radial distance during burning and g^* is the corresponding acceleration due to gravity. Equations (A.40) and (A.41) become

$$\ddot{y} + (g^*/r^*) y = (T/m) \cos \epsilon \quad (\text{A.46})$$

$$\ddot{x} + (g^*/r^*) x = (T/m) \sin \epsilon \quad (\text{A.47})$$

The use of assumption 3 to define η as

$$\eta \triangleq \frac{T}{m_o g^*} \quad (\text{A.48})$$

allows writing

$$\frac{m_o}{m} = \frac{c^*}{\eta g^*} \quad (\text{A.49})$$

where $T = c^* \dot{m}$, g_e is the gravitational attraction of the earth, and

$$c^* = g_e I_{sp} \quad (A. 50)$$

If ϵ_0 defines the initial thrust direction, the thrust attitude at any time is

$$\epsilon = \epsilon_0 + \dot{\epsilon} t \quad (A. 51)$$

where the pitch rate, $\dot{\epsilon}$, is constant (zero for constant attitude) by assumption 5.

Defining the inverse mass ratio at any time as

$$p \triangleq \frac{m}{m_0} \quad (A. 52)$$

it follows from Equation (A. 49) that

$$t = (1 - p) \frac{c^*}{\eta g^*} = (1 - p) \frac{g_e I_{sp}}{(T/m_0)} \quad (A. 53)$$

and in turn from Equation (A. 51) that

$$\epsilon = \nu + \xi p \quad (A. 54)$$

where

$$\nu = \epsilon_0 + \frac{c^* \dot{\epsilon}}{\eta g^*} \quad (A. 55)$$

$$\xi = - \frac{c^* \dot{\epsilon}}{\eta g^*} \quad (A. 56)$$

Equations (A. 46) and (A. 47) become

$$\ddot{y} + (g^*/r^*) y = \eta g^* \frac{\cos(\nu + \xi p)}{p}$$

$$\ddot{x} + (g^*/r^*) x = \eta g^* \frac{\sin(\nu + \xi p)}{p}$$

It is desirable at this point to make a change of independent variable from t to p :

$$\frac{dy}{dt} = \frac{dy}{dp} \left(\frac{dp}{dt} \right) = - \left(\frac{\eta g^*}{c^*} \right) \frac{dy}{dp} = - \frac{\eta g^*}{c^*} y'$$

$$\frac{d^2 y}{dt^2} = \left(\frac{\eta g^*}{c^*} \right)^2 \frac{d^2 y}{dp^2} = \left(\frac{\eta g^*}{c^*} \right)^2 y''$$

Under this change the differential equations become

$$y'' + \chi^2 y = \zeta f(p) \quad (\text{A. 57})$$

$$x'' + \chi^2 x = \zeta g(p) \quad (\text{A. 58})$$

where

$$\chi^2 = (g^*/r^*) \left(\frac{c^*}{\eta g^*} \right)^2 \quad (\text{A. 59})$$

$$\zeta = \frac{c^{*2}}{\eta g^*} \quad (\text{A. 60})$$

and

$$f(p) = \frac{\cos(\nu + \xi p)}{p} \quad (\text{A. 61})$$

$$g(p) = \frac{\sin(\nu + \xi p)}{p} \quad (\text{A. 62})$$

3.2 Solution of the Differential Equations

First take Equation (A. 57), which in operator form is

$$(D^2 + \chi^2) y = \zeta f(p)$$

or,

$$[(D - i\chi)(D + i\chi)] y = \zeta f(p)$$

Put $(D + i\chi) y \equiv \Delta$, so that

$$(D - i\chi) \Delta = \zeta f(p) \quad (\text{A. 63})$$

This is a linear first order differential equation which can be solved by the use of an integrating factor, in this case $e^{-i\chi p}$. Then the solution for Δ is

$$\Delta = \zeta e^{i\chi p} \int_1^p e^{-i\chi \tau} f(\tau) d\tau + C_1 e^{i\chi p} \quad (\text{A. 64})$$

$$= \zeta Z + C_1 e^{i\chi p} \quad (\text{A. 65})$$

where Z is defined by the expression

$$Z = e^{i\chi p} \int_1^p e^{-i\chi \tau} f(\tau) d\tau \quad (\text{A. 66})$$

and τ is the dummy variable of integration. If Equation (A.64) is substituted into the definition for Δ , the result is

$$(D + iX) y = \zeta e^{iXp} \int_1^P e^{-iX\tau} f(\tau) d\tau + C_1 e^{iXp} \quad (A.67)$$

which is again a linear first order equation and may be solved in the same manner as above. The integrating factor is e^{iXp} , and the resulting solution for y is

$$y = \zeta e^{-iXp} \int_1^P e^{i2X\tau} \int_1^P e^{-iX\tau} f(\tau) d\tau d\tau + \frac{C_1 \zeta}{2iX} e^{iXp} + C_2 e^{-iXp} \quad (A.68)$$

Upon performing a partial integration of the particular integral with respect to the quantity $\int_1^P e^{-iX\tau} f(\tau) d\tau$, the particular solution for y given by the first term of Equation (A.68) may be written as

$$y_p = \frac{\zeta}{2iX} \left(e^{iXp} \int_1^P e^{-iX\tau} f(\tau) d\tau - e^{-iXp} \int_1^P e^{iX\tau} f(\tau) d\tau \right) \quad (A.69)$$

The two terms of y_p are complex conjugates of each other, and using the variable Z defined by Equation (A-66), the particular solution is

$$y_p = \frac{\zeta}{2iX} (Z - \bar{Z})$$

The result for y may now be expressed as

$$y = \frac{\zeta}{2iX} (Z - \bar{Z}) + C'_1 e^{iXp} + C_2 e^{-iXp}$$

where the constant $C'_1 = (\zeta/2iX) C_1$. Differentiation of this expression gives

$$y' = \frac{\zeta}{2} (Z + \bar{Z}) + iX(C'_1 e^{iXp} - C_2 e^{-iXp})$$

Since $(Z - \bar{Z}) = 2i \operatorname{Im}(Z)$ and $(Z + \bar{Z}) = 2\operatorname{Re}(Z)$, y and y' may also be written in the form

$$y = \frac{\zeta}{X} \operatorname{Im}(Z) + C'_1 e^{iXp} + C_2 e^{-iXp} \quad (A.70)$$

$$y' = \zeta \operatorname{Re}(Z) + iX(C'_1 e^{iXp} - C_2 e^{-iXp}) \quad (A.71)$$

Under the initial conditions at $t = 0$: $p_0 = 1$, $y_0 = r_0$, $x_0 = 0$, $y'_0 = -(\xi/c^*) \dot{y}_0$, $x'_0 = -(\xi/c^*) \dot{x}_0$, the values for C'_1 and C_2 may be determined from the homogeneous equation and its derivative as represented in Equations (A.70) and (A.71). The results are

$$C'_1 = \frac{1}{Z} e^{-iX} \left(r_0 + \frac{i\xi}{c^*X} \dot{y}_0 \right)$$

and

$$C_2 = \frac{1}{Z} e^{iX} \left(r_0 - \frac{i\xi}{c^*X} \dot{y}_0 \right)$$

Substitution of these values into (A.70) and (A.71) gives

$$y = \frac{\xi}{X} \ln(Z) + r_0 \cos X(1-p) + \frac{\xi}{c^*X} \dot{y}_0 \sin X(1-p) \quad (A.72)$$

$$y' = \xi R(Z) + r_0 \sin X(1-p) - \frac{\xi}{c^*X} \dot{y}_0 \cos X(1-p) \quad (A.73)$$

To obtain a form for $\ln(Z)$ and $R(Z)$ which can be readily computed, take the integral associated with Z and expand the integrand $e^{-iXp} f(p)$:

$$\begin{aligned} Z e^{-iXp} &= \int_1^P e^{-iX\tau} \frac{\cos(\nu + \xi\tau)}{\tau} d\tau = \left(\cos \nu \int_1^P \cos \xi\tau \cos X\tau \frac{d\tau}{\tau} \right. \\ &\quad \left. - \sin \nu \int_1^P \cos X\tau \sin \xi\tau \frac{d\tau}{\tau} \right) \\ &\quad + i \left(-\cos \nu \int_1^P \sin X\tau \cos \xi\tau \frac{d\tau}{\tau} + \sin \nu \int_1^P \sin X\tau \sin \xi\tau \frac{d\tau}{\tau} \right) \end{aligned}$$

This can be further expanded to give

$$\begin{aligned} Z e^{-iXp} &= \frac{1}{Z} \left\{ \cos \nu \left[\int_1^P \frac{\cos \tau(\xi - X)}{\tau} d\tau + \int_1^P \frac{\cos \tau(\xi + X)}{\tau} d\tau \right] \right. \\ &\quad \left. - \sin \nu \left[\int_1^P \frac{\sin \tau(\xi - X)}{\tau} d\tau + \int_1^P \frac{\sin \tau(\xi + X)}{\tau} d\tau \right] \right\} \\ &\quad + \frac{i}{Z} \left\{ -\cos \nu \left[\int_1^P \frac{\sin \tau(\xi + X)}{\tau} d\tau - \int_1^P \frac{\sin \tau(\xi - X)}{\tau} d\tau \right] \right. \\ &\quad \left. + \sin \nu \left[\int_1^P \frac{\cos \tau(\xi - X)}{\tau} d\tau - \int_1^P \frac{\cos \tau(\xi + X)}{\tau} d\tau \right] \right\} \end{aligned}$$

By use of the dummy variables $m = \tau(\xi - \chi)$ and $n = \tau(\xi + \chi)$, the expression is

$$\begin{aligned} Z e^{-i\chi p} = \frac{1}{2} \left\{ \cos \nu \left[\int_{\xi-\chi}^{(\xi-\chi)p} \frac{\cos m}{m} dm + \int_{\xi+\chi}^{(\xi+\chi)p} \frac{\cos n}{n} dn \right] \right. \\ \left. - \sin \nu \left[\int_{\xi-\chi}^{(\xi-\chi)p} \frac{\sin m}{m} dm + \int_{\xi+\chi}^{(\xi+\chi)p} \frac{\sin n}{n} dn \right] \right\} \\ + \frac{i}{2} \left\{ \cos \nu \left[\int_{\xi-\chi}^{(\xi-\chi)p} \frac{\sin m}{m} dm - \int_{\xi+\chi}^{(\xi+\chi)p} \frac{\sin n}{n} dn \right] \right. \\ \left. + \sin \nu \left[\int_{\xi-\chi}^{(\xi-\chi)p} \frac{\cos m}{m} dm - \int_{\xi+\chi}^{(\xi+\chi)p} \frac{\cos n}{n} dn \right] \right\} \end{aligned}$$

The integrals in this form can be expressed as combinations of the sine integrals and cosine integrals whose standard forms are

$$\text{Si}(u) = \int_0^u \frac{\sin \sigma}{\sigma} d\sigma \quad (\text{A. 74})$$

$$\text{Ci}(u) = - \int_u^\infty \frac{\cos \sigma}{\sigma} d\sigma \quad (\text{A. 75})$$

The expression for Z is

$$\begin{aligned} Z = \frac{e^{i\chi p}}{2} \left[\left(\cos \nu \left[\text{Ci}[(\xi + \chi)p] - \text{Ci}(\xi + \chi) + \text{Ci}[(\xi - \chi)p] - \text{Ci}(\xi - \chi) \right] \right. \right. \\ \left. - \sin \nu \left[\text{Si}[(\xi + \chi)p] - \text{Si}(\xi + \chi) + \text{Si}[(\xi - \chi)p] - \text{Si}(\xi - \chi) \right] \right) \\ - i \left(\cos \nu \left[\text{Si}[(\xi + \chi)p] - \text{Si}(\xi + \chi) - \text{Si}[(\xi - \chi)p] + \text{Si}(\xi - \chi) \right] \right. \\ \left. \left. + \sin \nu \left[\text{Ci}[(\xi + \chi)p] - \text{Ci}(\xi + \chi) - \text{Ci}[(\xi - \chi)p] + \text{Ci}(\xi - \chi) \right] \right) \right] \end{aligned} \quad (\text{A. 76})$$

Separating into real and imaginary parts, the results

$$\text{Im}(Z) = A \sin \chi p - B \cos \chi p \quad (\text{A. 77})$$

$$\text{R}(Z) = A \cos \chi p + B \sin \chi p \quad (\text{A. 78})$$

may be written, where the following definitions hold:

$$A = \frac{1}{2} (E \cos v - F \sin v) \quad (\text{A. 79})$$

$$B = \frac{1}{2} (G \sin v + H \cos v) \quad (\text{A. 80})$$

and

$$E = \left[\text{Ci}[(\xi + \chi) p] - \text{Ci}(\xi + \chi) \right] + \left[\text{Ci}[(\xi - \chi) p] - \text{Ci}(\xi - \chi) \right] \quad (\text{A. 81})$$

$$F = \left[\text{Si}[(\xi + \chi) p] - \text{Si}(\xi + \chi) \right] + \left[\text{Si}[(\xi - \chi) p] - \text{Si}(\xi - \chi) \right] \quad (\text{A. 82})$$

$$G = \left[\text{Ci}(\xi + \chi) p] - \text{Ci}(\xi + \chi) \right] - \left[\text{Ci}[(\xi - \chi) p] - \text{Ci}(\xi - \chi) \right] \quad (\text{A. 83})$$

$$H = \left[\text{Si}[(\xi + \chi) p] - \text{Si}(\xi + \chi) \right] - \left[\text{Si}[(\xi - \chi) p] - \text{Si}(\xi - \chi) \right] \quad (\text{A. 84})$$

In a similar manner, the solution of the differential equation [Equation (A. 58)] may be found, since only the function $g(p)$ is interchanged for $f(p)$ in the particular solution [Equation (A. 69)] for y . The function corresponding to Z in the solution for x is

$$\omega = e^{i\chi p} \int_1^P \frac{\sin(v + \xi \tau)}{\tau} d\tau \quad (\text{A. 85})$$

and with the initial conditions $x'_0 = -(\xi/c^*)\dot{x}_0$, $x_0 = 0$ at $t = 0$, the resulting solution can be shown to be

$$x = \frac{\xi}{\chi} \text{Im}(\omega) + \frac{\xi}{c^*\chi} \dot{x}_0 \sin \chi(1 - p) \quad (\text{A. 86})$$

$$x' = \xi R(\omega) - \frac{\xi}{c^*} \dot{x}_0 \cos \chi(1 - p) \quad (\text{A. 87})$$

where

$$\text{Im}(\omega) = C \sin \chi p - D \sin \chi p \quad (\text{A. 88})$$

$$R(\omega) = C \cos \chi p + D \sin \chi p \quad (\text{A. 89})$$

and

$$C = \frac{1}{2} (E \sin v + F \cos v) \quad (\text{A. 90})$$

$$D = \frac{1}{2} (-G \cos v + H \sin v) \quad (\text{A. 91})$$

with E , F , G , and H defined by Equations (A. 82) through (A. 84).

Upon recalling that $\dot{y} = -(c^*/\xi)y'$ and $\dot{x} = -(c^*/\xi)x'$, expressions for the final solutions to the differential equations are

$$\left\{ \begin{aligned} y &= \frac{\xi}{\chi} \left[\text{Im}(Z) + \frac{\dot{y}_0}{c^*} \sin \chi(1-p) \right] + r_0 \cos \chi(1-p) \end{aligned} \right. \quad (\text{A. 92})$$

$$\left\{ \begin{aligned} x &= \frac{\xi}{\chi} \left[\text{Im}(\omega) + \frac{\dot{x}_0}{c^*} \sin \chi(1-p) \right] \end{aligned} \right. \quad (\text{A. 93})$$

$$\left\{ \begin{aligned} \dot{y} &= -c^* \left[R(Z) + \frac{r_0 \chi}{\xi} \sin \chi(1-p) \right] + \dot{y}_0 \cos \chi(1-p) \end{aligned} \right. \quad (\text{A. 94})$$

$$\left\{ \begin{aligned} \dot{x} &= -c^* R(\omega) + \dot{x}_0 \cos \chi(1-p) \end{aligned} \right. \quad (\text{A. 95})$$

These results can be used to find the altitude, h , velocity, V , flight path angle, β , and range angle, θ , by employing the following definitions:

$$h = \sqrt{x^2 + y^2} - y_0 = r - r_0 \quad (\text{A. 96})$$

$$V = \sqrt{\dot{x}^2 + \dot{y}^2} \quad (\text{A. 97})$$

$$\begin{aligned} V_R &= \sqrt{(\dot{x}^2 + \dot{y}^2) + 2g^* (\sqrt{x^2 + y^2} - r_0)} \\ &= \sqrt{V^2 + 2g^* h} \end{aligned} \quad (\text{A. 98})$$

$$\beta = \cos^{-1} \left[\frac{\dot{x}x + \dot{y}y}{\sqrt{(x^2 + y^2)(\dot{x}^2 + \dot{y}^2)}} \right] = \cos^{-1} \left(\frac{\dot{x}x + \dot{y}y}{Vr} \right) \quad (\text{A. 99})$$

$$\theta = \cos^{-1}(y/r) \quad (\text{A. 100})$$

Given an initial value, ϵ_0 , for the thrust attitude referenced to the initial vertical (at $t = 0$), the final attitude, ϵ , may be found by use of Equation (A. 51),

$$\epsilon = \epsilon_0 + \dot{\epsilon}t$$

and subsequently the angle of attack may be determined by the relationship

$$\alpha = \beta + \theta - \epsilon \quad (\text{A. 101})$$

with the angles having the signs indicated in Figure A-2.

Nomenclature

A-21

NOMENCLATURE

A	Reference area for aerodynamic coefficients
C_D	Aerodynamic drag coefficient
$C_{D_{max}}$	Maximum drag coefficient
c^*	$g_e I_{sp}$ = effective jet velocity
$Ci()$	Cosine integral of ()
D	Force due to aerodynamic drag
e	Orbital eccentricity
g	Acceleration due to gravity at distance r^* from the center of attraction
g_e	Acceleration due to gravity at the earth's surface
h	Height above initial reference (altitude)
h^*	Burnout altitude for nonatmospheric vertical ascent
h_a	Apogee altitude
h_{BO}	Altitude at burnout
h_p	Perigee altitude
$Im()$	Imaginary part of ()
I_{sp}	Specific impulse
$I_{sp_{sl}}$	Sea level specific impulse
$I_{sp_{vac}}$	Vacuum specific impulse
K_D	Drag loss constant
K_h	First-stage burnout altitude constant
m	Mass = W/g_e
\dot{m}	Mass flow rate
m_o	Initial mass = W_o/g_e
P	Orbital period

VEHICLE PERFORMANCE ESTIMATION TECHNIQUES

p	$\triangleq m/m_0 = W/W_0 =$ inverse mass ratio at any time
p_h	Atmospheric pressure at altitude h
p_{sl}	Atmospheric pressure at sea level
$R()$	Real part of $()$
r	Radial distance from center of attracting body
r^*	Effective radial distance from center of attracting body
r_e	Radius of earth = 3440.1818 n mi
r_h	$r_p + h =$ radial distance at altitude h
r_0	Initial radial distance
$Si()$	Sine integral of $()$
T	Thrust
T	Transit time for Hohmann transfer
T_{vac}	Vacuum thrust
T/W_0	Liftoff thrust-to-weight ratio
T_h	Thrust at altitude h
t	Time from initiation
t_B	Time of burning
v	Velocity along flight path
v_a	Apogee velocity
v_{BO}	Velocity at stage burnout
v_I	Inertial velocity
v_p	Perigee velocity
v_R	Reference potential velocity
w	Weight of vehicle
\dot{w}	Weight flow rate

Nomenclature

A-23

W_{BO}	Weight at burnout
W_O	Initial weight of vehicle
W_O/W_{BO}	r = stage mass ratio
W_P	Weight of propellant
Z	Defined by Equation (A. 66)
α	Angle of attack (angle between velocity and thrust vectors)
β	Flight path angle (velocity altitude referenced to the local vertical)
ΔV_{LD}	Velocity loss due to aerodynamic drag
ΔV_{Lg}	Velocity loss due to gravitational effects
ΔV_{LT}	Velocity loss due to thrust-atmospheric effects
ΔV_T	Total incremental velocity for Hohmann transfer
ΔV_1	Initial incremental velocity for Hohmann transfer
ΔV_2	Final incremental velocity for Hohmann transfer
ϵ	Angle thrust makes with initial local vertical
ϵ_0	Initial ϵ
$\dot{\epsilon}$	Rate of change of thrust attitude; pitch rate (pitch-down~ positive)
ζ	$c^{*2}/\eta g^* = g_e \text{ } I_{sp}^2 / (T/m_0)$
η	$\Delta \frac{T}{m_0 g^*}$
θ	Range angle
λ	$\frac{I_{sp_{sl}}}{I_{sp_{vac}}} = \text{ratio of sea level and vacuum specific impulses}$
μ_e	Gravitational-mass constant for earth = $1.40766 \times 10^{16} \text{ ft/sec}^2$

VEHICLE PERFORMANCE ESTIMATION TECHNIQUES

$$v = v_0 + \frac{g_e I_{sp}}{(T/m_0)}$$

$$\xi = \frac{g_e I_{sp}}{(T/m_0)}$$

p_h Atmospheric density at altitude h

$$X = \frac{L}{c^*} \sqrt{\frac{g^*}{r^*}} = \frac{g_e I_{sp}}{(T/m_0)} \sqrt{\frac{g^*}{r^*}}$$

ω Defined by Equation (A.85)

REFERENCES

1. P. Steiner, "Powered Flight Equations of Motion in the Absence of an Atmosphere-I: Equations of Motion," Space Technology Laboratories, Inc., STL/7861.5-32, 12 July 1961.
2. E. Jahnke and F. Emde, Tables of Functions with Formulae and Curves, Dover Publications Inc., New York, 1945.
3. Henry Margenau and George M. Murphy, The Mathematics of Physics and Chemistry, D. Van Nostrand Co., New York, 1943.
4. "Table of Sine and Cosine Integrals for Arguments from 10-100," U.S. National Bureau of Standards Applied Mathematics Series 32. U.S. Government Printing Office, Washington, 1954.
5. "Sine, Cosine and Exponential Integrals, Vol. I - Arguments Between Zero and 2 at Intervals of 0.0001," A. N. Lowan, Technical Director. Works Progress Administration (under sponsorship of the National Bureau of Standards) New York, 1940. (Reprinted by Western Periodicals Co., North Hollywood, California, 1956.)
6. "Sine, Cosine and Exponential Integrals, Vol. II - Arguments Between 2 and 10 at Intervals of 0.001," A. N. Lowan, Technical Director. Works Progress Administration (under sponsorship of the National Bureau of Standards) New York, 1940. (Reprinted by Western Periodicals Co., North Hollywood, California, 1956.)

APPENDIX B

SYSTEM CONSIDERATIONS

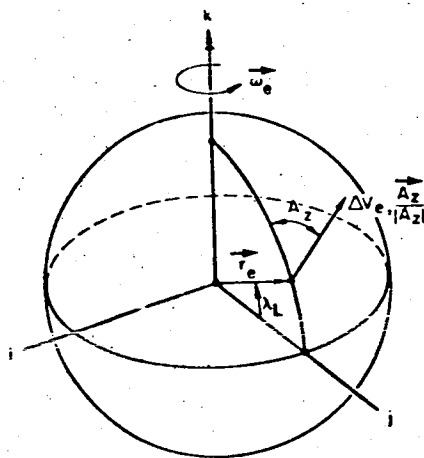
The following is a development of the equations and expressions used in Chapter 3.

1 LAUNCH SITE LIMITATIONS

1.1 Earth's Rotation

The earth's rotational velocity component at the launch site location in the launch azimuth plane is seen from the diagram below to equal,

$$\Delta V_e = (\vec{\omega}_e \times \vec{r}_e) \cdot \frac{\vec{A}_z}{|A_z|} \quad (B.1)$$



From the diagram,

$$\vec{\omega}_e = \vec{k} \omega_e \quad (B.2)$$

$$\vec{r}_e = \vec{j} r_e \cos \lambda_L + \vec{k} r_e \sin \lambda_L \quad (B.3)$$

$$\frac{\vec{A}_z}{|A_z|} = \vec{i} \sin A_z - \vec{j} \cos A_z \sin \lambda_L + \vec{k} \cos A_z \cos \lambda_L \quad (B.4)$$

B-2

SYSTEM CONSIDERATIONS

Substituting Equations (B. 2), (B. 3), and (B. 4) into Equation (B. 1) and performing the indicated operations,

$$\Delta V_e = \omega_e r_e \cos \lambda_L \sin A_z \quad (B.5)$$

where

$$\omega_e = 0.73100 \times 10^{-4} \text{ radians per second}$$

$$r_e = 0.209029 \times 10^8 \text{ feet.}$$

The velocity component normal to the launch azimuth plane, $\Delta V_{e\perp}$, is equal to

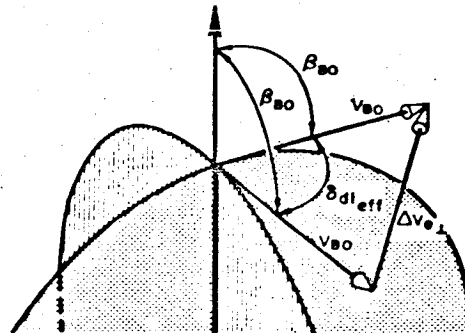
$$\Delta V_{e\perp} = \left| (\vec{\omega}_e \times \vec{r}_e) \times \frac{\vec{A}_z}{|\vec{A}_z|} \right| \quad (B.6)$$

substituting Equations (B. 2), (B. 3), and (B. 4) into Equation (B. 6) and performing the indicated operations,

$$\Delta V_{e\perp} = \omega_e r_e \cos \lambda \sin A_z \quad (B.7)$$

From the schematic below it is seen that the effective dog-leg angle, $\delta_{dl\text{eff}}$, is

$$\delta_{dl\text{eff}} = \frac{\Delta V_{e\perp}}{V_{BO} \sin \beta_{BO}} \text{ radians} \quad (B.8)$$



Launch Site Limitations

B-3

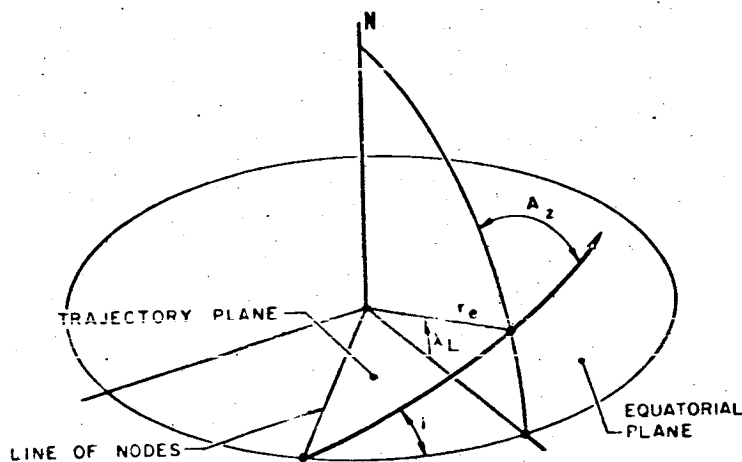
Substituting 1) Equation (B.7) into Equation (B.8) and 2) the values for ω_e and r_e specified above, and then converting to degrees,

$$\delta_{dl_{eff}} = \frac{87,548 \cos \lambda_L \cos A_Z}{V_{BO} \sin \beta_{BO}} \text{ degrees} \quad (\text{B. 9})$$

1.2 Trajectory Inclination

It can be seen from the diagram below that, by using spherical trigonometry, the trajectory inclination resulting from the particular launch site and the chosen launch azimuth equals

$$i = \cos^{-1}(\cos \lambda_L \sin A_Z) \quad (\text{B. 10})$$



where

i = inclination of the trajectory plane
with respect to the equatorial plane

λ_L = latitude of launch site

A_Z = launch azimuth measured from true North.

B-4

SYSTEM CONSIDERATIONS

1.3 Dog-Leg Maneuver

The dog-leg maneuver is accomplished as shown in the figure below.

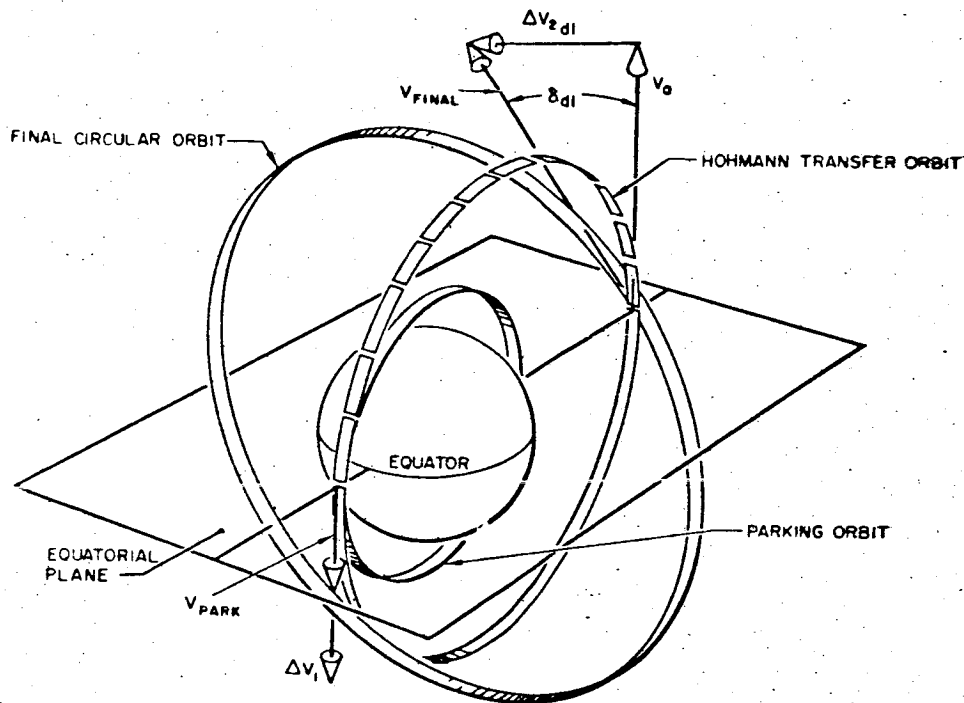


Figure B-1. Hohmann Transfer Dog-Leg Maneuver

The circular orbital velocity, V_o , at the parking orbit altitude is equal to

$$V_o = \sqrt{\frac{\mu_e}{r_o}} \quad (B.11)$$

where

$$r_o = r_e + h_o \quad (B.11a)$$

The perigee velocity for the transfer ellipse is then equal to

$$V_p = \sqrt{\frac{2\mu_e}{r_p} \left(\frac{r_a}{r_a + r_p} \right)} \quad (B.12)$$

Launch Site Limitations

B-5

where

$$r_a = r_e + h_2 \quad (\text{B. 12a})$$

$$r_p = r_e + h_1 \text{ and } h_1 = h_o \quad (\text{B. 12b})$$

$$\begin{aligned} \Delta V_1 &= V_p - V_o \\ &= \sqrt{\frac{2\mu_e}{r_p} \left(\frac{r_a}{r_a + r_p} \right)} - \sqrt{\frac{\mu_e}{r_p}} \end{aligned} \quad (\text{B. 13})$$

The velocity at the apogee of the transfer ellipse is equal to

$$V_a = \sqrt{\frac{2\mu_e}{r_a} \left(\frac{r_p}{r_a + r_p} \right)} \quad (\text{B. 14})$$

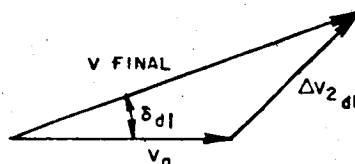
and the final circular orbit velocity at the apogee altitude is

$$V_{\text{final}} = \sqrt{\frac{\mu_e}{r_a}} \quad (\text{B. 15})$$

The incremental injection velocity, ΔV_{2dl} , is equal to

$$\Delta \vec{V}_{2dl} = \vec{V}_{\text{final}} - \vec{V}_a \quad (\text{B. 16})$$

The vector substitution is illustrated in the diagram below

where δ_{dl} is the desired dog-leg angle of the orbit plane.

B-6

SYSTEM CONSIDERATIONS

Performing the vector operation,

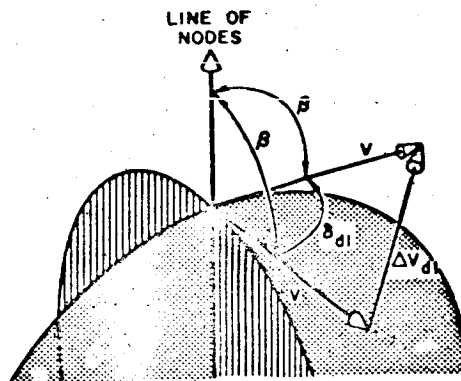
$$\begin{aligned}\Delta V_{2dl} &= \sqrt{(V_{\text{final}} \cos \delta_{dl} - V_a)^2 + (V_{\text{final}} \sin \delta_{dl})^2} \\ &= \sqrt{\frac{\mu_e}{r_a} \left[\left(\cos \delta_{dl} - \sqrt{\frac{r_p}{r_a + r_p}} \right)^2 + (\sin \delta_{dl})^2 \right]}\end{aligned}\quad (\text{B. 17})$$

The total injection velocity, ΔV_{Tdl} , is

$$\Delta V_{Tdl} = \Delta V_1 + \Delta V_{2dl} \quad (\text{B. 18})$$

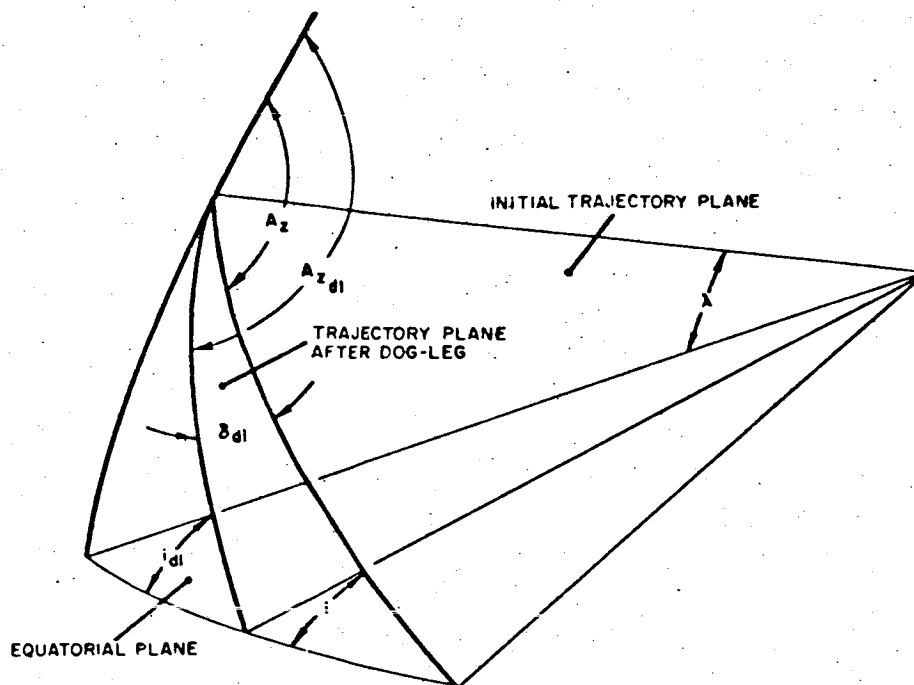
The velocity increment, ΔV_{dl} , required to accomplish the dog-leg after the orbital elements have been established (see diagram below) is equal to the projection of the velocity vector in its plane on the plane perpendicular to the line of nodes, times twice the product of the velocity and the sine of half the desired planar dog-leg angle; that is,

$$\Delta V_{dl} = 2V \sin \left| \frac{\delta_{dl}}{2} \right| \sin \beta \quad (\text{B. 19})$$



As seen from the diagram below, the dog-leg angle required to change the inclination of the trajectory plane is

$$\delta_{dl} = A_z - A_{zdl} \quad (\text{B. 20})$$



From spherical trigonometry,

$$A_z = \sin^{-1} \frac{\cos i}{\cos \lambda} \quad (\text{B. 21})$$

$$A_{z_{dl}} = \sin^{-1} \frac{\cos i_{dl}}{\cos \lambda} \quad (\text{B. 22})$$

$$\therefore \delta_{dl} = \sin^{-1} \frac{\cos i}{\cos \lambda} - \sin^{-1} \frac{\cos i_{dl}}{\cos \lambda} \quad (\text{B. 23})$$

where A_z and λ are the trajectory conditions at the execution of the dog-leg.

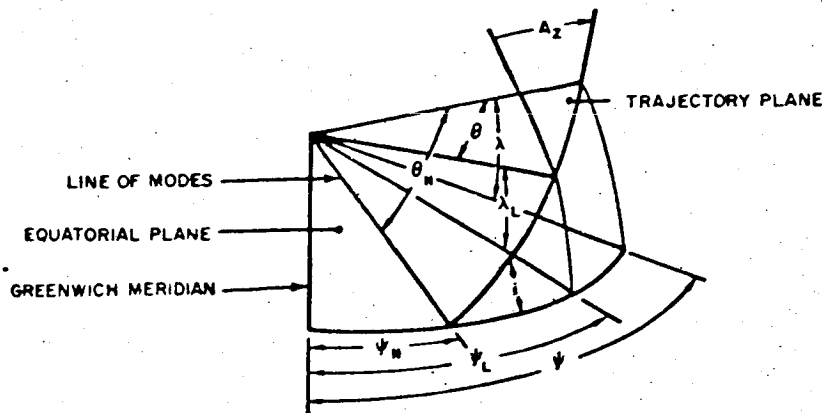
2 RANGE SAFETY

2.1 Impact Location

2.1.1 Range

Finding the nonrotating earth longitude as a function of the launch location and the launch azimuth is a matter of spherical trigonometry.

SYSTEM CONSIDERATIONS



From Equation (B.6),

$$i = \cos^{-1} (\cos \lambda_L \sin A_z) \quad (B.24)$$

$$\sin (\psi_L - \psi_N) = \frac{\tan \lambda_L}{\tan i} \quad (B.25)$$

$$\sin (\psi - \psi_N) = \frac{\tan \lambda}{\tan i} \quad (B.26)$$

Combining Equations (B.25) and (B.26) and solving for ψ ,

$$\psi = \psi_L + \sin^{-1} \left(\frac{\tan \lambda}{\tan i} \right) \sin^{-1} \left(\frac{\tan \lambda_L}{\tan i} \right) \quad (B.27)$$

Either geocentric or geographical latitude may be used since the maximum error to be incurred is 12 nautical miles.

The latitude impact for range of θ of the i th stage is derived as follows (see diagram above):

$$\sin \lambda_L = \sin i \sin (\theta_N - \theta_i) \quad (B.28)$$

$$\sin \lambda_i = \sin i \sin \theta_N \quad (B.29)$$

Solving Equation (B.28) for θ_N and Equation (B.29) for λ_i ,

$$\theta_N = \theta_i + \sin^{-1} \left(\frac{\sin \lambda_L}{\sin i} \right) \quad (B.30)$$

$$\lambda_i = \sin^{-1} (\sin i \sin \theta_N) \quad (B.31)$$

Substituting Equation (B.30) into Equation (B.31),

$$\lambda_i = \sin^{-1} \left[\sin i \sin \left(\theta_i + \sin^{-1} \frac{\sin \lambda_L}{\sin i} \right) \right] \quad (\text{B.32})$$

The equation for the ballistic range from burnout to impact, θ_{BR} , is

$$\frac{h_{BO} + r_e}{r_e} = \frac{1 - \cos \theta_{BR}}{c \sin^2 \beta_{BO}} + \frac{\sin (\beta_{BO} - \theta_{BR})}{\sin \beta_{BO}} \quad (\text{B.33})$$

where

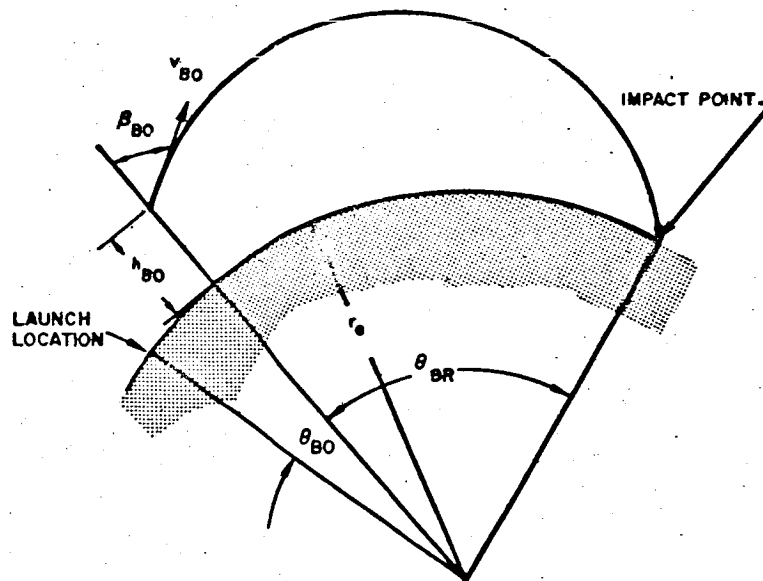
$$c = \frac{(h_{BO} + r_e) v_{BO}^2}{\mu_e}$$

$$h_{BO} = 400,000 \text{ feet}$$

$$r_e = 0.209029 \times 10^8 \text{ feet}$$

$$\mu_e = 1.40766 \times 10^{16} \text{ ft}^3/\text{sec}^2$$

The definitions of the symbols are found in the diagram below. The derivations of the equations presented here may be found in Reference 1.



2.1.2 Dispersions

To determine the dispersions, it is first necessary to determine the range sensitivity to the burnout errors. Only the equations are presented here; their derivations are found in Reference 1.

The range error due to burnout velocity dispersions equals

$$\frac{\partial R_{DR}}{\partial V_{BO}} = 2 \frac{r_e}{V_{BO}} \frac{1 - \cos \theta_{BR}}{\sin \theta_{BR} - c \sin \beta_{BO} \cos (\beta_{BO} - \theta_{BR})} \quad (B.34)$$

The range error due to burnout flight path angle dispersions equals

$$\frac{\partial R_{DR}}{\partial \beta_{BO}} = r_e \frac{\left[\cot \beta_{BO} \sin (\beta_{BO} - \theta_{BR}) - \cos (\beta_{BO} - \theta_{BR}) + \cos \beta_{BO} \frac{1 - \cos \theta_{BR}}{c \sin^2 \beta_{BO}} \right]}{\frac{\sin \theta_{BR}}{c \sin \beta_{BO}} - \cos (\beta_{BO} - \theta_{BR})} \quad (B.35)$$

For burnout altitude errors,

$$\frac{\partial R_{DR}}{\partial h_{BO}} = \frac{c \sin^2 \beta_{BO} + 1 - \cos \theta_{BR}}{\sin \theta_{BR} - c \sin \beta_{BO} \cos (\beta_{BO} - \theta_{BR})} \quad (B.36)$$

For burnout azimuth errors,

$$\frac{\partial R_{CR}}{\partial A_{zBO}} = r_e \frac{\sin \theta_{BR}}{\sin \beta_{BO}} \quad (B.37)$$

The time of ballistic flight from burnout until impact equals

$$t_{BR \rightarrow \text{impact}} = \frac{h_{BO} + r_e}{V_{BO} \sin \beta_{BO}} \left\{ \frac{(1 - \cos \theta_{BR}) \cot \beta_{BO} + (1 - c) \sin \theta_{BR}}{(2 - c) \left[\frac{1 - \cos \theta_{BR}}{c \sin^2 \beta_{BO}} + \frac{\sin (c - \theta_{BR})}{\sin \beta_{BO}} \right]} + \frac{2 \sin \beta_{BO}}{c \left(\frac{2}{c} - 1 \right)^{3/2}} \tan^{-1} \left(\frac{\sqrt{\frac{2}{c} - 1}}{\sin \beta_{BO} \cot \frac{\theta_{BR}}{2} - \cos \beta_{BO}} \right) \right\} \quad (B.38)$$

To define an impact zone, it is necessary to determine the shape and dimensions of a zone of equal probability density given the probability of impacting within the zone² (or vice versa). The downrange and crossrange dispersions associated with a boost vehicle are assumed to be distributed as a bivariate normal density function.

For the bivariate normal density function, the contours of equal probability density are ellipses. It will be shown, with $k\sqrt{\lambda_1}$ and $k\sqrt{\lambda_2}$ as semimajor and semiminor axes, respectively, that the probability of being within an equiprobability density ellipse is $P = 1 - e^{-.5k^2}$, where k is the number of standard deviations of the elliptical contour and λ_1 and λ_2 are the eigenvalues of the covariance matrix.

The equation for the bivariate normal density function is

$$f(x_1, x_2) = \frac{1}{2\pi\sigma_1\sigma_2\sqrt{1-\rho^2}} \exp \left[-\frac{1}{2(1-\rho^2)} \left(\frac{x_1^2}{\sigma_1^2} - \frac{2\rho}{\sigma_1\sigma_2} x_1x_2 + \frac{x_2^2}{\sigma_2^2} \right) \right] \quad (\text{B.39})$$

It should be noted the $f(x_1, x_2)$ is constant, corresponding to equal probability density, when

$$\frac{1}{(1-\rho^2)} \left(\frac{x_1^2}{\sigma_1^2} - \frac{2\rho}{\sigma_1\sigma_2} x_1x_2 + \frac{x_2^2}{\sigma_2^2} \right) = \text{constant} \quad (\text{B.40})$$

The above relation is the equation of a rotated ellipse. When $\sigma_1 \geq \sigma_2$, the major axis is rotated counterclockwise³ from the x_1 axis to form an angle equal to

$$\psi = \frac{1}{2} \tan^{-1} \frac{2\rho\sigma_1\sigma_2}{\sigma_1^2 - \sigma_2^2} \quad (\text{B.41})$$

In matrix notation, the bivariate density can be expressed

$$f(x_1, x_2) = \frac{1}{2\pi\sqrt{\Sigma_X}} \exp \left(-\frac{1}{2} X^T \Sigma_X^{-1} X \right) \quad (\text{B.42})$$

where

$$X = \begin{bmatrix} x_1 \\ x_2 \end{bmatrix}, \quad \Sigma_X = \begin{bmatrix} \sigma_1^2 & \sigma_{12} \\ \sigma_{12} & \sigma_2^2 \end{bmatrix}, \quad (\text{B.42a, b})$$

$$\Sigma_X^{-1} = \begin{bmatrix} \frac{1}{\sigma_1^2(1-\rho^2)} & \frac{-\rho}{\sigma_1\sigma_2(1-\rho^2)} \\ \frac{-\rho}{\sigma_1\sigma_2(1-\rho^2)} & \frac{1}{\sigma_2^2(1-\rho^2)} \end{bmatrix}, \text{ and } \rho = \frac{\sigma_{12}}{\sigma_1\sigma_2} \quad (\text{B.42c, d})$$

The quadratic form, $X^T \Sigma_X^{-1} X$, can be transformed⁴ by an orthogonal transformation to the form $U^T \Sigma_U^{-1} U$, where

$$U = \begin{bmatrix} u_1 \\ u_2 \end{bmatrix}, \quad \Sigma_U^{-1} = \begin{bmatrix} \lambda_1^{-1} & 0 \\ 0 & \lambda_2^{-1} \end{bmatrix}. \quad (\text{B.43a, b})$$

and λ_1^{-1} and λ_2^{-1} are the eigenvalues of the matrix Σ_X^{-1} . The bivariate density function now has the form

$$f(u_1, u_2) = \frac{\sqrt{\lambda_1^{-1}\lambda_2^{-1}}}{2\pi} \exp \left[-\frac{1}{2} (\lambda_1^{-1}u_1^2 + \lambda_2^{-1}u_2^2) \right] \quad (\text{B.44})$$

But the eigenvalues of Σ_X^{-1} are the reciprocals of the eigenvalues of Σ_X . Therefore,

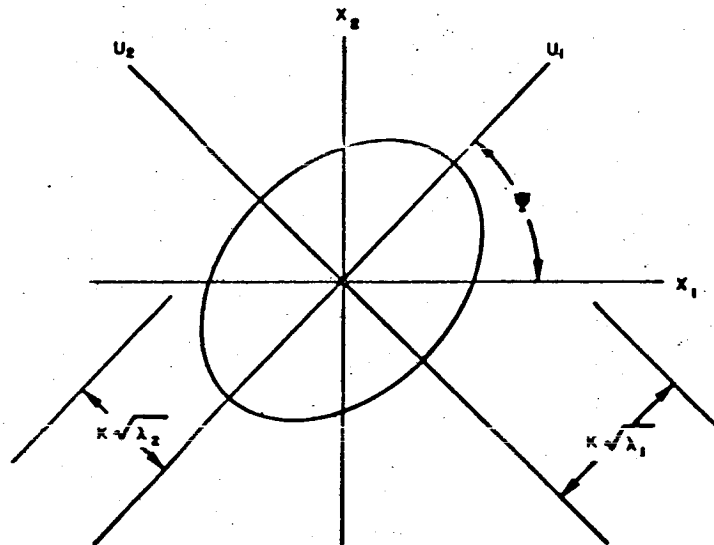
$$f(u_1, u_2) = \frac{1}{2\pi\sqrt{\lambda_1\lambda_2}} \exp \left[-\frac{1}{2} \left(\frac{u_1^2}{\lambda_1} + \frac{u_2^2}{\lambda_2} \right) \right] \quad (\text{B.45})$$

where λ_1 and λ_2 are the eigenvalues of the covariance matrix and can be expressed

$$\lambda_1 = \frac{\sigma_1^2}{2} \left\{ 1 + \left(\frac{\sigma_2}{\sigma_1} \right)^2 + \sqrt{\left[1 - \left(\frac{\sigma_2}{\sigma_1} \right)^2 \right]^2 + 4 \left(\rho \frac{\sigma_2}{\sigma_1} \right)^2} \right\} \quad (\text{B.45a})$$

$$\lambda_2 = \frac{\sigma_1^2}{2} \left\{ 1 + \left(\frac{\sigma_2}{\sigma_1} \right)^2 - \sqrt{\left[1 - \left(\frac{\sigma_2}{\sigma_1} \right)^2 \right]^2 + 4 \left(\rho \frac{\sigma_2}{\sigma_1} \right)^2} \right\} \quad (\text{B.45b})$$

The (x_1, x_2) and (u_1, u_2) coordinate systems are as shown below.



The probability of being within the ellipse

$$\frac{u_1^2}{\lambda_1} + \frac{u_2^2}{\lambda_2} = k^2 \quad (\text{B.46})$$

is

$$P = 4 \int_0^{\sqrt{\lambda_2 k}} \int_0^{\sqrt{\lambda_1 \left(k^2 - \frac{u_2^2}{\lambda_2} \right)}} \frac{1}{2\pi\sqrt{\lambda_1\lambda_2}} \exp \left[-\frac{1}{2} \left(\frac{u_1^2}{\lambda_1} + \frac{u_2^2}{\lambda_2} \right) \right] du_1 du_2 \quad (\text{B.47})$$

SYSTEM CONSIDERATIONS

After making the transformation of variables

$$u_1 = k\sqrt{\lambda_1} \cos \Psi \quad (\text{B.48})$$

$$u_2 = k\sqrt{\lambda_2} \sin \Psi, \quad (\text{B.49})$$

the probability can be expressed as

$$\begin{aligned} P &= 4 \int_0^k \int_0^{\pi/2} \frac{1}{2\pi\sqrt{\lambda_1\lambda_2}} e^{-\frac{1}{2}k^2} (k\sqrt{\lambda_1\lambda_2}) d\theta dk \\ &= \int_0^k k e^{-\frac{1}{2}k^2} dk = 1 - e^{-\frac{1}{2}k^2} \end{aligned} \quad (\text{B.50})$$

The above expression does not hold for $\sigma_2 = 0$ or $\rho = 1$.

For the dispersion analysis presented in Chapter 3, it was assumed that downrange and crossrange dispersions are uncorrelated; therefore, ρ is equal to zero. It is reasonable to assume that these errors are uncorrelated for a boost vehicle and for the particular coordinate system used.

To be conservative in the calculation of the downrange dispersions due to the burnout errors, it was assumed that the errors have unit positive correlation. This means that the downrange dispersion is simply the sum of the absolute values of each dispersion associated with an error source. If the individual dispersions were assumed to be uncorrelated then the total dispersion would have been the R.S.S. value. This would be an optimistic result, since burnout errors are correlated to a certain degree and the R.S.S. value is somewhat less than the algebraic sum.

3. LOADS AND AERODYNAMIC HEATING

The acceleration at burnout (in g's) for vacuum operations is simply,

$$a_{\text{BO}_{\text{vac}}} = \frac{T_{\text{vac}}}{W_{\text{BO}}} \quad (\text{B.51})$$

which can be written as,

$$a_{\text{BO}_{\text{vac}}} = \frac{T_{\text{vac}}}{W_O} r \quad (\text{B.52})$$

where

$$r = \frac{W_O}{W_{\text{BO}}}$$

and has been plotted and presented as Figure 39 in Chapter 3. To correct a_{BO} for atmospheric operation it is necessary to account for drag and nozzle back pressure. Acceleration at burnout now can be written as

$$a_{BO} = \frac{T_{BO} - D_{BO}}{W_{BO}} \quad (B.53)$$

The thrust equals,

$$T_{BO} = \left[1 - (1 - \lambda) \frac{P_{BO}}{P_o} \right] T_{vac} \quad (B.54)$$

where

$$\lambda = \frac{I_{spSL}}{I_{spvac}}$$

The drag equals,

$$D = q C_D A \quad (B.55)$$

where

$$q = 1/2 \rho V^2$$

substituting Equations (B.54) and (B.55) into Equation (B.53)

$$a_{BO} = \frac{\left[1 - (1 - \lambda) \frac{P_{BO}}{P_o} \right] T_{vac} - q C_D A}{W_{BO}} \quad (B.56)$$

multiplying the numerator and denominator by W_O , Equation (B.56) becomes

$$a_{BO} = \left\{ \left[1 - (1 - \lambda) \frac{P_{BO}}{P_o} \right] \frac{T_{vac}}{W_O} - q_{BO} \frac{C_D A}{W_O} \right\} r \quad (B.57)$$

The dynamic pressure, q_{BO} , as a function of altitude and velocity at burnout, the pressure ratio P_{BO}/P_o as a function of altitude, and the Mach number as a function of dynamic pressure for altitudes of 30 and 35,000 feet are plotted in Figures 40, 41 and 45 respectively, assuming The ARDC Model Atmosphere.⁵

To compute the acceleration at q_{max} , compute acceleration, a , assuming vacuum operation. The acceleration, a , equals

$$a = \frac{T_{vac}}{W} \quad (B.58)$$

SYSTEM CONSIDERATIONS

The vehicle weight equals,

$$W = W_0 - Wt \quad (B. 59)$$

$$= W_0 - \frac{T_{vac}}{I_{sp}} t \quad (B. 60)$$

substituting Equation (B. 60) into Equation (B. 58)

$$a = \frac{\frac{T_{vac}}{W_0}}{1 - \frac{T_{vac}}{W_0} \frac{t}{I_{sp}}} \quad (B. 61)$$

The parameter, a , is plotted as Figure 40 of Chapter 3. To correct for the atmospheric effects, the vacuum acceleration is adjusted in the same manner as was the acceleration at burnout

$$a_{q_{max}} = a \left\{ \left[1 - (1 - \lambda) \frac{p_{q_{max}}}{p_0} \right] - \frac{q_{max}}{\frac{T_{vac}}{W_0} \left(\frac{W}{C_D A} \right)} \right\} \quad (B. 62)$$

The nomographs for maximum dynamic pressure, q_{max} ; time of maximum dynamic pressure, $t_{q_{max}}$; maximum heating rate parameter, $(qV)_{max}$; and the total heating parameter, $\int qV dt$, were all derived empirically from machine computed trajectory calculations of one stage vehicles having parameters representative of current vehicles and vehicles anticipated in the near future. To develop the total heat input parameter, since heating is also experienced during second stage operation, it was assumed that the parameter was distributed symmetrically about $(qV)_{max}$ and twice the value of $\int qV dt$ at $(qV)_{max}$ was taken as the value for the total heat integral. This has been found to be a very good approximation. Though heating is experienced during second stage operation, the effect of its parameters on the total heat impact parameter has been found to be relatively small. The inaccuracy of these nomographs, from comparisons with many trajectory computations, has been found to be less than 10 percent.

The logic of the relationship between the parameter, $\int qV dt$, and aerodynamic heating is substantially as follows: At a particular location on a body and for a specific time during a vehicle's trajectory, the heat transfer rate from the boundary layer to the wall can be written as

$$\dot{q}_{BL} = C_H \rho_e V_e (h_r - h_w) \quad (\text{All quantities being time dependent functions of the trajectory})$$

where

C_H = the Stanton number (heat transfer coefficient)

ρ_e = the local density at the edge of the boundary layer

V_e = the local velocity at the edge of the boundary layer

h_r = the recovery enthalpy, $h_r = \frac{r V_e^2}{2J} + h_e$, with r being the recovery factor and J the mechanical equivalent of heat

h_e = the static enthalpy of the air at the edge of the boundary layer

h_w = the static enthalpy of the air at the wall, for a wall temperature T_w .

If it is assumed that

- 1) $(h_r - h_w) \sim V_e^2$, implying either that h_e and h_w are negligible in comparison to the V_e^2 term or that h_e and h_w essentially cancel each other and
- 2) the Stanton number is a very weak function of the flow conditions, then it follows that

$$\dot{q}_{BL} \sim \rho_e V_e^3$$

However, since ρ_e and V_e are directly related to ρ and V , respectively, for a given body geometry and free stream Mach number, it also follows that

$$\dot{q}_{BL} \sim \rho V^3$$

Finally, by integrating,

$$\int \dot{q}_{BL} dt \sim \int \rho V^3 dt \sim \int q V dt$$

In calculating the aerodynamic heating rate, it is customary to relate the Stanton number to the skin friction coefficient (c_f) via the Reynolds analogy; viz., $C_h = C_f/2$. It then follows that

$$C_h \sim \frac{1}{R_e^{1/5}} \sim \frac{1}{\rho_e^{1/5} V_e^{1/5}} \quad (\text{for turbulent flow})$$

and

$$C_h \sim \frac{1}{R_e^{1/2}} \sim \frac{1}{\rho_e^{1/2} V_e^{1/2}} \quad (\text{for laminar flow})$$

where R_e is the Reynolds number.

Strictly speaking, one might assume that $\dot{q}_{BL} \sim \rho_e^{0.8} V_e^{2.8}$ for turbulent flow, which is practically equal to $\rho_e V_e^3$; for laminar flow, on the other hand,

$q_{BL} \sim \rho_e^{0.5} V_e^{2.5}$. Hence the parameter $\int qV dt$ should be considered as a representative parameter for turbulent heating, and could be misleading if applied to trajectories where transition to laminar flow takes place early enough to significantly influence the skin temperatures.

The diagram illustrates the geometry of a rocket launch from a curved Earth surface. Key elements include:

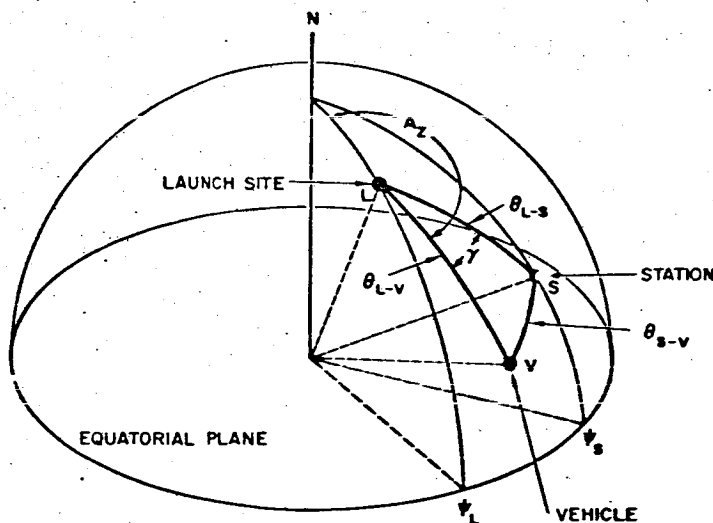
- Earth Surface:** A circular arc with center C and radius r_e .
- Launch Vertical:** A line passing through point D on the Earth's surface, labeled "LAUNCH VERTICAL".
- Launch Point:** Point A on the Earth's surface.
- Flight Path:** A line segment AB representing the rocket's trajectory, with distance \bar{R} from A to B .
- Altitude:** The distance h from the Earth's surface to point B .
- Angles:**
 - ϵ : Angle between the launch vertical and the line AD .
 - ϕ : Angle between the launch vertical and the flight path AB .
 - β : Angle between the flight path AB and the horizontal line through B .
 - α : Angle between the horizontal line through B and the vertical line through B .
 - θ : Central angle at C between the radii to points A and B .
 - γ : Angle between the flight path AB and the radius CA .
- Shaded Region:** A region between the Earth's surface and the flight path, shaded with a stippled pattern.

$$\sin (\zeta + 90^{\circ}) = \frac{\bar{R} \sin \theta}{r_c + h} \quad (\text{B. 63})$$
$$\bar{R} = \sqrt{(r_e + h)^2 + r_e^2 - 2r_e(r_e + h)\cos\theta} \quad (\text{B.64})$$
$$\zeta = \sin^{-1} \left(\frac{\bar{R} \sin \theta}{r_e + h} \right) - 90^\circ \quad (\text{B. 65})$$

The range angle, θ , is determined as the angle from launch site to the vehicle during the vehicle performance evaluation. However, when a tracking radar is located at a station other than the launch site, Equation B.61 can be used only when the range angle is the value measured from the given station to the vehicle, θ_{S-V} . It is assumed that the location of the auxiliary station, as well as the launch site, is known in terms of latitude and longitude.

With this information, θ_{S-V} can be found from the schematic below which shows that the range angle between the launch site and the station can be found using the law of cosines for a spherical triangle.

$$\theta_{L-S} = \cos^{-1} (\sin \lambda_L \sin \lambda_S + \cos \lambda_L \cos \lambda_S \cos |\psi_L - \psi_S|) \quad (B.66)$$



where

λ_L = launch site latitude

λ_S = station latitude

ψ_L = launch site longitude

ψ_S = station longitude

$||$ = absolute magnitude

Since θ_{L-S} is given above and θ_{L-V} is obtained from the performance evaluation, θ_{S-V} can be found from the spherical triangle LSV if the angle γ is known. Referring to the above figure, the angle γ is the difference between the vehicle launch azimuth,

SYSTEM CONSIDERATIONS

A_z , and the azimuth of the station with respect to the launch site. The azimuth of the station is

$$A_{z_S} = \sin^{-1} \left[\frac{\sin |\psi_L - \psi_S| \sin \theta_{L-S}}{\cos \lambda_S} \right] \quad (B.67)$$

Solving for γ ,

$$\left. \begin{aligned} \gamma &= |A_z - A_{z_S}| \\ &= \left| A_z - \sin^{-1} \left[\frac{\sin |\psi_L - \psi_S| \sin \theta_{L-S}}{\cos \lambda_S} \right] \right| \quad \text{for } \psi_L \geq \psi_S \\ \text{and} \\ &= \left| A_z - 360 + \sin^{-1} \left[\frac{\sin |\psi_L - \psi_S| \sin \theta_{L-S}}{\cos \lambda_S} \right] \right| \quad \text{for } \psi_L < \psi_S \end{aligned} \right\} \quad (B.68)$$

Using the law of cosines for the spherical triangle LSV,

$$\theta_{S-V} = \cos^{-1} \left[\cos \theta_{L-V} \cos \theta_{L-S} + \sin \theta_{L-V} \sin \theta_{L-S} \cos \gamma \right] \quad (B.69)$$

The elevation at the station, ζ_S , can be found from Equation (B.65) using the value of θ_{S-V} .

The vehicle angular displacement, ϵ , with respect to the launch vertical is shown in the diagram on Page B-18. Examining the triangle B the angle at D is $180^\circ - \epsilon$ while the angle at B can be represented $\beta - \alpha$. Summing the angles of BCD,

$$180^\circ - \epsilon + \theta + \beta - \alpha = 180^\circ \quad (B.70)$$

Solving for ϵ ,

$$\epsilon = \beta + \theta - \alpha \quad (B.71)$$

The look angle, ϕ , shown in diagram at the point B, is the angle between the vehicle axis and the slant range vector, \bar{R} . Summing of the interior angles of triangle ABD,

$$\phi + (90^\circ - \zeta) + (180^\circ - \epsilon) = 180^\circ \quad (B.72)$$

Solving for ϕ ,

$$\phi = \zeta + \epsilon - 90^\circ \quad (B.73)$$

5 PERFORMANCE MARGIN ANALYSIS

In this section analytical expressions are derived relating perturbations of booster vehicle performance parameters to perturbations of burnout velocity. Parameters considered include inert weight, propellant weight, burnout weight, specific impulse, and thrust. The results obtained here are summarized in Table B-1 on page B-26.

In the following derivations it is assumed that the total velocity losses due to atmospheric effects and thrust vector not acting along the flight path, ΔV_{L_a} , are not affected by perturbations of vehicle performance parameters. Velocity losses, ΔV_g , due to gravitational effects are approximated by $\Delta V_{g_i} = g t_{B_i} \cos \bar{\beta}_i$ where t_{B_i} is the burning time and $\bar{\beta}_i$ is the average flight path angle of the i th stage. With this approximation, vehicle velocity at burnout can be expressed as follows:

$$V = \sum_{i=1}^N \Delta V_i = \sum_{i=1}^N \left(\Delta V_{I_i} - \Delta V_{g_i} - \Delta V_{L_{a_i}} \right) = \sum_{i=1}^N \left[g I_{sp_i} \ln \left(\frac{W_O}{W_{BO}} \right)_i - g t_{B_i} \cos \bar{\beta}_i - \Delta V_{L_{a_i}} \right] \quad (B.74)$$

Taking the total differential,

$$\begin{aligned} dV = \sum_{i=1}^N \left\{ \left[\frac{\partial(\Delta V)}{\partial I_{sp}} \right]_i dI_{sp_i} + \left[\frac{\partial(\Delta V)}{\partial W_O} \right]_i dW_{O_i} + \left[\frac{\partial(\Delta V)}{\partial W_{BO}} \right]_i dW_{BO_i} \right. \\ \left. + \left[\frac{\partial(\Delta V)}{\partial t_B} \right]_i dt_{B_i} + \left[\frac{\partial(\Delta V)}{\partial \Delta V_{L_a}} \right]_i d\Delta V_{L_{a_i}} \right\} \quad (B.75) \end{aligned}$$

The last term on the right-hand side of Equation (B.75) is zero because of the assumption that the velocity losses, $\Delta V_{L_{a_i}}$, will remain constant. The partial derivatives in Equation (B.75) can be evaluated from Equation (B.74). These are

$$\left[\frac{\partial(\Delta V)}{\partial I_{sp}} \right]_i = g \ln r_i \quad (B.76a)$$

$$\text{where } r_i = (W_O/W_{BO})_i$$

SYSTEM CONSIDERATIONS

$$\left[\frac{\partial(\Delta V)}{\partial W} \right]_C = \left(\frac{g \text{ Isp}}{W_O} \right)_i \quad (\text{B. 76b})$$

$$\left[\frac{\partial(\Delta V)}{\partial W} \right]_{BO} = - \left(\frac{g \text{ Isp}}{W_{BO}} \right)_i \quad (\text{B. 76c})$$

$$\left[\frac{\partial(\Delta V)}{\partial t_B} \right]_i = -g \cos \bar{\beta}_i \quad (\text{B. 76d})$$

Variations of burnout velocity due to perturbations of vehicle performance parameters are derived through suitably combining Equations (B. 75a) and (76d).

Specific Impulse. The first parameter considered is stage specific impulse. A perturbation of specific impulse is assumed to correspond to a change in propellant mass flow rate resulting in a change of burning time.

$$\therefore d \text{ Isp}_i = d \text{ Isp}_n \quad (i = n) \quad (\text{B. 77a})$$

$$d \text{ Isp}_i = 0 \quad (i \neq n) \quad (\text{B. 77b})$$

$$d W_{O_i} = 0 \quad (1 \leq i < N) \quad (\text{B. 77c})$$

$$d W_{BO_i} = 0 \quad (1 \leq i \leq N) \quad (\text{B. 77d})$$

$$d t_{B_i} = \frac{\lambda_n}{(T/W_O)_n} \left(1 - \frac{1}{r_n} \right) d \text{ Isp} \quad (i = n) \quad (\text{B. 77e})$$

$$d t_{B_i} = 0 \quad (i \neq n) \quad (\text{B. 77f})$$

Substituting Equations (B. 77a) through (B. 77f) into Equation (B. 75),

$$dV = \left[\frac{\partial(\Delta V)}{\partial \text{Isp}} \right]_n d \text{ Isp}_n + \left[\frac{\partial(\Delta V)}{\partial t_B} \right]_n \frac{\lambda_n}{(T/W_O)_n} \left(1 - \frac{1}{r_n} \right) d \text{ Isp}_n \quad (\text{B. 78})$$

Substituting Equations (B. 76a) and (B. 76b),

$$\frac{dV}{d \text{ Isp}_n} = g \left[\ln r_n - \frac{\lambda_n \cos \bar{\beta}_n}{(T/W_O)_n} \left(1 - \frac{1}{r_n} \right) \right] \quad (\text{ft/sec/sec}) \quad (\text{B. 79})$$

Inert Weight. The next parameter considered is stage inert weight. It is assumed that initial and burnout weights are perturbed equally.

$$\therefore d I_{sp_i} = 0 \quad (1 \leq i \leq N) \quad (B. 80a)$$

$$d W_{O_i} = d W_{ST_n} \quad (1 \leq i \leq n) \quad (B. 80b)$$

$$d W_{O_i} = 0 \quad (n+1 \leq i \leq N) \quad (B. 80c)$$

$$d W_{BO_i} = d W_{ST_n} \quad (1 \leq i \leq n) \quad (B. 80d)$$

$$d W_{BO_i} = 0 \quad (n+1 \leq i \leq N) \quad (B. 80e)$$

$$d t_{B_i} = 0 \quad (1 \leq i \leq N) \quad (B. 80f)$$

Substituting Equations (B. 80a) through (B. 80f) into Equation (B. 75),

$$d V = \sum_{i=1}^n \left\{ \left[\frac{\partial (\Delta V)}{\partial W_O} \right] d W_{ST_n} + \left[\frac{\partial (\Delta V)}{\partial W_{BO}} \right]_i d W_{ST_n} \right\} \quad (B. 81)$$

Or substituting Equations (B. 76b) and (B. 76c),

$$\frac{d V}{d W_{ST_n}} = \sum_{i=1}^n \left(\frac{g I_{sp}}{W_O} \right)_i (1 - r_i) \quad (\text{ft/sec/lb}) \quad (B. 82)$$

For a one-stage vehicle,

$$\frac{d V}{d W_{ST}} = \frac{g I_{sp}}{W_O} (1 - r) \quad (\text{ft/sec/lb}) \quad (B. 83)$$

Payload Weight. A payload dispersion is identical to an inert weight dispersion of the nth stage.

$$\therefore \frac{d V}{d W_{PL}} = \frac{d V}{d W_{ST_N}} \quad (B. 84)$$

For a one-stage vehicle,

$$\frac{d V}{d W_{PL}} = \frac{d V}{d W_{ST}} \quad (B. 85)$$

SYSTEM CONSIDERATIONS

Burnout Weight. The next parameter considered is stage burnout weight. It is assumed that initial weight and propellant mass flow rate remain constant resulting in a change of burning time.

$$\therefore d Isp_i = 0 \quad (1 \leq i \leq N) \quad (B. 86a)$$

$$d W_{O_i} = 0 \quad (1 \leq i \leq N) \quad (B. 86b)$$

$$d W_{BO_i} = d W_{BO_n} \quad (i = n) \quad (B. 86c)$$

$$d W_{BO_i} = 0 \quad (i \neq n) \quad (B. 86d)$$

$$d t_{B_i} = - \frac{\lambda_n Isp_n d W_{BO_n}}{W_{O_n} (T/W_{O_n})} \quad (i = n) \quad (B. 86d)$$

$$d t_{B_i} = 0 \quad (i \neq n) \quad (B. 86f)$$

Substituting Equations (B. 86a) through (B. 86f) into Equation (B. 75),

$$d V = \left[\frac{\partial (\Delta V)}{\partial W_{BO}} \right]_n d W_{BO_n} - \left[\frac{\partial (\Delta V)}{\partial t_B} \right]_n \frac{\lambda_n Isp_n d W_{BO_n}}{W_{O_n} (T/W_{O_n})} \quad (B. 87)$$

or substituting Equations (B. 86c) and (B. 86d),

$$\frac{d V}{d W_{BO_n}} = - \left(\frac{g Isp}{W_{O_n}} \right)_n \left[r_n - \frac{\lambda_n \cos \bar{\beta}_n}{(T/W_{O_n})_n} \right] \quad (\text{ft/sec/lb}) \quad (B. 88)$$

Propellant Weight. The next parameter considered is stage propellant weight. It is assumed that structural weight is not varied.

$$\therefore d Isp_i = 0 \quad (1 \leq i \leq N) \quad (B. 89a)$$

$$d W_{O_i} = d W_{P_n} \quad (1 \leq i \leq n) \quad (B. 89b)$$

$$d W_{O_i} = 0 \quad (n+1 \leq i \leq N) \quad (B. 89c)$$

$$d W_{BO_i} = d W_{P_n} \quad (1 \leq i \leq n-1) \quad (B. 89c)$$

$$d W_{BO_i} = 0 \quad (n \leq i \leq N) \quad (B. 89e)$$

$$d t_{B_i} = \frac{\lambda_n Isp_n d W_{P_n}}{W_{O_n} (T/W_{O_n})_n} \quad (i = n) \quad (B. 89f)$$

$$d t_{B_i} = 0 \quad (i \neq n) \quad (B. 89g)$$

Substituting Equations (B. 89a) through (B. 89g) into Equation (B. 75),

$$d V = \left\{ \sum_{i=1}^n \left[\frac{\partial(\Delta V)}{\partial W_{O_i}} \right] + \left[\frac{\partial(\Delta V)}{\partial W_{BO_i}} \right] - \left[\frac{\partial(\Delta V)}{\partial W_{BO_n}} \right] + \left[\frac{\partial(\Delta V)}{\partial t_{B_n}} \right] \frac{\lambda_n Isp_n}{W_{O_n} (T/W_{O_n})_n} \right\} d W_{P_n} \quad (B. 90)$$

Or substituting Equations (B. 76b), (B. 76c), and (B. 76d),

$$\frac{d V}{d W_{P_n}} = \sum_{i=1}^n \left[\left(\frac{g Isp}{W_{O_i}} \right) (1 - r_i) \right] + \left(\frac{g Isp}{W_{O_n}} \right) \left[r_n - \frac{\lambda_n \cos \bar{\beta}_n}{(T/W_{O_n})_n} \right] \quad (\text{ft/sec/lb}) \quad (B. 91)$$

By substituting Equations (B. 82) and (B. 88), Equation (B. 91) can be written in terms of previously derived expressions.

$$\frac{d V}{d W_{P_n}} = \frac{d V}{d W_{ST_n}} - \frac{d V}{d W_{BO_n}} \quad (\text{ft/sec/lb}) \quad (B. 92)$$

For a one-stage vehicle Equation (B. 91) reduces to

$$\frac{d V}{d W_P} = \frac{g Isp}{W_O} \left[1 - \frac{\lambda \cos \bar{\beta}}{(T/W_O)} \right] \quad (\text{ft/sec/lb}) \quad (B. 93)$$

Stage Thrust. The last parameter considered is stage thrust. Specific impulse is assumed constant, therefore a thrust perturbation results in variations of propellant mass flow rate and burning time. Thrust perturbation, dT , is expressed as a percentage of nominal initial thrust.

$$\therefore d Isp_i = 0 \quad (1 \leq i \leq N) \quad (B. 94a)$$

$$d W_{O_i} = 0 \quad (1 \leq i \leq N) \quad (B. 94b)$$

SYSTEM CONSIDERATIONS

$$d W_{BO_i} = 0 \quad (1 \leq i \leq N) \quad (B. 94c)$$

$$d t_{B_i} = - \frac{\lambda_n Isp_n}{100 (T/W_O)_n} \left(1 - \frac{1}{r_n} \right) d T_n \quad (i = n) \quad (B. 94d)$$

$$d t_{B_i} = 0 \quad (i \neq n) \quad (B. 94e)$$

Substituting Equations (B. 94a) through (B. 94e) into Equation (B. 75),

$$d V = \left[\frac{\partial (\Delta V)}{\partial t_B} \right]_n \frac{\lambda_n Isp_n}{100 (T/W_O)_n} \left(1 - \frac{1}{r_n} \right) d T_n$$

Or substituting Equation (B. 76d),

$$\frac{d V}{d T_n} = \frac{\lambda_n g Isp_n \cos \bar{\beta}_n}{100 (T/W_O)_n} \left(1 - \frac{1}{r_n} \right) \quad (\text{ft/sec/percent}) \quad (B. 95)$$

Table B-1. Summary of Velocity Exchange Coefficients for Computing Vehicle Performance Margins

Stage Parameter	Coefficient	Units
Inert Weight	$\frac{d V}{d W_{ST_n}} = \sum_{i=1}^n \left(\frac{g Isp}{W_O} \right)_i \left(1 - r_i \right)$	(ft/sec/lb)
Payload Weight	$\frac{d V}{d W_{PL}} = \frac{d V}{d W_{ST_n}}$	(ft/sec/lb)
Burnout Weight	$\frac{d V}{d W_{BO_n}} = - \left(\frac{g Isp}{W_O} \right)_n \left[r_n - \frac{\lambda_n \cos \bar{\beta}_n}{(T/W_O)_n} \right]$	(ft/sec/lb)
Propellant Weight	$\frac{d V}{d W_{P_n}} = \frac{d V}{d W_{ST_n}} - \frac{d V}{d W_{BO_n}}$	(ft/sec/lb)
Specific Impulse	$\frac{d V}{d Isp_n} = g \left[\ln (r_n) - \frac{\lambda_n \cos \bar{\beta}_n}{(T/W_O)_n} \left(1 - \frac{1}{r_n} \right) \right]$	(ft/sec/sec)
Thrust	$\frac{d V}{d T_n} = \frac{\lambda_n g Isp_n \cos \bar{\beta}_n}{100 (T/W_O)_n} \left(1 - \frac{1}{r_n} \right)$	(ft/sec/percent)

Nomenclature

B-27

NOMENCLATURE

A	Reference area for aerodynamic coefficients
A_z	Launch azimuth measured clockwise from true North
A_{zdl}	Azimuth of the trajectory after dog-leg
A_{zs}	Azimuth of tracking station with respect to the launch site
a_{BO}	Axial acceleration at burnout of a stage
$a_{q_{max}}$	Axial acceleration at maximum dynamic pressure
C_D	Drag coefficient
C_H	Stanton number
c	$\left(\frac{h_{BO} + r_e}{\mu_e} \right) v_{BO}^2$
D	Drag force
h_1	Altitude of circular orbit at initiation of Hohmann transfer maneuver
h_2	Final altitude at the end of the Hohmann transfer
h_{BO}	Altitude at burnout
h_e	Static enthalpy of the air at the edge of the boundary layer
h_o	Altitude of circular orbit
h_r	Recovery enthalpy
h_w	Static enthalpy of the air at the wall for a wall temperature T_w
$I_{sp_{sl}}$	Sea level specific impulse
$I_{sp_{vac}}$	Vacuum specific impulse
i	Orbit inclination or integer corresponding to a particular stage
J	Mechanical equivalent of heat
k	Integer defining the number of standard deviation units (σ) from the mean
P	Probability
p_{BO}	Atmospheric pressure at burnout altitude
$p_{q_{max}}$	Atmospheric pressure at the altitude of maximum dynamic pressure

SYSTEM CONSIDERATIONS

p_c	Atmospheric pressure at sea level
q	Dynamic pressure
q_{BO}	Dynamic pressure at a stage burnout
q_{BL}	Heat transfer rate from the boundary layer to the wall
q_{max}	Maximum dynamic pressure
R	Slant range
R_{CR}	Range in the cross range direction
R_{DR}	Range in the down range direction
Re	Reynolds number
r	$\frac{W_O}{W_{BO}} =$ Mass ratio or recovery factor
r_a	Radius from the center of attraction to apogee
r_e	Radius of the earth
r_p	Radius from the center of attraction to perigee
T_{BO}	Thrust at burnout of a stage
T_w	Wall Temperature
$\frac{T}{W_O}$	Initial thrust to weight ratio at liftoff
t	Time
t_{BR}	Time during ballistic flight from burnout to impact
$t_{q_{max}}$	Time from liftoff to the occurrence of maximum dynamic pressure
T_{vac}	Vacuum thrust
v_a	Velocity at apogee
v_{BO}	Velocity at burnout
v_e	Local velocity at the edge of the boundary layer
v_{final}	Final circular orbit velocity at the apogee altitude
v_o	Circular orbital velocity at h_o
v_p	Velocity at perigee
w_{BO}	Burnout weight
w_o	Gross weight

Nomenclature

B-29

W_P	Propellant weight
W_{ST}	Structure weight
X_i	Variates in dispersion analysis
α	Angle of attack
β	Flight path angle
$\bar{\beta}$	Average flight path angle
β_{BO}	Flight path angle at burnout
γ	Angle defined on figure on Page B-19
ΔV_{dl}	Velocity increment required to rotate circular orbit plane through an angle
ΔV_e	Velocity increment due to the earth's rotation at a particular latitude along a particular azimuth
ΔV_g	Velocity losses due to gravity effects
ΔV_{L_a}	Velocity losses due to atmospheric effects
$\Delta V_{T_{dl}}$	$\Delta V_1 + \Delta V_{2_{dl}}$ = Total velocity increment for Hohmann transfer and dog-leg maneuver
$\Delta V_{2_{dl}}$	Increment of velocity required to circularize and dog-leg at the final injection of the Hohmann transfer maneuver
ϵ_{dl}	Dog-leg angle
ϵ	Angle defining the vehicle attitude with respect to the launch vertical
ζ	Elevation angle
θ	Range angle
θ_{BR}	Range angle traversed during ballistic flight
θ_{L-S}	Range angle between launch site and tracking station
θ_{L-V}	Range angle between launch site and vehicle
θ_{S-V}	Range angle between tracking station and vehicle
λ	Latitude or ratio of sea level specific impulse to vacuum specific impulse
λ_L	Latitude of the launch site
λ_S	Latitude of tracking station
μ_e	Gravitational constant of the earth

SYSTEM CONSIDERATIONS

ρ	Correlation coefficient or atmospheric density
ρ_e	Local density at the edge of the boundary layer
σ_i	Standard deviation of element i
σ_{ij}	Covariance of elements i and j
ϕ	Look angle
ψ	Defined by Equation (B.41)
ψ_L	Longitude of launch site
ψ_N	Longitude of nodes from Greenwich meridian
ψ_S	Longitude of tracking station
ω_e	Angular rate of rotation of the earth

REFERENCES

1. Albert D. Wheelon, "Free Flight of A Ballistic Missile," Trajectory Studies of Ballistic Missiles, Satellites, and Space Vehicles, Space Technology Laboratories, Inc.
2. L. J. Skidmore, "Equiprobability Density Ellipses of the Bivariate Normal Density Function," STL Memo 7340.3-131, 26 August 1960.
3. R. A. Meehl, "CEP for Correlated Errors with Unequal Standard Deviations," STL GM 41.2-108, 28 October 1957.
4. F. B. Hildebrand, Methods of Applied Mathematics, Prentice-Hall, Inc., 1952, pp. 35-42.
5. "A Table of the Atmospheric Functions," IBM 7090 Generated by RW MA5F Based on the Tables of The ARDC Model Atmosphere, 1959 Geophysics Directorate Air Force Cambridge Research Center, Air Research and Development Command, July 1, 1960.

APPENDIX C

DEVELOPMENT OF GENERALIZED EXCHANGE RATIOS

Presented herein is the derivation of the equations and relationships used in Chapter 4.

1 PAYLOAD EXCHANGE RATIOS

In this section analytical expressions are derived which relate the effect on vehicle payload capability of perturbations of booster performance parameters. Parameters considered include specific impulse, structural weight, initial stage gross weight, propellant weight, and thrust. Exchange ratios are derived for both single-stage and multistage vehicles.

For this analysis it is assumed that burnout velocity remains constant and the effect of a perturbation of a vehicle parameter is realized as a variation in the payload weight. It is assumed that the total velocity losses, ΔV_{L_i} , due to atmospheric effects and thrust components not acting along the flight path will remain constant. Velocity losses, V_{g_i} , due to gravitation effects are approximated by $V_{g_i} = g t_{B_i} \cos \bar{\beta}_i$, where t_{B_i} is the burning time and $\bar{\beta}_i$ is the average flight path angle of the i th stage. It is assumed that $\bar{\beta}_i$ is not affected by perturbing a single performance parameter.

The equation for the total velocity gained at burnout can be expressed as follows:

$$\begin{aligned} V &= \sum_{i=1}^N \Delta V_i = \sum_{i=1}^N \left(\Delta V_{I_i} - \Delta V_{g_i} - \Delta V_{L_{a_i}} \right) \\ &= \sum_{i=1}^N \left[g I_{sp_i} \ln \left(\frac{W_O}{W_{BO}} \right)_i - g t_{B_i} \cos \bar{\beta}_i - \Delta V_{L_{a_i}} \right] \end{aligned} \quad (C.1)$$

Taking the total differential,

$$\begin{aligned} dV &= \sum_{i=1}^N \left\{ \left[\frac{\partial(\Delta V)}{\partial I_{sp}} \right]_i dI_{sp_i} + \left[\frac{\partial(\Delta V)}{\partial W_O} \right]_i dW_{O_i} + \left[\frac{\partial(\Delta V)}{\partial W_{BO}} \right]_i dW_{BO_i} \right. \\ &\quad \left. + \left[\frac{\partial(\Delta V)}{\partial t_B} \right]_i dt_{B_i} + \left[\frac{\partial(\Delta V)}{\partial \Delta V_{L_a}} \right]_i d\Delta V_{L_{a_i}} \right\} \end{aligned} \quad (C.2)$$

The last term on the right-hand side of Equation (C.2) being zero because of the assumption that the velocity losses, ΔV_{La} will remain constant. It is assumed the total velocity gained remains constant.

$$\therefore dV = 0 \quad (C.3)$$

The equation, combining Equations (C.2) and (C.3),

$$\sum_{i=1}^N \left\{ \left[\frac{\partial(\Delta V)}{\partial Isp} \right]_i dIsp_i + \left[\frac{\partial(\Delta V)}{\partial W_O} \right]_i dW_{O_i} + \left[\frac{\partial(\Delta V)}{\partial W_{BO}} \right]_i dW_{BO_i} + \left[\frac{\partial(\Delta V)}{\partial t_B} \right]_i dt_{B_i} \right\} = 0 \quad (C.4)$$

becomes the foundation for the development of the exchange ratios. The partial derivatives in Equation (C.4) can be evaluated from the term on the right in Equation (C.1). These are:

$$\left[\frac{\partial(\Delta V)}{\partial Isp} \right]_i = g \ln r_i \quad (C.5a)$$

where

$$r_i = \left(\frac{W_O}{W_{BO_i}} \right)$$

$$\left[\frac{\partial(\Delta V)}{\partial W_O} \right]_i = \left(\frac{g Isp}{W_O} \right) \quad (C.5b)$$

$$\left[\frac{\partial(\Delta V)}{\partial W_{BO}} \right]_i = - \left(\frac{g Isp}{W_{BO}} \right) \quad (C.5c)$$

$$\left[\frac{\partial(\Delta V)}{\partial t_B} \right]_i = - g \cos \bar{\beta}_i \quad (C.5d)$$

Having developed these equations, the exchange ratios can be derived. The partial derivatives, rather than their functions, will be used in the development since this gives the reader a better understanding of the importance of each partial.

The first exchange ratio to be developed is

$$\left(\frac{dW_{PL}}{dIsp} \right)_n$$

A change in vacuum Isp for a particular stage is assumed to correspond to a change in propellant mass flow rate. No change in either the structural weight or propellant weight is assumed.

Payload Exchange Ratios

C-3

$$\therefore dIsp_i = dIsp_n, \quad (i = n) \quad (C. 6a)$$

$$dIsp_i = 0, \quad (i \neq n) \quad (C. 6b)$$

$$dW_{O_i} = dW_{PL}, \quad (1 \leq i \leq N) \quad (C. 6c)$$

$$dW_{BO_i} = dW_{PL}, \quad (1 \leq i \leq N) \quad (C. 6d)$$

$$dt_{B_i} = \left(1 - \frac{1}{r_n}\right) \frac{\lambda_n dIsp_n}{(T/W_O)_n}, \quad (i = n) \quad (C. 6e)$$

$$dt_{B_i} = 0, \quad (i \neq n) \quad (C. 6f)$$

Substituting Equations (C. 6a) through (C. 6f) into Equation (C. 4) and rearranging,

$$\frac{dW_{PL}}{dIsp_n} = - \frac{\left[\frac{\partial(\Delta V)}{\partial Isp} \right]_n + \left[\frac{\partial(\Delta V)}{\partial t_B} \right]_n \lambda_n \left(1 - \frac{1}{r_n}\right) \frac{1}{(T/W_O)_n}}{\sum_{i=1}^N \left[\frac{\partial(\Delta V)}{\partial W_O} \right]_i + \left[\frac{\partial(\Delta V)}{\partial W_{BO}} \right]_i} \quad (C. 7)$$

Substituting Equations (C. 5a) through (C. 5d),

$$\frac{dW_{PL}}{dIsp_n} = - \frac{g \ln r_n - \frac{\lambda_n g \cos \bar{\beta}_n \left(1 - \frac{1}{r_n}\right)}{(T/W_O)_n}}{\sum_{i=1}^N \left[\left(\frac{g Isp}{W_O} \right)_i - \left(\frac{g Isp}{W_{BO}} \right)_i \right]} \quad (C. 8)$$

Define the following parameter:

$$\theta = \frac{\lambda \cos \bar{\beta}}{T/W_O} \quad (C. 9)$$

$$\frac{dW_{PL}}{dIsp_n} = \frac{\ln r_n - \theta_n \left(1 - \frac{1}{r_n}\right)}{\sum_{i=1}^N \left(\frac{Isp}{W_O} \right)_i (r_i - 1)} \quad (C. 10)$$

For a one-stage vehicle, Equation (C.10) reduces to

$$\frac{dW_{PL}}{dIsp} = \frac{\ln r - \theta \left(1 - \frac{1}{r}\right)}{\frac{Isp}{W_0} (r - 1)} \quad (C.11)$$

The next exchange ratio to be developed is

$$\left(\frac{dW_{PL}}{dW_{ST_n}} \right)$$

It is assumed that with a change in structural weight, the propellant weight and specific impulse remain constant.

$$\therefore dIsp_i = 0, \quad (1 \leq i \leq N) \quad (C.12a)$$

$$dW_{O_i} = dW_{ST_n} + dW_{PL}, \quad (1 \leq i \leq n) \quad (C.12b)$$

$$dW_{O_i} = dW_{PL}, \quad (n+1 \leq i \leq N) \quad (C.12c)$$

$$dW_{BO_i} = dW_{ST_n} + dW_{PL}, \quad (1 \leq i \leq n) \quad (C.12d)$$

$$dW_{BO_i} = dW_{PL}, \quad (n+1 \leq i \leq N) \quad (C.12e)$$

$$dt_{B_i} = 0, \quad (1 \leq i \leq N) \quad (C.12f)$$

Substituting Equations (C.12a) through (C.12f) into Equation (C.4) and rearranging,

$$\frac{dW_{PL}}{dW_{ST_n}} = - \frac{\sum_{i=1}^n \left[\frac{\partial(\Delta V)}{\partial W_{O_i}} \right] + \left[\frac{\partial(\Delta V)}{\partial W_{BO_i}} \right]}{\sum_{i=1}^N \left[\frac{\partial(\Delta V)}{\partial W_{O_i}} \right] + \left[\frac{\partial(\Delta V)}{\partial W_{BO_i}} \right]} \quad (C.13)$$

Substituting Equations (C.5a), (C.5b), and (C.5c),

Payload Exchange Ratios

C-5

$$\frac{dW_{PL}}{dW_{ST_n}} = - \frac{\sum_{i=1}^n \left[\left(\frac{g_{isp}}{W_{O_i}} \right) - \left(\frac{g_{isp}}{W_{BO_i}} \right) \right]}{\sum_{i=1}^N \left[\left(\frac{g_{isp}}{W_{O_i}} \right) - \left(\frac{g_{isp}}{W_{BO_i}} \right) \right]} \quad (C.14)$$

Rearranging,

$$\frac{dW_{PL}}{dW_{ST_n}} = - \frac{\sum_{i=1}^n \left[\left(\frac{isp}{W_{O_i}} \right) (r_i - 1) \right]}{\sum_{i=1}^N \left[\left(\frac{isp}{W_{O_i}} \right) (r_i - 1) \right]} \quad (C.15)$$

For a one-stage vehicle, Equation (15) reduces to

$$\frac{dW_{PL}}{dW_{ST}} = -1 \quad (C.16)$$

The next exchange ratio to be considered is

$$\frac{dW_{PL}}{dW_{O_n}}$$

Here, it is assumed that both the propellant and structure weight are perturbed corresponding with an amount to accommodate the propellant weight change. The specific impulse is assumed to be constant.

$$\therefore d_{isp_i} = 0, \quad (1 \leq i \leq N) \quad (C.17a)$$

$$dW_{O_i} = dW_{O_n}, \quad (1 \leq i \leq n) \quad (C.17b)$$

$$dW_{O_i} = dW_{PL}, \quad (n+1 \leq i \leq N) \quad (C.17c)$$

$$dW_{BO_i} = dW_{O_n}, \quad (1 \leq i \leq n-1) \quad (C.17d)$$

$$dW_{BO_i} = dW_{PL} + dW_{ST_n}, \quad (i = n) \quad (C.17e)$$

C-6

DEVELOPMENT OF GENERALIZED EXCHANGE RATIOS

where from the definition of W_{ST_n} ,

$$W_{ST_n} = \sigma_n (W_{O_n} - W_{O_{n+1}})$$

$$\therefore dW_{ST_n} = \sigma_n (dW_{O_n} - dW_{O_{n+1}})$$

From Equation (C.17c),

$$dW_{O_{n+1}} = dW_{PL}$$

Substituting into Equation (C.17e) and rearranging,

$$dW_{BO_i} = (1 - \sigma_n) dW_{PL} + \sigma_n dW_{O_n}, \quad (i = n) \quad (C.17f)$$

$$dW_{BO_i} = dW_{PL}, \quad (n+1 \leq i \leq N) \quad (C.17g)$$

$$dt_{B_i} = \frac{\lambda_n Isp_n (1 - \sigma_n)}{W_{O_n} (T/W_{O_n})} (dW_{O_n} - dW_{PL}), \quad (i = n) \quad (C.17h)$$

$$dt_{B_i} = 0, \quad (i \neq n) \quad (C.17i)$$

Substituting Equations (C.17a) through (C.17i) into Equation (C.4) and rearranging,

$$\frac{dW_{PL}}{dW_{O_n}} = \frac{\sum_{i=1}^n \left[\left[\frac{\partial(\Delta V)}{\partial W_{O_i}} \right] + \left[\frac{\partial(\Delta V)}{\partial W_{BO_i}} \right] - (1 - \sigma_n) \left[\frac{\partial(\Delta V)}{\partial W_{BO_n}} \right] + \left[\frac{\partial(\Delta V)}{\partial t_B} \right] \frac{\lambda_n Isp_n (1 - \sigma_n)}{W_{O_n} (T/W_{O_n})} \right]}{\sum_{i=n+1}^N \left[\left[\frac{\partial(\Delta V)}{\partial W_{O_i}} \right] + \left[\frac{\partial(\Delta V)}{\partial W_{BO_i}} \right] \right] + (1 - \sigma_n) \left[\left[\frac{\partial(\Delta V)}{\partial W_{BO_n}} \right] - \left[\frac{\partial(\Delta V)}{\partial t_B} \right] \frac{\lambda_n Isp_n}{W_{O_n} (T/W_{O_n})} \right]} \quad (C.18)$$

Substituting Equations (C.5b), (C.5c), and (C.5d),

$$\frac{dW_{PL}}{dW_{O_n}} = \frac{\sum_{i=1}^n \left[\left(\frac{g Isp}{W_{O_i}} \right) - \left(\frac{g Isp}{W_{BO_i}} \right) \right] + (1 - \sigma_n) \left[\left(\frac{g Isp}{W_{BO_n}} \right) - \frac{\lambda_n g Isp_n \cos \bar{\beta}_n}{W_{O_n} (T/W_{O_n})} \right]}{\sum_{i=n+1}^N \left[\left(\frac{g Isp}{W_{O_i}} \right) - \left(\frac{g Isp}{W_{BO_i}} \right) \right] - (1 - \sigma_n) \left[\left(\frac{g Isp}{W_{BO_n}} \right) - \frac{g \lambda_n Isp_n \cos \bar{\beta}_n}{W_{O_n} (T/W_{O_n})} \right]} \quad (C.19)$$

Payload Exchange Ratios

C-7

Rearranging and substituting Equation (C.10),

$$\frac{dW_{PL}}{dW_{O_n}} = - \frac{\sum_{i=1}^n \left[\left(\frac{I_{sp}}{W_{O_i}} \right) (1 - r_i) \right] + (1 - \sigma_n) \left(\frac{I_{sp}}{W_{O_n}} \right) (r_n - \theta_n)}{\sum_{i=n+1}^N \left[\left(\frac{I_{sp}}{W_{O_i}} \right) (1 - r_i) \right] - (1 - \sigma_n) \left(\frac{I_{sp}}{W_{O_n}} \right) (r_n - \theta_n)} \quad (C.20)$$

For a one-stage vehicle, Equation (C.20) reduces to

$$\frac{dW_{PL}}{dW_O} = \frac{1 - \sigma r - (1 - \sigma)\theta}{(1 - \sigma)(r - \theta)} \quad (C.21)$$

If one assumes a constant T/W_O is maintained and the velocity losses due to both gravitational and atmospheric effects are not affected by a perturbation of stage gross weight, then Equation (C.21) reduces to the following form:

$$\begin{aligned} \frac{dW_{PL}}{dW_O} &= \frac{1 - \sigma r}{(1 - \sigma)r} \\ &= \frac{W_{PL}}{W_O} \end{aligned} \quad (C.22)$$

The next exchange ratio to be evaluated is

$$\frac{dW_{PL}}{dW_P}$$

Here, two cases will be considered. One will consider only a perturbation of the propellant weight, while the other will assume a proportional variation in structural weight to accommodate the change in propellant. The specific impulse in both cases is assumed constant.

For the first case,

$$\left(\frac{dW_{PL}}{dW_{P_n}} \right)_{W_{ST_n}}$$

$$dI_{sp_i} = 0, \quad (1 \leq i \leq N) \quad (C.22a)$$

$$dW_{O_i} = dW_{PL} + dW_{P_n}, \quad (1 \leq i \leq n) \quad (C.22b)$$

C-8

DEVELOPMENT OF GENERALIZED EXCHANGE RATIOS

$$dW_{O_i} = dW_{PL}, \quad (n+1 \leq i \leq N) \quad (C.22c)$$

$$dW_{BO_i} = dW_{PL} + dW_{P_n}, \quad (1 \leq i \leq n-1) \quad (C.22d)$$

$$dW_{BO_i} = dW_{PL}, \quad (n \leq i \leq N) \quad (C.22e)$$

$$dt_{B_i} = \frac{\lambda_n Isp_n}{W_{O_n} (T/W_{O_n})} dW_{P_n}, \quad (i = n) \quad (C.22f)$$

$$dt_{B_i} = 0, \quad (i \neq n) \quad (C.22g)$$

Substituting Equations (C.22a) through (C.22g) into Equation (C.4) and rearranging,

$$\left(\frac{dW_{PL}}{dW_{P_n}} \right)_{W_{ST_n}} = - \frac{\sum_{i=1}^n \left[\frac{\partial(\Delta V)}{\partial W_{O_i}} \right] + \sum_{i=1}^{n-1} \left[\frac{\partial(\Delta V)}{\partial W_{BO_i}} \right] + \left[\frac{\partial(\Delta V)}{\partial t_B} \right]_n \frac{\lambda_n Isp_n}{W_{O_n} (T/W_{O_n})}}{\sum_{i=1}^N \left[\frac{\partial(\Delta V)}{\partial W_{O_i}} \right] + \left[\frac{\partial(\Delta V)}{\partial W_{BO_i}} \right]} \quad (C.23)$$

Substituting Equations (C.5b), (C.5c), (C.5d), and (C.10),

$$\left(\frac{dW_{PL}}{dW_{P_n}} \right)_{W_{ST_n}} = \frac{\left(\frac{Isp}{W_{O_n}} \right) (1 - \theta_n) - \sum_{i=1}^{n-1} \left[\left(\frac{Isp}{W_{O_i}} \right) (r_i - 1) \right]}{\sum_{i=1}^N \left[\left(\frac{Isp}{W_{O_i}} \right) (r_i - 1) \right]} \quad (C.24)$$

For a one-stage vehicle, Equation (C.24) reduces to

$$\left(\frac{dW_{PL}}{dW_P} \right)_{W_{ST}} = \frac{(1 - \theta)}{(r - 1)} \quad (C.25)$$

Payload Exchange Ratios

C-9

For the second case,

$$\frac{dW_{PL}}{dW_{P_n}}$$

$$dI_{sp} = 0, \quad (1 \leq i \leq N) \quad (C.26a)$$

$$dW_{O_i} = dW_{O_n}, \quad (1 \leq i \leq n) \quad (C.26b)$$

$$dW_{O_i} = dW_{PL}, \quad (n+1 \leq i \leq N) \quad (C.26c)$$

$$dW_{BO_i} = dW_{O_n}, \quad (1 \leq i \leq n-1) \quad (C.26d)$$

$$dW_{BO_i} = dW_{PL} + dW_{ST_n}, \quad (i = n) \quad (C.26e)$$

$$dW_{BO_i} = dW_{PL}, \quad (n+1 \leq i \leq N) \quad (C.26f)$$

Now,

$$dW_{O_n} = dW_{P_n} + dW_{ST_n} + dW_{PL} \quad (C.27)$$

as before, and from Equation (C.26c),

$$dW_{ST_n} = \sigma_n (dW_{O_n} - dW_{PL}) \quad (C.28)$$

$$\therefore dW_{O_n} = \frac{dW_{P_n}}{1 - \sigma_n} + dW_{PL} \quad (C.29)$$

Substituting Equation (C.29) into Equation (C.26b) and Equation (C.28) into Equation (C.26e),

$$dW_{O_i} = \frac{dW_{P_n}}{1 - \sigma_n} + dW_{PL}, \quad (1 \leq i \leq n) \quad (C.30a)$$

$$dW_{BO_i} = \frac{dW_{P_n}}{1 - \sigma_n} + dW_{PL}, \quad (1 \leq i \leq n-1) \quad (C.30b)$$

C-10

DEVELOPMENT OF GENERALIZED EXCHANGE RATIOS

$$dW_{BO_i} = \left(\frac{\sigma_n}{1 - \sigma_n} \right) dW_{P_n} + dW_{PL}, \quad (i = n) \quad (C.30c)$$

$$dt_{B_i} = \frac{\lambda_n I_{sp_n}}{W_{O_n} (T/W_{O_n})} dW_{P_n}, \quad (i = n) \quad (C.30d)$$

$$dt_{B_i} = 0, \quad (i \neq n) \quad (C.30e)$$

Substituting Equations (C.26c) and (C.26e) and Equations (C.30a) through (C.30e) into Equation (C.4), and rearranging and solving for dW_{PL}/dW_{P_n} ,

$$\frac{dW_{PL}}{dW_{P_n}} = - \frac{\frac{1}{1 - \sigma_n} \sum_{i=1}^n \left[\frac{\partial(\Delta V)}{\partial W_{O_i}} \right] + \left[\frac{\partial(\Delta V)}{\partial W_{BO_i}} \right] - \left[\frac{\partial(\Delta V)}{\partial W_{BO_n}} \right] + \left[\frac{\partial(\Delta V)}{\partial t_B} \right] \frac{\lambda_n I_{sp_n}}{W_{O_n} (T/W_{O_n})}}{\sum_{i=1}^N \left[\left[\frac{\partial(\Delta V)}{\partial W_{O_i}} \right] + \left[\frac{\partial(\Delta V)}{\partial W_{BO_i}} \right] \right]} \quad (C.31)$$

Substituting Equations (C.5b), (C.5c), (C.5d), and (C.10),

$$\frac{dW_{PL}}{dW_{P_n}} = \frac{\left(\frac{I_{sp}}{W_{O_n}} \right) (r_n - \theta_n) - \frac{1}{1 - \sigma_n} \sum_{i=1}^n \left[\left(\frac{I_{sp}}{W_{O_i}} \right) (r_i - 1) \right]}{\sum_{i=1}^N \left[\left(\frac{I_{sp}}{W_{O_i}} \right) (r_i - 1) \right]} \quad (C.32)$$

For a one-stage vehicle, Equation (C.32) reduces to

$$\frac{dW_{PL}}{dW_P} = \frac{1 - \sigma r - (1 - \sigma)\theta}{(1 - \sigma)(r - 1)} \quad (C.33)$$

The last payload exchange ratio to be evaluated is

$$\left(\frac{dW_{PL}}{dT} \right)_n$$

Specific impulse is assumed constant, and therefore a thrust perturbation results in variations of both propellant mass flow rate and burning time. Structural weight also is assumed constant. Thrust perturbation, dT , is expressed as a percentage of nominal initial thrust.

Vehicle Gross Weight Exchange Ratios

C-11

$$\therefore d I_{sp_i} = 0, \quad (1 \leq i \leq N) \quad (C. 34a)$$

$$d W_{O_i} = d W_{PL}, \quad (1 \leq i \leq N) \quad (C. 34b)$$

$$d W_{BO_i} = d W_{PL}, \quad (1 \leq i \leq N) \quad (C. 34c)$$

$$d t_{B_i} = - \frac{\lambda_n I_{sp_n}}{100 (T/W_O)_n} \left(1 - \frac{1}{r_n} \right) d T_n, \quad (i = n) \quad (C. 34d)$$

$$d t_{B_i} = 0, \quad (i \neq n) \quad (C. 34e)$$

Substituting Equations (C. 34a) through (C. 34e) into Equation (C. 4) and rearranging,

$$\frac{d W_{PL}}{d T} = \frac{\left[\frac{\partial (\Delta V)}{\partial t_B} \right]_n \frac{\lambda_n I_{sp_n} (1 - 1/r_n)}{100 (T/W_O)_n}}{\sum_{i=1}^N \left[\left[\frac{\partial (\Delta V)}{\partial W_O} \right]_i + \left[\frac{\partial (\Delta V)}{\partial W_{BO}} \right]_i \right]}$$

Substituting Equations (C. 5b), (C. 5c), and (C. 5d),

$$\frac{d W_{PL}}{d T} = \frac{\lambda_n I_{sp_n} \cos \bar{\beta}_n (1 - 1/r_n)}{100 (T/W_O)_n \sum_{i=1}^N \left[\left(\frac{I_{sp}}{W_O} \right)_i (r_i - 1) \right]} \quad (C. 36)$$

For a one-stage vehicle, Equation (C. 36) reduces to

$$\frac{d W_{PL}}{d T} = \frac{\lambda W_{BO} \cos \bar{\beta}}{100 (T/W_O)} \quad (C. 37)$$

2 VEHICLE GROSS WEIGHT EXCHANGE RATIOS

In this section, analytical expressions are derived which relate perturbations of booster performance parameters to the amounts that stage gross weight must be varied in order to maintain a fixed payload capability. Performance parameters considered include specific impulse, inert weight, and thrust. The derivations follow directly from Equations (C.4) and (C.5) and, therefore, the assumptions made

DEVELOPMENT OF GENERALIZED EXCHANGE RATIOS

in deriving these equations are applicable in this section. In addition, a constant stage structure factor is assumed in deriving all stage gross weight exchange ratios.

The first exchange ratio to be developed for a single-stage vehicle is

$$\left(\frac{dW_O}{dI_{sp}}\right)_{W_{PL}}$$

A change in vacuum I_{sp} is assumed to correspond to a change in propellant mass flow rate. Burning time is assumed to vary in proportion to the changes in I_{sp} and stage propellant weight. Thrust is assumed constant.

$$\therefore dI_{sp} = dI_{sp} \quad (C.38a)$$

$$dW_O = dW_O \quad (C.38b)$$

$$dW_{BO} = \sigma dW_O \quad (C.38c)$$

$$dt_B = \frac{\lambda(1 - 1/r)}{T/W_O} dI_{sp} + \frac{(1 - \sigma) \lambda I_{sp}}{W_O(T/W_O)} dW_O \quad (C.38d)$$

Substituting Equations (C.38a) through (C.38d) into Equation (C.4) and rearranging,

$$\left(\frac{dW_O}{dI_{sp}}\right)_{W_{PL}} = - \frac{\left[\frac{\partial(\Delta V)}{\partial I_{sp}}\right] + \left[\frac{\partial(\Delta V)}{\partial t_B}\right] \frac{\lambda(1 - 1/r)}{T/W_O}}{\frac{\partial(\Delta V)}{\partial W_O} + \sigma \frac{\partial(\Delta V)}{\partial W_{BO}} + \frac{(1 - \sigma) \lambda I_{sp}}{W_O(T/W_O)} \left[\frac{\partial(\Delta V)}{\partial t_B}\right]} \quad (C.39)$$

Substituting Equations (C.5a) through (C.5d) and (C.10),

$$\left(\frac{dW_O}{dI_{sp}}\right)_{W_{PL}} = - \frac{\ln r - \theta(1 - 1/r)}{I_{sp} [1 - \sigma r - \theta(1 - \sigma)]} \quad (C.40)$$

The next exchange ratio to be developed is

$$\left(\frac{dW_O}{dW_{ST}^*}\right)_{W_{PL}}$$

where W_{ST}^* corresponds to a change of stage inert weight. Thrust and specific impulse are assumed constant. Then,

Vehicle Gross Weight Exchange Ratios

C-13

$$dIsp = 0 \quad (C.41a)$$

$$dW_O = dW_{ST} \quad (C.41b)$$

$$dW_{BO} = dW_{ST}^* + dW_{ST} \quad (C.41c)$$

where dW_{ST} represents the change in structure weight required to vary stage gross weight. For an assumed constant structure factor,

$$dW_{ST} = \sigma(dW_O - dW_{ST}^*) \quad (C.41d)$$

$$\therefore dW_{BO} = (1 - \sigma) dW_{ST}^* + \sigma dW_O \quad (C.41e)$$

$$dt_B = \frac{\lambda Isp}{W_O(T/W_O)} \left[(1 - \sigma) (dW_O - dW_{ST}^*) \right] \quad (C.41f)$$

Substituting Equations (C.41a) through (C.41f) into Equation (C.4) and rearranging,

$$\left(\frac{dW_O}{dW_{ST}^*} \right)_{W_{PL}} = - \frac{(1 - \sigma) \frac{\partial(\Delta V)}{\partial W_{BO}} - (1 - \sigma) \frac{\lambda Isp}{W_O(T/W_O)} \left[\frac{\partial(\Delta V)}{\partial t_B} \right]}{\frac{\partial(\Delta V)}{\partial W_O} + \sigma \frac{\partial(\Delta V)}{\partial W_{BO}} + (1 - \sigma) \frac{\lambda Isp}{W_O(T/W_O)} \left[\frac{\partial(\Delta V)}{\partial t_B} \right]} \quad (C.42)$$

Substituting Equations (C.5b) through (C.5d) and (C.10),

$$\left(\frac{dW_O}{dW_{ST}^*} \right)_{W_{PL}} = \frac{(1 - \sigma)(r - \theta)}{1 - \sigma r - (1 - \sigma)\theta} \quad (C.43)$$

The next exchange ratio to be developed is

$$\left(\frac{dW_O}{dT} \right)_{W_{PL}}$$

Specific impulse and structure factor are assumed constant. Burning time is assumed to vary in proportion to the changes in thrust and stage gross weight. Thrust perturbation, dT , is expressed as a percentage of nominal initial thrust.

$$dIsp = 0 \quad (C.44a)$$

$$dW_O = dW_{ST} \quad (C.44b)$$

$$dW_{BO} = dW_{ST} = \sigma dW_O \quad (C.44c)$$

$$dt_B = \frac{\lambda_{isp}(1-\sigma)}{W_O(T/W_O)} dW_O - \frac{\lambda_{isp}(1-1/r)}{100(T/W_O)} dT \quad (C.44d)$$

Substituting Equations (C.44a) through (C.44d) into Equation (C.4) and rearranging,

$$\left(\frac{dW_O}{dT}\right)_{W_{PL}} = \frac{\frac{\lambda_{isp}(1-1/r)}{100(T/W_O)} \left[\frac{\partial(\Delta V)}{\partial t_B}\right]}{\frac{\partial(\Delta V)}{\partial W_O} + \sigma \frac{\partial(\Delta V)}{\partial W_{BO}} + \frac{\lambda_{isp}(1-\sigma)}{W_O(T/W_O)} \left[\frac{\partial(\Delta V)}{\partial t_B}\right]} \quad (C.45)$$

Substituting Equations (C.5b) through (C.5d) and (C.10)

$$\left(\frac{dW_O}{dT}\right)_{W_{PL}} = - \frac{W_O \Theta(1-1/r)}{100 [1-\sigma r - (1-\sigma)\Theta]} \quad (C.46)$$

The last exchange ratio to be developed relates the change in gross weight of the nth stage of a multistage vehicle to the change in gross weight of the n + 1 stage.

$$\left(\frac{dW_{O_n}}{dW_{O_{n+1}}}\right)$$

It is assumed that the increment of velocity, ΔV_i , which each stage provides does not vary when the stage gross weights are varied. This corresponds to a fixed payload capability when the gross weight of the n + 1 stage has been varied to account for a perturbation of another stage parameter, such as thrust or specific impulse. Constant thrusts, specific impulse, and structure factors are assumed for the nth stage. Then

$$dW_{O_n} = dW_{O_n} \quad (C.47a)$$

$$dW_{BO_n} = dW_{ST_n} + dW_{O_{n+1}}$$

since

$$dW_{ST_n} = \sigma_n (dW_{O_n} - dW_{O_{n+1}}) \quad (C.47b)$$

$$dW_{BO_n} = \sigma_n dW_{O_n} + (1-\sigma_n) dW_{O_{n+1}}$$

$$dt_{B_n} = \frac{\lambda_n I_{sp_n}}{W_{O_n}(T/W_{O_n})} (1-\sigma_n) (dW_{O_n} - dW_{O_{n+1}}) \quad (C.47c)$$

Substituting Equations (C.47a) through (C.47c) into Equation (C.4) and rearranging,

$$\left(\frac{dW_{O_n}}{dW_{O_{n+1}}} \right)_{W_{PL}, T_n} = - \frac{(1 - \sigma_n) \left[\left[\frac{\partial(\Delta V)}{\partial W_{BO}} \right]_n - \frac{\lambda_n Isp_n}{W_{O_n} (T/W_{O_n})} \left[\frac{\partial(\Delta V)}{\partial t_B} \right]_n \right]}{\left[\left[\frac{\partial(\Delta V)}{\partial W_O} \right]_n + \sigma_n \left[\frac{\partial(\Delta V)}{\partial W_{BO}} \right]_n + (1 - \sigma_n) \frac{\lambda_n Isp_n}{W_{O_n} (T/W_{O_n})} \left[\frac{\partial(\Delta V)}{\partial t_B} \right]_n \right]} \quad (C.48)$$

Substituting Equations (C.5b) through (C.5d) and (C.10),

$$\left(\frac{dW_{O_n}}{dW_{O_{n+1}}} \right)_{W_{PL}, T_n} = \frac{(1 - \sigma_n)(r_n - \theta_n)}{1 - \sigma_n r_n - (1 - \sigma_n)\theta_n} \quad (C.49)$$

If instead of assuming a fixed thrust, a constant thrust-to-weight ratio, (T/W_{O_n}) , and specific impulse are assumed for the nth stage, then $dt_B = C$ and Equation (C.49) reduces to

$$\left(\frac{dW_{O_n}}{dW_{O_{n+1}}} \right)_{W_{PL}, (T/W_{O_n})} = \frac{(1 - \sigma_n)r_n}{1 - \sigma_n r_n} = \frac{W_{O_n}}{W_{O_{n+1}}} \quad (C.50)$$

Equation (C.51) can be used to determine the change in gross weight of the kth stage of a multistage vehicle required to maintain a fixed payload capability due to a perturbation of gross weight of the nth stage, as follows:

$$\begin{aligned} dW_{O_k} &= \frac{W_{O_k}}{W_{O_{k+1}}} \frac{W_{O_{k+1}}}{W_{O_{k+2}}} \frac{W_{O_{k+2}}}{W_{O_{k+3}}} \cdots \frac{W_{O_{n-2}}}{W_{O_{n-1}}} \frac{W_{O_{n-1}}}{W_{O_n}} dW_{O_n} \\ &= W_{O_k} \left(\frac{dW_{O_n}}{W_{O_n}} \right) \end{aligned} \quad (C.51)$$

or rewriting

$$\left(\frac{dW_{O_k}}{dW_{O_n}} \right)_{W_{PL}, (T/W_{O_i})} = \frac{W_{O_k}}{W_{O_n}} \quad \begin{matrix} (k \leq n) \\ (1 \leq i \leq n - 1) \end{matrix} \quad (C.52)$$

Equation (C. 53) can be used to estimate the change in vehicle liftoff weight required to maintain a fixed payload capability due to a perturbation of gross weight of the n th stage.

$$\left(\frac{dW_{L_O}}{dW_{O_n}} \right)_{W_{PL}, (T/W_O)_k} = \frac{1}{W_{O_n}} \sum_{i=1}^n W_{O_i} \quad \begin{matrix} (1 \leq i \leq n) \\ (1 \leq k \leq n-1) \end{matrix} \quad (C. 53)$$

Conversely, Equation (C. 53) can be used when the payload weight is perturbed to estimate the change in vehicle liftoff weight required to achieve a fixed mission velocity requirement.

APPENDIX D

DEVELOPMENT OF EQUATIONS FOR VEHICLE SIZING

The following is the development of equations and expressions for Chapter 5, Vehicle Sizing.

1 VEHICLE PAYLOAD RATIO

The usual parameter of interest for vehicle sizing is the ratio of vehicle gross weight to payload weight for the particular mission of interest.

1.1 One Stage

The ideal velocity, mission burnout velocity plus losses, for a one-stage vehicle is defined as

$$V_I = g \text{ Isp} \ln \frac{W_O}{W_{BO}} \quad (\text{D.1})$$

$$= g \text{ Isp} \ln \frac{W_O}{W_O - W_P} \quad (\text{D.2})$$

The structure factor, σ , is defined as

$$\sigma = \frac{W_O - W_P - W_{PL}}{W_O - W_{PL}} = \frac{W_{ST}}{W_O - W_{PL}} \quad (\text{D.3})$$

Solving for W_P in Equation (D.3),

$$W_P = (1 - \sigma)(W_O - W_{PL}) \quad (\text{D.4})$$

Substituting into a nondimensional form of Equation (D.2),

$$\frac{V_I}{g \text{ Isp}} = \ln \frac{W_O}{\sigma W_O + (1 - \sigma) W_{PL}} \quad (\text{D.5})$$

$$= \ln \frac{\frac{W_O}{W_{PL}}}{\sigma \frac{W_O}{W_{PL}} + (1 - \sigma)} = \ln \frac{x}{\sigma x + (1 - \sigma)} \quad (\text{D.6})$$

D-2

DEVELOPMENT OF EQUATIONS FOR VEHICLE SIZING

where

$$x = \frac{W_O}{W_{PL}}, \quad x \text{ is the ratio of interest.}$$

Solving for x ,

$$x = \frac{1 - \sigma}{\frac{V_I}{e^{-g Isp} - \sigma}} \quad (D.7)$$

Realizing W_{PL} can be the gross weight of an additional stage $W_{O_{n+1}}$,

$$x_n = \frac{1 - \sigma_n}{\frac{V_{I_n}}{e^{-g Isp_n} - \sigma_n}} \quad (D.8)$$

1.2 Multiple Staging

Like Parameters. For a multiple-stage vehicle whose stages have equal specific impulses and structure factors, the optimum payload ratio can be obtained by using the optimum criteria presented by Equation (D.39) in this appendix:

$$x_{n+1} = \frac{\frac{Isp_{n+1}}{Isp_n} (1 - \sigma_{n+1}) [x_n \sigma_n + (1 - \sigma_n)] - (1 - \sigma_{n+1})(1 - \sigma_n)}{(1 - \sigma_n)(\sigma_{n+1})}, \quad (1 \leq n \leq N-1) \quad (D.9)$$

where x_n represents the payload ratio of a particular stage n . Substitution of equal specific impulses and structure factors in the above reduces the expression to

$$x_1 = x_2 = \dots x_n = \dots x_N \quad (D.10)$$

which implies equal ideal velocities per stage:

$$V_{I_n} = \frac{V_{I_N}}{N} \quad (D.11)$$

The total gross weight to payload weight ratio, X_N , for a multiple-stage vehicle is

$$X_N = x_1 \cdot x_2 \cdot \dots x_n \cdot \dots x_N \quad (D.12)$$

Vehicle Payload Ratio

D-3

Combining Equations (D.10) and (D.12) gives

$$X_N = (x_n)^N \quad (D.13)$$

Substituting Equation (D.8) into (D.13) gives

$$X_N = \left[\frac{1 - \sigma}{\left(\frac{V_{I_N}}{e^{NgIsp}} \right) - \sigma} \right]^N \quad (D.14)$$

for a multiple-stage vehicle of equal specific impulses and structure factors.

Unlike Parameters. Equation (D.9) can also be used for a multiple-stage vehicle whose stages have equal specific impulses and different structure factors. Assume a vehicle of two stages for this case. Equation (D.9) becomes

$$x_2 = \frac{(1 - \sigma_2)(x_1 \sigma_1)}{(1 - \sigma_1)(\sigma_2)} \quad (D.15)$$

Multiplying both sides by x_2 and rearranging gives

$$\frac{V_N}{\sigma_1} - \frac{\sigma_2}{\sigma_1} \left(\frac{x_1}{x_2} \right)^2 \left(\frac{1 - \sigma_1}{1 - \sigma_2} \right) = \frac{\sigma_1}{\sigma_2} \left(\frac{x_1}{x_2} \right)^2 \left(\frac{1 - \sigma_2}{1 - \sigma_1} \right) \quad (D.16)$$

Equation (D.6), expressed in a form for a two-stage vehicle with equal specific impulses, gives

$$\frac{V_{I_N}}{e^{gIsp}} = \left(\frac{x_1}{\sigma_1 x_1 + 1 - \sigma_1} \right) \left(\frac{x_2}{\sigma_2 x_2 + 1 - \sigma_2} \right) \quad (D.17)$$

Substitution of Equation (D.16) into (D.17) and solving for X_N gives

$$X_N = \frac{(1 - \sigma_1)(1 - \sigma_2)}{\left(\frac{V_{I_N}}{e^{2gIsp} - \sqrt{\sigma_1 \sigma_2}} \right)^2} \quad (D.18)$$

1.3 Infinite Staging

For vehicles of infinite stages of like parameters, the gross weight to payload weight ratio can be determined from Equation (D.14). As N approaches infinity, Equation (D.14) approaches 1^∞ , which is an indeterminate form; therefore the use of L' Hospital's Rule for indeterminate forms applies.

Taking the logarithm of both sides of Equation (D.14) gives

$$\lim_{N \rightarrow \infty} \ln X_N = \lim_{N \rightarrow \infty} \frac{\ln \left[\frac{1 - \sigma}{e^{\left(\frac{V_{I_N}}{Ng \text{ Isp}} \right)} - \sigma} \right]}{N} \quad (\text{D.19})$$

L' Hospital's rule states that if the fraction $f(u)/g(u)$ assumes the form

$$\frac{0}{0} \text{ when } u = a, \text{ then } \lim_{x \rightarrow a} \frac{f(u)}{g(u)} = \lim_{x \rightarrow a} \frac{\frac{df}{dx}}{\frac{dg}{dx}} \quad (\text{D.20})$$

Applying the above to Equation (D.19) gives

$$\lim_{N \rightarrow \infty} \ln X_N = \lim_{N \rightarrow \infty} \frac{V_{I_N}}{\text{Isp} g} \left[\frac{-\left(\frac{V_{I_N}}{Ng \text{ Isp}} \right)}{e^{\left(\frac{V_{I_N}}{Ng \text{ Isp}} \right)} - \sigma} \right] \quad (\text{D.21})$$

In the limit Equation (D.21) becomes

$$\ln X_N = \frac{V_{I_N}}{g \text{ Isp} (1 - \sigma)} \quad (\text{D.22})$$

Solving for X_N gives

$$X_N = e^{\left[\frac{V_{I_N}}{g \text{ Isp} (1 - \sigma)} \right]} \quad (\text{D.23})$$

for a vehicle of infinite stages of like parameters.

2 STAGE MASS RATIO

In order to determine the stage characteristics, it is of interest to solve for the stage mass ratios r_n

where

$$r_n = \frac{W_{O_n}}{W_{BO_n}}$$

after having found the payload ratio.

2.1 One Stage

For a one-stage vehicle Equations (D.1) and (D.6) can be combined to give

$$r = e^{\frac{V_I}{g I_{sp}}} = \frac{\frac{W_O}{W_{PL}}}{\sigma \frac{W_O}{W_{PL}} + (1 - \sigma)} = \frac{x}{\sigma x + (1 - \sigma)} \quad (D.24)$$

2.2 Multiple Stage

Like Parameters. For a vehicle of multiple stages with like specific impulses and structure factors, Equation (D.11) indicated equal ideal velocities per stage for optimum staging, thereby requiring equal mass ratios per stage. This results in the following:

$$r_n = e^{\frac{V_{I_N}}{Ng I_{sp}}} = \frac{(X_N)^{\frac{1}{N}}}{\sigma (X_N)^{\frac{1}{N}} + (1 - \sigma)} \quad (D.25)$$

Two-Stage Vehicle with Unlike Structure Factors. For two-stage vehicles of equal specific impulses but different structure factors, the individual stage mass ratios can be found as follows from Equation (D.24):

$$r_1 = \frac{x_1}{\sigma_1 x_1 + (1 - \sigma_1)} \quad (D.26)_1$$

or

$$r_2 = \frac{x_2}{\sigma_2 x_2 + (1 - \sigma_2)} \quad (D.26)_2$$

Combining the above with Equation (D.16) gives

$$r_{1 \text{ or } 2} = \frac{\sqrt{\frac{\sigma_{2 \text{ or } 1}}{\sigma_{1 \text{ or } 2}} \left(\frac{1 - \sigma_{1 \text{ or } 2}}{1 - \sigma_{2 \text{ or } 1}} \right) X_N}}{\sigma_{1 \text{ or } 2} \sqrt{\frac{\sigma_{2 \text{ or } 1}}{\sigma_{1 \text{ or } 2}} \left(\frac{1 - \sigma_{1 \text{ or } 2}}{1 - \sigma_{2 \text{ or } 1}} \right) X_N + (1 - \sigma_{1 \text{ or } 2})}} \quad (\text{D.27})$$

for a two-stage vehicle of like specific impulses and unlike structure factors.

3 OPTIMUM SIZING FOR MINIMUM GROSS WEIGHT PAYLOAD RATIO

The analytic expressions used in Chapter 5, Section 3 are derived below.

3.1 Constant Structure Factor

In optimally sizing a vehicle for minimum initial gross weight-to-payload weight ratio W_{O1}/W_{PL} , the simplest and most commonly used approximation for structural weight is to assume that it is linearly proportional to the stage weight.

Thus

$$\sigma_i = \text{constant} \quad (\text{D.28})$$

where

$$\sigma_i = \frac{W_{ST_i}}{W_{O_i} - W_{O_{i+1}}} \quad (\text{D.28a})$$

The solution is discussed in Chapter 5, Section 4.1. It is desired to minimize the ratio W_{O1}/W_{PL} represented by X_N and constrained by a required ideal velocity, V_{IN} .

To obtain the solution, both X_N and V_{IN} must be represented as functions of $(x_1, x_2, \dots, x_{i=N})$ where $x_i = W_{O_i}/W_{O_{i+1}}$ and $W_{O_{N+1}} = W_{PL}$

$$X_N = \prod_{i=1}^N x_i \quad (\text{D.29})$$

The total ideal velocity by definition and using the classic Rocket Equation equals

$$V_{IN} = \sum_{i=1}^N I_{sp_i} g \ln \left(\frac{W_O}{W_{BO_i}} \right) \quad (\text{D.30})$$

where

$$(W_O/W_{BO})_i = W_{O_i}/(W_{O_i} - W_{P_i}) \quad (\text{D.30a})$$

The propellant weight, W_{P_i} equals

$$W_{P_i} = W_{O_i} - W_{O_{i+1}} - W_{ST_i} \quad (D.31)$$

Substituting Equation (D.28a),

$$W_{P_i} = (1 - \sigma_i)(W_{O_i} - W_{O_{i+1}}) \quad (D.32)$$

Substituting into Equations (D.30) and (D.30a),

$$V_{I_N} = \sum_{i=1}^N I_{sp_i} g \ln \frac{x_i}{x_i \sigma_i + (1 - \sigma_i)} \quad (D.33)$$

The solution for the minimum, from Chapter 5, Section 4.1, Equations (40), is

$$\frac{\partial X_N}{\partial x_1} + \phi \frac{\partial V_{I_N}}{\partial x_1} = 0 \quad (D.34)_1$$

$$\frac{\partial X_N}{\partial x_2} + \phi \frac{\partial V_{I_N}}{\partial x_2} = 0 \quad (D.34)_2$$

$$\vdots \quad \vdots \quad \vdots$$

$$\frac{\partial X_N}{\partial x_n} + \phi \frac{\partial V_{I_N}}{\partial x_n} = 0 \quad (D.34)_n$$

$$\vdots \quad \vdots \quad \vdots$$

$$\frac{\partial X_N}{\partial x_N} + \phi \frac{\partial V_{I_N}}{\partial x_N} = 0 \quad (D.34)_N$$

Solving Equation (D.29) for $\partial X_N / \partial x_i$,

$$\frac{\partial X_N}{\partial x_i} = \frac{1}{x_i} \prod_{i=1}^N x_i \quad (D.36)$$

Similarly solving Equation (D.30) for $\partial V_{I_N} / \partial x_i$,

$$\frac{\partial V_{I_N}}{\partial x_i} = \frac{I_{sp_i} g}{x_i} \frac{[x_i \sigma_i + (1 - \sigma_i)] - x_i \sigma_i}{[x_i \sigma_i + (1 - \sigma_i)]} \quad (D.37)$$

Substituting into Equations (D.34) and solving simultaneously,

$$\frac{I_{sp_i}(1 - \sigma_i)}{[x_i \sigma_i + (1 - \sigma_i)]} = \frac{I_{sp_{i+1}}(1 - \sigma_{i+1})}{[x_{i+1} \sigma_{i+1} + (1 - \sigma_{i+1})]}, \quad (1 \leq i \leq N - 1) \quad (D.38)$$

solving for x_{n+1} ,

$$x_{n+1} = \frac{\frac{I_{sp_{n+1}}}{I_{sp_n}} (1 - \sigma_{n+1}) [x_n \sigma_n + (1 - \sigma_n)] - (1 - \sigma_{n+1})(1 - \sigma_n)}{\sigma_{n+1}(1 - \sigma_n)}, \quad (1 \leq n \leq N - 1) \quad (D.39)$$

To solve for x_1, x_2, \dots, x_N it is first necessary to assume an x_n for a particular stage and solve Equation (D.39) for the other values of x_i . Then substituting those values into Equation (D.30), test the fulfillment of the constraint.

3.2 Variable Structure Factor

3.2.1 Linear Approximation

A linear representation is the next simplest approximation for the variation of structure factor with stage weight. Thus

$$\sigma_i = A_i (W_{O_i} - W_{O_{i+1}}) + B_i \quad (D.40)$$

where

$$\sigma_i = \frac{W_{ST_i}}{W_{O_i} - W_{O_{i+1}}} \quad (D.40a)$$

There are two solutions for this problem, one where initial gross weight of the vehicle is given and the other where the payload weight of the vehicle is given. Of course, there are other solutions where the initial gross weight of a particular stage other than the first stage is given but this would be rather unlikely and therefore the solutions are not presented here.

Given Initial Gross Weight. Again, it is desired to minimize the ratio W_{O_1}/W_{PL} represented by X_N and constrained by a required velocity, V_{I_N} . To obtain the solution both X_N and V_{I_N} must be represented as functions of (x_1, x_2, \dots, x_N) where $x_i = W_{O_i}/W_{O_{i+1}}$ and $W_{O_{N+1}} = W_{PL}$

$$X_N = \prod_{i=1}^N x_i \quad (D.41)$$

The total ideal velocity by definition and using the classic Rocket Equation equals

$$V_{I_N} = \sum_{i=1}^N I_{sp_i} g \ln \left(\frac{W_O}{W_{BO}} \right)_i \quad (D.42)$$

where

$$\left(W_O / W_{BO} \right)_i = W_{O_i} / (W_{O_i} - W_{P_i}) \quad (D.42a)$$

The propellant weight equals

$$W_{P_i} = W_{O_i} - W_{O_{i+1}} - W_{ST_i} \quad (D.43)$$

Substituting Equation (D.40a),

$$W_{P_i} = (1 - \sigma_i) (W_{O_i} - W_{O_{i+1}}) \quad (D.44)$$

Substituting Equation (D.40),

$$W_{P_i} = (1 - B_i) (W_{O_i} - W_{O_{i+1}}) - A_i (W_{O_i} - W_{O_{i+1}})^2 \quad (D.45)$$

Then substituting into Equation (D.42a) and as before letting $x_i = W_{O_i} / W_{O_{i+1}}$,

$$\left(W_O / W_{BO} \right)_i = \frac{x_i}{x_i - (1 - B_i)(x_i - 1) - \frac{A_i W_{O_i}}{i} (x_i - 1)^2, \quad \prod_{k=1}^i x_k} \quad (D.46)$$

Equation (D.42) now can be written

$$V_{I_N} = \sum_{i=1}^N I_{sp_i} g \ln \frac{x_i}{x_i - (1 - B_i)(x_i - 1) - \frac{A_i W_{O_i}}{i} (x_i - 1)^2, \quad \prod_{k=1}^i x_k} \quad (D.47)$$

The solution for the minimum is the same as presented in Equations (D.34)₁, (D.34)₂, ..., (D.34)_n, ..., (D.34)_N. Solving Equation (D.41) for $\partial X_N / \partial x_i$,

$$\frac{\partial X_N}{\partial x_i} = \frac{1}{x_i} \prod_{i=1}^N x_i \quad (D.48)$$

Similarly solving Equation (D.47) for $\partial V_{IN} / \partial x_i$.

$$\frac{\partial V_{IN}}{\partial x_i} = \frac{Isp_i \left\{ (1 - B_i) + \frac{A_i W_{O_i}}{\prod_{k=1}^i x_k} [2x_i(x_i - 1)] \right\}}{x_i \left[x_i - (1 - B_i)(x_i - 1) - \frac{A_i W_{O_i}}{\prod_{k=1}^i x_k} (x_i - 1)^2 \right]} \quad (D.49)$$

Substituting Equations (D.48) and (D.49) into Equation (D.34),

$$\begin{aligned} & \frac{Isp_n \left\{ (1 - B_n) + \frac{A_n W_{O_1}}{\prod_{k=1}^n x_k} [2x_n(x_n - 1)] \right\}}{x_n - (1 - B_n)(x_n - 1) - \frac{A_n W_{O_1}}{\prod_{k=1}^n x_k} (x_n - 1)^2} \\ &= \frac{Isp_{n-1} \left\{ (1 - B_{n-1}) + \frac{A_{n-1} W_{O_1}}{\prod_{k=1}^{n-1} x_k} [2x_{n-1}(x_{n-1} - 1)] \right\}}{x_{n-1} - (1 - B_{n-1})(x_{n-1} - 1) - \frac{A_{n-1} W_{O_1}}{\prod_{k=1}^{n-1} x_k} (x_{n-1} - 1)^2} \quad (2 \leq n \leq N) \quad (D.50) \end{aligned}$$

To solve for x_1, x_2, \dots, x_N it is easiest to assume a value for x_1 and iterate on x_2 until Equation (D.50) is fulfilled. Having found x_2 , iterate on x_3 and so on. After finding all the values of x_i substitute into Equation (D.47) to test fulfillment of the constraint. Iterate on x_1 until the constraint is fulfilled.

Given Payload Weight. Given the payload weight, then Equation (D.46) becomes

$$\left(\frac{W_O}{W_{BC}} \right)_i = \frac{x_i}{x_i - (1 - B_i)(x_i - 1) - \frac{A_i W_{PL}}{\prod_{k=i+1}^{N+1} x_k}} \quad (D.51)$$

where

$$x_{k=N+1} = \frac{W_{PL}}{W_{PL}} = 1 \quad (D.51a)$$

Then Equation (D.49) becomes

$$\frac{\partial V_{I_N}}{\partial x_i} = \frac{Isp_i g \left[(1 - B_i) + A_i W_{PL} (x_i^2 - 1) \prod_{k=i+1}^{N+1} x_k \right]}{x_i \left[x_i - (1 - B_i)(x_i - 1) - A_i W_{PL} (x_i - 1)^2 \prod_{k=i+1}^{N+1} x_k \right]} \quad (D.52)$$

Substituting Equations (D.49) and (D.52) into Equation (D.34),

$$\begin{aligned} & \frac{Isp_n \left[(1 - B_n) + A_n W_{PL} (x_n^2 - 1) \prod_{k=n+1}^{N+1} x_k \right]}{x_n - (1 - B_n)(x_n - 1) - A_n W_{PL} (x_n - 1)^2 \prod_{k=n+1}^{N+1} x_k} \\ &= \frac{Isp_{n-1} \left[(1 - B_{n-1}) + A_{n-1} W_{PL} (x_{n-1}^2 - 1) \prod_{k=n}^{N+1} x_k \right]}{x_{n-1} - (1 - B_{n-1})(x_{n-1} - 1) - A_{n-1} W_{PL} (x_{n-1} - 1)^2 \prod_{k=n}^{N+1} x_k} \quad (2 \leq n \leq N) \end{aligned} \quad (D.53)$$

To solve for x_1, x_2, \dots, x_N first assume a value for x_N and iterate on x_{N-1} until Equation (D.53) is fulfilled. Having found x_{N-1} , iterate on x_{N-2} and so on. After finding all the values of x_i , substitute into Equation (D.53) to test fulfillment of the constraint. Iterate on x_N until the constraint is fulfilled.

3.2.2 Higher Order Approximation

The next approximation to be considered is a higher order curve fit. The one assumed is

$$\sigma_i = C_i (W_{O_i} - W_{O_{i+1}})^{a_i - 1} \quad (D.54)$$

where

$$\sigma_i = \frac{W_{ST_i}}{W_{O_i} - W_{O_{i+1}}} \quad (D.54a)$$

There are also two solutions for this problem, one where the initial gross weight of the vehicle is given and the other where the payload weight of the vehicle is given.

Given Initial Gross Weight. As before, it is desired to minimize the ratio W_{O1}/W_{PL} represented by X_N and constrained by a required ideal velocity, V_{IN} . To obtain the solution both X_N and V_{IN} must be represented as functions of $(x_1, x_2, \dots, x_{i=N})$ where $x_i = W_{O_i}/W_{O_{i+1}}$ and $W_{O_{N+1}} = W_{PL}$

$$X_N = \prod_{i=1}^N x_i \quad (D. 55)$$

The total ideal velocity by definition and using the classic Rocket Equation equals

$$V_{IN} = \sum_{i=1}^N I_{sp_i} g \ln \left(\frac{W_{O_i}}{W_{BO_i}} \right) \quad (D. 56)$$

where

$$\left(\frac{W_{O_i}}{W_{BO_i}} \right) = \frac{W_{O_i}}{W_{O_i} - W_{P_i}} \quad (D. 56a)$$

The propellant weight equals

$$W_{P_i} = W_{O_i} - W_{O_{i+1}} - W_{ST_i} \quad (D. 57)$$

Substituting Equation (D. 54a),

$$W_{P_i} = (1 - \sigma_i) (W_{O_i} - W_{O_{i+1}}) \quad (D. 58)$$

Substituting Equation (D. 54),

$$W_{P_i} = (W_{O_i} - W_{O_{i+1}}) - C_i (W_{O_i} - W_{O_{i+1}})^{a_i} \quad (D. 59)$$

Then substituting into Equation (D. 56a) and as before letting $x_i = W_{O_i}/W_{O_{i+1}}$,

$$W_{O_i}/W_{BO_i} = \frac{x_i}{1 + C_i \left(\frac{W_{O_i}}{\prod_{k=1}^i x_k} \right)^{a_i - 1} (x_i - 1)^{a_i}} \quad (D. 60)$$

Equation (D.56) now can be written

$$V_{I, \dots} = \sum_{i=1}^N I_{sp_i} g \ln \frac{x_i}{1 + C_i \left(\frac{W_{O_i}}{\prod_{k=1}^i x_k} \right)^{a_i-1} (x_i - 1)^{a_i}} \quad (D.61)$$

The solution for the minimum is the same as presented in Equations (D.34)₁ through (D.34)_N.

Solving Equation (D.55) for $\partial X_N / \partial x_i$,

$$\frac{\partial X_N}{\partial x_i} = \frac{1}{x_i} \prod_{i=1}^N x_i \quad (D.62)$$

Similarly solving Equation (D.61) for $\partial V_{I_N} / \partial x_i$,

$$\frac{\partial V_{I_N}}{\partial x_i} = \frac{I_{sp_i} g \left\{ 1 + C_i \left(\frac{W_{O_i}}{\prod_{k=1}^i x_k} \right)^{a_i-1} \left[(x_i - 1)^{a_i} - x_i (x_i - 1)^{a_i-1} \right] \right\}}{x_i \left[1 + C_i \left(\frac{W_{O_i}}{\prod_{k=1}^i x_k} \right)^{a_i-1} (x_i - 1)^{a_i} \right]} \quad (D.63)$$

Substituting Equations (D.62) and (D.63) into Equation (D.34),

$$\begin{aligned} & \frac{I_{sp_n} \left\{ 1 + C_n \left(\frac{W_{O_1}}{\prod_{k=1}^n x_k} \right)^{a_n-1} \left[(x_n - 1)^{a_n} - x_n (x_n - 1)^{a_n-1} \right] \right\}}{x_n \left[1 + C_n \left(\frac{W_{O_1}}{\prod_{k=1}^n x_k} \right)^{a_n-1} (x_n - 1)^{a_n} \right]} \\ &= \frac{I_{sp_{n-1}} \left\{ 1 + C_{n-1} \left(\frac{W_{O_1}}{\prod_{k=1}^{n-1} x_k} \right)^{a_{n-1}-1} \left[(x_{n-1} - 1)^{a_{n-1}} - x_{n-1} (x_{n-1} - 1)^{a_{n-1}-1} \right] \right\}}{x_{n-1} \left[1 + C_{n-1} \left(\frac{W_{O_1}}{\prod_{k=1}^{n-1} x_k} \right)^{a_{n-1}-1} (x_{n-1} - 1)^{a_{n-1}} \right]} \quad (2) \end{aligned} \quad (D.64)$$

As before, to solve for x_1, x_2, \dots, x_N , first assume a value for x_1 and iterate on x_2 until Equation (D.64) is fulfilled. Having found x_2 , iterate on x_3 and so on. After finding all the values of x_i , substitute into Equation (D.61) to test fulfillment of the constraint. Iterate on x_1 until the constraint is fulfilled.

Given Payload Weight. Given the payload weight, then Equation (D.60) becomes

$$V_{I_N} = \sum_{i=1}^N I_{sp} g \ln \frac{x_i}{1 + C_i \left(W_{PL} \prod_{k=1}^{N+1} x_k \right)^{a_i-1} (x_i - 1)^{a_i}} \quad (D.65)$$

where

$$x_{k=N+1} = W_{PL}/W_{PL} = 1 \quad (D.65a)$$

Now Equation (D.61) becomes

$$\frac{\partial V_{I_N}}{\partial x_i} = \frac{I_{sp_i} g \left\{ 1 + C_i \left(W_{PL} \prod_{k=i+1}^{N+1} x_k \right)^{a_i-1} \left[(x_i - 1)^{a_i} - a_i x_i (x_i - 1)^{a_i-1} \right] \right\}}{x_i \left[1 + C_i \left(W_{PL} \prod_{k=i+1}^{N+1} x_k \right)^{a_i-1} (x_i - 1)^{a_i} \right]} \quad (D.66)$$

Substituting Equations (D.62) and (D.66) into Equation (D.34).

$$\begin{aligned} & \frac{I_{sp_n} \left\{ 1 + C_n \left(W_{PL} \prod_{k=n+1}^{N+1} x_k \right)^{a_n-1} \left[(x_{n-1})^{a_n} - a_n x_n (x_{n-1})^{a_n-1} \right] \right\}}{1 + C_n \left(W_{PL} \prod_{k=n+1}^{N+1} x_k \right)^{a_n-1} (x_n - 1)^{a_n}} \\ &= \frac{I_{sp_{n-1}} \left\{ 1 + C_{n-1} \left(W_{PL} \prod_{k=n}^{N+1} x_k \right)^{a_{n-1}-1} \left[(x_{n-1} - 1)^{a_{n-1}} - a_{n-1} x_{n-1} (x_{n-1} - 1)^{a_{n-1}-1} \right] \right\}}{\left[1 + C_{n-1} \left(W_{PL} \prod_{k=n}^{N+1} x_k \right)^{a_{n-1}-1} (x_{n-1} - 1)^{a_{n-1}} \right]} \quad (2 \leq n \leq N) \end{aligned} \quad (D.67)$$

To solve for x_1, x_2, \dots, x_N first assume a value for x_N and iterate on x_{N-1} until Equation (D.67) is fulfilled. Having found x_{N-1} iterate on x_{N-2} and so on. After finding all the values of x_i substitute into Equation (D.65) to test fulfillment of the constraint. Iterate on x_N until the constraint is fulfilled.

3.3 Development of Optimum Sizing Nomograph

The optimum vehicle sizing equations (developed in Section 3.1), assuming a vehicle with a finite number of stages of different constant structure factors and specific impulses, are readily adaptable to a nomograph form of presentation. This type of presentation allows the rapid optimum sizing of vehicles using a graphical means.

Equation (D.38) presents the optimum sizing relationship in terms of the payload ratio for each stage:

$$\frac{Isp_1 (1 - \sigma_1)}{[x_1 \sigma_1 + (1 - \sigma_1)]} = \dots = \frac{Isp_n (1 - \sigma_n)}{[x_n \sigma_n + (1 - \sigma_n)]} = \frac{Isp_{n+1} (1 - \sigma_{n+1})}{[x_{n+1} \sigma_{n+1} + (1 - \sigma_{n+1})]} \\ = \frac{Isp_N (1 - \sigma_N)}{x_1 \sigma_N + (1 - \sigma_N)} \quad (D.68)$$

Realizing that stage payload ratio can be expressed in terms of stage mass ratio as

$$x_n = \frac{r_n (1 - \sigma_n)}{1 - r_n \sigma_n} \quad (D.69)$$

where $r = W_O / W_{BO}$

Equation (D.68) can be rewritten as

$$Isp_1 (1 - r_1 \sigma_1) = \dots = Isp_n (1 - r_n \sigma_n) = Isp_{n+1} (1 - r_{n+1} \sigma_{n+1}) \dots \\ = Isp_N (1 - r_N \sigma_N) \quad (D.70)$$

This equation is graphically presented to represent optimum sizing criteria. Also, Equation (D.69) and the equation

$$V_{I_n} = g Isp_n \ln r_n \quad (D.71)$$

are presented to indicate the stage payload ratio and ideal velocity, respectively.

4 GENERAL OPTIMUM SIZING

The solution for general optimum sizing, with respect to any criteria, are aptly developed within the text of Chapter 5 and therefore are not repeated here. The reader is referred to the reference material for further assistance.

DEVELOPMENT OF EQUATIONS FOR VEHICLE SIZING

NOMENCLATURE

A	Coefficients for structure factor curve fit
B	
C	
g	Acceleration due to gravity
I_{sp}	Vacuum specific impulse
i	Integer corresponding to a particular stage
k	Integer corresponding to a particular stage
N	Integer corresponding to the total number of stages
n	Integer corresponding to a particular stage
r	$\frac{W_O}{W_{BO}} = \text{Stage mass ratio}$
V_I	Ideal velocity
W_{BO}	Burnout weight
W_O	Gross weight
W_P	Propellant weight
W_{PL}	Payload weight
W_{ST}	Structure weight
X_N	Total vehicle gross weight-to-payload weight ratio
x	$\frac{W_{O_i}}{W_{O_{i+1}}} = \text{Stage gross weight-to-stage payload weight ratio}$
α	Exponent for structure factor curve fit
σ	Structure factor—structure weight-to-stage weight ratio

APPENDIX E

LUNAR/PLANETARY DEBOOST AND LUNAR LANDING

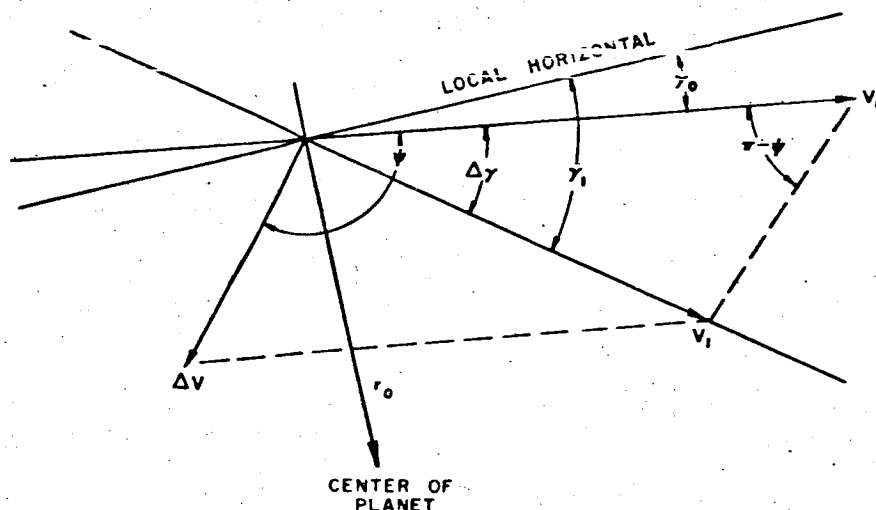
This appendix presents the derivation of the equations presented in Chapter 6.

1 EQUATIONS FOR IMPULSIVE VACUUM DEBOOST

The primary debost problem is to solve for entry angle, γ_E , entry velocity, V_E , range angle, θ , and time of flight $t_{I \rightarrow E}$, in terms of velocity impulse, ΔV , and thrust direction, ψ . Other independent variables include velocity in initial orbit, V_o ; initial flight path angle, γ_o ; the distance from the center of the planet to the point of impulse application and to the point of entry, r_o and r_E , respectively; and the gravitational constant, μ_p .

At the instant of impulse application, vectors V_o and ΔV add vectorially to yield V_1 , as shown in the diagram below. V_1 is determined in nondimensional form by application of the Law of Cosines:

$$\left(\frac{V_1}{V_o}\right)^2 = \left[1 + \left(\frac{\Delta V}{V_o}\right)^2 + 2 \frac{\Delta V}{V_o} \cos \psi\right] \quad (E.1)$$



E-2

LUNAR/PLANETARY DEBOOST AND LUNAR LANDING

Energy relationships are used to determine V_E .

$$V_1^2 = \mu_p \left(\frac{2}{r_o} - \frac{1}{a} \right); \quad V_E^2 = \mu_p \left(\frac{2}{r_E} - \frac{1}{a} \right) \quad (E.2)$$

Solving simultaneously to eliminate a yields

$$\left(\frac{V_E}{V_o} \right)^2 = \frac{2}{V_o^2} \left(\frac{\mu_p}{r_E} - \frac{\mu_p}{r_o} \right) + \left(\frac{V_1}{V_o} \right)^2 \quad (E.3)$$

Reference to the diagram shows that

$$\begin{aligned} \gamma_1 &= \gamma_o + \Delta\gamma = \gamma_o + \tan^{-1} \frac{\Delta V \sin \psi}{V_o + \Delta V \cos \psi} \\ &= \gamma_o + \tan^{-1} \frac{\frac{\Delta V}{V_o} \sin \psi}{1 + \frac{\Delta V}{V_o} \cos \psi} \end{aligned} \quad (E.4)$$

Since angular momentum is constant in the deboost trajectory,

$$\bar{h} = V_1 r_o \cos \gamma_1 = V_E r_E \cos \gamma_E \quad ()$$

Therefore,

$$\begin{aligned} \cos \gamma_E &= \frac{V_o}{V_E} \frac{r_o}{r_E} \cos (\gamma_o + \Delta\gamma) \\ \gamma_E &= \cos^{-1} \left(\frac{V_1}{V_o} \right) \left(\frac{V_o}{V_E} \right) \left(\frac{r_o}{r_E} \right) (\cos \gamma_o \cos \Delta\gamma - \sin \gamma_o \sin \Delta\gamma) \end{aligned} \quad (E.6)$$

The error equations are determined by taking the derivative of V_E and γ_E in Equations (E.3) and (E.6) with respect to the independent variables ψ and ΔV , holding all others constant.

$$\frac{\partial V_E}{\partial \psi} = - \left(\frac{V_o}{V_E} \right) \left(\frac{\Delta V}{V_o} \right) V_o \sin \psi \quad (E.7)$$

$$\frac{\partial V_E}{\partial \Delta V} = \left(\frac{V_o}{V_E} \right) \left(\frac{\Delta V}{V_o} + \cos \psi \right) \quad (E.8)$$

Equations for Impulsive Vacuum Deboost

E-3

$$\frac{\partial \gamma_E}{\partial \psi} = \csc \gamma_E \left(\frac{r_o}{r_E} \right) \left\{ \frac{\frac{\Delta V}{V_o} (\sin \psi \cos \gamma_o + \cos \psi \sin \gamma_o)}{\frac{V_E}{V_o}} - \frac{\left[\left(1 + \frac{\Delta V}{V_o} \cos \psi \right) \cos \gamma_o - \frac{\Delta V}{V_o} \sin \psi \sin \gamma_o \right] \frac{\Delta V}{V_o} \sin \psi}{\left(\frac{V_E}{V_o} \right)^3} \right\} \quad (E.9)$$

$$\frac{\partial \gamma_E}{\partial \Delta V} = - \csc \gamma_E \left(\frac{r_o}{r_E} \right) \left\{ \frac{\cos \gamma_o \cos \psi + \sin \gamma_o \sin \psi}{V_o \left(\frac{V_E}{V_o} \right)} - \frac{\left[\left(1 + \frac{\Delta V}{V_o} \cos \psi \right) (\cos \gamma_o) - \frac{\Delta V}{V_o} \sin \psi \sin \gamma_o \right] \left(\frac{\Delta V}{V_o} + \cos \psi \right)}{V_o \left(\frac{V_E}{V_o} \right)^3} \right\} \quad (E.10)$$

The equations presented in the text for \bar{h} , a , e , γ , E , and t are all standard definitions of these elements. The range angle, θ , is the difference between the true anomaly at time of impulse application and the true anomaly at atmospheric entry, since the true anomaly is the angle from these points to perigee of the deboost orbit. The time computed is the time at each point from perigee passage in the deboost orbit, and therefore, time of flight is the difference between t_1 and t_E .

The "miss equations," which describe the effect of ΔV and ψ on the range angle, θ , are found by taking the derivative of θ with respect to these two variables. This in turn, necessitates obtaining the derivatives of \bar{h} , γ_1 , and γ_E . However, the derivative of γ_E has already been determined.

$$\frac{\partial \bar{h}}{\partial \psi} = -V_o r_o \left[\left(\frac{V_1}{V_o} \right) \sin \gamma_1 \frac{\partial \gamma_1}{\partial \psi} + \frac{\left(\frac{\Delta V}{V_o} \right) \sin \psi \cos \gamma_1}{\left(\frac{V_1}{V_o} \right)} \right] \quad (E.11)$$

$$\frac{\partial \gamma_1}{\partial \psi} = \frac{\frac{\Delta V}{V_o} \left(\frac{\Delta V}{V_o} + \cos \psi \right)}{\left(V_1/V_o \right)^2} \quad (E.12)$$

E-4

LUNAR/PLANETARY DEBOOST AND LUNAR LANDING

$$\frac{\partial \theta}{\partial \psi} = \frac{\bar{h} \cos^2 \gamma_1}{\mu_p} \left[\frac{\left(\frac{\bar{h}^2}{\mu_p} - r_o \right) \left(2 \tan \gamma_1 \frac{\partial \bar{h}}{\partial \psi} + \bar{h} \sec^2 \gamma_1 \frac{\partial \gamma_1}{\partial \psi} \right) - 2 \frac{\bar{h}^2}{\mu_p} \tan \gamma_1 \frac{\partial \bar{h}}{\partial \psi}}{\left(\frac{\bar{h}^2}{\mu_p} - r_o \right)^2} \right] \\ - \frac{\bar{h} \cos^2 \gamma_E}{\mu_p} \left[\frac{\left(\frac{\bar{h}^2}{\mu_p} - r_E \right) \left(2 \tan \gamma_E \frac{\partial \bar{h}}{\partial \psi} + \bar{h} \sec^2 \gamma_E \frac{\partial \gamma_E}{\partial \psi} \right) - 2 \frac{\bar{h}^2}{\mu_p} \tan \gamma_E \frac{\partial \bar{h}}{\partial \psi}}{\left(\frac{\bar{h}^2}{\mu_p} - r_E \right)^2} \right] \quad (E.13)$$

$$\frac{\partial \bar{h}}{\partial (\Delta V)} = V_o r_o \left[\frac{\left(\frac{\Delta V}{V_o} + \cos \psi \right) \cos \gamma_1}{V_o \left(\frac{V_1}{V_o} \right)} - \left(\frac{V_1}{V_o} \right) \sin \gamma_1 \frac{\partial \gamma_1}{\partial (\Delta V)} \right] \quad (E.14)$$

$$\frac{\partial \gamma_1}{\partial (\Delta V)} = \frac{\sin \psi}{V_o (V_1/V_o)^2} \quad (E.15)$$

$$\frac{\partial \theta}{\partial (\Delta V)} = \frac{\bar{h} \cos^2 \gamma_1}{\mu_p} \left[\frac{\left(\frac{\bar{h}^2}{\mu_p} - r_o \right) \left(2 \tan \gamma_1 \frac{\partial \bar{h}}{\partial (\Delta V)} + \bar{h} \sec^2 \gamma_1 \frac{\partial \gamma_1}{\partial (\Delta V)} \right) - 2 \frac{\bar{h}^2}{\mu_p} \tan \gamma_1 \frac{\partial \bar{h}}{\partial (\Delta V)}}{\left(\frac{\bar{h}^2}{\mu_p} - r_o \right)^2} \right] \\ - \frac{\bar{h} \cos^2 \gamma_E}{\mu_p} \left[\frac{\left(\frac{\bar{h}^2}{\mu_p} - r_E \right) \left(2 \tan \gamma_E \frac{\partial \bar{h}}{\partial (\Delta V)} + \bar{h} \sec^2 \gamma_E \frac{\partial \gamma_E}{\partial (\Delta V)} \right) - 2 \frac{\bar{h}^2}{\mu_p} \tan \gamma_E \frac{\partial \bar{h}}{\partial (\Delta V)}}{\left(\frac{\bar{h}^2}{\mu_p} - r_E \right)^2} \right] \quad (E.16)$$

To determine the optimum ψ for a minimum value of ΔV with γ_E specified, solve implicitly for

$$\frac{\partial (\Delta V/V_o)}{\partial \psi}$$

by taking the derivative of the equation for γ_E , (E.6). The derivative,

$$\frac{\partial (\Delta V/V_o)}{\partial \psi}$$

Equations for Impulsive Vacuum Deboost

E-5

is set equal to zero, giving a relationship between ΔV and ψ . For the sake of simplicity, let $\Delta V/V_0 = \Gamma$.

$$\frac{\partial \Gamma}{\partial \psi} = 0 = \frac{\left[\frac{2\mu_p}{V_0^2} \left(\frac{1}{r_E} - \frac{1}{r_0} \right) + (1 + \Gamma^2 + 2\Gamma \cos \psi) \right]^{\frac{1}{2}} \left[\cos \gamma_0 (1 + \Gamma \cos \psi) - \sin \gamma_0 (\Gamma \sin \psi) \right] \Gamma \sin \psi}{\left[\frac{2\mu_p}{V_0^2} \left(\frac{1}{r_E} - \frac{1}{r_0} \right) + (1 + \Gamma^2 + 2\Gamma \cos \psi) \right]} - \frac{\left[\frac{2\mu_p}{V_0^2} \left(\frac{1}{r_E} - \frac{1}{r_0} \right) + (1 + \Gamma^2 + 2\Gamma \cos \psi) \right]^{\frac{1}{2}} \left[(\Gamma \sin \psi \cos \gamma_0 + \Gamma \cos \psi \sin \gamma_0) \right]}{\left[\frac{2\mu_p}{V_0^2} \left(\frac{1}{r_E} - \frac{1}{r_0} \right) + (1 + \Gamma^2 + 2\Gamma \cos \psi) \right]} \quad (E.17)$$

Since the denominator,

$$\left[\frac{2\mu_p}{V_0^2} \left(\frac{1}{r_E} - \frac{1}{r_0} \right) + (1 + \Gamma^2 + 2\Gamma \cos \psi) \right]$$

cannot equal infinity, the numerator must be identically equal to zero or

$$\begin{aligned} & \sin \psi \left[\cos \gamma_0 (1 + \Gamma \cos \psi) - \sin \gamma_0 (\Gamma \sin \psi) \right] \\ &= \left[\frac{2\mu_p}{V_0^2} \left(\frac{1}{r_E} - \frac{1}{r_0} \right) + (1 + \Gamma^2 + 2\Gamma \cos \psi) \right] (\cos \gamma_0 \sin \psi + \sin \gamma_0 \cos \psi) \end{aligned}$$

Expanding and eliminating terms,

$$\begin{aligned} & \left[\frac{2\mu_p}{V_0^2} \left(\frac{1}{r_E} - \frac{1}{r_0} \right) + \Gamma^2 \right] (\cos \gamma_0 \sin \psi + \sin \gamma_0 \cos \psi) + \Gamma \sin \gamma_0 + \Gamma \cos^2 \psi \sin \gamma_0 \\ & + \Gamma \cos \psi \sin \psi \cos \gamma_0 + \sin \gamma_0 \cos \psi = 0 \quad (E.18) \end{aligned}$$

This is a quadratic equation in Γ . If we solve for Γ , the expression under the radical may be simplified by use of trigonometric identities to

$$\sin^2 \psi \left[\cos (\psi - \gamma_o) \cos (\psi + \gamma_o) \right] - \cos \gamma_o \sin \gamma_o \cos \psi \sin \psi (1 + 2 \sin^2 \psi) \\ - 4 \sin^2 (\psi + \gamma_o) \left[\frac{2\mu_p}{V_o^2} \left(\frac{1}{r_E} - \frac{1}{r_o} \right) \right]$$

Calling this quantity S , the solution for Γ is

$$\Gamma = \frac{\Delta V}{V_o} = \frac{-[\cos \psi \sin (\psi + \gamma_o) + \sin \gamma_o] \pm \sqrt{S}}{2 \sin (\psi + \gamma_o)} \quad (E.19)$$

Solving this equation simultaneously with the equation for γ_E , (E.6), provides an expression for optimum ψ to minimize ΔV for a specified γ_E .

If it is desired to specify V_E and disregard γ_E , the derivative

$$\frac{\partial(\Delta V/V_o)}{\partial \psi}$$

is again solved for implicitly by taking the derivative of Equation (E.3), holding all variables except $\Delta V/V_o$ and ψ constant. (Again, $\Delta V/V_o = \Gamma$)

$$\frac{\partial \Gamma}{\partial \psi} = \frac{-\Gamma \sin \psi}{\left[\frac{2\mu_p}{V_o^2} \left(\frac{1}{r_E} - \frac{1}{r_o} \right) \right]} \quad (E.20)$$

Setting $\partial \Gamma / \partial \psi$ equal to zero, and noticing that the denominator cannot be infinite, then

$$\Gamma \sin \psi = 0$$

Since $\Gamma = 0$ gives no solution, ψ must be either 0 or π . It also follows that ΔV must be turned opposite to the direction of flight to deboost for entry purposes. By substituting $\psi = \pi$ into Equation (E.1) and using the results in Equation (E.3), the equation for minimum ΔV is

$$\frac{\Delta V}{V_o} = 1 - \left[\left(\frac{V_E}{V_o} \right)^2 - \frac{2\mu_p}{V_o^2} \left(\frac{1}{r_E} - \frac{1}{r_o} \right) \right]^{\frac{1}{2}} \quad (E.21)$$

2 VELOCITY REQUIREMENTS FOR A VERTICAL-DESCENT LUNAR LANDING

This section is devoted to the development of equations for a nonatmospheric vertical descent with a single retrolanding maneuver. Since atmospheric effects are not present, the analysis can be useful in simulating a vertical landing on the lunar surface. It is assumed that the approach to the moon is along a hyperbolic impact trajectory, where the impact velocity, V_{IMP} , is defined as

$$V_{IMP} = \sqrt{\frac{2\mu_m}{r_m} + (V_\infty)^2} \quad (E.22)$$

where

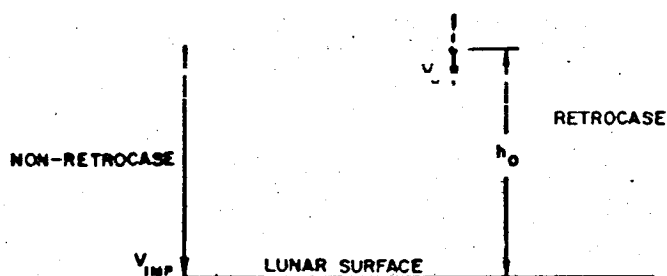
μ_m = lunar gravitational constant

r_m = radius of the moon

V_∞ = approach velocity at an infinite distance from the lunar surface

The velocity, V_∞ , is determined by the earth burnout velocity at the end of boost and by any midcourse maneuvers performed during the circumlunar flight.

As can be seen from the diagram below, the landing vehicle will begin its retrolanding maneuver at some point, h_o , above the lunar surface.



In the non-retrocase, the impact velocity, V_{IMP} , is the sum of the initial velocity, V_o , plus the gain in potential energy,

$$V_{IMP} = \sqrt{V_o^2 + 2g_m h_o} \quad (E.23)$$

where g_m is the acceleration of lunar gravity, which is assumed constant. In the case where retrovelocity is added, the ideal or total velocity is defined as

$$V_I = V_o + g_m t_B = g_e I_{sp} \ln \frac{W_o}{W_{BO}} \quad (E.24)$$

E-3

LUNAR/PLANETARY DEBOOST AND LUNAR LANDING

where g_e represents the acceleration of gravity of the earth. It was assumed that at time t_B the vehicle had landed on the lunar surface with zero velocity.

The altitude, h_o , or distance traveled during burning can be expressed as

$$h_o = v_o t_B + \frac{1}{2} g_m t_B^2 - g_e \text{Isp} t_B \left(1 - \frac{\ln \frac{W_o}{W_{BO}}}{\frac{W_o}{W_{BO}} - 1} \right) \quad (\text{E.25})$$

Combining Equations (E.23), (E.24), and (E.25) gives

$$v_{\text{IMP}} = \sqrt{g_e^2 \text{Isp}^2 \left(\ln \frac{W_o}{W_{BO}} \right)^2 - 2 g_e g_m \text{Isp} t_B \left(1 - \frac{\ln \frac{W_o}{W_{BO}}}{\frac{W_o}{W_{BO}} - 1} \right)} \quad (\text{E.26})$$

Realizing that

$$t_B = \frac{\text{Isp}}{\frac{T}{W_o}} \left(1 - \frac{W_{BO}}{W_o} \right) \quad (\text{E.27})$$

Equation (E.26) in nondimensional form gives

$$\frac{v_{\text{IMP}}}{g_e \text{Isp}} = \sqrt{\left(\ln \frac{W_o}{W_{BO}} \right)^2 - \frac{2 g_m}{g_e \frac{T}{W_o}} \left(\frac{\frac{W_o}{W_{BO}} - 1 - \ln \frac{W_o}{W_{BO}}}{\frac{W_o}{W_{BO}}} \right)} \quad (\text{E.28})$$

Equation (E.28) is seen to give the vehicle mass ratio, W_o/W_{BO} , required to perform the landing maneuver as a function of the specific impulse and the initial thrust-to weight ratio, where T_{vac}/W_o is measured in earth standards.

Nomenclature

E-9

NOMENCLATURE

a	Semimajor axis of deboost orbit
g_e	Earth gravitational acceleration
g_m	Lunar gravitational acceleration
\bar{h}	Angular momentum of deboost orbit
h_o	Altitude at the start of retrophase
I_{sp}	Vacuum specific impulse
r_E	Radius from planet center to outer edge of atmosphere
r_m	Radius of the moon
r_o	Radius from planet center to deboost impulse application point
T_{vac}	Vacuum thrust
t_B	Vehicle burning time during retrophase
V_1	Velocity immediately after impulse application
V_E	Velocity at atmospheric entry
V_{imp}	Impact velocity with no retrophase
V_o	Velocity at the start of retrophase
V_∞	Velocity at an infinite distance
W_{BO}	Vehicle burnout weight
W_o	Vehicle initial weight
Γ	$\Delta V/V_o$
γ_1	Flight path angle immediately after impulse application
γ_E	Flight path angle at atmospheric entry
γ_o	Flight path angle in initial orbit at impulse application point
$\Delta\gamma$	Change in flight path angle due to velocity impulse application
ΔV	Velocity impulse applied for deboost
μ_m	Lunar gravitational constant
μ_p	Planet gravitational constant
ψ	Angle between initial orbit velocity vector and velocity impulse vector

ADDENDUM

TRAJECTORY OPTIMIZATION FOR POWERED
FLIGHT IN TWO OR THREE DIMENSIONS

Although powered flight trajectory design constitutes a large area of study which requires special attention, no discussion of this subject is complete without consideration of the optimization aspects of the problem. The following discussion is based upon "Trajectory Optimization for Powered Flight in Two or Three Dimensions," by Dr. Burton D. Fried, which was published as Chapter 4 in the book Space Technology (edited by Howard Seifert), published by John Wiley and Sons, Inc., 1959. Incorporated with this article are portions of the following:

Culler, Glen J. and Burton D. Fried, "Universal Gravity Turn Trajectories," Journal of Applied Physics, Vol. 28, No. 6, pp. 672-676, June 1957.

Culler, Glen J. and Burton D. Fried, "Universal Gravity Turn Curves," Ramo-Wooldridge Corporation, Report ARL-5-2, 1 November 1955.

Culler, Glen J. and Burton D. Fried, "Supplement to Universal Gravity Turn Trajectories," Ramo-Wooldridge Corporation, Report ARL-7-32, 14 August 1957.

In addition, at the conclusion of the addendum, a bibliography is presented which contains references pertaining to the general problem of trajectory optimization (as differentiated from vehicle design optimization; references which pertain strictly to design optimization are given at the conclusion of Chapter 5). The list is by no means complete; those publications selected for the bibliography are intended, to some extent, to complement the discussion, as well as to call attention to developments in other approaches to the problem. Many of the articles logically complement developments in the material herein, while other researchers, whose work chronologically post-dates that performed by Fried, et. al., have further developed arguments and ideas found in the addendum. Also, several of the articles referenced in the bibliography demonstrate the use of direct methods such as dynamic programming and the method of steepest descent for optimization analyses of trajectory problems, in addition to further exploitation of the approach in which the disciplines of the calculus of variations are utilized.

1 INTRODUCTION

Problems of missile analysis may conveniently be divided into two categories. In the first, a missile with given characteristics is assumed and its performance is studied, whereas in the second it is the performance requirements that are specified in advance, the problem being one of designing a missile to satisfy them.

To carry out either kind of analysis, it is necessary to use some kind of model for a missile. The simplest is a point particle, confined to motion in one direction and subject to thrust forces, gravity, and, perhaps, drag. This model is quite satisfactory for many purposes and allows the study of the effects of mass ratios, exhaust velocities, burning time, staging, thrust programming, etc. Of course, it cannot, by its very nature, provide any information regarding the spatial trajectory of the missile (with the exception of a sounding rocket). Thus, it is necessary to consider the generalization of this model to include motion in at least two dimensions, since such typical space technology missions as the long-range surface-to-surface delivery of a given payload and the launching of an earth satellite require that the missile be given a large horizontal component of velocity as well as the vertical acceleration which carries it to high altitudes. The present discussion will be largely concerned with the extension of the point particle model to include motion in two or three dimensions, although a full description of the trajectory problem will require a brief discussion of the more complex models that better describe the actual system.

One of the most important questions a two- or three-dimensional model must answer is simply, "What trajectory should the missile follow, i. e., how should it be steered?" A careful formulation of this leads, of course, to problems of optimization. What choice of trajectory will maximize (or minimize) some criterion of performance W , where W might be the range, the altitude of a satellite orbit, the payload, the cost, etc.? However, it is important to distinguish here between two classes of optimization problems, corresponding to the suggested categorization of missile problems. Only those of the first variety, in which all characteristics of the missile (e. g., mass and thrust as functions of time for the point model in vacuum) are specified and the trajectory that optimizes some aspect of the performance is sought, constitute pure trajectory problems. Those of the second kind, in which the mission rather than the missile is specified, and in which payload weight, take-off weight, or the like is to be optimized, are really problems of missile design. A brief discussion of this latter type will nonetheless be appropriate here since they are often classed as trajectory problems; trajectory considerations—in particular, solutions of the first type of problem—play an

important part in their solution; and they provide an excellent illustration of an appropriate use for large computers in missile problems. Consideration will also be given to a third type of problem, intermediate between these two, in which not only the thrust direction but also the mass and the exhaust velocity are allowed to vary in the optimization, the criterion being, for instance, maximum burnout weight for given initial weight and performance. These problems are more general than those of the pure trajectory type, with mass and thrust specified functions of time, but since it is generally the payload that we seek to maximize, rather than the total burnout weight, these intermediate formulations do not solve the design problem, although they can provide upper limits of interest.

In many engineering problems optimization procedures are of small importance, the performance not being particularly sensitive to the choice of operating parameters so that experience provides a satisfactory guide. This is not the case with large ballistic missiles because (a) their performance is extremely sensitive to small changes in design; (b) they are large, overwhelmingly complex systems with strong interactions between the different subsystems; and (c) the number of variables that have a significant effect on any one quantity is generally so large as to make intuitive judgments difficult and/or incorrect. Experience has shown that system optimization, far from being an academic luxury, is frequently a vital part of the analysis and therefore worth considering in detail.

Some general comments regarding the role of numerical analysis in trajectory problems are in order. It is clearly a straightforward matter to write down complete equations of motion for very sophisticated vehicle models, including rigid-body rotations, aerodynamic forces and moments, the servo loop of the steering system, etc., and modern digital computers can provide solutions in a matter of minutes. Why then bother with the analysis of simple models? In the first place, a straight numerical approach is unwieldy for optimization problems, in which the (infinite dimensional) space of all possible trajectories must be explored. This is true even for the pure trajectory problems, whereas for the fixed mission or design type of problem, in which the trajectory must be codetermined with the characteristics of the missile itself, the capabilities of even the largest computers would be taxed should the trajectory part of the optimization be handled numerically. Moreover, machine calculations generally provide far more detail than is actually required unless the problem at hand is simply one of computing firing tables. For purposes of a general survey or an understanding of the relation of trajectory to performance, simple analytical, albeit approximate, results can be far more informative than a long series of machine calculations.

The general philosophy of approach adopted here stresses the use of models that can give simple analytical results, avoiding the use of computing machines for the "brute force" solution of trajectory optimization problems. It is felt that more sophisticated models and the concomitant numerical methods should be used only where they are really required, e. g. for the solution of the fixed-mission, design type of problem.

The general subject of trajectories is, of course, quite extensive, and qualitatively different methods of analysis are required for various cases. The emphasis in the present discussion will be on ballistic missiles, i. e., those characterized by a short period of powered flight followed by a long free-flight period, although the general analysis of Section 3 applies as well to trajectories for which thrust is exerted throughout the flight. In any case, attention here will be confined to the powered-flight portion of the trajectory, since only for it are characteristics peculiar to missiles involved. The free-flight portion of the trajectory, which is amenable to conventional analytical dynamics, is treated in the companion volume, Reference 1.

Although many trajectory optimization problems involve straightforward application of well-established techniques of the calculus of variations, a number of important results can be deduced without invoking the full power of that discipline. Such is the case for ballistic missiles with chemical propulsion systems and terrestrial missions (distance covered during powered flight not large compared to the earth's radius), for which it is a good approximation to treat the gravitational force field as uniform throughout the powered flight. This is discussed in Section 2, in which elementary considerations are used to deduce a general, nearly optimum trajectory pattern for ballistic missiles with either long-range surface-to-surface or satellite missions. The more general formulation required to study the effects of a nonuniform force field during the powered flight and to treat problems in which the mass and thrust are not specified is presented in Section 3, and some soluble examples are cited. Section 4 deals with the problem of optimization of missile design.

2 TRAJECTORY OPTIMIZATION FOR BALLISTIC MISSILES

By definition, a ballistic missile is characterized by a period of powered flight, $0 \leq t \leq T$, followed by a free flight during which the missile is subject to no thrust. Let \vec{r}_1 and \vec{v}_1 denote the position and velocity of the missile at burnout ($t = T$) and W the quantity to be optimized, e. g., range for a surface-to-surface missile, orbit altitude, or perigee altitude for a satellite, etc. Classical dynamics gives W as a function of the burnout variables, $W(\vec{r}_1, \vec{v}_1)$.

The simplest model for the missile is a point particle with mass and thrust as functions of time, $M(t)$ and $F(t)$. For the pure-trajectory or fixed-missile type of problem, these are to be regarded as given, albeit arbitrary,* functions. The flight path then depends on the orientation of the thrust vector, and for a planar trajectory (i. e., one for which the thrust vector is confined to a plane passing through the vertical and the initial velocity vector) this is specified by the attitude angle $\psi(t)$ between the thrust vector at time t and the horizontal direction at launch. For each choice of $\psi(t)$ we can compute the burnout variables \bar{r}_1 and \bar{v}_1 and hence the value of W ; W , \bar{r}_1 and \bar{v}_1 are functionals of $\psi(t)$.

The problem is to find the particular function $\psi(t)$ that maximizes (or minimizes) W . A necessary condition on $\psi(t)$ is that a small change, $\psi(t) \rightarrow \psi(t) + \delta\psi(t)$, not produce a first-order change in W , i. e., that in the expansion of $W(\psi + \epsilon\eta)$ in powers of ϵ , the term linear in ϵ should vanish for any function η . A function $\psi(t)$ satisfying this condition is said to be a stationary solution† and the coefficient of $\epsilon\eta$ in such an expansion is sometimes called the variational derivative of W with respect to ψ . It is a function of t which may be denoted by $\delta W/\delta\psi(t)$ and is related to the analogously defined variational derivatives $\delta\bar{r}_1/\delta\psi$ and $\delta\bar{v}_1/\delta\psi$ by the equation

$$\delta W/\delta\psi(t) = \nabla_r W \cdot \delta\bar{r}_1/\delta\psi(t) + \nabla_v W \cdot \delta\bar{v}_1/\delta\psi(t) \quad (1)$$

where $\nabla_r W$ is the vector with components $\partial W/\partial x_1$, $\partial W/\partial y_1$ evaluated for the arguments \bar{r}_1 , \bar{v}_1 and $\nabla_v W$ is defined in an analogous fashion.

Each term in equation (1) is a product of a factor determined only from an analysis of the ballistic or free-flight portion of the trajectory ($\nabla_r W$, $\nabla_v W$) and a factor that depends only on the powered-flight trajectory ($\delta\bar{r}_1/\delta\psi$, $\delta\bar{v}_1/\delta\psi$). Of course, $\nabla_r W$ and $\nabla_v W$ are functions of the burnout quantities \bar{r}_1 , \bar{v}_1 , which in turn depend on the powered flight.

* The term "arbitrary function" is to be understood here, and in the following, in a physical rather than a mathematical sense, i. e., as a function which is arbitrary except for such restrictions of continuity, differentiability, positive definiteness, etc., as may be necessary to exclude situations that are clearly not sensible in view of the physical significance of the function. For instance, M and F would have jump discontinuities in a multistage missile.

† The present discussion, as well as that of Section 3, will be concerned chiefly with such stationary solutions. As will be shown later, a trajectory optimization problem may have a stationary solution which is not a maximum (or minimum) or it may have a maximum (or minimum) which is not a stationary solution.

The variational derivatives needed for the right-hand side of (1) cannot be computed in closed form, in general, since the functional relation between \vec{r} and ψ is specified by differential equations. This difficulty may be resolved by using Lagrange multipliers, as shown in Section 3. However, a direct computation of $\delta\vec{r}_1/\delta\psi$ and $\delta\vec{v}_1/\delta\psi$ can be made by neglecting aerodynamic effects and variations in the gravitation force and assuming that the acceleration is due only to the thrust and a uniform gravitational force field. To evaluate the variational derivatives of \vec{r}_1 and \vec{v}_1 in that case, note that if only the direction of the thrust is varied, and not its magnitude, the increment of thrust must be normal to the thrust \vec{F} . This extra impulse produces, per unit time, a velocity increment

$$\delta\vec{v}(t) = F(t) \delta\psi \vec{N}_0(t)/M(t) \quad (2)$$

where \vec{N}_0 is a unit vector normal to \vec{F} , and this velocity increment appears as an equal increment in the burnout velocity \vec{v}_1 , since the force field is constant. Thus,

$$\delta\vec{v}_1/\delta\psi(t) = n(t)\vec{N}_0(t) \quad (3)$$

where $n = F/M$ is the magnitude of the acceleration due to thrust. Since the change in burnout position is just the velocity increment multiplied by the time remaining until burnout,

$$\delta\vec{r}_1/\delta\psi(t) = (T - t) \delta\vec{v}_1/\delta\psi(t) \quad (4)$$

where T is the total burning time.

It then follows at once from the vanishing of (1) that the direction of thrust at time t should be along the vector

$$\vec{f}(t) = \nabla_v W + (T - t) \nabla_r W \quad (5)$$

(We need not bother to normalize \vec{f} since only its direction is of interest.) This is a linear vector function of time since the gradients of W , although unknown a priori [since \vec{r}_1 and \vec{v}_1 are functionals of $\psi(t)$], are nonetheless independent of t . We thereby obtain the implicit result (noted also by Lawden²),

$$\tan \psi(t) = \frac{\partial W/\partial v_y + (T - t)\partial W/\partial y}{\partial W/\partial v_x + (T - t)\partial W/\partial x} = \frac{a + bt}{c + dt} \quad (6)$$

implicit because the gradients of W are functions of \vec{r}_1 and \vec{v}_1 which in turn depend on ψ . It is to be emphasized that the result (5) or (6) is completely independent of the form of the functions $F(t)$ and $M(t)$ and remains valid for an arbitrary (see footnote, * p. 5A) program of staging, throttling, or the like.

The simplest example of this general formalism is the case where W is the range of a surface-to-surface missile. If the total range is small compared to the earth's radius, R_e , so that the Kepler field can be well approximated by a uniform gravitational force field during the entire flight, free as well as powered, the two gradients of W are exactly parallel,

$$\nabla_v W = \tau \nabla_r W$$

where τ is the free-flight time—burnout to impact. (In a uniform field the same change in range is produced by a variation $\delta \vec{v}_1$ in velocity or a variation $\delta \vec{r}_1 = \tau \delta \vec{v}_1$ in position.) According to (6) the direction of \vec{r} is then independent of time, i. e., the optimum thrust attitude program is $\psi = \text{constant}$. *

This continues to be very nearly the optimum program when the free flight occurs in the inverse-square, central force field of the earth. Except for such special cases as a sounding flight or a near satellite orbit (range nearly equal to the earth's circumference), the change in range due to an increment $\delta \vec{v}_1$ in burnout velocity will then be of the same order of magnitude as the change due to an increment $\delta \vec{r}_1 = (R_e/v_1) \delta \vec{v}_1$ in burnout position. This means

$$|\nabla_v W| \approx |\nabla_r W| R_e/v_1 \quad (7)$$

If $R_e/v_1 \gg T$, as is true, for instance, when the distance covered during powered flight is small compared to R_e , it follows at once from (5) that the optimum thrust orientation is very nearly parallel to the fixed direction $\nabla_v W$. [Of course, if $v_1 T$ is not small compared to R_e , we can always return to the complete expression (6) but since the distance covered during powered flight is of order $v_1 T$, the assumption of a uniform gravitational field, used in deriving (5) and (6), is generally not valid for cases where $v_1 T > R_e$.] Explicit equations for the optimum value of ψ in terms of $F(t)$ and $M(t)$ may be obtained from (5) and (6),³ but the most important feature of the result is simply the knowledge that a constant or nearly constant thrust attitude maximizes the range.

Another pertinent example is provided by missiles used for satellite launching. If the performance of the vehicle is marginal, it might, for instance, be important to maximize the perigee altitude in order to prevent excessive slowing down due

to drag. Other alternatives of possible interest are to minimize the apogee altitude, maximize the mean of perigee and apogee altitudes, etc. For any of these cases W is a function only of y and \vec{v} , so that (6) gives $\tan \psi$ as a linear function of t .⁴ An iterative process is necessary to find the actual values of the two coefficients in this linear expression but, as in the maximum-range problem, the chief value of the result is that it gives the functional form of $\psi(t)$.

Of all the possible trajectories, one corresponding to each choice of $\psi(t)$, a single family— $\psi = \psi_0 = \text{constant}$ in the surface-to-surface problem, $\tan \psi = a - bt$ for the satellite launcher—has been selected. Even if it proves expedient to determine the parameters ψ_0 , a , b , by numerical optimization, as is often the case, the task of determining the values of one or two parameters is enormously simpler than that of selecting a $\psi(t)$ from the class of all admissible functions.

At this point it is in order to examine the validity of the approximations used in deriving (5) and (6). The error involved in treating the gravitational force field as constant, in magnitude and direction, during the powered flight will be small provided the powered flight extends over a distance small compared to R_e . To verify this, we use the result (derived in Section 3) that for a general force field the optimum direction of thrust is along a vector $\vec{\lambda}$ which satisfies the differential equation

$$\ddot{\vec{\lambda}} + \nabla U \cdot \vec{\lambda} = 0 \quad (8)$$

and the initial conditions

$$\vec{\lambda}(T) = -\nabla_{\vec{v}} W, \quad \dot{\vec{\lambda}}(T) = \nabla_{\vec{r}} W \quad (9)$$

where U is the potential of the gravitational force field, e. g.,

$$U = -gR_e^2/r \quad (10)$$

In the case of a uniform force field, $\nabla U = 0$ and (8) and (9) give

$$\vec{\lambda} = -[\nabla_{\vec{v}} W + (T - t)\nabla_{\vec{r}} W] \quad (11)$$

in agreement with (5). As a first correction to this result, we can expand in powers of $|\vec{p}|/R_e$ where \vec{p} is the position vector measured from launch,

$$\vec{p} = \vec{r} - \vec{r}(0)$$

Since

$$\nabla U = gR_e^2 (\vec{r}^2 - 3\vec{r}\vec{r})/r^5$$

for the Kepler field, where \hat{I} is the unit dyad, we have, to lowest order in $|\vec{p}|/R_e$,

$$\nabla\nabla U = (g/R_e) \begin{pmatrix} 1 & 0 \\ 0 & -2 \end{pmatrix}$$

Substituting in (8) and using the initial conditions (9), we find

$$\begin{aligned} \lambda_x &= -(\partial W/\partial v_x) \cos \omega_x(t - T) + (\partial W/\partial x) [\sin \omega_x(t - T)] / \omega_x \\ \lambda_y &= -(\partial W/\partial v_y) \cosh \omega_y(t - T) + (\partial W/\partial y) [\sinh \omega_y(t - T)] / \omega_y \end{aligned} \quad (12)$$

with

$$\omega_x^2 = \omega_y^2/2 = g/R_e$$

Since (12) reduces to (11) for $\omega_y t \ll 1$, the uniform-field results are certainly valid provided the length of powered flight is small compared to R_e and the burning time is small compared to

$$(R_e/2g)^{1/2} = 9.5 \text{ min}$$

If these conditions are not satisfied, there is no recourse but to solve the full variational problem, i. e., equations (8) and (9) together with the equations of motion

$$\ddot{\vec{r}} = n\vec{N} - \nabla U$$

as explained in Section 3.

The discussion so far has neglected the aerodynamic forces, which have a twofold effect. While the missile is traversing the denser parts of the atmosphere, it will experience drag and lift forces, which may change the total impulse delivered to the missile by a few percent. Of far more practical importance, however, is the fact that an attempt to follow a program like (5) or (6) with a real missile will generally result in a large angle of attack (defined, for instance, as the angle between the velocity vector and the symmetry axis of the missile). This in turn gives rise to large bending moments and excessive structural loads on the missile body. It is possible, of course, to take account of all these effects in formulating the optimization problem, adding to the equations of motion for the center of mass those for the rigid rotation about it, etc., but the result is too complicated to be of much value. A simpler but generally satisfactory procedure is as follows.

The penalties (in terms of extra structural weight) associated with a large angle of attack are so great that it is essential to keep the angle of attack almost zero during the portion of the flight in which aerodynamic forces and moments are significant. This may be accomplished by following a "gravity turn" (sometimes referred to as a "zero angle of attack" or "zero lift" trajectory), defined as the trajectory that results from simply keeping the thrust always parallel to the velocity, starting from some nonzero, nonvertical initial velocity \vec{v}_0^* for a given $n(t)$ the path is then completely specified by the choice of \vec{v}_0 . This eliminates the large bending moments and so takes care of the major effect of aerodynamic forces. Of course, there will remain some aerodynamic forces, but these are often small enough so that it is a good approximation to integrate the equations for motion in a vacuum and then take account of the drag forces by an iteration.

Unfortunately, the equations for a gravity turn trajectory are nonlinear and have so far defied all attempts at a solution in closed form, even if we neglect aerodynamic forces, treat the gravitational force field as uniform (a good approximation since the length of the atmospheric portion of the flight is generally small compared to the earth's radius), and assume a single-stage rocket with constant thrust and mass flow rate. The necessity of repeatedly integrating these same gravity turn equations on a computing machine for each new missile problem is annoying and wasteful, particularly since extreme accuracy is frequently not required. It would be desirable to integrate them once and for all and compile the results in a convenient form. One difficulty is that even for planar motion the trajectories constitute a three-parameter family with the magnitude \vec{v}_0 of the initial velocity; the angle β_0 (often called the "initial-kick angle") of \vec{v}_0 with the vertical; and (assuming constant thrust and mass flow rate) the initial thrust to weight ratio, η , as parameters. The representation, in convenient form, of a three-parameter family of trajectories for a range of parameter values is somewhat difficult. However, the number of parameters can be reduced to two by taking advantage of the fact that in practice the gravity turn generally begins soon after launch when v_0 and β_0 are both very small. This suggests consideration of the gravity turn equations

$$\dot{v} = n - g \cos \beta \quad (13a)$$

$$v\dot{\beta} = g \sin \beta \quad (13b)$$

* The name "gravity turn" presumably comes from the fact that with the thrust, \vec{F} , parallel to \vec{v} , the trajectory would be a straight line were it not for the force of gravity which turns \vec{v} downward.

for the limiting case $v_0, \beta_0 \rightarrow 0$. The singularity in (13b) at $v = 0$ makes numerical integration of the limiting case difficult. However, the equivalent integral equation⁵

$$\psi(\tau) = \tanh \left[\int_{\tau}^1 \frac{ds}{\eta \log(1-s) - \int_0^s \psi(s') ds'} - k \right] \quad (14)$$

which already incorporates the initial conditions $v_0 = \beta_0 = 0$, presents no such difficulties. Here

$$\psi \equiv \tanh \ln \tan(\beta/2)$$

k is a constant of integration,

$$k = -\tanh^{-1} \psi(1)$$

τ is the time in units of $M(0)/|\dot{M}|$ (initial mass divided by mass flow rate) and $\eta = F/M(0)g$ is the initial-thrust-to-weight ratio. The parameter k plays a role analogous to the initial-kick angle for nonsingular gravity turns. Equation (14) is well adapted to numerical solution by iteration, starting with the initial choice $\psi \equiv -1$. From it we find $z = \tan(\beta/2)$ as a function of τ , while the velocity in units of c/η (c being the exhaust velocity, $c = F/|\dot{M}|$) is given by

$$u(\tau) = -\eta \log(1-\tau) + \int_0^{\tau} \psi(s) ds \quad (15a)$$

By expressing the velocity and time in dimensionless units, results are obtained which are "universal" in the sense that they do not depend upon specific impulse, mass flow rate or initial mass. The value of τ corresponding to burnout is simply the quantity

$$v = \frac{\text{initial propellant weight}}{\text{initial gross weight}}$$

frequently used to characterize a missile stage. The parameter k does not have a direct physical significance, but is related to the velocity attitude angle (β) at burnout, since

$$k = (-\ln z)_{\tau=1} \approx (-\ln z)_{\tau=v}$$

provided v lies in the range $0.65 \lesssim v \lesssim 1$.

Plots of the velocity attitude variable, z , versus time, τ , are shown in Figures 1 through 8 for discrete values of initial thrust-to-weight ratio, η , between 1 and 4, and for several values of the parameter $k = -[\ln \tan(\beta/2)]_{\tau=1}$ which replaces the initial kick angle. For the same values of η and k , plots of the velocity, u , versus velocity attitude, z , are shown in Figure 9 through 16. From the lines of constant τ shown on the latter curves, it is clear that u as a function of τ will be almost independent of k . It is therefore convenient to split $u(t)$ into two parts,

$$u(\tau) = u_s(\tau) + \tilde{u}(\tau)$$

where

$$u_s(\tau) \equiv -\eta \log(1 - \tau) - \tau \quad (15b)$$

is the velocity corresponding to a vertical "sounding" flight ($z \equiv 0$) and is thus independent of k , while

$$\tilde{u}(\tau) \equiv \int_0^\tau [\psi(s) + 1] ds, \quad (15c)$$

like the total u , is a function of k as well as of η . Since $|\tilde{u}(\tau)| \ll |u_s(\tau)|$ in almost all the examples that have been calculated, $u_s(\tau)$ provides a good first approximation, which can be corrected, if necessary, by adding $\tilde{u}(\tau)$. Figure 17 shows the sounding velocity, u_s , as a function of time, τ , for several values of the initial thrust-to-weight ratio, η . The correction velocity, \tilde{u} , is shown in Figures 18 through 25 as a function of time, τ , for each value of η in Figure 17 and for several values of k .

The trajectories resulting from use of these curves are sufficiently accurate for most missile problems, particularly if corrected (by a first numerical iteration) for drag forces and variations in thrust or mass flow rate.

These considerations show that with the use of a few reasonable assumptions and simplifications it is possible to obtain a general, nearly optimum trajectory pattern: a gravity turn through the atmosphere, followed by a linear fraction program, equation (6), for $\tan \psi$ during the remainder of powered flight. This pattern is characterized by a few parameters—initial-kick angle or k for the gravity turn and the coefficients in (6)—whose values may be determined either by iteration, making use of the relation of these parameters to the burnout variables, or by numerical optimization within the framework of this pattern. In the latter case,

an optimization problem in the (infinite dimensional) function space of all possible $\psi(t)$ is reduced to one in an algebraic space of at most five dimensions. The value of this is particularly apparent in the fixed-mission problems discussed in Section 4, where the trajectory must be codetermined along with the design of the vehicle itself.

3 A GENERAL FORMULATION OF TRAJECTORY OPTIMIZATION PROBLEMS

The simple optimization problems discussed in Section 2 may be generalized in several ways:

1. The uniform force field during powered flight may be replaced with a nonuniform force field or even a velocity-dependent one.
2. In addition to seeking the optimum thrust attitude program, we can also look for the best way of programming the mass and thrust.
3. For problems of type 2, we can choose the initial or final mass as a criterion for optimization in place of the function $W(\vec{r}_1, \vec{v}_1)$ studied earlier.

The mathematical methods appropriate to these questions are well known in the calculus of variations (the problem of Bolza⁶), and it is possible to give a complete and general formulation that includes all these cases. However, it seems better, for pedagogic reasons, to defer this and study first modifications 1, 2, and 3 in turn, finally summarizing and unifying them with a general statement.

Consider first the generalization of the problem of Section 2 to the case where the external force field is no longer uniform. The restriction to planar trajectories may also be dropped, the three-dimensional problem being formally no harder than the two-dimensional one. The equation of motion for a point mass missile is

$$\ddot{\vec{r}} = n(t) \vec{N}(t) + \vec{a}(\vec{r}, \dot{\vec{r}}, M) \quad (16)$$

where n is the ratio of thrust to mass, \vec{N} is a unit vector specifying the direction of thrust, and \vec{a} is the acceleration from all nonthrust forces, such as gravity or drag. For example, for motion in the earth's inverse-square field, \vec{a} would be given by

$$\vec{a}_g = -gR_e^2 \vec{r}/r^3 \quad (17)$$

and drag might contribute a term of the form

$$\vec{a}_d = 1/2 C_D(v) S \rho v \dot{\vec{r}}/M$$

As in Section 2, we seek the steering program, $\vec{N}(t)$, which makes stationary some function $W(\vec{r}_1, \vec{v}_1)$ of the burnout position and velocity, the mass and thrust being

given functions of time, so that $n(t)$ is known. Because of the dependence of \vec{a} on \vec{r} and \vec{v} it is no longer possible to give explicit expressions for the variational derivatives of \vec{r}_1 and \vec{v}_1 . To take account of the relation between \vec{r} and \vec{N} implied by the constraint (16), it is then convenient to use Lagrange multipliers. To satisfy both the condition that W be stationary for variations in the thrust attitude $\delta\vec{N}$,

$$\delta W = \nabla_{\vec{v}} W \cdot \delta\vec{v}_1 + \nabla_{\vec{r}} W \cdot \delta\vec{r}_1 = 0 \quad (18)$$

and also the constraint equation

$$\delta\vec{r} - n \delta\vec{N} - \delta\vec{a} = 0 \quad (19)$$

with

$$\delta\vec{a} = \delta\vec{r} \cdot \nabla_{\vec{r}} \vec{a} + \delta\vec{v} \cdot \nabla_{\vec{v}} \vec{a} \quad (20)$$

multiply (19) with an arbitrary vector function of the time $\vec{\lambda}(t)$, sum over all times, and add it to (18), giving

$$\delta W + \int_0^T dt \vec{\lambda} \cdot (\delta\vec{r} - n \delta\vec{N} - \delta\vec{a}) = 0 \quad (21)$$

If the initial position and velocity are fixed, the usual integration by parts gives

$$\delta\vec{v}_1 \cdot [\vec{\lambda}(T) + \nabla_{\vec{v}} W] + \delta\vec{r}_1 \cdot [\nabla_{\vec{r}} W - \vec{\lambda}(T) - \nabla_{\vec{v}} \vec{a} \cdot \vec{\lambda}(T)] + \int_0^T dt \left\{ \delta\vec{r} \cdot \left[\vec{\lambda} - \nabla_{\vec{r}} \vec{a} \cdot \vec{\lambda} + \frac{d}{dt} (\nabla_{\vec{v}} \vec{a} \cdot \vec{\lambda}) \right] - n \vec{\lambda} \cdot \delta\vec{N} \right\} = 0 \quad (22)$$

The variations $\delta\vec{r}$ and $\delta\vec{N}$ are related by (19) and cannot in general be treated as independent. However, equation (22) must be satisfied for any $\vec{\lambda}$, so if $\vec{\lambda}(t)$ is chosen to make the coefficient of $\delta\vec{r}$ in the integrand vanish for all t , and if $\vec{\lambda}(T)$, $\vec{\lambda}(T)$ are chosen to make the end point quantities vanish, equation (22) requires that

$$\vec{\lambda} \cdot \delta\vec{N} = 0 \quad \text{for all } t \quad (23)$$

Since \vec{N} is a unit vector,

$$N^2 = 1, \quad \vec{N} \cdot \delta\vec{N} = 0$$

its three components are not independent and (23) implies that, unless $\lambda \equiv 0$, the thrust direction \vec{N} must be parallel to $\vec{\lambda}$,

$$\vec{\lambda} = \lambda \vec{N} \quad (24)$$

Summarizing, the optimum direction of thrust is along a vector $\vec{\lambda}$ determined by the differential equation

$$\ddot{\vec{\lambda}} + \frac{d}{dt} (\nabla_{\vec{v}} \vec{a} \cdot \vec{\lambda}) - \nabla_{\vec{r}} \vec{a} \cdot \vec{\lambda} = 0 \quad (25)$$

and the boundary conditions

$$\begin{aligned} \vec{\lambda}(T) &= -\nabla_{\vec{v}} W \\ \dot{\vec{\lambda}}(T) &= \nabla_{\vec{r}} W + \nabla_{\vec{v}} \vec{a} \cdot \nabla_{\vec{v}} W \end{aligned} \quad (26)$$

In (25), \vec{a} is a function of \vec{r} , \vec{v} and $M(t)$, where $M(t)$ is a given function of time and $\vec{r}(t)$ is determined by the differential equation

$$\ddot{\vec{r}} - n\vec{\lambda}/\lambda - \vec{a} = 0 \quad (27)$$

with the initial conditions

$$\vec{r}(0) = \vec{r}_0 \quad \text{and} \quad \dot{\vec{r}}(0) = \vec{v}_0 \quad (28)$$

given. In (26), the arguments of $\nabla_{\vec{v}} \vec{a}$ are to be evaluated at the burnout time, $t = T$.

The equations (25) through (28) constitute a system of two, coupled, second-order (vector) differential equations, with two (vector) boundary conditions for each. This system is, in general, soluble in principle, although solutions in closed form are usually not possible. However, some special cases are worth noting.

1. For a uniform force field,

$$\nabla_{\vec{r}} \vec{a} = \nabla_{\vec{v}} \vec{a} = 0$$

and (25) gives

$$\vec{\lambda} = -\nabla_{\vec{v}} W + (T-t) \nabla_{\vec{r}} W$$

in agreement with (5).

2. If the force is independent of velocity and a linear function of \vec{r} , so that $\nabla_{\vec{v}} \vec{a} = 0$ and $\nabla_{\vec{r}} \vec{a}$ is constant, then $\vec{\lambda}$ can be expressed in terms of trigonometric and hyperbolic functions. This situation arises in finding the first corrections caused by nonuniformity of the force field, as pointed out in Section 2. In particular, if $\nabla_{\vec{r}} \vec{a}$ is diagonal, a result like that of equation (12) is obtained.

3. As pointed out by C. Porter in a private communication, the case where both $\nabla_{\mathbf{v}} \bar{\alpha}$ and $\nabla_{\mathbf{r}} \bar{\alpha}$ are constant also permits an explicit closed form solution for $\bar{\lambda}$ in terms of exponentials.

As the next generalization, consider problems in which the mass and thrust magnitude programs are to be varied. Leaving both mass and thrust, or mass and exhaust velocity, free does not lead to interesting problems, for the final mass, the range, and the like generally increase indefinitely with increasing exhaust velocity. To obtain optima of physical interest, it is necessary to add some constraint, for instance by assuming the exhaust velocity, c , to be a specified function of time or by imposing some functional relation between $c(t)$ and $M(t)$. In the following, it will be assumed that c is a given function of M and t . This might be the case, for instance, in a propulsion system in which the propellant gas is heated as it flows through a heat source. The rate of propellant flow may affect the heat balance, causing the working temperature, and with it the exhaust velocity, to depend on M . If the heat source is a fission reactor, the propellant might provide part of the neutron moderation, which would also make the temperature a function of M . Since the assumption $c = c(M, t)$ in addition covers the elementary cases in which exhaust velocity, thrust, or power are specified functions of time, it does not seem necessary to consider a more general functional relation between M and c , although this would not cause any particular difficulty.

With $M(t)$ variable, a number of interesting problems can be formulated. As a first example, suppose that the burning time is fixed and that the quantity to be made stationary is again $W(\bar{\mathbf{r}}_1, \bar{\mathbf{v}}_1)$. Equation (19) must now be replaced by

$$\delta \bar{\mathbf{r}} - n \delta \bar{\mathbf{N}} - \bar{\mathbf{N}} \delta n - \delta \bar{\alpha} = 0 \quad (29)$$

where

$$\delta n = - \delta(\dot{M}c/M) = (\dot{M}c/M^2) \delta M - [c/M + (\dot{M}/M)(\partial c / \partial \dot{M})] \delta \dot{M} \quad (30)$$

and $\delta \bar{\alpha}$ contains an additional term,

$$\delta \bar{\alpha} = \delta \bar{\mathbf{r}} \cdot \nabla_{\mathbf{r}} \bar{\alpha} + \delta \bar{\mathbf{v}} \cdot \nabla_{\mathbf{v}} \bar{\alpha} + \delta M \partial \bar{\alpha} / \partial M \quad (31)$$

Otherwise the procedure is the same as before: introduce the Lagrange multiplier $\bar{\lambda}$ and integrate by parts. The result is the same as (22) but with some extra terms added, namely [taking note of (24)],

$$- \int_0^T dt \delta M \left\{ \lambda \dot{M}c/M^2 + \frac{d}{dt} [\lambda c/M + (\lambda \dot{M}/M)(\partial c / \partial \dot{M})] + \bar{\lambda} \cdot \frac{\partial \bar{\alpha}}{\partial \dot{M}} \right\} + \left[\lambda [c/M + (\dot{M}/M)(\partial c / \partial \dot{M})] \delta M \right]_0^T \quad (32)$$

Therefore to equations (25) through (28) must be added the differential equation

$$\vec{\lambda} \cdot \frac{\partial \vec{a}}{\partial \dot{M}} + \lambda \dot{M} c / M^2 + \frac{d}{dt} [\lambda c / M + (\lambda \dot{M} / M) (\partial c / \partial \dot{M})] = 0 \quad (33)$$

and the boundary conditions

$$\lambda [c + \dot{M} (\partial c / \partial \dot{M})] = 0 \quad \text{at } t = 0, T \quad (34)$$

which determine M in terms of λ , giving again a coupled and (in principle) closed system for determining M , \vec{N} , and \vec{r} .

Next, suppose that M_1 , the mass at burnout, is to be made stationary for a given value of $W(\vec{r}_1, \vec{v}_1)$ and the initial mass, M_0 . We now require $\delta M_1 = 0$ with equations (18), (29), and $M(0) = M_0$ as constraints. If Lagrange multipliers, $\vec{\lambda}(t)$, μ_1 , and μ_2 , are introduced to take care of these constraints, (21) is replaced by

$$\delta M_1 + \mu_1 \delta W + \mu_2 \delta M_0 + \int_0^T dt \vec{\lambda} (\delta \vec{r} - \delta(n\vec{N}) - \delta \vec{a}) = 0 \quad (35)$$

Integration by parts gives the same differential equations as before—(25), (27), and (33). The boundary conditions for $\vec{\lambda}$ are changed only in that $W \rightarrow \mu_1 W$, and those for M are

$$\begin{aligned} (\lambda / M) [c + \dot{M} \partial c / \partial \dot{M}]_0 - \mu_2 &= 0 \\ (\lambda / M) [c + \dot{M} \partial c / \partial \dot{M}]_T + 1 &= 0 \end{aligned} \quad (36)$$

As before, there is, in principle, sufficient information to determine all the unknowns, for although the latter now include μ_1 and μ_2 , we also have the two conditions that M_0 and W have assigned values.

All the other variations of the problem lead again to the same differential equations, the only differences being in the boundary conditions. With the inclusion of (33) for $M(t)$, this coupled set of equations is one step more complicated than when $M(t)$ is prescribed, so that solutions in closed form are even rarer than for the simpler set (25) through (28). However, a few special cases are worth noting.

1. If c is a specified function of time, so that $\partial c / \partial \dot{M} = 0$, and also $\partial \vec{a} / \partial \dot{M} = 0$ (no drag), then (33) gives

$$M^{-1} d(\lambda c) / dt = 0 \quad (37)$$

or

$$\lambda c = \text{const} \quad (38)$$

In general, it will not be possible to satisfy this equation, since the specified $c(t)$ may be quite different from $1/\lambda(t)$ as determined from (25) through (28). For instance, in a uniform gravitational field,

$$\ddot{\lambda} = 0$$

$$\dot{\lambda} = \vec{A}t + \vec{B} \quad (39)$$

$$\lambda = (A^2 t^2 + 2\vec{A} \cdot \vec{B}t + B^2)^{1/2} \quad (40)$$

where \vec{A} and \vec{B} are fixed vectors. Unless c^{-1} happens to have the particular form of the square root of a quadratic function of t , (38) and (40) are clearly inconsistent. Moreover, even if (38) can be satisfied, no information about the optimum $M(t)$ is obtained.

This example illustrates very pointedly the fact that the formalism developed here provides only a necessary condition for a stationary solution. These equations may have solutions which, although stationary, are not maxima or minima, and on the other hand there may exist optima of such a character that they are not included among these solutions. How this comes about in the present case can be understood from the following simple problem: For one dimensional, gravity-free motion, $0 \leq t \leq T$, with given $c(t)$, find the $M(t)$ which maximizes M_1 for given M_0 , T , $x(0)$, $\dot{x}(0)$, $x(T)$, $\dot{x}(T)$. Intuitive arguments make it seem almost certain that a solution exists, yet application of this formalism gives

$$\ddot{\lambda} = 0$$

$$\dot{\lambda} = At + B$$

[the one dimensional analog of (39)] and

$$\lambda c = \text{const} \quad (41)$$

If c^{-1} happens to be a linear function of the time, equation (38) can be satisfied but nothing is said about $M(t)$; if not, there is no way of even satisfying (38), let alone finding a stationary solution.

To see what is really going on, return to the equation of motion,

$$\ddot{x} = -\dot{M}c/M \quad (42)$$

Dividing by c and integrating we find

$$\log(M_0/M_1) = \int_0^T dt \, \ddot{x}/c = \left[\dot{x}/c - x \frac{d}{dt}(c^{-1}) \right]_0^T + \int_0^T dt \, x \frac{d^2(c^{-1})}{dt^2}$$

followed by a period of coasting until $t = T$, and then an impulsive firing to bring the velocity to $\dot{x}(T)$. For the general case, where $d^2(c^{-1})/dt^2$ changes sign, the optimum program may also involve impulsive firings at times other than 0, t' , or T .

This example illustrates the situations that can arise, when $c(t)$ is specified, also in more complicated problems — three-dimensional motion in an external force field, etc. There may be no optimum because the quantity to be optimized is really independent of $M(t)$, or there may be an optimum of the sort described here, one that is not stationary and hence escapes the general formalism.

2. In the particular case where c is specified as constant, equation (38) implies that if there is a stationary solution (as there may be for more complicated examples than that just considered), the associated $\vec{\lambda}(t)$ will have constant magnitude. It then follows from (25) that

$$\vec{N} + \frac{d}{dt} (\nabla_{\vec{v}} \vec{a} \cdot \vec{N}) - \nabla_{\vec{r}} \vec{a} \cdot \vec{N} = 0 \quad (44)$$

from which certain information can be obtained without actually solving the problem. For instance, with motion in a Kepler field,

$$\vec{a} = -K\vec{r}/r^3$$

(44) gives

$$\vec{N} \cdot \vec{N} - Kr^{-3}(3 \cos^2 \theta - 1) = 0 \quad (45)$$

where θ is the angle between \vec{N} and \vec{r} . Since \vec{N} is a unit vector,

$$\vec{N} \cdot \vec{N} + \dot{\vec{N}}^2 = 0$$

(45) requires

$$\cos^2 \theta < 1/3$$

i. e., the optimum direction of firing is always at an angle θ with the local vertical where

$$125^\circ 16' > \theta > 54^\circ 44'$$

a result first pointed out by Corben.⁷

3. If the relation between c and \dot{M} has the form

$$c = \Gamma(t) \dot{M}^p \quad (46)$$

where $\Gamma(t)$ is a prescribed function of time and p is a real number, a first integral of the mass equation (33) can be found when $\partial a / \partial M = 0$. We obtain

$$\lambda \Gamma = KM^{p/(p+1)} / \dot{M}^p \text{ for } p \neq 0 \text{ or } -1 \quad (47)$$

where K is constant of integration. The case $p = 0$ corresponds to $c(t)$ specified, which has already been discussed, whereas for $p = -1$, which corresponds to the thrust being specified, equation (33) gives

$$\lambda \Gamma / M^2 = 0$$

so that again no stationary solution exists. The case $p = -1/2$ is of particular interest, since it corresponds to the power being a specified function of time. Then (47) gives

$$\lambda \Gamma = KM^{1/2} / \dot{M}$$

and if, in particular, the power is independent of time, then

$$\lambda(t) = -K' \dot{M} c / M = K' n(t) \quad (48)$$

where K' is another, a priori unknown, constant. With the help of (48), it is possible to eliminate λ from (25) and (27) to obtain a fourth-order equation involving \vec{r} alone*

$$\ddot{\vec{r}} - \ddot{\vec{a}} + \nabla_{\vec{a}} \ddot{\vec{a}} \cdot (\ddot{\vec{r}} - \ddot{\vec{a}}) + \left(\frac{d}{dt} \nabla_{\vec{a}} \ddot{\vec{a}} - \nabla_{\vec{r}} \ddot{\vec{a}} \right) \cdot (\ddot{\vec{r}} - \ddot{\vec{a}}) = 0 \quad (49)$$

Finally, it may be noted that (47) can be integrated again to give an explicit expression for M in terms of λ ,

$$M(t)^\gamma = M(0)^\gamma + K'' \int_0^t (\lambda \Gamma)^{-1/p} \quad (50)$$

where

$$\gamma = p(p+1)^{-1}$$

and K'' is a constant of integration.

To unify the various problems and examples that have been considered in this section, it may be of help to give a general formulation which embraces all these cases and many more besides, including those with variable burning time. The trajectory analysis involves seven scalar functions of the time: $\vec{r}(t)$, $\vec{N}(t)$ with $N^2 = 1$, $M(t)$, and $c(t)$. These may not be varied independently but must satisfy four constraining relations, namely the differential equations of motion

* This generalizes slightly a result first obtained by J.H. Irving, "Optimum Program for Single-Stage Rockets," The Ramo-Wooldridge Corporation, October 7, 1956.

$$\ddot{\vec{r}} = -Mc\vec{N}/M + \vec{a}(\vec{r}, \dot{\vec{r}}, M) \equiv \vec{a} \quad (51)$$

and a functional relation between $c(t)$ and $M(t)$, assumed here to have the particular form

$$c = c[\dot{M}(t), t] \quad (52)$$

Let (ξ_i) denote the set of end point values

$$\vec{r}(t_0), \vec{r}(t_1), \dot{\vec{r}}(t_0), \dot{\vec{r}}(t_1), M(t_0), M(t_1), t_0, t_1$$

where t_0 and t_1 denote initial and final times for the powered flight. The optimization problem consists in making some function W_0 —range, final mass, etc.—of the ξ_i stationary, while holding certain other functions of the ξ_i — W_1, W_2, \dots, W_n —constant. Eliminating c by means of (52) leaves six functional variables with the three constraints (51), so three Lagrange multipliers, $\vec{\lambda}(t)$, are introduced, together with m constant Lagrange multipliers, μ_σ , $\sigma = 1, \dots, m$, corresponding to each of the end point constraints W_σ . The quantity

$$\sum_{\sigma=0}^n W_\sigma \mu_\sigma + \int_{t_0}^{t_1} \vec{\lambda} \cdot (\ddot{\vec{r}} - \vec{a})$$

with $\mu_0 \equiv 1$, is then made stationary; i. e., we set

$$\sum_{\sigma,i} \mu_\sigma (\partial W_\sigma / \partial \xi_i) \Delta \xi_i + \delta \int_{t_0}^{t_1} \vec{\lambda} \cdot (\ddot{\vec{r}} - \vec{a}) = 0 \quad (53)$$

Carrying out the variations of the integral and integrating by parts as before leads to

$$\begin{aligned} \sum \Delta \xi_i (\partial W / \partial \xi_i) + \left[\vec{\lambda} \cdot (\ddot{\vec{r}} - \vec{a}) \delta t - \delta \vec{r} \cdot (\nabla_{\vec{v}} \vec{a} \cdot \vec{\lambda} + \dot{\vec{\lambda}}) + \vec{\lambda} \cdot \delta \dot{\vec{r}} + \lambda \left(\frac{c}{M} + \frac{\dot{M}}{M} \frac{\partial c}{\partial \dot{M}} \right) \delta M \right]_{t_0}^{t_1} \\ + \int_{t_0}^{t_1} dt \left\{ \delta \vec{r} \cdot \left[\ddot{\vec{\lambda}} - \nabla_{\vec{r}} \vec{a} \cdot \vec{\lambda} + \frac{d}{dt} (\nabla_{\vec{v}} \vec{a} \cdot \vec{\lambda}) \right] - n \vec{\lambda} \cdot \delta \vec{N} - \delta M \left[\vec{\lambda} \cdot \partial \vec{a} / \partial M - \lambda \dot{M} c / M^2 \right. \right. \\ \left. \left. - \frac{d}{dt} \left[\lambda \left(\frac{c}{M} + \frac{\dot{M}}{M} \frac{\partial c}{\partial \dot{M}} \right) \right] \right] \right\} = 0 \quad (54) \end{aligned}$$

where

$$\bar{W} = \sum_{\sigma} \mu_{\sigma} W_{\sigma}$$

Thanks to the Lagrange multipliers, the coefficients of each variation may be set equal to zero. In doing so, it must be remembered that the variations of the ξ_i

appearing in the first term of (54) are total variations. For instance, $\Delta \vec{r}(t_0)$ is due both to the variation in the function $\vec{r}(t)$,

$$\vec{r}(t) \rightarrow \vec{r}(t) + \delta \vec{r}(t)$$

and to the variation in t_0 ,

$$t_0 \rightarrow t_0 + \delta t_0$$

so that

$$\Delta \vec{r}(t_0) = \delta \vec{r}(t_0) + \dot{\vec{r}}(t_0) \delta t_0 \quad (55)$$

and similarly for the other ξ_i .

The final result is a set of seven scalar coupled differential equations

$$\left. \begin{aligned} \ddot{\vec{r}} &= -\dot{M}c\vec{\lambda}/M\lambda + \vec{a} \\ \ddot{\vec{\lambda}} - \nabla_{\vec{r}} \vec{a} \cdot \vec{\lambda} + \frac{d}{dt} (\nabla_{\vec{v}} \vec{a} \cdot \vec{\lambda}) &= 0 \\ \lambda \dot{M}c/M^2 + \frac{d}{dt} \left[\lambda \left(\frac{c}{M} + \frac{\dot{M}}{M} \frac{\partial c}{\partial M} \right) \right] - \vec{\lambda} \cdot \partial \vec{a} / \partial M &= 0 \end{aligned} \right\} \quad (56)$$

for the seven functions \vec{r} , $\vec{\lambda}$, and M , together with boundary conditions

$$\left. \begin{aligned} \left(\frac{\partial}{\partial t_0} + \dot{\vec{r}} \nabla_{\vec{r}_0} + \dot{\vec{r}} \cdot \nabla_{\vec{r}_0} + \dot{M} \frac{\partial}{\partial M_0} \right) \bar{W} &= 0 \\ \lambda \left(\frac{c}{M} + \frac{\dot{M}}{M} \frac{\partial c}{\partial M} \right) \partial \bar{W} / \partial M_0 &= 0 \\ \vec{\lambda} - \nabla_{\vec{r}_0} \bar{W} &= 0 \\ \vec{\lambda} + \nabla_{\vec{v}} \vec{a} \cdot \vec{\lambda} + \nabla_{\vec{r}_0} \bar{W} &= 0 \end{aligned} \right\} \quad t = t_0 \quad (57)$$

with a similar set for $t = t_1$.

The number of boundary conditions is just sufficient to determine fully a solution (if one exists), for we have the seven second-order differential equations (56) together with the eight boundary conditions (57) at t_0 and eight similar ones at t_1 from which to find the seven trajectory functions $\vec{r}(t)$, $\vec{\lambda}(t)$, $M(t)$, and the (in general unspecified) initial and final times, t_0 and t_1 . The unknown constants μ_1 through μ_n appearing in the boundary conditions are determined by requiring that W_1 through W_n take on their prescribed values.

From this general formulation, it can be seen that the manifold of problems included in it, special cases of which have been examined, will all have in common

the same differential equations (56) and will only differ in the form of the boundary conditions, according to the particular choice of the W_0 . Of course, we always have the freedom of specifying one or more of the seven trajectory functions in advance, in which case the corresponding Euler-Lagrange equations and boundary conditions are simply omitted from (56) and (57). Thus, in the problems of Section 2 we fixed $M(t)$ as well as $c(t)$, so that the third of equations (56) and the second of equations (57) were not used, and we studied problems in which W_0 was a given function (e. g. range or orbit altitude) of \vec{r}_1 and \vec{v}_1 . In the present section (starting on p. 13A) we considered problems with variable $M(t)$, taking W_0 again to be a function of \vec{r}_1 , \vec{v}_1 in the first example (p. 16A), whereas in the second (p. 17A) we took W_0 to be M_1 , with M_0 and a function of \vec{r}_1 , \vec{v}_1 as the constraints W_1 , W_2 . We may, as in these examples, consider t_0 and/or t_1 as given, in which case the first of equations (57), obtained by equating to zero the coefficient of δt_0 , and/or its analog at t_1 are simply omitted. Finally, it is clear that problems such as maximizing the kinetic energy per unit burnout mass for fixed burnout altitude are also encompassed in our formalism (for instance, by taking W_0 to be v_1^2 , W_1 to be v_1 or r_1).

4 DESIGN OPTIMIZATION

As has been suggested already, there are optimization problems of considerable practical importance which are not included in the formalism developed in Section 3. For instance, it is generally the payload rather than the total burnout weight, M_1 , that we should like to optimize (or hold constant while optimizing something else). Even aside from this, to program $M(t)$ as dictated by (56) requires much greater flexibility than seems possible with the chemical propulsion systems currently available, although these considerations may be of considerable importance for advanced propulsion systems, for example, those involving electromagnetic acceleration mechanisms, in which exhaust velocity and mass flow rate can more easily be varied.

For the chemical propulsion systems currently available, however, it is more realistic to assume the exhaust velocity to be a given function of the time. Optimization of $M(t)$ generally leads to programs involving one or more impulsive thrusts because of the tendency to fire when c is large, as in the one-dimensional example considered on page 18A, and also because of the advantage of exhausting mass in a region of low potential. It is therefore necessary to consider the less elegant but nevertheless very important problem of how to choose the number of stages, the mass flow rates, the burning times for each stage, etc. Although these questions lie outside the domain of pure trajectory problems, the choice of trajectory is sufficiently involved in the task of fixing these design parameters for some brief comments to be in order.

As a first step, we might attempt a simple model in which the total missile is considered to consist of fuel, tanks, motor, and payload. By assuming simple scaling laws such as tank weight linearly proportional to fuel weight, motor weight linearly proportional to thrust, etc., it is possible to reduce the design problem to a set of algebraic relations together with the trajectory equations. Such a formulation is in fact of little help, for although the assumptions are drastic enough to make the validity of the results open to serious question, we do not, even at this price, obtain a simple and tractable analysis. For even a two-stage missile the resulting set of equations is sufficiently complicated that numerical methods are necessary and we gain little insight into the nature of the design interactions.

A more profitable approach is a generalized design analysis which may be characterized as follows. Engineering analyses for each part of the missile are set up. These might include an analysis of the propulsion system, an analysis of the fuel tank weight, an analysis of the skin heating and thermodynamics, an analysis of the guidance and control systems, etc., together with the differential equations for the trajectory. It is a fairly straightforward matter to develop the equations constituting any one of these analyses. However, it must be understood that

1. Each group of equations is sufficiently complicated to make solutions in closed form impossible.
2. There is a very close coupling between the various analyses, so that, for example, a change in trajectory alters the acceleration, which in turn affects the tank pressure program, which changes the tank weight, which alters the trajectory, etc.
3. Each analysis requires certain input variables (where the term variable may include an entire function—tank pressure as a function of time, allowable stress as a function of skin temperature, etc.) and from these yields certain output variables.
4. The "coupling" referred to arises because the outputs of each analysis serve as inputs for the others.

The situation can best be represented by a large block diagram, typical parts of which are depicted in Table 1. By connecting together the various inputs and outputs in an appropriate way we obtain not only a picture of the interrelations of the various parts of the design analysis but also a kind of rough flow diagram useful for organizing the computations, which can be appropriately carried out by a large digital computer. Some variables in the scheme, e. g. altitude as a function of time, are wholly internal, being generated in one analysis and fed to another. Others, called Principal Variables (P. V.), must be supplied from outside, examples

Table 1. Examples of two of the component blocks involved in the generalized design analysis. "Input" variables (i. e., those received from some other part of the block diagram) are shown on the left, "output" variables on the right.

Analysis of Tank Weight			
→ l	Slenderness ratio	Tank weight	W_T
→ \dot{m}_j	Mass flow rates for each stage	Tank radius	R
→ t_j	Burning and staging times	Tank length	L
→ τ_m	Minimum gage for tank wall thickness	Tank wall thickness at various stations	τ_{io}, τ_{if}
→ k_m	Mixture ratio, oxidizer to fuel		
→ $\sigma(T)$	Allowable stress of wall material as a function of temperature		
→ ρ_m, ρ_o, ρ_f	Densities of wall material, oxidizer, fuel		
→ $W(t)$	Gross weight as a function of time		
→ $F(t)$	Thrust		
→ $p_o(t), p_f(t)$	Tank pressures		
→ $T_o(t), T_f(t)$	Temperature of exposed tank walls		

Trajectory Equations			
→ $F(h)$	Thrust vs altitude	Range	R
→ R	Tank radius	Altitude	$h(t)$
→ β_o	Initial kick angle of gravity turn	Velocity	$v(t)$
→ \dot{m}_j	Mass flow rates	Air density	$\rho(t)$
→ t_j	Burning and staging times	Drag and lift	$C_D(t), C_L(t)$
→ t_g	End of gravity turn		
→ W_{io}	Weight at beginning of stage i	Acceleration due to thrust	$n(t)$
→ $C_D(M, \alpha)$	Lift and drag coefficients as functions of Mach number and angle of attack		
→ $C_L(M, \alpha)$			

being natural parameters, such as characteristics of materials or properties of the atmosphere, and independent design variables, such as staging times or combustion chamber pressure, etc.

A set of P. V. values is chosen and the machine then finds a self-consistent solution for the whole set of coupled equations, e. g. by iteration among the various analyses. The result is that for each set of P. V. we find the associated values of gross weight and total range together with the values of any internal variables of interest—tank pressures, tank dimensions, engine weights, skin temperatures, etc. This machinery can be used in a variety of ways. For instance, the P. V. can be varied to find an optimum where the criterion might be minimum gross weight, dry weight, or cost for given range, payload, etc. We can also find the penalties imposed by constraints on engine sizes, the effects of changes in skin material, etc. Finally, at any given point in the P. V. space we can make small changes in the P. V., thereby obtaining "exchange ratios."

Despite its complexity, an analysis of this kind is feasible, provided a high-speed digital computer is available. In fact, just this kind of problem constitutes an appropriate and efficient use for such computers in missile design work. However, to keep the problem within the capabilities of even the largest computers, it is essential to have some convenient characterization of the trajectory, for the trajectory "box" in the block diagram plays a central role in the analysis, accepting inputs from and feeding outputs to many other parts of the system (cf. Table 1). If it were necessary to search a large section of the trajectory space at each iteration, the calculation would bog down completely. Fortunately, the results of Section 2 show that a nearly optimum trajectory can be adequately described by a few parameters. For instance, a trajectory pattern consisting of a gravity turn (specified by the parameter k corresponding to initial-kick angle), followed by a thrust attitude program of the form of (6), might be adopted. The four parameters a , b , c , and d (which may, as in the examples discussed on pages 7A and 8A, reduce to one or two in particular cases) together with k would be treated as principal variables and their values determined along with those of other design parameters.

5 SUMMARY

The one-dimensional, point particle model of a missile has here been generalized to include motion in two or three dimensions. This leads naturally to a study of trajectory optimization, a subject which includes a variety of related, but different, problems. The simplest are the pure trajectory or steering problems, in which the dynamic characteristics of the missile are specified and the trajectory

that optimizes some aspect of the performance is sought. A general formulation, applicable to force fields depending on velocity as well as position, is possible, and in the particular case where the force field is either constant or a linear function of position, solutions in closed form can be found. These are of considerable practical importance for ballistic missiles with terrestrial missions (e. g., long-range surface-to-surface missiles or satellite launchers) where the distance covered during powered flight is small compared to the earth's radius. A simple and nearly optimum trajectory pattern for such cases uses a gravity turn through the atmosphere followed by a thrust attitude program as given by (6). Although no solution in closed form for the gravity turn equations exists, a set of universal curves, adequate for most purposes, can be prepared.

Optimization problems in which the mass and exhaust velocity programs and the burning time are varied, as well as the steering program, can also be handled by classical variational methods, insofar as we only seek stationary solutions. To find solutions that actually provide maxima or minima requires, of course, a special investigation for each problem, since there may well be a stationary solution which is not optimum or an optimum solution which is not stationary.

When the exhaust velocity is a prescribed function of time (e. g., constant as is, approximately, the case for chemical propulsion systems) the sophisticated analysis for finding the optimum $M(t)$ is of little help, since it generally says only that impulsive burning is optimal. A more detailed analysis, in which the characteristics of the rocket motors, propellant tanks, et al. are taken into account simultaneously with the trajectory optimization, is then necessary. A practical method of carrying this out involves the logical interconnection of a number of detailed engineering analyses, of which one is the set of differential equations of motion for the trajectory. With the aid of a high-speed digital computer, a self-consistent solution of this scheme of equations can be obtained, each such solution representing a possible and realistic missile. By variation of the input parameters, a number of optimization problems may be studied.

In the field of missile analysis, there is a need for both very complicated models, like this design optimization analysis, and for very simple models, like the point particle. In fact, these tend to complement each other. The latter provide analytical solutions in closed form, from which valuable insights regarding trajectories can be obtained. They also furnish simple trajectory patterns which are of great value for the problems involving the simultaneous optimization of design and trajectory. The more complicated models, in turn, make it possible to take into account many effects which must of necessity be omitted from the simple models and also provide a good illustration of the proper use of high-speed computers in missile design.

Graphical Presentation

29A

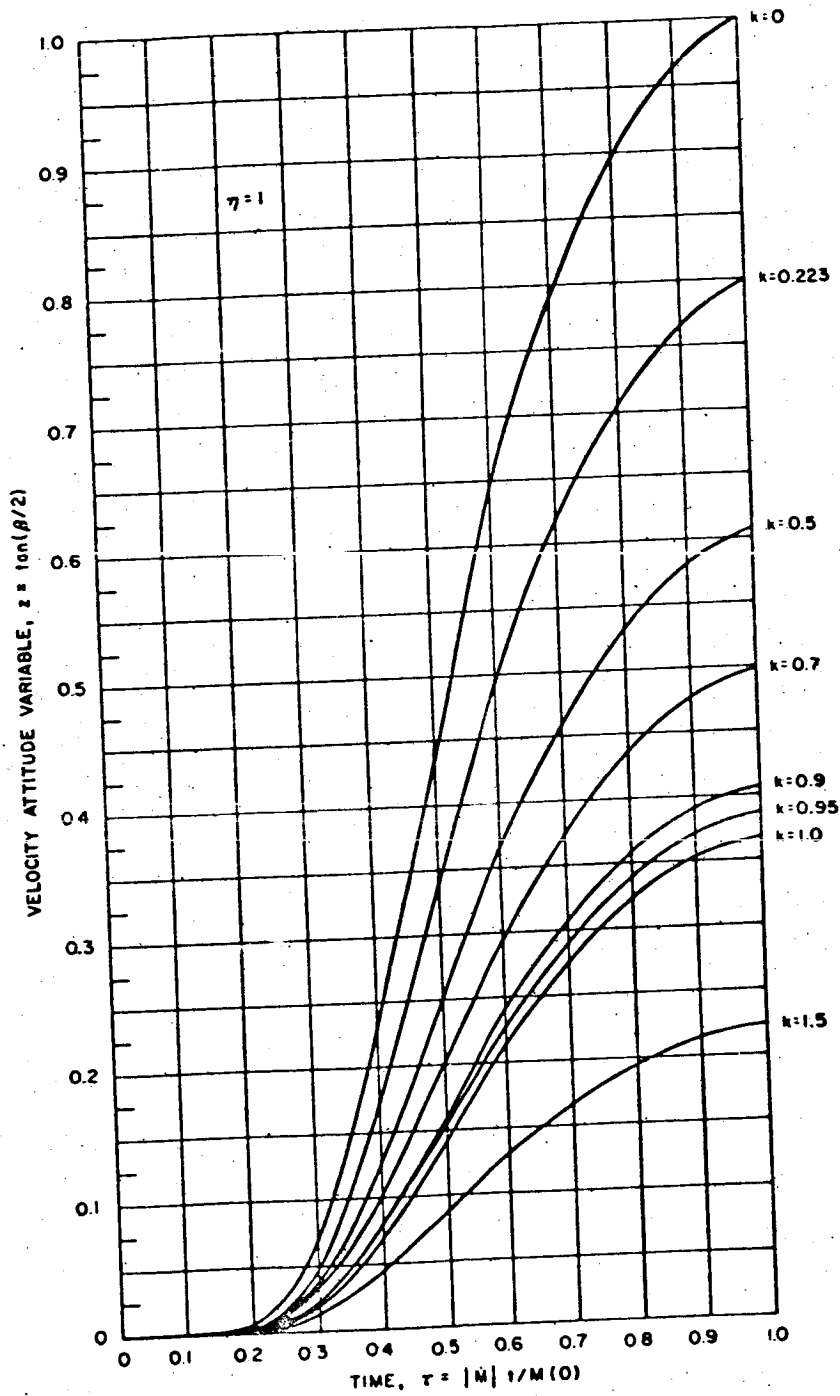


Figure 1. Velocity Attitude Variable for a Gravity Turn Trajectory

30A

TRAJECTORY OPTIMIZATION FOR POWERED FLIGHT

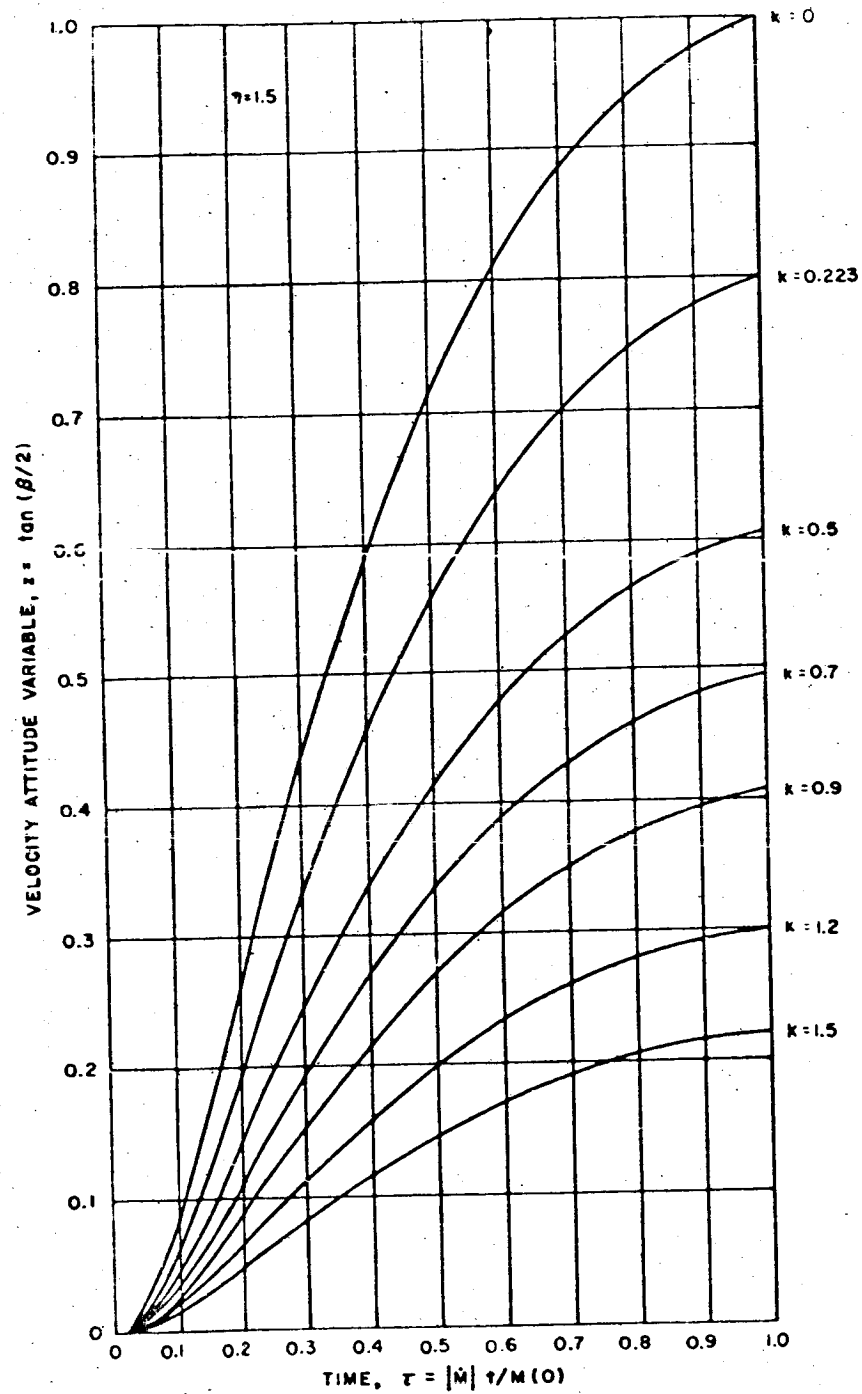


Figure 2. Velocity Attitude Variable for a Gravity Turn Trajectory

Graphical Presentation

31A

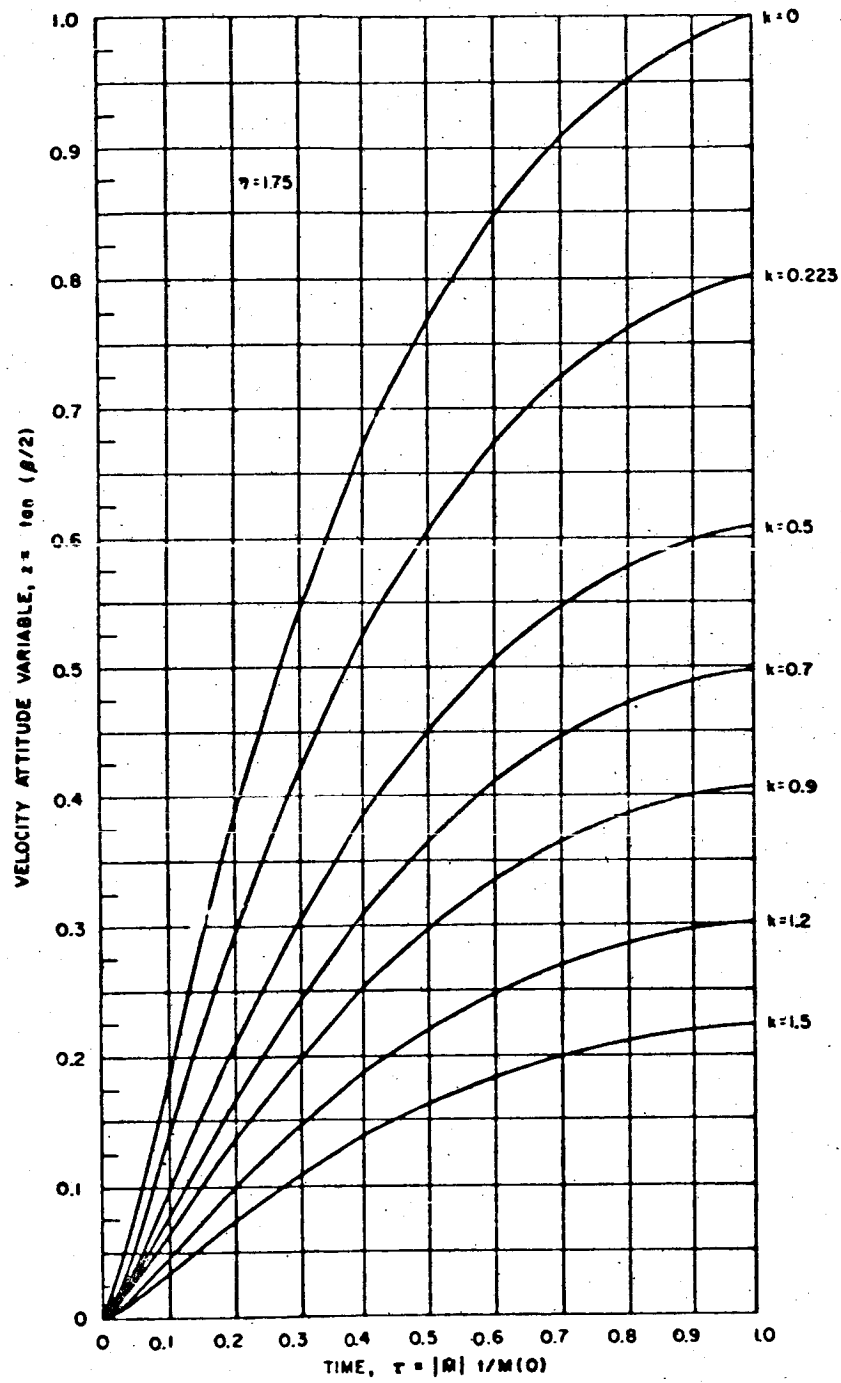


Figure 3. Velocity Attitude Variable for a Gravity Turn Trajectory

32A

TRAJECTORY OPTIMIZATION FOR POWERED FLIGHT

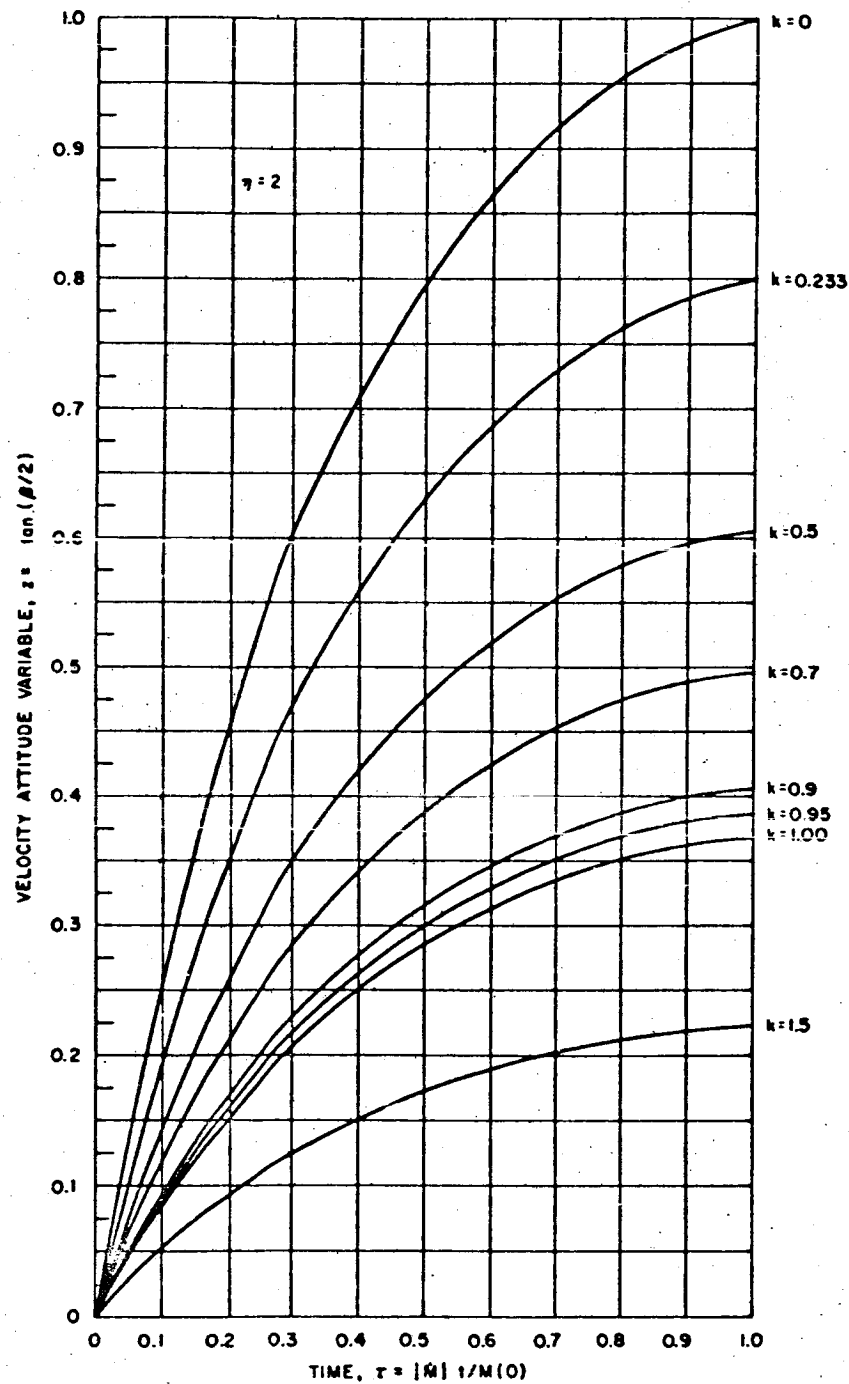


Figure 4. Velocity Attitude Variable for a Gravity Turn Trajectory

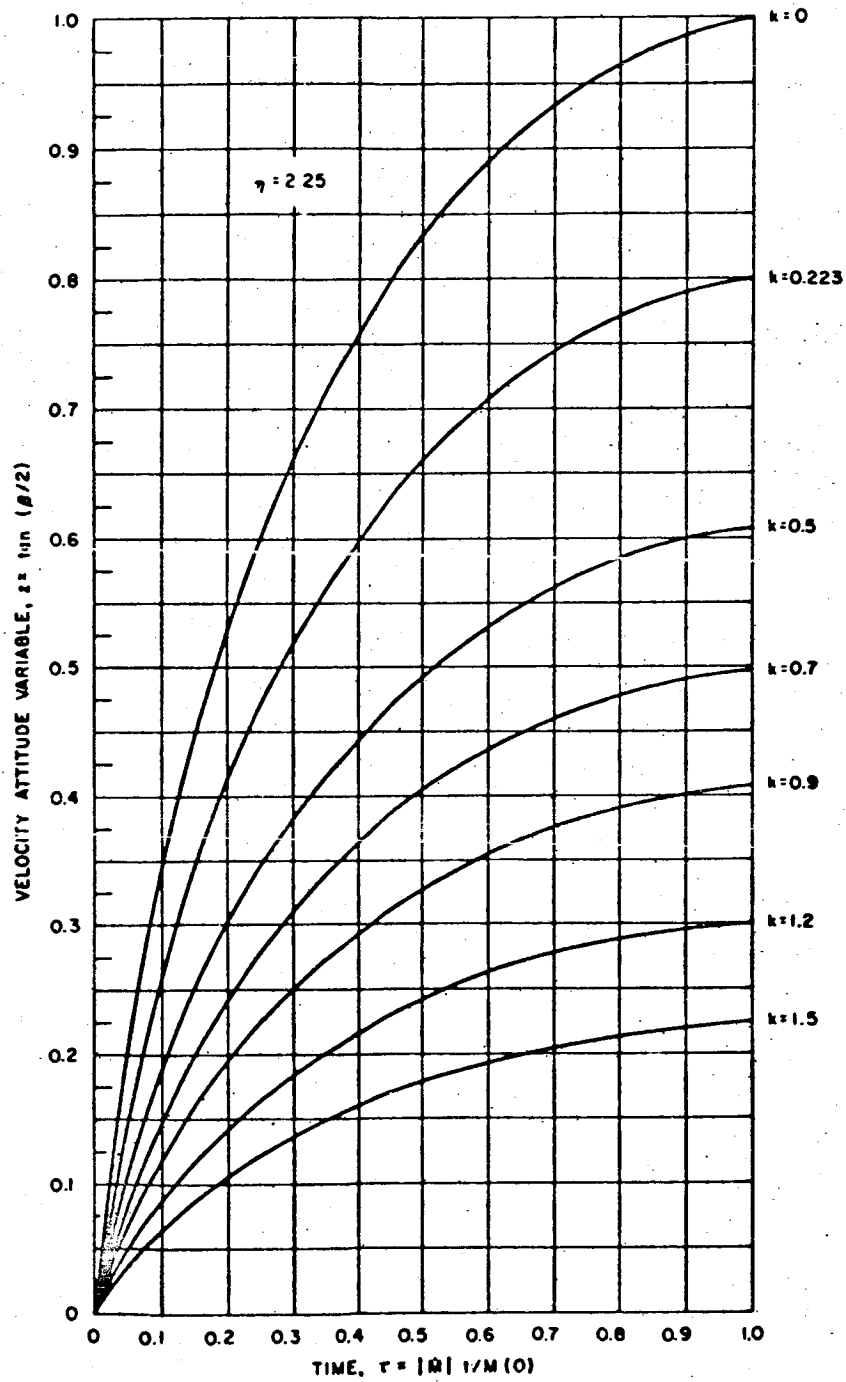


Figure 5. Velocity Attitude Variable for a Gravity Turn Trajectory

TRAJECTORY OPTIMIZATION FOR POWERED FLIGHT

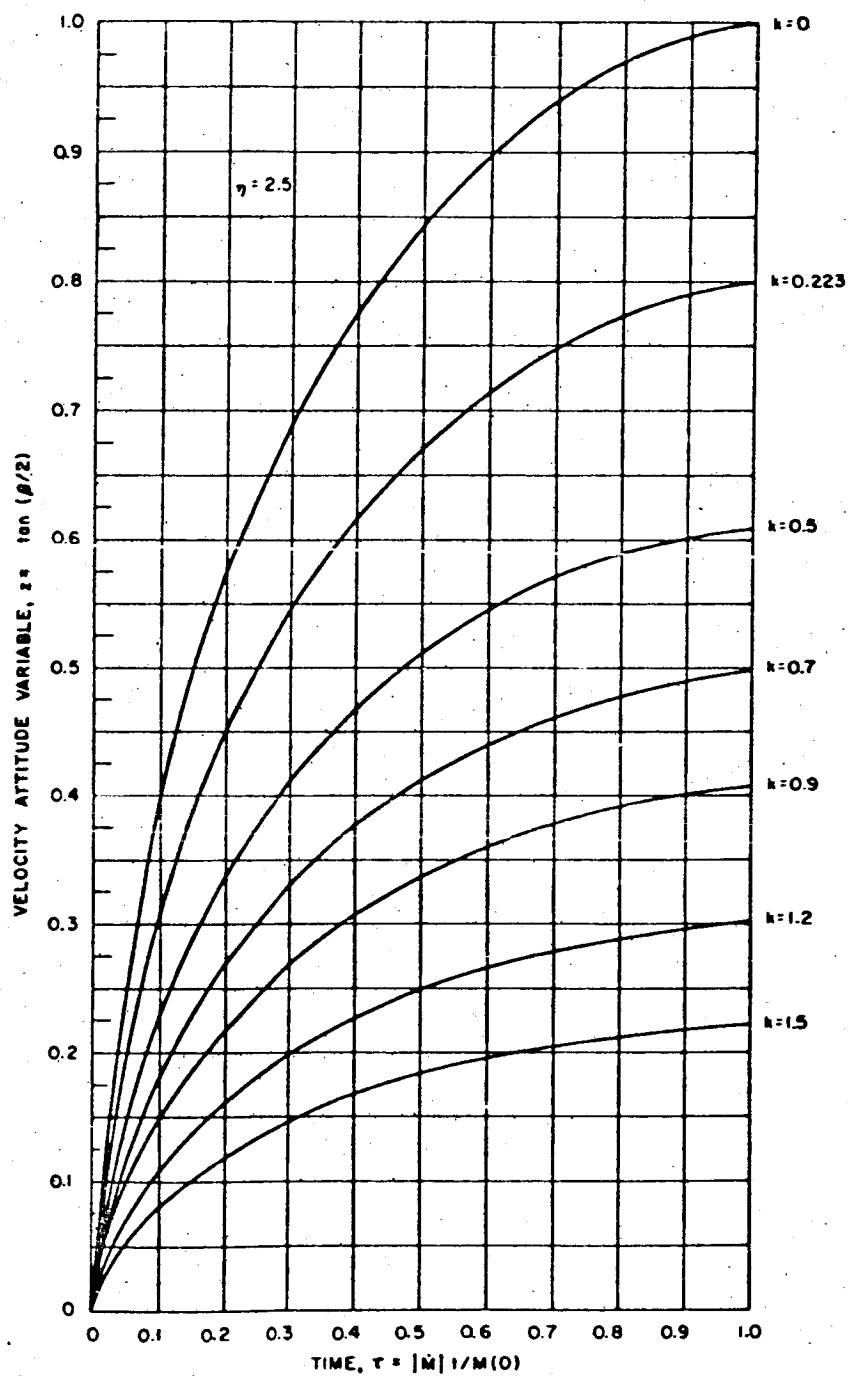


Figure 6. Velocity Attitude Variable for a Gravity Turn Trajectory

Graphical Presentation

35A

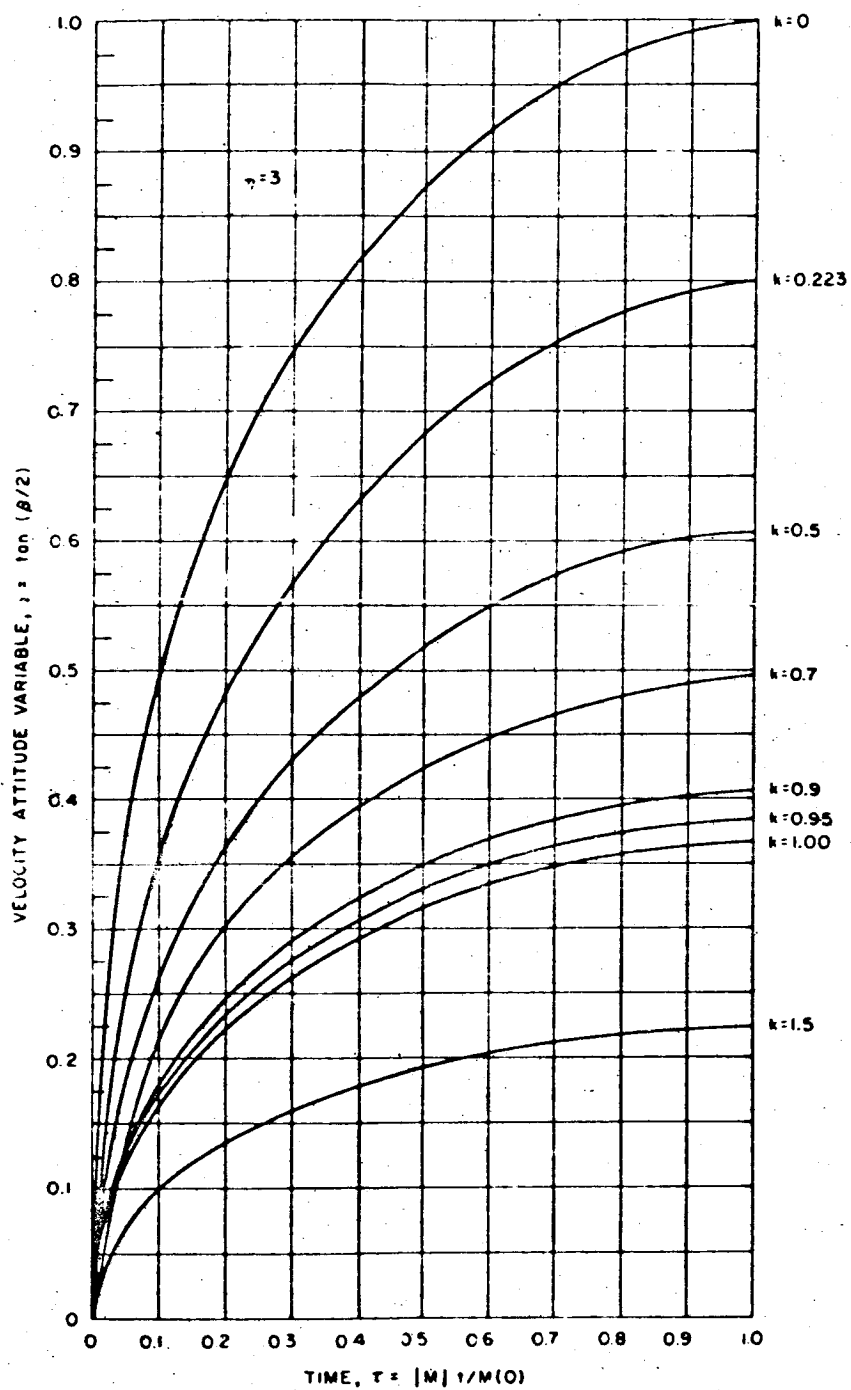


Figure 7. Velocity Attitude Variable for a Gravity Turn Trajectory

TRAJECTORY OPTIMIZATION FOR POWERED FLIGHT

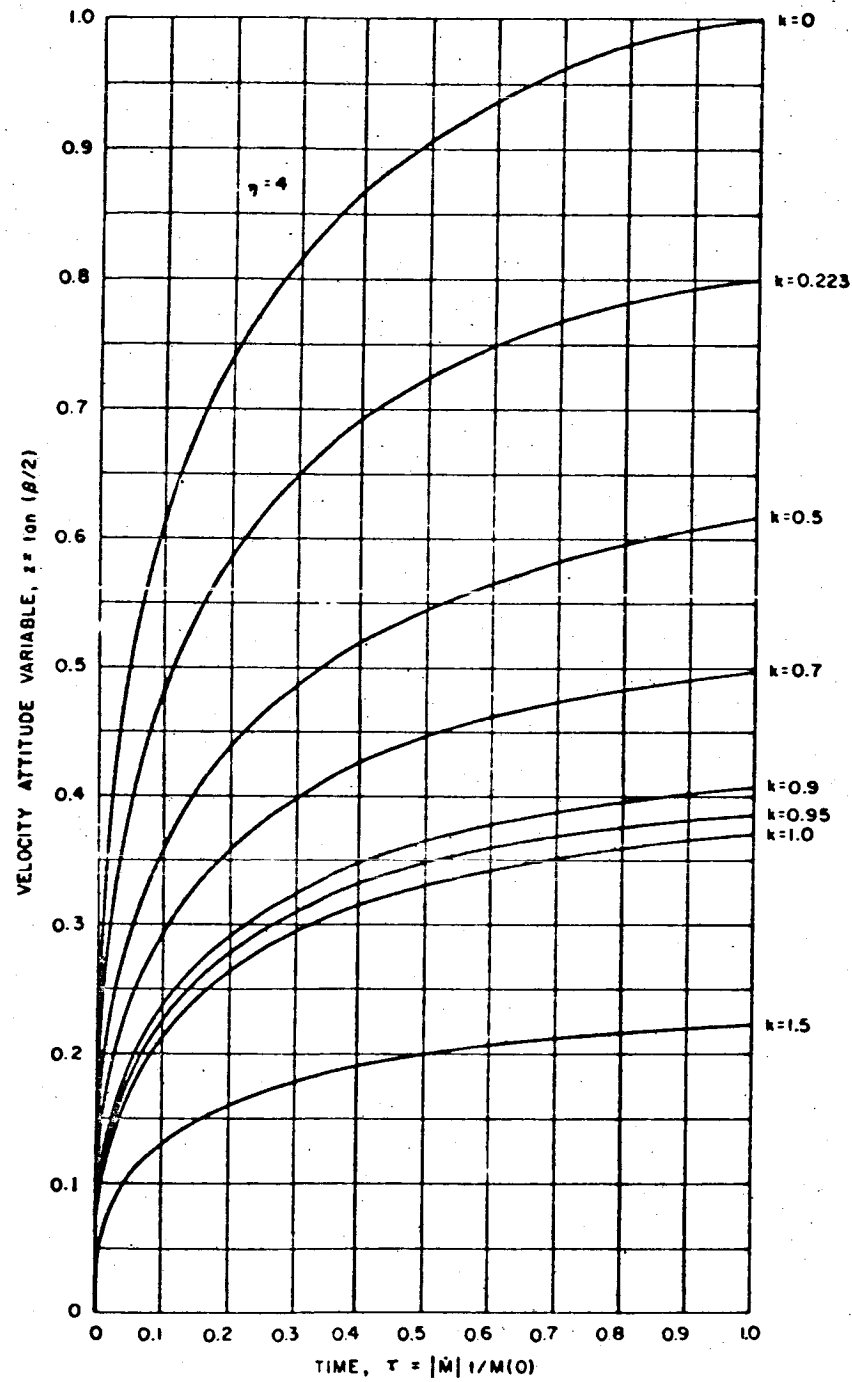


Figure 8. Velocity Attitude Variable for a Gravity Turn Trajectory

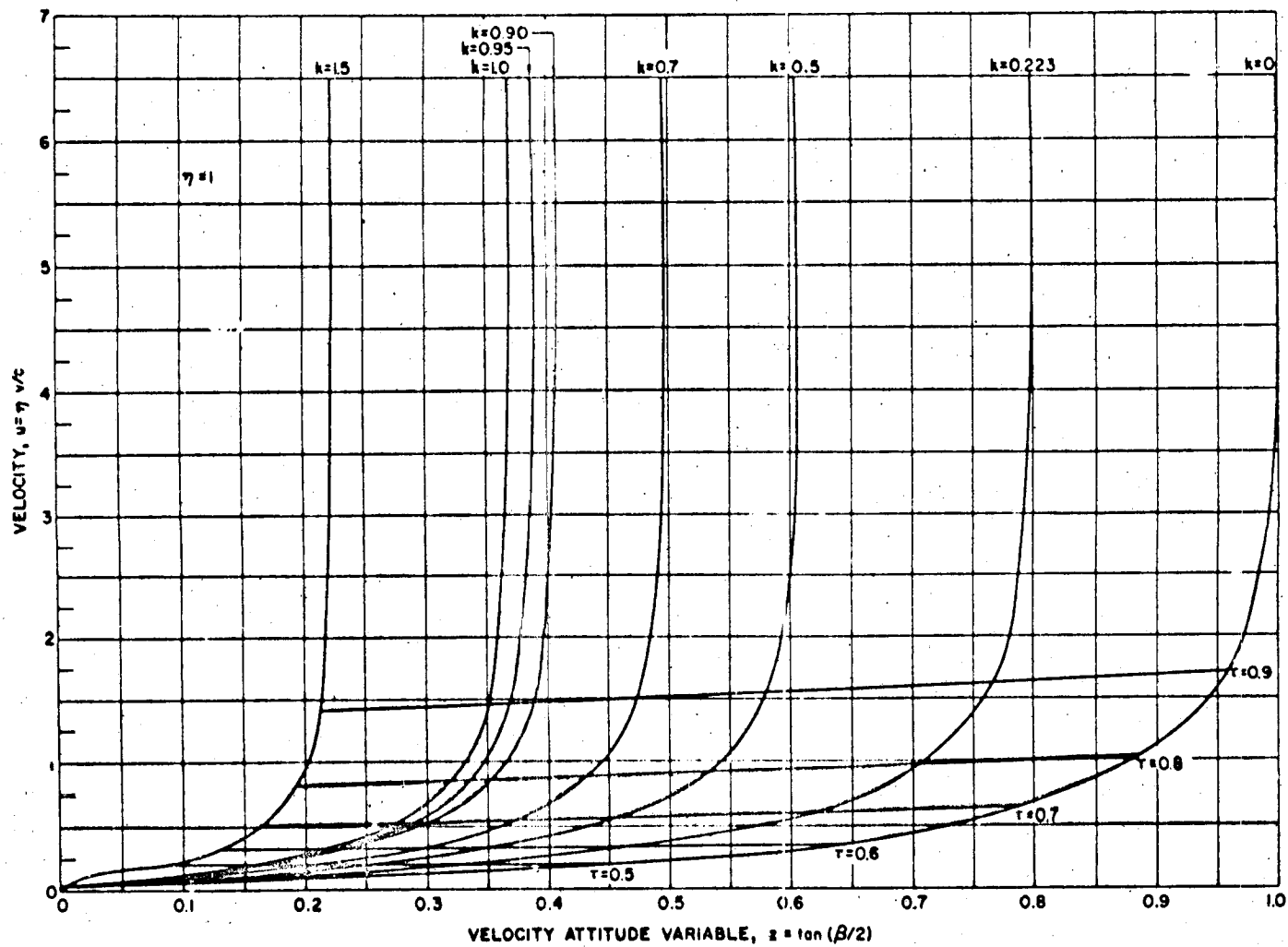


Figure 9. Velocity for a Gravity Turn Trajectory Versus Velocity Attitude

Graphical Presentation

37A

REORDER No. 62-286

535

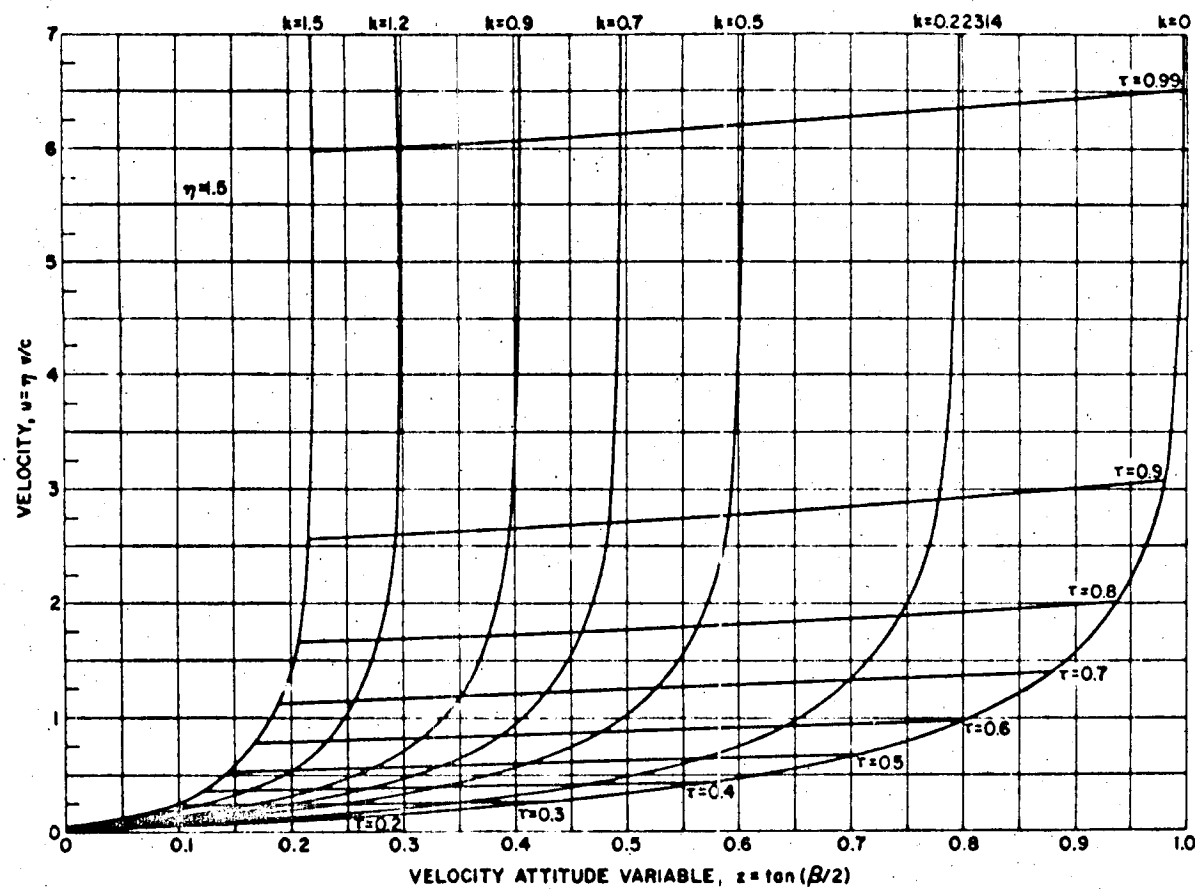


Figure 10. Velocity for a Gravity Turn Trajectory Versus Velocity Attitude

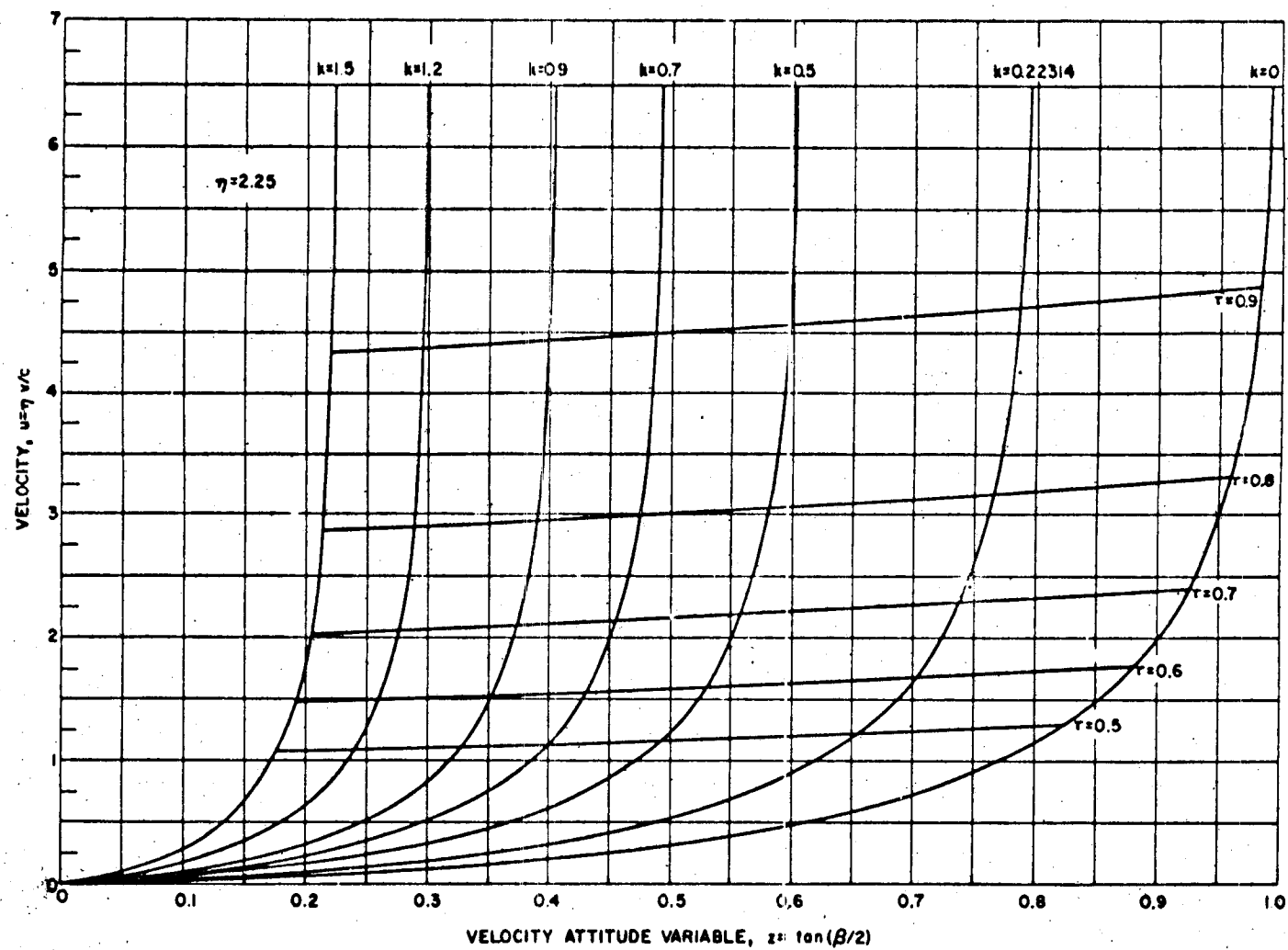


Figure 11. Velocity for a Gravity Turn Trajectory Versus Velocity Attitude

Graphical Presentation

39A

RECEIVED NO. 62-286

537

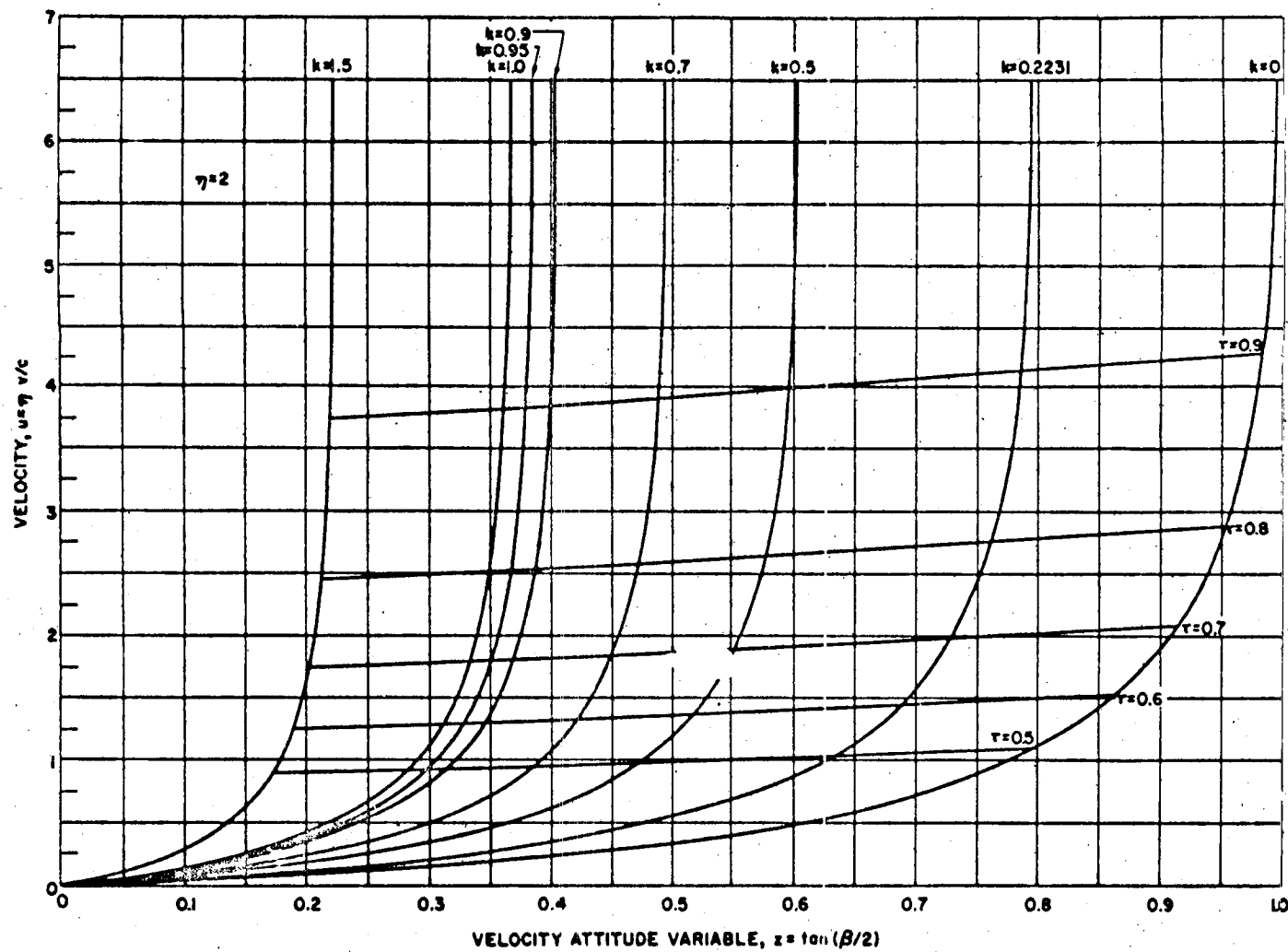


Figure 12. Velocity for a Gravity Turn Trajectory
Versus Velocity Attitude

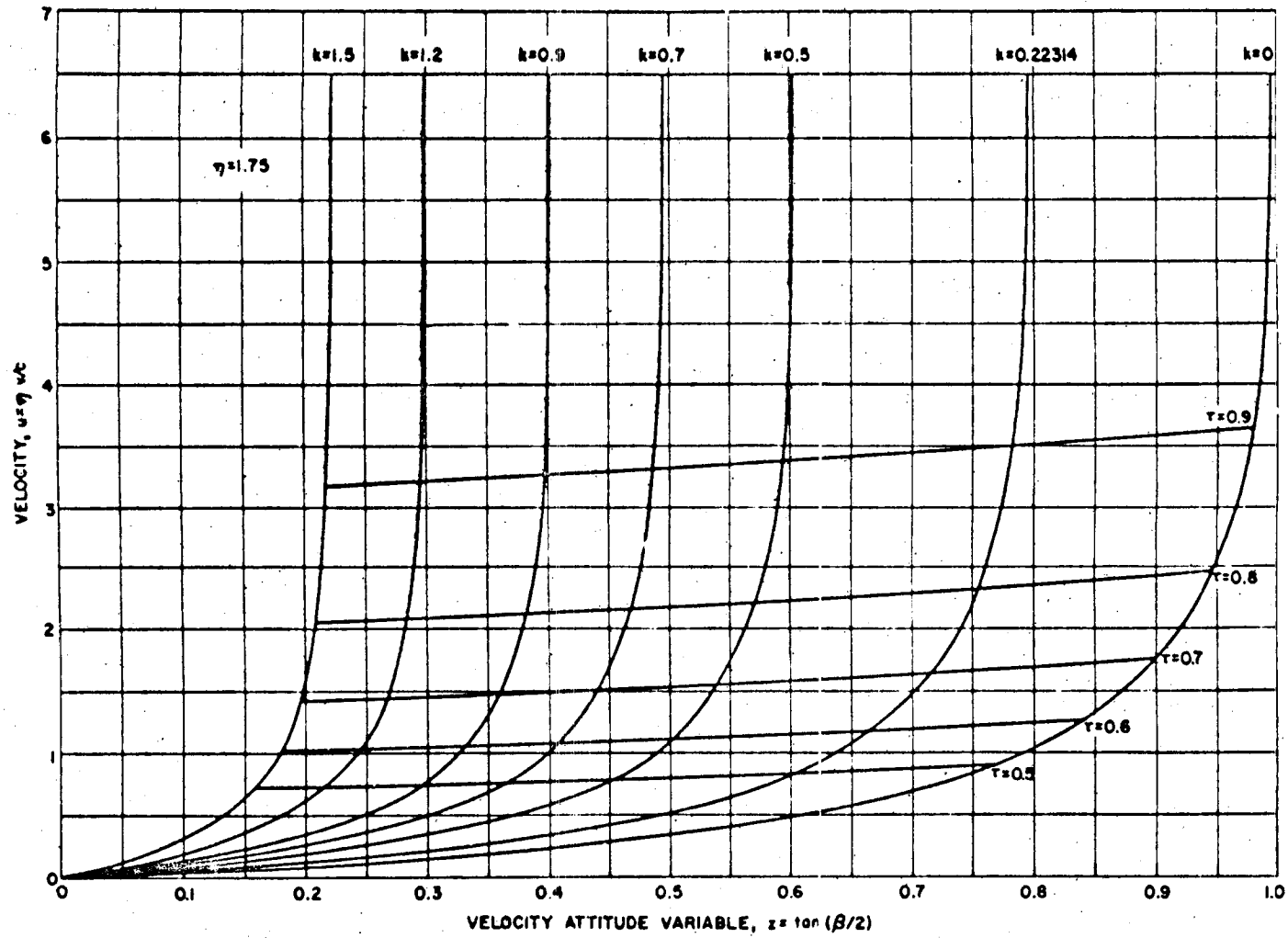


Figure 13. Velocity for a Gravity Turn Trajectory Versus Velocity Attitude

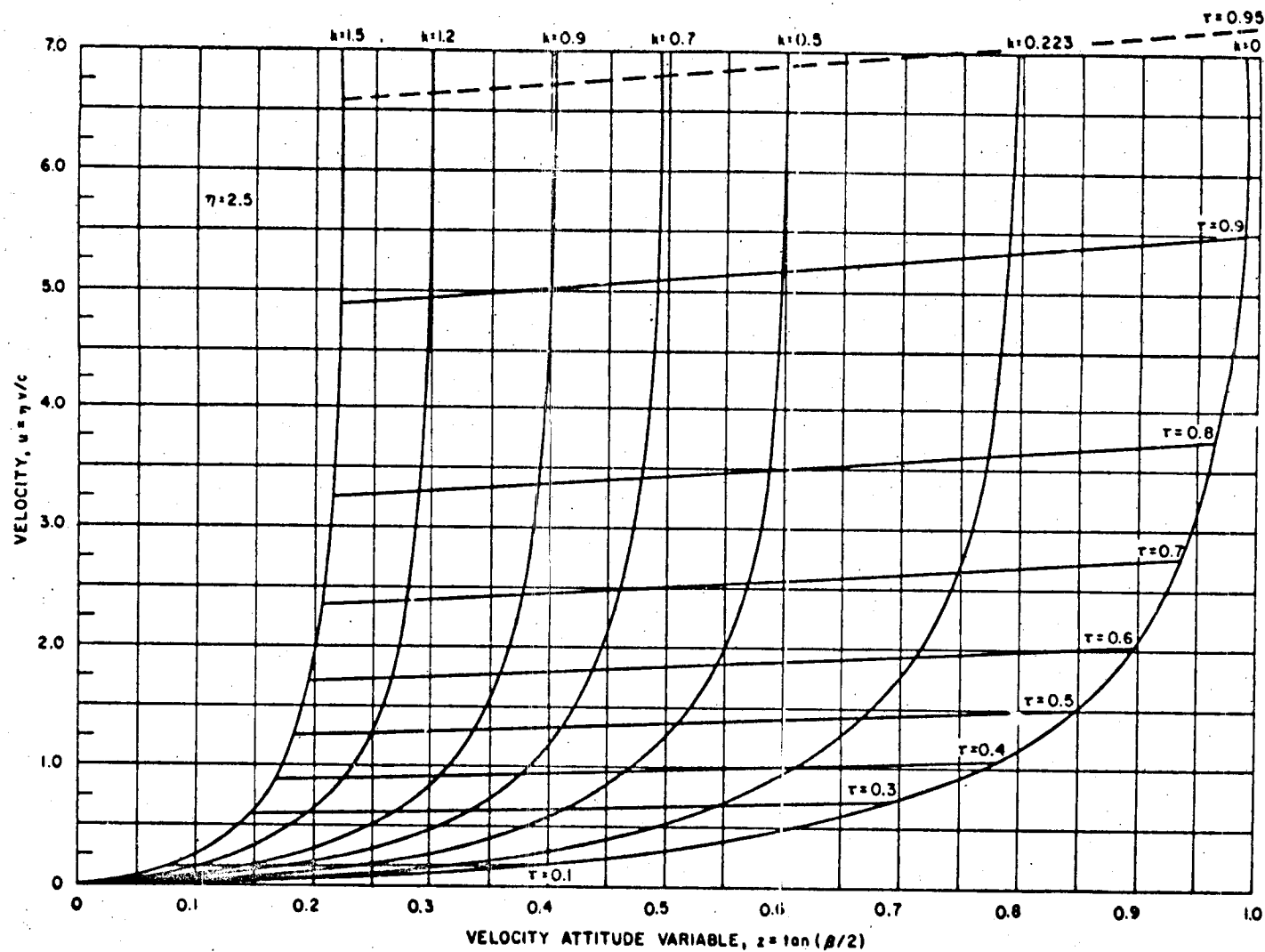


Figure 14. Velocity for a Gravity Turn Trajectory Versus Velocity Attitude

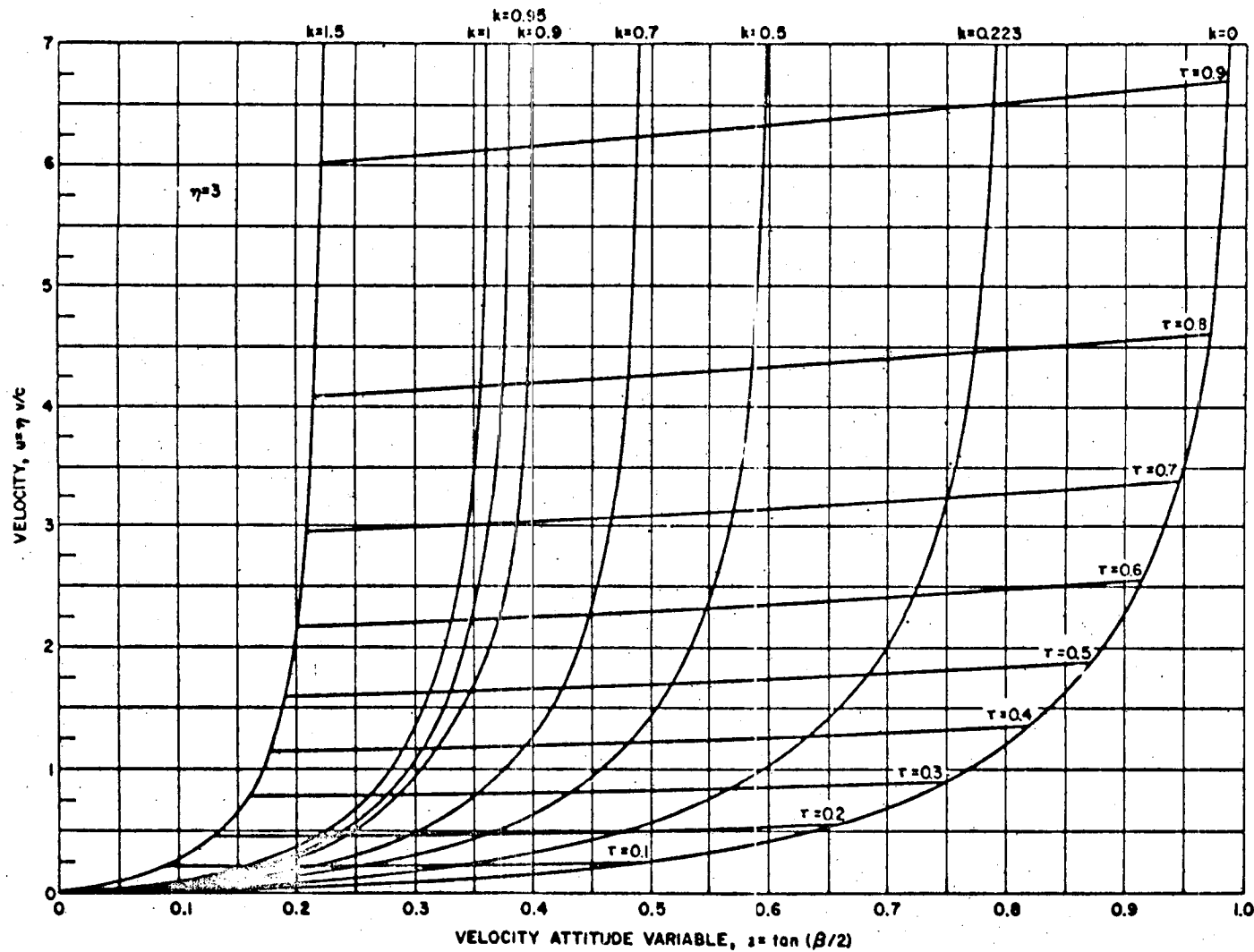


Figure 15. Velocity for a Gravity Turn Trajectory Versus Velocity Attitude

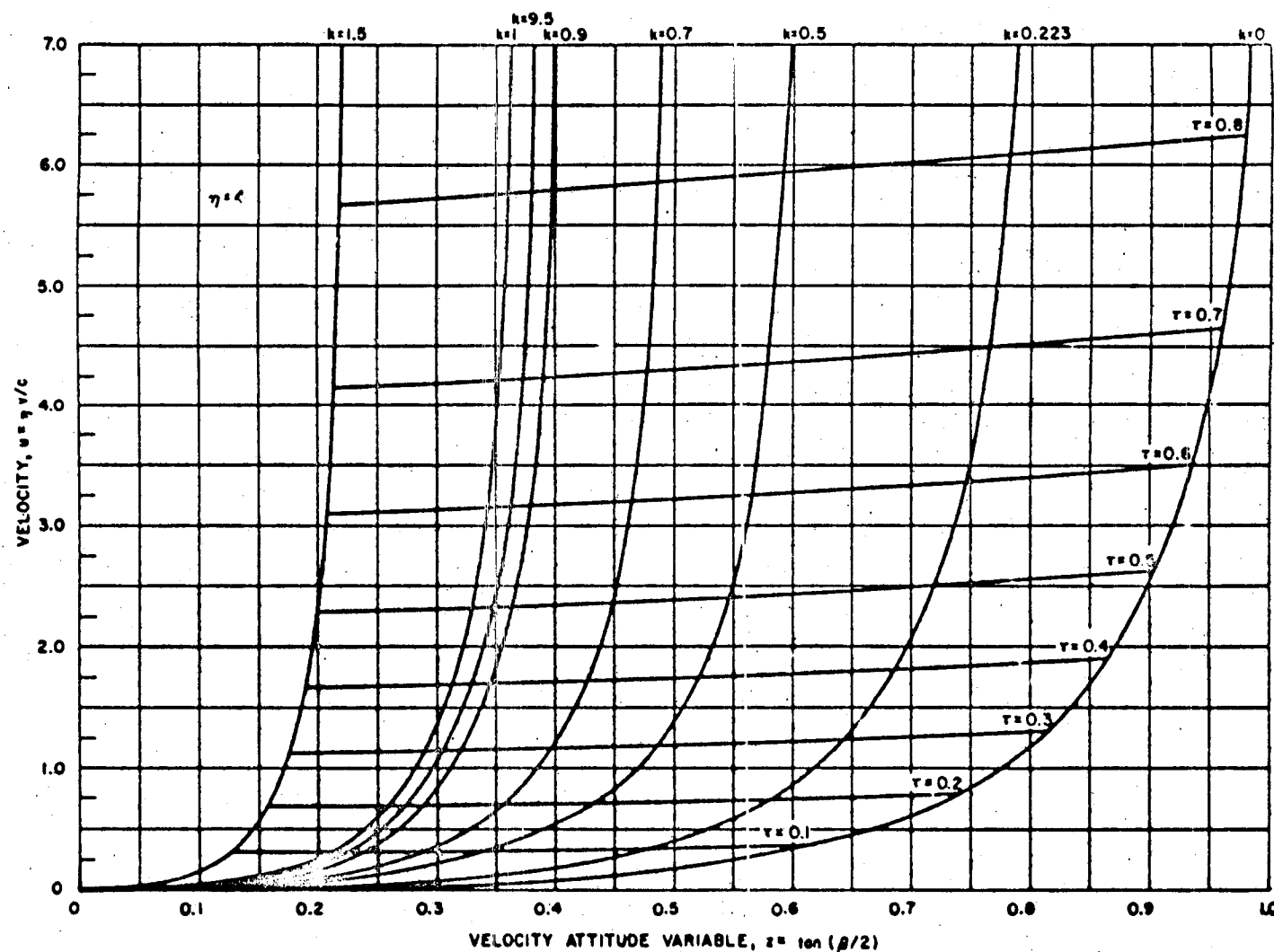


Figure 16. Velocity for a Gravity Turn Trajectory Versus Velocity Attitude

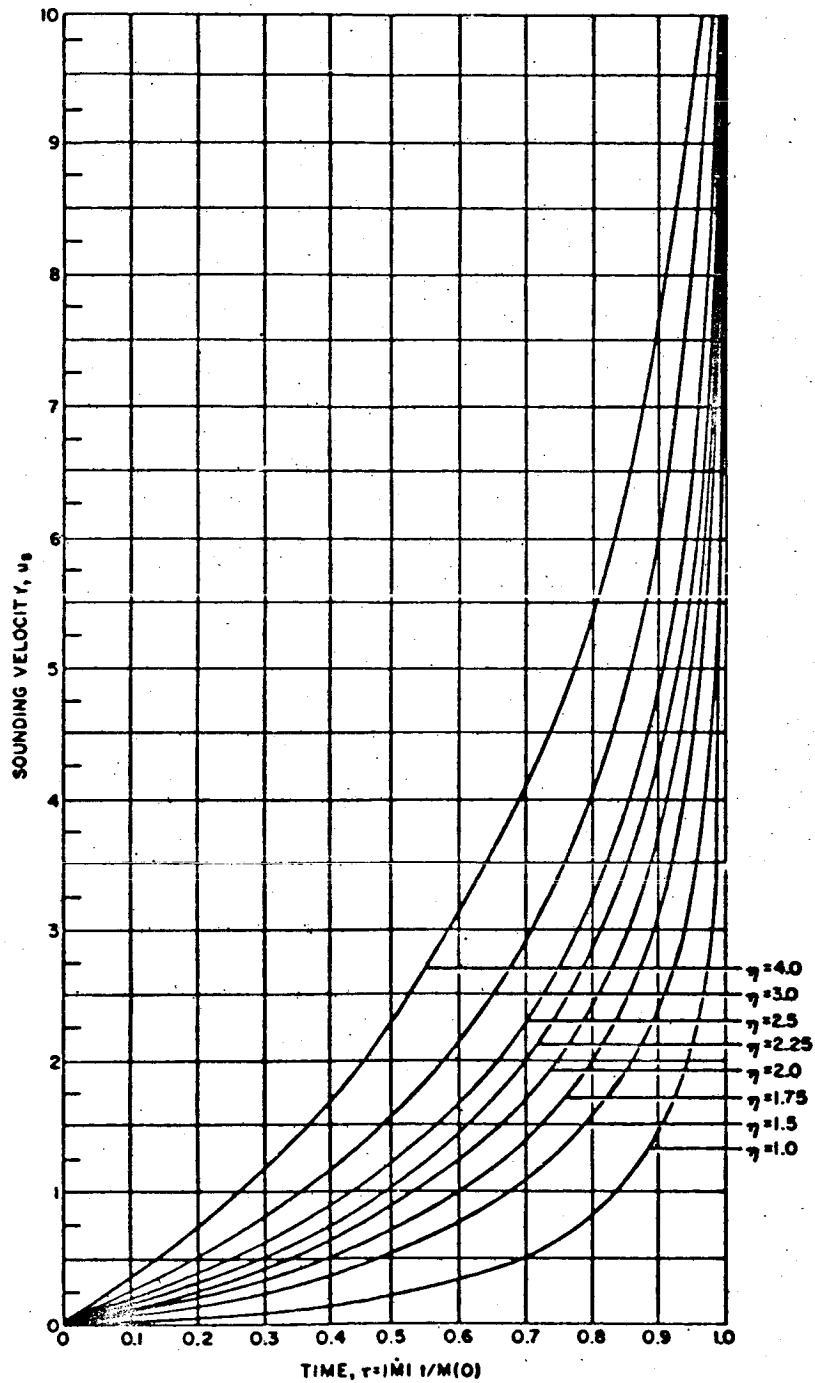


Figure 17. Velocity for a Vertical Sounding Flight

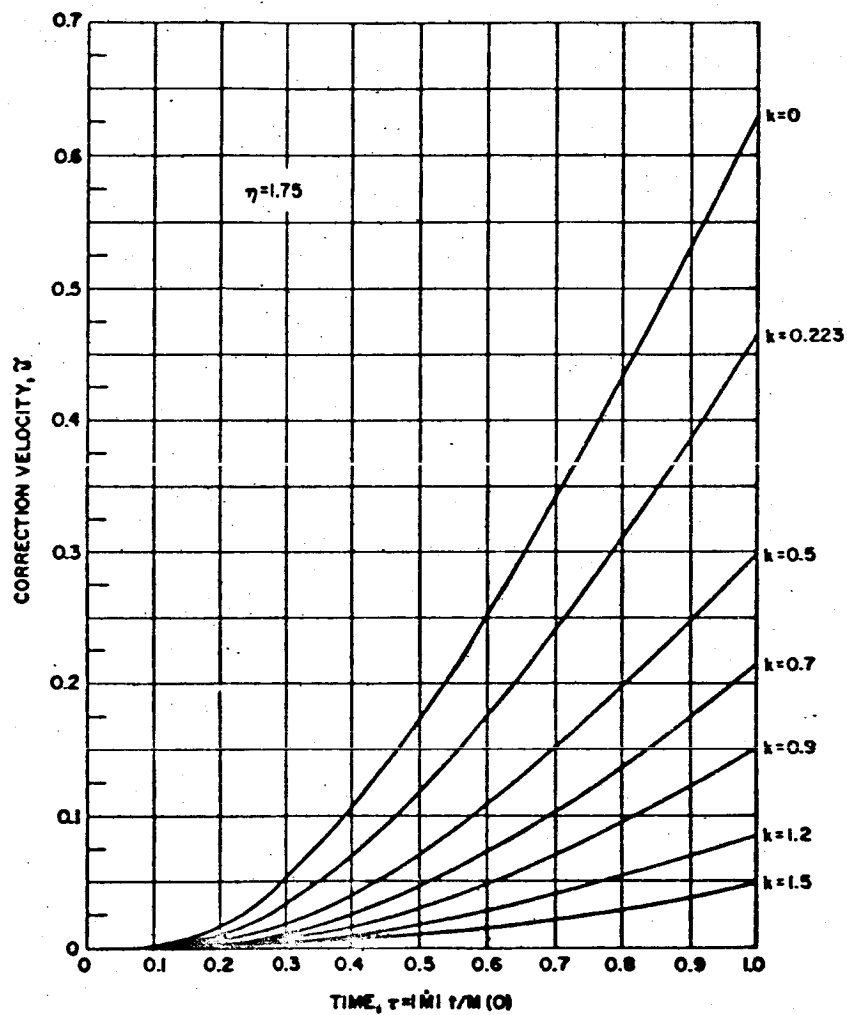


Figure 18. Correction to Sounding Velocity for a Gravity Turn Trajectory

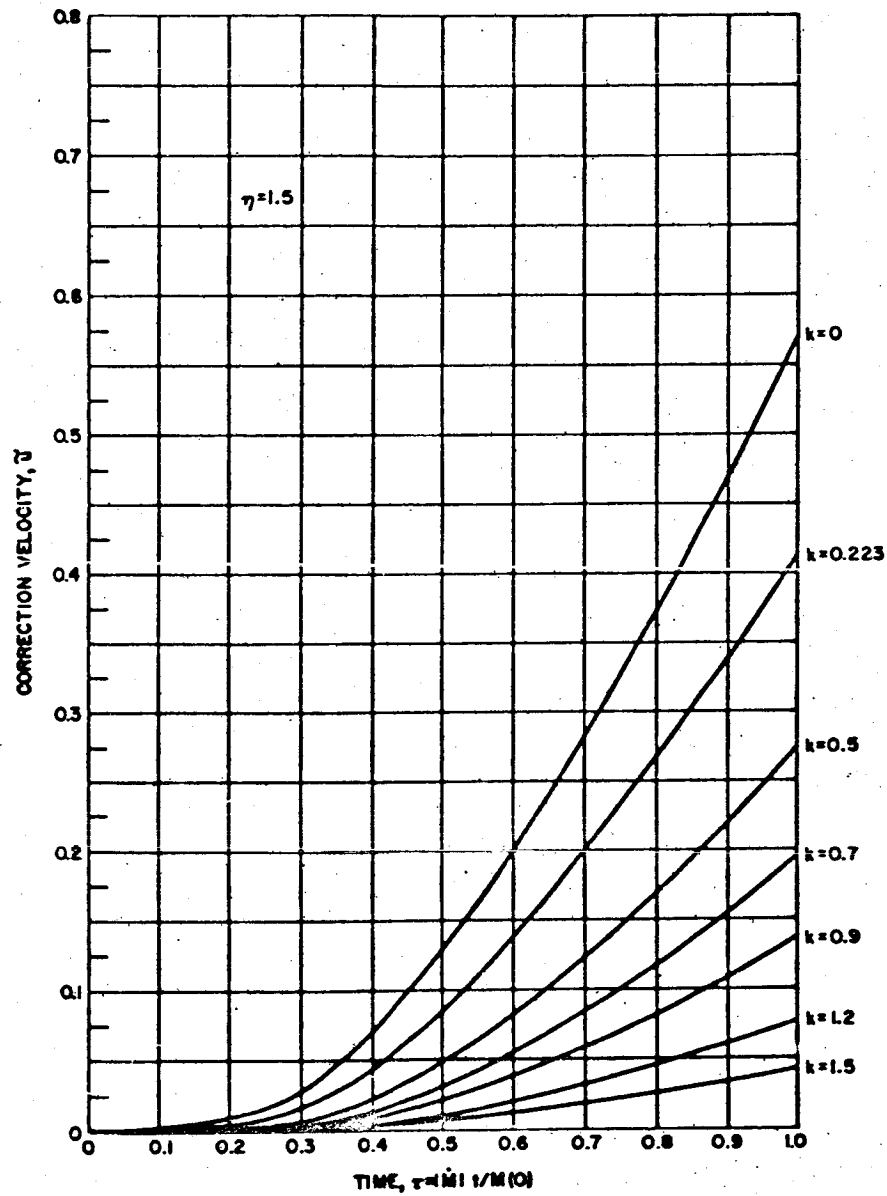


Figure 19. Correction to Sounding Velocity for a Gravity Turn Trajectory

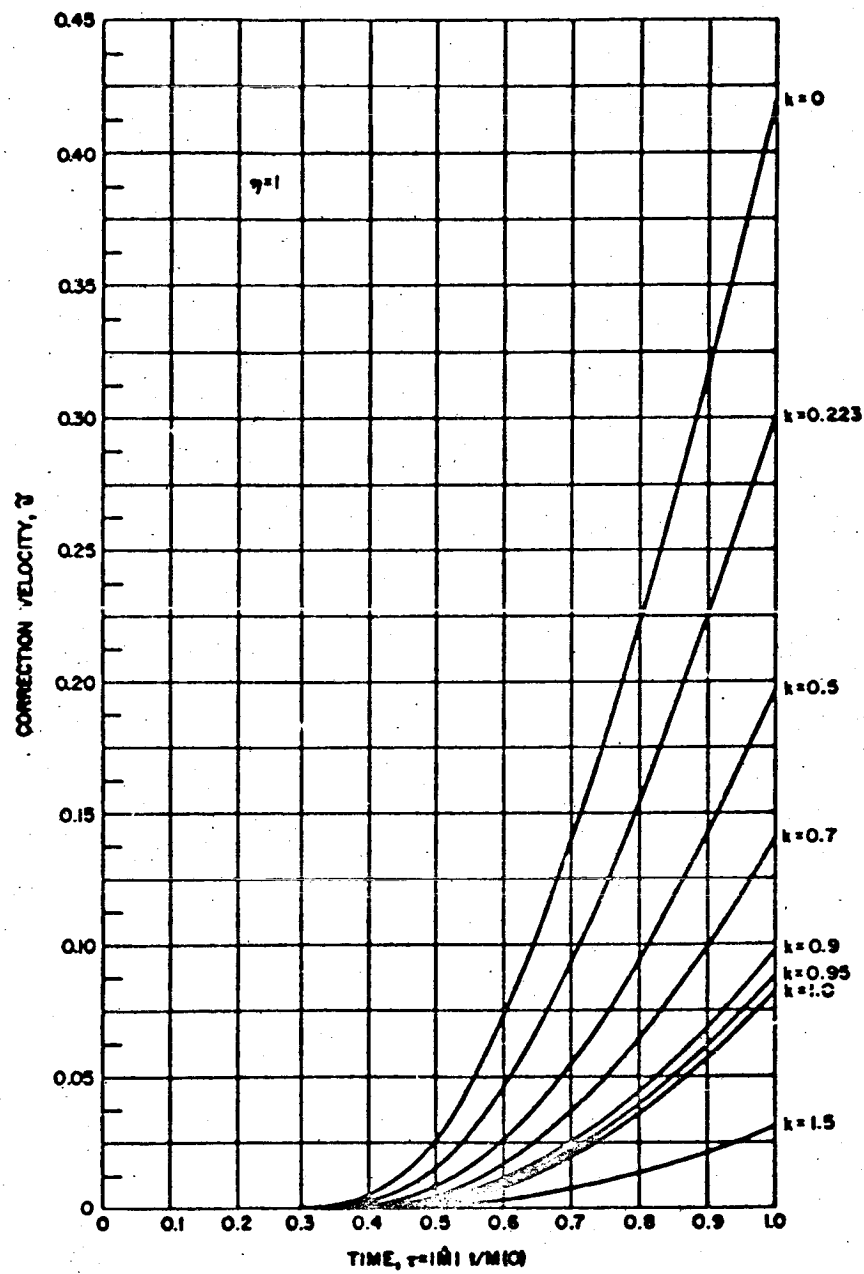


Figure 20. Correction to Sounding Velocity for a Gravity Turn Trajectory

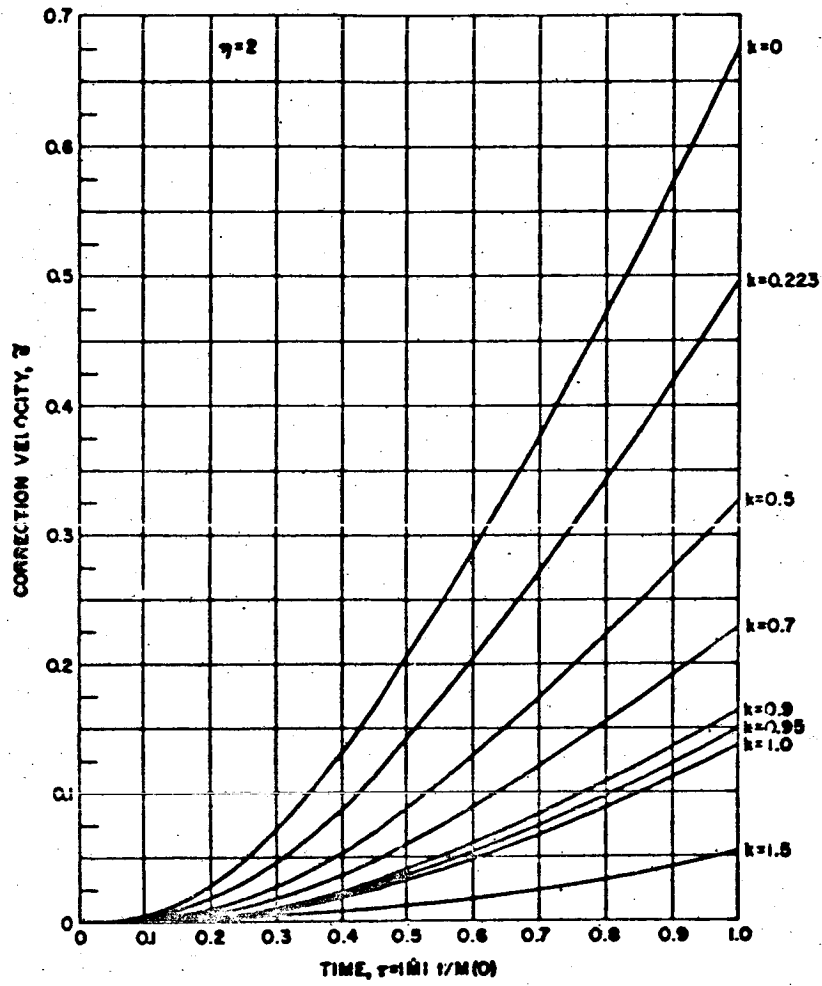


Figure 21. Correction to Sounding Velocity for a Gravity Turn Trajectory

50A

TRAJECTORY OPTIMIZATION FOR POWERED FLIGHT

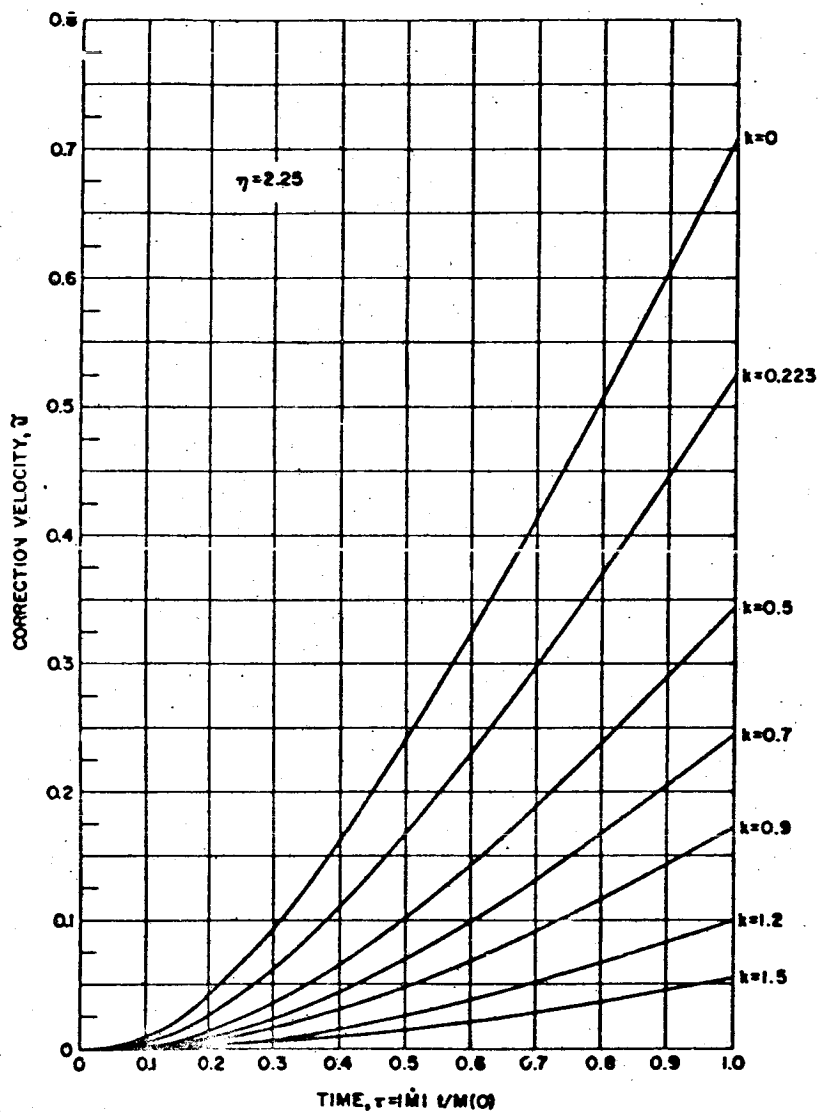


Figure 22. Correction to Sounding Velocity for a Gravity Turn Trajectory

Graphical Presentation

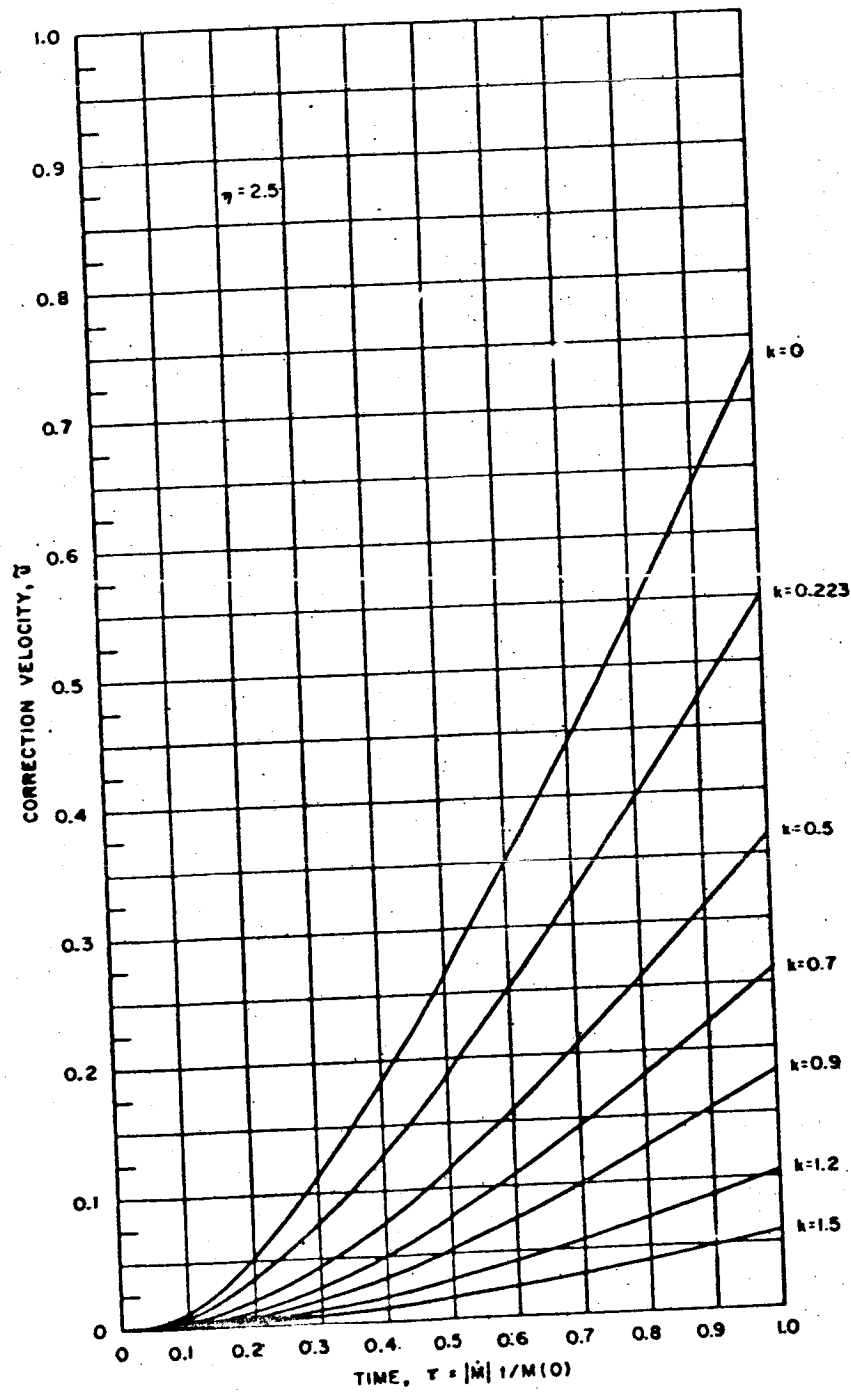


Figure 23. Correction to Sounding Velocity for a Gravity Turn Trajectory

TRAJECTORY OPTIMIZATION FOR POWERED FLIGHT

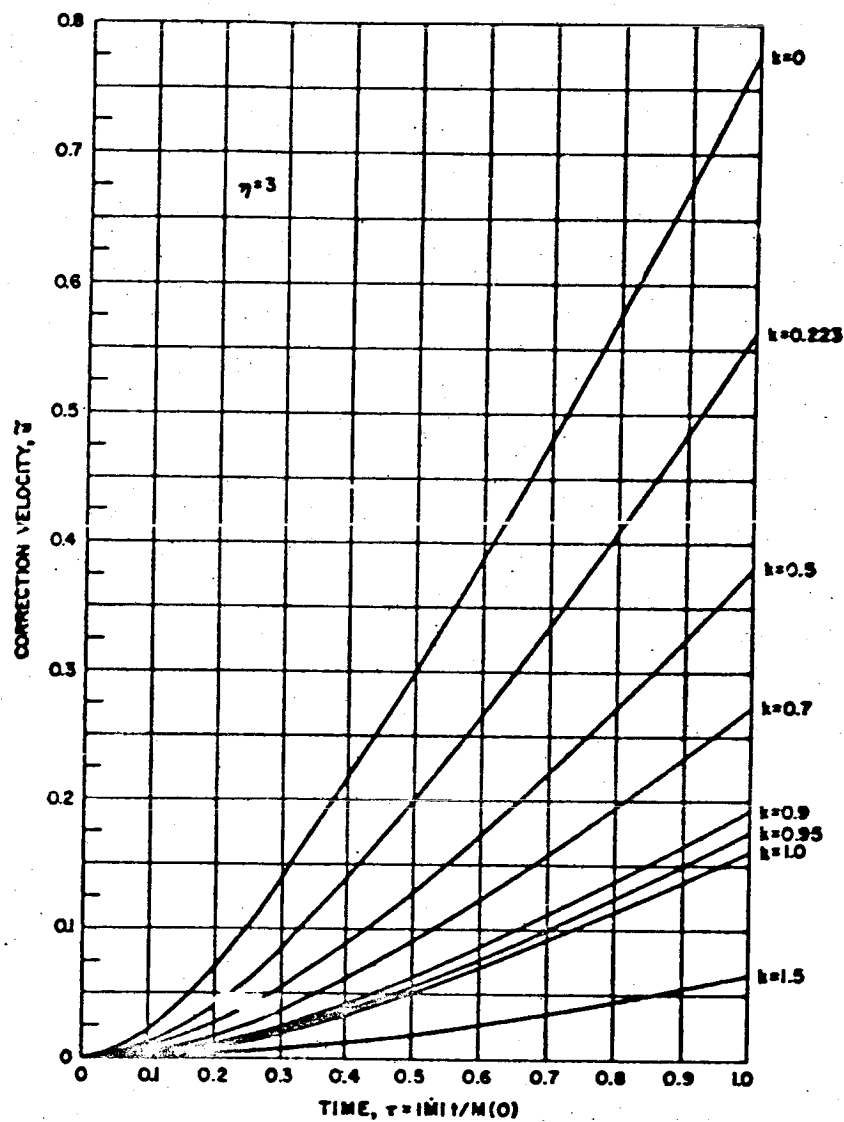


Figure 24. Correction to Sounding Velocity for a Gravity Turn Trajectory

Graphical Presentation

53A

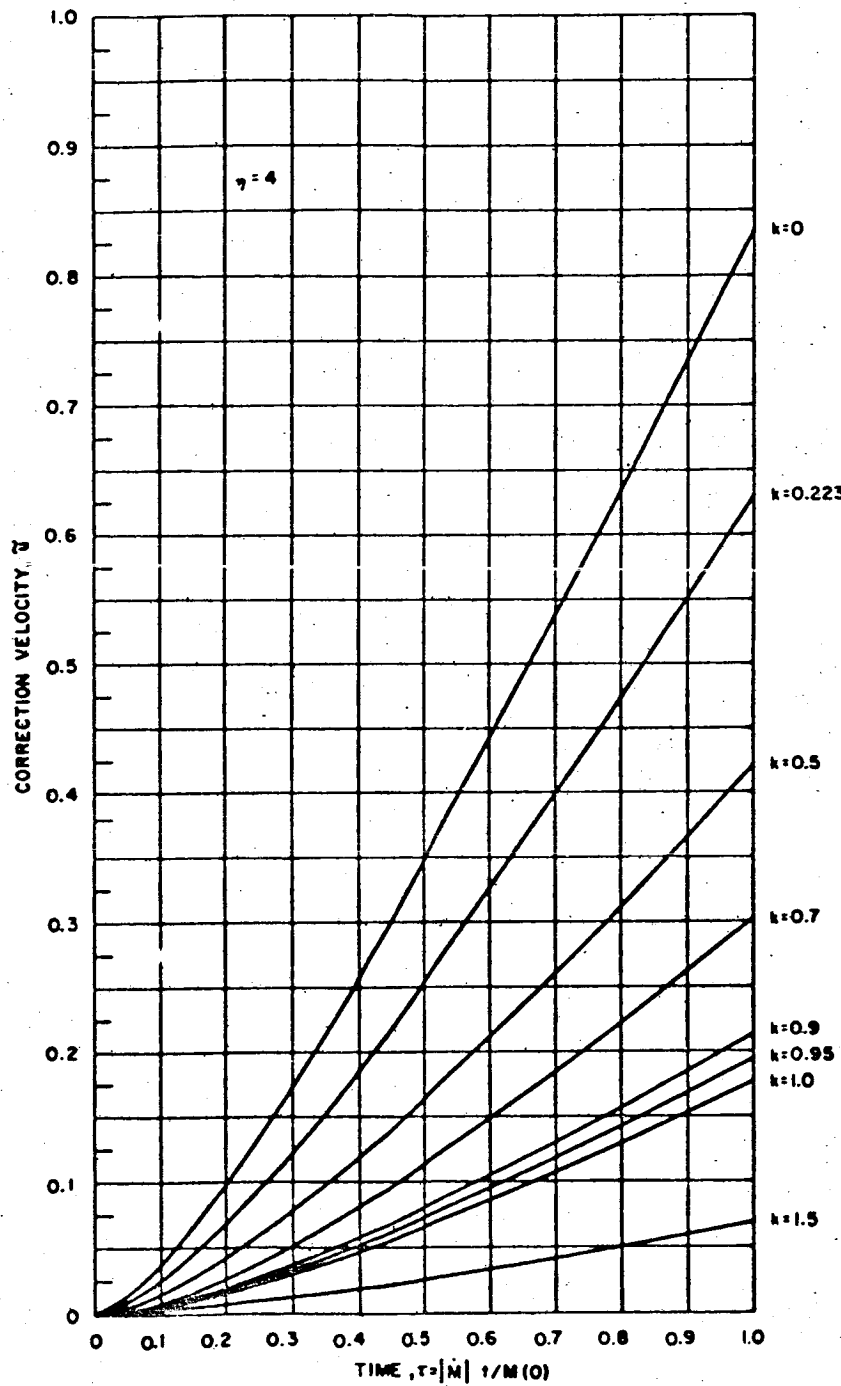


Figure 25. Correction to Sounding Velocity for a Gravity Turn Trajectory

NOMENCLATURE

\vec{A} \vec{B}	{ Fixed vectors
C_D	Aerodynamic drag coefficient
c	Exhaust velocity; $c = F/ \dot{M} $
F	Thrust
\vec{f}	Direction of thrust
g	Force of gravity
\vec{I}	Unit dyad
K	Constant of integration
k	Parameter analogous to the initial kick angle for nonsingular gravity turns; $k = [-\ln \tan (\beta/2)]_{\tau=1}$
M	Mass
\dot{M}	Mass flow rate
\vec{N}	A unit vector specifying thrust direction
\vec{N}_0	A unit vector normal to the thrust vector
n	Magnitude of the acceleration due to thrust; $n = \text{ratio of thrust to mass, } F/M$
p	A real number
R_e	Radius of the earth
r	Radial distance
S	Drag reference area
s	Variable of integration
T	Time at burnout; total burning time
t	Time
U	Potential of the gravitational force field
u	Velocity in units of c/η
\tilde{u}	Correction to sounding velocity
u_s	Sounding velocity
v	Velocity

Nomenclature

55A

v_o	Initial velocity
W	Any given criterion of performance
X	} Position variables
Y	
z	Velocity attitude variable; $z = \tan (\beta/2)$
a	Acceleration from all non-thrust forces
a_d	Acceleration due to drag
a_g	Acceleration due to gravity
β	Angle of the velocity vector with the vertical
β_o	"Initial-kick angle" of gravity turn; angle of v_o with the vertical.
Γ	A prescribed function of time
γ	$p/(p+1)$
δ	A small quantity
ϵ	A small quantity
η	Initial thrust-to-weight ratio; $\eta = F/M(o)g$
θ	Angle between the vectors \vec{N} and \vec{r}
λ	Optimum direction of thrust for a general force field
μ_o	Lagrange multipliers
v	Initial propellant weight/Initial gross weight
ξ_i	Denotes set of i end point values for a powered flight trajectory
ρ	Atmospheric density
\vec{p}	Position vector measured from launch
τ	Free flight time (burnout to impact)
τ	Time in units of initial mass divided by mass flow rate: $= \dot{M} t/M(0)$
ψ	Thrust attitude angle referenced to horizontal direction at launch
ω_y	$\sqrt{2g/R_e}$
ω_x	$\sqrt{g/R_e}$

REFERENCES

1. Raymond W. Wolverton, ed., Flight Performance Handbook for Orbital Operations, Space Technology Laboratories, Inc., Redondo Beach, California, September 1961.
2. D. F. Lawden, "Optimal Rocket Trajectories," Jet Propulsion, Vol. 27, No. 12, December 1957.
3. B. D. Fried and J. M. Richardson, "Optimum Rocket Trajectories," Journal of Applied Physics, Vol. 27, 955 (1956).
4. B. D. Fried, "On the Powered Flight Trajectory of an Earth Satellite," Jet Propulsion, Vol. 27, No. 6, 1957.
5. B. D. Fried and G. J. Culler, "Universal Gravity Turn Trajectories," Journal of Applied Physics, Vol. 28, No. 672, 1957.
6. G. A. Bliss, Lectures on the Calculus Variations, University of Chicago Press, 1946.
7. H. C. Corben, "A Note on the Optimization of Powered Trajectories," Ramo-Wooldridge Corporation, Report ERL-LM-150, 4 December 1957.

BIBLIOGRAPHY

- Baker, G. A., Jr., K. W. Ford and C. E. Porter, "Optimal Accuracy Rocket Trajectories," Journal of Applied Physics, Vol. 30, No. 12, December 1959.
- Bellman, R. and S. Dreyfus, "An Application of Dynamic Programming to the Determination of Optimal Satellite Trajectories," Journal of the British Interplanetary Society, Vol. 17, Nos. 3 - 4, May-August 1959.
- Bellman, R. and S. E. Dreyfus, "Computational Solutions of Dynamic Programming; VI - On the Optimal Trajectory Problem," Rand Corp., Report RM-1750, 16 April 1957.
- Bergqvist, Björn, "The Optimization Problem for Rocket Vehicles Subjected to Medium and High Accelerations: A Literature Survey," Astronautik, Vol. 1, No. 3, 1959.
- Bliss, G. A., Lectures on the Calculus Variations, University of Chicago Press, 1946.
- Breakwell, J. V., "The Optimization of Trajectories," Journal of the Society for Industrial and Applied Mathematics, Vol. 7, No. 2, June 1959.
- Breakwell, J. V. "Optimum Ascent Into a Circular Orbit," presented at: IAS Symposium on Vehicle Systems Optimization, 28-29 November 1961, Garden City, N. Y.
- Bryson, A. E. and S. E. Ross, "Optimum Rocket Trajectories with Aerodynamic Drag," Jet Propulsion, Vol. 28, No. 7, July 1958.
- Burns, Rowland E. "Correlative Survey Report on Powered Flight Trajectory Optimization Including An Extensive Critical Bibliography," ARS Space Flight Report to the Nation, Preprint No. 2071-61, 9-15 October 1961, New York, N. Y.

Corben, H. C. "A Note on the Optimization of Powered Trajectories in an Arbitrary Gravitational Field," Ramo-Wooldrige Corp., Report ERL-LM-150, 4 December 1957.

Ehlers, E. Edward, "Missile Trajectories With Linear Time Variation of the Sine or Tangent of the Thrust Angle," ARS Journal, Vol. 31, No. 5, May 1961.

Ewing, George M. "A Fundamental Problem of Navigation in Free Space," Quarterly of Applied Mathematics, Vol. 18, No. 4, January 1961.

Faulkner, Frank D. "Some Results From Direct Methods Applied to Optimum Rocket Trajectories," Proceedings of the 10th International Astronautical Congress, Vol. II, 1959. Springer - Verlag, Vienna.

Faulkner, Frank D. "Complete Elementary Solution to Some Optimum Trajectory Problems," ARS Journal, Vol. 31, No. 1, January 1961.

Ford, Kenneth W. "Optimization of Rocket Orbits: Part I. Idealized Calculations," University of California, Los Alamos Scientific Laboratory, Report No. LA-2166, 10 February 1958.

Fried, B. D., "General Formulation of Powered Flight Trajectory Optimization Problems," Journal of Applied Physics, Vol. 29, No. 8, 1958.

Fried, B. D., "On the Powered Flight Trajectory of an Earth Satellite," Jet Propulsion, Vol. 27, No. 6, 1957.

Fried, B. D. and G. J. Culler, "Universal Gravity Turn Trajectories," Journal of Applied Physics, Vol. 28, No. 672, 1957.

Fried, B. D. and J. M. Richardson, "Optimum Rocket Trajectories," Journal of Applied Physics, Vol. 27, No. 8, August 1956.

Graham, E. W. and B. J. Beane, "Optimum Trajectories with Atmospheric Resistance," Douglas Aircraft Company, Inc. Report No. SM-23745, November 1959.

Graham, E. W., "A Class of Optimum Trajectory Problems in Gravitational Fields," Douglas Aircraft Company, Inc. Report No. SM-23640, July 1959.

Hestenes, M. R., "A General Problem in the Calculus of Variations with Applications to Paths of Least Time," The Rand Corporation, Report No. RM-100, 1950.

Hibbs, A. R., "Optimum Burning Program for Horizontal Flight," ARS Journal, Vol. 22, No. 4, July-August 1952.

Jurovics, Stephen, "Optimum Steering Program for the Entry of a Multistage Vehicle Into a Circular Orbit," ARS Journal, Vol. 31, No. 4, April 1961.

Jurovics, Stephen, and John E. McIntyre, "The Adjoint Method and Its Application to Trajectory Optimization," ARS Preprint 2064-61. ARS Space Flight Report to the Nation, 9-15 October 1961.

Kelley, H. J., "Gradient Theory of Optimal Flight Paths," ARS Journal, Vol. 30, No. 10, October 1960.

Kulakowski, L. J. and R. T. Stancil, "Rocket Boost Trajectories for Maximum Burnout Velocity," ARS Journal, Vol. 30, No. 7, July 1960.

Lawden, D.F., "Interplanetary Rocket Trajectories," Chapter 1 of Advances in the Space Sciences; Vol. 1 (edited by F.L. Ordway III), 1959, Academic Press, New York, N.Y.

Lawden, D.F., "Dynamic Problems of Interplanetary Flight," The Aeronautical Quarterly, Vol. 6, Nos. 1 - 4, 1955.

Lawden, D.F., "Optimal Rocket Trajectories," Jet Propulsion, Vol. 27, No. 12, December 1957.

Lawden, D.F., "Optimal Programming of Rocket Thrust Direction," Astronautica Acta, Vol. 1, 1955.

Lawden, D.F., "Optimum Launching of a Rocket into an Orbit about the Earth," Astronautica Acta, Vol. 1, No. 4, 1955.

Lawden, D.F., "Minimal Rocket Trajectories," ARS Journal, November - December 1953.

Lawden, D.F., "Optimal Powered Arcs in an Inverse Square Law Field," ARS Journal, Vol. 31, No. 4, April 1961.

Lawden, D.F., "Necessary Conditions for Optimal Rocket Trajectories," Quarterly Journal of Mechanics and Applied Mathematics, Vol. 12, No. 4, November 1959.

Leitmann, George, "Extremal Rocket Trajectories in Position and Time Dependent Force Fields," Preprint No. 61-30, 7th Annual Meeting of the American Astronautical Society, 16-18 January 1961.

Leitmann, George, "Trajectory Programming for Maximum Range," Journal of the Franklin Institute, Vol. 264, No. 6, December 1957.

Leitmann, George, "Optimal Thrust Direction For Maximum Range," Journal of the British Interplanetary Society, Vol. 16, No. 9, September-October 1958.

Leitmann, George, "Stationary Trajectories for a High-Altitude Rocket with Drop-Away Booster," Astronautica Acta, Vol. 2, No. 3, 1956.

Leitmann, George, "The Optimization of Rocket Trajectories. A Survey," Progress in the Astronautical Sciences, 1961.

Leitmann, George, "On Some Optimum Rocket Trajectories," Presented at: Institute of the Aerospace Sciences Symposium on Vehicle Systems Optimization, 28-29 November 1961, Garden City, N.Y.

Leitmann, George, "On a Class of Variational Problems in Rocket Flight," Journal of the Aero/Space Sciences, Vol. 26, No. 9, September 1959.

MacKay, John S., "Approximate Solution for Rocket Flight with Linear - Tangent Thrust Attitude Control," ARS Journal, Vol. 30, No. 11, November 1960.

McIntyre, John E. "Optimum Trajectory Analysis," North American Aviation Report MD 60-309, 6 October 1960.

Bibliography

59A

McIntyre, John E., Stephen A. Jurovics, William P. Gardill, and Barbara Johnson, "The Application of Optimum Trajectory Analysis to Boost Vehicle Design," presented at: Institute of the Aerospace Sciences Symposium on Vehicle Systems Optimization, 28-29 November 1961, Garden City, N. Y.

Miele, Angelo, and Carlos R. Cavotti, "Generalized Variational Approach to the Optimum Thrust Programming for the Vertical Flight of a Rocket. Part II: Application of Green's Theorem to the Development of Sufficiency Proofs for Particular Classes of Solutions," Purdue University, School of Engineering, Report A-57-2, August 1957.

Miele, Angelo, "General Variational Theory of the Flight Paths of Rocket-Powered Aircraft, Missiles and Satellite Carriers," Astronautica Acta, Vol. 4, No. 4, 1958.

Miele, Angelo, and J. O. Cappellari, "Some Variational Solutions to Rocket Trajectories over a Spherical Earth," Purdue University, School of Aeronautical Engineering, Report No. A-58-9, November 1958.

Miele, Angelo, and J. O. Cappellari, "Topics in Dynamic Programming for Rockets," Zeitschrift für Flugwissenschaften, Vol. 7, No. 1, 1959.

Moskowitz, S. and L. Ting, "An Approach to Problem of Optimum Rocket Trajectories," ARS Journal, Vol. 31, No. 4, April 1961.

Newton, R. R., "On the Optimum Trajectory of a Rocket," Journal of the Franklin Institute, Vol. 266, No. 3, September 1958.

Okhotsimskii, D. E. and T. M. Eneev, "Some Variational Problems Connected with the Launching of Artificial Satellites of the Earth," Journal of the British Interplanetary Society, Vol. 16, No. 5, January-February 1958.

Pfeiffer, Carl G. "Theory and Applications of the Critical Direction Method of Trajectory Optimization," Presented at: IAS Symposium on Vehicle Systems Optimization, 28-29 November 1961, Garden City, N. Y.

Ross, Stanley, "Composite Trajectories Yielding Maximum Coasting Apogee Velocity," ARS Journal, Vol. 29, No. 11, November 1959.

Ross, Stanley, "Minimality for Problems in Vertical and Horizontal Rocket Flight," Jet Propulsion, Vol. 28, No. 1, 1958.

Stancil, R. T. and L. J. Kulakowski, "Rocket Boost Vehicle Mission Optimizations," Preprint No. 1449-60, ARS 15th Annual Meeting, 1960, New York, N. Y.

Tsien, H. S. and R. L. Evans, "Optimum Thrust Programming for a Sounding Rocket," Jet Propulsion, Vol. 21, No. 5, September 1951.

Wolverton, Raymond W., ed., Flight Performance Handbook for Orbital Operations, Space Technology Laboratories, Inc., Redondo Beach, California, September 1961.

SUBJECT INDEX

A

ABLATING MATERIALS 7-2

ACCELERATION, AXIAL

Burnout at (Staging) 3-49

(Derivation) B-14

(Graphical Presentation) 3-50

Dynamic Pressure

(Graphical Presentation) 3-51

Pressure Ratio, at 3-49, B-15

(Graphical Presentation) 3-52

Dynamic Pressure, Maximum 3-53

(Derivation) B-15

(Graphical Presentation) 3-54, 3-55

Mach Number, at 3-53

(Derivation) B-15

(Graphical Presentation) 3-58

Time, at 3-53

(Derivation) B-16

(Graphical Presentation) 3-56

Entry, During 7-9, 7-26

(also see DECELERATION DURING
PLANETARY ENTRY)

Stage Operation, During

(Graphical Presentation) 3-57

Pressure Ratio at

(Graphical Presentation) 3-52

AERODYNAMIC

Drag (see DRAG)

Heating 2-3, 3-49, 7-32

(also see HEATING)

Loads 3-49

(also see LOADS)

AIR 7-34

Equation of State for

(Graphical Presentation) 7-35

Viscosity of

(Graphical Presentation) 7-38

ALTITUDE

Apogee 2-4, A-2

Perigee 2-4, A-1

Range Error Coefficient 3-36

(Analytical Expression) B-10

(Graphical Presentation) 3-39, 3-40

APOGEE, ALTITUDE 2-4, A-2

ASCENT, DIRECT 2-4

ATLANTIC MISSILE RANGE 3-33

Firing Sector

(Map) 3-31

Range Safety Summary

(Tabular Presentation) 3-30

ATMOSPHERE

Earth 7-5

(also see AIR)

Exponential, Comparison with ARDC 1959
Model 7-6

Pressure Ratio

(Graphical Presentation) 3-49

Mars 7-5

Venus 7-8

ATTITUDE

Constant 2-93, A-14

Constant Pitch Rate 2-93, A-12

Control During Entry 7-1

Optimum (see TRAJECTORY OPTIMIZATION)

Stabilization 2-3

AZIMUTH

Dispersions 3-48

Exit Launch Limits, Permissible 3-29

(Graphical Presentation) 3-31, 3-32

(Tabular Presentation) 3-30

Range Error Coefficient 3-48

(Analytical Expression) 3-48, B-10

B

BACKWARD ENTRY 7-1

BALLISTIC COEFFICIENT (BALLISTIC PARAMETERS), $W/C_D A$ 2-3, 7-27, A-9

BI-ELLIPTICAL TRANSFER MANEUVER 3-27

BOUNDARY LAYER TRANSITION 7-41

Reynolds Number

Below Transition 7-41

Definition 7-41

Maximum 7-41

BURNOUT ALTITUDE, COMPUTATION OF

First-Stage 2-89, A-11

Constant 2-89, A-12

(Graphical Presentation) 2-90

Upper Stage 2-103, A-20

C

CARBON DIOXIDE 7-34

Equation of State for

(Graphical Presentation) 7-37

Viscosity of

(Graphical Presentation) 7-38

CIRCULAR ORBITS

Period 2-4, A-2

(Graphical Presentation) 2-12 through 2-19

(Tabular Presentation) 2-20

Transfer (see HOHMANN TRANSFER)

Velocity 2-4, A-1

(Graphical Presentation) 2-5 through 2-10

(Tabular Presentation) 2-11

COAST PHASE 2-3, 2-62, 2-103

Long Phase 2-104

Specified Change in Altitude 2-104

Specified Coasting Time 2-107

Short Phase 2-103

CROSSRANGE DISPERSION 3-48

(also see DISPERSIONS)

CURSORY ESTIMATION OF PERFORMANCE 2-68, A-5

Earth's Rotational Velocity 2-70

First-Stage Velocity Losses 2-68, A-5

(Graphical Presentation) 2-71 through 2-76

Corrections 2-70, A-7

Drag Characteristics, Change in 2-70, A-7

Mass Ratio, Change in 2-70, A-5

Sea Level-Vacuum Specific Impulse Ratio, Change in 2-70, A-6

Drag 2-68, A-4, A-5

Gravity 2-68, A-4, A-5

Thrust-Atmosphere Effects 2-68, A-4, A-5

Upper-Stage Velocity Losses 2-77, A-7

Angles of Attack 2-77

Average Flight Path Angle 2-77, A-7

Single Upper Stage

(Graphical Presentation) 2-78

Two Upper Stages

(Graphical Presentation) 2-79

Velocity

Burnout 2-68, A-5

Ideal, Total 2-68, A-5

D

DEBOOST (see LUNAR/PLANETARY DEBOOST)

DECELERATION, DURING PLANETARY ENTRY 7-26

Alleviation During Entry 7-1

Ballistic Trajectories, for 7-26

Equations of Motion 7-26

General Entry Functions 7-9

Maximum During Entry

(Analytical Expression) 7-27

(Graphical Presentation) 7-28

Modulated 7-27

Continuous

(Analytical Expression) 7-29

(Graphical Presentation) 7-31

Discrete

(Analytical Expression) 7-29

(Graphical Presentation) 7-30

Subject Index

1-3

- DE LAVAL NOZZLE 2-81, A-11
 DESIGN-SIZING TRAJECTORY PROGRAM 5-66
 DESIGN OPTIMIZATION 24A
 Example 26A
 DIRECT ASCENT 2-4
 DISCRETE MODULATION, PARAMETERS FOR 7-29
 (Graphical Presentation) 7-30
 DISPERSIONS 3-41, B-10
 Altitude-Range Error Coefficients 3-48
 (A analytical Expression) B-10
 (Graphical Presentation) 3-39, 3-40
 Azimuth-Range Error Coefficients 3-48
 (A analytical Expression) 3-48, B-10
 Downrange-Crossrange Dispersion, Correlation of, 3-48, B-14
 Downrange Dispersions, Correlation of, 3-48, B-14
 Flight Path Angle-Range Error Coefficient 3-43
 (A analytical Expression) B-10
 (Graphical Presentation) 3-46, 3-47
 Impact Location 3-33
 Performance 3-67
 (also see PERFORMANCE MARGIN CONCEPT)
 Velocity-Range Error Coefficient 3-43
 (A analytical Expression) B-10
 (Graphical Presentation) 3-44, 3-45
 DOG-LEG MANEUVER 3-6, B-4
 (Illustration) 3-7
 Bi-elliptical Dog-Leg Transfer Maneuver 3-27
 Final Injection Velocity 3-7
 (Graphical Presentation) 3-8 through 3-18
 Initial Injection Velocity 3-7
 (Graphical Presentation) 2-22 through 2-28
 Total Injection Velocity 3-7
 (Graphical Presentation) 3-19 through 3-26
 Transit Time 2-22
 (Graphical Presentation) 2-40 through 2-51
 DOWNRANGE DISPERSIONS 3-43
 (also see DISPERSIONS)
 DRAG 2-68, A-4, A-5, 10A
 Loss 2-80, 2-81, 2-110, A-9
 Constant 2-81, 2-87
 Modulation 7-1, 7-27
 DYNAMIC MOTION DURING ENTRY 7-3
 DYNAMIC PRESSURE
 Burnout, at 3-49, B-15
 Maximum 3-53, B-15
 (Graphical Presentation) 3-54, 3-55
 Altitude at 3-53
 Axial Acceleration at 3-53
 Drag Coefficient, at 3-53
 Mach Number, at 3-53, B-15
 (Graphical Presentation) 3-58
 Time, at 3-53, B-16
 (Graphical Presentation) 3-56
 E
 EARTH
 Atmosphere 7-5
 Exponential ARDC Atmosphere of 1959, Comparison 7-6
 Pressure Ratio-Altitude
 (Graphical Presentation) 3-52
 Rotation 3-1, B-1
 Effects of 2-76, 2-89
 Velocity, due to
 (Graphical Presentation) 3-2
 Track 3-35
 Velocity Requirements to
 Mars 2-56
 (Graphical Presentation) 2-58
 Moon 2-51
 (Graphical Presentation) 2-53, 2-54
 Venus 2-56
 (Graphical Presentation) 2-57
 ELEVATION ANGLE 2-3, 3-62, B-18
 Launch Site, from 3-62
 Radar Station, from 3-64, B-19
 Slant Range 3-62, B-18

Subject Index

ELLIPTICAL ORBITS

- Period 2-4
 - (Graphical Presentation) 2-12, 2-13
- Velocity 2-4, A-12
 - (Graphical Presentation) 2-5, 2-6

ENTRY ANGLE EFFECT ON

- Aerodynamic Heat Transfer 7-2
- Radiant Heat Transfer 7-2

ENTRY FUNCTION (GENERAL) 7-1, 7-9

- Constants
 - (Tabular Presentation) 7-9
- Deceleration for Ballistic Trajectories 7-9, 7-26
- Example 7-17
- Exponential Integral
 - (Graphical Presentation) 7-12
- Heat Rate, Laminar 7-9
- Heat Rate, Turbulent 7-9
- Integrated Value (of Entry Functions) 7-14
- Radiant Heat Rate Function 7-9
- Reynolds Number 7-41
 - Maximum for ($W/C_D A$, R_N)
 - (Analytical Expression) 7-41
 - Transition, Below 7-42
- Time
 - Between Two Maximums of Different Phenomenon 7-17
 - t/t_{\max} of
 - (Analytical Expression) 7-17
 - (Graphical Presentation) 7-21 through 7-24
 - Pressure Change for
 - (Analytical Expression) 7-10
- Total/Maximum Relationship 7-14
- Parameter
 - (Analytical Expression) 7-17
- Variation of t/t_{\max} 7-11
 - (Graphical Presentation) 7-15, 7-16
- Velocity at Maximum 7-11
 - (Analytical Expression) 7-11
 - (Graphical Presentation) 7-13

ERROR COEFFICIENTS

- Altitude-Range 3-48
 - (Analytical Expression) B-9
 - (Graphical Presentation) 3-39, 3-40
- Azimuth-Range 3-48
 - (Analytical Expression) 3-48, B-10
- Flight Path Angle-Range 3-43
 - (Analytical Expression) B-9
 - (Graphical Presentation) 3-46, 3-47
- Velocity-Range 3-43
 - (Analytical Expression) B-10
 - (Graphical Presentation) 3-44, 3-45

ERRORS, PERFORMANCE (see DISPERSIONS, EXCHANGE RATIO ANALYSIS, and PERFORMANCE MARGIN CONCEPT)

ESCAPE VELOCITY, EARTH 2-55

EXAMPLES

- Exchange Ratio Computation 4-15
- General Design Analysis 26A
- General Entry Function 7-17
- Performance Evaluation, Precise 2-108
- Comparison of Results 2-121
- Determination of
 - Earth's Rotational Effects 2-112
- First-Stage
 - Burnout Altitude 2-111
 - Burnout Flight Path Angle 2-109
 - Burnout Range Angle and Vehicle Attitude 2-112
 - Burnout Velocities 2-109
- Second-Stage
 - Burnout Conditions 2-113
- Performance Margin Computation 3-67
- Sizing
 - Cost 5-85
 - Nomograph, Use of 5-74
 - Parallel Staging 5-80

EXCHANGE RATIO ANALYSIS, GENERAL 4-1, 27A

- Analytical Relationships 4-1
- Development of Generalized Exchange Ratios C-1

Subject Index

15

EXCHANGE RATIO ANALYSIS, GENERAL
(Continued)

Example 4-51
 Graphical Presentation 4-6
 Gross Weight Exchange Ratios
 (Derivation) C-11
 kth Stage to Gross Weight of nth Stage, of
 (A analytical Expression) 4-4
 (Derivation) C-15
 nth Stage to Gross Weight of
 $n + 1$ Stage, of
 (A analytical Expression) 4-3
 (Derivation) C-14
 (Graphical Presentation) 4-13
 One-Stage Vehicle, of
 Inert Weight, to
 (A analytical Expression) 4-5
 (Derivation) C-12
 (Graphical Presentation) 4-13
 Initial Thrust, to
 (A analytical Expression) 4-5
 (Derivation) C-13
 (Graphical Presentation) 4-14
 Payload, to
 (A analytical Expression) 4-5
 (Derivation) C-7
 (Graphical Presentation) 4-13
 Specific Impulse, to
 (A analytical Expression) 4-5
 (Derivation) C-12
 (Graphical Presentation) 4-12
 Payload
 (A analytical Expression) 4-3
 (Derivation) C-5
 Payload Exchange Ratios 4-2
 (Derivation) C-1
 Initial Gross Weight, to
 nth Stage, of
 (A analytical Expression) 4-3
 (Derivation) C-5
 One-Stage Vehicle, of
 (A analytical Expression) 4-5
 (Derivation) C-7
 (Graphical Presentation) 4-7

EXCHANGE RATIO ANALYSIS, GENERAL
(Continued)

Vehicle, of
 (A analytical Expression) 4-3
 (Derivation) C-5
 Initial Thrust, to
 (Derivation) C-11
 nth Stage, of
 (A analytical Expression) 4-3
 Payload Exchange Ratios (Continued)
 Initial Thrust, to (Continued)
 One Stage, of
 (A analytical Expression) 4-5
 (Graphical Presentation) 4-11
 Propellant
 Loading, to
 (Derivation) C-9
 nth Stage, of
 (A analytical Expression) 4-3
 One Stage, of
 (A analytical Expression) 4-5
 (Graphical Presentation) 4-9
 Weight, to
 Derivation C-9
 nth Stage, of
 (A analytical Expression) 4-3
 One Stage, of
 (A analytical Expression) 4-5
 (Graphical Expression) 4-10
 Specific Impulse, to
 (Derivation) C-2
 nth Stage of
 (A analytical Expression) 4-4
 One Stage, of
 (A analytical Expression) 4-5
 (Graphical Presentation) 4-7
 Structural Weight, to
 (Derivation) C-4
 nth Stage, of
 (A analytical Expression) 4-3
 One Stage, of
 (A analytical Expression) 4-5
 N-Stage Vehicle 4-2
 One-Stage Vehicle 4-4

Subject Index

EXCHANGE RATIO ANALYSIS, GENERAL
(Continued)

Velocity Exchange Coefficients 3-69
(also see PERFORMANCE MARGIN ANALYSIS)

Burnout Weight
(Analytical Expression) 3-69
(Derivation) B-24
(Graphical Presentation) 3-71

Velocity Exchange Coefficients (Continued)

Inert Weight
(Analytical Expression) 3-69
(Derivation) B-23
One Stage, of
(Graphical Presentation) 3-70

Payload Weight
(Analytical Expression) 3-69
(Derivation) B-23
One Stage, of
(Graphical Presentation) 3-70

Propellant Weight
(Analytical Expression) 3-69
(Derivation) B-24
(Graphical Presentation) 3-70, 3-71

Specific Impulse
(Analytical Expression) 3-69
(Derivation) B-22
(Graphical Presentation) 3-72

Thrust
(Analytical Expression) 3-69
(Derivation) B-25
(Graphical Presentation) 3-73

EXPANSION-DEFLECTION NOZZLE 2-81, A-11

EXPONENTIAL INTEGRAL
(Graphical Presentation) 7-12

F

FIRING SECTOR

Atlantic Missile Range
(Graphical Presentation) 3-31
Pacific Missile Range
(Graphical Presentation) 3-32

FIRST-STAGE PERFORMANCE COMPUTATION
(see CURSORY ESTIMATION OF PERFORMANCE, and PRECISE EVALUATION OF PERFORMANCE)

FLIGHT PATH ANGLE-RANGE ERROR COEFFICIENT 3-43

(A analytical Expression) B-10
(Graphical Presentation) 3-46, 3-47

FLIGHT TIME (FROM BURNOUT TO IMPACT) 3-41

(A analytical Expression) B-10
(Graphical Presentation) 3-42

FLIGHT, VERTICAL (see VERTICAL)

G

GENERAL DESIGN-SIZING TRAJECTORY PROGRAM 5-66

GENERAL ENTRY FUNCTIONS (see ENTRY FUNCTIONS, GENERAL)

GRAVITY TURN 2-62, A-3, 10A

Equations 10A

Sounding Velocity

(Graphical Presentation) 45A

Correction to, for a Gravity turn

(Graphical Presentation) 46A
through 53A

Velocity Attitude Variable

(Graphical Presentation) 29A through 36A

Velocity Versus Velocity Attitude

(Graphical Presentation) 37A through 44A

GRAVITATIONAL

Constants

(Tabular Presentation) 6-9

Velocity Losses 2-81, A-4, A-8

Constant 2-81

(Graphical Presentation) 2-83

Variation Correction 2-81, A-5

Constant 2-81

(Graphical Presentation) 2-82

GROSS WEIGHT EXCHANGE RATIO (see EXCHANGE RATIO ANALYSIS)

GUIDANCE AND TRACKING 3-59, B-18
 Elevation Angle 2-3, 3-62, B-18
 Look Angle 3-66, B-20
 Radio 2-3, 3-62
 Slant Range 3-62, B-18
 Vehicle Angular Displacement 3-66, B-20

H

HEATING DURING BOOST TRAJECTORY
3-53, B-16

Input, Total 3-59, B-16
 (Graphical Presentation) 3-61
 Rate, Maximum 3-59
 (Graphical Presentation) 3-60

HEATING DURING PLANETARY ENTRY 7-32

Boundary Layer Transition 7-41
 Reynolds Number
 Below Transition 7-42
 (Analytical Expression) 7-42
 Definition 7-41
 Maximum 7-41
 (Analytical Expression) 7-41
 Convective Total, at Stagnation Point 7-40
 (Analytical Expression) 7-40
 Radiation 7-42
 Rate
 (Analytical Expression) 7-42
 Total
 (Analytical Expression) 7-42
 Rate, 7-9, 7-39
 Laminar 7-9
 Turbulent 7-9
 Sink 7-2
 Stagnation Point Heating 7-42
 Air
 Equation of State for 7-34
 (Graphical Presentation) 7-35
 Viscosity of 7-34
 (Graphical Presentation) 7-38
 Average Heating Rate 7-39
 Carbon Dioxide 7-39
 Equation of State for 7-39

HEATING DURING PLANETARY ENTRY
(Continued)

Stagnation Point Heating (Continued)
 (Graphical Presentation) 7-37
 Viscosity of
 (Graphical Presentation) 7-38
 Convective Heating, Total 7-40
 Nitrogen
 Equation of State for 7-34
 (Graphical Presentation) 7-36
 Viscosity, of
 (Graphical Presentation) 7-38
 Total (Radiation and Aerodynamic)
 (Graphical Presentation) 7-43
 Viscosity of Air, Nitrogen, and Carbon
 Dioxide
 (Graphical Presentation) 7-38

HOHMANN TRANSFER 2-21, A-2

(Illustration) A-1
 Dog-Leg Maneuver 3-7, B-3
 Final Injection Velocity 3-7
 (Graphical Presentation) 3-8
 through 3-18
 Initial Injection Velocity 3-7
 (Graphical Presentation) 2-22
 through 2-28
 Total Injection Velocity 3-7
 (Graphical Presentation) 3-19
 through 3-26
 Transit Time 2-22
 (Graphical Presentation) 2-40
 through 2-51
 Injection Velocity
 Final Injection Velocity 2-22
 (Graphical Presentation) 2-29
 through 2-32
 Initial Injection Velocity 2-21
 (Graphical Presentation) 2-22
 through 2-28
 Total Injection Velocity 2-22
 (Graphical Presentation) 2-34
 through 2-39
 Transit Time 2-22, A-2
 (Graphical Presentation) 2-40 through 2-51

I

IDEAL VELOCITY (Impulsive) 2-68, A-5

IMPACT

Dispersion 3-33

(also see DISPERSIONS)

Downrange, Correlation of 3-48

Downrange-Crossrange, Correlation of 3-48

Location 3-33, B-7

Nonrotating Earth Range 3-36

(Graphical Presentation) 3-37, 3-38

Range 3-35

Correction, Rotating Earth 3-41

From Burnout (Nonrotating Earth)

(Graphical Presentation) 3-37, 3-38

Range Computation 3-36

Latitude of Impact 3-36, B-8

Longitude of Impact 3-41, B-7

Zone 3-43, B-11

(Illustration) 3-34

Probability 3-43, B-11

INJECTION VELOCITY

Dog-Leg Maneuver (see DOG-LEG MANEUVER)

Hohmann Transfer (see HOHMANN TRANSFER)

INTERPLANETARY MISSIONS 2-50

Deboost (see LUNAR/PLANETARY DEBOOST)

Direct Ascent 2-4

Parking Orbit-Transfer 2-3

Trajectory Inclination 3-3

Velocity Requirement

Escape 2-55

Lunar 2-52

(Graphical Presentation) 2-53, 2-54

Mars 2-55

(Graphical Presentation) 2-58

Venus 2-55

(Graphical Presentation) 2-57

K

KICK ANGLE 2-62, 10A

Low Altitude Parking Orbit, for

(Graphical Presentation) 2-66

L

LAGRANGE SOLUTION, FOR CONSTRAINED
MAXIMUM AND MINIMUM PROBLEMS 5-78

LAUNCH SITE

Limitations 3-1, B-1

Earth's Rotation 3-1, B-1

(Graphical Presentation) 3-2

Exit Azimuth

(Tabular Presentation) 3-30

Location

(Tabular Presentation) 3-30

Trajectory Inclination 3-3

(Graphical Presentation) 3-4

Velocity Penalty for Equatorial Orbits 3-5

(Tabular Presentation) 3-5

Window 2-4, 2-55

LIFTING VEHICLE 7-1

LOADING OF THE STRUCTURAL SYSTEM 7-3

(also see ACCELERATION, DECELERATION,
and SYSTEM CONSIDERATIONS)

LOADS AND AERODYNAMIC HEATING

3-49, B-14

Dynamic Pressure, Maximum 3-53, B-16

(also see DYNAMIC PRESSURE)

Heat Input Total 3-59, B-16

(also see HEATING DURING BOOST
TRAJECTORY)

Heating Rate, Maximum 3-59, B-16

(also see HEATING DURING BOOST
TRAJECTORY)

Staging 3-49, B-15

(also see STAGING)

LOOK ANGLE 3-66, B-20

LUNAR

Impact Velocity 6-9

(Derivation) E-7

(Graphical Presentation) 6-11

Landing, Vertical Descent 6-9, E-7

Effect of Thrust-to-Weight Ratio

(Graphical Presentation) 6-16

Mass Ratio

(Graphical Presentation) 6-12

Total Ideal Velocity

(Graphical Presentation) 6-13
through 6-15

LUNAR (Continued)

Missions

Requirements 2-52, 2-55

System Considerations

Trajectory Inclination 3-3

Velocity Requirements, for 2-52

(Graphical Presentation) 2-53, 2-54

LUNAR/PLANETARY DEBOOST

Deboost Angle for Minimum Velocity 6-8

Deboost Equations 6-3

(Derivation) E-1

Planetary Data for 6-8

(Tabular Presentation) 6-9

Error Equations

(Analytical Expression) 6-4

(Derivation) E-2

Miss Equations

(Analytical Expression) 6-6

(Derivation) E-3

Optimum Deboost Angle for Minimum Velocity (Proof) E-4

Planetary Data for Deboost Equations 6-8

(Tabular Presentation) 6-9

Specified Deboost Conditions for Equations 6-3

M

MACH NUMBER AT PEAK DRAG

(Graphical Presentation) 2-86

MARGIN, PERFORMANCE (see PERFORMANCE MARGIN CONCEPT)

MARS

Atmosphere 7-5

Entry (see LUNAR/PLANETARY DEBOOST, and PLANETARY ENTRY)

Mission Requirements 2-52, 2-55

Velocity Requirements 2-55

(Graphical Presentation) 2-58

MINIMUM ENERGY ORBITAL TRANSFER (see HOHMANN TRANSFER)

MISSION PROFILE, OPTIMIZING THE 2-2

MISSION REQUIREMENTS 2-2

(also see LUNAR, ORBITAL, MARS and VENUS)

N

NITROGEN 7-34

Equation of State for 7-34

(Graphical Presentation) 7-36

Viscosity of 7-34

(Graphical Presentation) 7-38

NONATMOSPHERIC POWERED FLIGHT (see PRECISE EVALUATION OF PERFORMANCE)

NONROTATING EARTH IMPACT RANGE 3-36, B-9

(Graphical Presentation) 3-37, 3-38

NOZZLES

DeLaval 2-81, A-11

Expansion-Deflection 2-81, A-11

Plug 2-81, A-11

Spike 2-81, A-11

O

OPTIMUM

Attitude, Thrust (see TRAJECTORY OPTIMIZATION)

Sizing (see SIZING)

ORBITAL SATELLITE

Deboost (see LUNAR/PLANETARY DEBOOST)

Dog-Leg (see DOG-LEG)

Lifetime 2-3

Missions 2-2, A-1

Trajectory Inclination 3-3

Parking 2-3

Period 2-4, A-2

(Graphical Presentation) 2-12 through 2-19

(Tabular Presentation) 2-20

Rendezvous 2-3

Transfer (see BI-ELLIPTICAL TRANSFER MANEUVER, and HOHMANN TRANSFER MANEUVER)

Velocity 2-4, A-1

(Graphical Presentation) 2-5 through 2-10

(Tabular Presentation) 2-11

OUTAGE, PROPELLANT 3-68

P

PACIFIC MISSILE RANGE

Firing Sector

(Map) 3-32

Range Safety Summary

(Tabular Presentation) 3-30

PAD, PERFORMANCE (see PERFORMANCE MARGIN CONCEPT)

PARALLEL STAGING 5-80

PARKING ORBIT 2-3

Hohmann Transfer Maneuver, from 2-3

(also see HOHMANN TRANSFER)

Interplanetary Transfer, from 2-3

Lunar Transfer, from 2-3

PATRICK AIR FORCE BASE (see ATLANTIC MISSILE RANGE)

PAYLOAD

Considerations During Entry 7-1

Attitude Control 7-1

Backward Entry 7-1

Deceleration, Alleviation During Entry 7-1

Normal Force, Alleviation During Entry 7-1

Temperature Limitations 7-2

Exchange Ratios (see EXCHANGE RATIO ANALYSIS, GENERAL)

PERFORMANCE

Cursory Estimation (see CURSORY ESTIMATION OF PERFORMANCE)

Dispersions (see DISPERSIONS)

Margin Concept 3-67, B-19

Analysis 3-67, B-21

Discussion 3-67

Exchange Coefficients, Velocity 3-68

(Derivation) B-26

Summary

(Tabular Presentation) 3-68, B-26

Numerical Example 3-74

Optimization (see TRAJECTORY OPTIMIZATION)

Pad, (Reserve) 3-67

(also see PERFORMANCE MARGIN CONCEPT)

Precise Evaluation (see PRECISE EVALUATION OF PERFORMANCE)

Tradeoffs (see EXCHANGE RATIO ANALYSIS, GENERAL)

PERIGEE 2-4

Altitude 2-4, A-1

Period, Versus 2-4, A-2

(Graphical Presentation) 2-12, 2-13

Velocity, Versus 2-4, A-1

(Graphical Presentation) 2-5, 2-6

PLANETARY

Data, Constants 6-8

(Tabular Presentation) 6-9

Deboost (see LUNAR/PLANETARY DEBOOST)

PLANETARY ENTRY

Atmospheres of the Planets 7-4

Earth 7-5

Exponential Atmosphere - ARDC
Atmosphere of 1959 Comparison

(Graphical Presentation) 7-6

Mars 7-5

Venus 7-8

Deboost (see LUNAR/PLANETARY DEBOOST)

Deceleration (see DECELERATION DURING PLANETARY ENTRY)

Entry Function (General) (see ENTRY FUNCTION, GENERAL)

Heating (see HEATING DURING PLANETARY ENTRY)

Vehicle Design Considerations 7-1

Accuracy of Impact Point Prediction 7-4

Load and Structural System 7-3

Payload Considerations 7-1

Stability and Dynamic Motions 7-3

Thermal Protection 7-2

PLANETS (see EARTH, MARS, or VENUS)

PLUG, NOZZLE 2-81, A-11

POINT ARGUELLO (see PACIFIC MISSILE RANGE)

POWERED FLIGHT 2-59, A-2

(also see LUNAR/PLANETARY DEBOOST, and TRAJECTORY OPTIMIZATION)

Atmospheric 2-59, A-2

Nonatmospheric 2-92, A-12

Equations of Motion A-12

Performance (see CURSORY ESTIMATION OF PERFORMANCE, and PRECISE EVALUATION OF PERFORMANCE)

PRECISE EVALUATION OF PERFORMANCE
2-77

Coasting 2-103

Long Coast Phase 2-104

Short Coast Phase 2-103

Earth's Rotation, Effects of 2-89

Effective Acceleration of Gravity 2-97, A-13

Effective Radius 2-97, A-13

Example of Precise Performance
Estimation 2-108

First-Stage 2-80

Burnout Altitude 2-89

Burnout Altitude Constant 2-89

(Graphical Presentation) 2-90

Burnout Range Angle 2-89

(Graphical Presentation) 2-91

Drag Loss 2-81

Gravitational Loss 2-81

Mach Number at Peak Drag 2-81

(Graphical Presentation) 2-86

Mass Ratio Correction Factor 2-81

(Graphical Presentation) 2-85

Performance 2-80

Range Angle at Burnout 2-89

(Graphical Presentation) 2-91

Thrust - Atmosphere Losses 2-81

Losses

Drag 2-81, A-9

Constant 2-81

(Graphical Presentation) 2-87

Gravitational 2-81, A-8

Variation Correction 2-81, A-9

(Graphical Presentation) 2-81

Gravity Constant 2-81, A-8

(Graphical Presentation) 2-82

Thrust-Atmospheric 2-81, A-10

(Graphical Presentation) 2-88

Nonatmospheric Powered Flight Performance
Computation 2-92, A-12Constant Pitch Rate (Includes Constant
Attitude) 2-93Final Trajectory Parameters,
Computation of 2-97

Input Parameters 2-94

Iteration on Pitch Rate 2-101

Velocity Loss Computation 2-101

PRECISE EVALUATION OF PERFORMANCE
(Continued)

Differential Equations, Solution of A-15

Operation Out of Orbit 2-102

Range Angle 2-102

Velocity, Final 2-102

PRESSURE RATIO VERSUS ALTITUDE,
STANDARD ATMOSPHERE, FOR

(Graphical Presentation) 3-52

PROGRESSIVE BURNING 2-64

PROPELLANT DISTRIBUTION, OPTIMUM
(see SIZING)

R

RADIATION HEATING

Total 7-42

(Graphical Presentation) 7-43

RADIANT HEAT RATE, STAGNATION 7-9

RADIO GUIDANCE 2-3, 3-62

RANGE ANGLE AT BURNOUT, FIRST-STAGE
2-89

(Graphical Presentation) 2-91

RANGE ERROR COEFFICIENTS (see
DISPERSIONS)

RANGE SAFETY

Constraints and Considerations 3-28

Launch Site

Summary

(Tabular Presentation) 3-30

Orbit Inclination, Realizable

(Tabular Presentation) 3-30

Dog-Leg Maneuver 3-6, 3-40, B-4

Dispersions (see DISPERSIONS)

Exit Azimuth 3-30

Limitations 3-30

Firing Sector

Atlantic Missile Range

(Map) 3-31

Pacific Missile Range

(Map) 3-32

Hazards 3-29

Impact

Location 3-30, 3-33, B-7

Point Prediction, Accuracy of, During
Atmospheric Entry 7-4

RANGE SAFETY (Continued)

Impact (Continued)

Range Computation 3-36

Zone 3-43, B-11

Range 3-36, B-7

Summary

(Tabular Presentation) 3-30

Template 3-34

RANGE, SLANT 3-62, B-18

REGRESSIVE (OR PROGRESSIVE) BURNING 2-64

RESTART CAPABILITY 2-3

REYNOLDS NUMBER 7-41, 7-42

Below Transition 7-42

Definition 7-41

Maximum for $(W/C_{DA}, R_N)$ 7-42

(Analytical Expression) 7-42

ROTATING EARTH, IMPACT RANGE
CORRECTION 3-41

S

SATELLITE 2-3, A-1

(also see ORBITAL, SATELLITE)

SIZING

Examples 5-80

Minimum Cost 5-89

Parallel Staging 5-80

Sizing Nomograph 5-74

General Design - Sizing Trajectory Program
5-66

General Optimum Sizing 5-78

Development of Solution 5-78

Examples 5-80

Lagrange Solution (for Constrained Maximum
and Minimum Problems) 5-78Optimum Sizing for Maximum Payload
Weight 5-64, D-6

Constant Structure Factor 5-67

(Derivation) D-6

Optimum Sizing Nomograph 5-73

(Derivation) D-15

(Graphical Presentation) inside back
cover

Illustrated Example 5-74

SIZING (Continued)

Variable Structure Factor 5-68

Higher Order Approximation 5-71

(Derivation) D-11

Given Initial Gross Weight 5-71

Given Payload Weight 5-72

Linear Structure Factor 5-69, D-8

(Derivation) D-8

Given Initial Gross Weight 5-69

Given Payload Weight 5-70

Payload Ratio 5-3, D-1

Infinite Staging 5-3

(Derivation) D-4

(Graphical Presentation) 5-9, 5-10

One Stage 5-3

(Derivation) D-1

(Graphical Presentation) 5-7, 5-8

Multiple Staging 5-4

Like Parameters 5-4

(Derivation) D-2

(Graphical Presentation) 5-11
through 5-42Unlike Structure Factors (Two Stages)
5-5

(Derivation) D-3

(Graphical Presentation) 5-43
through 5-58

Stage Mass Ratio 5-5, D-5

Infinite Staging 5-6

Multiple Staging

Like Parameters 5-6

(Derivation) D-5

(Graphical Presentation) 5-61
through 5-63Unlike Structure Factors (Two Stages)
5-6

(Derivation) D-5

(Graphical Presentation) 5-59,
5-61 through 5-63

One Stage 5-5

(Derivation) D-5

(Graphical Presentation) 5-60

SLANT RANGE 3-62, B-18

SOUNDING FLIGHT 12A

Velocity for

(Graphical Presentation) 45A

Velocity Correction for Gravity Turn

(Graphical Presentation) 46A through 53A

SPIKE NOZZLE 2-81, A-11**SPIN STABILIZATION 2-3****STABILITY AND DYNAMIC MOTION 7-3**

During Entry 7-3

STAGING 3-49

Axial Acceleration, at 3-49, B-15

Dynamic Pressure, at 3-49

Parallel 5-80

Tandem 5-80

STRUCTURE FACTOR 5-64, D-1

Curve Fits 5-65

SYSTEM CONSIDERATIONS 3-1, B-1(also see GUIDANCE AND TRACKING,
LAUNCH SITE LIMITATIONS,
LOADS AND AERODYNAMIC HEATING,
PERFORMANCE MARGIN CONCEPT, and
RANGE SAFETY)**T****TANDEM STAGING 5-80****THERMAL PROTECTION SYSTEM 7-2**

Ablating Materials 7-2

Heat Sink 7-2

**THRUST-ATMOSPHERE, LOSSES 2-68, 2-81,
A-4, A-10****THRUST ATTITUDE PROGRAM, OPTIMUM**

Ballistic Missile, for 7A

General Case 9A

Constant Specific Impulse 20A

Variable Specific Impulse (Function of
Flowrate) 20AVariable Specific Impulse (Function of
Time) 17A

Satellite Launcher 7A

Aerodynamic Forces Effect 9A

Correction for Uniform Force Field 15A

TIME 7-17Between Two Maximums of Different
Phenomenon 7-17 t/t_{max} of 7-17

(Graphical Presentation) 7-21 through 7-24

For Pressure Change 7-10

Maximum Dynamic Pressure 3-53

(Graphical Presentation) 3-54, 3-55

TRACES (or Earth Track)

Trajectory 3-35

TRACKING 2-3, 3-59, B-18**TRADEOFFS, PERFORMANCE (see EXCHANGE
RATIO ANALYSIS, GENERAL)****TRAJECTORY**

Earth Track 3-35

Inclination 3-3, B-3

Interplanetary Missions 3-6

Lunar Missions 3-5

Orbital Missions 3-3

Range Safety

Dog-Leg Maneuver 3-6

Optimization 1A

Ballistic Missiles 4A

Thrust Attitude Program, Optimum 7A

Bibliography 57A

Design Optimization 24A

General Formulation of Problems 13A

Powered Flight in Two or Three
Dimensions, for 1A

Satellite Launcher

Optimum Thrust Attitude Program,
for 8AThrust Attitude Program, Optimum (see
THRUST ATTITUDE PROGRAM)Trajectory Analysis, Block Diagram for
26A

Variational Solution 13A

Velocity

Attitude Variable 12A

(Graphical Presentation) 29A
through 36A

Gravity Turn, for

(Graphical Presentation) 37A
through 44A

Subject Index

TRAJECTORY (Continued)

Velocity (Continued)

Vertical Flight 12A

(Graphical Presentation) 45A

Correction to, for Gravity Turn

(Graphical Presentation) 46A
through 53A

Profile, Typical 2-62

(Graphical Presentation) 2-61

TRANSFER, ORBITAL (see BI-ELLIPTICAL
TRANSFER, and HOHMANN TRANSFER)

TRANSIT TIME, HOHMANN TRANSFER 2-22

(Graphical Presentation) 2-40 through 2-51

U

UPPER STAGE

Losses 2-77

Average Flight Path Angle 2-77

Operating Out of Orbit 2-102

Range Angle 2-102

Velocity Computation 2-102

Performance Computation (see CURSORY
ESTIMATION OF PERFORMANCE, and
PRECISE EVALUATION OF PERFORMANCE)

V

VANDENBURG AIR FORCE BASE (see PACIFIC
MISSILE RANGE)

VEHICLE

Angular Displacement 3-66, B-20

Design Considerations

Atmospheric Entry, for 7-1

Systems Consideration, for (see SYSTEMS
CONSIDERATIONS)

Performance, Estimation Techniques 2-1

(also see CURSORY ESTIMATION OF
PERFORMANCE, and PRECISE
EVALUATION OF PERFORMANCE)

Sizing 5-1, D-1

(also see SIZING)

VELOCITY

Attitude Variable 12A

(Graphical Presentation) 29A through 36A

VELOCITY (Continued)

Exchange Coefficients

Burnout Weight

(Analytical Expression) 3-69

(Derivation) B-24

(Graphical Presentation) 3-71

Inert Weight

(Analytical Expression) 3-69

(Derivation) B-23

(Graphical Presentation) 3-70

Payload Weight

(Analytical Expression) 3-69

(Derivation) B-23

(Graphical Presentation) 3-70

Propellant Weight

(Analytical Expression) 3-69

(Derivation) B-24

(Graphical Presentation) 3-70, 3-71

Specific Impulse

(Analytical Expression) 3-69

(Derivation) B-22

(Graphical Presentation) 3-72

Thrust

(Analytical Expression) 3-69

(Derivation) B-25

(Graphical Presentation) 3-73

Gravity Turn, for 12A

(Graphical Presentation) 37A through 44A

Losses for First Stage 2-68, A-2

Losses for Upper Stages 2-77, A-7

Range Error Coefficient 3-43

(Graphical Presentation) 3-44, 3-45

Requirements for

Lunar Mission 2-52

(Graphical Presentation) 2-53, 2-54

Mars 2-55

(Graphical Presentation) 2-58

Venus 2-55

(Graphical Presentation) 2-57

Vertical Flight, for 12A

(Graphical Presentation) 45A

Correction for Gravity Turn Flight

(Graphical Presentation) 46A
through 53A

Subject Index

I-15

VENUS

Atmosphere 7-8
 Entry (see LUNAR/PLANETARY DEBOOST,
 and PLANETARY ENTRY)
 Mission Requirements 2-52, 2-55
 Velocity Requirements 2-55
 (Graphical Presentation) 2-57

VERTICAL

Ascent
 Burnout Altitude A-11
 Flight A-11, 17A
 Rise Time 2-62
 (Graphical Presentation) 2-67

VERTICAL (Continued)

Velocity for 12A
 (Graphical Presentation) 46A
 Correction for Gravity Turn Flight
 (Graphical Presentation) 47A
 through 53A
 Descent (see LUNAR LANDING)

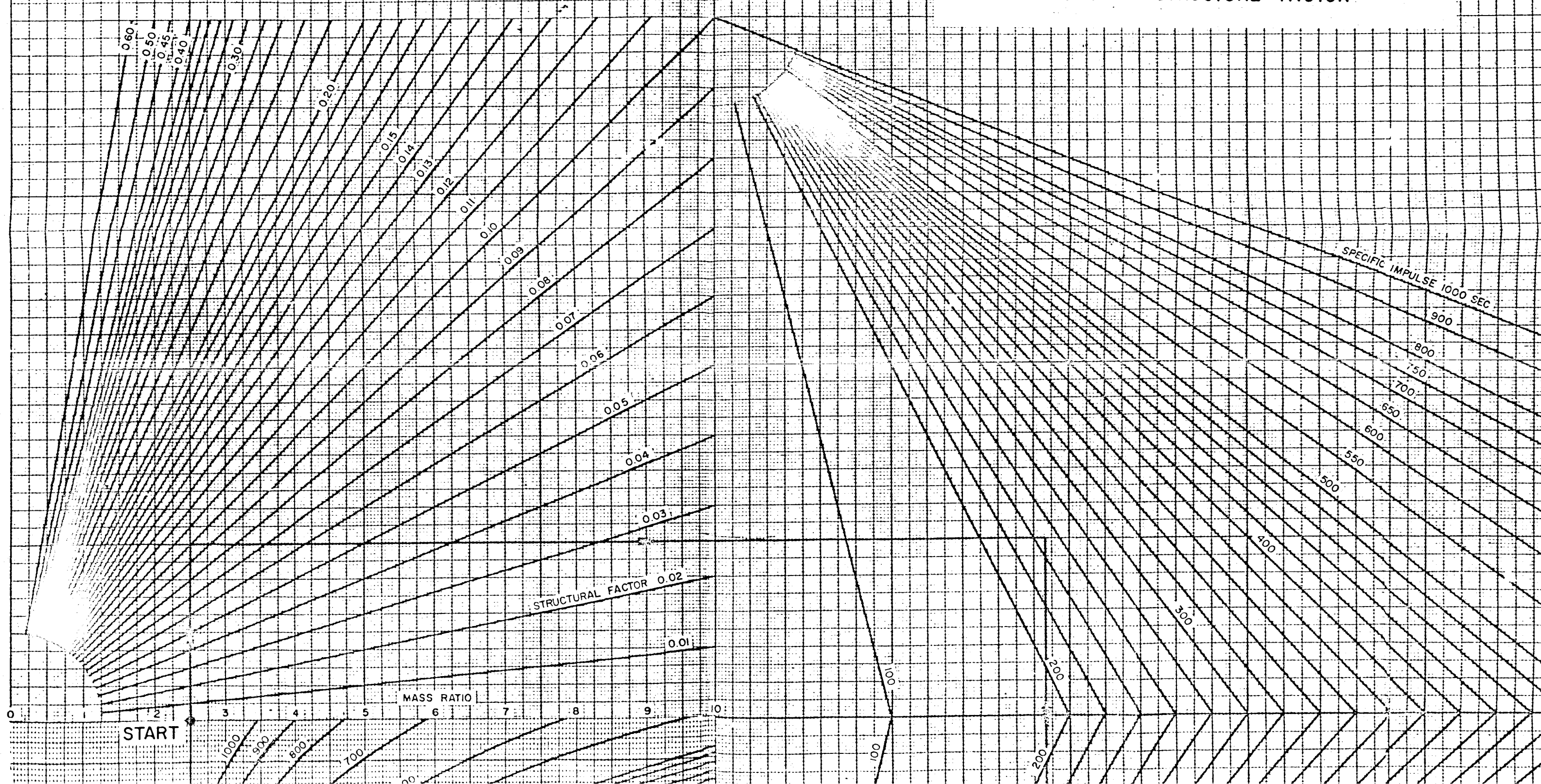
W
WALLOPS ISLAND

Range Safety Summary
 (Tabular Presentation) 3-30

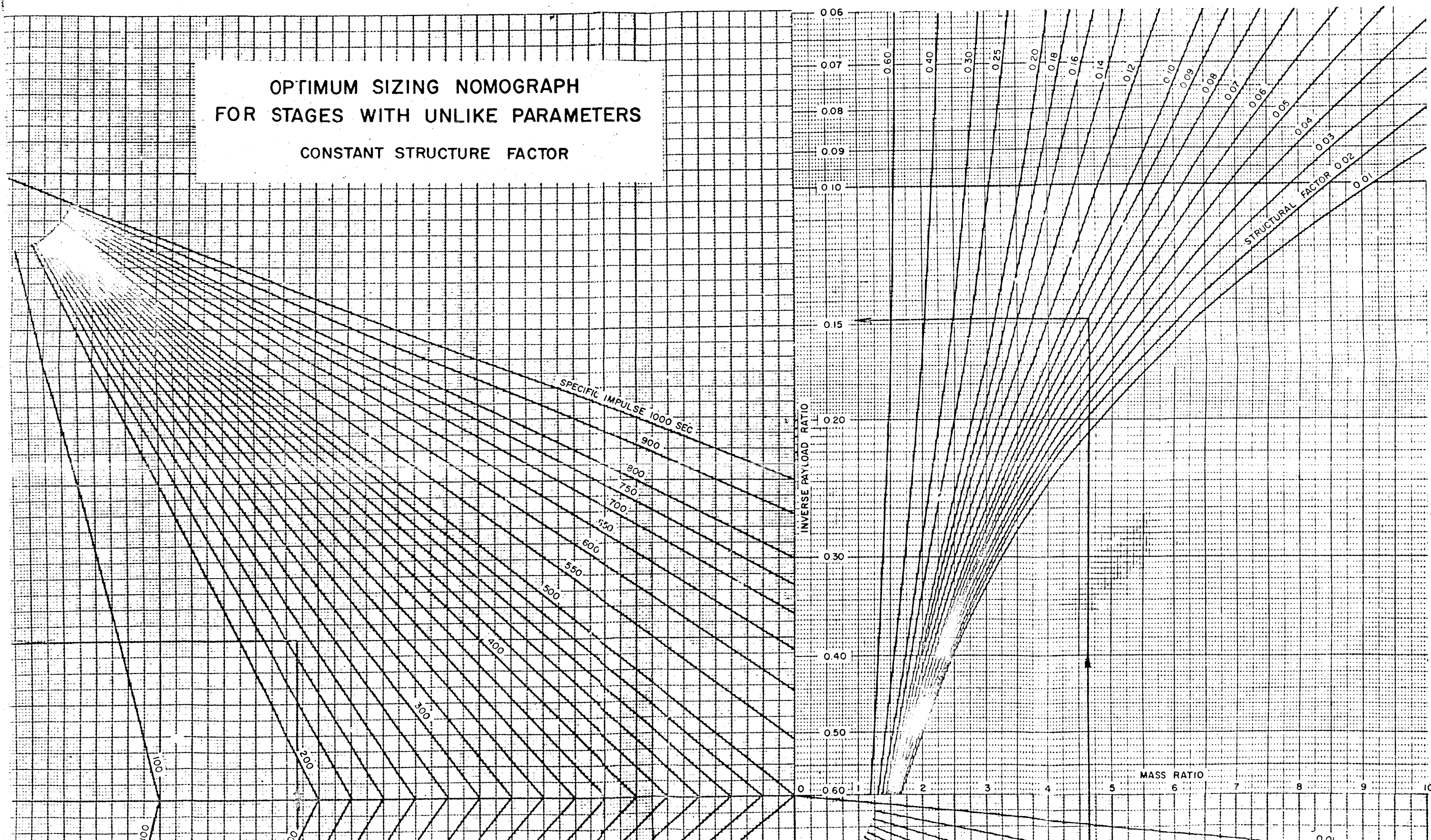
Z

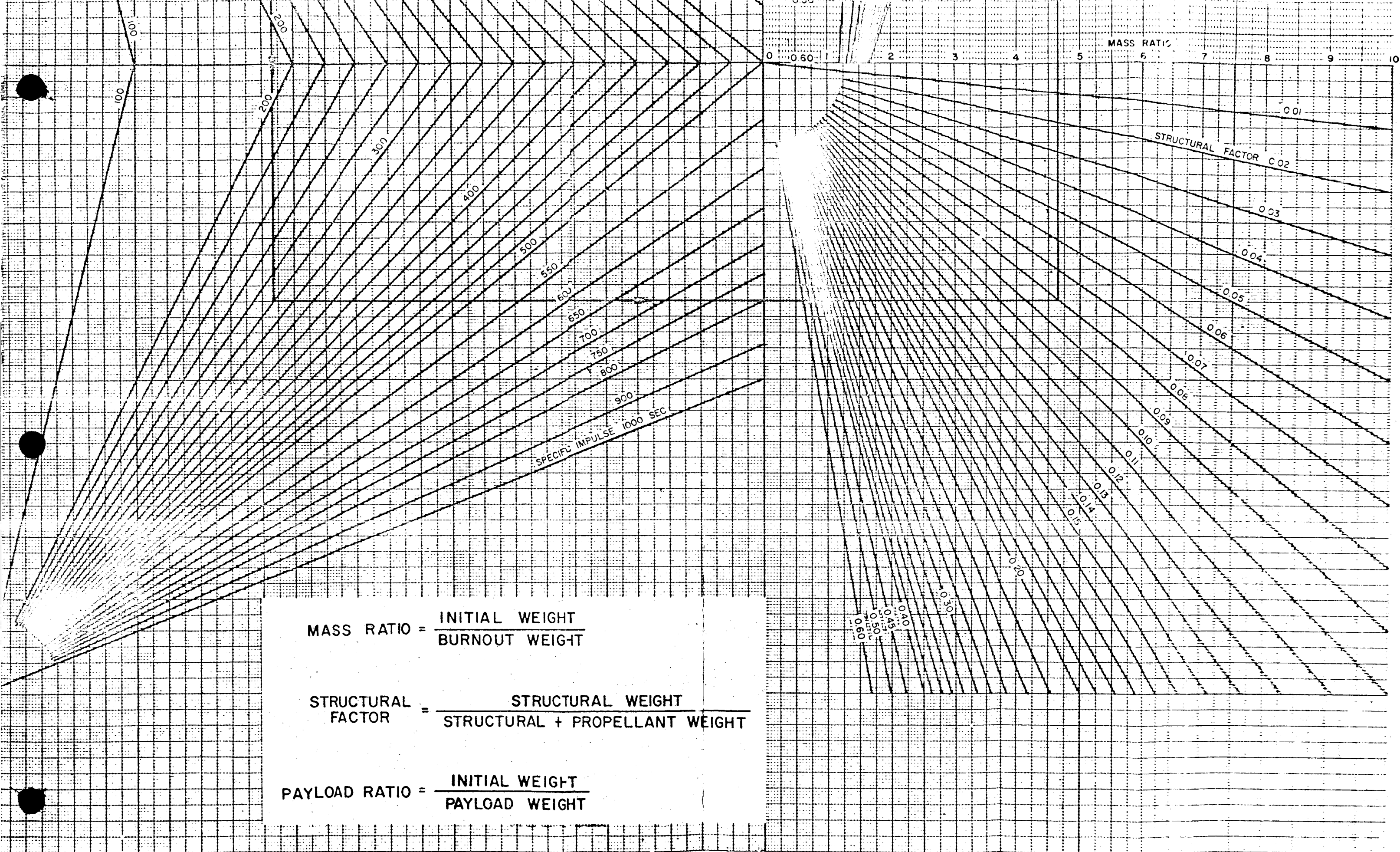
ZONE, IMPACT (see IMPACT)

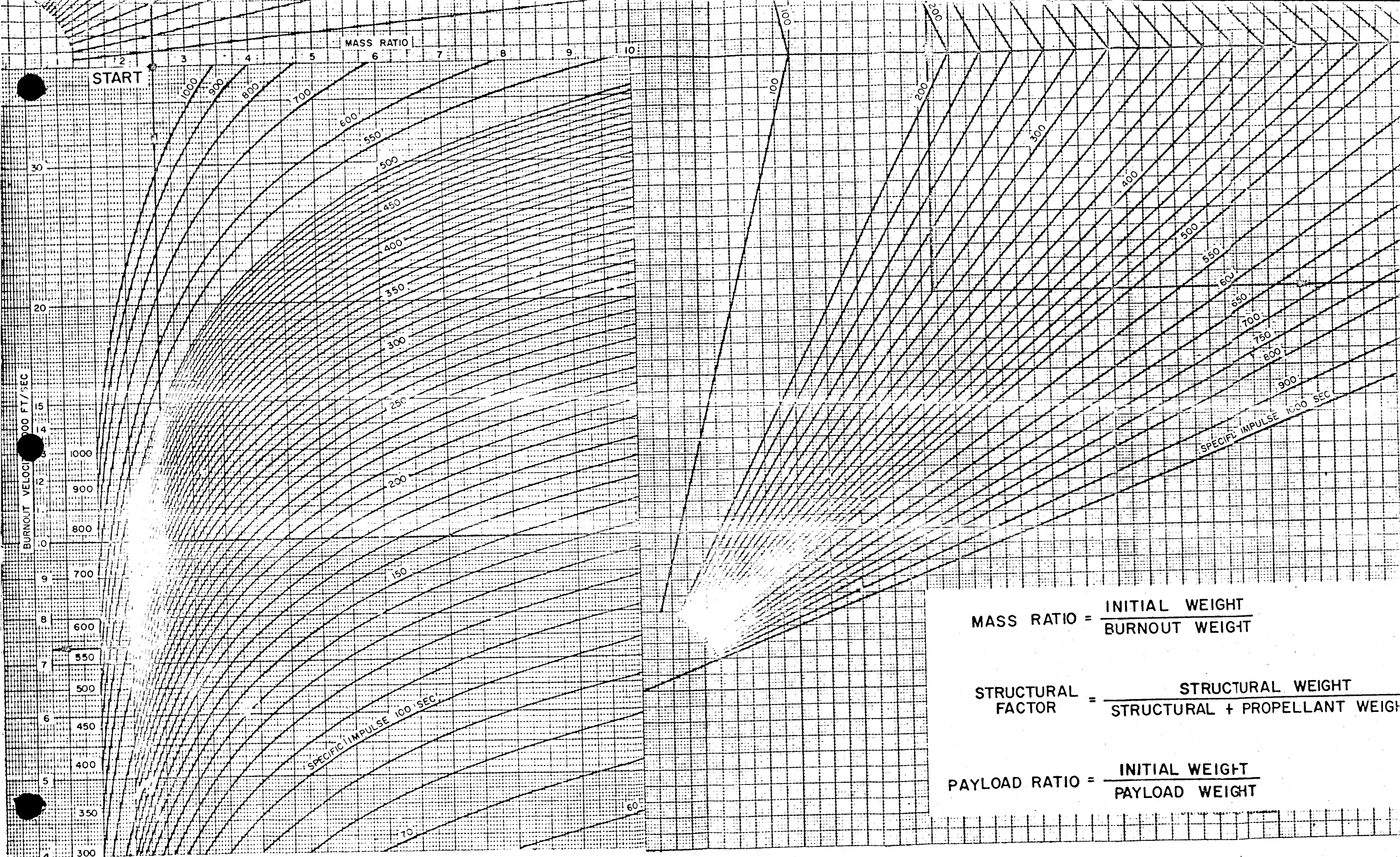
OPTIMUM SIZING NOMOGRAPH
FOR STAGES WITH UNLIKE PARAMETERS
CONSTANT STRUCTURE FACTOR



OPTIMUM SIZING NOMOGRAPH FOR STAGES WITH UNLIKE PARAMETERS CONSTANT STRUCTURE FACTOR







$$\text{MASS RATIO} = \frac{\text{INITIAL WEIGHT}}{\text{BURNOUT WEIGHT}}$$

$$\text{STRUCTURAL FACTOR} = \frac{\text{STRUCTURAL WEIGHT}}{\text{STRUCTURAL + PROPELLANT WEIGHT}}$$

$$\text{PAYLOAD RATIO} = \frac{\text{INITIAL WEIGHT}}{\text{PAYLOAD WEIGHT}}$$